Electronic Supplementary Material (ESI) for Dalton Transactions.

Supporting Information

Tuning the Spin-Crossover Properties of $Fe^{II}_4L_6$ Cages via the Interplay of Coordination Motif and Linker Modifications

Tobias Paschelke,[a] Eicke Trumpf,[a] David Grantz,[a] Malte Pankau,[a] Niclas Grocholski,[a] Christian Näther,[b] Frank D. Sönnichsen[a] and Anna J. McConnell*[a],†

[a] Otto Diels Institute of Organic Chemistry, Kiel University, Otto-Hahn-Platz 4, Kiel 24098, Germany

[b] Institute of Inorganic Chemistry, Kiel University, Max-Eyth-Strasse 2, Kiel 24118, Germany

† Current address: Department of Chemistry and Biology, University of Siegen, Adolf-Reichwein-Strasse 2, Siegen 57068, Germany

* Email: anna.mcconnell@uni-siegen.de

Table of Contents

1 Materials and Methods

Reagents and solvents were purchased from commercial suppliers and used without further purification, unless otherwise specified. Deionised water was used in all cases and for Suzuki reactions, the water was degassed using three freeze-pump-thaw cycles. Tetrahydrofuran was dried using a Pure Solv MD-5 apparatus. Tetrakis(triphenylphosphine)palladium(0) was purchased commercially and stored under a nitrogen atmosphere. CD_3CN for the preparation of the $Fe^{II}_4L_6$ cages was dried using the following procedure: using dried glassware, 50 mL of CD_3CN was dried over 1 g of CaH_2, distilled and stored over molecular sieves (3-4 Å).

Fluorescence indicator plates (Polygram® SIL G/UV_{254}) from Macherey Nagel were used for thin-layer chromatography measurements having a coating thickness of 0.2 mm. Column flash chromatography was performed using an Isolera One from Biotage® with Biotage® SNAP Ultra (10g, 25g) and Biotage® Sfär Silica HC D columns (10g, 25g).

1.1 NMR Spectroscopy

NMR spectra were recorded on Bruker Avance 200, Bruker AvanceNeo 500, or Bruker Avance 600 spectrometers. Chemical shifts for ^{1}H, ^{13}C, and ^{19}F spectra are expressed in parts per million (ppm) and coupling constants (*J*) are reported in Hertz (Hz). ^{1}H and ^{13}C spectra were referenced to TMS at 0.00 ppm and ^{19}F spectra were referenced to C_6F_6 at -164.9 ppm. All measurements were carried out at 298 K unless reported otherwise. The following abbreviations are used to describe signal multiplicity for ^{1}H, ^{13}C and ^{19}F NMR spectra: s: singlet, d: doublet, t: triplet, m: multiplet, b: broad, unres.: unresolved.

The following pulse programs were used for diamagnetic compounds: zg30 (^{1}H), zgfhigqn (^{19}F), cosygpmfppqf (COSY), hsqcedetgpsp.3 (HSQC), hmbcgplpndqf (HMBC), zgpg30 (^{13}C).

The following pulse programs were used for the paramagnetic complexes: zg30 (^{1}H), zg (^{1}H), zgfhigqn (^{19}F), cosyqf90 (COSY), cosygpqf (COSY), cosyqpmfqf (COSY), hmqcgpqf (HMQC), zg (^{13}C).[1]

1.2 Mass Spectrometry

Electron Ionisation (EI) mass spectrometry was carried out on a Jeol AccuTOF. High resolution electrospray ionisation mass spectrometry (ESI-MS) was carried out on a ThermoFisher Orbitrap (spray voltage 3-4 eV, capillary temperature 40-50 °C) infused from a Harvard syringe pump at a rate of 5-10 µL per minute.

2 Ligand Synthesis

2.1 Imidazole-Based Ligand

Imidazole-based ligand **14** was synthesized according to Scheme S1 using our recently developed one-pot Sonogashira-type reaction.[2] Precursor **12** was prepared using a literature-known procedure,[3] while precursor **13** was obtained after methylation adapting a procedure from Ling and co-workers.[4]

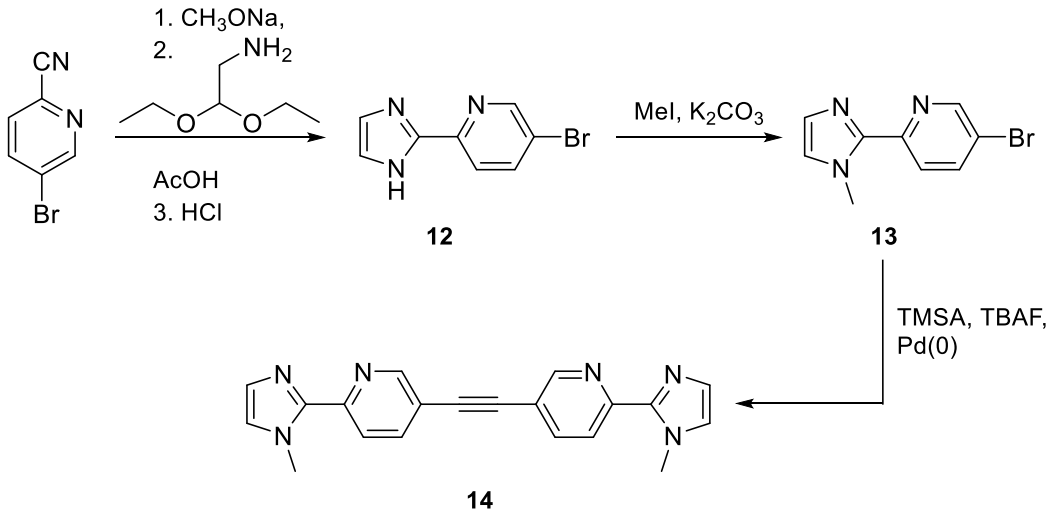

Scheme S1. Synthesis of imidazole-based ligand **14**.

2.1.1 5'-Bromo-2'-(1*H*-imidazol-2-yl)pyridine (**12**)

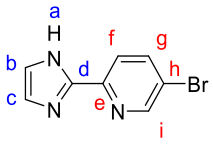

Adapted from Zhang, Ma and co-workers.[3a] 5-Bromo-2-cyanopyridine (1.83 g, 10.0 mmol) was dissolved in methanol (10 mL). The reaction mixture was treated with sodium methoxide solution (190 µL, 1.03 mmol, 5.4 M in methanol) and stirred at 40 °C for 2 h. Afterwards, aminoacetalaldehyde diethyl acetal (1.45 mL, 10 mmol) and glacial acetic acid (1.10 mL) were added at 40 °C, the mixture heated to 70 °C and stirring was continued for 0.5 h. The reaction mixture was cooled to room temperature, methanol (5 mL) and hydrochloric acid (5 mL, 6 M) were added and the mixture was heated at 75 °C for 20 h. After cooling to room temperature, methanol was removed *in vacuo* and the remaining solution cooled to 0 °C. Dropwise addition of potassium carbonate solution (5.00 g in 5.00 mL water) resulted in precipitation of the product, which was filtered and washed with water (400 mL). The product was obtained as a colourless solid (2.00 g, 8.93 mmol, 89%).

Note: After the addition of sodium methoxide, stirring at 40 °C for 2 h is necessary to ensure imidate formation.[3b]

The analytical data was consistent with literature data.[3a]

^{1}H NMR (500 MHz, DMSO-d_6, 298 K) δ (ppm): 12.9 (br, 1H, H_a), 8.71 (d, ^{4}J = 2.3 Hz, 1H, H_i), 8.12 (dd, ^{3}J = 8.5 Hz, ^{4}J = 2.3 Hz, 1H, H_g), 7.98 (d, ^{3}J = 8.5 Hz, 1H, H_f), 7.19 (s, 2H, $H_{b,c}$).

^{13}C NMR (151 MHz, DMSO-d_6, 298 K) δ (ppm): 149.6 (C_i), 147.5 (C_e), 144.5 (C_d), 139.8 (C_g), 125.5 ($C_{b,c}$), 121.01 (C_f), 118.9 (C_h).

EI-MS *m/z*: 222.97442 (calculated for $C_8H_6{}^{79}BrN_3$: 222.97451), 224.97246 (calculated for $C_8H_6{}^{81}BrN_3$: 224.97246).

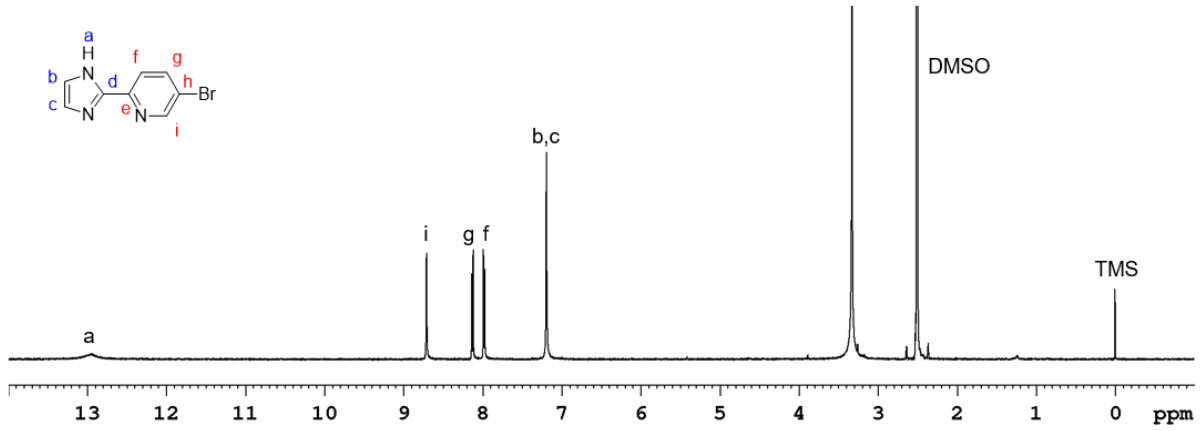

Figure S1. ^{1}H NMR spectrum (500 MHz, DMSO-d_6, 298 K) of 5'-bromo-2'-(1*H*-imidazol-2-yl)pyridine (**12**).

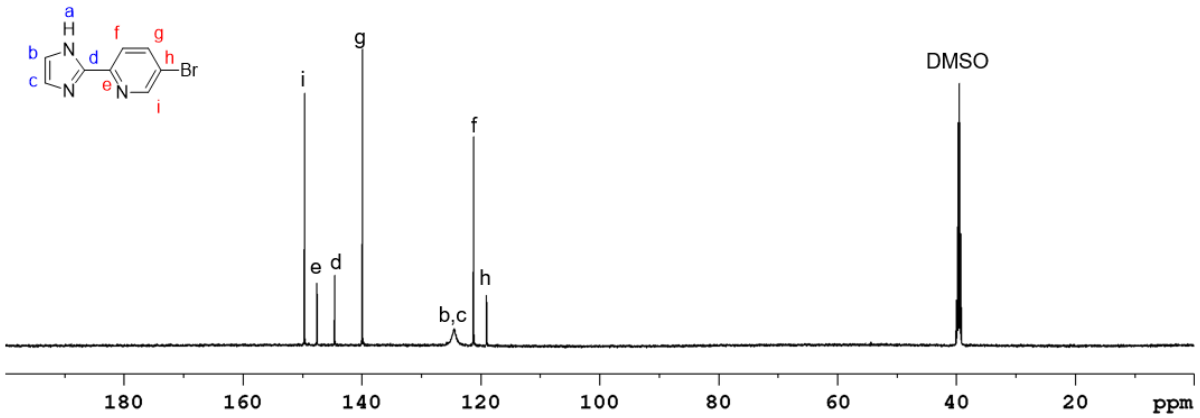

Figure S2. ^{13}C NMR spectrum (151 MHz, DMSO-d_6, 298 K) of 5'-bromo-2'-(1*H*-imidazol-2-yl)pyridine (**12**).

2.1.2 5'-Bromo-2'-(1-methyl-1*H*-imidazol-2-yl)pyridine (**13**)

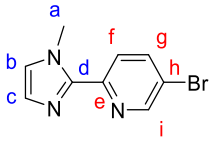

Adapted from Ling and co-workers.[4] 5'-Bromo-2'-(1*H*-imidazol-2-yl)pyridine (**12**) (1.30 g, 5.80 mmol) and potassium carbonate (2.50 g, 18.1 mmol, milled) were dissolved in dimethylformamide (50 mL). After the addition of methyl iodide (500 µL, 8.04 mmol), the mixture was stirred at room temperature for 24 h. The solution was poured into water (300 mL), the aqueous layer extracted with ethyl acetate (200 mL) and the layers separated. The organic layer was washed with brine (250 mL) and sodium hydroxide solution (200 mL, 10%) and dried over magnesium sulfate. The solvent was removed *in vacuo* and the product obtained as a brown solid (930 mg, 3.91 mmol, 67%).

^{1}H NMR (500 MHz, DMSO-d_6, 298 K) δ (ppm): 8.74 (dt, ^{4}J = 2.4 Hz, ^{6}J = 0.7 Hz, 1H, H_i), 8.13 (ddd, ^{3}J = 8.5 Hz, ^{4}J = 2.4 Hz, ^{6}J = 0.7 Hz, 1H, H_g), 8.03 (dd, ^{3}J = 8.5 Hz, ^{5}J = 0.7 Hz, 1H, H_f), 7.35 (s, 1H, H_b), 7.05 (s, 1H, H_c), 4.03 (d, ^{6}J = 0.7 Hz, 3H, H_a).

^{13}C NMR (125 MHz, DMSO-d_6, 298 K) δ (ppm): 149.0 (C_e), 148.9 (C_i), 142.9 (C_d), 139.6 (C_g), 128.0 (C_c), 125.6 (C_b), 123.7 (C_f), 118.8 (C_h), 35.9 (C_a).

ESI-MS *m/z*: 237.99731 (calculated for $C_9H_9{}^{79}BrN_3$: 237.99744).

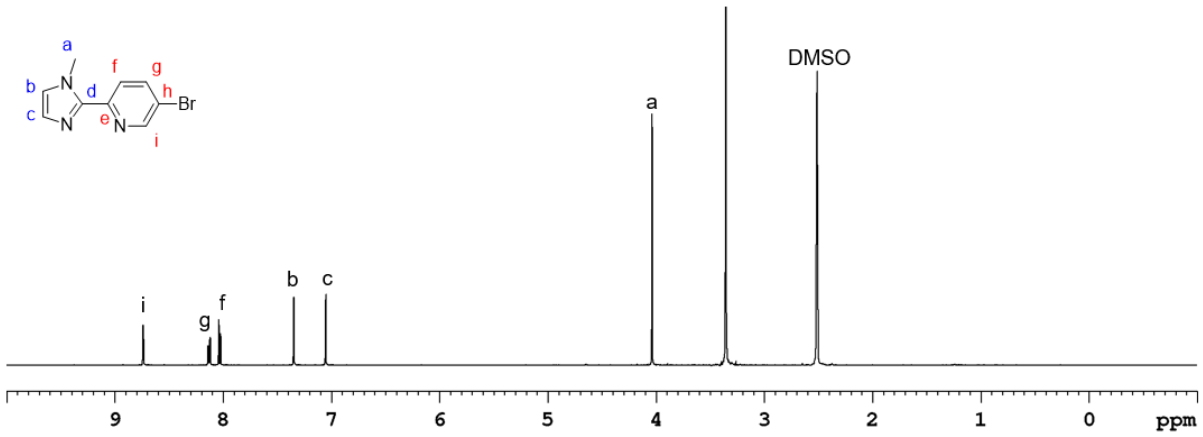

Figure S3. ^{1}H NMR spectrum (500 MHz, DMSO-d_6, 298 K) of 5'-bromo-2'-(1-methyl-1*H*-imidazol-2-yl)pyridine (**13**).

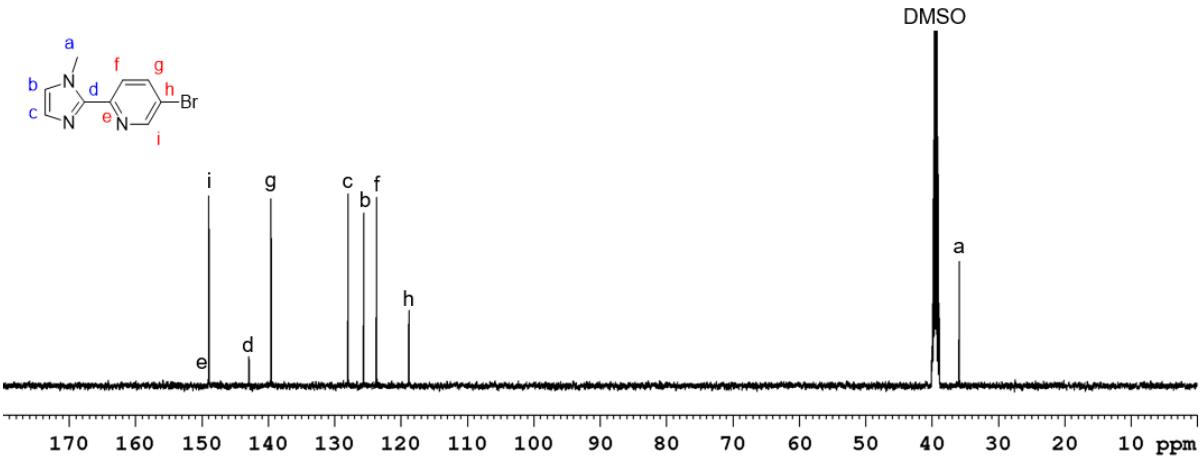

Figure S4. ^{13}C NMR spectrum (125 MHz, DMSO-d_6, 298 K) of 5'-bromo-2'-(1-methyl-1*H*-imidazol-2-yl)pyridine (**13**).

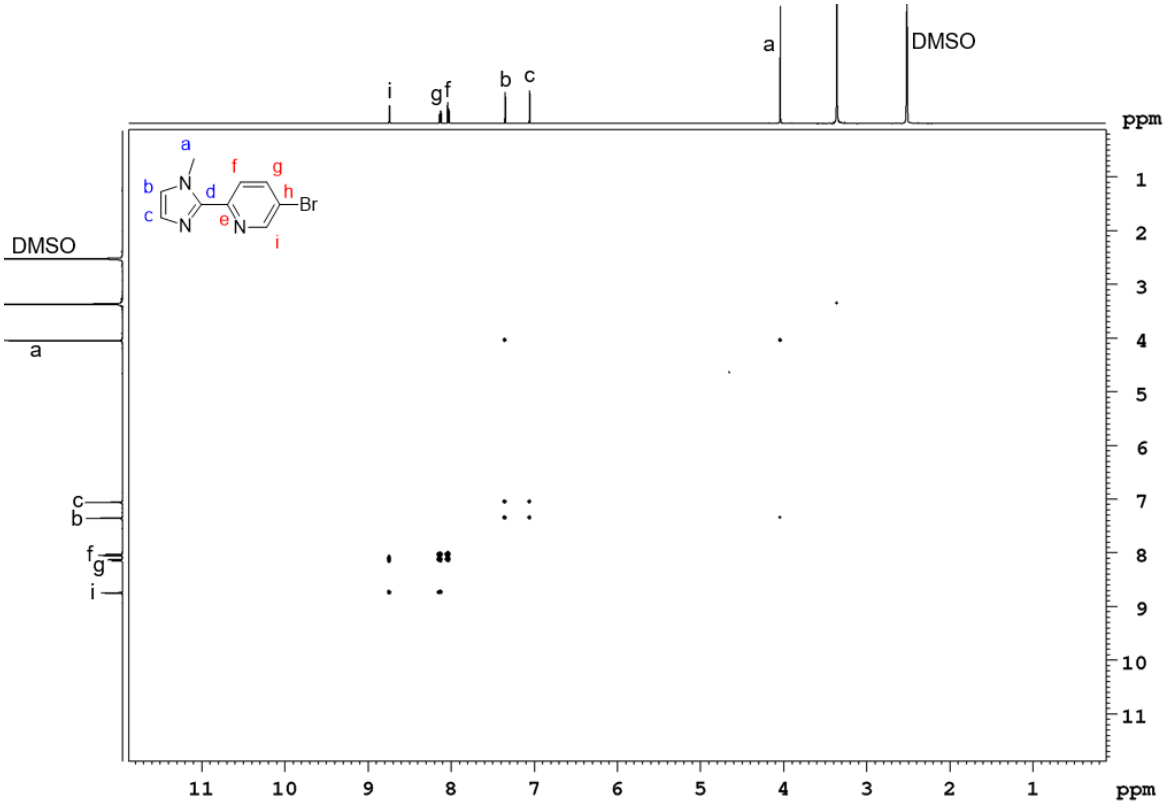

Figure S5. ^{1}H-^{1}H COSY NMR spectrum (500 MHz, DMSO-d_6, 298 K) of 5'-bromo-2'-(1-methyl-1*H*-imidazol-2-yl)pyridine (**13**).

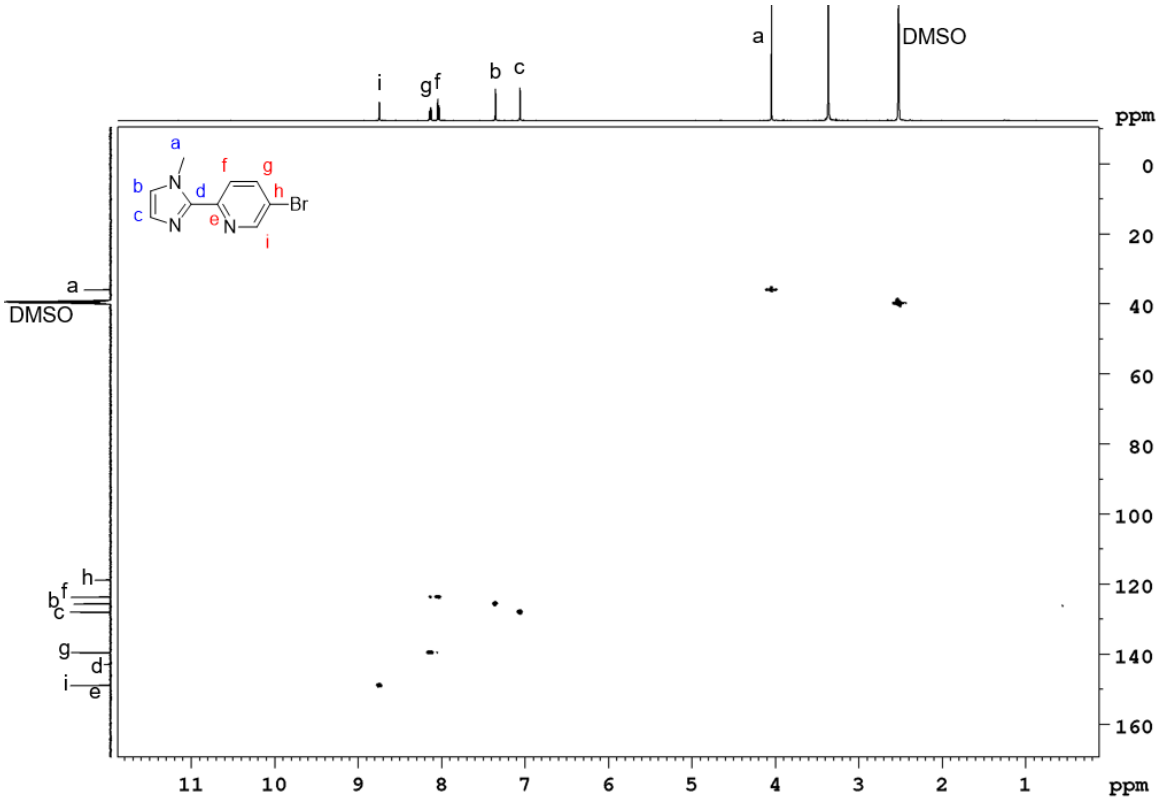

Figure S6. ^{1}H-^{13}C HSQC NMR spectrum (500 MHz/125 MHz, DMSO-d_6, 298 K) of 5'-bromo-2'-(1-methyl-1*H*-imidazol-2-yl)pyridine (**13**).

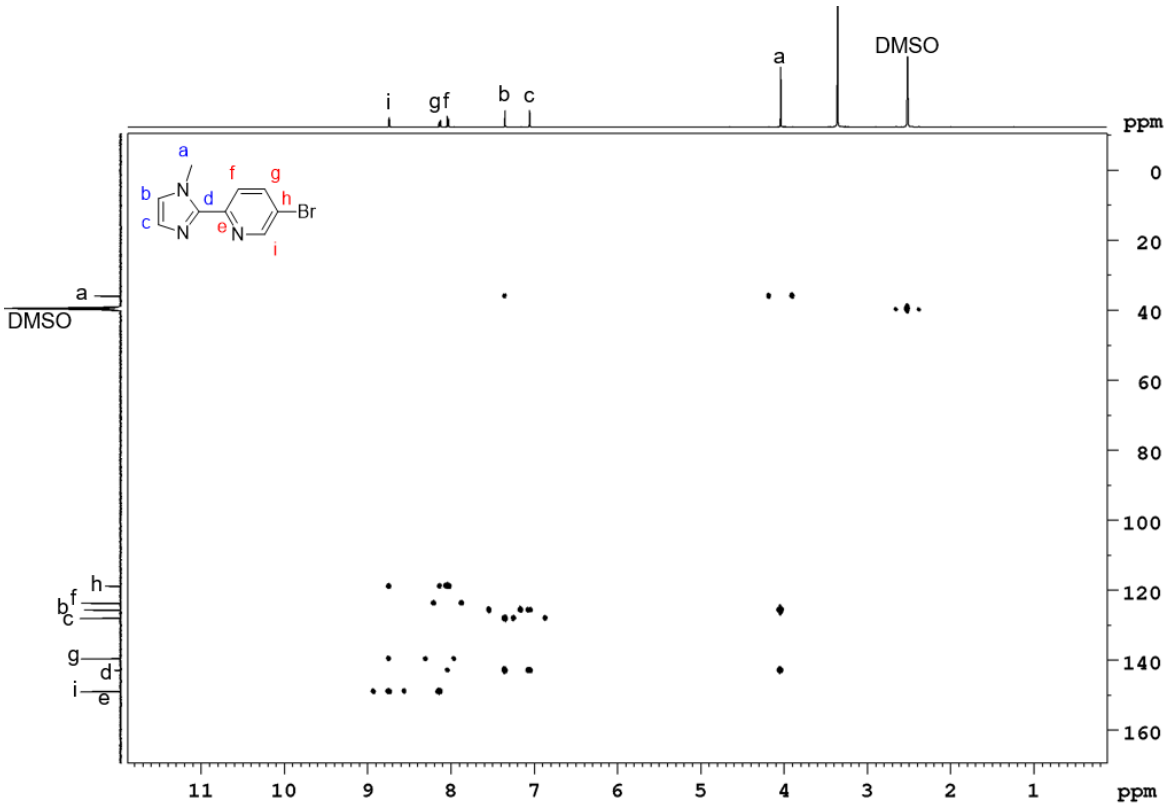

Figure S7. ^{1}H-^{13}C HMBC NMR spectrum (500 MHz/125 MHz, DMSO-d_6, 298 K) of 5'-bromo-2'-(1-methyl-1*H*-imidazol-2-yl)pyridine (**13**).

2.1.3 1,2-Bis(6''-(1'-methyl-1*H*-imidazol-2'-yl)pyridin-3''-yl)ethyne (**14**)

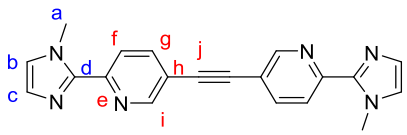

Adapted from McConnell and co-workers.[2] 5'-Bromo-2'-(1-methyl-1*H*-imidazol-2-yl)pyridine (**13**) (172 mg, 722 µmol) and $Pd(PPh_3)_4$ (41.8 mg, 5 mol%) were added to a pressure tube and the tube was evacuated for 5 min. Tetrabutylammonium fluoride (4.30 mL, 4.30 mmol) and trimethylsilylacetylene (100 µL, 723 µmol) were added, the tube immediately closed and the reaction mixture was heated at 70 °C for 19 h. After cooling to room temperature, water (50 mL) was added and the aqueous layer was extracted with dichloromethane (150 mL). The layers were separated, and the organic layer dried over magnesium sulfate and dried *in vacuo*. The crude product was further purified by flash chromatography (silica gel, 3% methanol/chloroform) and afterwards by an acid extraction where the impure product was dissolved in dichloromethane (10 mL) and the organic layer was extracted with hydrochloric acid (3 x 10 mL, 6 M). The layers were separated and the pH value of the aqueous layer adjusted to 12-14 using ammonia solution (25%). The precipitated product was collected by filtration as a yellow solid (78.5 mg, 231 µmol, 64%).

^{1}H NMR (500 MHz, $CDCl_3$, 298 K) δ (ppm): 8.74 (dd, ^{4}J = 2.1 Hz, ^{5}J = 0.8 Hz, 2H, H_i), 8.22 (dd, ^{3}J = 8.3 Hz, ^{5}J = 0.8 Hz, 2H, H_f), 7.89 (dd, ^{3}J = 8.3 Hz, ^{4}J = 2.1 Hz, 2H, H_g), 7.16 (d, ^{3}J = 1.1 Hz, 2H, H_c), 7.00 (d, ^{3}J = 1.1 Hz, 2H, H_b), 4.16 (s, 6H, H_a).

^{13}C NMR (125 MHz, $CDCl_3$, 298 K) δ (ppm): 150.8 (C_i), 149.7 (C_e), 144.2 (C_d), 139.0 (C_g), 128.7 (C_c), 125.0 (C_b), 121.8 (C_f), 118.1 (C_h), 90.2 (C_j), 36.6 (C_a).

ESI-MS *m/z*: 341.15077 (calculated for $C_{20}H_{17}N_6$: 341.15092).

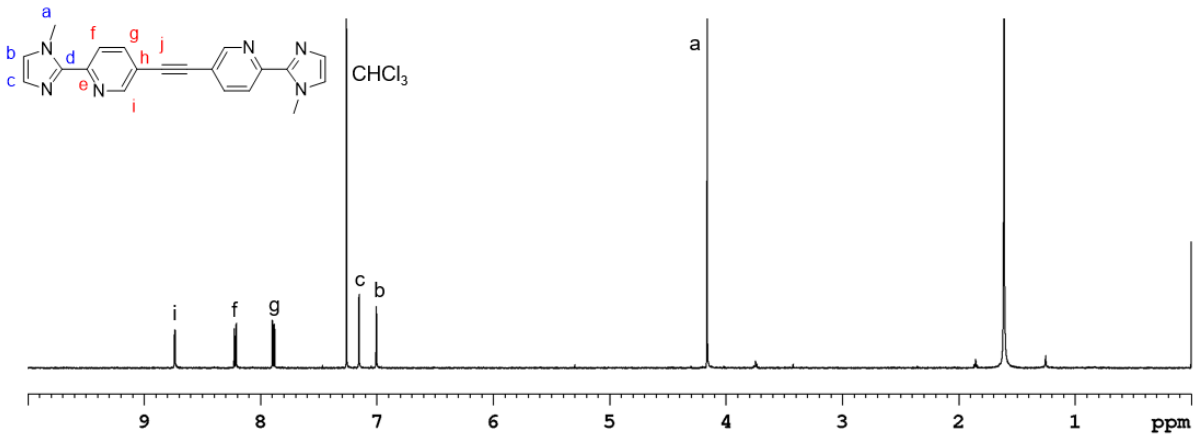

Figure S8. ^{1}H NMR spectrum (500 MHz, $CDCl_3$, 298 K) of 1,2-bis(6''-(1'-methyl-1*H*-imidazol-2'-yl)pyridine-3''-yl)ethyne (**14**).

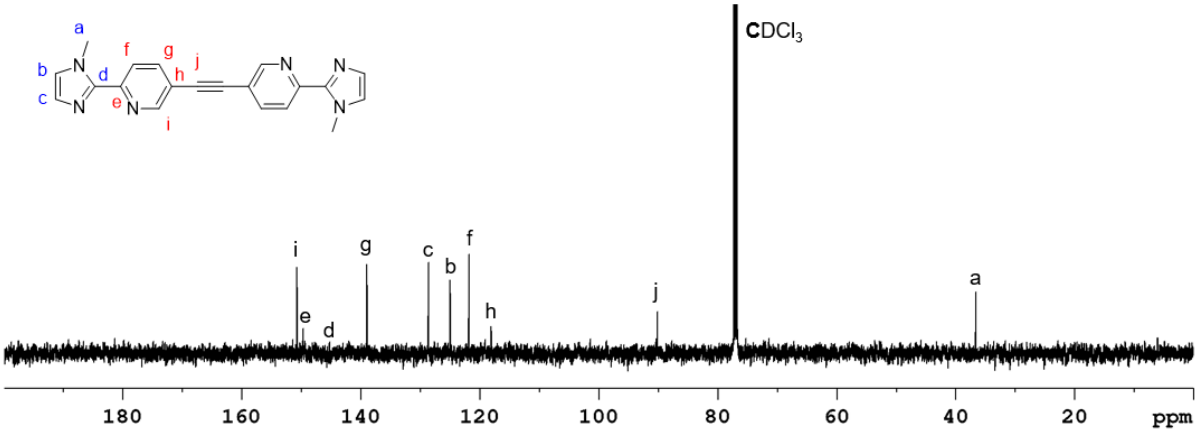

Figure S9. ^{13}C NMR spectrum (125 MHz, $CDCl_3$, 298 K) of 1,2-bis(6''-(1'-methyl-1*H*-imidazol-2'-yl)pyridine-3''-yl)ethyne (**14**).

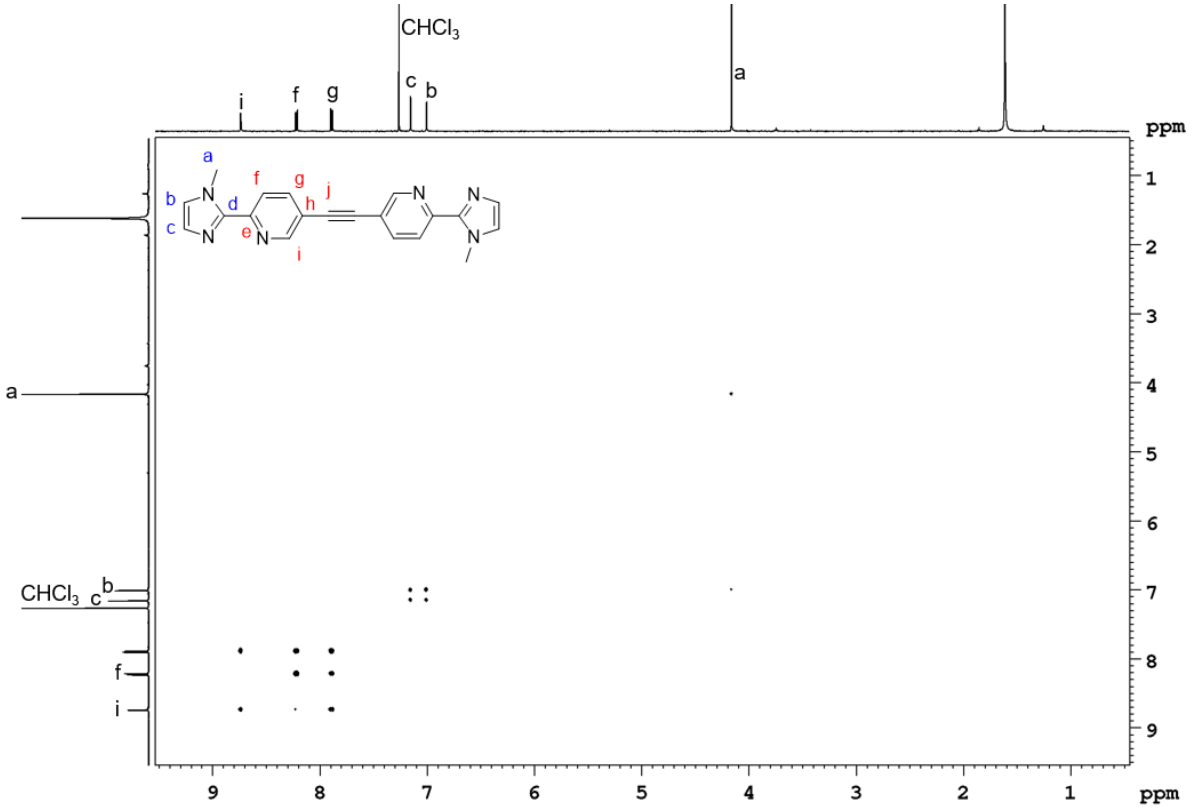

Figure S10. ^{1}H-^{1}H COSY NMR spectrum (500 MHz, $CDCl_3$, 298 K) of 1,2-bis(6''-(1'-methyl-1*H*-imidazol-2'-yl)pyridine-3''-yl)ethyne (**14**).

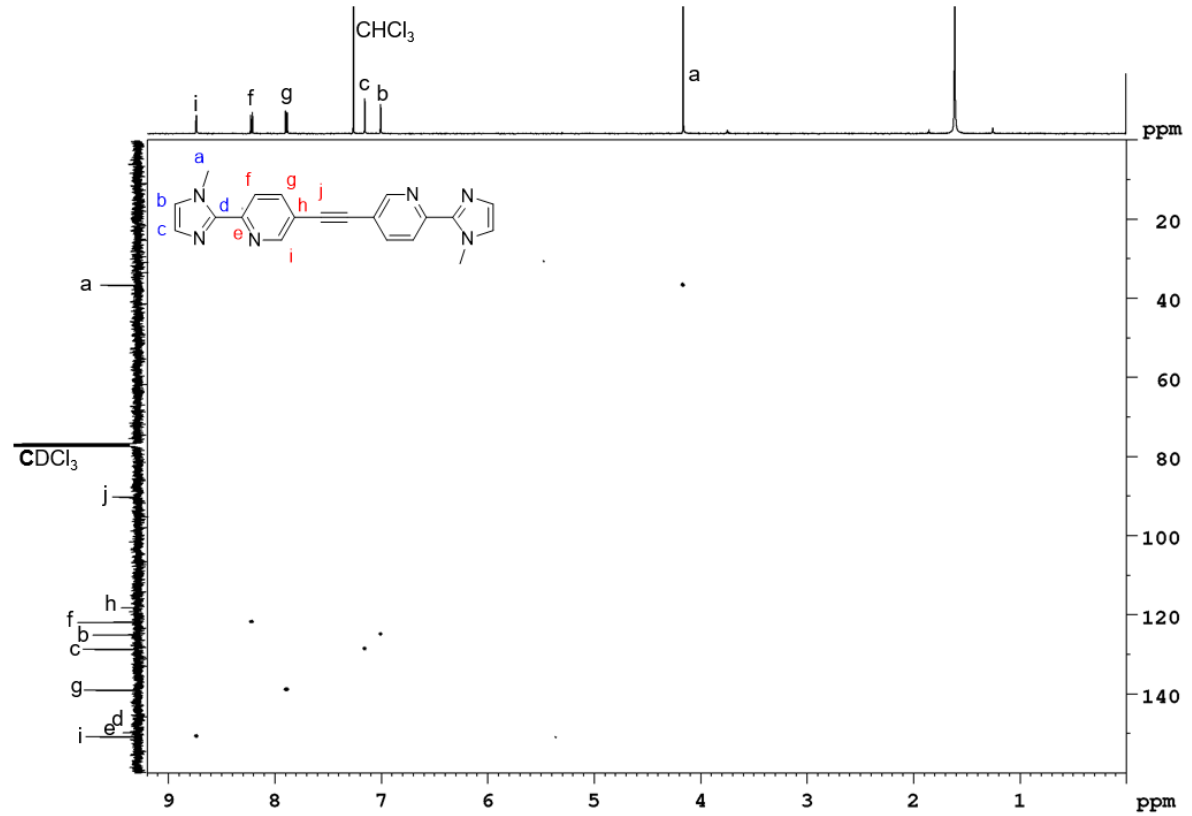

Figure S11. ^{1}H-^{13}C HSQC NMR spectrum (500 MHz/125 MHz, $CDCl_3$, 298 K) of 1,2-bis(6''-(1'-methyl-1*H*-imidazol-2'-yl)pyridine-3''-yl)ethyne (**14**).

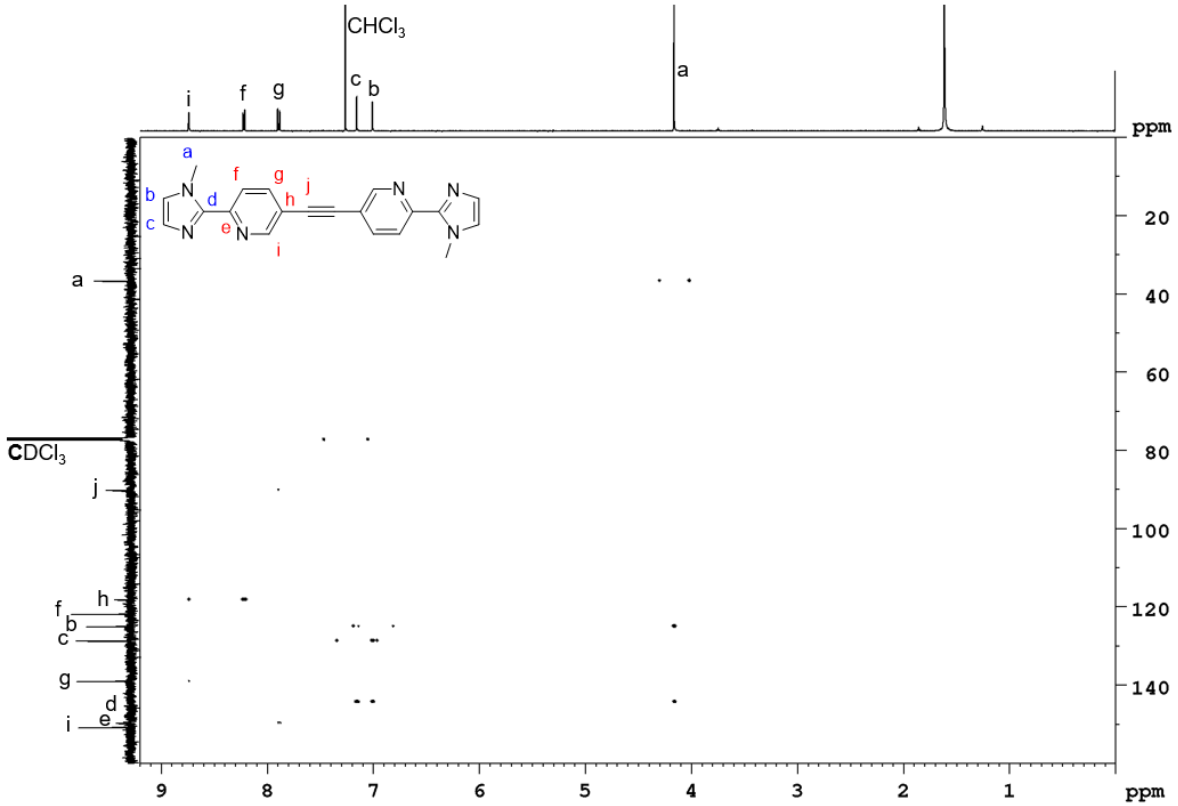

Figure S12. ^{1}H-^{13}C HMBC NMR spectrum (500 MHz/125 MHz, $CDCl_3$, 298 K) of 1,2-bis(6''-(1'-methyl-1*H*-imidazol-2'-yl)pyridine-3''-yl)ethyne (**14**).

2.2 Benzimidazole-Based Ligands with an Alkyne Linker

Benzimidazole-based ligands with an alkyne spacer were prepared according to Scheme S2. The appropriate picolinic acid and amine were reacted according to a procedure from Zhang, Ma and co-workers to obtain the precursors **15** and **20**.[3a] Methylation or benzylation reactions were adapted from literature-known procedures.[4-5] Ligands **17**, **19** and **22** were prepared using our previously reported one-pot Sonogashira-type method.[2]

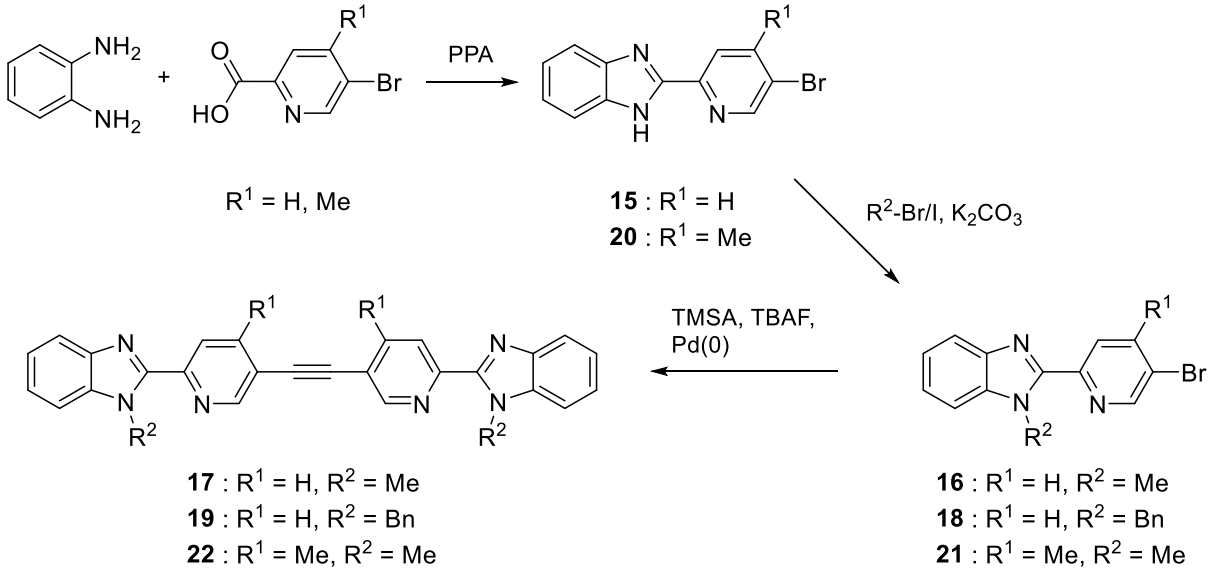

Scheme S2. Synthesis of benzimidazole-based ligands **17**, **19** and **22**.

2.2.1 Compounds **15-19**

Compounds **15-19** were synthesised according to a literature procedure and the analytical data was consistent with the literature data.[2]

2.2.2 2-(5'-Bromo-4'-methylpyridin-2'-yl)-1*H*-benzo[*d*]imidazole (**20**)

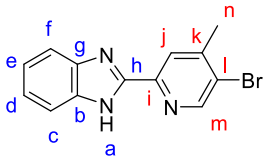

Adapted from Zhang, Ma and co-workers.[3a] Polyphosphoric acid (40 ml) was added to a three-neck flask and heated to 140 °C. *o*-Phenylenediamine (536 mg, 4.96 mmol) and 5-bromo-4-methylpyridine-2-carboxylic acid (1.07 g, 4.95 mmol) were added and the reaction was stirred at 180 °C for 23.5 h. After cooling to 140 °C, the reaction mixture was poured into water (300 mL), neutralised with ammonia solution (25%) and the precipitate collected by filtration. After washing the precipitate with water (200 mL), product **20** was obtained as a pink solid (1.03 g, 3.57 mmol, 72%).

^{1}H NMR (600 MHz, DMSO-d_6, 298 K) δ (ppm): 13.15 (s, 1H, H_a), 8.81 (s, 1H, H_m), 8.34 (s, 1H, H_j), 7.69 (unres. dt, ^{3}J = 8.0 Hz, 1H, H_c), 7.53 (unres. dt, ^{3}J = 8.0 Hz, 1H, H_f), 7.26 (td, ^{3}J = 8.0 Hz, ^{4}J = 1.2 Hz, 1H, H_e), 7.22 (td, ^{3}J = 8.0 Hz, ^{4}J = 1.2 Hz, 1H, H_d), 2.49 (s, 3H, H_n).

^{13}C NMR (151 MHz, DMSO-d_6, 298 K) δ (ppm): 150.5 (C_m), 149.9 (C_h), 148.1 (C_i), 147.5 (C_k), 143.8 (C_b), 135.0 (C_g), 123.8 (C_l), 123.6 (C_j), 123.3 (C_e), 122.0 (C_d), 119.3 (C_c), 112.1 (C_f), 21.8 (C_n).

EI-MS *m/z*: 287.00591 (calculated for $C_{13}H_{10}{}^{79}BrN_3$: 287.00581), 289.00392 (calculated for $C_{13}H_{10}{}^{81}BrN_3$: 289.00376).

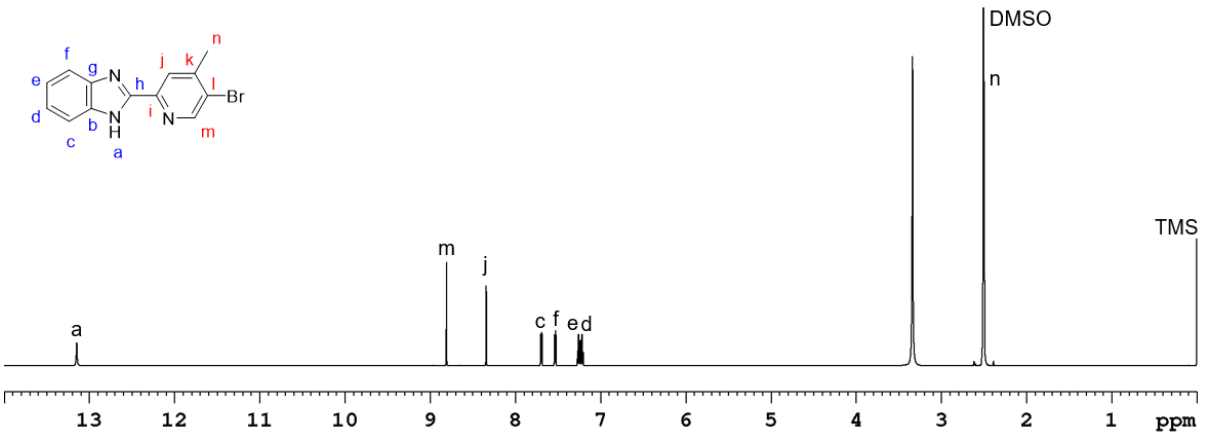

Figure S13. ^{1}H NMR spectrum (600 MHz, DMSO-d_6, 298 K) of 2-(5'-bromo-4'-methylpyridin-2'-yl)-1*H*-benzo[*d*]imidazole (**20**).

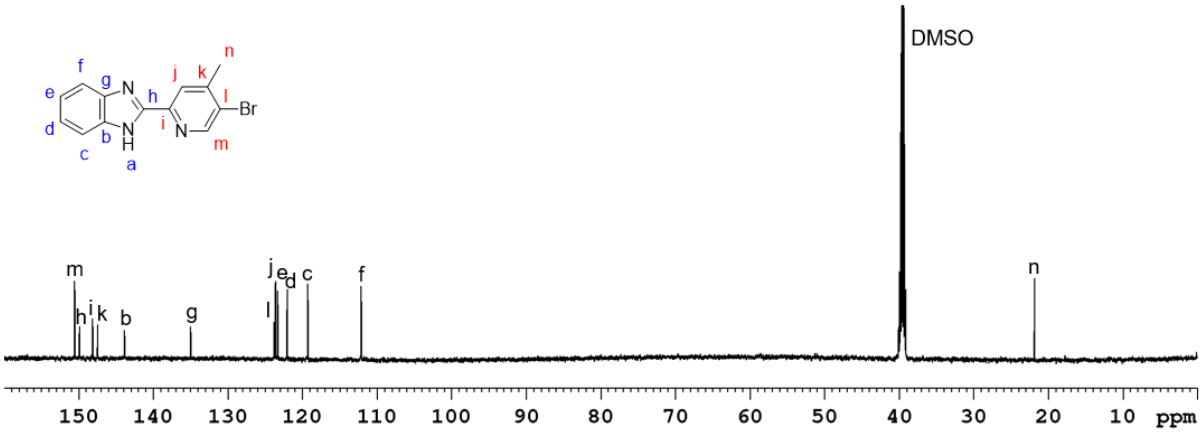

Figure S14. ^{13}C NMR spectrum (151 MHz, DMSO-d_6, 298 K) of 2-(5'-bromo-4'-methylpyridin-2'-yl)-1*H*-benzo[*d*]imidazole (**20**).

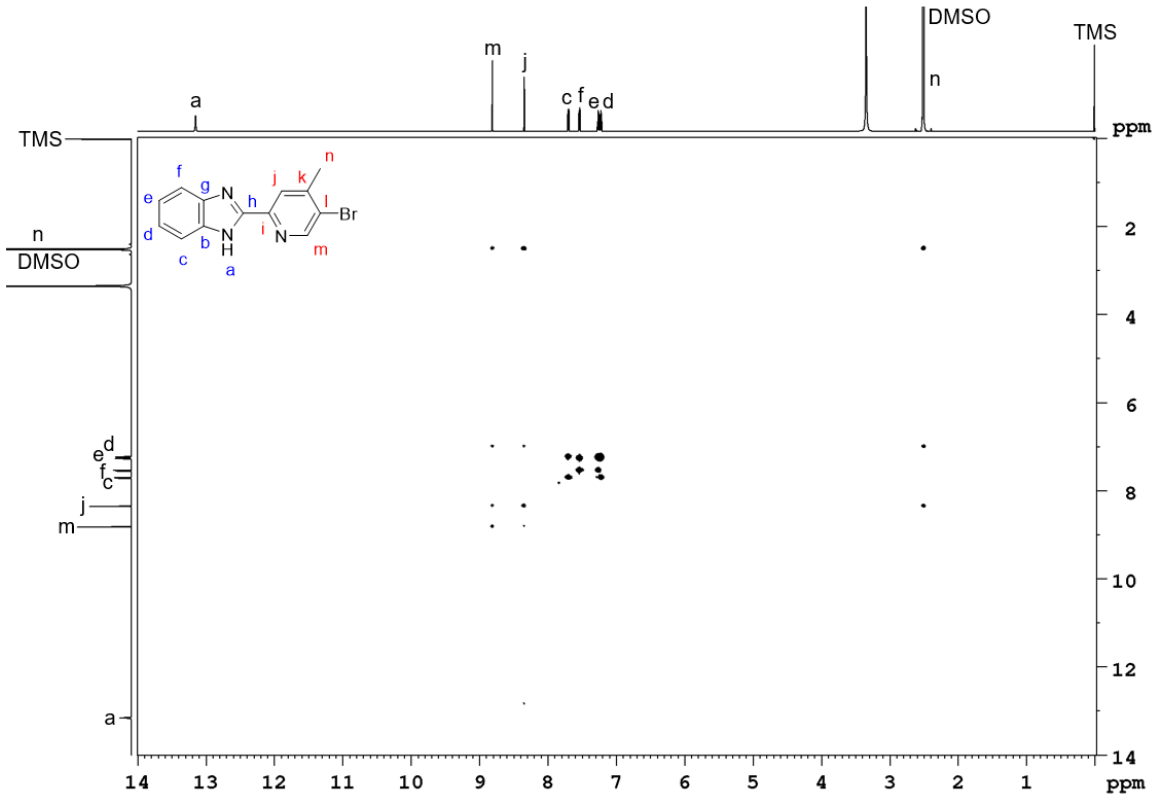

Figure S15. ^{1}H-^{1}H COSY NMR spectrum (600 MHz, DMSO-d_6, 298 K) of 2-(5'-bromo-4'-methylpyridin-2'-yl)-1*H*-benzo[*d*]imidazole (**20**).

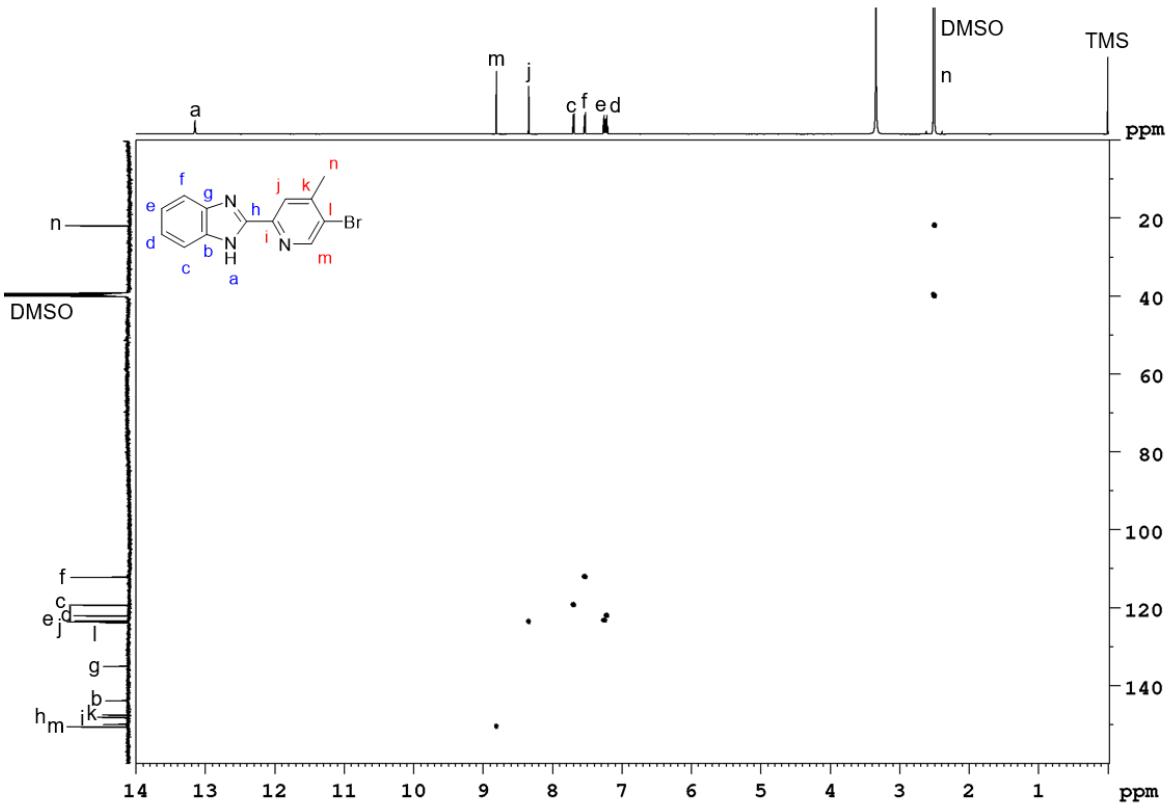

Figure S16. ^{1}H-^{13}C HSQC NMR spectrum (600 MHz/151 MHz, DMSO-d_6, 298 K) of 2-(5'-bromo-4'-methylpyridin-2'-yl)-1*H*-benzo[*d*]imidazole (**20**).

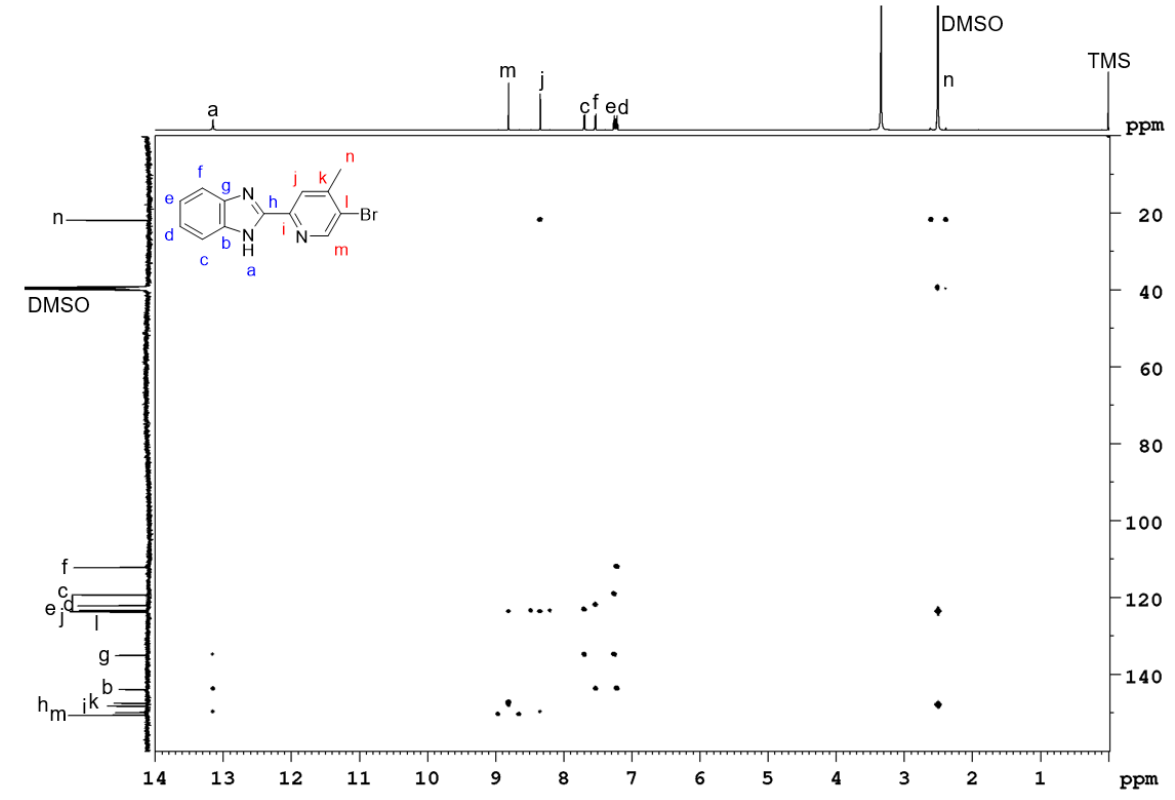

Figure S17. ^{1}H-^{13}C HMBC NMR spectrum (600 MHz/151 MHz, DMSO-d_6, 298 K) of 2-(5'-bromo-4'-methylpyridin-2'-yl)-1*H*-benzo[*d*]imidazole (**20**).

2.2.3 2-(5'-Bromo-4'-methylpyridin-2'-yl)-1-methyl-1*H*-benzo[*d*]imidazole (**21**)

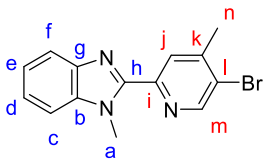

Adapted from Ling and co-workers.[4] 2-(5'-Bromo-4'-methylpyridin-2'-yl)-1*H*-benzo[*d*]imidazole (**21**) (670 mg, 2.33 mmol), methyl iodide (200 µL, 3.21 mmol) and potassium carbonate (998 mg, 7.22 mmol, milled) were dissolved in dimethylformamide (20 mL) and stirred at room temperature for 17 h. The reaction mixture was poured into water (100 mL) and the aqueous layer was extracted with ethyl acetate (150 mL). The layers were separated and the organic layer was washed with brine (250 mL), sodium hydroxide solution (100 mL, 10%) and dried over magnesium sulfate. The solvent was removed *in vacuo* and the product obtained as a brown solid (547 mg, 1.81 mmol, 78%).

^{1}H NMR (600 MHz, DMSO-d_6, 298 K) δ (ppm): 8.82 (s, 1H, H_m), 8.32 (s, 1H, H_j), 7.71 (dt, ^{3}J = 7.7 Hz, ^{4}J = 1.1 Hz, 1H, H_f), 7.65 (dt, ^{3}J = 7.7 Hz, ^{4}J = 1.1 Hz, 1H, H_c), 7.34 (unres. ddd, ^{3}J = 7.7 Hz, ^{4}J = 1.1 Hz, 1H, H_d), 7.28 (unres. ddd, ^{3}J = 7.6 Hz, ^{4}J = 1.1 Hz, 1H, H_e), 4.20 (s, 3H, H_a), 2.48 (s, 3H, H_n).

^{13}C NMR (151 MHz, DMSO-d_6, 298 K) δ (ppm): 150.0 (C_m), 148.9 ($C_{h,i}$), 148.0 (C_k), 142.0 (C_g), 137.1 (C_b), 126.5 (C_j), 123.7 (C_l), 123.3 (C_d), 122.5 (C_e), 119.4 (C_c), 110.9 (C_f), 32.6 (C_a), 21.8 (C_n).

ESI-MS *m/z*: 302.02863 (calculated for $C_{14}H_{13}N_3Br$: 302.02874).

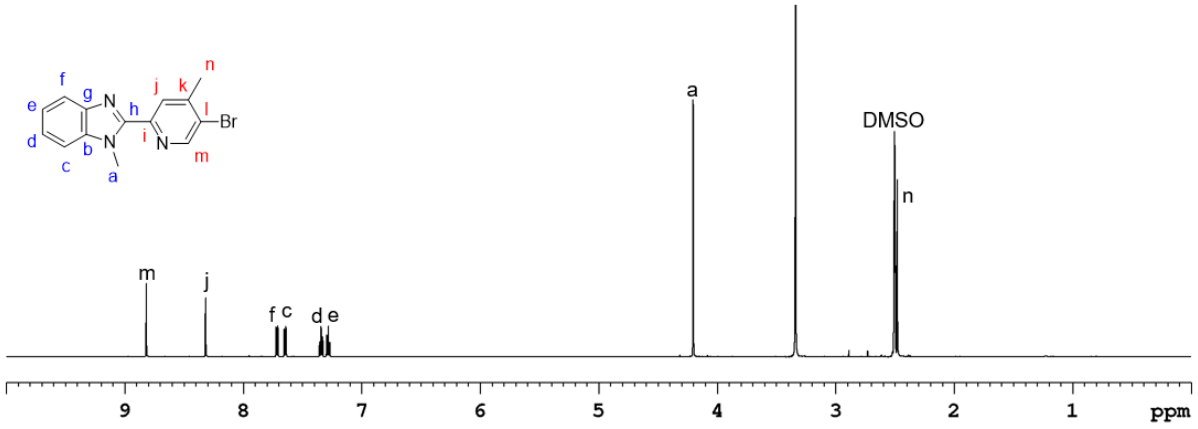

Figure S18. ^{1}H NMR spectrum (600 MHz, DMSO-d_6, 298 K) of 2-(5'-bromo-4'-methylpyridin-2'-yl)-1-methyl-1*H*-benzo[*d*]imidazole (**21**).

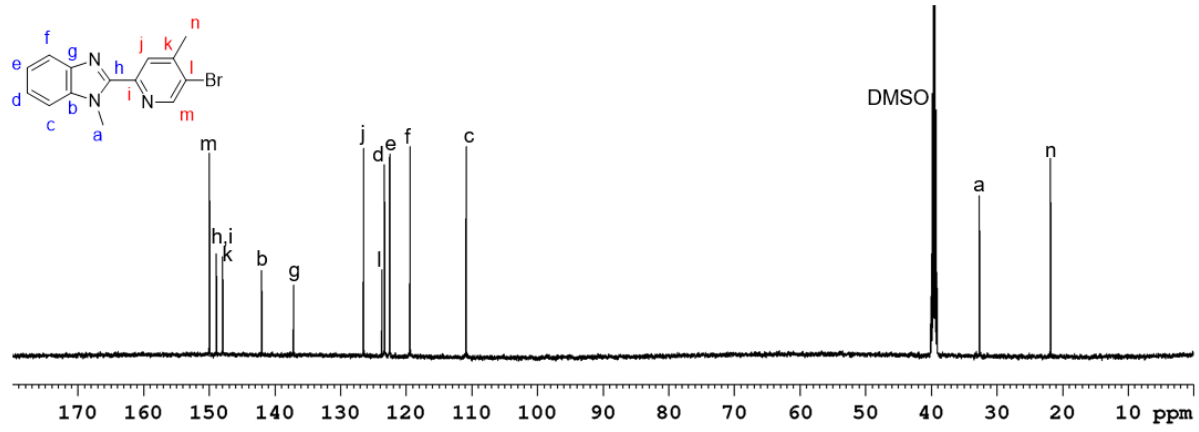

Figure S19. ^{13}C NMR spectrum (151 MHz, DMSO-d_6, 298 K) of 2-(5'-bromo-4'-methylpyridin-2'-yl)-1-methyl-1*H*-benzo[*d*]imidazole (**21**).

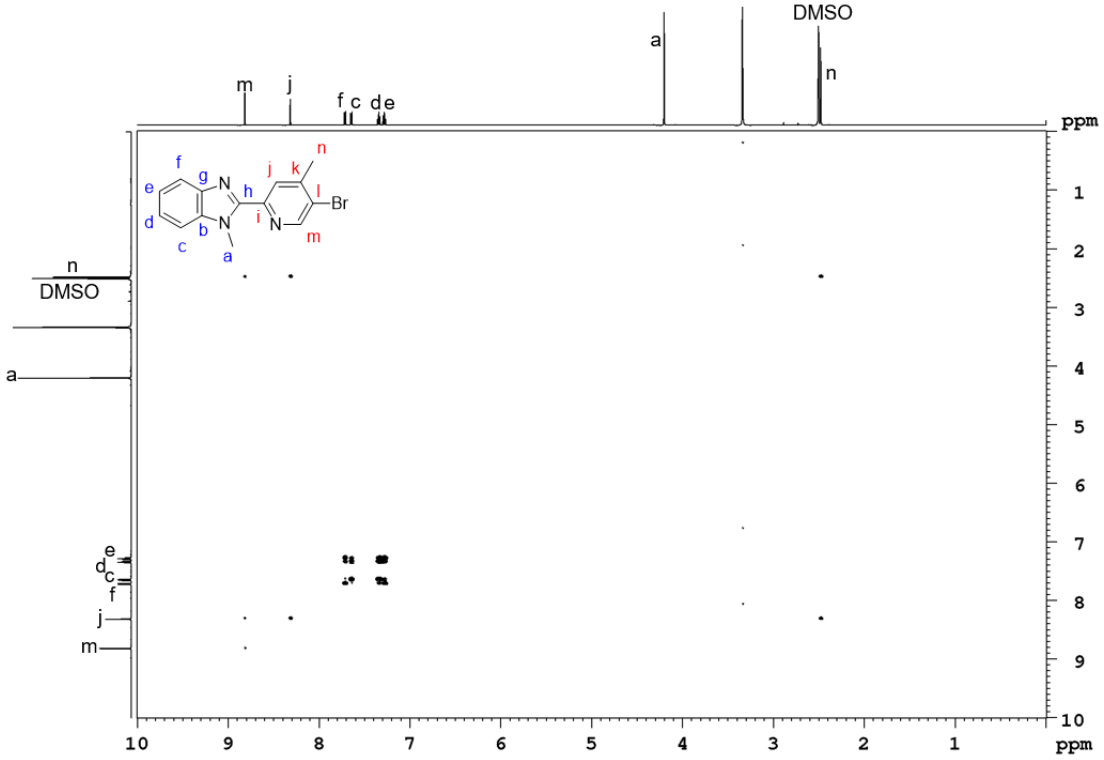

Figure S20. ^{1}H-^{1}H COSY NMR spectrum (600 MHz, DMSO-d_6, 298 K) of 2-(5'-bromo-4'-methylpyridin-2'-yl)-1-methyl-1*H*-benzo[*d*]imidazole (**21**).

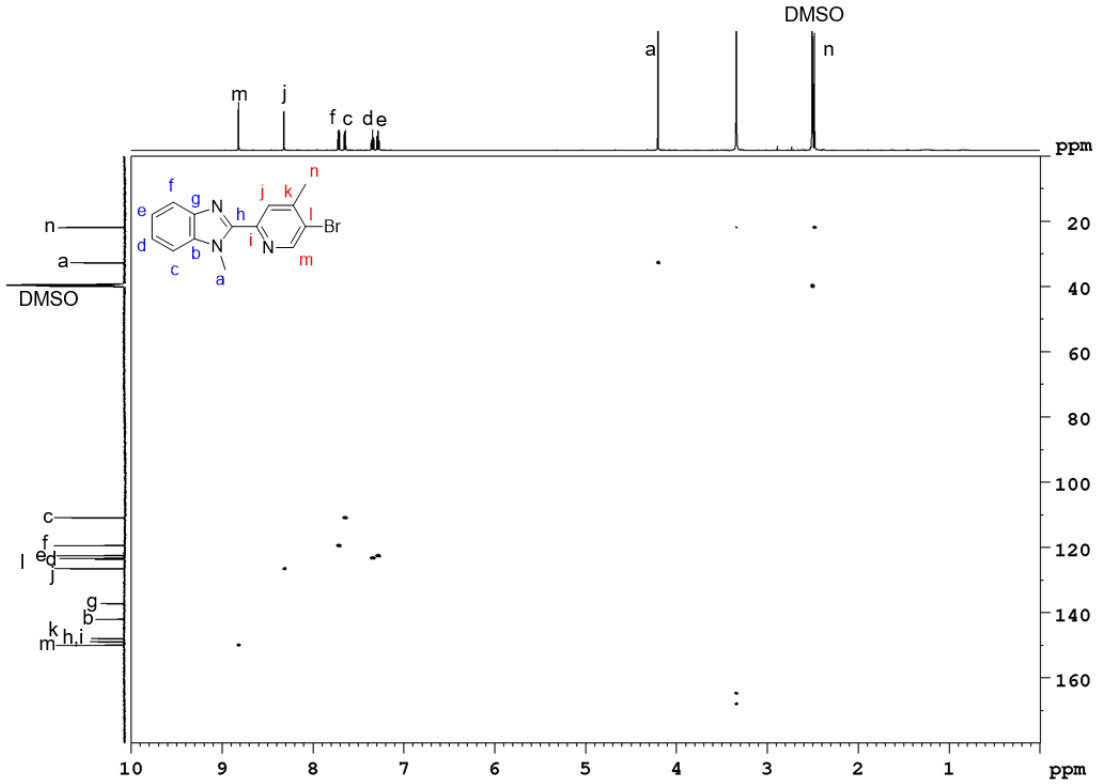

Figure S21. ^{1}H-^{13}C HSQC NMR spectrum (600 MHz/151 MHz, DMSO-d_6, 298 K) of 2-(5'-bromo-4'-methylpyridin-2'-yl)-1-methyl-1*H*-benzo[*d*]imidazole (**21**).

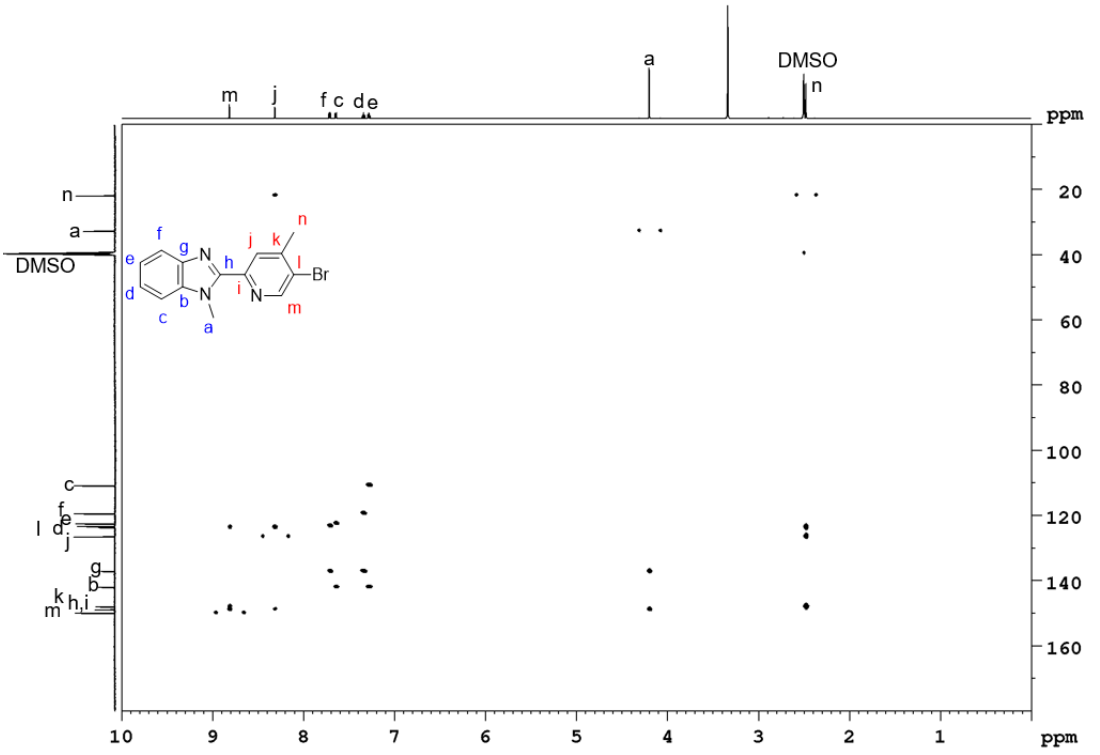

Figure S22. ^{1}H-^{13}C HMBC NMR spectrum (600 MHz/151 MHz, DMSO-d_6, 298 K) of 2-(5'-bromo-4'-methylpyridin-2'-yl)-1-methyl-1*H*-benzo[*d*]imidazole (**21**).

2.2.4 1,2-Di(4''-methyl-6″-(1′-methyl-1*H*-benzo[*d*]imidazol-2′-yl)pyridin-3″-yl)ethyne (**22**)

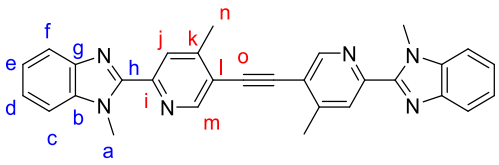

Adapted from McConnell and co-workers.[2] 2-(5'-Bromo-4'-methylpyridin-2'-yl)-1-methyl-1*H*-benzo[*d*]imidazole (**21**) (218 mg, 712 µmol) and $Pd(PPh_3)_4$ (41.8 mg, 5 mol%) were added to a pressure tube and the tube was evacuated for 5 min. Tetrabutylammonium fluoride (4.30 mL, 4.30 mmol) and trimethylsilylacetylene (100 µL, 723 µmol) were added, the tube immediately closed and the reaction mixture heated at 70 °C for 21 h. After cooling to room temperature, the precipitate was collected by filtration and washed with cold tetrahydrofuran (250 mL). The product was obtained as a yellow solid (120 mg, 256 µmol, 71%).

^{1}H NMR (600 MHz, TFA-d_1, 298 K) δ (ppm): 9.29 (s, 2H, H_m), 8.40 (s, 2H, H_j), 7.95-7.82 (m, 8H, $H_{c,d,e,f}$), 4.34 (s, 6H, H_a), 2.97 (s, 6H, H_n).

^{13}C NMR (151 MHz, TFA-d_1, 298 K) δ (ppm): 161.7 (C_k), 152.8 (C_m), 144.6 (C_h), 139.1 (C_i), 135.8 (C_b), 132.5 (C_g), 132.0 ($C_{c/d/e/f}$), 131.5 (C_j), 131.4 ($C_{c/d/e/f}$), 127.3 (C_l), 114.3 ($C_{c/d/e/f}$), 112.2 ($C_{c/d/e/f}$), 96.0 (C_o), 35.0 (C_a), 22.7 (C_n).

EI-MS *m/z*: 468.20493 (calculated for $C_{30}H_{24}N_6$: 468.20624).

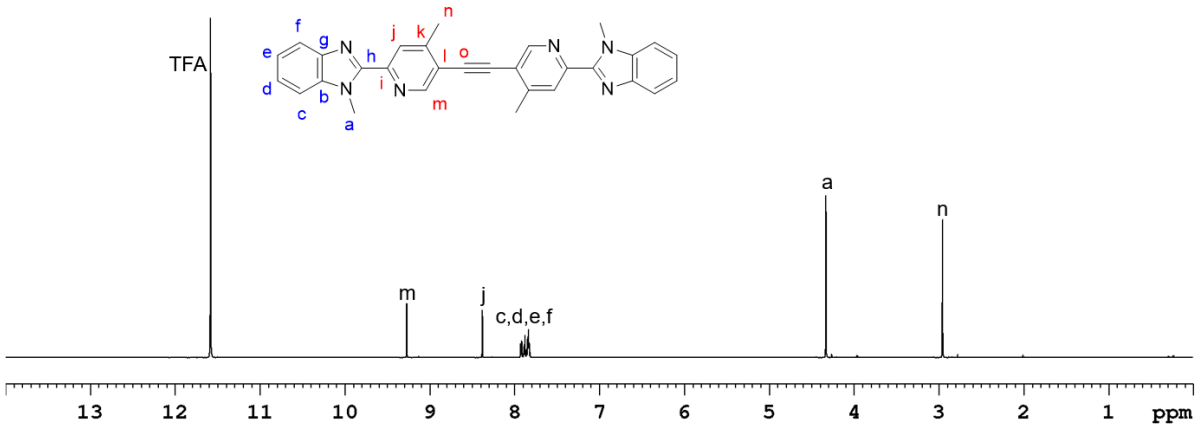

Figure S23. ^{1}H NMR spectrum (600 MHz, TFA-d_1, 298 K) of 1,2-di(4''-methyl-6″-(1′-methyl-1*H*-benzo[*d*]imidazol-2′-yl)pyridin-3″-yl)ethyne (**22**).

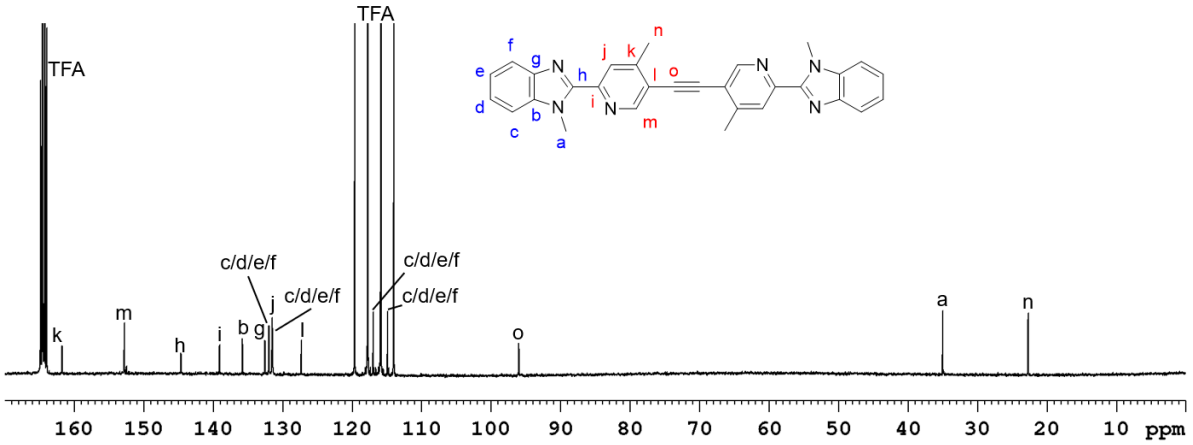

Figure S24. ^{13}C NMR spectrum (151 MHz, TFA-d_1, 298 K) of 1,2-di(4''-methyl-6″-(1′-methyl-1*H*-benzo[*d*]imidazol-2′-yl)pyridin-3″-yl)ethyne (**22**).

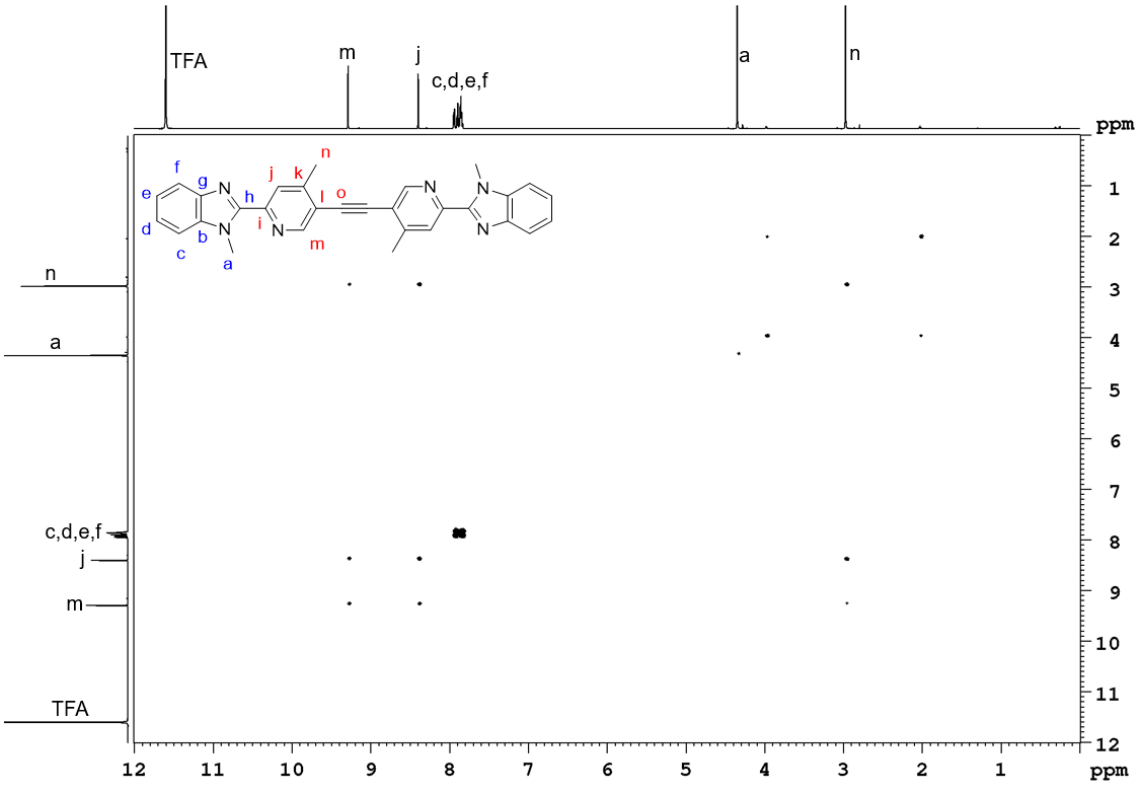

Figure S25. ^{1}H-^{1}H COSY NMR spectrum (600 MHz, TFA-d_1, 298 K) of 1,2-di(4''-methyl-6″-(1′-methyl-1*H*-benzo[*d*]imidazol-2′-yl)pyridin-3″-yl)ethyne (**22**).

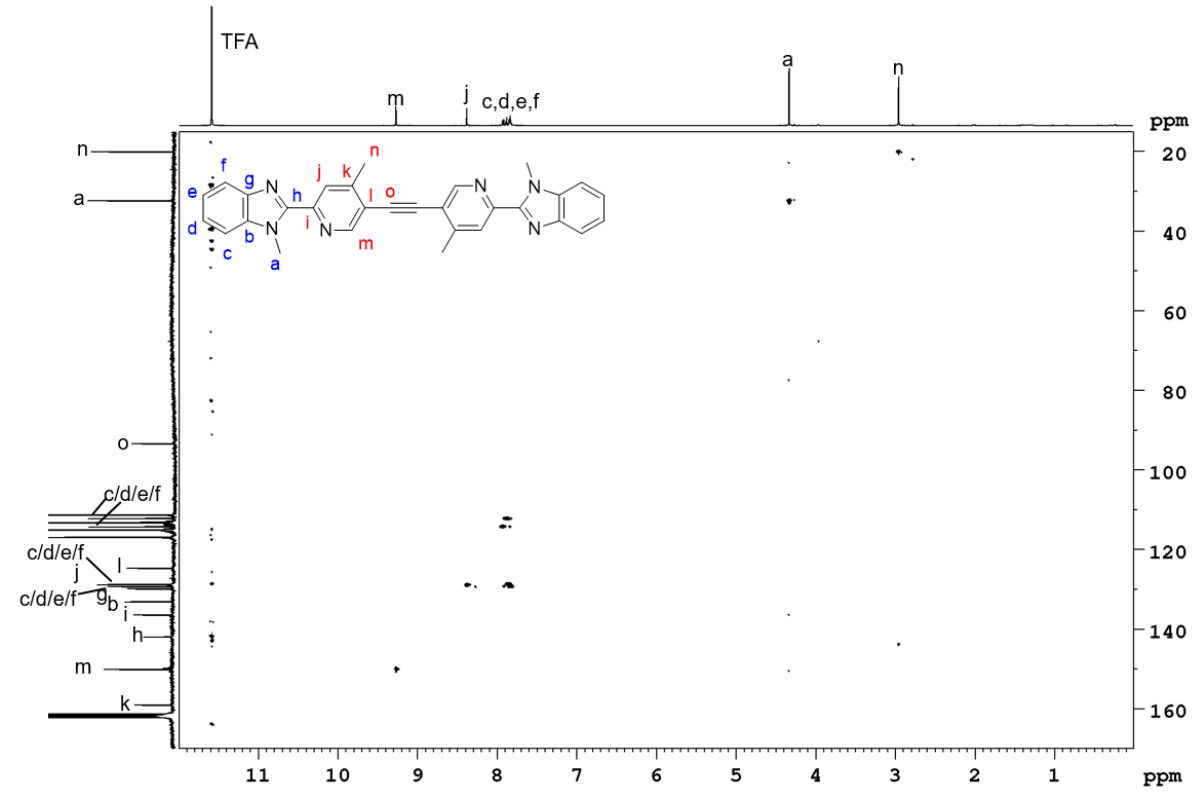

Figure S26. ^{1}H-^{13}C HSQC NMR spectrum (600 MHz/151 MHz, TFA-d_1, 298 K) of 1,2-di(4''-methyl-6″-(1′-methyl-1*H*-benzo[*d*]imidazol-2′-yl)pyridin-3″-yl)ethyne (**22**).

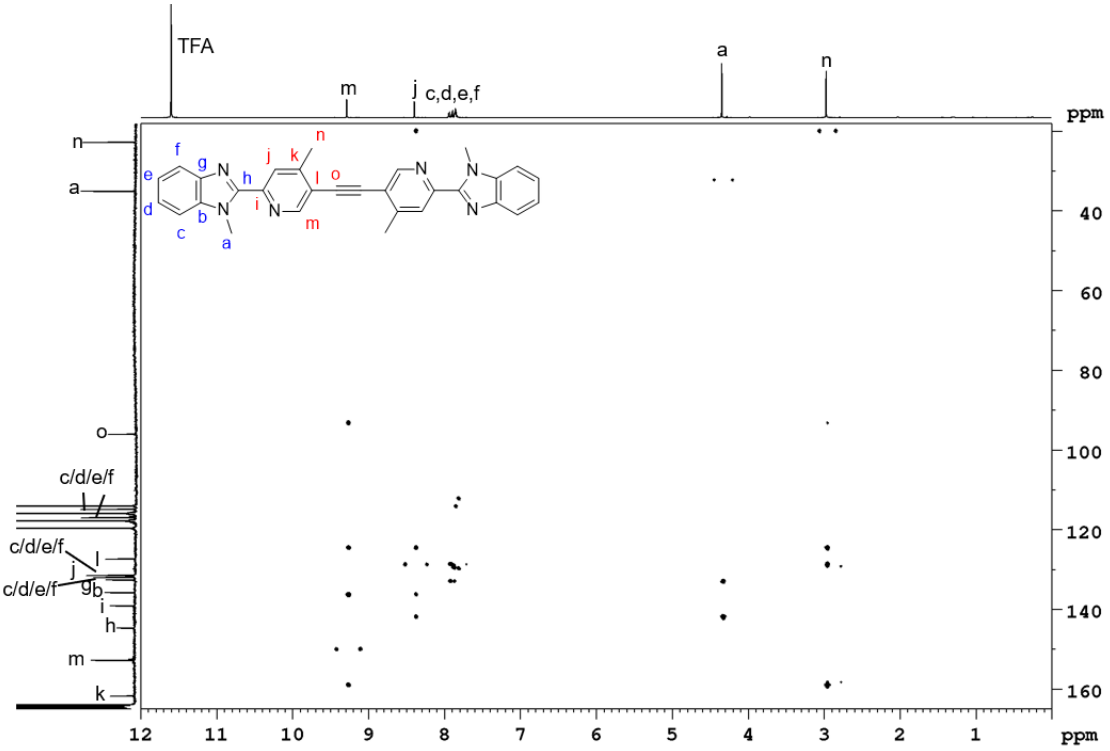

Figure S27. ^{1}H-^{13}C HMBC NMR spectrum (600 MHz/151 MHz, TFA-d_1, 298 K) of 1,2-di(4''-methyl-6″-(1′-methyl-1*H*-benzo[*d*]imidazol-2′-yl)pyridin-3″-yl)ethyne (**22**).

2.3 Benzimidazole-based Ligands with no Linker

Benzimidazole-based ligands without a spacer group were synthesised according to Scheme S3. Boronic acid **23** was prepared adapting the synthesis of thiophene-based boronic acids.[6] In addition, boronic ester **25** was prepared according to Severin and co-workers.[7]

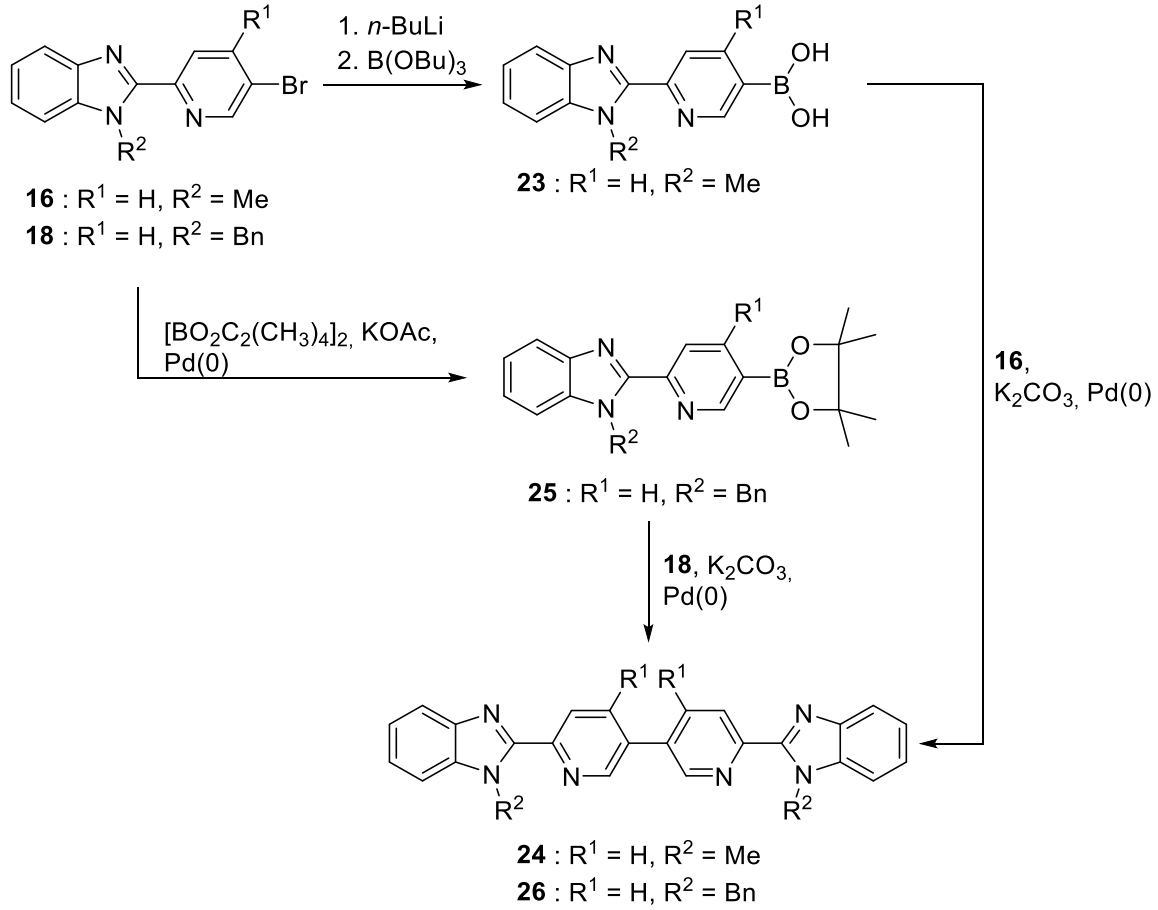

Scheme S3. Synthesis of ligands **24** and **26**.

2.3.1 (6'-(1-Methyl-1*H*-benzo[*d*]imidazol-2-yl)pyridin-3'-yl)boronic acid (**23**)

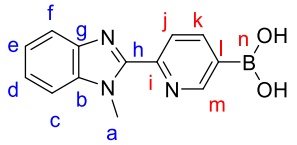

Adapted from Phillips and co-workers.[6] 2-(5'-Bromo-4'-methylpyridin-2'-yl)-1-methyl-1*H*-benzo[*d*]imidazole (**16**) (985 mg, 3.42 mmol) was added to a three-neck flask and the flask was evacuated for 5 min. After the addition of anhydrous tetrahydrofuran (15 mL), the solution was cooled to -78 °C. *n*-Butyllithium (1.50 mL, 3.75 mmol, 2.5 M in hexanes) was added dropwise, the reaction mixture stirred at -78 °C for 2 h before tributyl borate (1.02 mL, 3.78 mmol) was added. Stirring was continued at -78 °C for 2 h. Hydrochloric acid (12 mL, 24 mmol, 2 M) was added and the reaction mixture warmed to room temperature and stirred for 18 h. The precipitate was collected by filtration and washed with cold tetrahydrofuran (3 mL). The product was obtained as a colourless solid (705 mg, 2.79 mmol, 81%).

^{1}H NMR (500 MHz, DMSO-d_6, 298 K) δ (ppm): 9.15 (s, 1H, H_m), 8.44 (dt, ^3J = 7.8 Hz, ^4J = 1.9 Hz, 1H, H_k), 8.33 (dd, ^3J = 7.8 Hz, ^6J = 1.3 Hz, 1H, H_j), 7.97 (d, ^3J = 7.9 Hz, 1H, H_c), 7.86 (d, ^3J = 8.1 Hz, 1H, H_f), 7.62-7.54 (m, 2H, $H_{d,e}$), 4.32 (d, ^6J = 1.3 Hz, 3H, H_a).

^{13}C NMR (125 MHz, DMSO-d_6, 298 K) δ (ppm): 154.6 (C_m), 147.6 (C_h), 145.6 (C_i), 143.1 (C_k), 134.7 (C_b), 133.8 (C_g), 131.6 (C_l), 125.6 ($C_{d/e}$), 125.4 ($C_{d/e}$), 124.6 (C_j), 115.9 (C_f), 112.6 (C_c), 33.2 (C_a).

^{11}B NMR (160 MHz, DMSO-d_6, 298 K) δ (ppm): 28.3 (B_n).

ESI-MS *m/z*: 253.11327 (calculated for $C_{13}H_{13}N_3O_2B$: 253.11317).

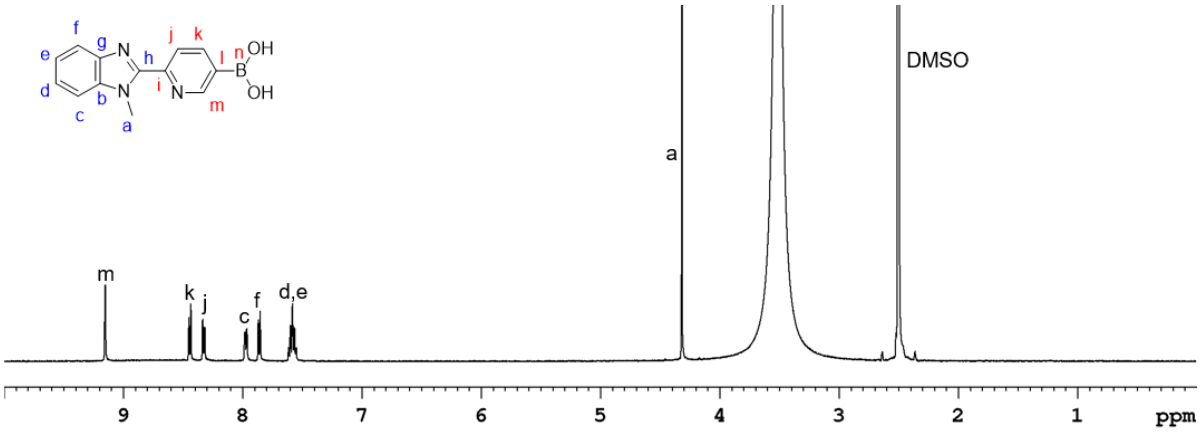

Figure S28. ^{1}H NMR spectrum (500 MHz, DMSO-d_6, 298 K) of (6'-(1-methyl-1*H*-benzo[*d*]imidazol-2-yl)pyridin-3'-yl)boronic acid (**23**).

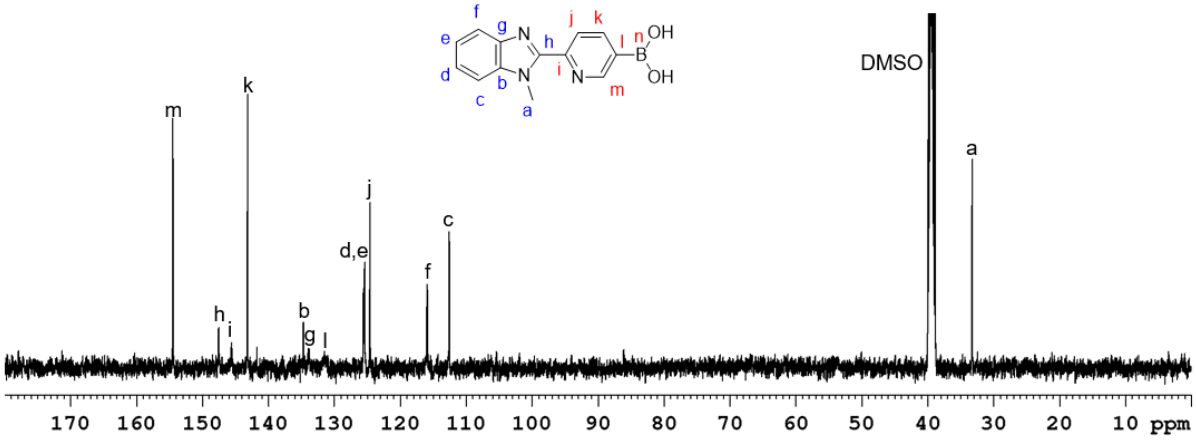

Figure S29. ^{13}C NMR spectrum (125 MHz, DMSO-d_6, 298 K) of (6'-(1-methyl-1*H*-benzo[*d*]imidazol-2-yl)pyridin-3'-yl)boronic acid (**23**).

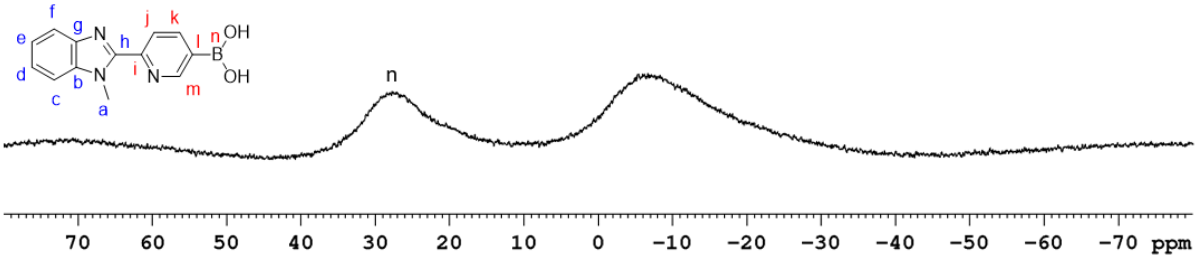

Figure S30. ^{11}B NMR spectrum (160 MHz, DMSO-d_6, 298 K) of (6'-(1-methyl-1*H*-benzo[*d*]imidazol-2-yl)pyridin-3'-yl)boronic acid (**23**).

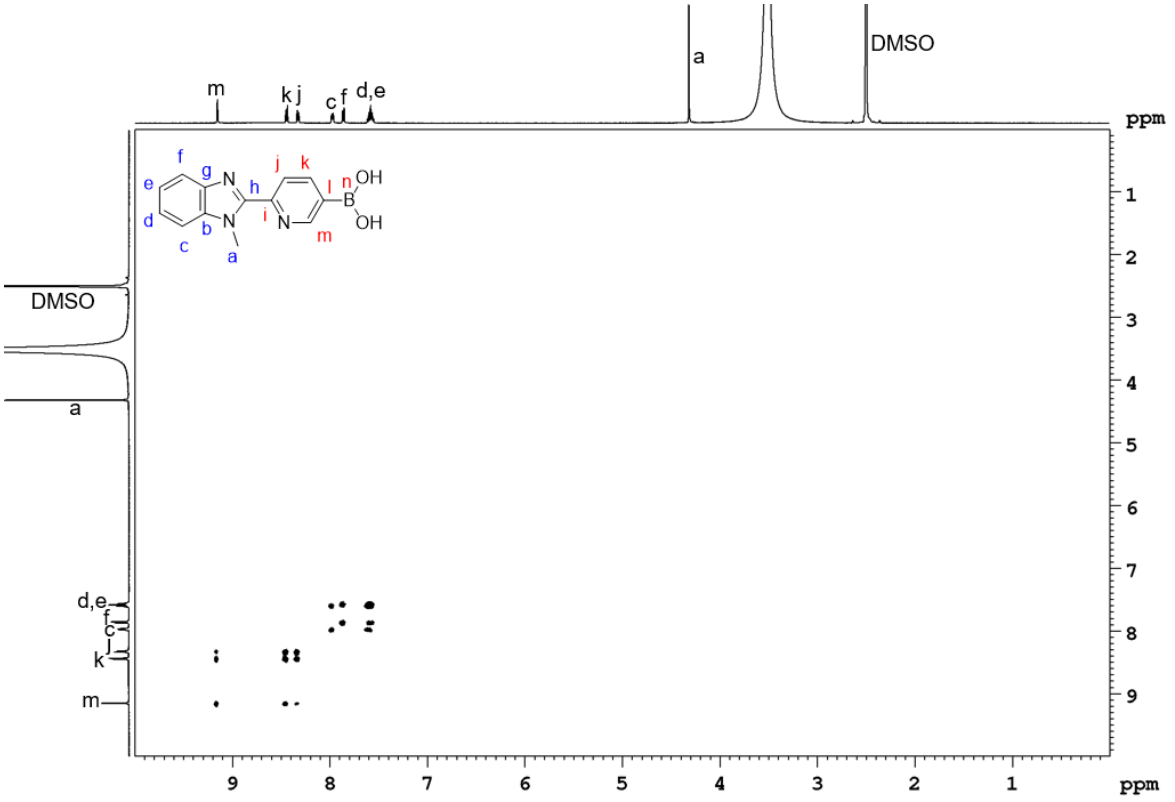

Figure S31. ^{1}H-^{1}H COSY NMR spectrum (500 MHz, DMSO-d_6, 298 K) of (6'-(1-methyl-1*H*-benzo[*d*]imidazol-2-yl)pyridin-3'-yl)boronic acid (**23**).

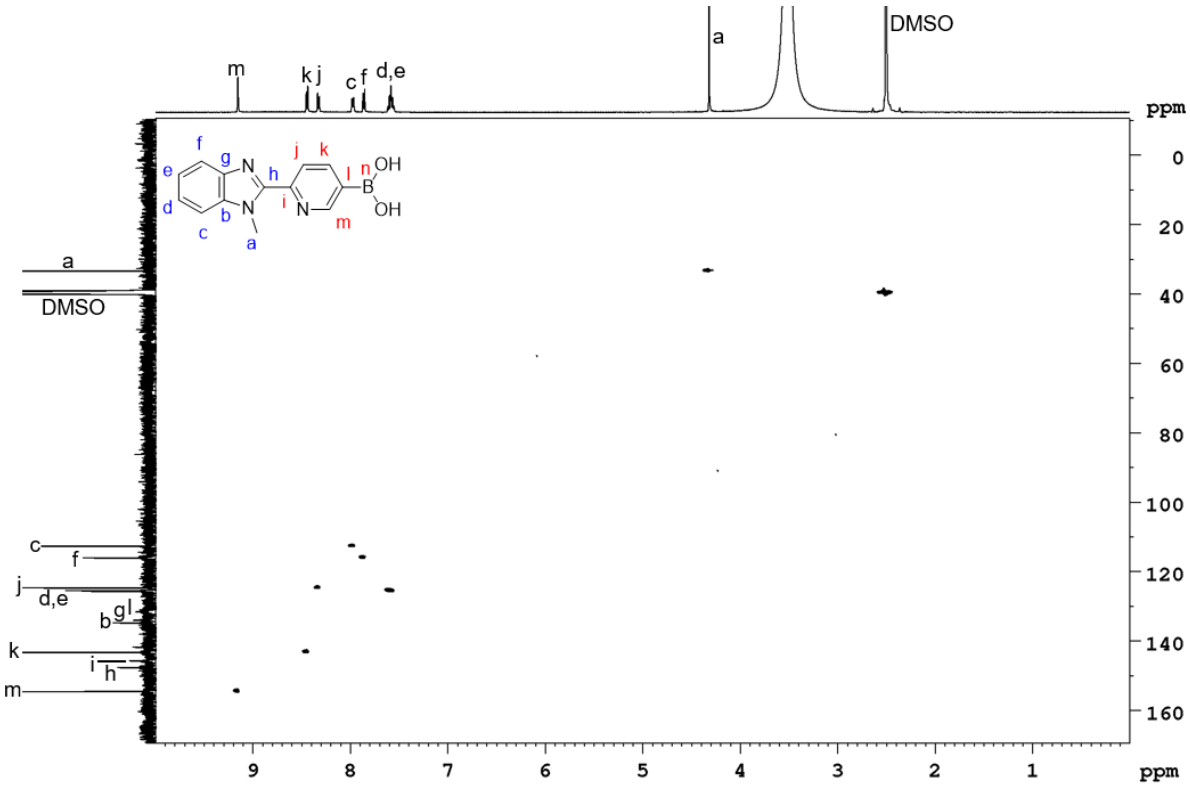

Figure S32. ^{1}H-^{13}C HSQC NMR spectrum (500 MHz/125 MHz, DMSO-d_6, 298 K) of (6'-(1-methyl-1*H*-benzo[*d*]imidazol-2-yl)pyridin-3'-yl)boronic acid (**23**).

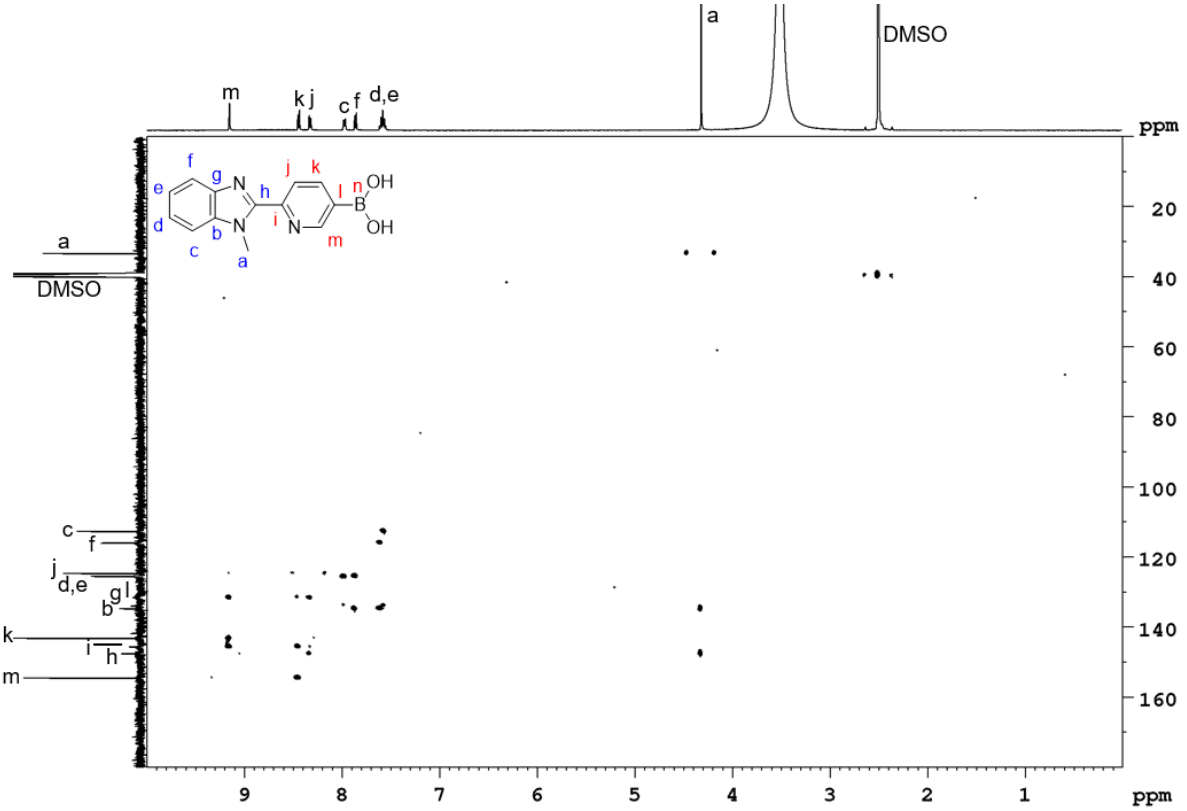

Figure S33. ^{1}H-^{13}C HMBC NMR spectrum (500 MHz/125 MHz, DMSO-d_6, 298 K) of (6'-(1-methyl-1*H*-benzo[*d*]imidazol-2-yl)pyridin-3'-yl)boronic acid (**23**).

2.3.2 6',6''-Di(1-methyl-1*H*-benzo[*d*]imidazol-2-yl)-3',3''-bipyridine (**24**)

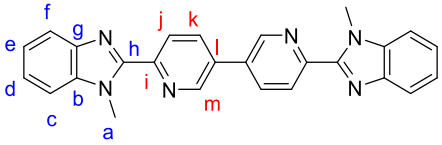

Adapted from Lusby and co-workers.[8] 2-(5'-Bromopyridin-2'-yl)-1-methyl-1*H*-benzo[*d*]imidazole (**16**) (350 mg, 1.22 mmol), (6'-(1-methyl-1*H*-benzo[*d*]imidazol-2-yl)pyridin-3'-yl)boronic acid (**23**) (309 mg, 1.22 mmol), potassium carbonate (422 mg, 3.05 mmol, milled) and $Pd(PPh_3)_4$ (70.5 mg, 5 mol%) were added to a three-neck flask and the flask was evacuated for 5 min. Ethanol (4 mL, dry), water (4 mL, degassed) and tetrahydrofuran (9 mL, dry) were added and the reaction mixture was stirred at 80 °C for 19.75 h. The solution was cooled to room temperature and the precipitate was collected by filtration and washed with cold tetrahydrofuran (250 mL). The product was obtained as a colourless solid (374 mg, 898 µmol, 74%)

The analytical data was consistent with literature data.[8]

^{1}H NMR (600 MHz, $CDCl_3$, 298 K) δ (ppm): 9.03 (dd, ^{4}J = 2.4 Hz, ^{5}J = 0.7 Hz, 2H, H_m), 8.58 (dd, ^{3}J = 8.2 Hz, ^{5}J = 0.7 Hz, 2H, H_j), 8.15 (dd, ^{3}J = 8.2 Hz, ^{4}J = 2.4 Hz, 2H, H_k), 7.87 (unres. dt, 2H, H_f), 7.48 (unres. dt, 2H, H_c), 7.38 (td, ^{3}J = 7.1 Hz, ^{4}J = 1.3 Hz, 2H, H_d), 7.35 (td, ^{3}J = 7.1 Hz, ^{4}J = 1.3 Hz, 2H, H_e), 4.36 (s, 6H, H_a).

^{13}C NMR (151 MHz, $CDCl_3$, 298 K) δ (ppm): 150.5 (C_i), 149.7 (C_h), 146.8 (C_m), 142.7 (C_g), 137.5 (C_b), 135.0 (C_k), 132.7 (C_l), 124.9 (C_j), 123.6 (C_d), 122.9 (C_e), 120.2 (C_f), 110.0 (C_c), 32.9 (C_a).

EI-MS *m/z*: 416.17383 (calculated for $C_{26}H_{20}N_6$: 416.17494).

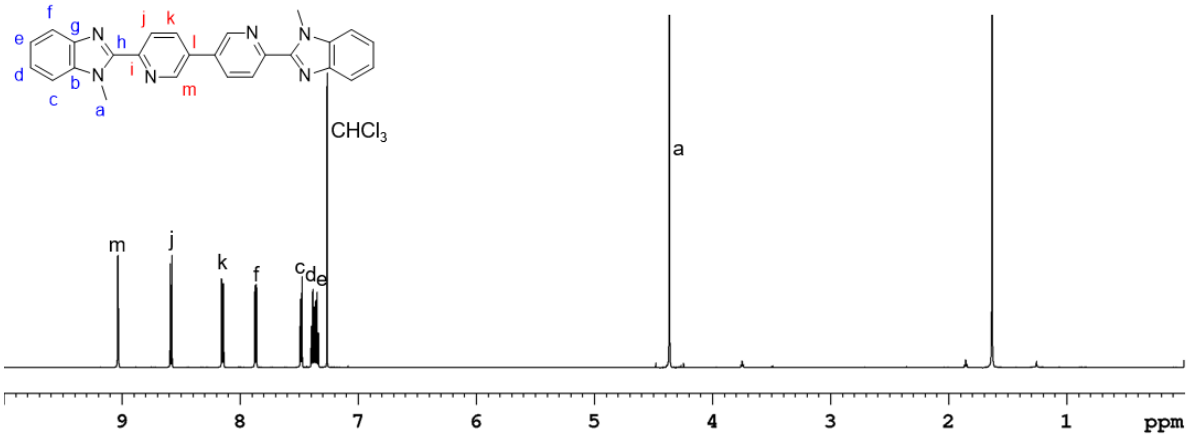

Figure S34. ^{1}H NMR spectrum (600 MHz, $CDCl_3$, 298 K) of 6',6''-di(1-methyl-1*H*-benzo[*d*]imidazol-2-yl)-3',3''-bipyridine (**24**).

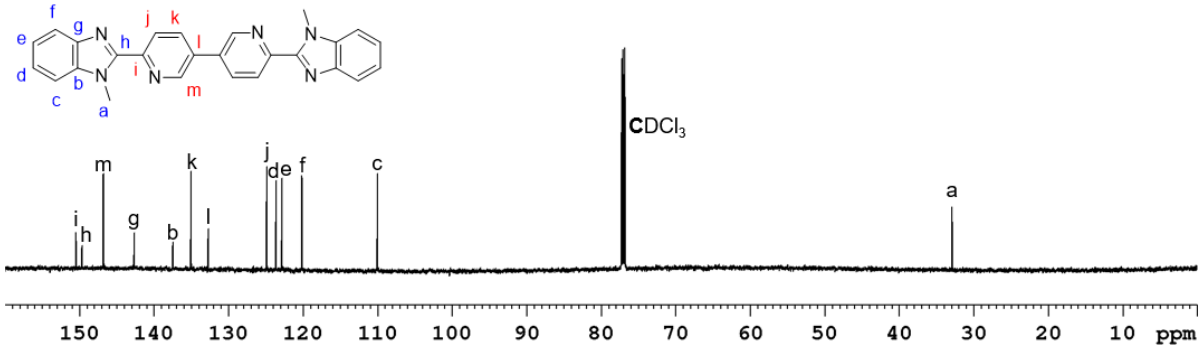

Figure S35. ^{13}C NMR spectrum (151 MHz, $CDCl_3$, 298 K) of 6',6''-di(1-methyl-1*H*-benzo[*d*]imidazol-2-yl)-3',3''-bipyridine (**24**).

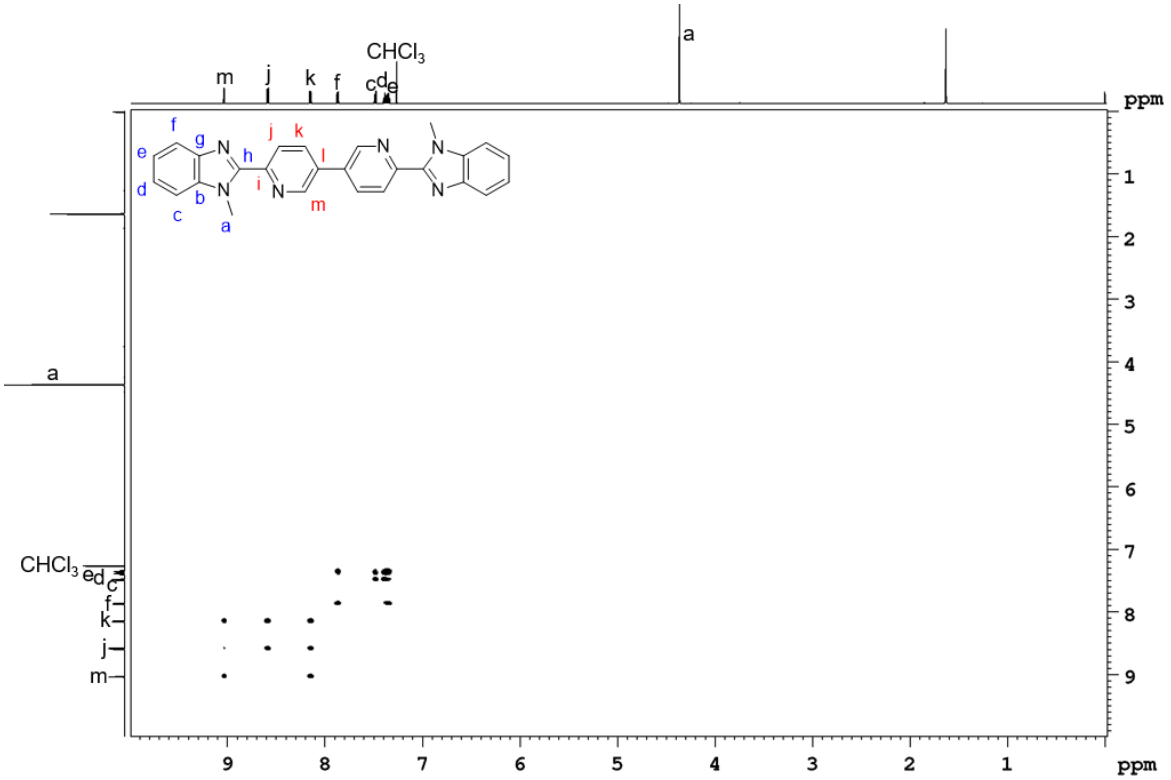

Figure S36. ^{1}H-^{1}H COSY NMR spectrum (600 MHz, $CDCl_3$, 298 K) of 6',6''-di(1-methyl-1*H*-benzo[*d*]imidazol-2-yl)-3',3''-bipyridine (**24**).

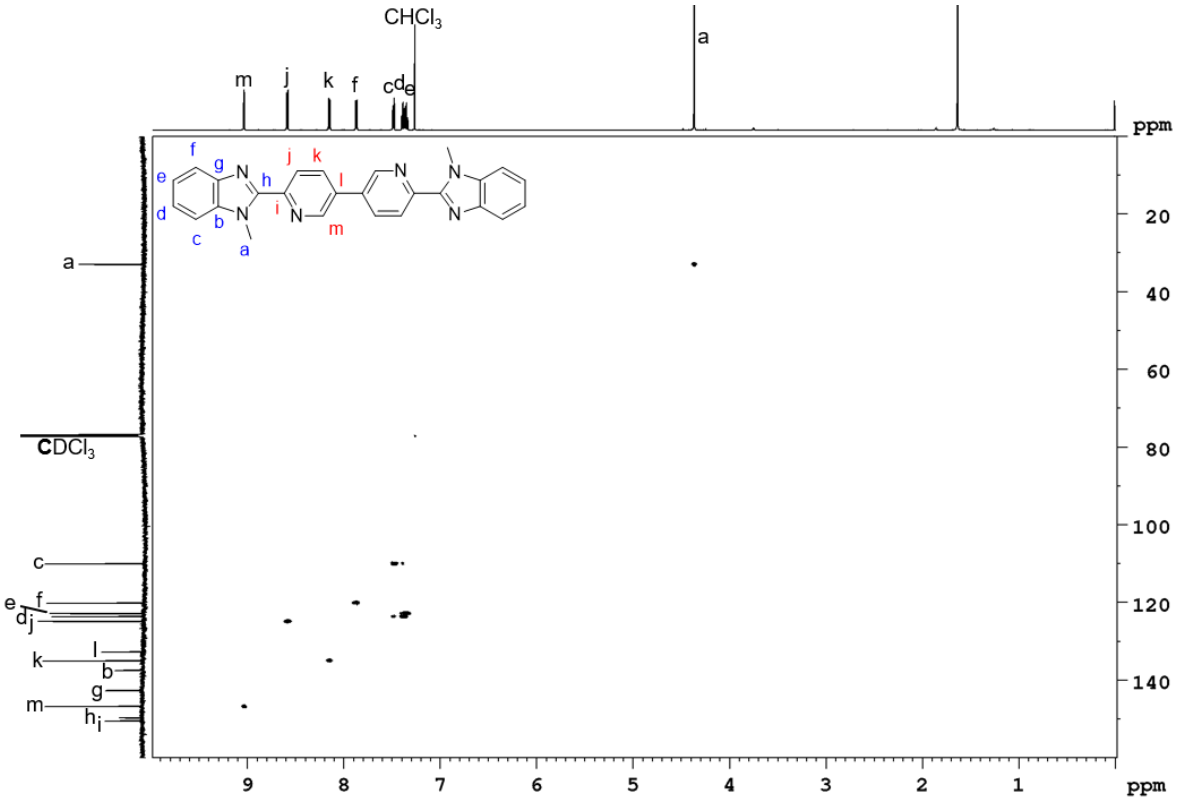

Figure S37. ^{1}H-^{13}C HSQC NMR spectrum (600 MHz/151 MHz, $CDCl_3$, 298 K) of 6',6''-di(1-methyl-1*H*-benzo[*d*]imidazol-2-yl)-3',3''-bipyridine (**24**).

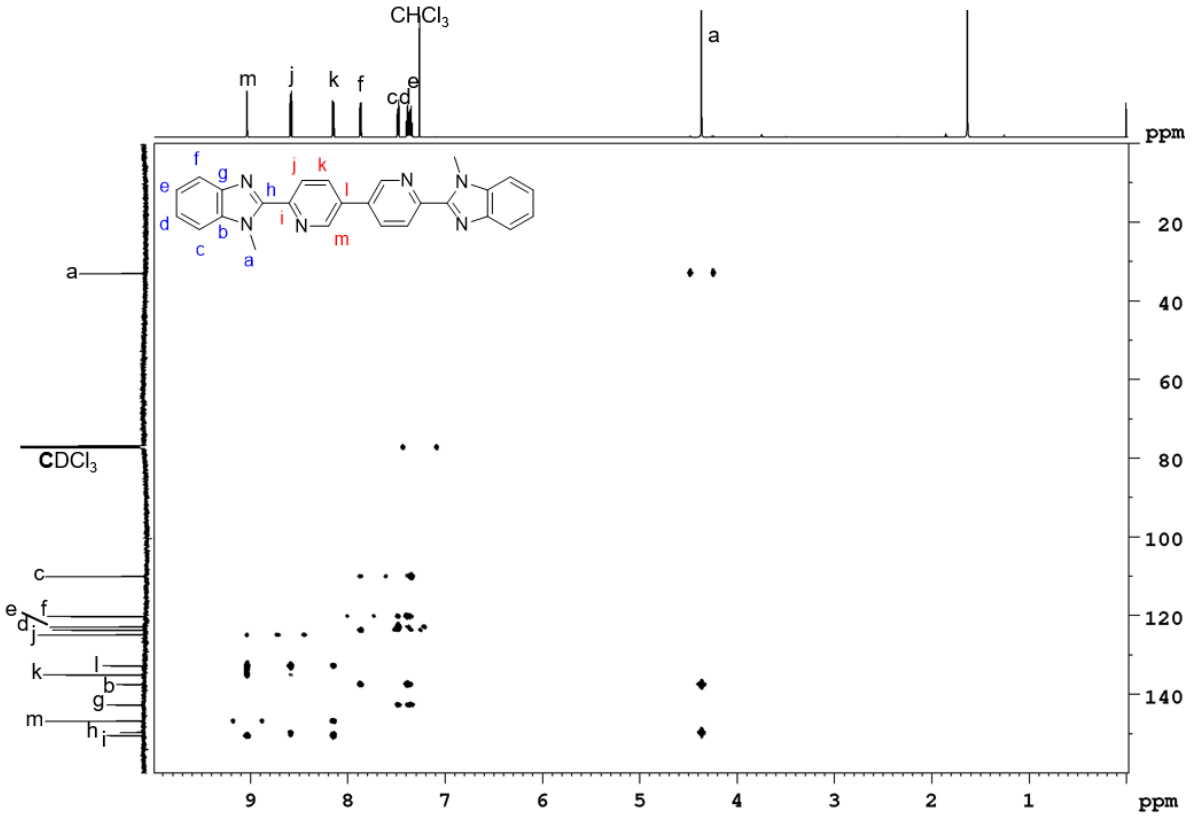

Figure S38. ^{1}H-^{13}C HMBC NMR spectrum (600 MHz/151 MHz, $CDCl_3$, 298 K) of 6',6''-di(1-methyl-1*H*-benzo[*d*]imidazol-2-yl)-3',3''-bipyridine (**24**).

2.3.3 1-Benzyl-2-(5'-(4'',4'',5'',5''-tetramethyl-1'',3'',2''-dioxaborolan-2''-yl)pyridin-2'-yl)-1*H*-benzo[*d*]imidazole (**25**)

Adapted from Severin and co-workers.[7] 2-(5'-Bromopyridin-2'-yl)-1-benzyl-1*H*-benzo[*d*]imidazole (**18**) (300 mg, 824 µmol), bis(pinacolato)diboron (437 mg, 1.72 mmol), potassium acetate (404 mg, 4.12 mmol) and $Pd(dppf)Cl_2 \cdot CH_2Cl_2$ (33.7 mg, 5 mol%) were added to a three-neck flask and the flask was evacuated for 5 min. Anhydrous 1,4-dioxane (9 mL) was added and the reaction mixture was stirred at 90 °C for 19 h. The solution was cooled to room temperature and the crude reaction mixture was filtered through a silica gel plug (1:1 cyclohexane/ethyl acetate). The solvent was removed *in vacuo*. The impure product was used in the next step without further purification.

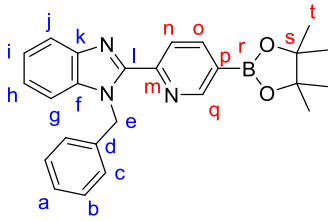

^{1}H NMR (500 MHz, DMSO-d_6, 298 K) δ (ppm): 8.85 (dd, ^{4}J = 1.8 Hz, ^{5}J = 1.0 Hz, 1H, H_q), 8.40 (dd, ^{3}J = 7.9 Hz, ^{5}J = 1.0 Hz, 1H, H_n), 8.19 (dd, ^{3}J = 7.9 Hz, ^{4}J = 1.8 Hz, 1H, H_o), 7.78-7.75 (m, 1H, $H_{g/j}$), 7.65-7.62 (m, 1H, $H_{g/j}$), 7.33-7.26 (m, 2H, $H_{h,i}$), 7.26-7.21 (m, 2H, H_b), 7.20-7.16 (m, 1H, H_a), 7.14-7.10 (m, 2H, H_c), 6.25 (s, 2H, H_e), 1.33 (s, 12H, H_t).

^{13}C NMR (125 MHz, DMSO-d_6, 298 K) δ (ppm): 153.7 (C_q), 152.0 (C_m), 148.7 (C_l), 143.0 (C_o), 142.1 (C_k), 137.7 (C_d), 136.6 (C_f), 128.4 (C_b), 127.1 (C_a), 126.6 (C_c), 123.6 ($C_{h/i}$), 123.5 (C_n), 122.7 ($C_{h/i}$), 119.7 ($C_{g/j}$), 111.3 ($C_{g/j}$), 84.3 (C_s), 47.9 (C_e), 24.6 (C_t).

Note: C_p was not observed.

^{11}B NMR (160 MHz, DMSO-d_6, 298 K) δ (ppm): Unambiguous assignment of the two signals was not possible due to the presence of a boron-containing impurity.

EI-MS *m/z*: 411.21174 (calculated for $C_{25}H_{26}N_3B_1O_2$: 411.21181).

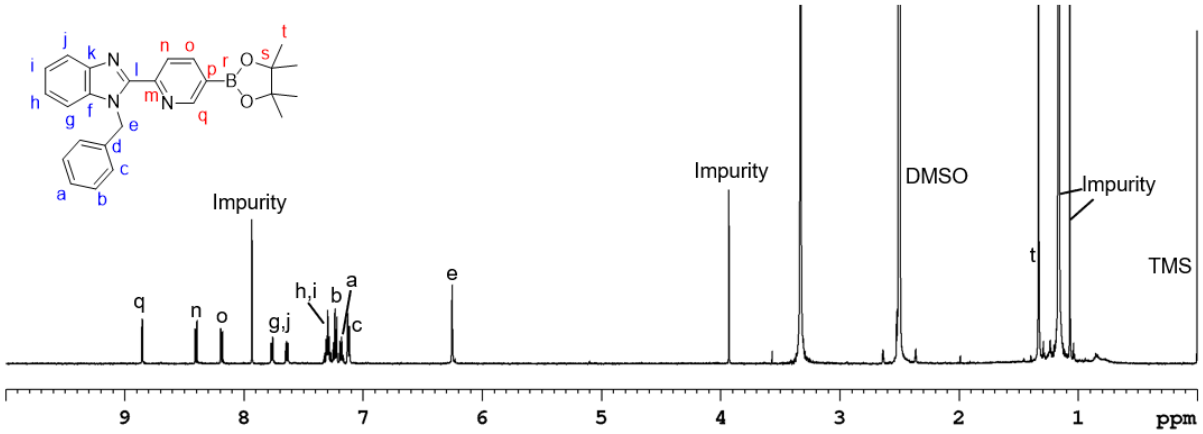

Figure S39. ^{1}H NMR spectrum (500 MHz, DMSO-d_6, 298 K) of 1-benzyl-2-(5'-(4'',4'',5'',5''-tetramethyl-1'',3'',2''-dioxaborolan-2''-yl)pyridin-2'-yl)-1*H*-benzo[*d*]imidazole (**25**).

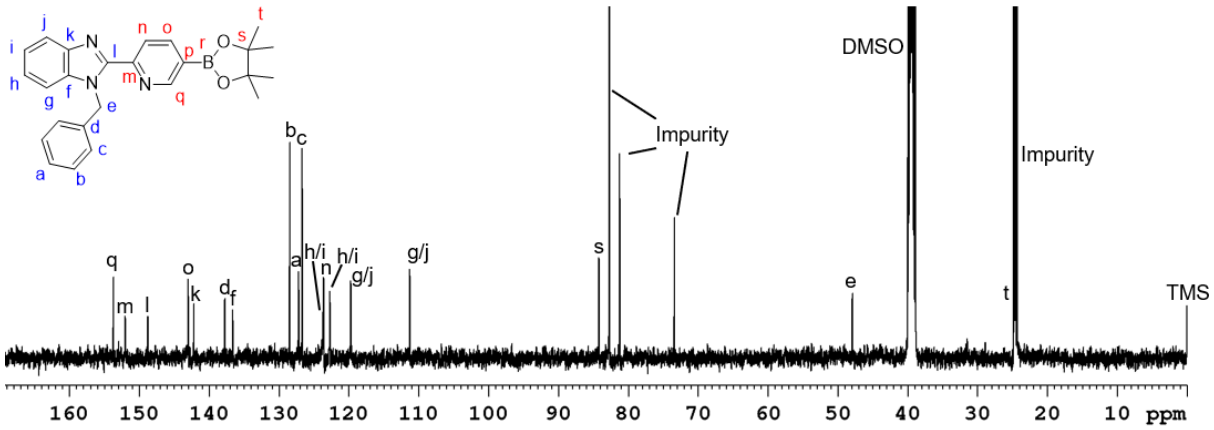

Figure S40. ^{13}C NMR spectrum (125 MHz, DMSO-d_6, 298 K) of 1-benzyl-2-(5'-(4'',4'',5'',5''-tetramethyl-1'',3'',2''-dioxaborolan-2''-yl)pyridin-2'-yl)-1*H*-benzo[*d*]imidazole (**25**).

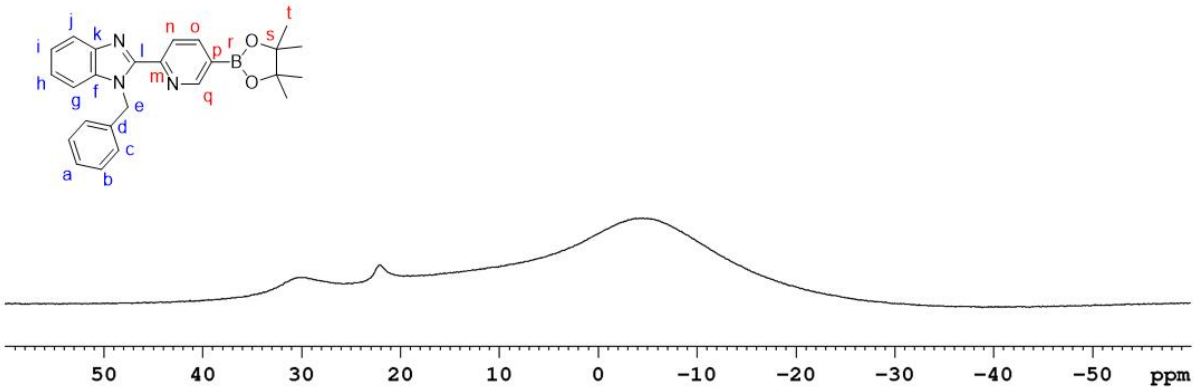

Figure S41. ^{11}B NMR spectrum (160 MHz, DMSO-d_6, 298 K) of 1-benzyl-2-(5'-(4'',4'',5'',5''-tetramethyl-1'',3'',2''-dioxaborolan-2''-yl)pyridin-2'-yl)-1*H*-benzo[*d*]imidazole (**25**).

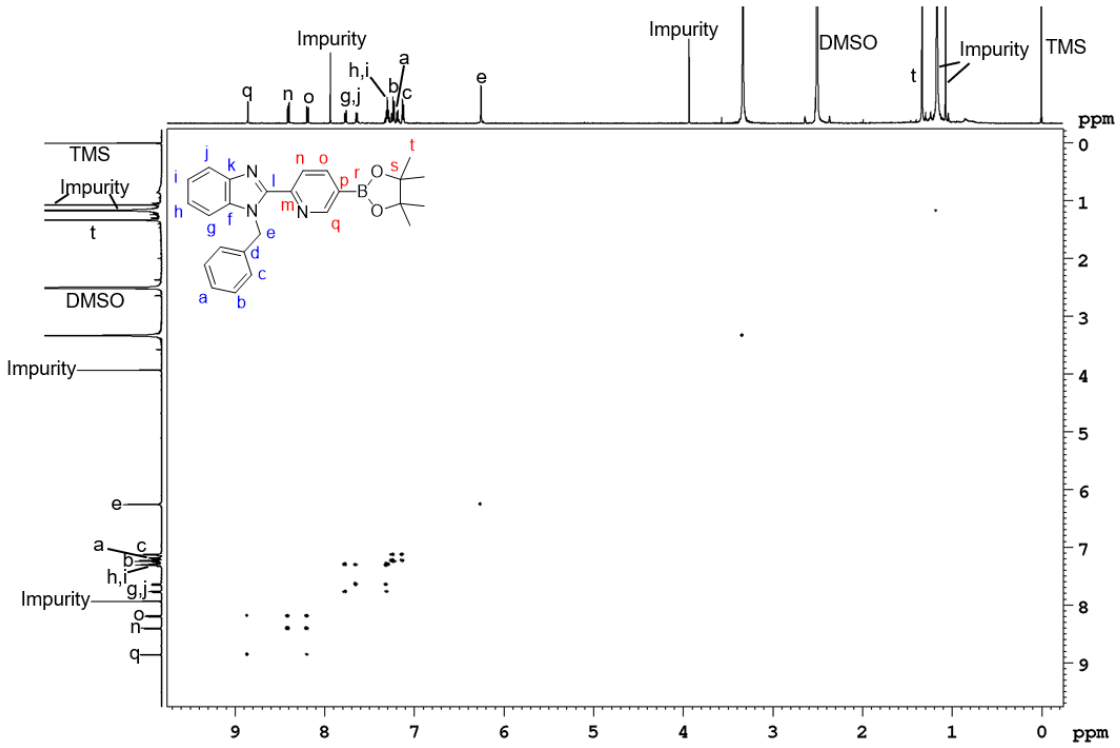

Figure S42. ^{1}H-^{1}H COSY NMR spectrum (500 MHz, DMSO-d_6, 298 K) of 1-benzyl-2-(5'-(4'',4'',5'',5''-tetramethyl-1'',3'',2''-dioxaborolan-2''-yl)pyridin-2'-yl)-1*H*-benzo[*d*]imidazole (**25**).

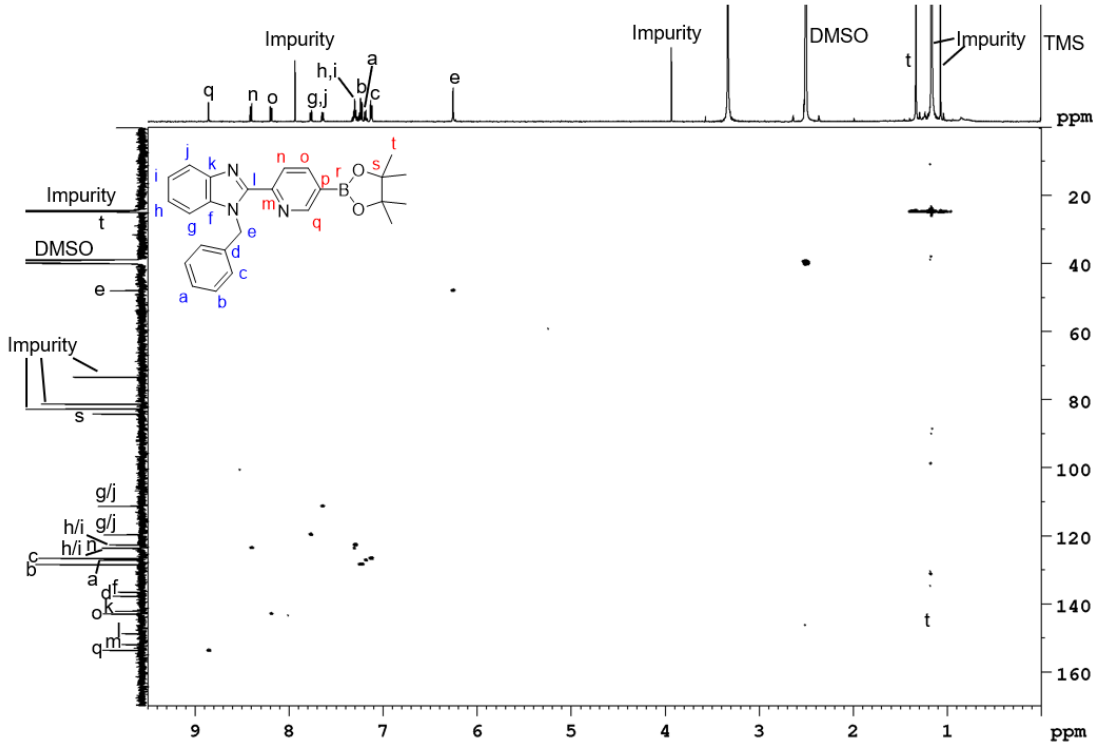

Figure S43. ^{1}H-^{13}C HSQC NMR spectrum (500 MHz/125 MHz, DMSO-d_6, 298 K) of 1-benzyl-2-(5'-(4'',4'',5'',5''-tetramethyl-1'',3'',2''-dioxaborolan-2''-yl)pyridin-2'-yl)-1*H*-benzo[*d*]imidazole (**25**).

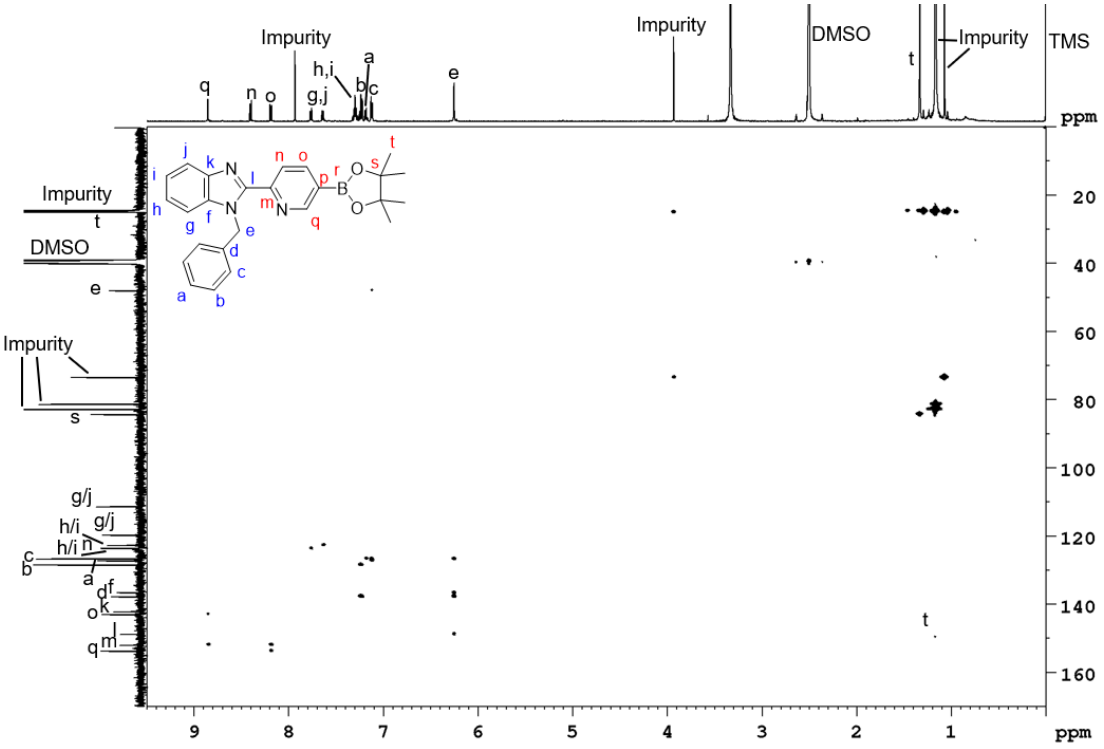

Figure S44. ^{1}H-^{13}C HMBC NMR spectrum (500 MHz/125 MHz, DMSO-d_6, 298 K) of 1-benzyl-2-(5'-(4'',4'',5'',5''-tetramethyl-1'',3'',2''-dioxaborolan-2''-yl)pyridin-2'-yl)-1*H*-benzo[*d*]imidazole (**25**).

2.3.4 6',6''-Di(1-benzyl-1*H*-benzo[*d*]imidazol-2-yl)-3',3''-bipyridine (**26**)

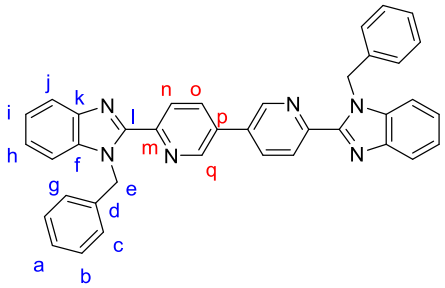

Adapted from Lusby and co-workers.[8] 2-(5'-Bromopyridin-2'-yl)-1-benzyl-1*H*-benzo[*d*]imidazole (**18**) (79.0 mg, 217 µmol), 1-benzyl-2-(5'-(4'',4'',5'',5''-tetramethyl-1'',3'',2''-dioxaborolan-2''-yl)pyridin-2'-yl)-1*H*-benzo[*d*]imidazole (**25**) (89.3 mg, 217 µmol), potassium carbonate (150 mg, 1.09 mmol, milled) and $Pd(PPh_3)_4$ (25.1 mg, 5 mol%) were added to a three-neck flask and the flask was evacuated for 5 min. Anhydrous ethanol (2 mL), water (2 mL, degassed) and anhydrous tetrahydrofuran (5 mL) were added and the reaction mixture was stirred at 80 °C for 23.5 h. The solution was cooled to room temperature, filtered and the precipitate was washed with cold tetrahydrofuran (250 mL). The product was obtained as a colourless solid (59.7 mg, 105 µmol, 49%).

^{1}H NMR (600 MHz, TFA-d_1, 298 K) δ (ppm): 9.41 (dd, ^{4}J = 2.2 Hz, ^{5}J = 0.7 Hz, 2H, H_q), 8.64 (dd, ^{3}J = 8.2 Hz, ^{4}J = 2.2 Hz, 2H, H_o), 8.34 (dd, ^{3}J = 8.2 Hz, ^{5}J = 0.7 Hz, 2H, H_n), 7.97 (unres. dt, 2H, H_j), 7.84-7.74 (m, 6H, $H_{g,h,i}$), 7.39-7.32 (m, 6H, $H_{a,b}$), 7.21-7.16 (m, 4H, H_c), 6.05 (s, 4H, H_e).

^{13}C NMR (151 MHz, TFA-d_1, 298 K) δ (ppm): 150.7 (C_q), 146.7 (C_l), 142.9 (C_m), 141.7 (C_o), 138.4 (C_p), 135.6 (C_f), 134.5 (C_d), 132.6 (C_k), 131.9 (C_b), 131.8 (C_a), 131.6 (C_i), 131.2 (C_h), 129.7 (C_n), 128.5 (C_c), 117.0 (C_j), 115.6 (C_g), 52.8 (C_e).

EI-MS *m/z*: 568.23722 (calculated for $C_{38}H_{28}N_6$: 568.23754).

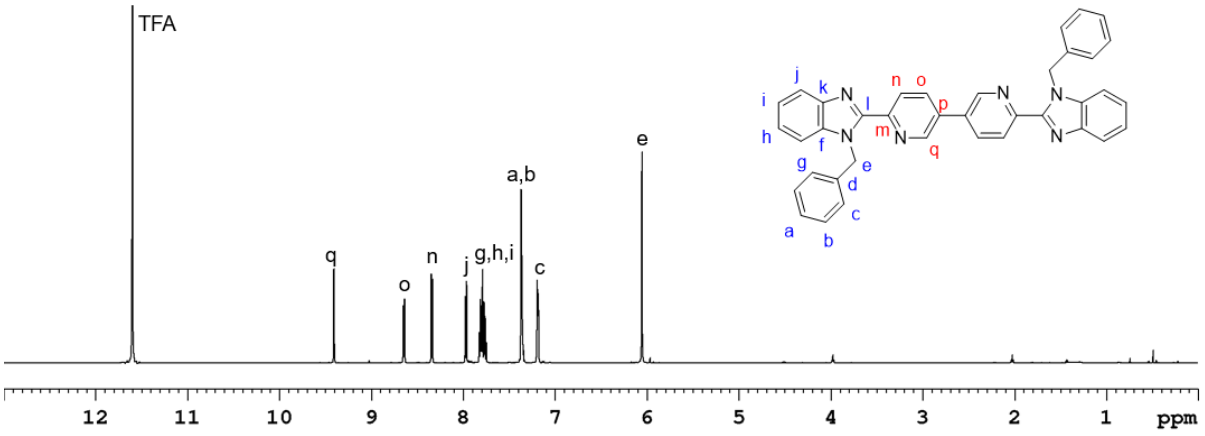

Figure S45. ^{1}H NMR spectrum (600 MHz, TFA-d_1, 298 K) of 6',6''-di(1-benzyl-1*H*-benzo[*d*]imidazol-2-yl)-3',3''-bipyridine (**26**).

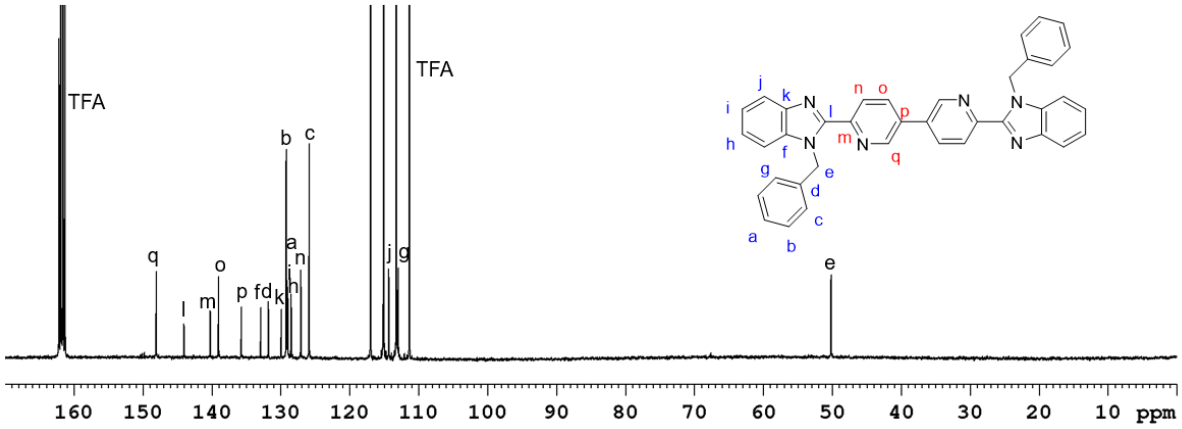

Figure S46. ^{13}C NMR spectrum (151 MHz, TFA-d_1, 298 K) of 6',6''-di(1-benzyl-1*H*-benzo[*d*]imidazol-2-yl)-3',3''-bipyridine (**26**).

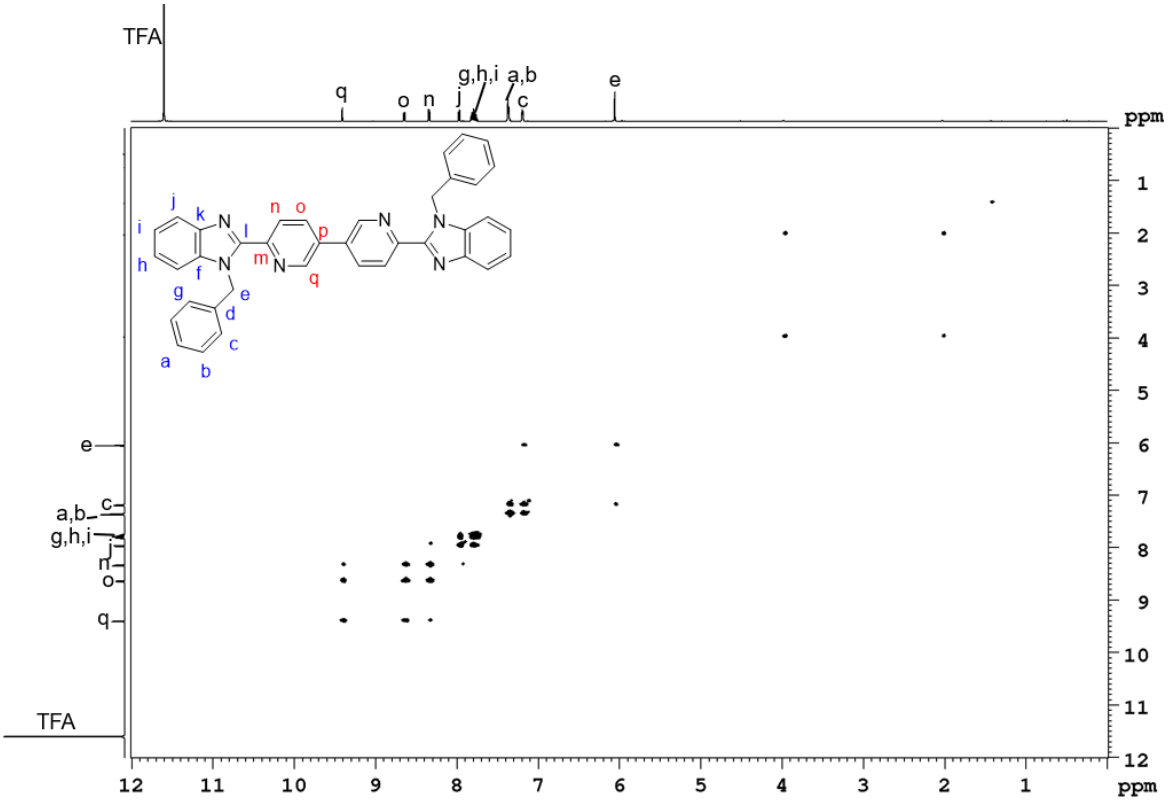

Figure S47. ^{1}H-^{1}H COSY NMR spectrum (600 MHz, TFA-d_1, 298 K) of 6',6''-di(1-benzyl-1*H*-benzo[*d*]imidazol-2-yl)-3',3''-bipyridine (**26**).

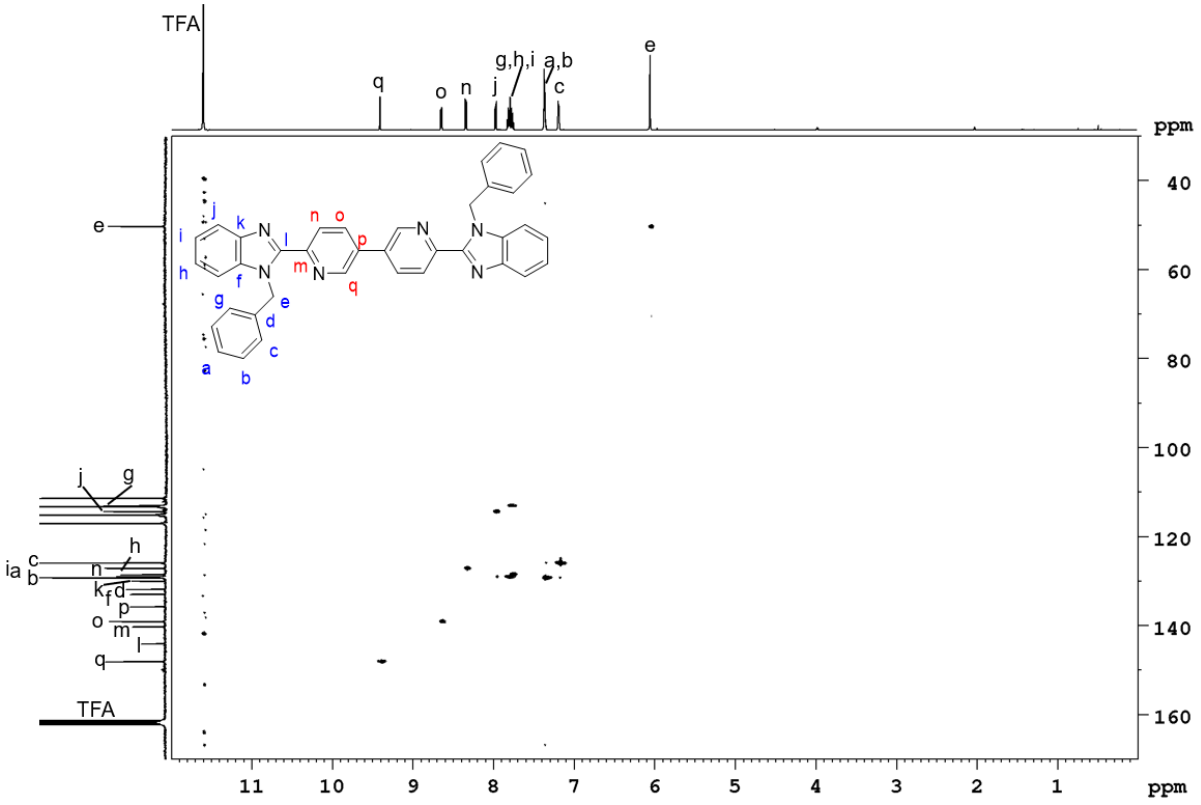

Figure S48. ^{1}H-^{13}C HSQC NMR spectrum (600 MHz/151 MHz, TFA-d_1, 298 K) of 6',6''-di(1-benzyl-1*H*-benzo[*d*]imidazol-2-yl)-3',3''-bipyridine (**26**).

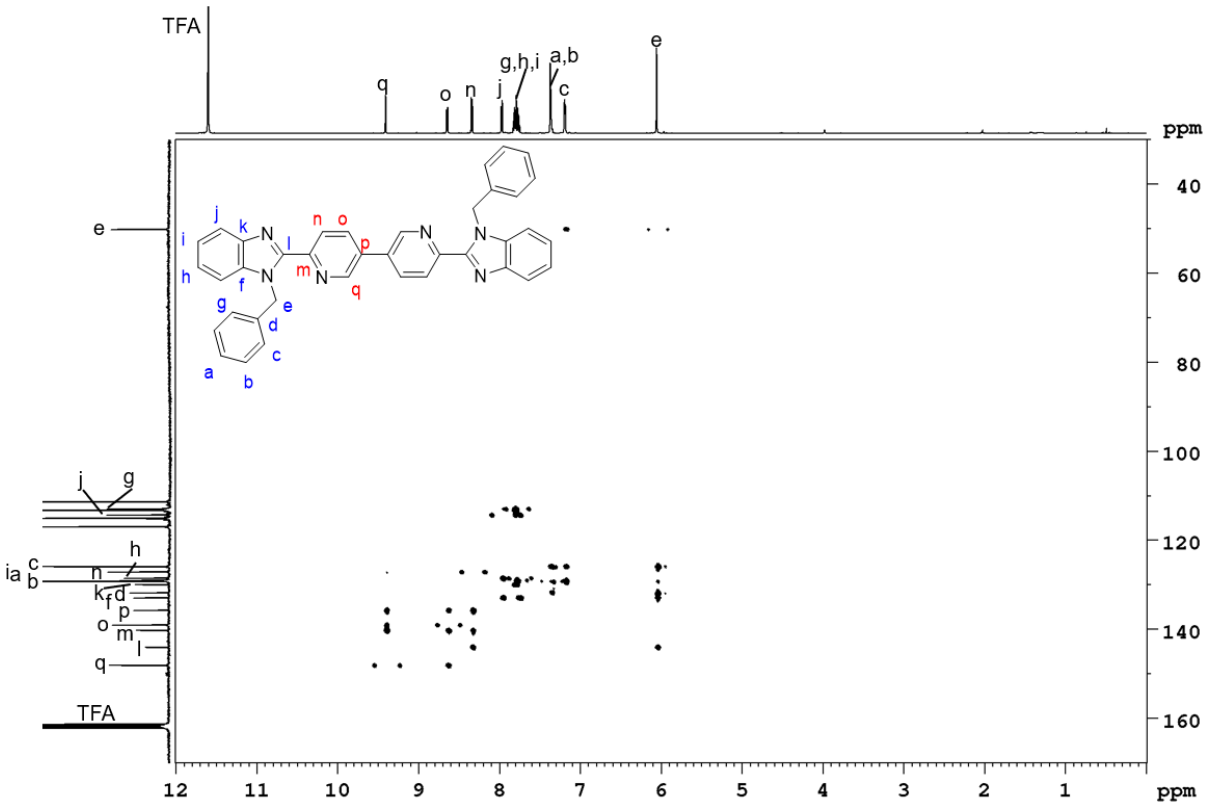

Figure S49. ^{1}H-^{13}C HMBC NMR spectrum (600 MHz/151 MHz, TFA-d_1, 298 K) of 6',6''-di(1-benzyl-1*H*-benzo[*d*]imidazol-2-yl)-3',3''-bipyridine (**26**).

2.4 Benzimidazole-based Ligands with a Phenylene-Based Spacer

Benzimidazole-based ligands with a phenylene-based spacer were synthesised according to Scheme S4. The boronic esters were prepared adapting a literature-known procedure.[7]

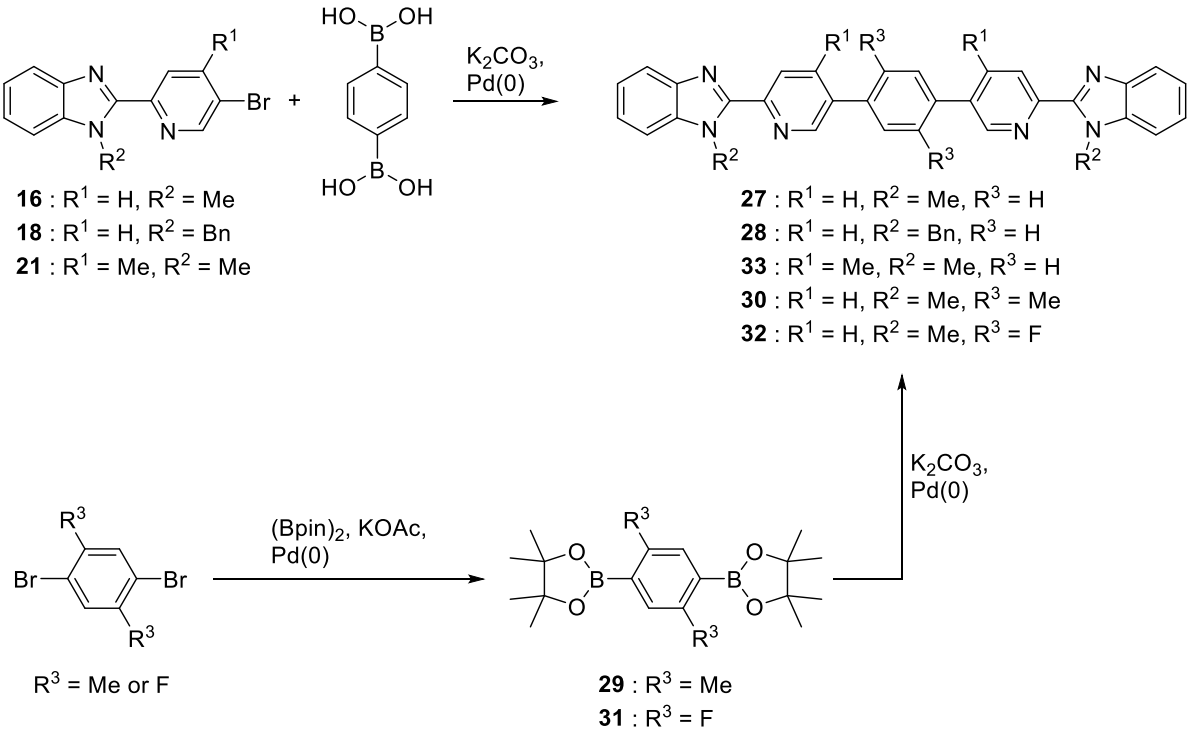

Scheme S4. Synthesis of ligands **27**, **28**, **30**, **32** and **33**.

2.4.1 1,4-Di(6''-(1'-methyl-1*H*-benzo[*d*]imidazol-2'-yl)pyridin-3''-yl)benzene (**27**)

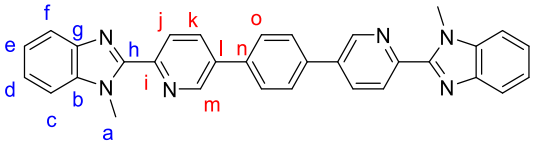

Adapted from Lusby and co-workers.[8] 2-(5'-Bromopyridin-2'-yl)-1-methyl-1*H*-benzo[*d*]imidazole (**16**) (250 mg, 868 µmol), *p*-phenylenediboronic acid (71.9 mg, 434 µmol), potassium carbonate (300 mg, 2.17 mmol, milled) and $Pd(PPh_3)_4$ (50.2 mg, 10 mol%) were added to a three-neck flask and the flask was evacuated for 5 min. Anhydrous ethanol (3 mL), water (3 mL, degassed) and anhydrous tetrahydrofuran (7 mL) were added and the reaction mixture stirred at 80 °C for 20 h. The solution was cooled to room temperature and the precipitate was collected by filtration and washed with cold tetrahydrofuran (200 mL). The product was obtained as a colourless solid (152 mg, 309 µmol, 71%).

^{1}H NMR (600 MHz, $CDCl_3$, 298 K) δ (ppm): 9.02 (d, ^4J =2.3 Hz, 2H, H_m), 8.53 (d, ^3J = 8.2 Hz, 2H, H_j), 8.13 (dd, ^3J = 8.2 Hz, ^4J = 2.3 Hz, 2H, H_k), 7.86 (d, ^3J = 7.7 Hz, 2H, H_f), 7.84 (s, 4H, H_o), 7.48 (d, ^3J = 7.6 Hz, 2H, H_c), 7.39-7.36 (m, 2H, H_d), 7.36-7.33 (m, 2H, H_e), 4.36 (s, 6H, H_a).

^{13}C NMR (151 MHz, $CDCl_3$, 298 K) δ (ppm): 150.0 (C_h), 149.7 (C_i), 146.9 (C_m), 142.7 (C_g), 137.5 (C_b), 137.4 (C_n), 135.6 (C_l), 135.0 (C_k), 127.9 (C_o), 124.8 (C_j), 123.5 (C_d), 122.7 (C_e), 120.0 (C_f), 110.0 (C_c), 32.9 (C_a).

EI-MS *m/z*: 492.20465 (calculated for $C_{32}H_{24}N_6$: 492.20624).

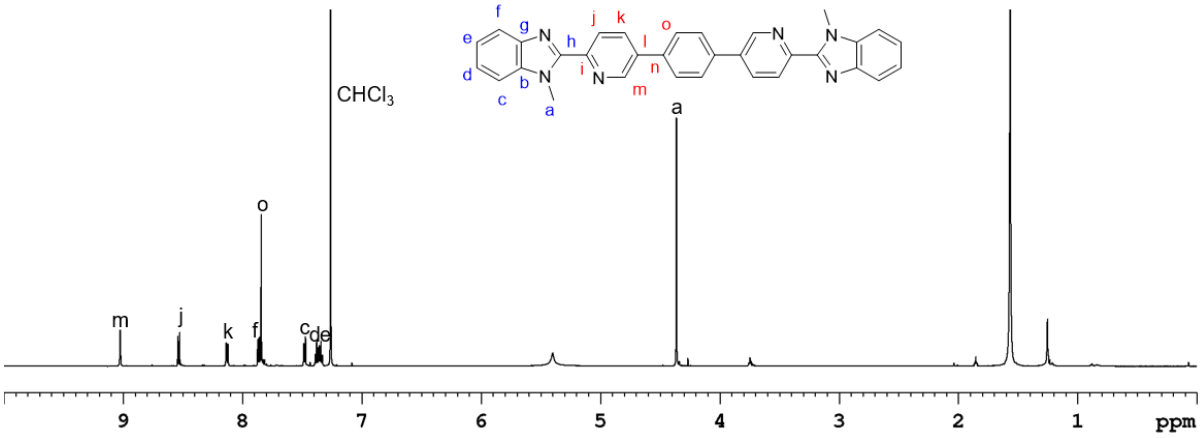

Figure S50. ^{1}H NMR spectrum (600 MHz, $CDCl_3$, 298 K) of 1,4-di(6''-(1'-methyl-1*H*-benzo[*d*]imidazol-2'-yl)pyridin-3''-yl)benzene (**27**).

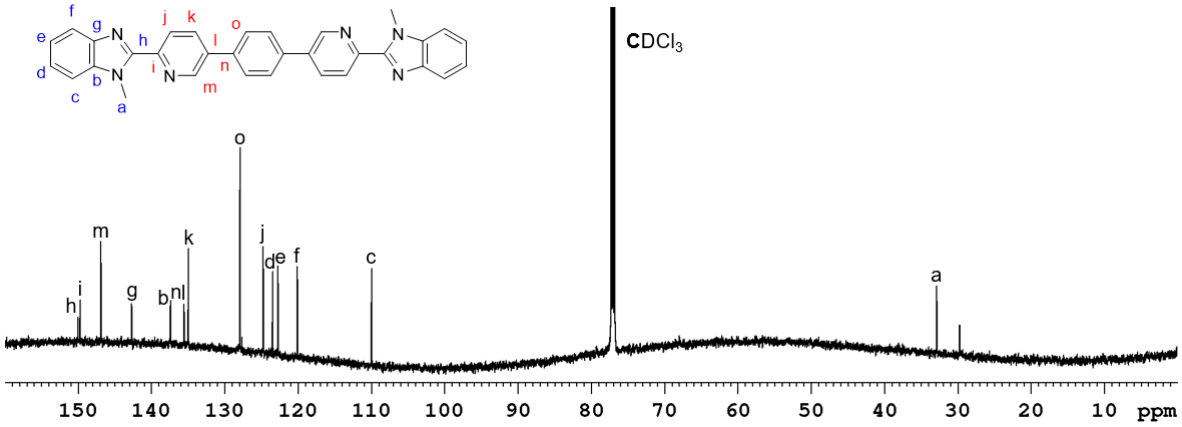

Figure S51. ^{13}C NMR spectrum (151 MHz, $CDCl_3$, 298 K) of 1,4-di(6''-(1'-methyl-1*H*-benzo[*d*]imidazol-2'-yl)pyridin-3''-yl)benzene (**27**).

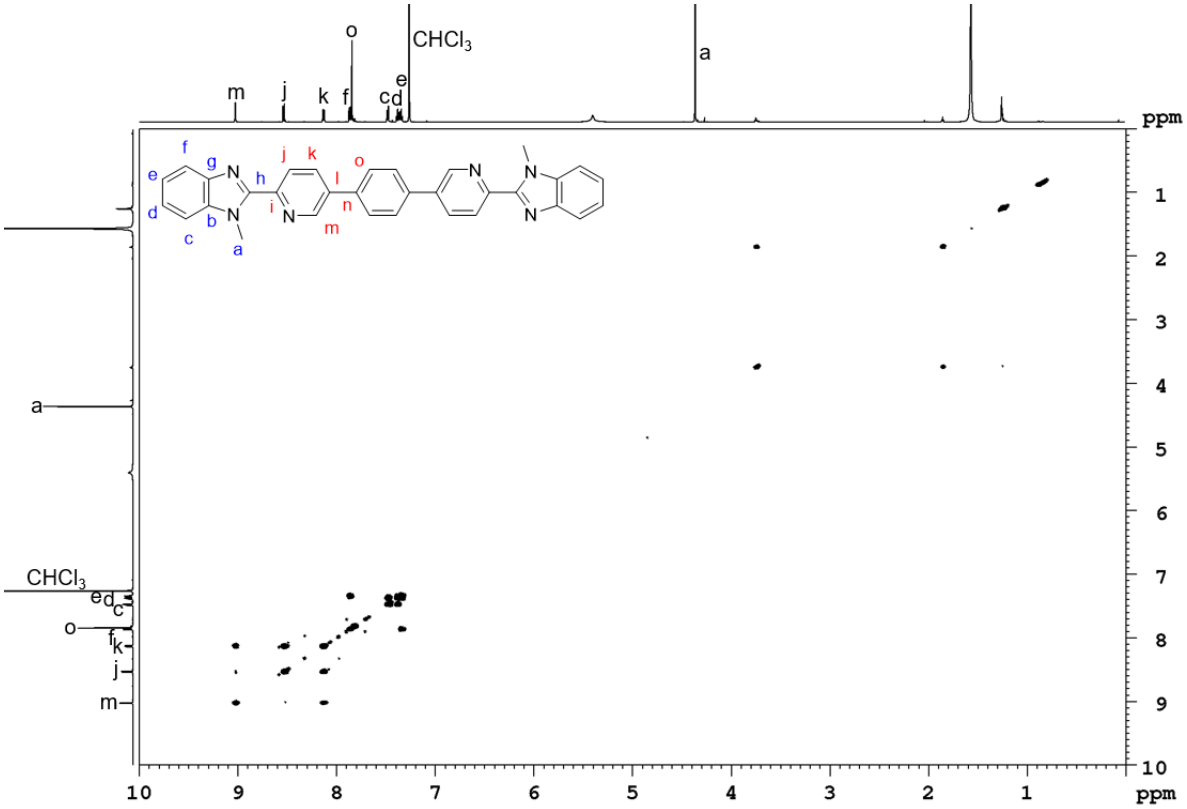

Figure S52. ^{1}H-^{1}H COSY NMR spectrum (600 MHz, $CDCl_3$, 298 K) of 1,4-di(6''-(1'-methyl-1*H*-benzo[*d*]imidazol-2'-yl)pyridin-3''-yl)benzene (**27**).

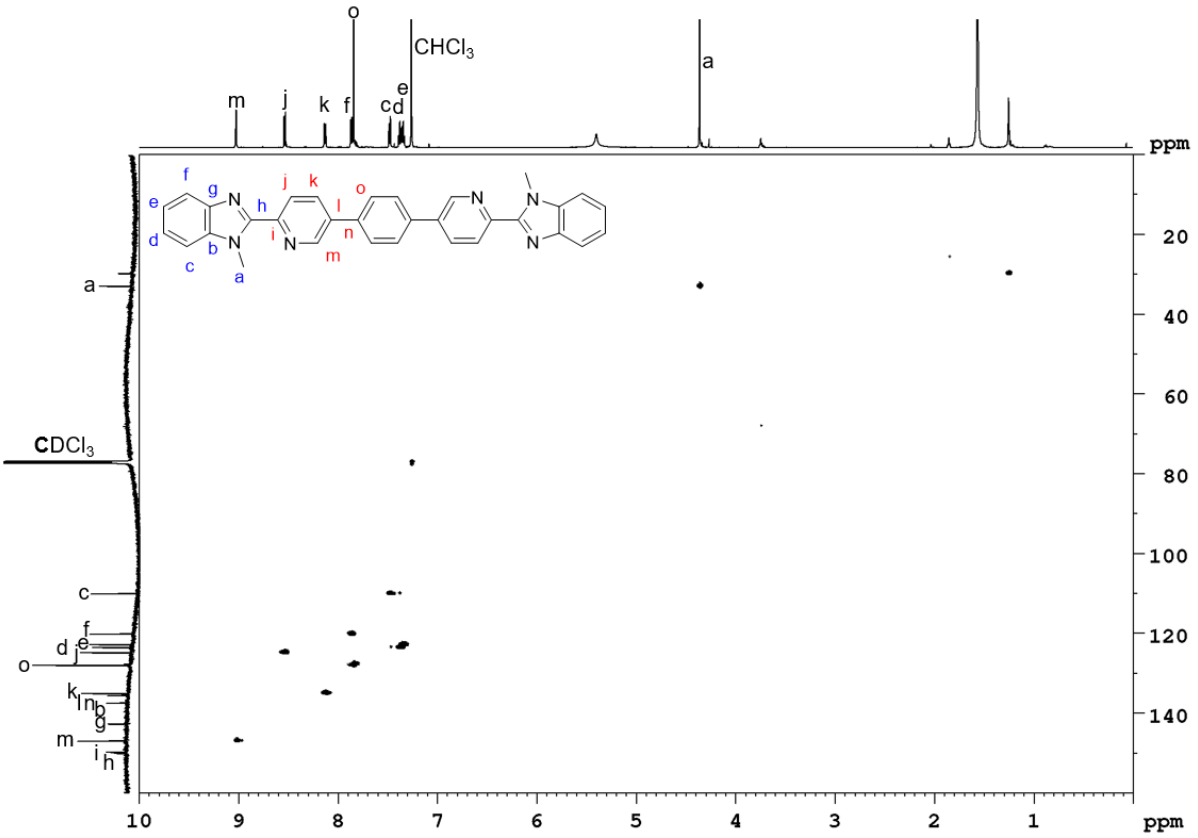

Figure S53. ^{1}H-^{13}C HSQC NMR spectrum (600 MHz/151 MHz, $CDCl_3$, 298 K) of 1,4-di(6''-(1'-methyl-1*H*-benzo[*d*]imidazol-2'-yl)pyridin-3''-yl)benzene (**27**).

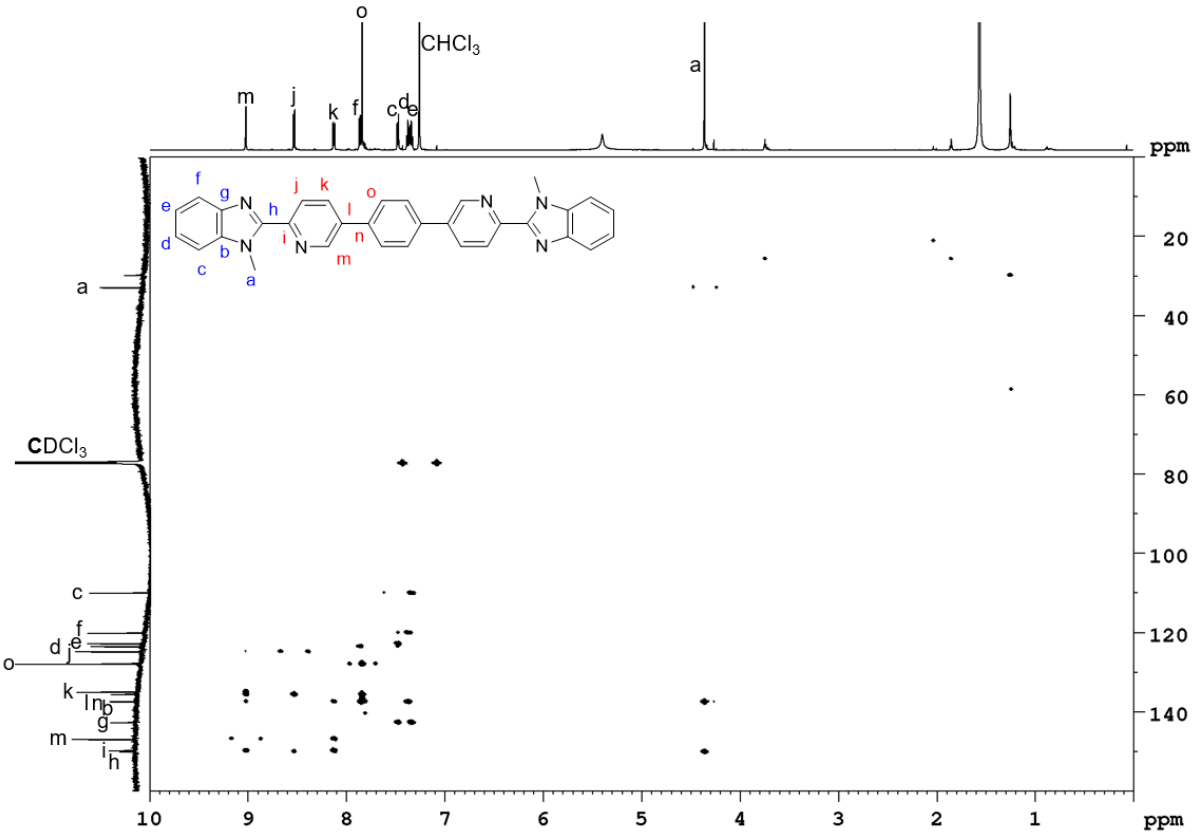

Figure S54. ^{1}H-^{13}C HMBC NMR spectrum (600 MHz/151 MHz, $CDCl_3$, 298 K) of 1,4-di(6''-(1'-methyl-1*H*-benzo[*d*]imidazol-2'-yl)pyridin-3''-yl)benzene (**27**).

2.4.2 1,4-Di(6''-(1'-benzyl-1*H*-benzo[*d*]imidazol-2'-yl)pyridin-3''-yl)benzene (**28**)

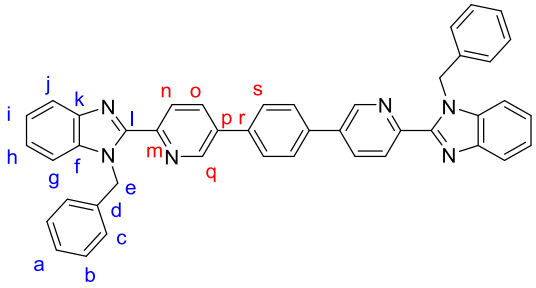

Adapted from Lusby and co-workers.[8] 2-(5'-Bromopyridin-2'-yl)-1-benzyl-1*H*-benzo[*d*]imidazole (**18**) (158 mg, 434 µmol), *p*-phenylenediboronic acid (36.0 mg, 217 µmol), potassium carbonate (150 mg, 1.09 mmol, milled) and $Pd(PPh_3)_4$ (25.1 mg, 10 mol%) were added to a three-neck flask and the flask was evacuated for 5 min. Anhydrous ethanol (1.5 mL), water (1.5 mL, degassed) and anhydrous tetrahydrofuran (3.5 mL) were added and the reaction mixture stirred at 80 °C for 18 h. The solution was cooled to room temperature and the precipitate was collected by filtration and washed with cold tetrahydrofuran (250 mL). The product was obtained as a colourless solid (101 mg, 157 µmol, 72%).

^{1}H NMR (500 MHz, TFA-d_1, 298 K) δ (ppm): 9.46 (d, ^4J = 2.1 Hz, 2H, H_q), 8.86 (dd, ^3J = 8.3 Hz, ^4J = 2.1 Hz, 2H, H_o), 8.38 (d, ^3J = 8.3 Hz, 2H, H_n), 8.04 (s, 4H, H_s), 7.99 (d, ^3J = 8.3 Hz, 1H, H_j), 7.88-7.80 (m, 3H, $H_{g,h,i}$), 7.42-7.34 (m, 3H, $H_{a,b}$), 7.16 (d, ^3J = 8.0 Hz, 2H, H_c), 5.94 (s, 2H, H_e).

^{13}C NMR (151 MHz, TFA-d_1, 298 K) δ (ppm): 147.6 (C_q), 145.0 ($C_{p/r}$), 144.9 (C_o), 143.3 (C_l), 137.8 ($C_{p/r}$), 136.9 (C_m), 135.3 (C_f), 133.8 (C_d), 132.7 (C_k), 132.0 (C_a), 132.0 (C_i), 131.9 (C_b), 131.7 (C_n), 131.6 (C_h), 131.2 (C_s), 128.6 (C_c), 117.1 (C_j), 115.5 (C_g), 53.0 (C_e).

EI-MS *m/z*: 644.26771 (calculated for $C_{44}H_{32}N_6$: 644.26884).

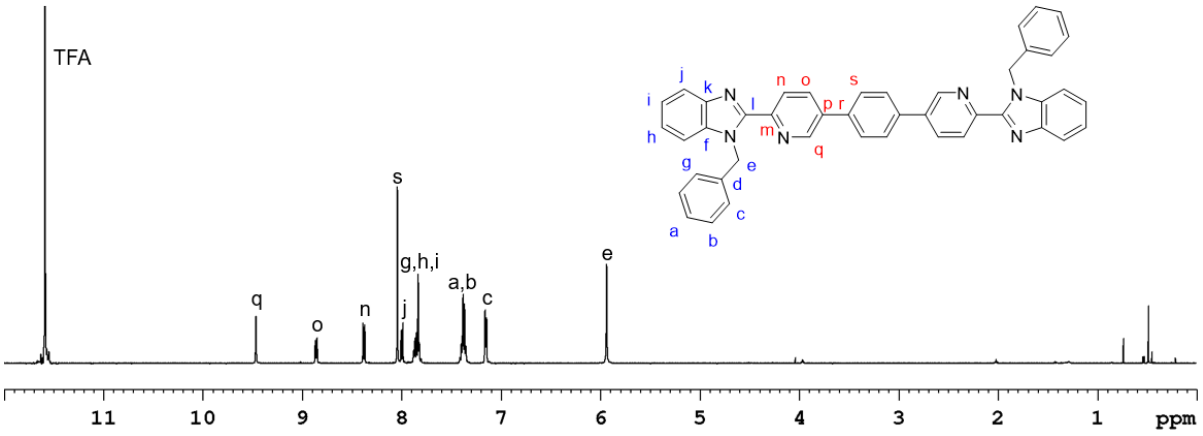

Figure S55. ^{1}H NMR spectrum (500 MHz, TFA-d_1, 298 K) of 1,4-di(6''-(1'-benzyl-1*H*-benzo[*d*]imidazol-2'-yl)pyridin-3''-yl)benzene (**28**).

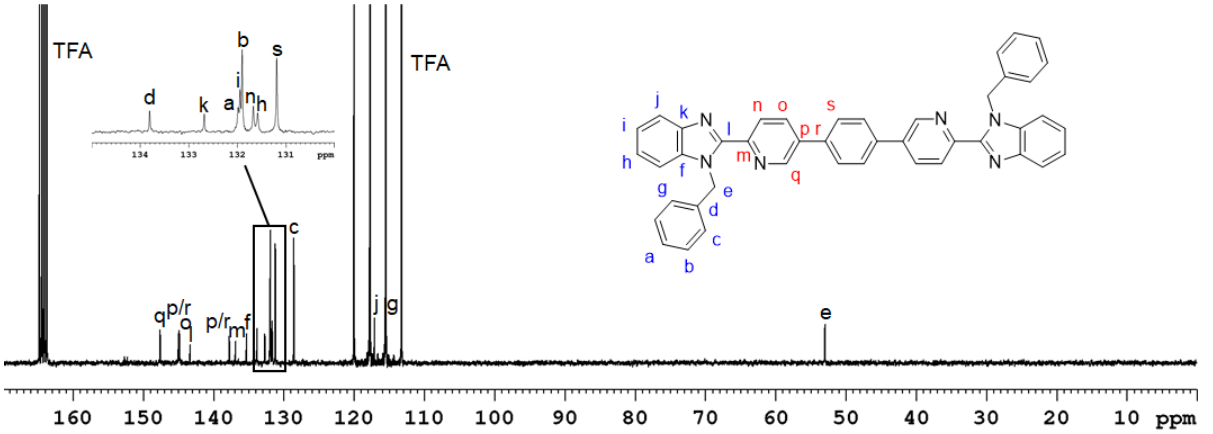

Figure S56. ^{13}C NMR spectrum (125 MHz, TFA-d_1, 298 K) of 1,4-di(6''-(1'-benzyl-1*H*-benzo[*d*]imidazol-2'-yl)pyridin-3''-yl)benzene (**28**).

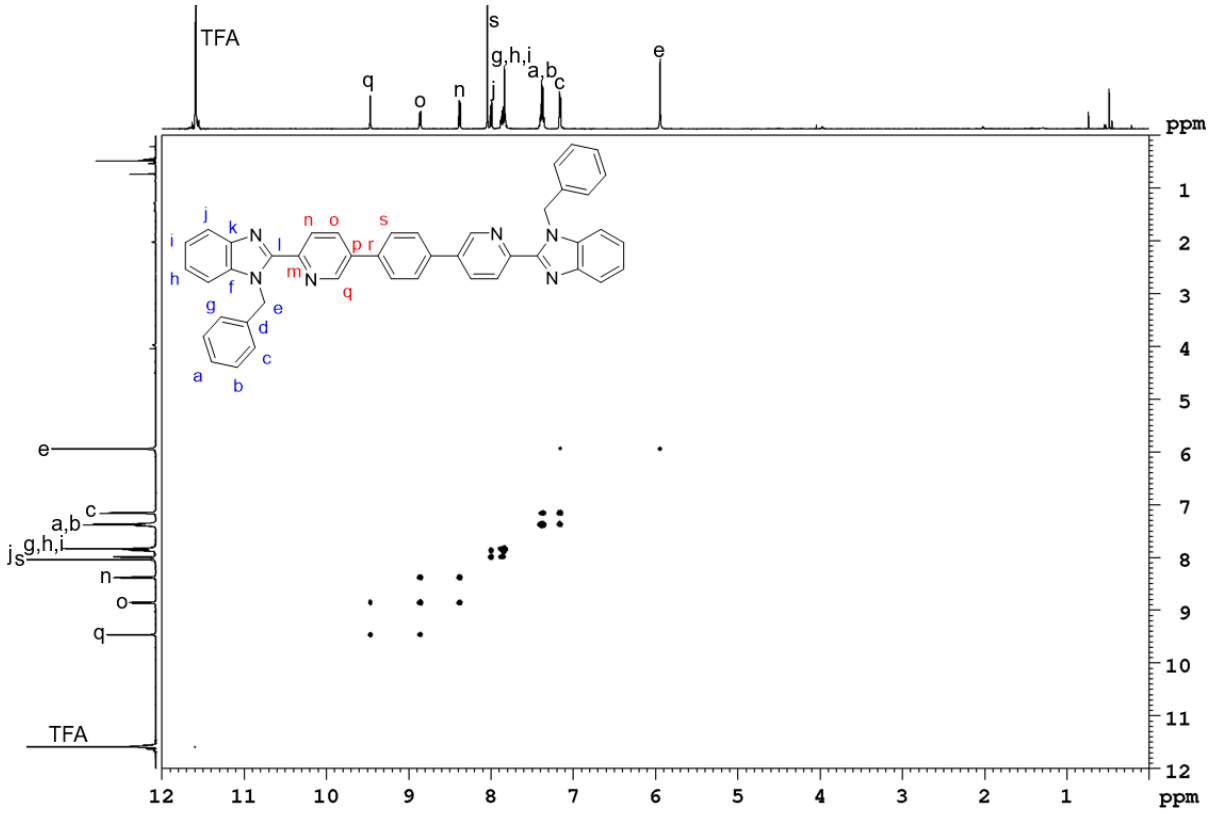

Figure S57. ^{1}H-^{1}H COSY NMR spectrum (500 MHz, TFA-d_1, 298 K) of 1,4-di(6''-(1'-benzyl-1*H*-benzo[*d*]imidazol-2'-yl)pyridin-3''-yl)benzene (**28**).

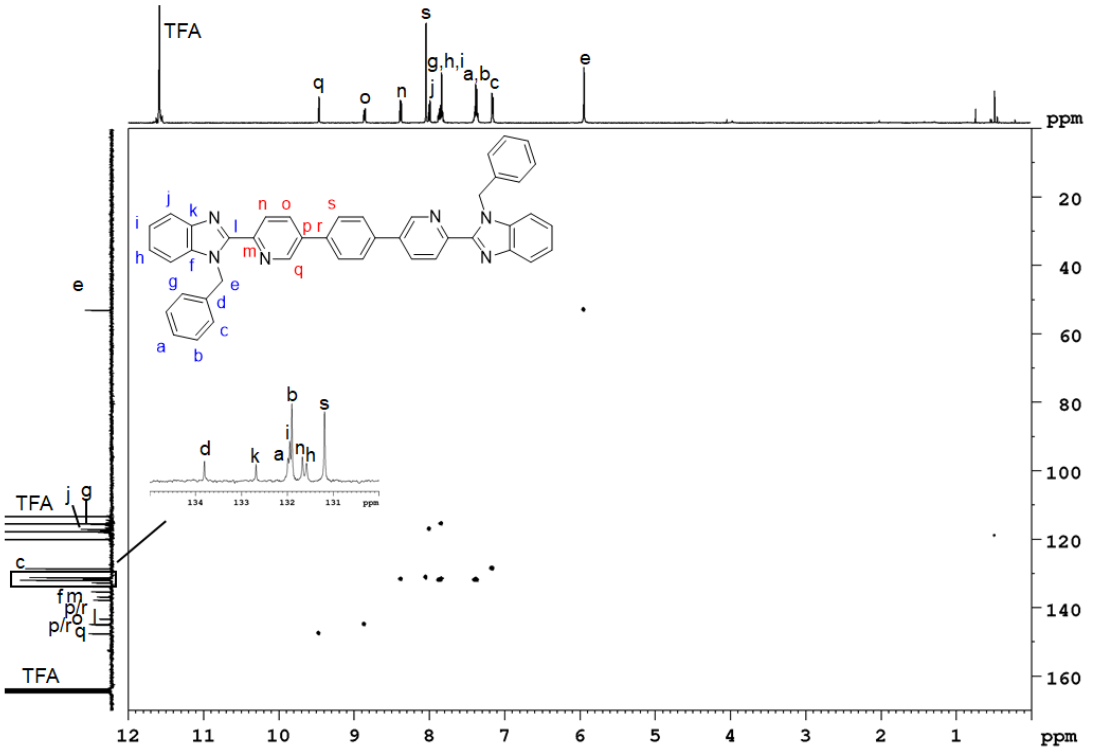

Figure S58. ^{1}H-^{13}C HSQC NMR spectrum (500 MHz/125 MHz, TFA-d_1, 298 K) of 1,4-di(6''-(1'-benzyl-1*H*-benzo[*d*]imidazol-2'-yl)pyridin-3''-yl)benzene (**28**).

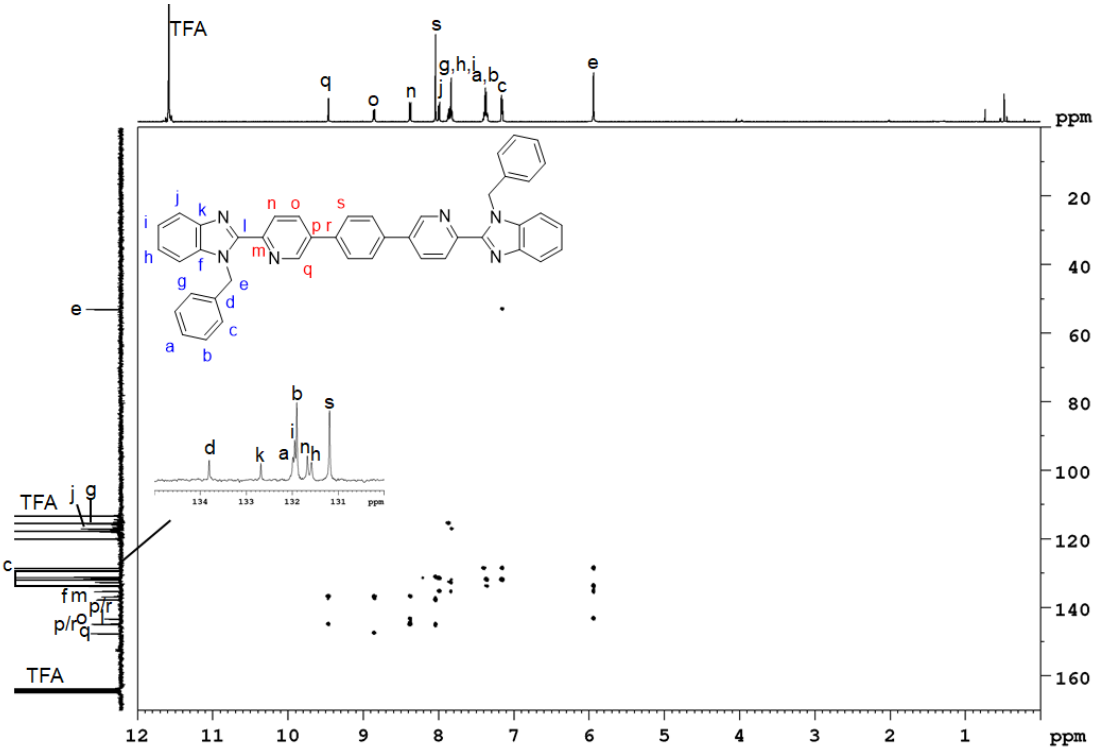

Figure S59. ^{1}H-^{13}C HMBC NMR spectrum (500 MHz/125 MHz, TFA-d_1, 298 K) of 1,4-di(6''-(1'-benzyl-1*H*-benzo[*d*]imidazol-2'-yl)pyridin-3''-yl)benzene (**28**).

2.4.3 2,2'-(2,5-Dimethyl-1,4-phenylene)di(4'',4'',5'',5''-tetramethyl-1'',3'',2''-dioxaborolane) (**29**)

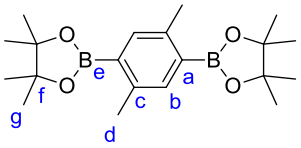

Adapted from Severin and co-workers.[7] 1,4-Dibromo-2,5-dimethylbenzene (500 mg, 1.89 mmol), bis(pinacolato)diboron (1.00 g, 3.94 mmol), potassium acetate (925 mg, 9.42 mmol) and Pd(dppf)Cl_2·CH_2Cl_2 (77.2 mg, 5 mol%) were added to a three-neck flask and the flask was evacuated for 5 min. Anhydrous 1,4-dioxane (20 mL) was added and the mixture was stirred at 90 °C for 23 h. The reaction mixture was cooled to room temperature and the solvent was removed *in vacuo*. Purification by flash chromatography (silica gel, 33% dichloromethane/cyclohexane) gave the product as a colourless solid (196 mg, 547 µmol, 29%).

The analytical data was consistent with literature data.[7]

^{1}H NMR (500 MHz, $CDCl_3$, 298 K) δ (ppm): 7.54 (s, 2H, H_b), 2.48 (s, 6H, H_d), 1.34 (s, 24H, H_g).

^{13}C NMR (125 MHz, $CDCl_3$, 298 K) δ (ppm): 140.5 (C_c), 136.9 (C_b), 83.4 (C_f), 24.9 (C_g), 21.5 (C_d). C_a was not observed.

EI-MS *m/z*: 358.24906 (calculated for $C_{20}H_{28}{}^{11}B_2O_4$: 358.24867).

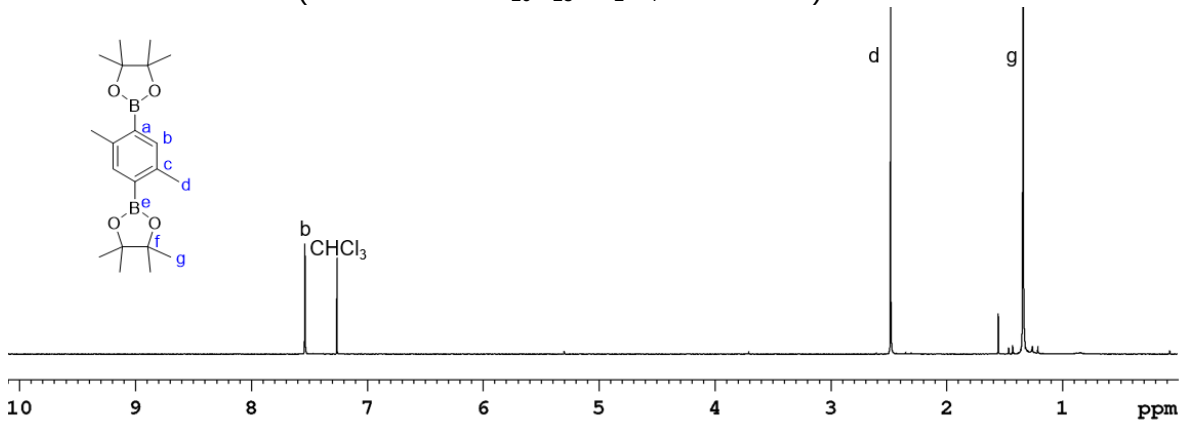

Figure S60. ^{1}H NMR spectrum (500 MHz, $CDCl_3$, 298 K) of 2,2'-(2,5-dimethyl-1,4-phenylene)di(4'',4'',5'',5''-tetramethyl-1'',3'',2''-dioxaborolane) (**29**).

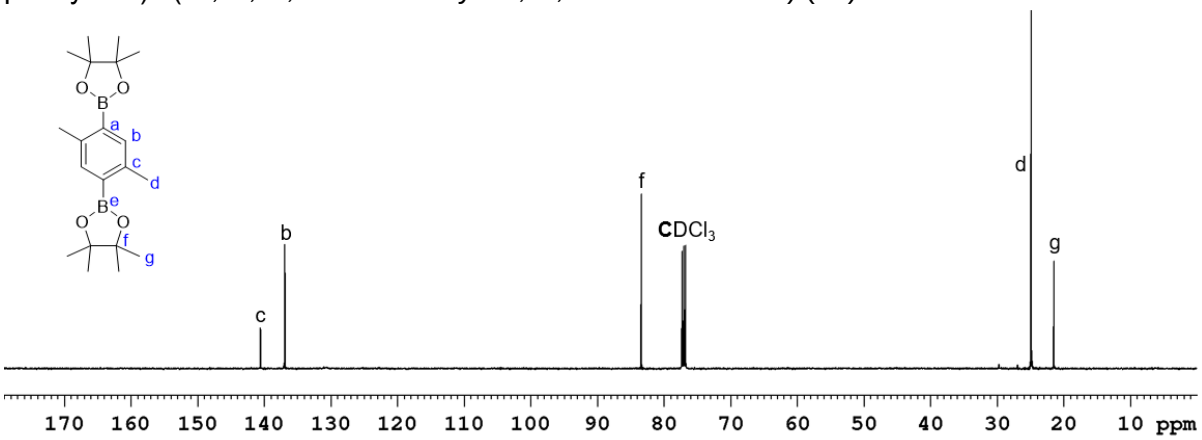

Figure S61. ^{13}C NMR spectrum (125 MHz, $CDCl_3$, 298 K) of 2,2'-(2,5-dimethyl-1,4-phenylene)di(4'',4'',5'',5''-tetramethyl-1'',3'',2''-dioxaborolane) (**29**).

2.4.4 1,4-Di(6''-(1'-methyl-1*H*-benzo[*d*]imidazol-2'-yl)pyridin-3''-yl)-2,5-dimethylbenzene (**30**)

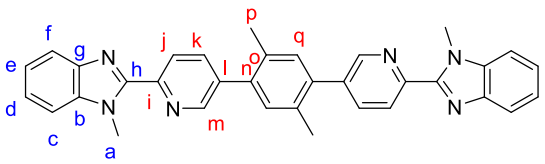

Adapted from Lusby and co-workers.[8] 2-(5'-Bromopyridin-2'-yl)-1-benzyl-1*H*-benzo[*d*]imidazole (**16**) (80.7 mg, 280 µmol), 2,2'-(2,5-dimethyl-1,4-phenylene)di(4'',4'',5'',5''-tetramethyl-1'',3'',2''-dioxaborolane) (**29**) (50.0 mg, 140 µmol), potassium carbonate (96.7 mg, 700 µmol, milled) and $Pd(PPh_3)_4$ (16.2 mg, 10 mol%) were added to a three-neck flask and the flask was evacuated for 5 min. Anhydrous ethanol (1 mL, dry), water (1 mL, degassed) and anhydrous tetrahydrofuran (3 mL) were added and the reaction mixture was stirred at 80 °C for 23 h. The solution was cooled to room temperature and the precipitate was collected by filtration and washed with cold tetrahydrofuran (250 mL, cooled to -18 °C) to obtain the product as a beige solid (56.0 mg, 108 µmol, 77%).

^{1}H NMR (500 MHz, $CDCl_3$, 298 K) δ (ppm): 8.75 (dd, ^4J = 2.3 Hz, ^5J = 0.8 Hz, 2H, H_m), 8.50 (dd, ^3J = 8.1 Hz, ^5J = 0.8 Hz, 2H, H_j), 7.89 (dd, ^3J = 8.1 Hz, ^4J = 2.3 Hz, 2H, H_k), 7.87-7.85 (m, 2H, H_f), 7.49-7.47 (m, 2H, H_c), 7.37 (td, ^3J = 7.2 Hz, ^4J =1.3 Hz, 2H, H_d), 7.34 (td, ^3J = 7.2 Hz, ^4J =1.3 Hz, 2H, H_e), 7.28 (s, 2H, H_q), 4.36 (s, 6H, H_a), 2.38 (s, 6H, H_p).

^{13}C NMR (125 MHz, $CDCl_3$, 298 K) δ (ppm): 150.2 (C_h), 149.2 (C_i), 148.6 (C_m), 142.7 (C_g), 137.7 (C_n), 137.4 (C_b), 137.3 (C_k), 136.9 (C_l), 133.5 (C_o), 132.2 (C_q), 124.1 (C_j), 123.4 (C_d), 122.7 (C_e), 120.0 (C_f), 110.0 (C_c), 32.8 (C_a), 19.9 (C_p).

EI-MS *m/z*: 520.23624 (calculated for $C_{34}H_{28}N_6$: 520.23754).

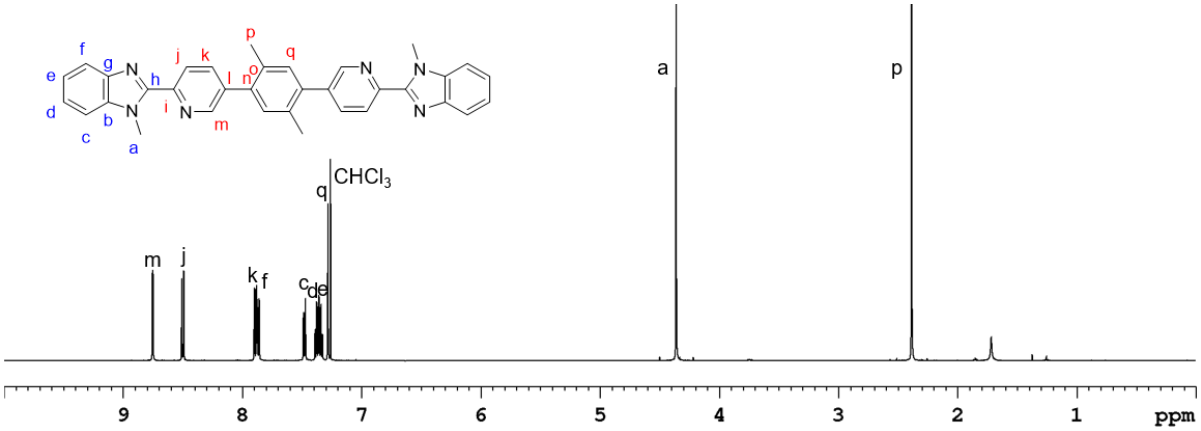

Figure S62. ^{1}H NMR spectrum (500 MHz, $CDCl_3$, 298 K) of 1,4-di(6''-(1'-methyl-1*H*-benzo[*d*]imidazol-2'-yl)pyridin-3''-yl)-2,5-dimethylbenzene (**30**).

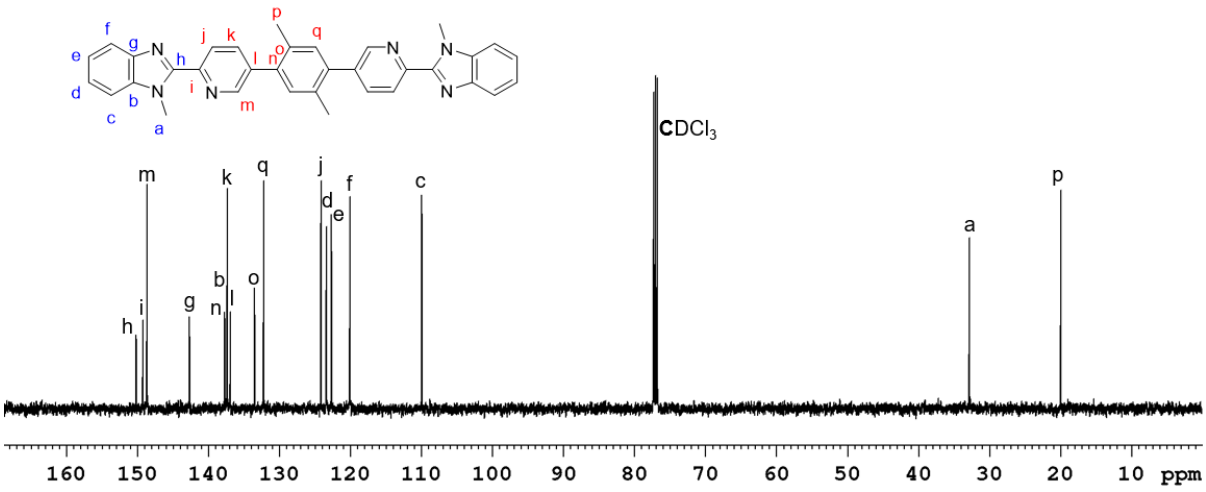

Figure S63. ^{13}C NMR spectrum (125 MHz, $CDCl_3$, 298 K) of 1,4-di(6''-(1'-methyl-1*H*-benzo[*d*]imidazol-2'-yl)pyridin-3''-yl)-2,5-dimethylbenzene (**30**).

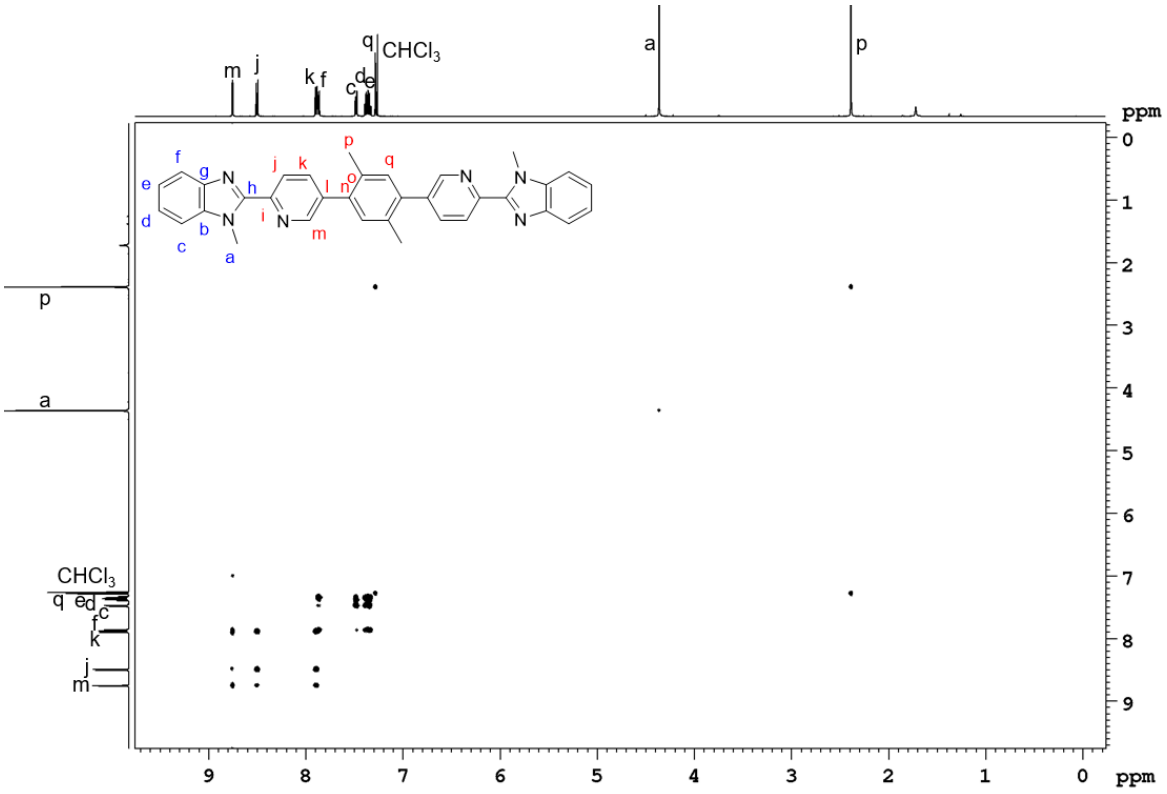

Figure S64. ^{1}H-^{1}H COSY NMR spectrum (500 MHz, $CDCl_3$, 298 K) of 1,4-di(6''-(1'-methyl-1*H*-benzo[*d*]imidazol-2'-yl)pyridin-3''-yl)-2,5-dimethylbenzene (**30**).

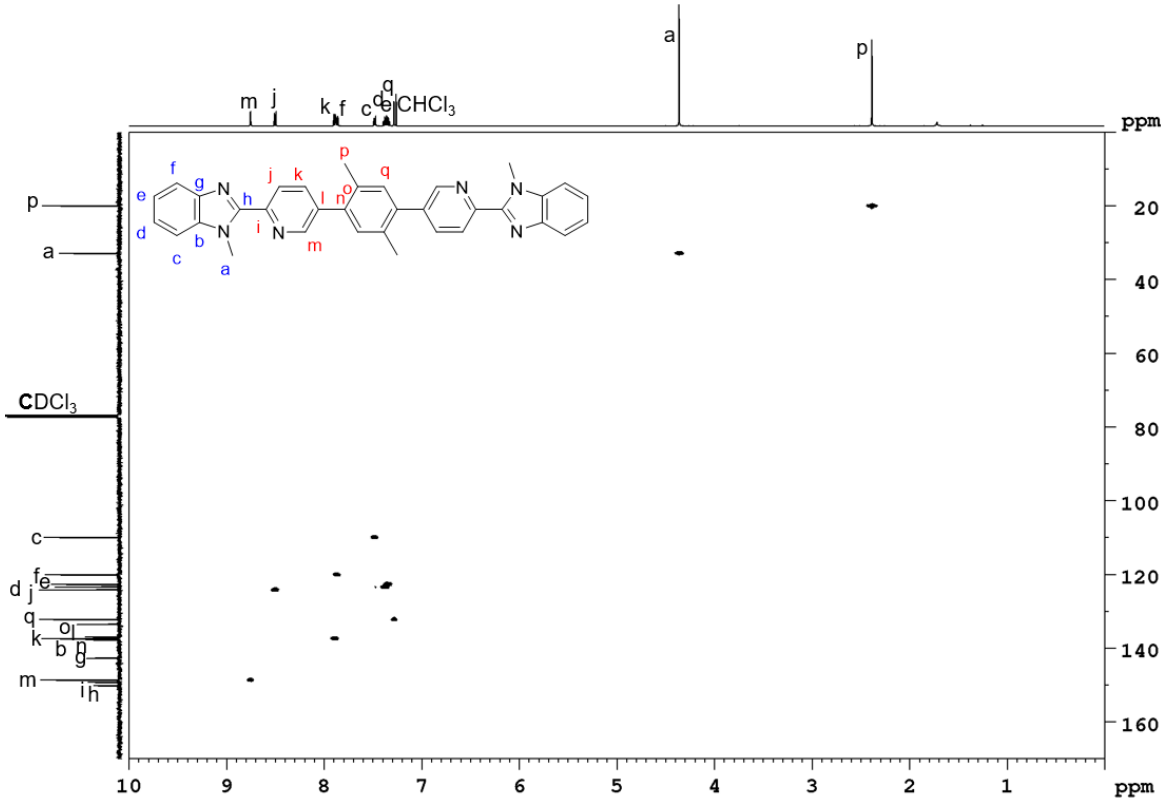

Figure S65. ^{1}H-^{13}C HSQC NMR spectrum (500 MHz/125 MHz, $CDCl_3$, 298 K) of 1,4-di(6''-(1'-methyl-1*H*-benzo[*d*]imidazol-2'-yl)pyridin-3''-yl)-2,5-dimethylbenzene (**30**).

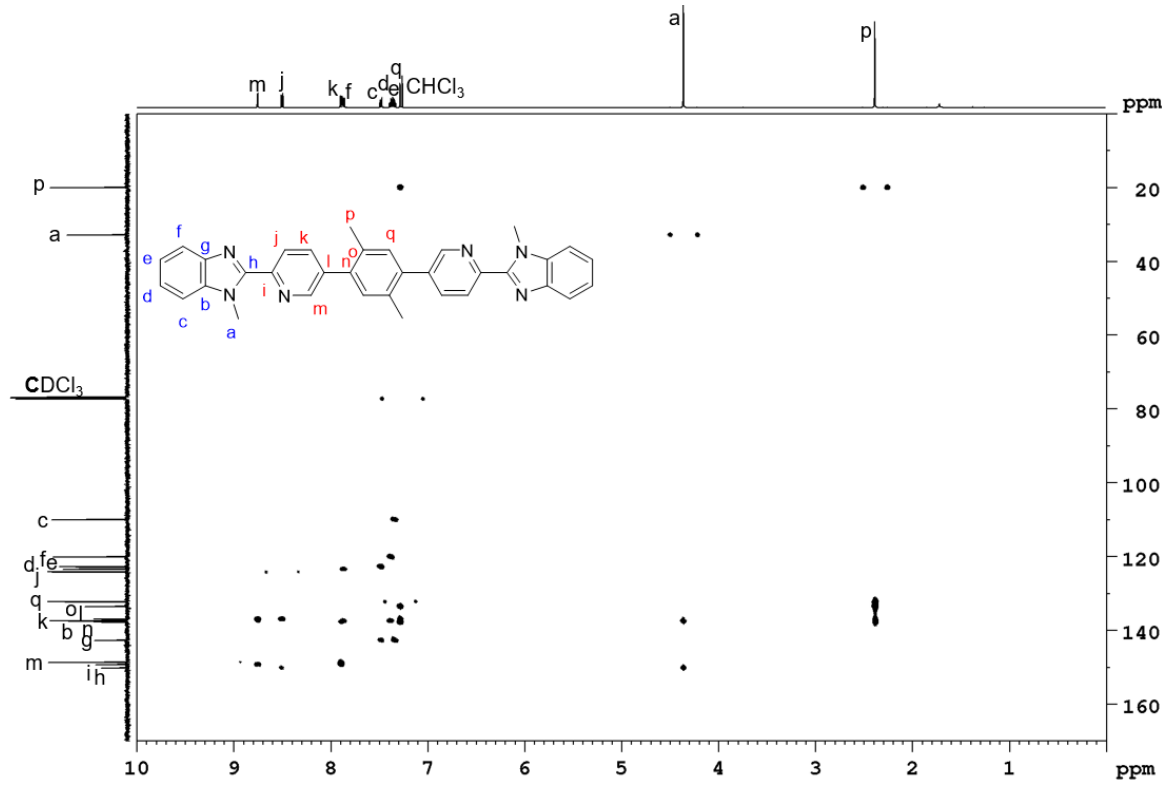

Figure S66. ^{1}H-^{13}C HMBC NMR spectrum (500 MHz/125 MHz, $CDCl_3$, 298 K) of 1,4-di(6''-(1'-methyl-1*H*-benzo[*d*]imidazol-2'-yl)pyridin-3''-yl)-2,5-dimethylbenzene (**30**).

2.4.5 2,2'-(2,5-Difluoro-1,4-phenylene)di(4'',4'',5'',5''-tetramethyl-1'',3'',2''-dioxaborolane) (**31**)

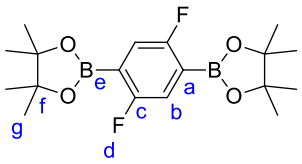

Adapted from Severin and co-workers.[7] 1,4-Dibromo-2,5-difluorobenzene (514 mg, 1.89 mmol), bis(pinacolato)diboron (1.00 g, 3.94 mmol), potassium acetate (925 mg, 9.42 mmol) and Pd(dppf)Cl_2·CH_2Cl_2 (77.2 mg, 5 mol%) were added to a three-neck flask and the flask was evacuated for 5 min. Anhydrous 1,4-dioxane (20 mL) was added and the mixture was stirred at 90 °C for 23 h. The reaction mixture was cooled to room temperature and the solvent was removed *in vacuo*. Purification by flash chromatography (silica gel, 33% dichloromethane/cyclohexane) gave the product as a colourless solid (143 mg, 391 µmol, 21%).

^{1}H NMR (500 MHz, $CDCl_3$, 298 K) δ (ppm): 7.35 (t, ^{3}J = 6.5 Hz, 2H, H_b), 1.35 (s, 24H, H_g).

^{13}C NMR (125 MHz, $CDCl_3$, 298 K) δ (ppm): 162.5 (d, $^{1}J_{CF}$ = 249.2 Hz, C_c), 122.4 (dd, $^{2}J_{CF}$ = 20.5 Hz, $^{3}J_{CF}$ = 13.7 Hz, C_b), 84.3 (C_f), 24.8 (C_g). A signal for C_a was not observed.

^{11}B NMR (160 MHz, $CDCl_3$, 298 K) δ (ppm): 29.5 (B_e).

^{19}F NMR (470 MHz, $CDCl_3$, 298 K) δ (ppm): -114.2 (F_d).

EI-MS *m/z*: 366.19828 (calculated for $C_{18}H_{26}{}^{11}B_2{}^{19}F_2O_4$: 366.19853).

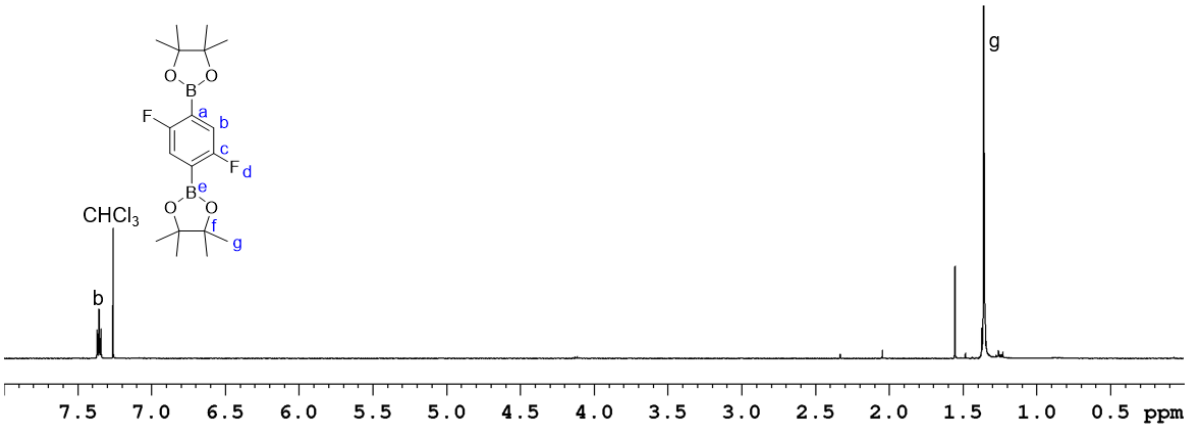

Figure S67. ^{1}H NMR spectrum (500 MHz, $CDCl_3$, 298 K) of 2,2'-(2,5-difluoro-1,4-phenylene)di(4'',4'',5'',5''-tetramethyl-1'',3'',2''-dioxaborolane) (**31**).

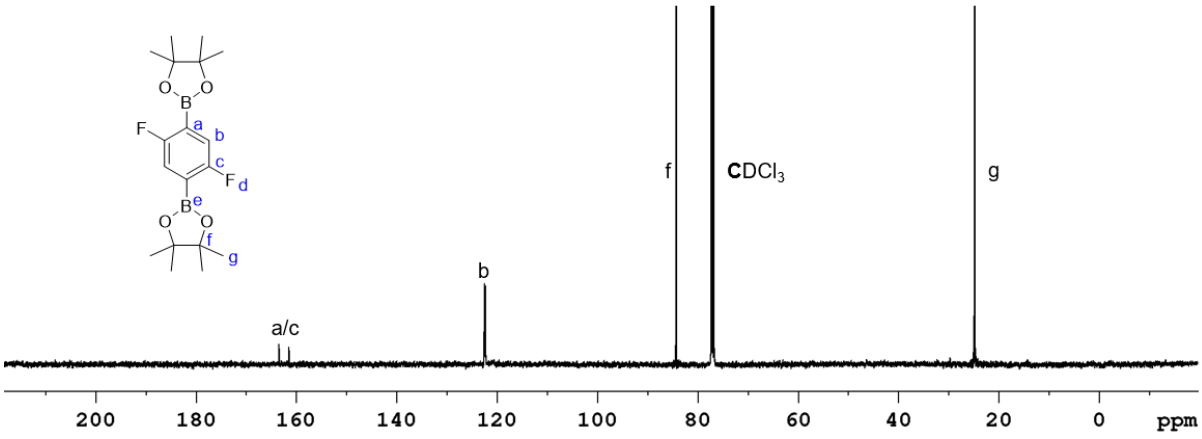

Figure S68. ^{13}C NMR spectrum (125 MHz, $CDCl_3$, 298 K) of 2,2'-(2,5-difluoro-1,4-phenylene)di(4'',4'',5'',5''-tetramethyl-1'',3'',2''-dioxaborolane) (**31**).

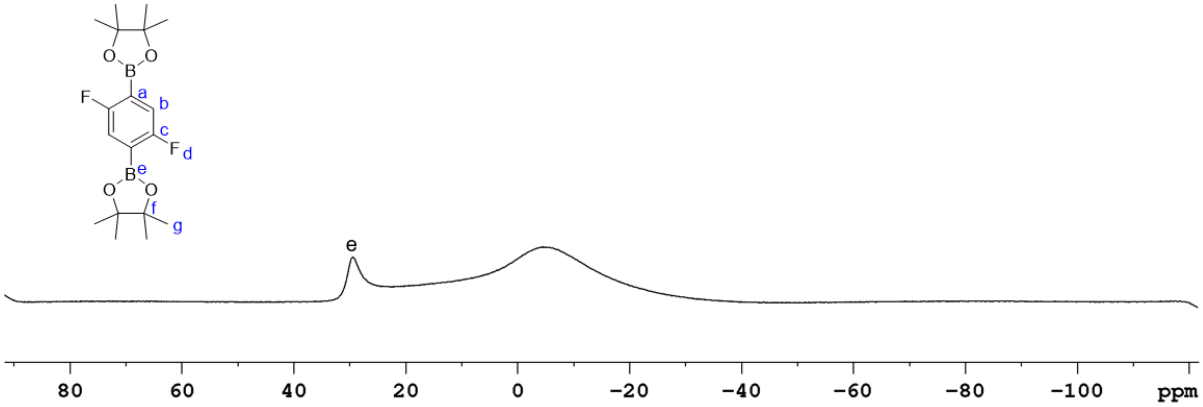

Figure S69. ^{11}B NMR spectrum (160 MHz, $CDCl_3$, 298 K) of 2,2'-(2,5-difluoro-1,4-phenylene)di(4'',4'',5'',5''-tetramethyl-1'',3'',2''-dioxaborolane) (**31**).

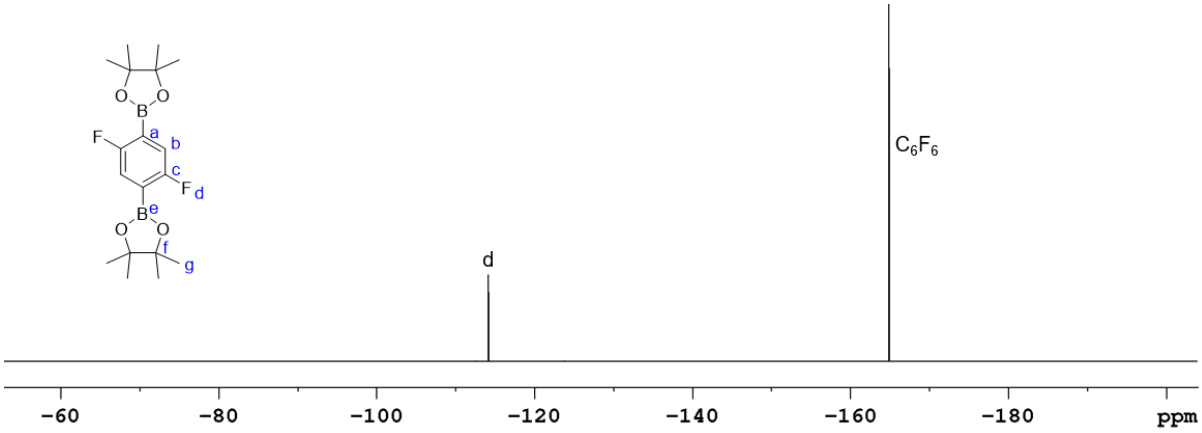

Figure S70. ^{19}F NMR spectrum (470 MHz, $CDCl_3$, 298 K) of 2,2'-(2,5-difluoro-1,4-phenylene)di(4'',4'',5'',5''-tetramethyl-1'',3'',2''-dioxaborolane) (**31**).

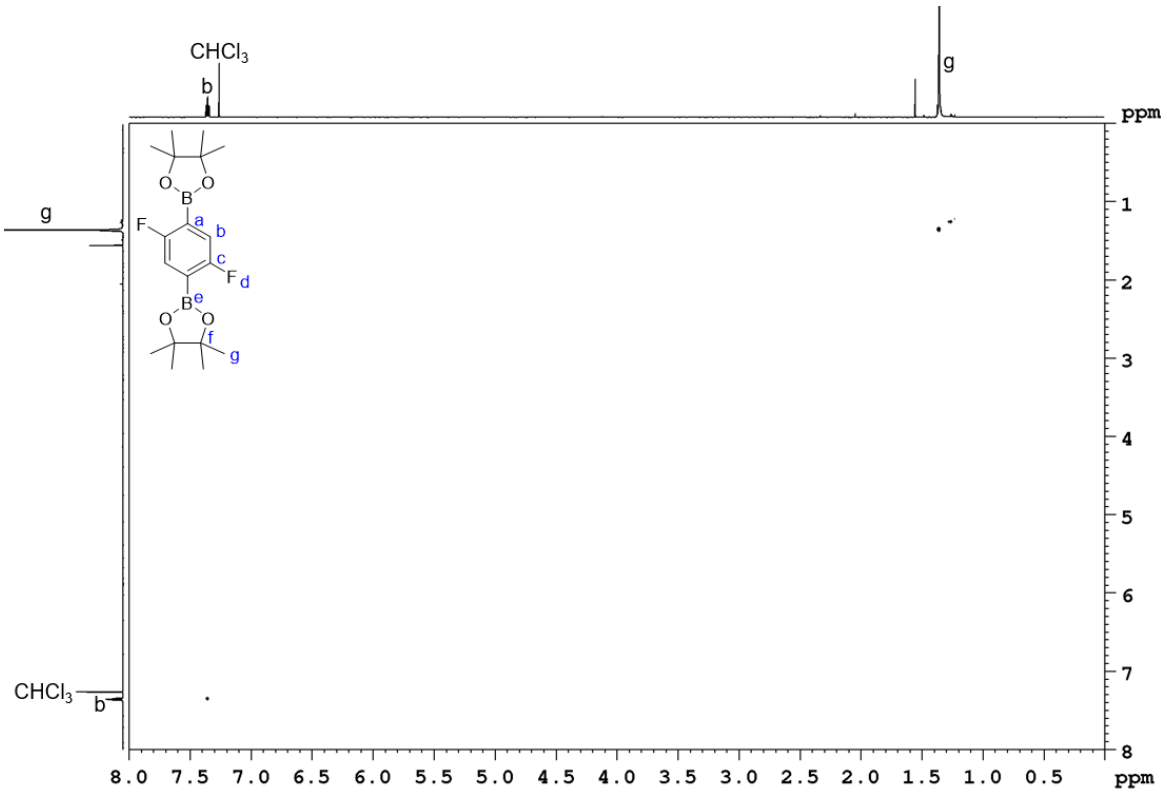

Figure S71. ^{1}H-^{1}H COSY NMR spectrum (500 MHz, $CDCl_3$, 298 K) of 2,2'-(2,5-difluoro-1,4-phenylene)di(4'',4'',5'',5''-tetramethyl-1'',3'',2''-dioxaborolane) (**31**).

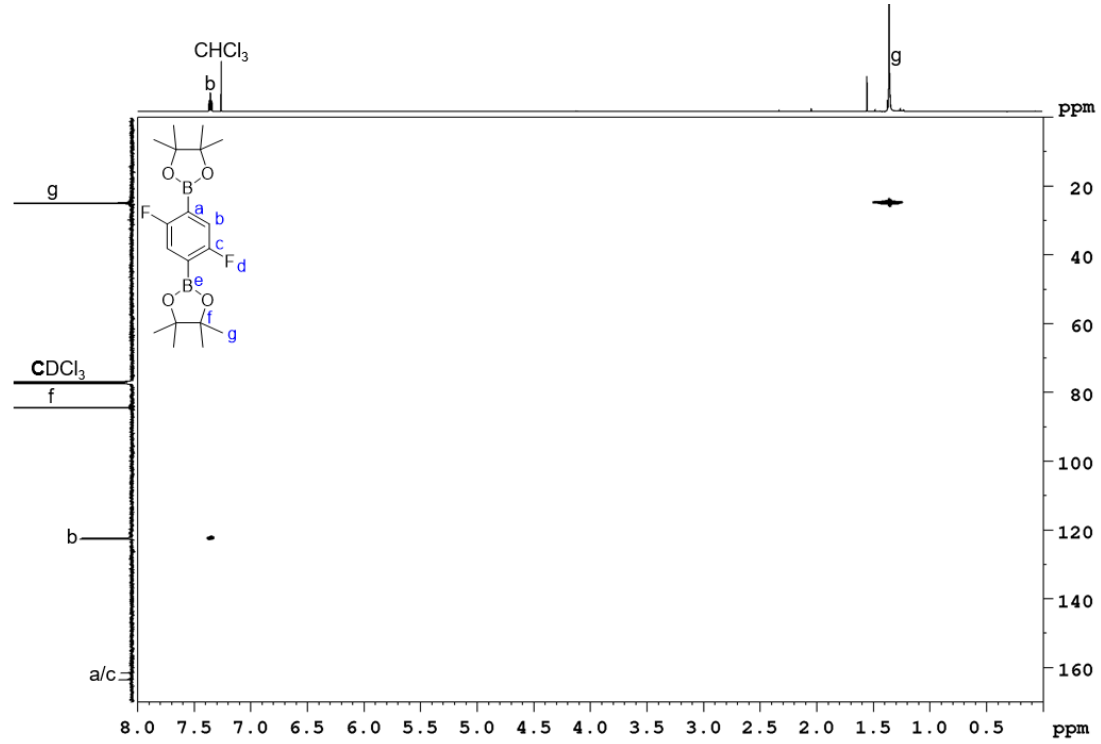

Figure S72. ^{1}H-^{13}C HSQC NMR spectrum (500 MHz/125 MHz, $CDCl_3$, 298 K) of 2,2'-(2,5-difluoro-1,4-phenylene)di(4'',4'',5'',5''-tetramethyl-1'',3'',2''-dioxaborolane) (**31**).

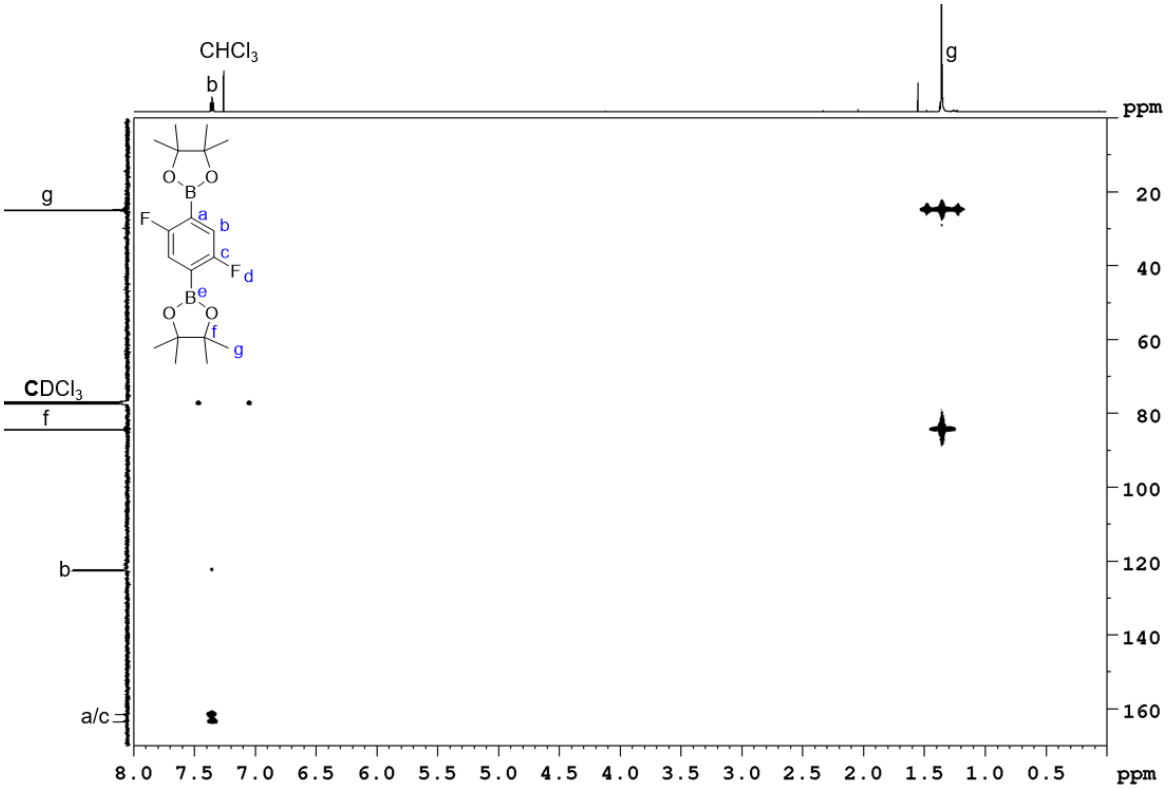

Figure S73. ^{1}H-^{13}C HMBC NMR spectrum (500 MHz/125 MHz, $CDCl_3$, 298 K) of 2,2'-(2,5-difluoro-1,4-phenylene)di(4'',4'',5'',5''-tetramethyl-1'',3'',2''-dioxaborolane) (**31**).

2.4.6 1,4-Di(6''-(1'-methyl-1*H*-benzo[*d*]imidazol-2'-yl)pyridin-3''-yl)-2,5-difluorobenzene (**32**)

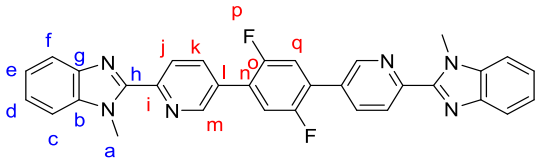

Adapted from Lusby and co-workers.[8] 2-(5'-Bromopyridin-2'-yl)-1-benzyl-1*H*-benzo[*d*]imidazole (**16**) (80.7 mg, 280 µmol), 2,2'-(2,5-difluoro-1,4-phenylene)di(4'',4'',5'',5''-tetramethyl-1'',3'',2''-dioxaborolane) (**31**) (51.2 mg, 140 µmol), potassium carbonate (96.7 mg, 700 µmol, milled) and $Pd(PPh_3)_4$ (16.2 mg, 10 mol%) were added to a three-neck flask and the flask was evacuated for 5 min. Anhydrous ethanol (1 mL), water (1 mL, degassed) and anhydrous tetrahydrofuran (3 mL) were added and the reaction mixture was stirred at 80 °C for 23 h. The solution was cooled to room temperature and the precipitate was collected by filtration and washed with cold tetrahydrofuran (200 mL, cooled to -18 °C) to obtain the product as a brown solid (38.7 mg, 73.2 µmol, 52%).

^{1}H NMR (500 MHz, TFA-d_1, 298 K) δ (ppm): 9.46 (d, ^{4}J =2.1 Hz, 2H, H_m), 8.88 (dd, ^{3}J = 8.2 Hz, ^{4}J = 2.1 Hz, 2H, H_k), 8.61 (d, ^{3}J = 8.2 Hz, 2H, H_j), 7.97-7.83 (m, 4H, $H_{c,d,e,f}$), 7.72 (t, ^{3}J = 8.2 Hz, 2H, H_q), 4.37 (s, 6H, H_a).

^{13}C NMR (125 MHz, TFA-d_1, 298 K) δ (ppm): 157.7 (d, $^{1}J_{CF}$ = 251.6 Hz, C_o), 150.3 (C_m), 145.3 (C_k), 144.5 (C_h), 139.1 (C_i), 138.6 (C_l), 135.6 (C_b), 132.4 (C_g), 131.8 ($C_{d/e}$), 131.3 ($C_{d/e}$), 130.9 (C_j), 127.7 (C_n), 120.5 (dd, $^{2}J_{CF}$ = 19.4 Hz,$^{3}J_{CF}$ = 10.2 Hz, C_q), 116.8 ($C_{c/f}$), 114.7 ($C_{c/f}$), 34.8 (C_a).

^{19}F NMR (470 MHz, TFA-d_1, 298 K) δ (ppm): -120.7 (F_p).

EI-MS *m/z*: 528.18648 (calculated for $C_{32}H_{22}{}^{19}F_2N_6$: 528.18740).

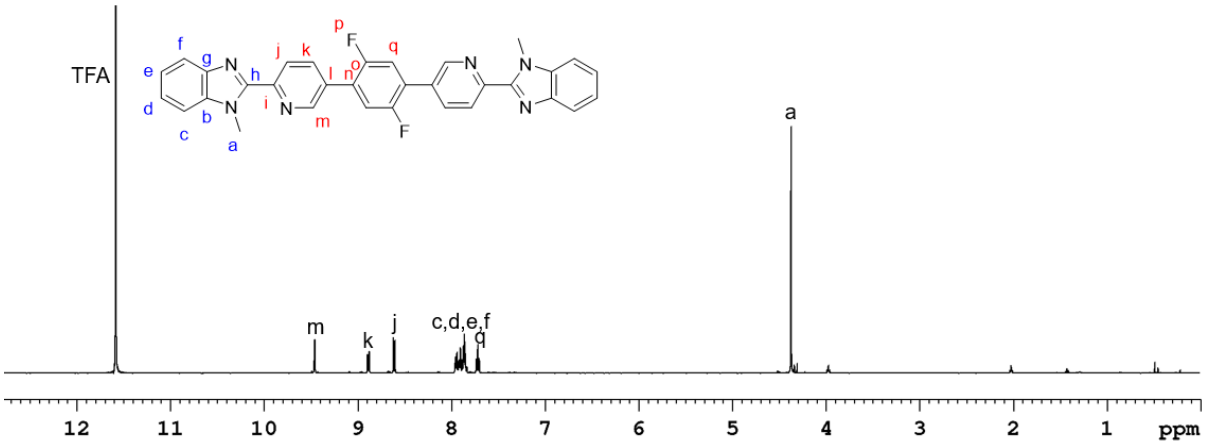

Figure S74. ^{1}H NMR spectrum (500 MHz, $CDCl_3$, 298 K) of 1,4-di(6''-(1'-methyl-1*H*-benzo[*d*]imidazol-2'-yl)pyridin-3''-yl)-2,5-difluorobenzene (**32**).

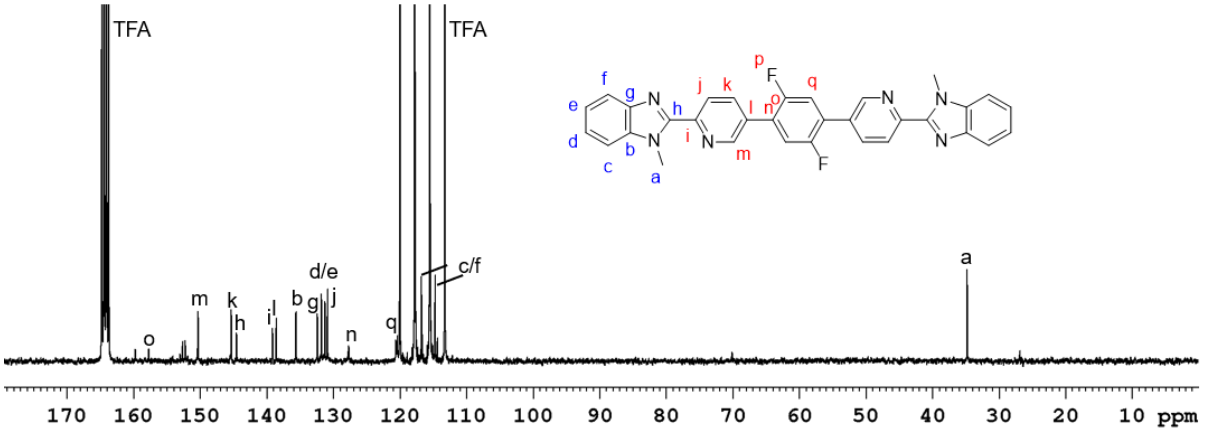

Figure S75. ^{13}C NMR spectrum (125 MHz, $CDCl_3$, 298 K) of 1,4-di(6''-(1'-methyl-1*H*-benzo[*d*]imidazol-2'-yl)pyridin-3''-yl)-2,5-difluorobenzene (**32**).

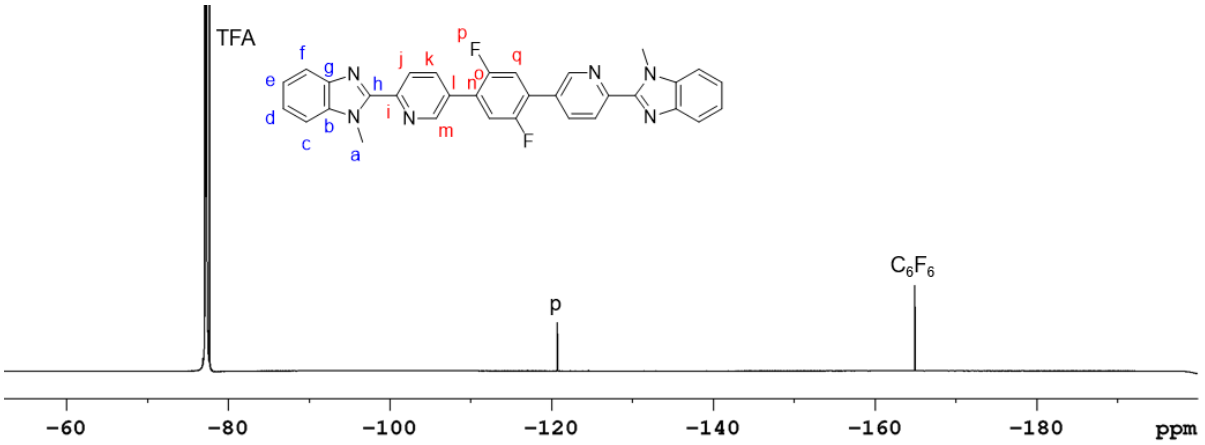

Figure S76. ^{19}F NMR spectrum (471 MHz, $CDCl_3$, 298 K) of 1,4-di(6''-(1'-methyl-1*H*-benzo[*d*]imidazol-2'-yl)pyridin-3''-yl)-2,5-difluorobenzene (**32**).

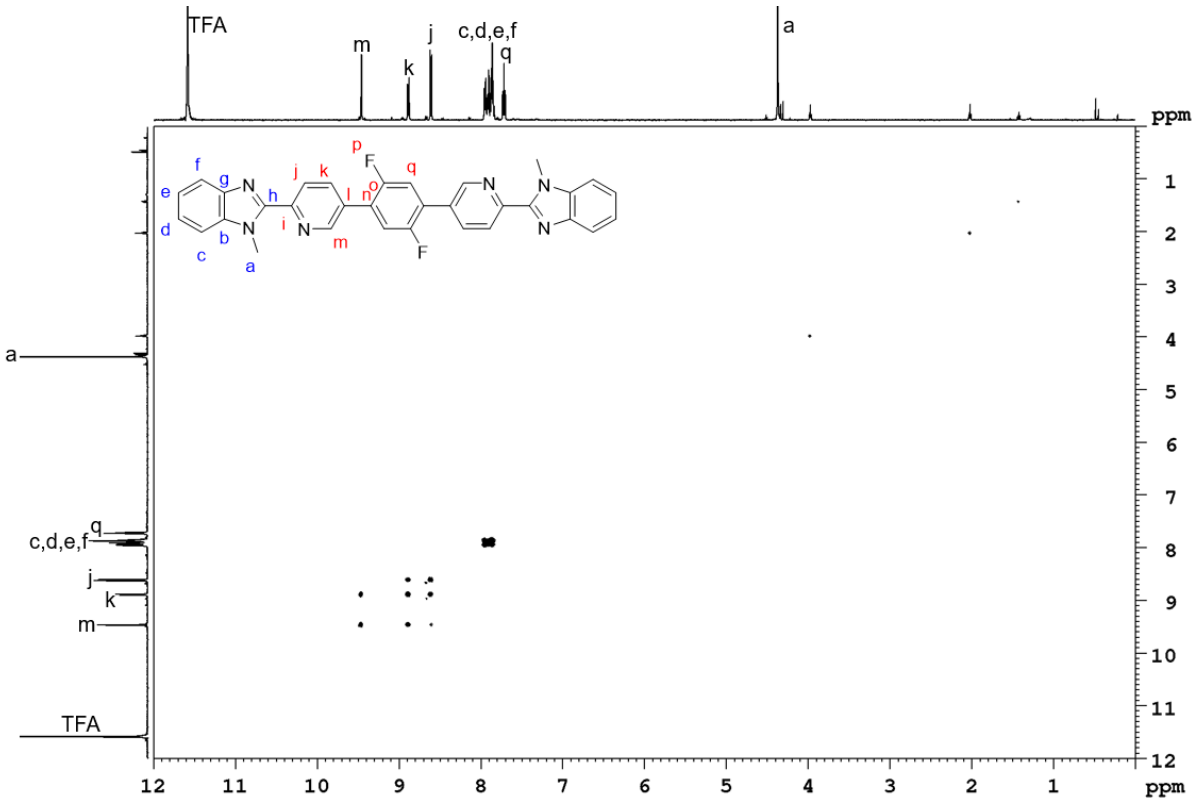

Figure S77. ^{1}H-^{1}H COSY NMR spectrum (500 MHz, $CDCl_3$, 298 K) of 1,4-di(6''-(1'-methyl-1*H*-benzo[*d*]imidazol-2'-yl)pyridin-3''-yl)-2,5-difluorobenzene (**32**).

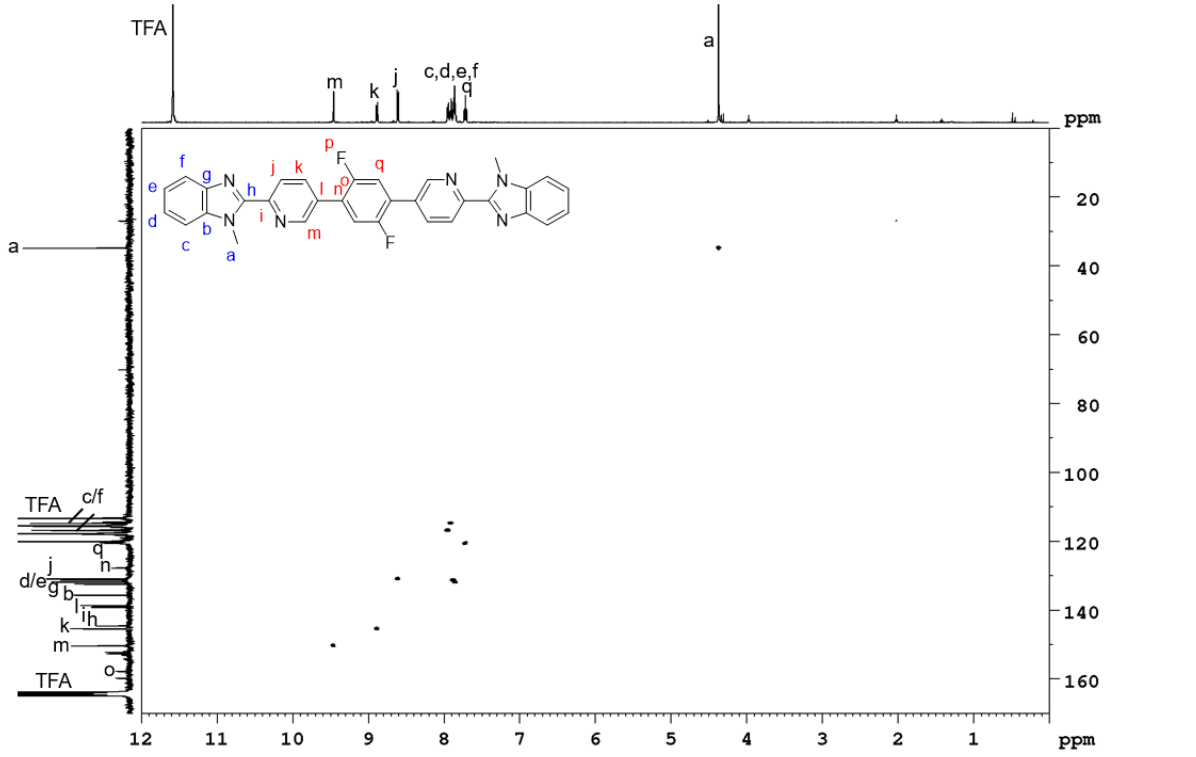

Figure S78. ^{1}H-^{13}C HSQC NMR spectrum (500 MHz/125 MHz, $CDCl_3$, 298 K) of 1,4-di(6''-(1'-methyl-1*H*-benzo[*d*]imidazol-2'-yl)pyridin-3''-yl)-2,5-difluorobenzene (**32**).

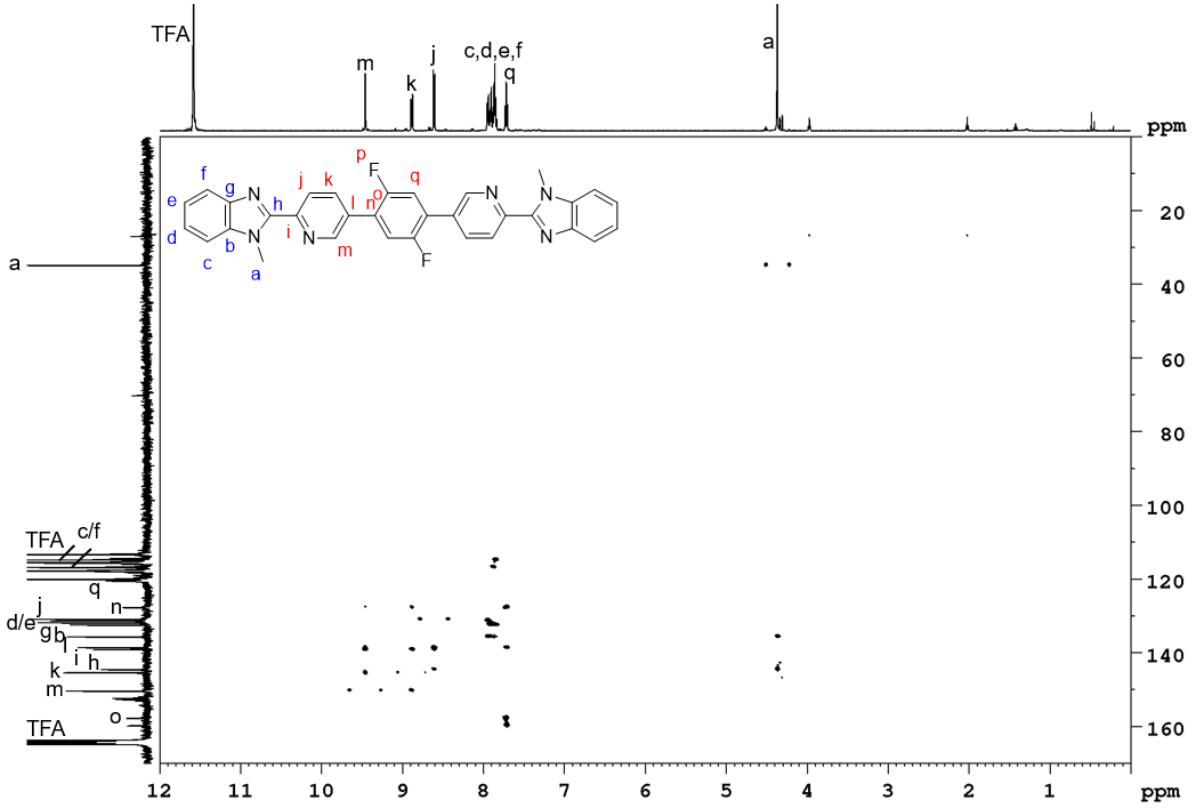

Figure S79. ^{1}H-^{13}C HMBC NMR spectrum (500 MHz/125 MHz, $CDCl_3$, 298 K) of 1,4-di(6''-(1'-methyl-1*H*-benzo[*d*]imidazol-2'-yl)pyridin-3''-yl)-2,5-difluorobenzene (**32**).

2.4.7 1,4-Bis(4''-methyl-6''-(1'-methyl-1*H*-benzo[*d*]imidazol-2'-yl)pyridin-3''-yl)benzene (**33**)

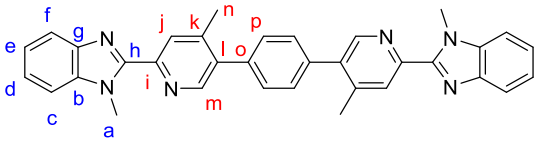

Adapted from Lusby and co-workers.[8] 2-(5'-Bromo-4'-methylpyridin-2'-yl)-1-methyl-1*H*-benzo[*d*]imidazole (**21**) (32.2 mg, 107 µmol), 1,4-phenylenediboronic acid (8.84 mg, 53.4 µmol), potassium carbonate (36.9 mg, 267 µmol, milled) and $Pd(PPh_3)_4$ (5.34 mg, 5 mol%) were added to a three-neck flask and the flask was evacuated for 30 min. Anhydrous ethanol (370 µL), water (370 µL, degassed) and anhydrous tetrahydrofuran (860 µL) were added and the reaction mixture was stirred at 80 °C for 21 h. The solution was cooled to room temperature and the precipitate was collected by filtration and washed with cold (0 °C) tetrahydrofuran (20 mL). The product was obtained as a colourless solid (16.8 mg, 32.3 µmol, 30%).

^{1}H NMR (600 MHz, $CDCl_3$, 298 K) δ (ppm): 8.62 (s, 2H, H_m), 8.38 (s, 2H, H_j), 7.87 (unres. dd, 2H, H_f), 7.53 (s, 2H, H_p), 7.48 (unres. dd, 2H, H_c), 7.37 (td, ^{3}J = 7.2 Hz, ^{4}J = 1.2 Hz, 2H, H_d), 7.34 (td, ^{3}J = 7.8 Hz, ^{4}J = 1.4 Hz, 2H, H_e), 4.35 (s, 6H, H_a), 2.49 (s, 6H, H_n).

^{13}C NMR (151 MHz, $CDCl_3$, 298 K) δ (ppm): 150.3 (C_h), 149.4 (C_i), 148.9 (C_m), 145.6 (C_k), 142.6 (C_g), 137.4 (C_b), 137.3 (C_o), 137.1 (C_l), 129.5 (C_p), 126.1 (C_j), 123.3 (C_d), 122.7 (C_e), 120.0 (C_f), 110.0 (C_c), 32.8 (C_a), 20.0 (C_n).

EI-MS *m/z*: 520.23705 (calculated for $C_{34}H_{28}N_6$: 520.23754).

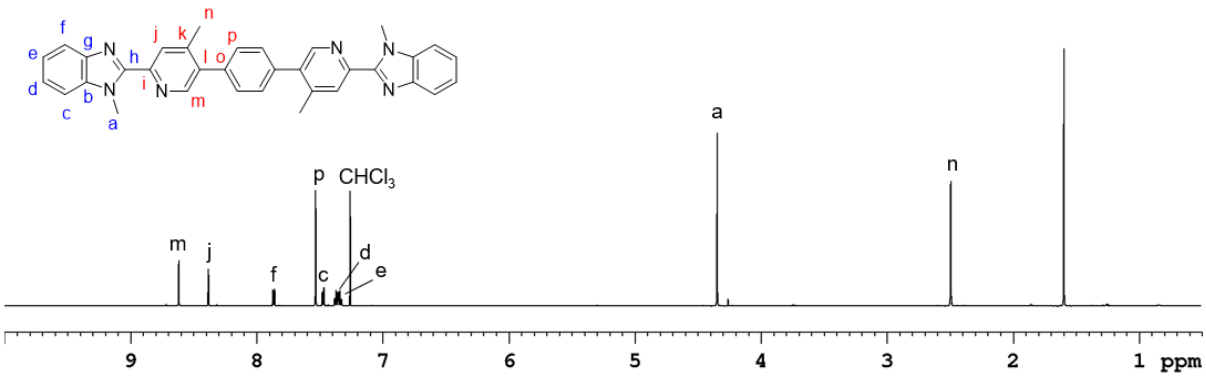

Figure S80. ^{1}H NMR spectrum (600 MHz, $CDCl_3$, 298 K) of 1,4-bis(4''-methyl-6''-(1'-methyl-1*H*-benzo[*d*]imidazol-2'-yl)pyridin-3''-yl)benzene (**33**).

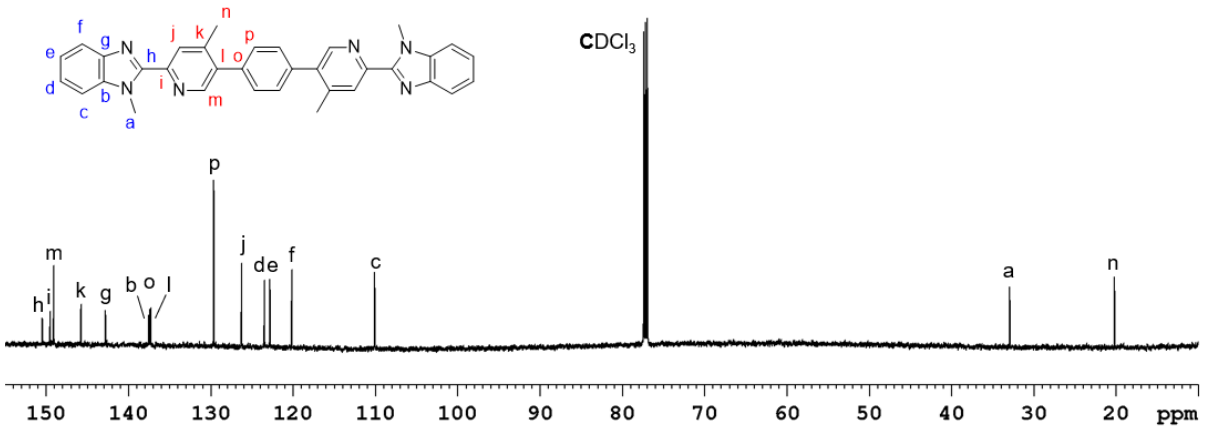

Figure S81. ^{13}C NMR spectrum (151 MHz, $CDCl_3$, 298 K) of 1,4-bis(4''-methyl-6''-(1'-methyl-1*H*-benzo[*d*]imidazol-2'-yl)pyridin-3''-yl)benzene (**33**).

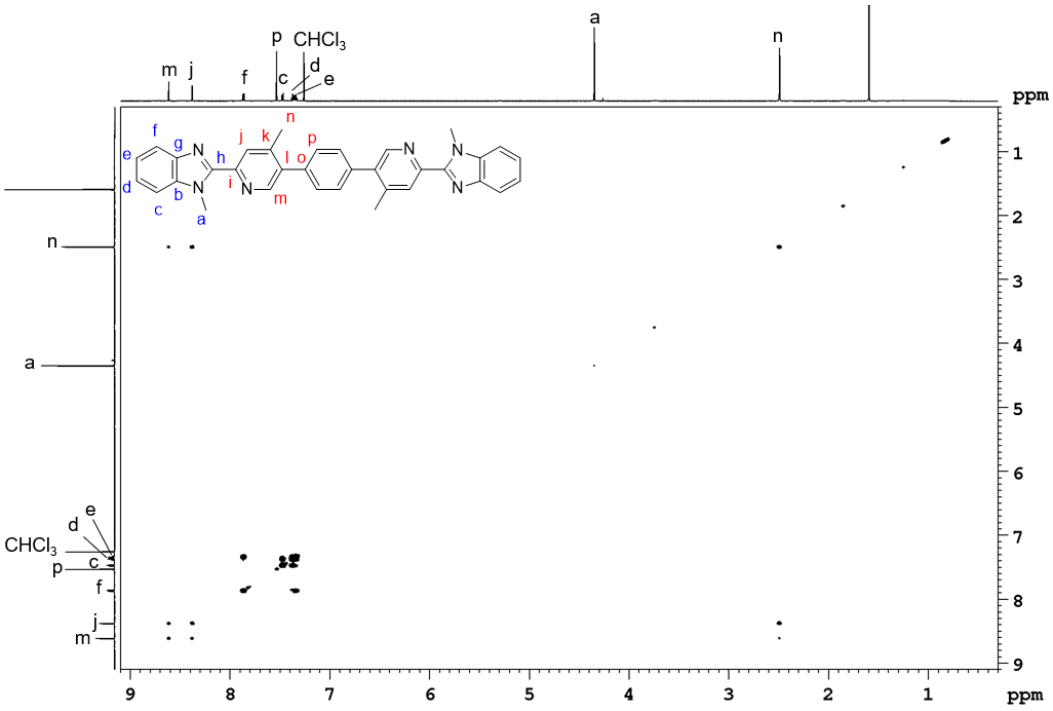

Figure S82. ^{1}H-^{1}H COSY NMR spectrum (600 MHz, $CDCl_3$, 298 K) of 1,4-bis(4''-methyl-6''-(1'-methyl-1*H*-benzo[*d*]imidazol-2'-yl)pyridin-3''-yl)benzene (**33**).

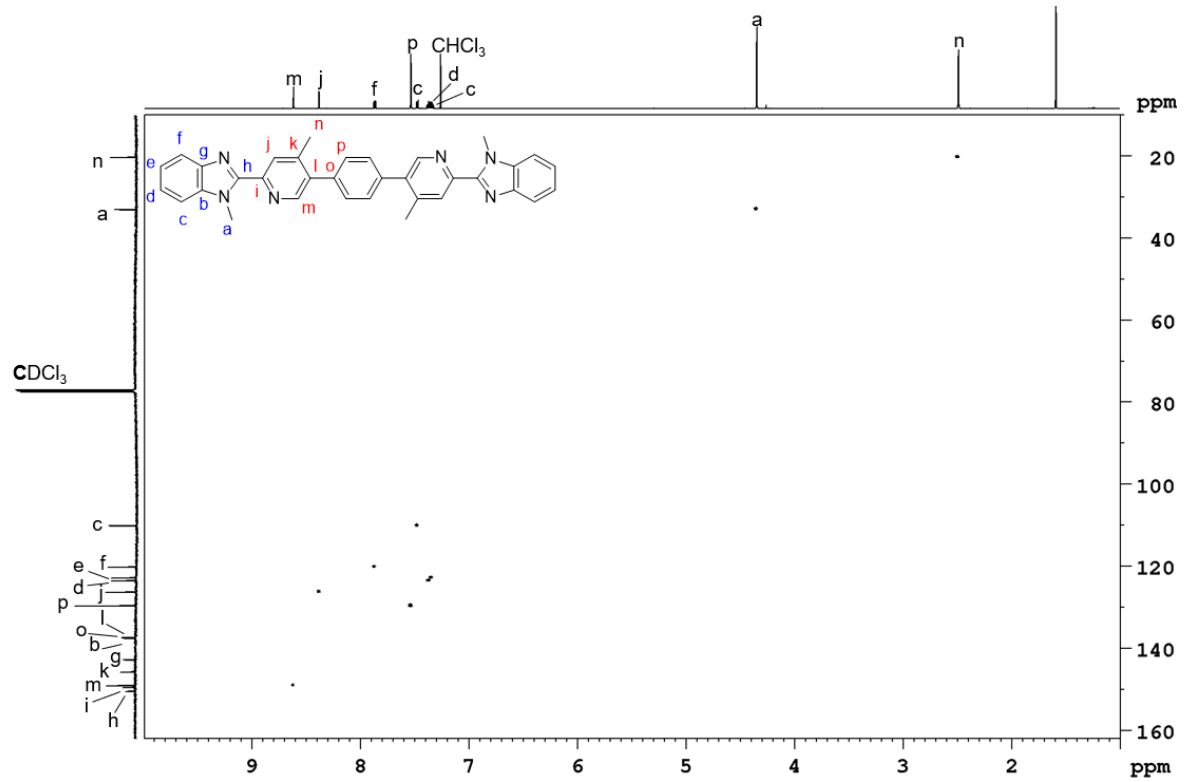

Figure S83. ^{1}H-^{13}C HSQC NMR spectrum (600 MHz/151 MHz, $CDCl_3$, 298 K) of 1,4-bis(4''-methyl-6''-(1'-methyl-1*H*-benzo[*d*]imidazol-2'-yl)pyridin-3''-yl)benzene (**33**).

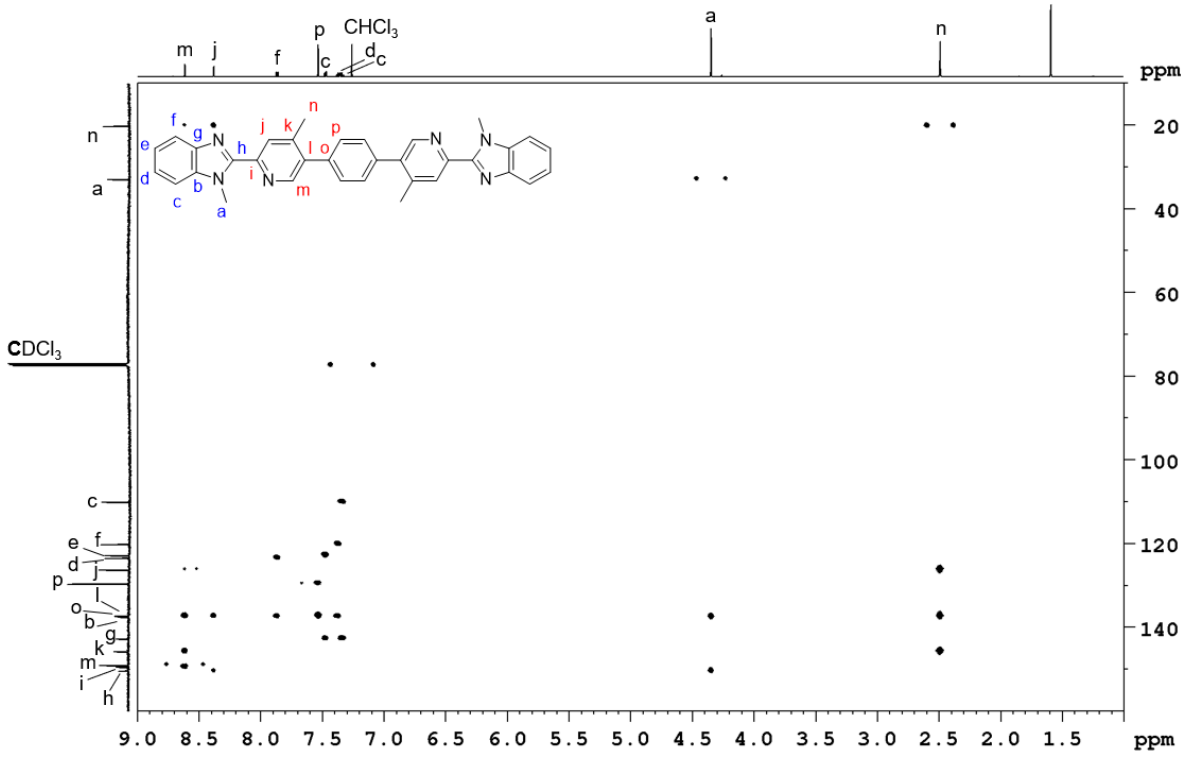

Figure S84. ^{1}H-^{13}C HMBC NMR spectrum (600 MHz/151 MHz, $CDCl_3$, 298 K) of 1,4-bis(4''-methyl-6''-(1'-methyl-1*H*-benzo[*d*]imidazol-2'-yl)pyridin-3''-yl)benzene (**33**).

3 Zn_4L_6 Metal-Organic Cages

Metal-organic cages based on Zn^{II} were self-assembled using six equivalents of the appropriate ligand and four equivalents zinc(II) triflate. The cages were prepared *in situ* and characterisation using NMR spectroscopy and ESI-MS were consistent with the self-assembly of Zn_4L_6 cages. However, a discrete cage did not form with ligand **14** (Section 3.1). Zn_2L_3 structures were also self-assembled with ligands **22**, **27** and **32** (Section 3.7, 3.8 and 3.10).

3.1 Attempted Self-Assembly of Cage 34

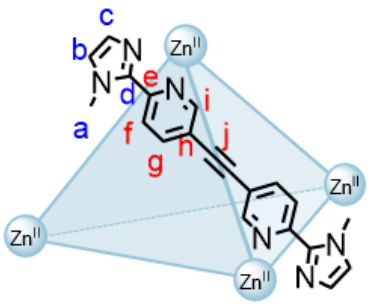

Zinc(II) triflate (1.95 mg, 5.36 µmol) and 1,2-bis(6''-(1'-methyl-1*H*-imidazol-2'-yl)pyridin-3''-yl)ethyne (**14**) (2.74 mg, 8.05 µmol) were dissolved in CD_3CN (500 µL) in an attempt to prepare cage **34** *in situ*. However, a discrete cage did not form, even after heating for 117 h at 50 °C, and therefore, assignment of the ^{1}H NMR spectrum was not possible (Figure S85). In addition, signals consistent with the expected cage were not observed in the ESI mass spectrum.

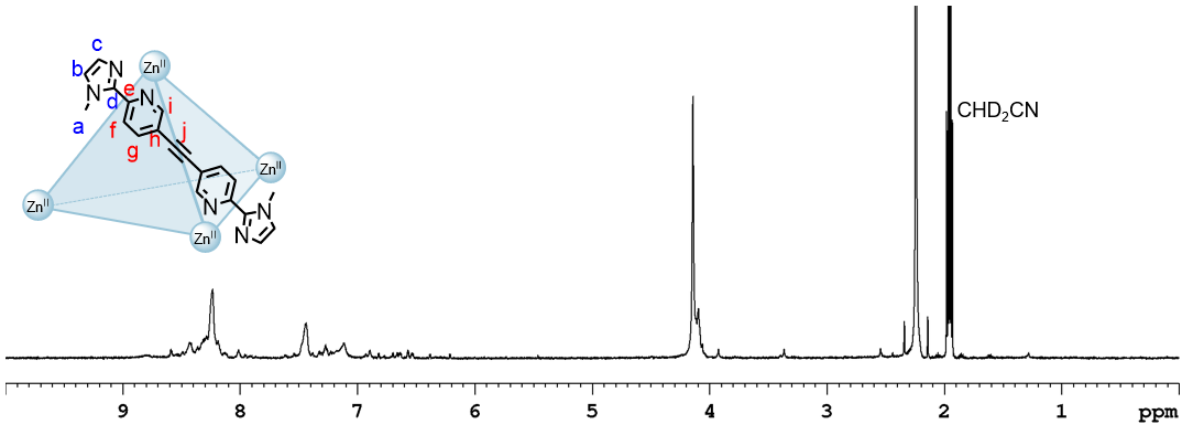

Figure S85. ^{1}H NMR spectrum (200 MHz, CD_3CN, 298 K) of the self-assembly for cage **34**.

3.2 Cage 35

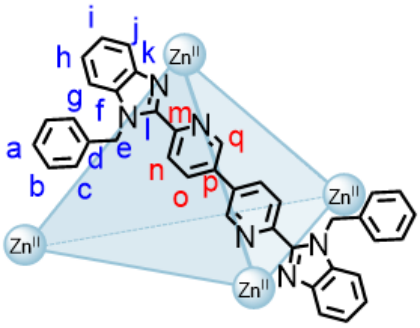

Zinc(II) triflate (2.02 mg, 5.56 µmol) and 6',6''-di(1-benzyl-1*H*-benzo[*d*]imidazol-2-yl)-3',3''-bipyridine (**26**) (4.70 mg, 8.25 µmol) were dissolved in CD_3CN (500 µL) and heated for 24 h at 50 °C to prepare cage **35** *in situ*.

^{1}H NMR (500 MHz, CD_3CN, 298 K) δ (ppm): 8.16 (dd, ^4J = 2.2 Hz, ^5J = 0.7 Hz, 12H, H_q), 7.78 (d, ^3J = 8.4 Hz, 12H, H_n), 7.60 (dd, ^3J = 8.4 Hz, ^4J = 2.2 Hz, 12H, H_o), 7.58 (dt, ^3J = 8.4 Hz, ^4J = 1.0 Hz, 12H, H_g), 7.42 (ddd, ^3J = 8.4 Hz, ^3J = 7.3 Hz, ^4J = 1.0 Hz, 12H, H_h), 7.37-7.32 (m, 24H, H_b), 7.31-7.27 (m, 12H, H_a), 7.22 (ddd, ^3J = 8.4 Hz, ^3J = 7.3 Hz, ^4J = 1.0 Hz, 12H, H_i), 7.14-7.11 (m, 24H, H_c), 6.95 (dt, ^3J = 8.4 Hz, ^4J = 1.0 Hz, 12H, H_j), 6.06 (d, ^2J = 18.0 Hz, 12H, H_e), 5.81 (d, ^2J = 18.0 Hz, 12H, H_e).

^{13}C NMR (125 MHz, CD_3CN, 298 K) δ (ppm): 149.7 (C_q), 149.5 (C_l), 143.0 (C_m), 141.9 (C_o), 138.8 (C_k), 138.5 (C_f), 136.7 (C_p), 135.6 (C_d), 130.3 (C_b), 129.3 (C_a), 127.4 (C_h), 127.1 (C_i), 126.8 (C_c), 124.4 (C_n), 118.1 (C_j), 113.7 (C_g), 49.7 (C_e).

^{19}F NMR (471 MHz, CD_3CN, 298 K, C_6F_6) δ (ppm): -79.3 (OTf^-).

HRMS (ESI): *m/z* = 2283.4282 [**35** + 6OTf]$^{2+}$, 1472.6331 [**35** + 5OTf]$^{3+}$, 1067.2363 [**35** + 4OTf]$^{4+}$, 823.7981 [**35** + 3OTf]$^{5+}$, 661.5064 [**35** + 2OTf]$^{6+}$.

While the signal at *m/z* 661.5064 is consistent with the 6+ charge for the cage, the theoretical isotopic pattern does not match, possibly due to fragmentation in the gas phase or overlap with other signals.

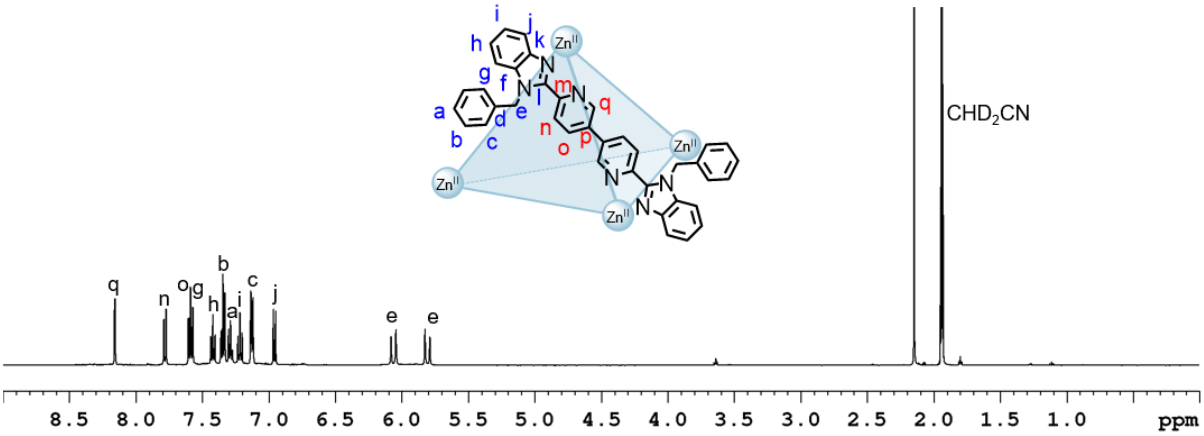

Figure S86. ^{1}H NMR spectrum (500 MHz, CD_3CN, 298 K) of cage **35**.

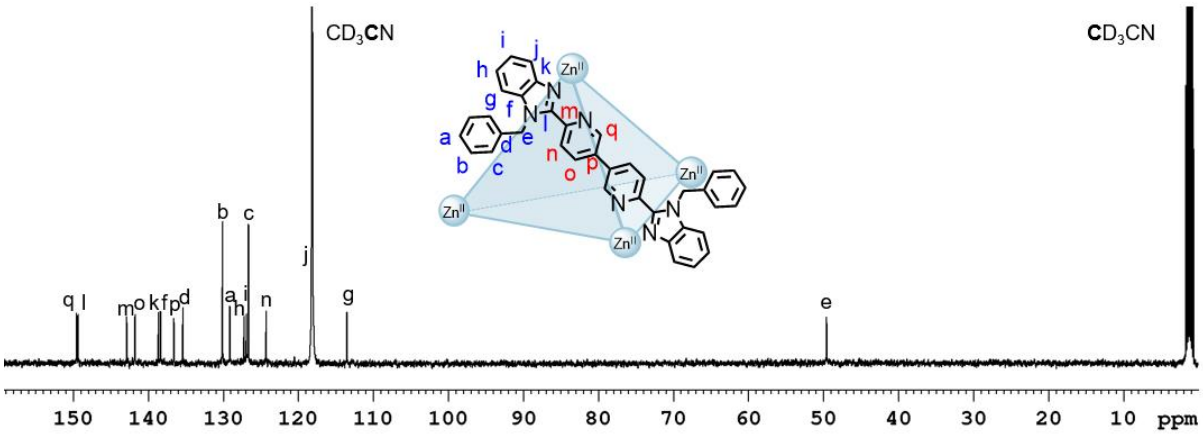

Figure S87. ^{13}C NMR spectrum (125 MHz, CD_3CN, 298 K) of cage **35**.

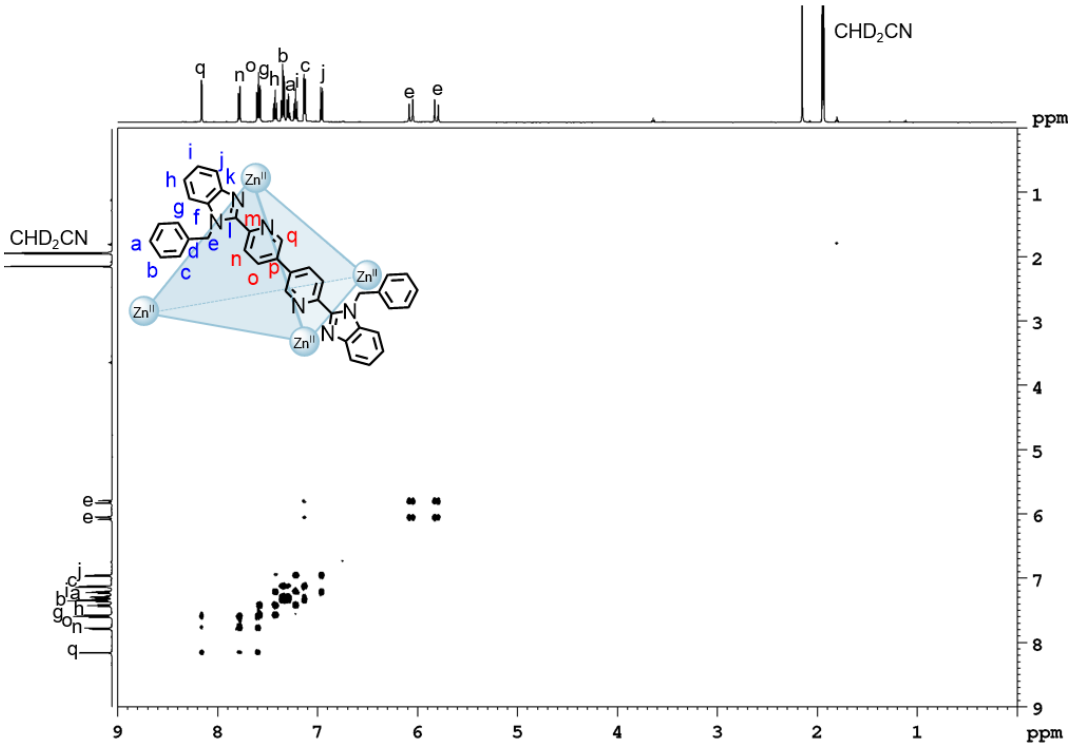

Figure S88. ^{1}H-^{1}H COSY NMR spectrum (500 MHz, CD_3CN, 298 K) of cage **35**.

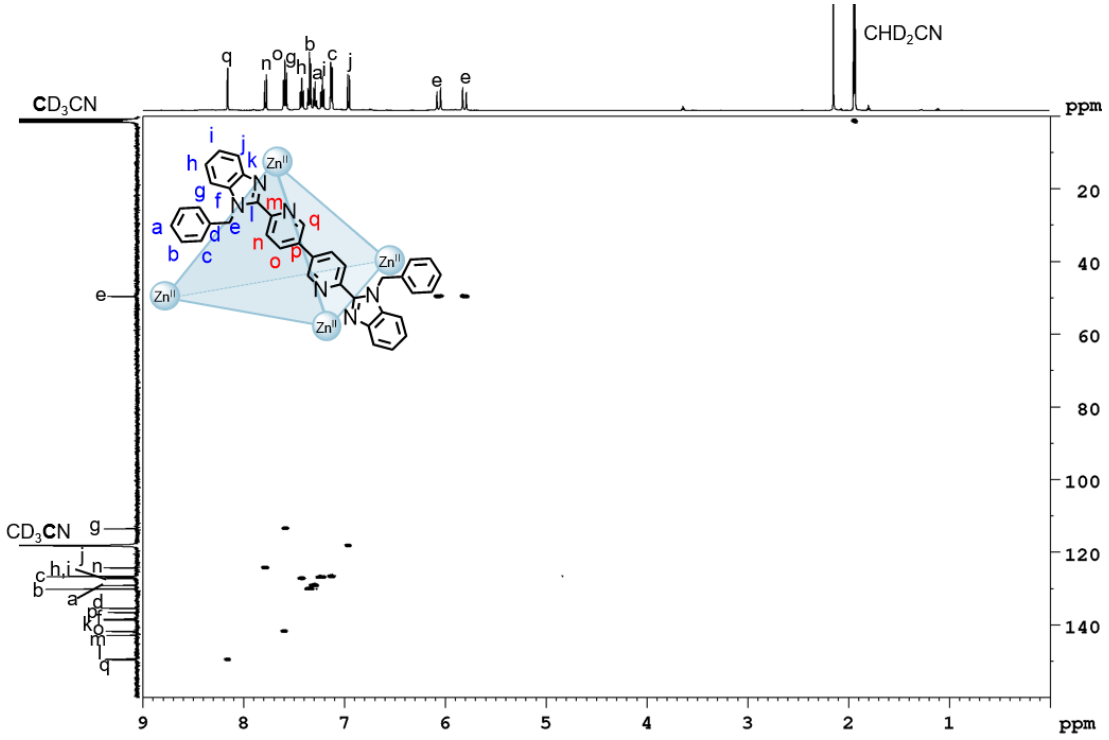

Figure S89. ^{1}H-^{13}C HSQC NMR spectrum (500 MHz/125 MHz, CD_3CN, 298 K) of cage **35**.

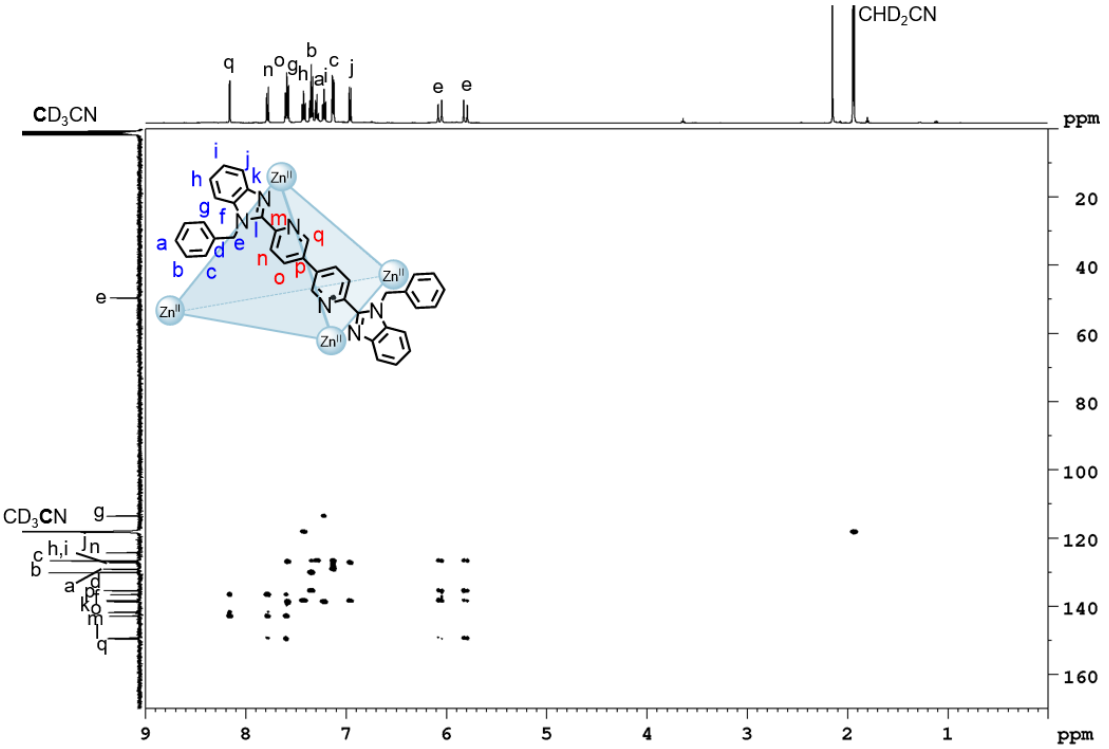

Figure S90. ^{1}H-^{13}C HMBC NMR spectrum (500 MHz/125 MHz, CD_3CN, 298 K) of cage **35**.

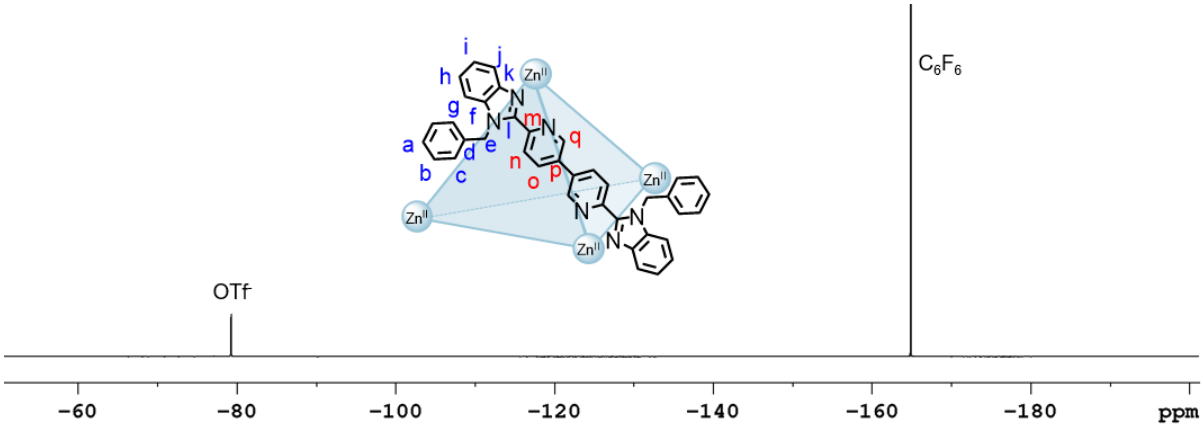

Figure S91. ^{19}F NMR spectrum (471 MHz, CD_3CN, 298 K, C_6F_6) of cage **35**.

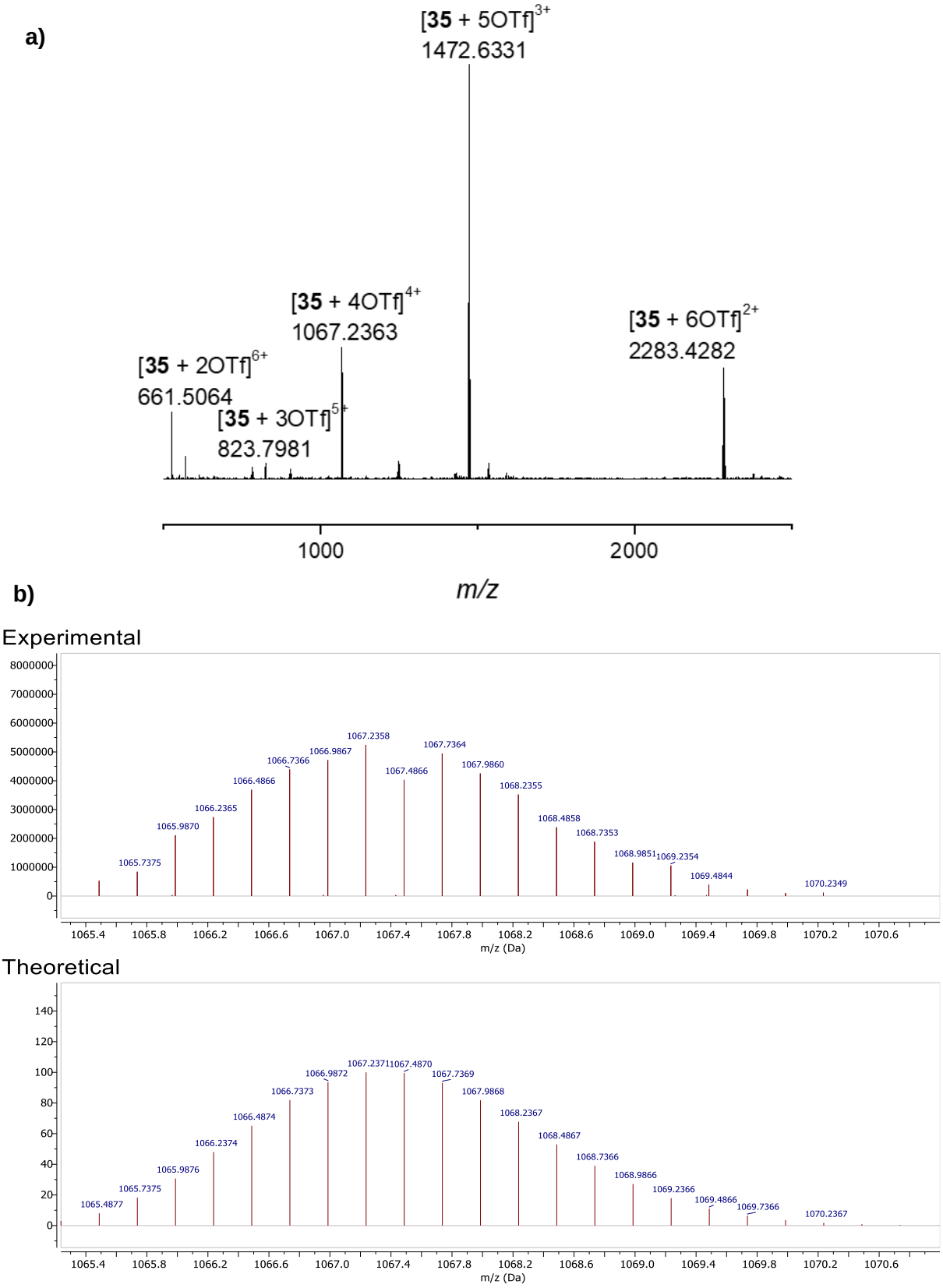

Figure S92. a) High resolution ESI mass spectrum of cage **35** and b) isotopic patterns of cage **35**: experimental (top) and theoretical (bottom).

3.3 Cage 36

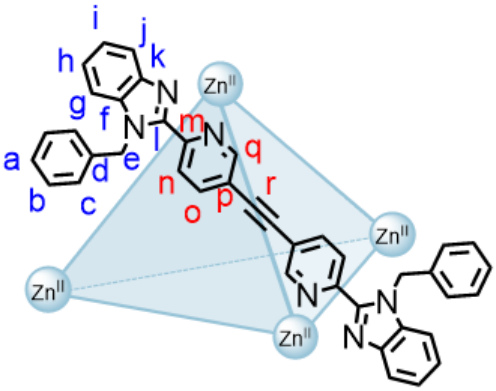

Zinc(II) triflate (1.96 mg, 5.39 µmol) and 1,2-di(6''-(1'-benzyl-1*H*-benzo[*d*]imidazole-2'-yl)pyridin-3''-yl)ethyne (**19**) (4.79 mg, 8.08 µmol) were dissolved in CD_3CN (500 µL) to prepare cage **36** *in situ*.

^{1}H NMR (600 MHz, CD_3CN, 298 K) δ (ppm): 8.02 (dd, ^3J = 8.5 Hz, ^5J = 0.7 Hz, 12H, H_n), 7.95 (dd, ^3J = 8.5 Hz, ^4J = 2.0 Hz, 12H, H_o), 7.84 (dd, ^4J = 2.0 Hz, ^5J = 0.7 Hz, 12H, H_q), 7.69 (unres. dt, 12H, H_g), 7.50 (ddd, ^3J = 8.5 Hz, ^3J = 7.4 Hz, ^4J = 0.8 Hz, 12H, H_h), 7.31 (t, ^3J = 7.7 Hz, 24H, H_b), 7.25 (ddd, ^3J = 8.3 Hz, ^3J = 7.4 Hz, ^4J = 0.8 Hz, 12H, H_i), 7.20 (t, ^3J = 7.4 Hz, 12H, H_a), 7.06 (d, ^3J = 7.6 Hz, 24H, H_c), 6.99 (dt, ^3J = 8.3 Hz, ^4J = 0.8 Hz, 12H, H_j), 6.06-5.98 (m, 24H, H_e).

^{13}C NMR (151 MHz, CD_3CN, 298 K) δ (ppm): 152.3 (C_q), 148.8 (C_l), 145.0 (C_o), 142.7 (C_m), 138.7 (C_k), 138.6 (C_f), 135.4 (C_d), 130.3 (C_b), 129.3 (C_a), 127.8 (C_h), 127.4 (C_i), 126.8 (C_c), 124.7 (C_n), 122.8 (C_p), 118.3 (C_j), 113.7 (C_g), 91.4 (C_r), 50.1 (C_e).

^{19}F NMR (471 MHz, CD_3CN, 298 K, C_6F_6) δ (ppm): -79.5 (OTf^-).

HRMS (ESI): *m/z* = 2355.4280 [**36** + 6OTf]$^{2+}$, 1520.9655 [**36** + 5OTf]$^{3+}$, 1103.4861 [**36** + 4OTf]$^{4+}$, 852.7982 [**36** + 3OTf]$^{5+}$, 686.1721 [**36** + 2OTf]$^{6+}$.

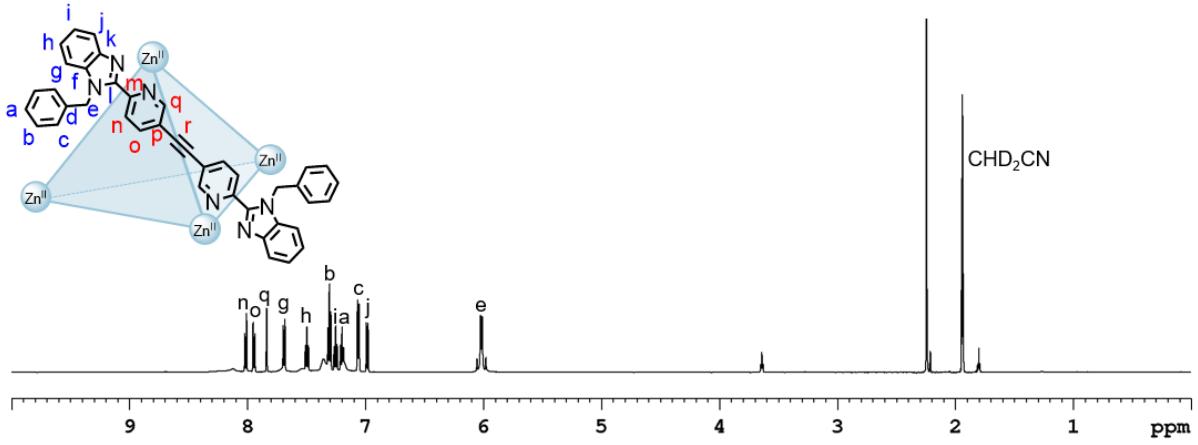

Figure S93. ^{1}H NMR spectrum (600 MHz, CD_3CN, 298 K) of cage **36**.

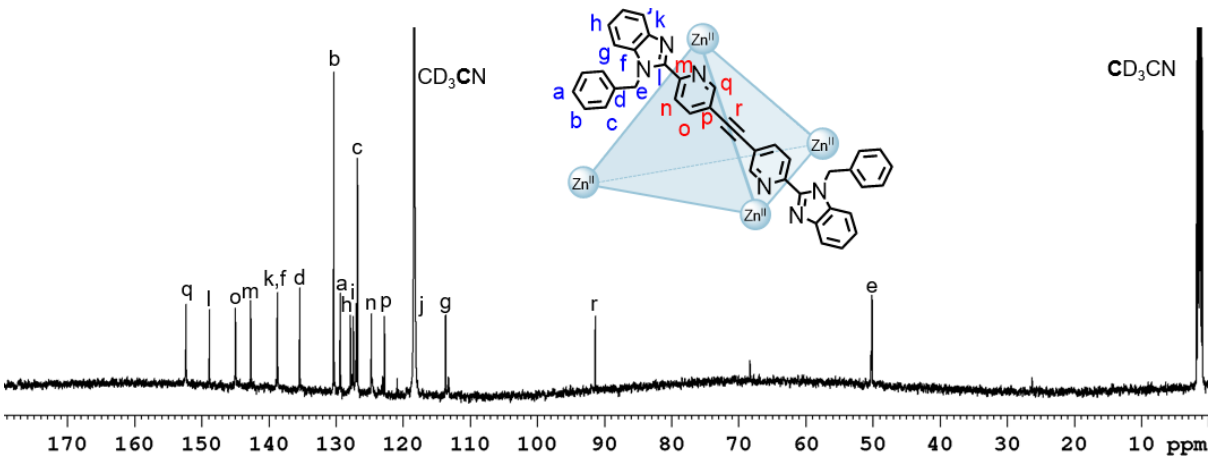

Figure S94. ^{13}C NMR spectrum (151 MHz, CD_3CN, 298 K) of cage **36**.

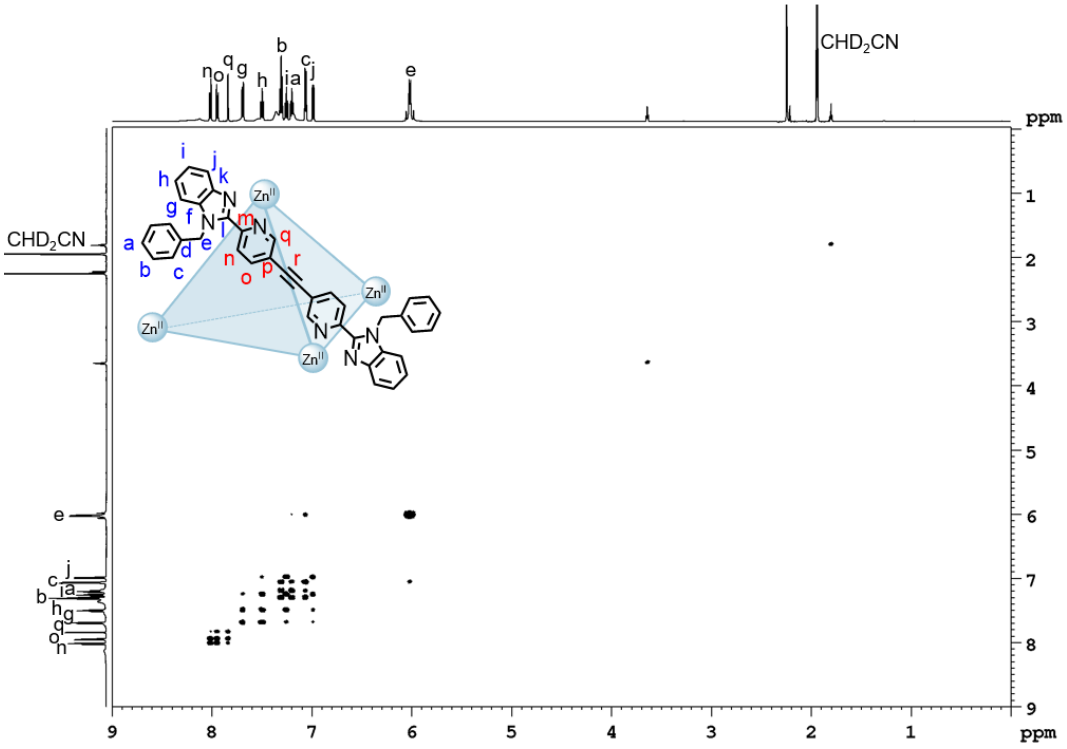

Figure S95. ^{1}H-^{1}H COSY NMR spectrum (600 MHz, CD_3CN, 298 K) of cage **36**.

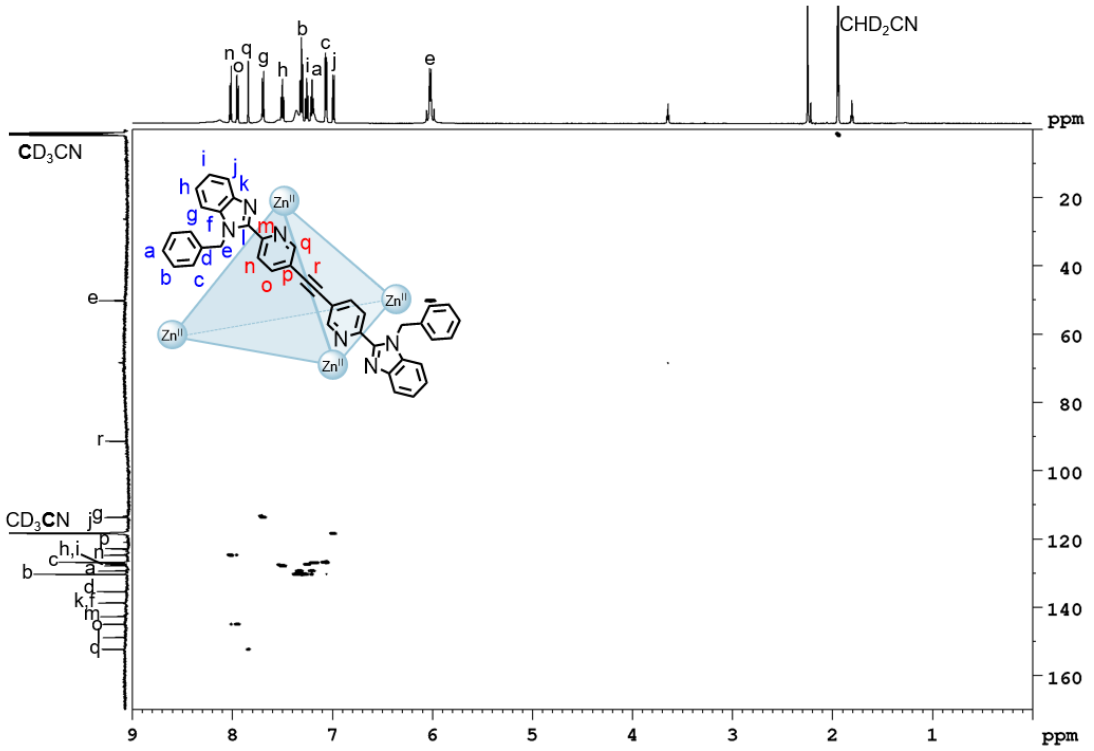

Figure S96. ^{1}H-^{13}C HSQC NMR spectrum (600 MHz/151 MHz, CD_3CN, 298 K) of cage **36**.

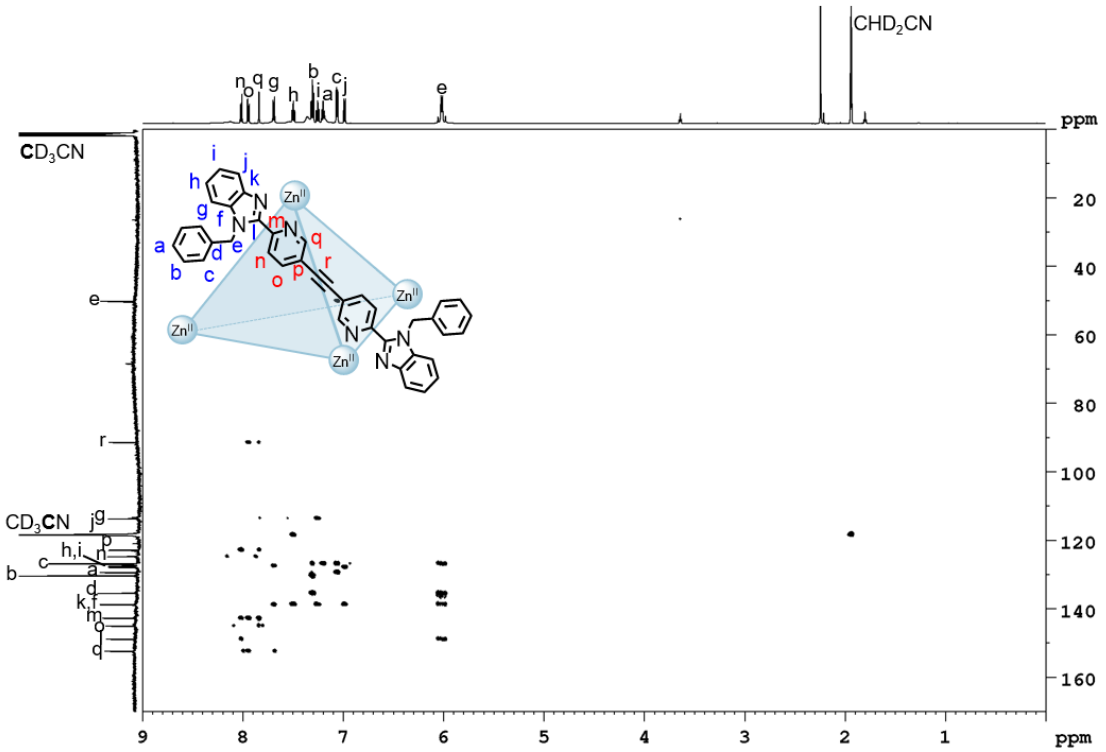

Figure S97. ^{1}H-^{13}C HMBC NMR spectrum (600 MHz/151 MHz, CD_3CN, 298 K) of cage **36**.

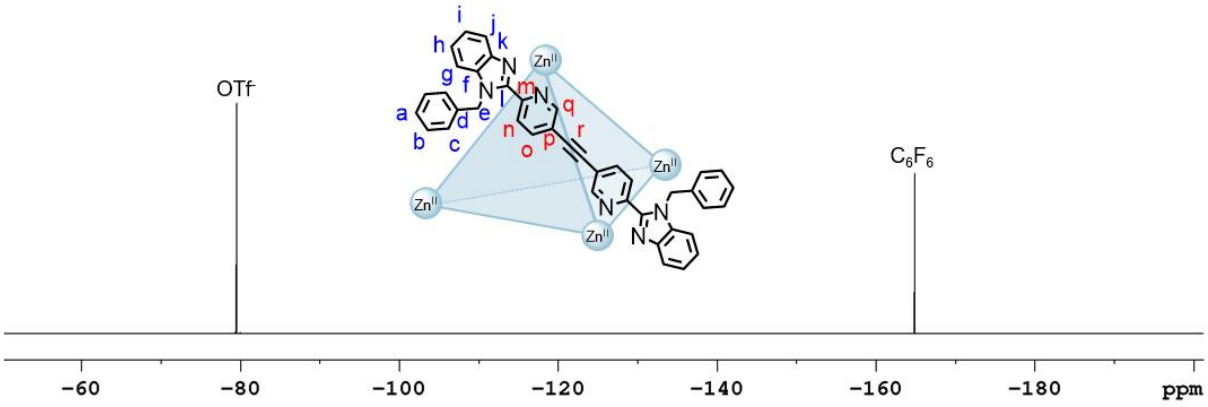

Figure S98. ^{19}F NMR spectrum (471 MHz, CD_3CN, 298 K, C_6F_6) of cage **36**.

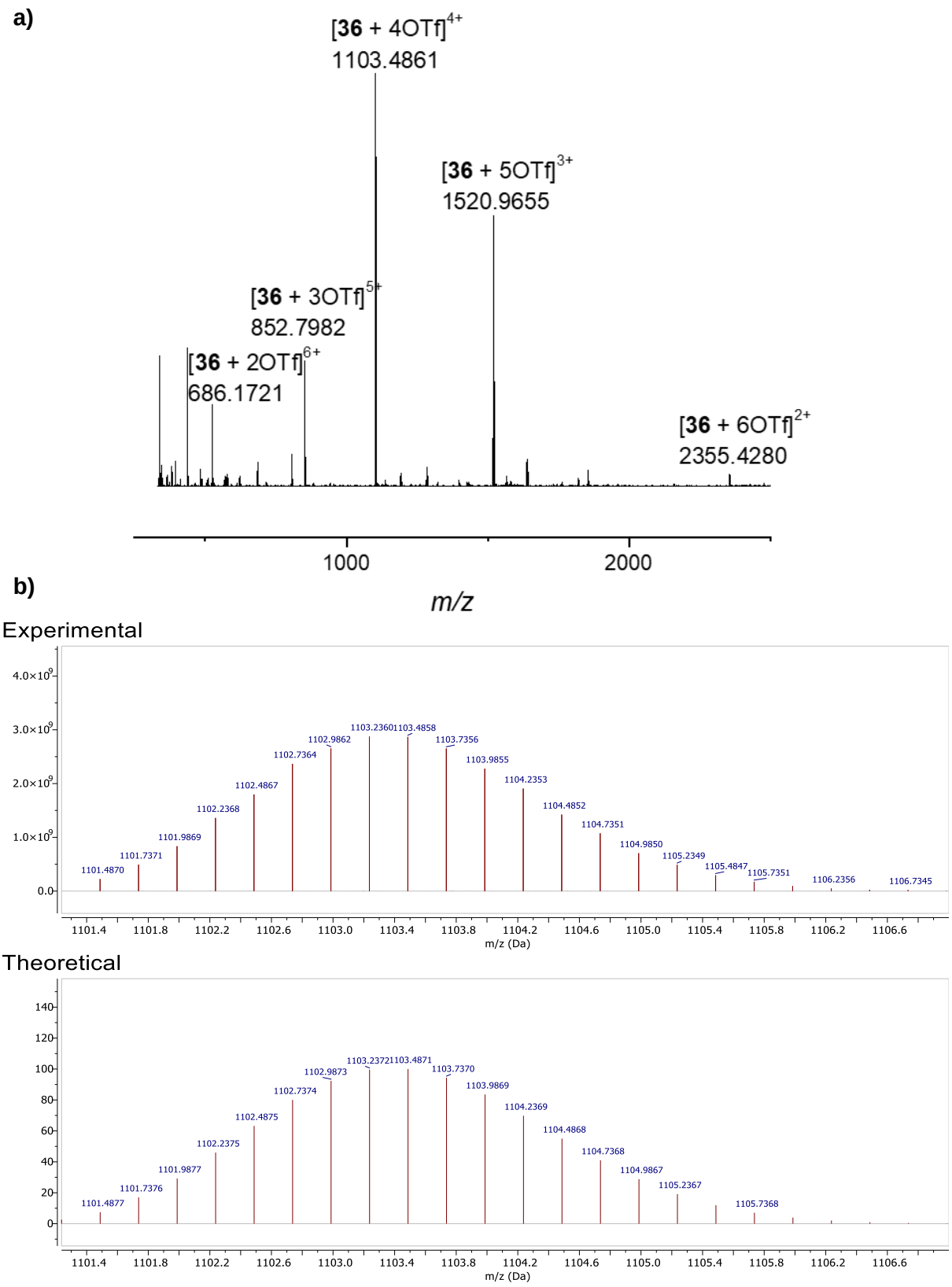

Figure S99. a) High resolution ESI mass spectrum of cage **36** and b) isotopic patterns of cage **36**: experimental (top) and theoretical (bottom).

3.4 Cage 37

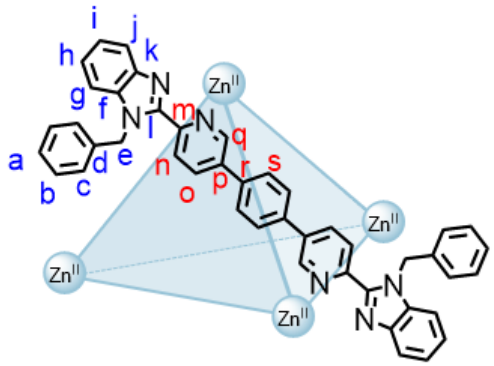

Zinc(II) triflate (2.08 mg, 5.72 µmol) and 1,4-di(6''-(1'-benzyl-1*H*-benzo[*d*]imidazol-2'-yl)pyridin-3''-yl)benzene (**28**) (5.53 mg, 8.58 µmol) were dissolved in CD_3CN (500 µL) and heated for 74.5 h at 50 °C to prepare cage **37** *in situ*.

^{1}H NMR (500 MHz, CD_3CN, 298 K) δ (ppm): 8.38 (dd, ^3J = 8.5 Hz, ^4J = 2.3 Hz, 12H, H_o), 8.18 (dd, ^3J = 8.5 Hz, ^5J = 0.6 Hz, 12H, H_n), 8.06 (dd, ^4J = 2.3 Hz, ^5J = 0.6 Hz, 12H, H_q), 7.74 (dt, ^3J = 8.5 Hz, ^4J = 0.8 Hz, 12H, H_g), 7.51 (ddd, ^3J = 8.5 Hz, ^3J = 7.3 Hz, ^4J = 0.9 Hz, 12H, H_h), 7.26 (ddd, ^3J = 8.3 Hz, ^3J = 7.3 Hz, ^4J = 0.8 Hz, 12H, H_i), 7.22-7.18 (m, 24H, H_b), 7.11-7.08 (m, 36H, $H_{a,c}$), 7.09 (s, 24H, H_s), 7.02 (dt, ^3J = 8.3 Hz, ^4J = 0.8 Hz, 12H, H_j), 6.00 (s, 24H, H_e).

^{13}C NMR (125 MHz, CD_3CN, 298 K) δ (ppm): 149.1 (C_l), 147.8 (C_q), 142.0 (C_m), 139.9 (C_o), 139.1 (C_p), 138.8 (C_f), 138.6 (C_k), 136.0 (C_r), 135.4 (C_d), 130.1 (C_b), 129.0 (C_a), 128.4 (C_s), 127.4 (C_h), 127.0 (C_i), 126.6 (C_c), 124.9 (C_n), 118.2 (C_j), 113.3 (C_g), 49.9 (C_e).

^{19}F NMR (471 MHz, CD_3CN, 298 K, C_6F_6) δ (ppm): -79.5 (OTf^-).

HRMS (ESI): *m/z* = 2512.0241 [**37** + 6OTf]$^{2+}$, 1625.0290 [**37** + 5OTf]$^{3+}$, 1181.2836 [**37** + 4OTf]$^{4+}$, 915.2358 [**37** + 3OTf]$^{5+}$, 737.8710 [**37** + 2OTf]$^{6+}$.

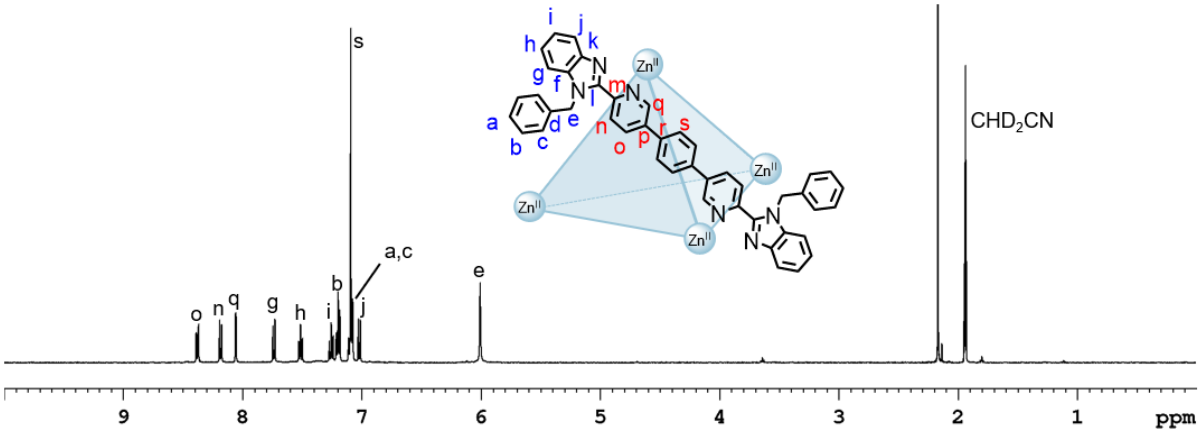

Figure S100. ^{1}H NMR spectrum (500 MHz, CD_3CN, 298 K) of cage **37**.

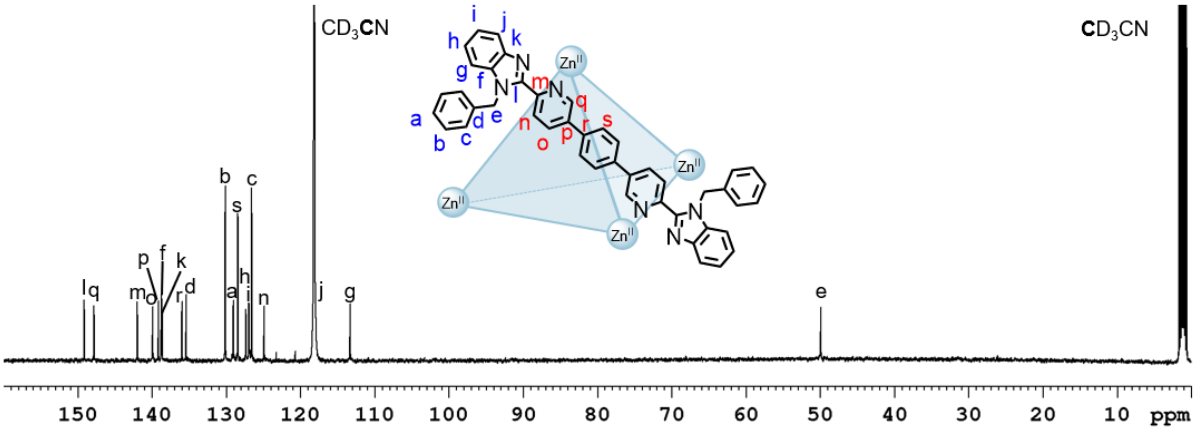

Figure S101. ^{13}C NMR spectrum (125 MHz, CD_3CN, 298 K) of cage **37**.

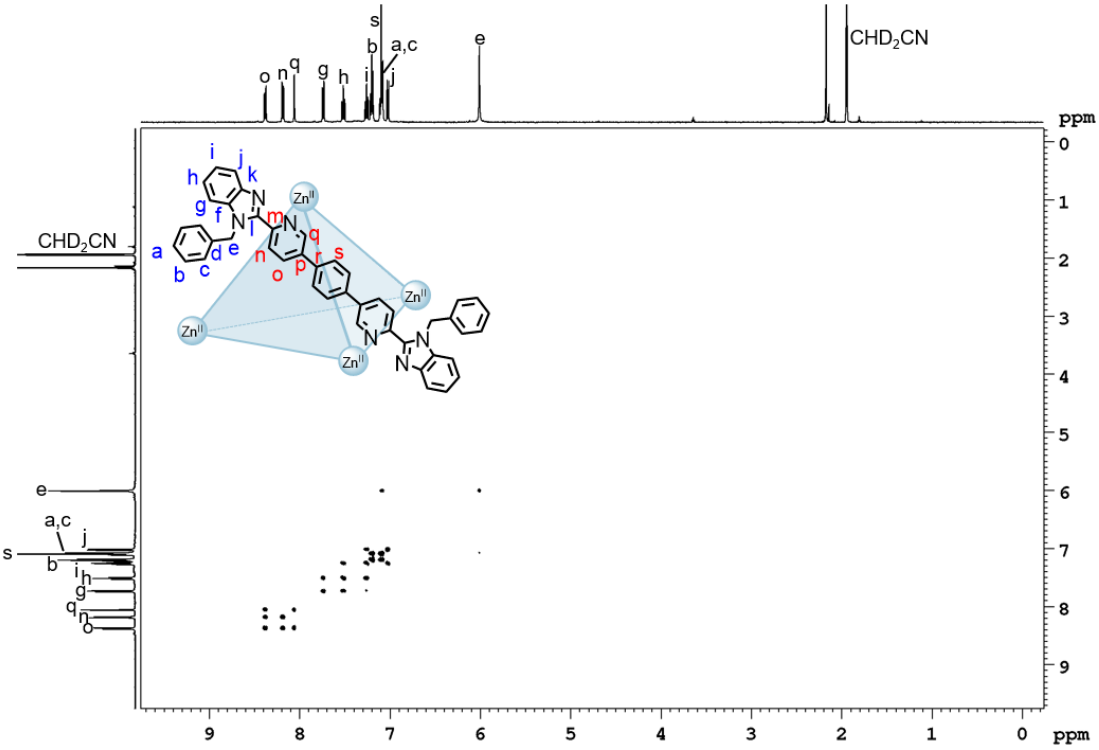

Figure S102. ^{1}H-^{1}H COSY NMR spectrum (500 MHz, CD_3CN, 298 K) of cage **37**.

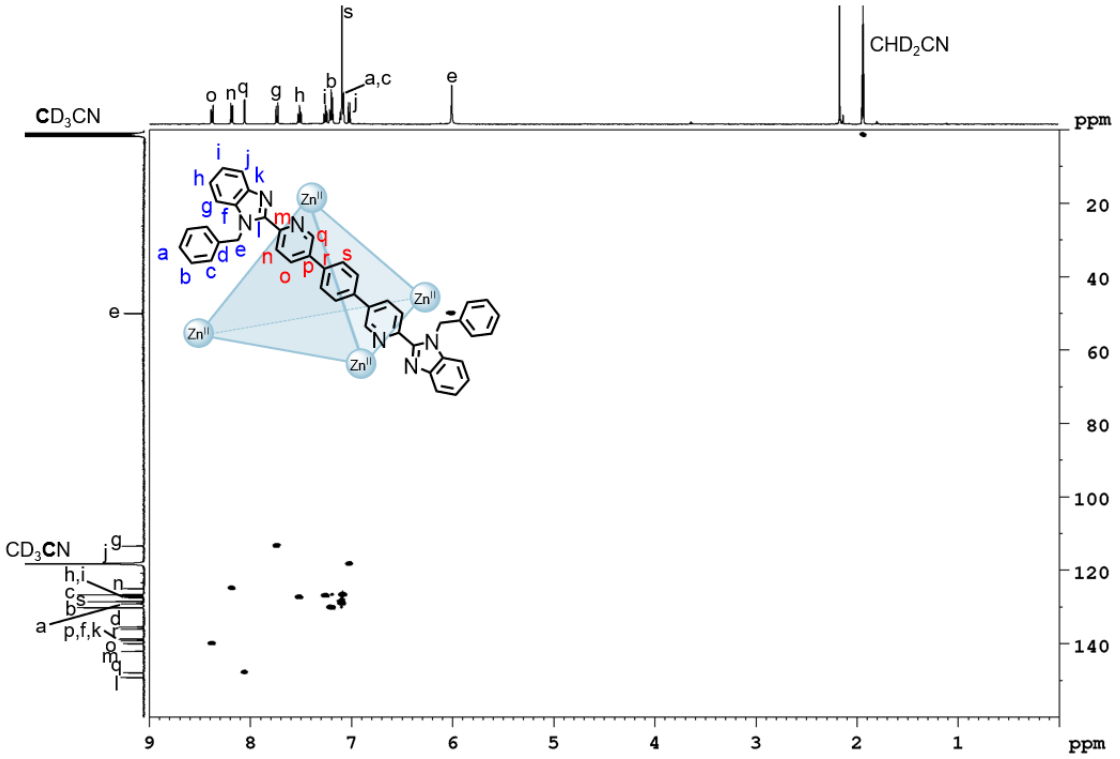

Figure S103. ^{1}H-^{13}C HSQC NMR spectrum (500 MHz/125 MHz, CD_3CN, 298 K) of cage **37**.

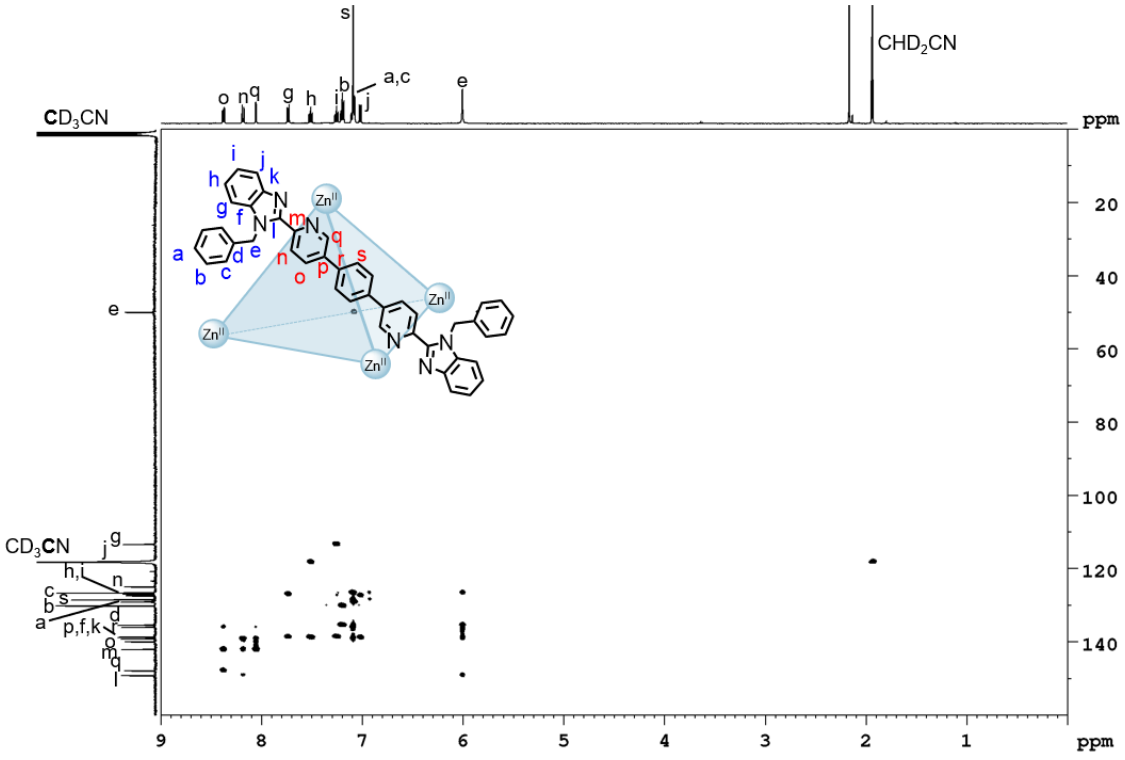

Figure S104. ^{1}H-^{13}C HMBC NMR spectrum (500 MHz/125 MHz, CD_3CN, 298 K) of cage **37**.

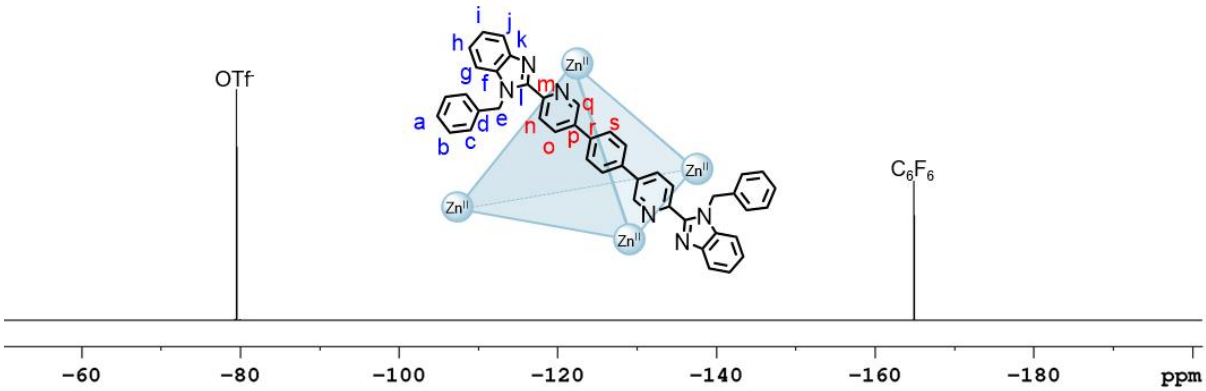

Figure S105. ^{19}F NMR spectrum (471 MHz, CD_3CN, 298 K, C_6F_6) of cage **37**.

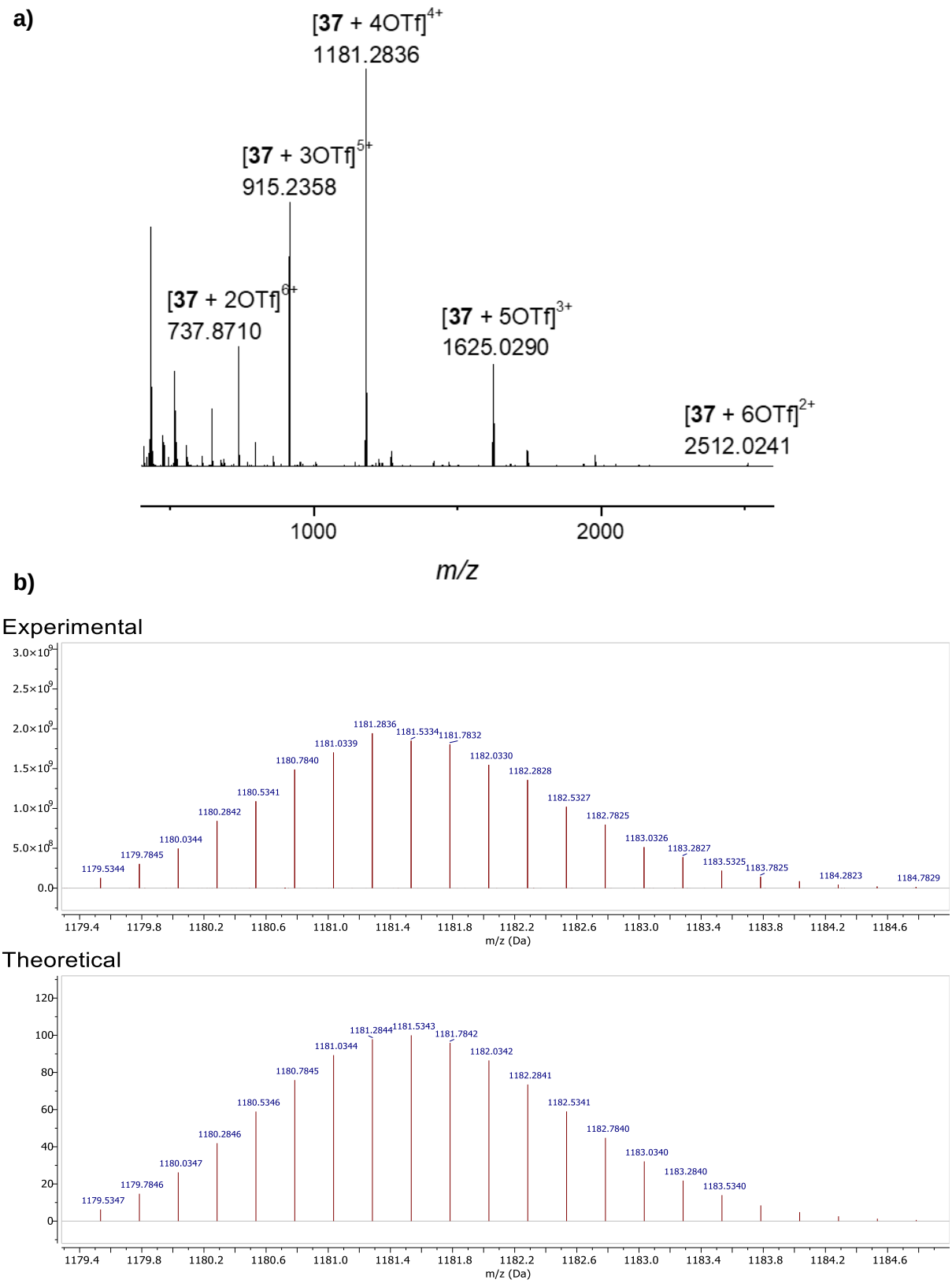

Figure S106. a) High resolution ESI mass spectrum of cage **37** and b) isotopic patterns of cage **37**: experimental (top) and theoretical (bottom).

3.5 Cage 38

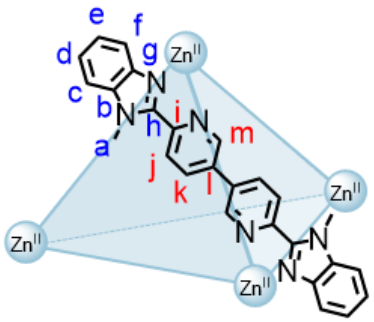

Zinc(II) triflate (1.97 mg, 5.42 µmol) and 6',6''-di(1-methyl-1*H*-benzo[*d*]imidazol-2-yl)-3',3''-bipyridine (**24**) (3.39 mg, 8.14 µmol) were dissolved in CD_3CN (500 µL) and heated for 22 h at 50 °C to prepare cage **38** *in situ*.

^{1}H NMR (600 MHz, CD_3CN, 298 K) δ (ppm): 8.34 (dd, ^3J = 8.4 Hz, ^5J = 0.6 Hz, 12H, H_j), 8.03 (dd, ^4J = 2.3 Hz, ^5J = 0.6 Hz, 12H, H_m), 7.84 (dd, ^3J = 8.4 Hz, ^4J = 2.3 Hz, 12H, H_k), 7.77 (unres. ddd, 12H, H_c), 7.47 (ddd, ^3J = 8.5 Hz, ^3J = 7.2 Hz, ^4J = 0.8 Hz, 12H, H_d), 7.11 (ddd, ^3J = 8.3 Hz, ^3J = 7.2 Hz, ^4J = 0.8 Hz, 12H, H_e), 6.92 (unres. ddd, 12H, H_f), 4.26 (s, 36H, H_a).

^{13}C NMR (151 MHz, CD_3CN, 298 K) δ (ppm): 149.5 (C_h), 149.3 (C_m), 143.7 (C_i), 141.3 (C_k), 138.7 (C_b), 138.6 (C_g), 136.3 (C_l), 126.8 (C_d), 126.5 (C_e), 125.0 (C_j), 118.2 (C_f), 113.4 (C_c), 34.4 (C_a).

^{19}F NMR (471 MHz, CD_3CN, 298 K, C_6F_6) δ (ppm): -79.6 (OTf^-).

HRMS (ESI): *m/z* = 1827.2372 [**38** + 6OTf]$^{2+}$, 1168.5063 [**38** + 5OTf]$^{3+}$, 839.1410 [**38** + 4OTf]$^{4+}$, 641.3225 [**38** + 3OTf]$^{5+}$, 509.4439 [**38** + 2OTf]$^{6+}$.

While the signal at *m/z* 509.4439 is consistent with the 6+ charge for the cage, the theoretical isotopic pattern does not match, possibly due to fragmentation in the gas phase or overlap with other signals.

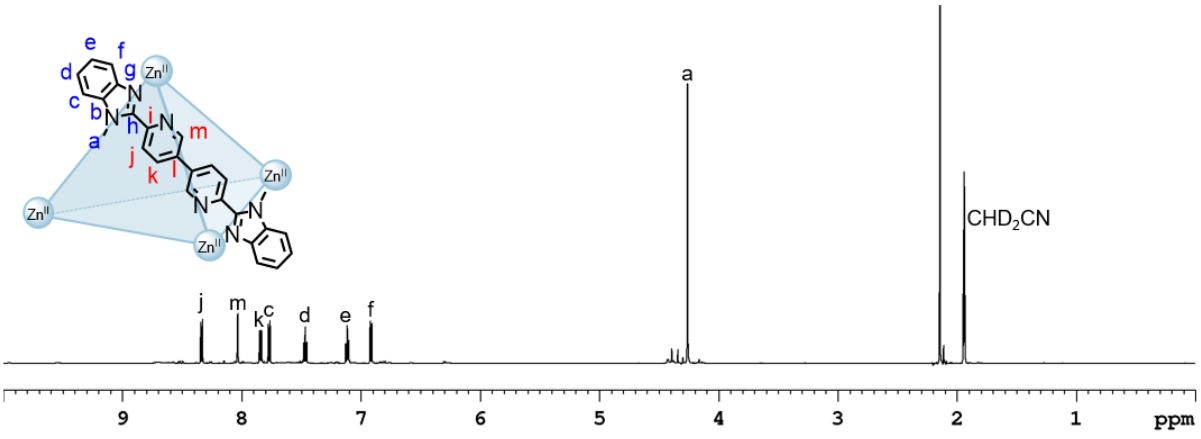

Figure S107. ^{1}H NMR spectrum (600 MHz, CD_3CN, 298 K) of cage **38**.

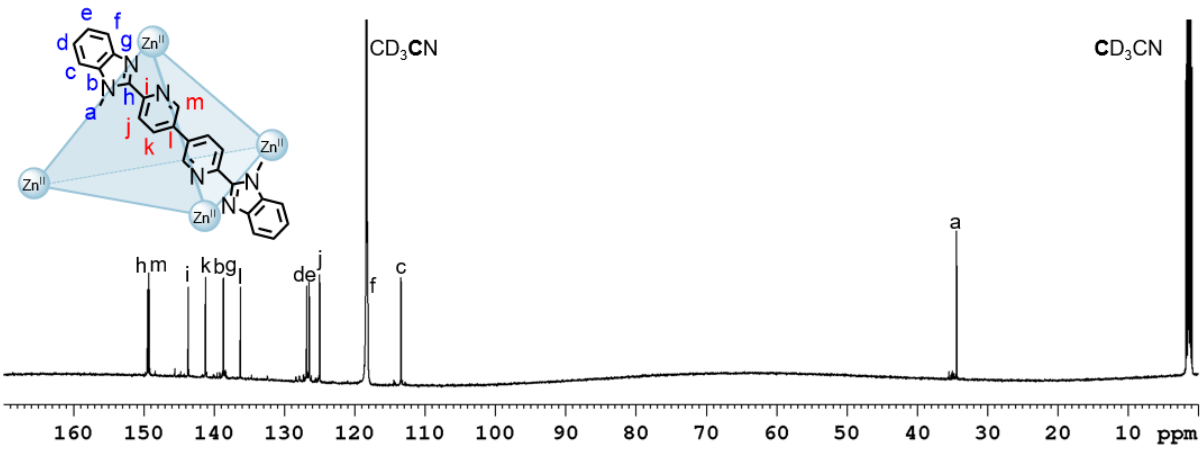

Figure S108. ^{13}C NMR spectrum (151 MHz, CD_3CN, 298 K) of cage **38**.

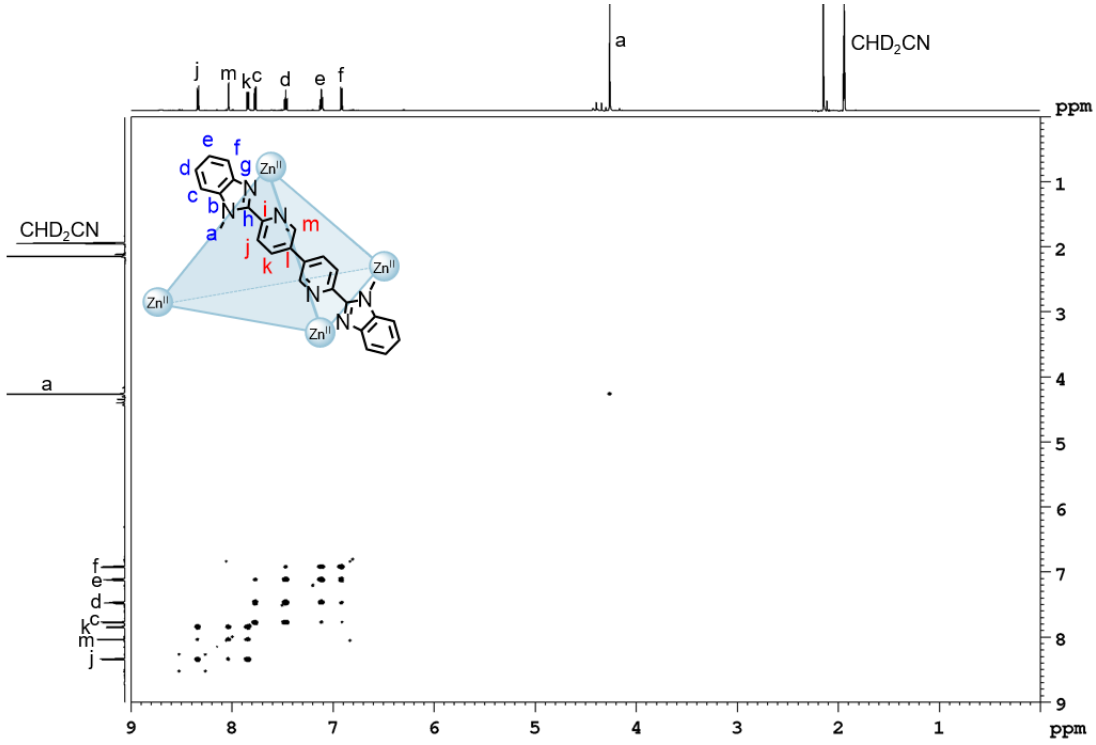

Figure S109. ^{1}H-^{1}H COSY NMR spectrum (600 MHz, CD_3CN, 298 K) of cage **38**.

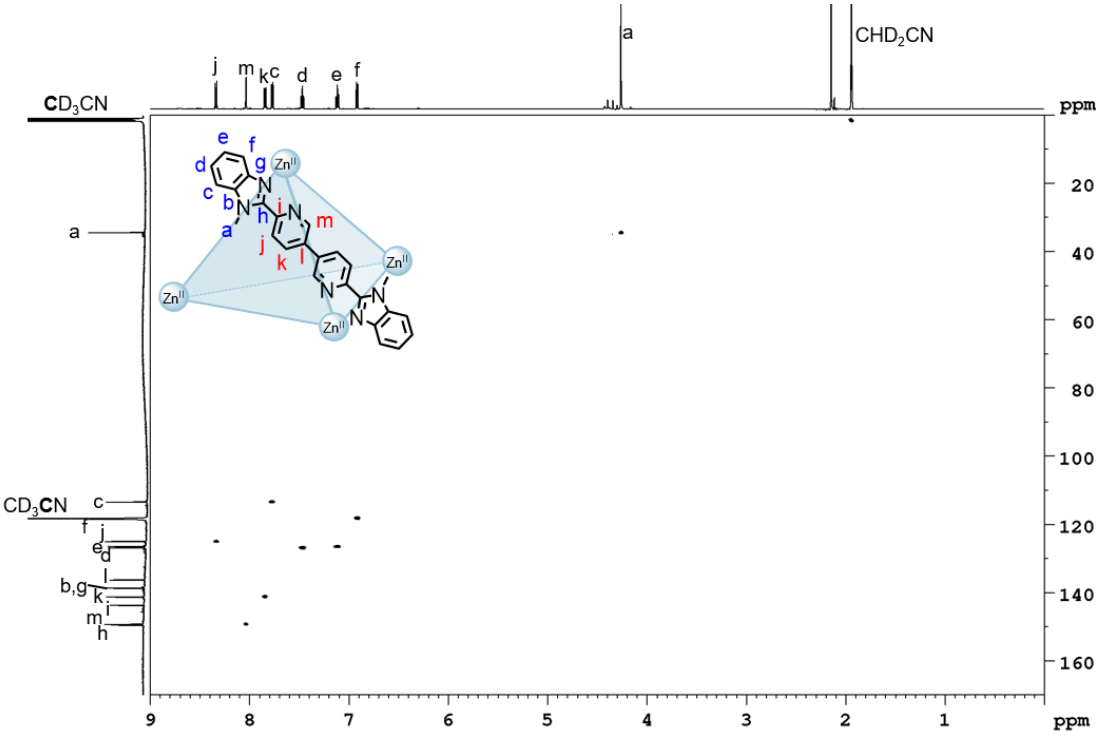

Figure S110. ^{1}H-^{13}C HSQC NMR spectrum (600 MHz/151 MHz, CD_3CN, 298 K) of cage **38**.

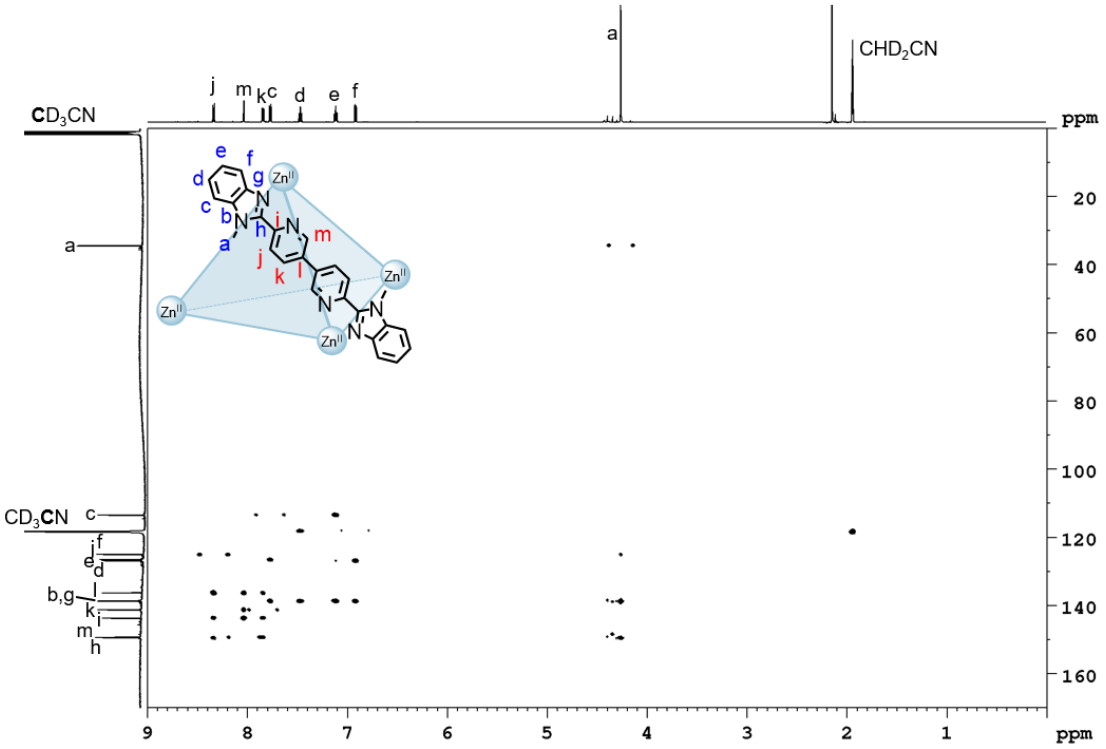

Figure S111. ^{1}H-^{13}C HMBC NMR spectrum (600 MHz/151 MHz, CD_3CN, 298 K) of cage **38**.

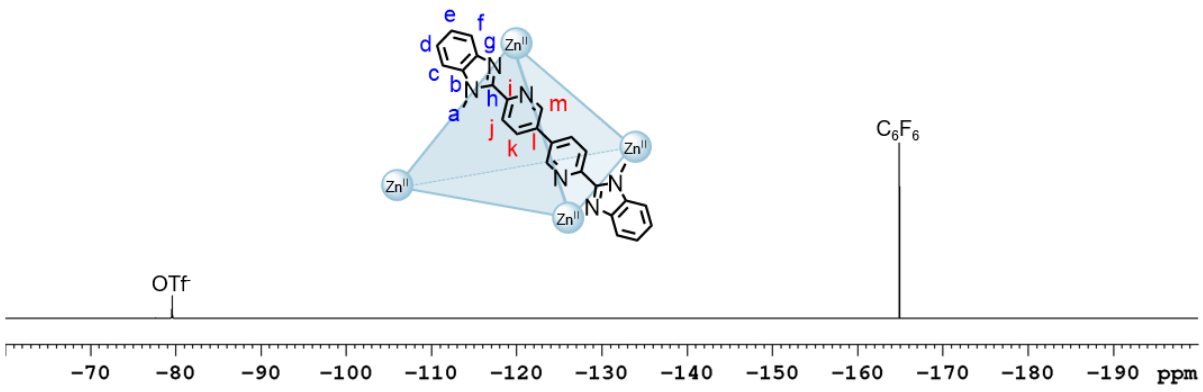

Figure S112. ^{19}F NMR spectrum (471 MHz, CD_3CN, 298 K, C_6F_6) of cage **38**.

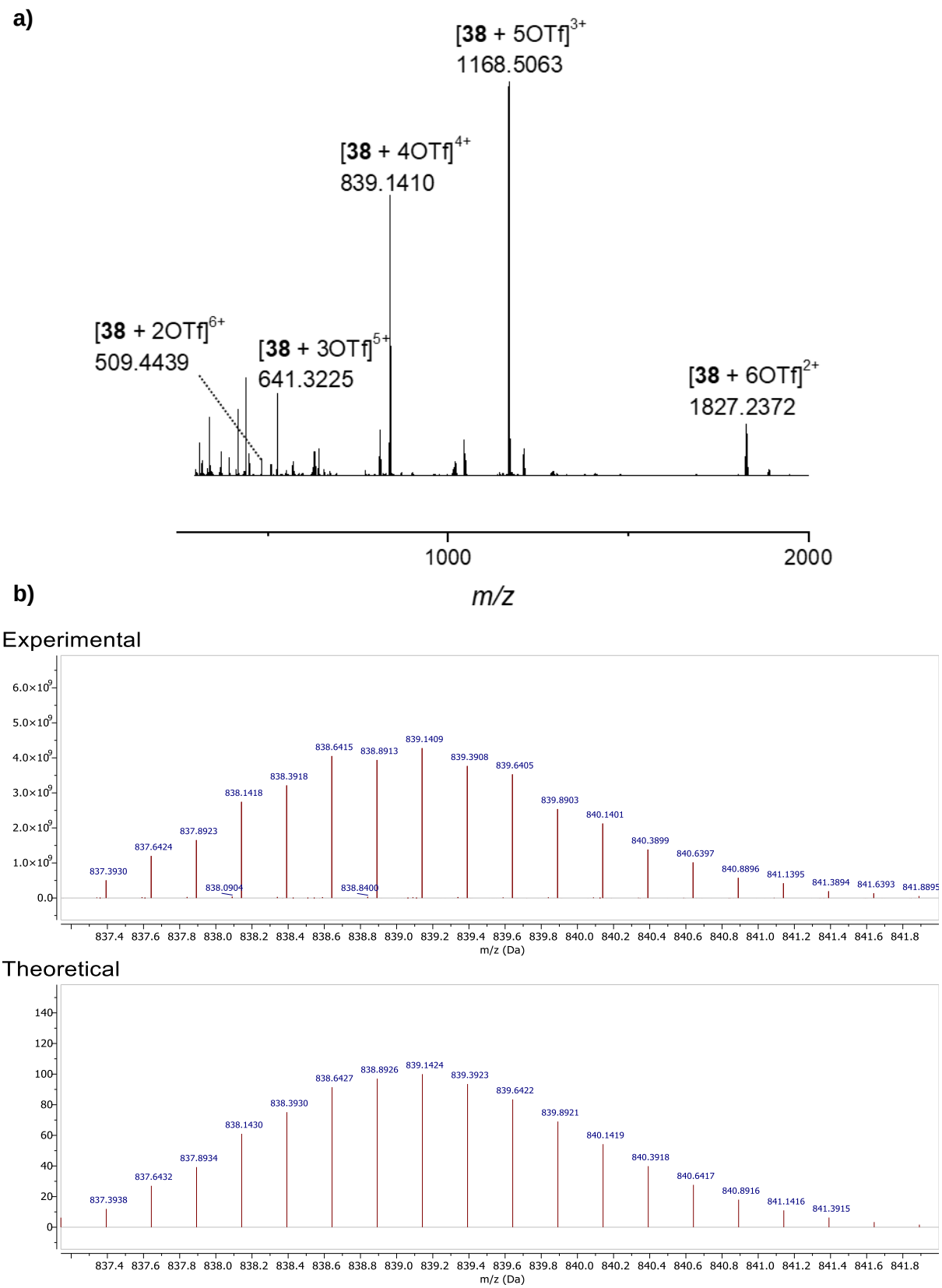

Figure S113. a) High resolution ESI mass spectrum of cage **38** and b) isotopic patterns of cage **38**: experimental (top) and theoretical (bottom).

3.6 Cage 39

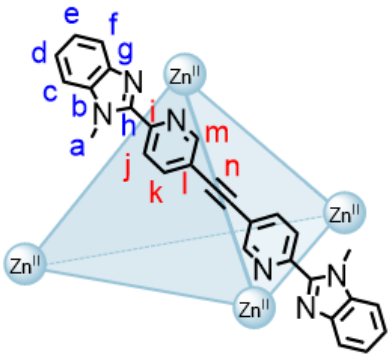

Zinc(II) triflate (2.04 mg, 5.61 µmol) and 1,2-di(6''-(1'-methyl-1*H*-benzo[*d*]imidazole-2'-yl)pyridin-3''-yl)ethyne (**17**) (3.71 mg, 8.42 µmol) were dissolved in CD_3CN (500 µL) to prepare cage **39** *in situ*.

^{1}H NMR (500 MHz, CD_3CN, 298 K) δ (ppm): 8.43 (dd, ^3J = 8.6 Hz, ^5J = 0.8 Hz, 12H, H_j), 8.25 (dd, ^3J = 8.6 Hz, ^4J = 2.0 Hz, 12H, H_k), 7.99 (dd, ^4J = 2.0 Hz, ^5J = 0.8 Hz, 12H, H_m), 7.77 (dt, ^3J = 8.6 Hz, ^4J = 0.9 Hz, 12H, H_c), 7.47 (ddd, ^3J = 8.6 Hz, ^3J = 7.3 Hz, ^4J = 0.9 Hz, 12H, H_d), 7.08 (ddd, ^3J = 8.4 Hz, ^3J = 7.3 Hz, ^4J = 0.9 Hz, 12H, H_e), 6.73 (dt, ^3J = 8.4 Hz, ^4J = 0.9 Hz, 12H, H_f), 4.29 (s, 36H, H_a).

^{13}C NMR (125 MHz, CD_3CN, 298 K) δ (ppm): 152.4 (C_m), 149.2 (C_h), 144.6 (C_k), 143.4 (C_i), 138.7 (C_g), 138.6 (C_b), 127.2 (C_d), 126.8 (C_e), 125.2 (C_j), 122.9 (C_l), 118.2 (C_f), 113.4 (C_c), 91.5 (C_n), 34.7 (C_a).

^{19}F NMR (471 MHz, CD_3CN, 298 K, C_6F_6) δ (ppm): -79.6 (OTf^-).

HRMS (ESI): *m/z* = 1899.7373 [**39** + 6OTf]$^{2+}$, 1216.1738 [**39** + 5OTf]$^{3+}$, 875.1411 [**39** + 4OTf]$^{4+}$, 670.3225 [**39** + 3OTf]$^{5+}$, 533.4437 [**39** + 2OTf]$^{6+}$.

While the signal at *m/z* 533.4437 is consistent with the 6+ charge for the cage, the theoretical isotopic pattern does not match, possibly due to fragmentation in the gas phase or overlap with other signals.

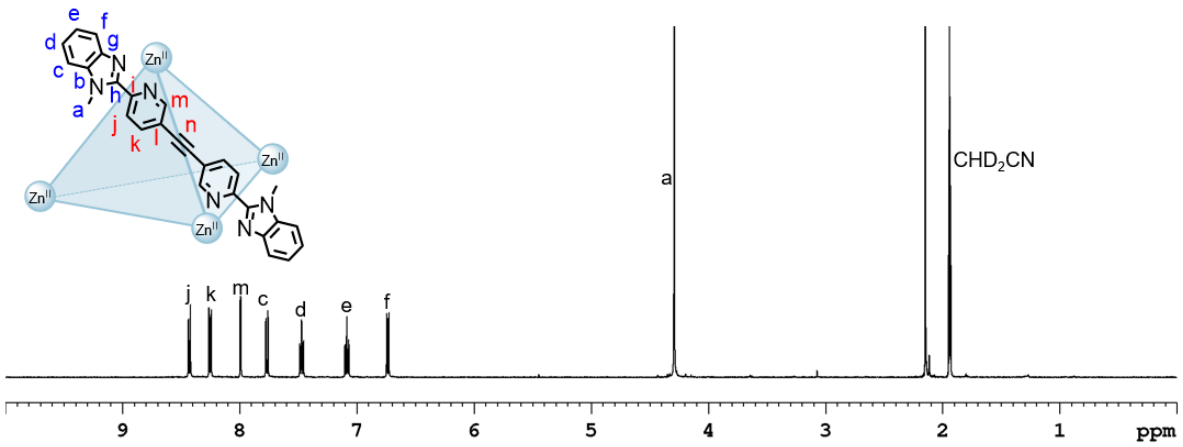

Figure S114. ^{1}H NMR spectrum (500 MHz, CD_3CN, 298 K) of cage **39**.

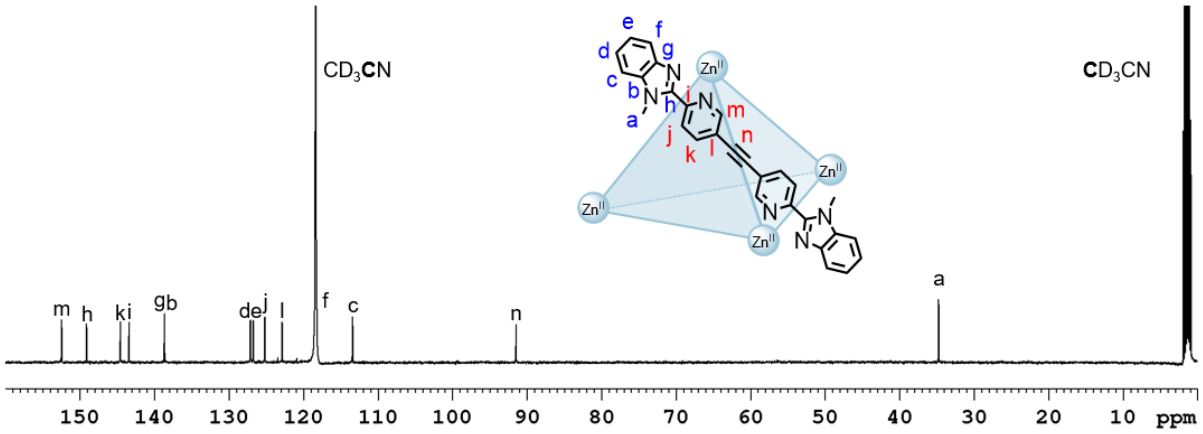

Figure S115. ^{13}C NMR spectrum (125 MHz, CD_3CN, 298 K) of cage **39**.

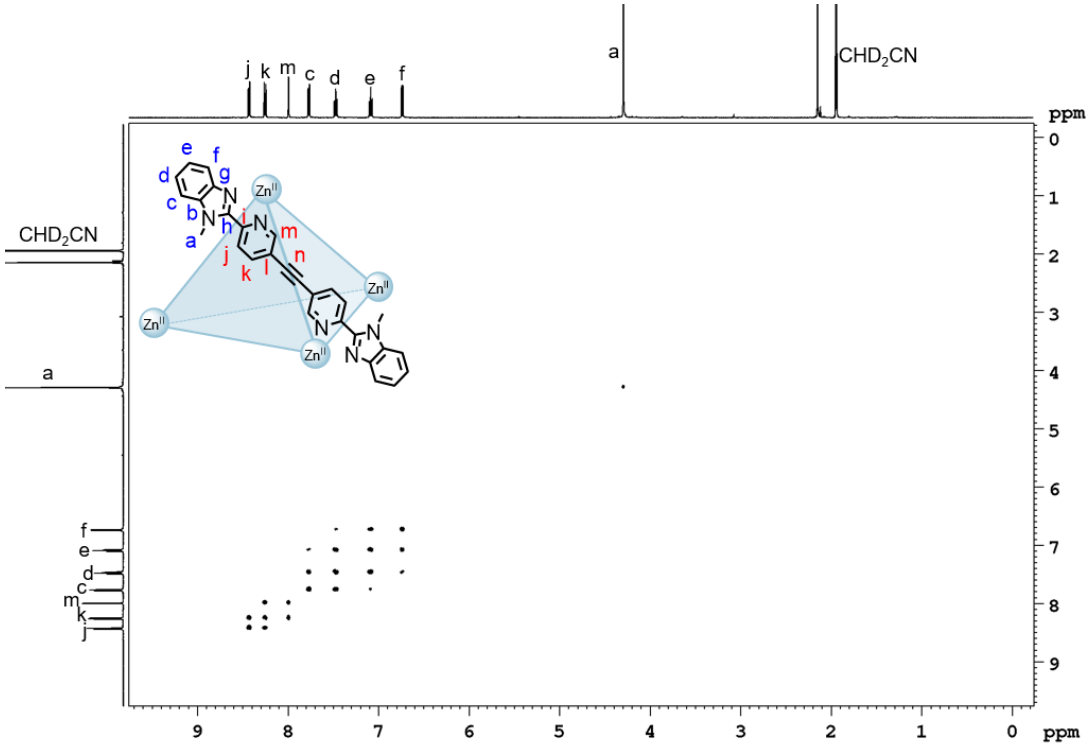

Figure S116. ^{1}H-^{1}H COSY NMR spectrum (500 MHz, CD_3CN, 298 K) of cage **39**.

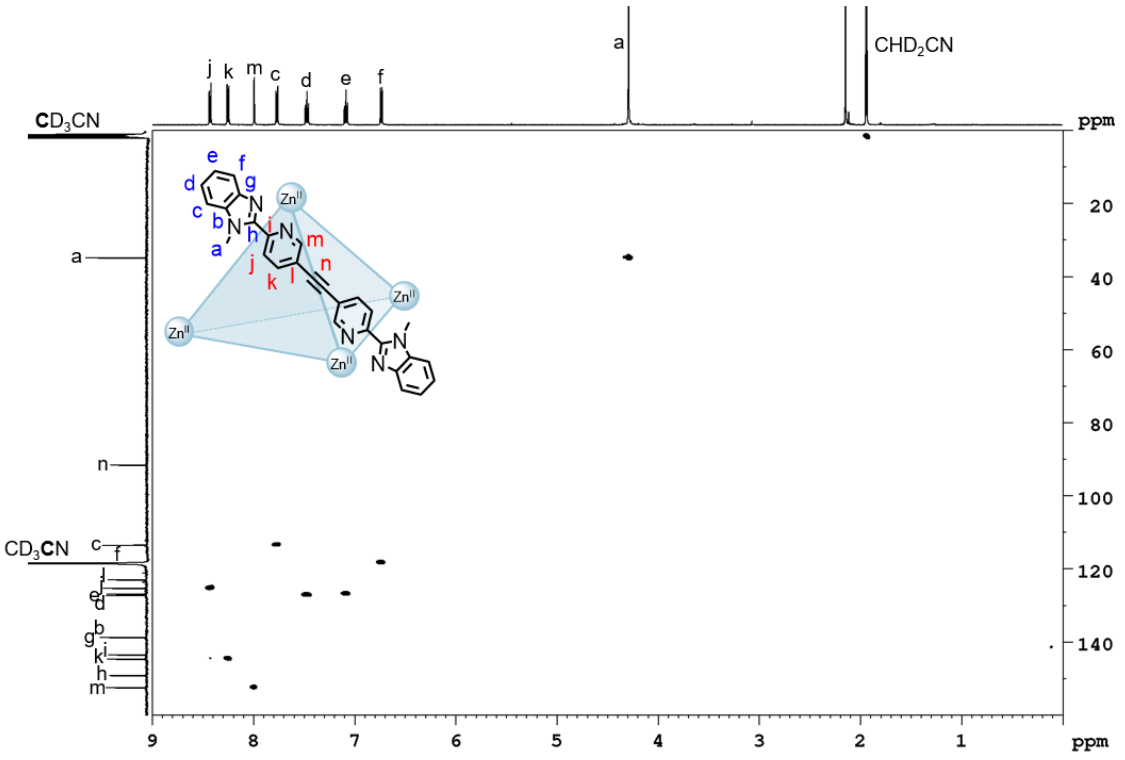

Figure S117. ^{1}H-^{13}C HSQC NMR spectrum (500 MHz/125 MHz, CD_3CN, 298 K) of cage **39**.

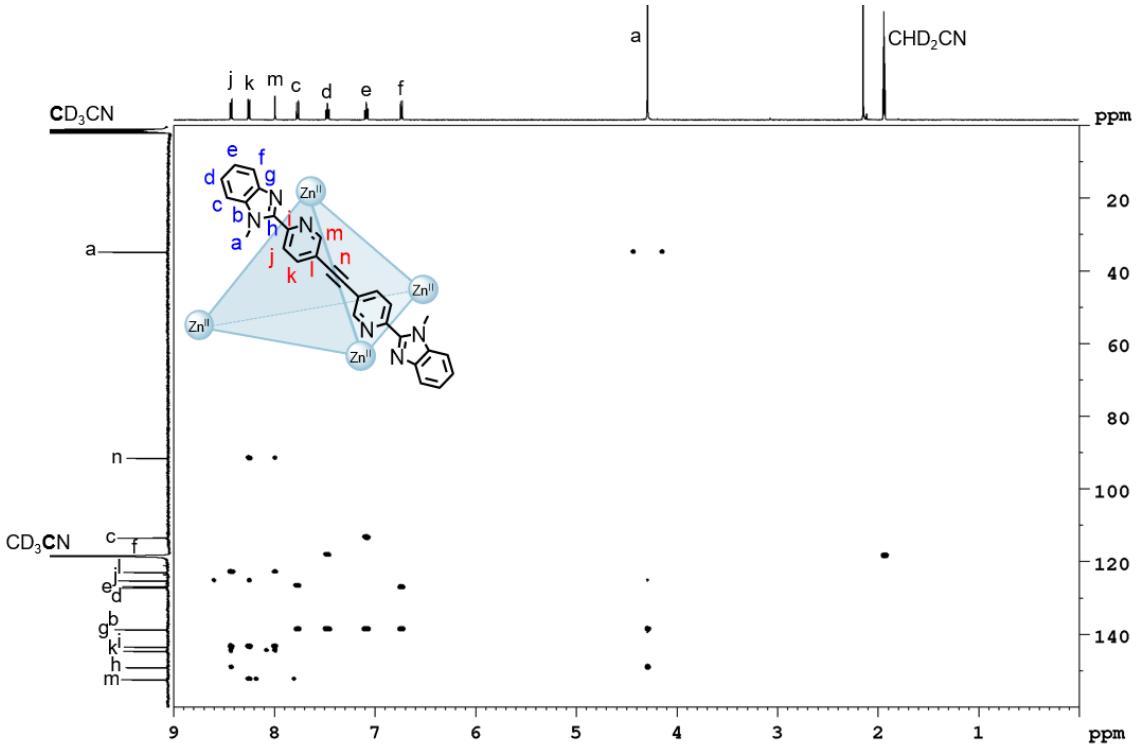

Figure S118. ^{1}H-^{13}C HMBC NMR spectrum (500 MHz/125 MHz, CD_3CN, 298 K) of cage **39**.

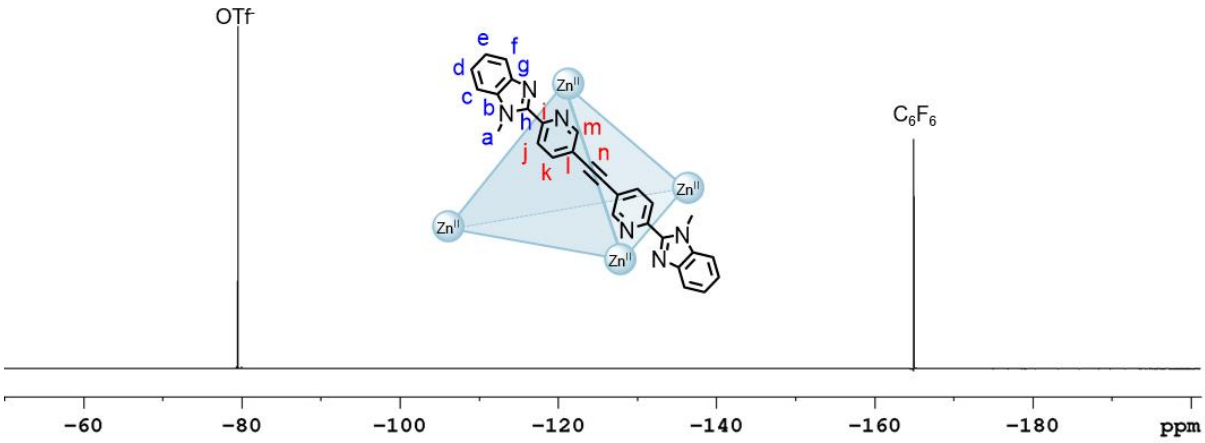

Figure S119. ^{19}F NMR spectrum (471 MHz, CD_3CN, 298 K, C_6F_6) of cage **39**.

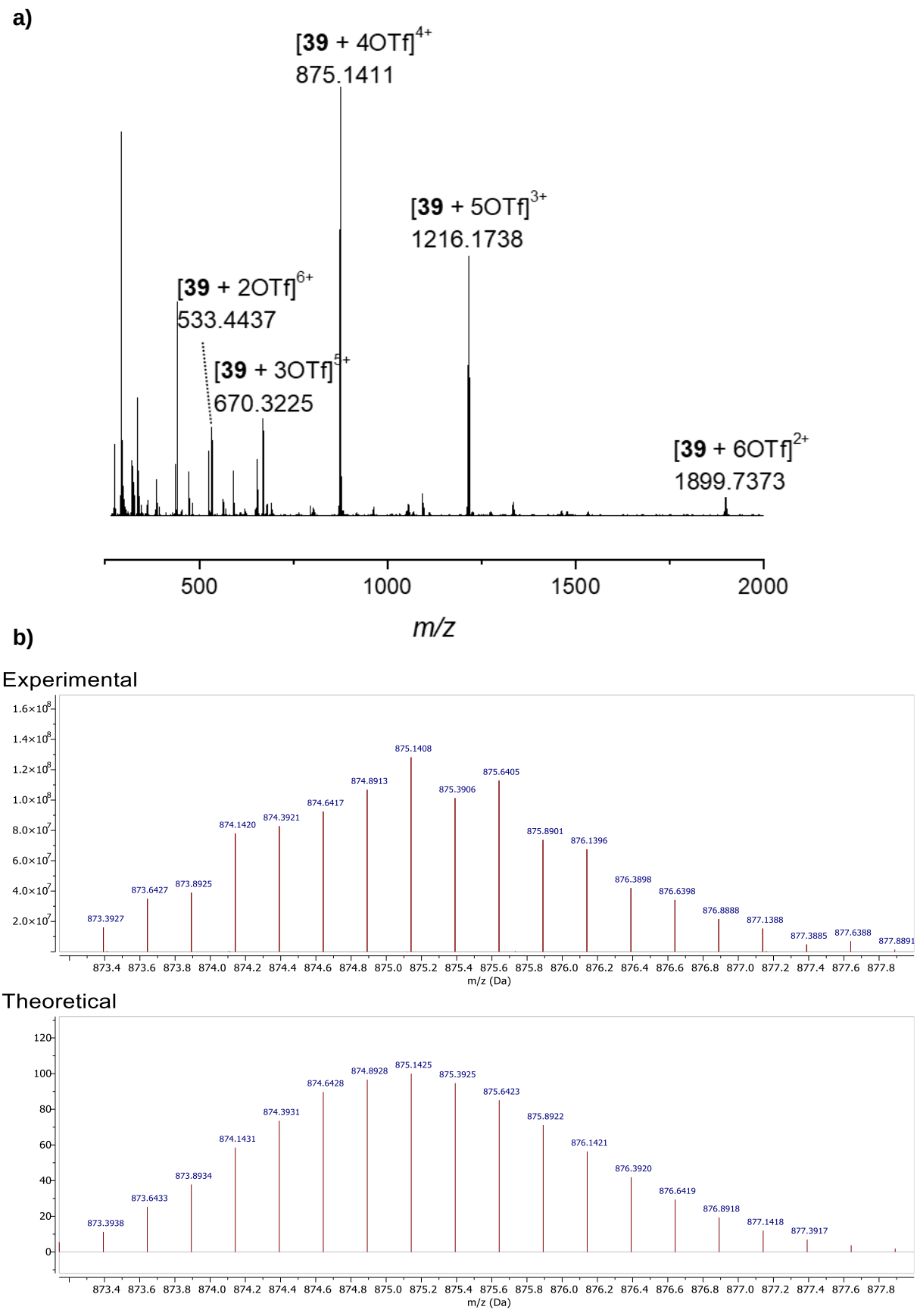

Figure S120. a) High resolution ESI mass spectrum of cage **39** and b) isotopic patterns of cage **39**: experimental (top) and theoretical (bottom).

3.7 Cage 40a and Helicate 40b

Zinc(II) triflate (2.03 mg, 5.58 µmol) and 1,4-di(6''-(1'-methyl-1*H*-benzo[*d*]imidazol-2'-yl)pyridin-3''-yl)benzene (**27**) (4.13 mg, 8.38 µmol) were dissolved in CD_3CN (500 µL) and heated for 117 h at 50 °C to prepare cage **40a** and helicate **40b** *in situ*.

3.7.1 Cage **40a**

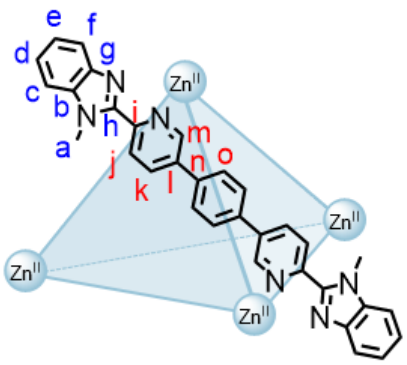

^{1}H NMR (600 MHz, CD_3CN, 298 K) δ (ppm): 8.54 (unres. dd, 12H, H_j), 8.53 (unres. dd, 12H, H_m), 8.24 (unres. dd, 12H, H_k), 7.76 (d, ^3J = 8.5 Hz, 12H, H_c), 7.48 (s, 24H, H_o), 7.46 (unres. ddd, 12H, H_d), 7.07 (unres. ddd, 12H, H_e), 6.78 (d, ^3J = 8.4 Hz, 12H, H_f), 4.29 (s, 36H, H_a).

^{13}C NMR (151 MHz, CD_3CN, 298 K) δ (ppm): 149.6 (C_h), 148.2 (C_k), 142.9 (C_i), 139.8 (C_j), 139.1 (C_n), 138.8 (C_b), 138.7 (C_g), 136.5 (C_l), 128.9 (C_o), 126.7 (C_d), 126.4 (C_e), 125.3 (C_m), 118.1 (C_f), 113.3 (C_c), 34.7 (C_a).

^{19}F NMR (471 MHz, CD_3CN, 298 K, C_6F_6) δ (ppm): -79.6 (OTf^-).

HRMS (ESI): *m/z* = 2055.3310 [**40a** + 6OTf]$^{2+}$, 1320.5694 [**40a** + 5OTf]$^{3+}$, 953.1881 [**40a** + 4OTf]$^{4+}$, 732.7601 [**40a** + 3OTf]$^{5+}$, 585.8077 [**40a** + 2OTf]$^{6+}$.

While the signal at *m/z* 585.8077 is consistent with the 6+ charge for the cage, the theoretical isotopic pattern does not match, possibly due to fragmentation in the gas phase or overlap with other signals.

3.7.2 Helicate **40b**

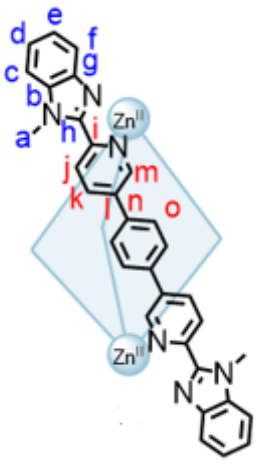

^{1}H NMR (600 MHz, CD_3CN, 298 K) δ (ppm): 8.72 (d, ^3J = 8.3 Hz, 6H, H_j), 8.67 (dd, ^3J = 8.3 Hz, ^4J = 1.8 Hz, 6H, H_k), 7.87 (d, ^3J = 8.4 Hz, 6H, H_c), 7.55 (unres. ddd, 6H, H_d), 7.34 (s, 12H, H_o),

7.24 (d, ^4J = 1.8 Hz, 6H, H_m), 7.11 (unres. ddd, 6H, H_e), 6.85 (d, ^3J = 8.2 Hz, 6H, H_f), 4.38 (s, 18H, H_a).

^{13}C NMR (151 MHz, CD_3CN, 298 K) δ (ppm): 149.9 (C_h), 148.2 (C_k), 144.0 (C_i), 139.0 (C_k), 138.9 (C_g), 138.8 (C_n), 138.8 (C_b), 136.3 (C_l), 128.8 (C_o), 126.9 (C_d), 126.8 (C_j), 126.4 (C_e), 118.5 (C_f), 113.4 (C_c), 34.9 (C_a).

^{19}F NMR (471 MHz, CD_3CN, 298 K, C_6F_6) δ (ppm): -79.6 (OTf^-).

HRMS (ESI): *m/z* = 2054.3328 [**40b** + 3OTf]$^+$, 952.6901 [**40b** + 2OTf]$^{2+}$, 585.4759 [**40b** + 1OTf]$^{3+}$, 401.8688 [**40b**]$^{4+}$.

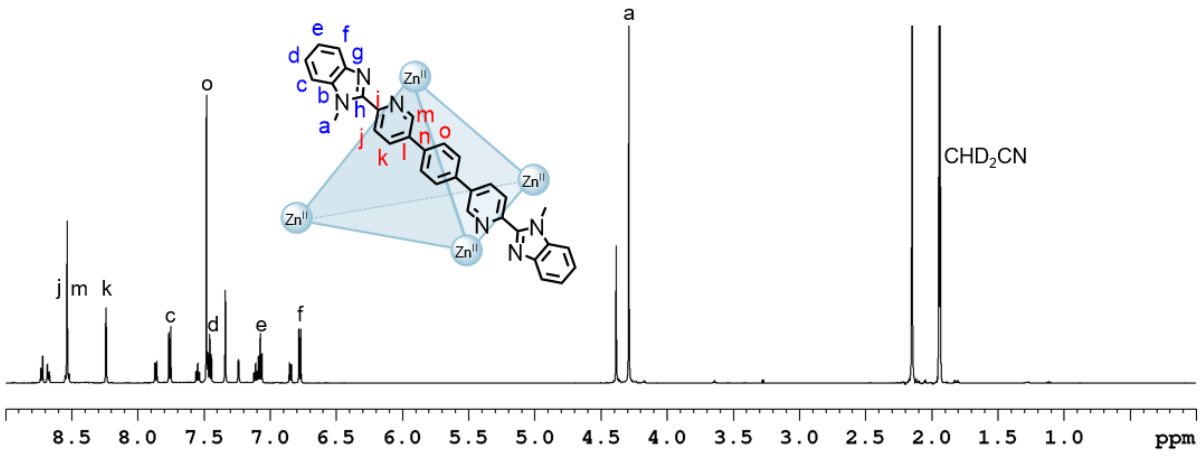

Figure S121. ^{1}H NMR spectrum (600 MHz, CD_3CN, 298 K) of cage **40a** and helicate **40b**. For clarity, only the signals for cage **40a** are labelled.

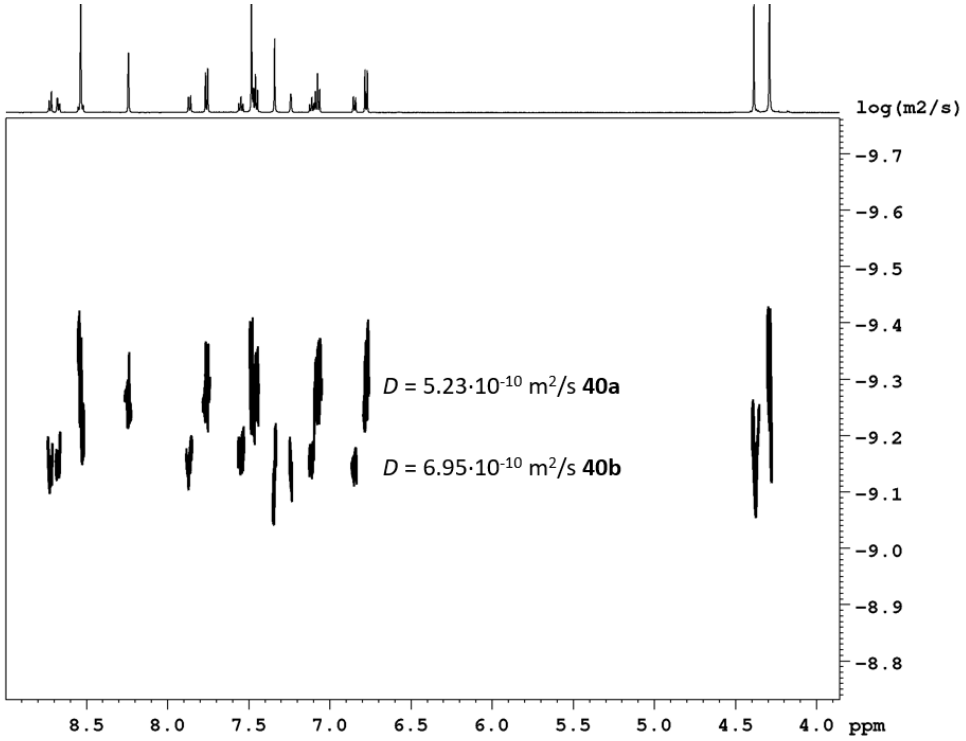

Figure S122. ^{1}H DOSY spectrum (600 MHz, CD_3CN, 298 K) of cage **40a** (D = 5.23·10^{-10} m^2/s) and helicate **40b** (D = 6.95·10^{-10} m^2/s).

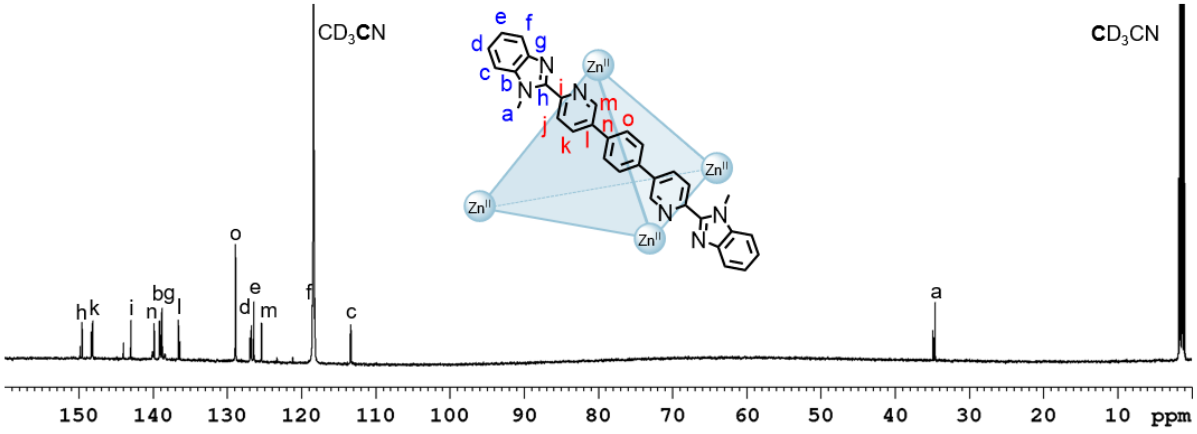

Figure S123. ^{13}C NMR spectrum (151 MHz, CD_3CN, 298 K) of cage **40a** and helicate **40b**. For clarity, only the signals for cage **40a** are labelled.

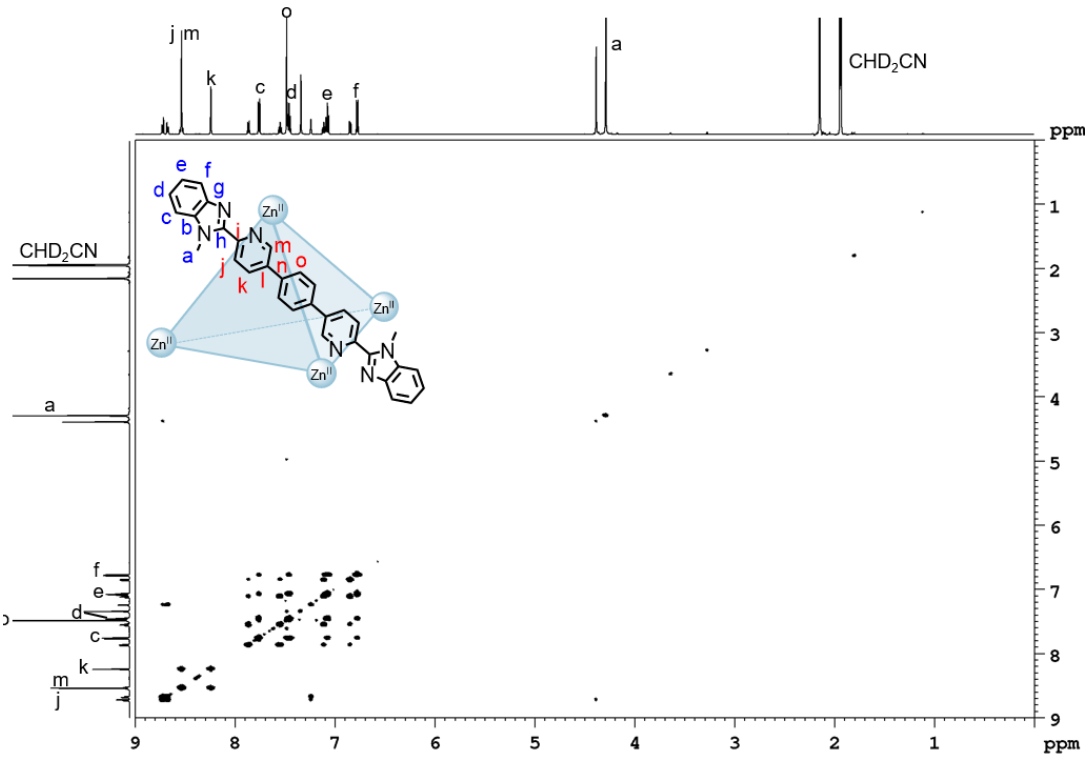

Figure S124. ^{1}H-^{1}H COSY NMR spectrum (600 MHz, CD_3CN, 298 K) of cage **40a** and helicate **40b**. For clarity, only the signals for cage **40a** are labelled.

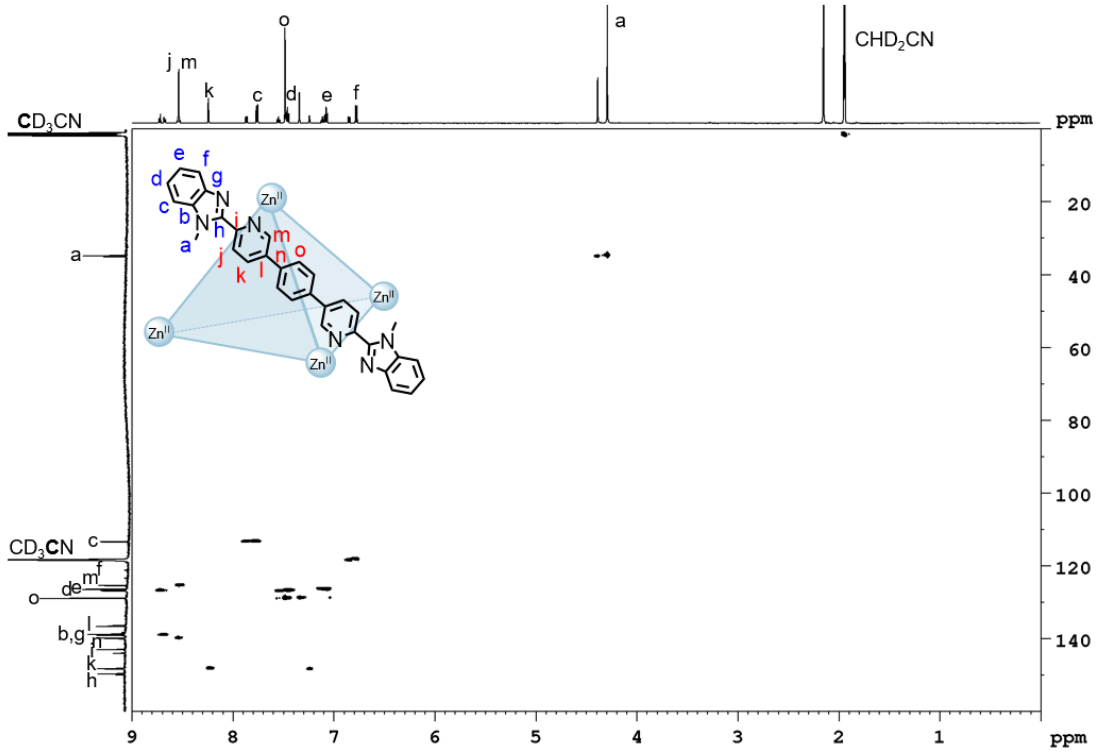

Figure S125. ^{1}H-^{13}C HSQC NMR spectrum (600 MHz/151 MHz, CD_3CN, 298 K) of cage **40a** and helicate **40b**. For clarity, only the signals for cage **40a** are labelled.

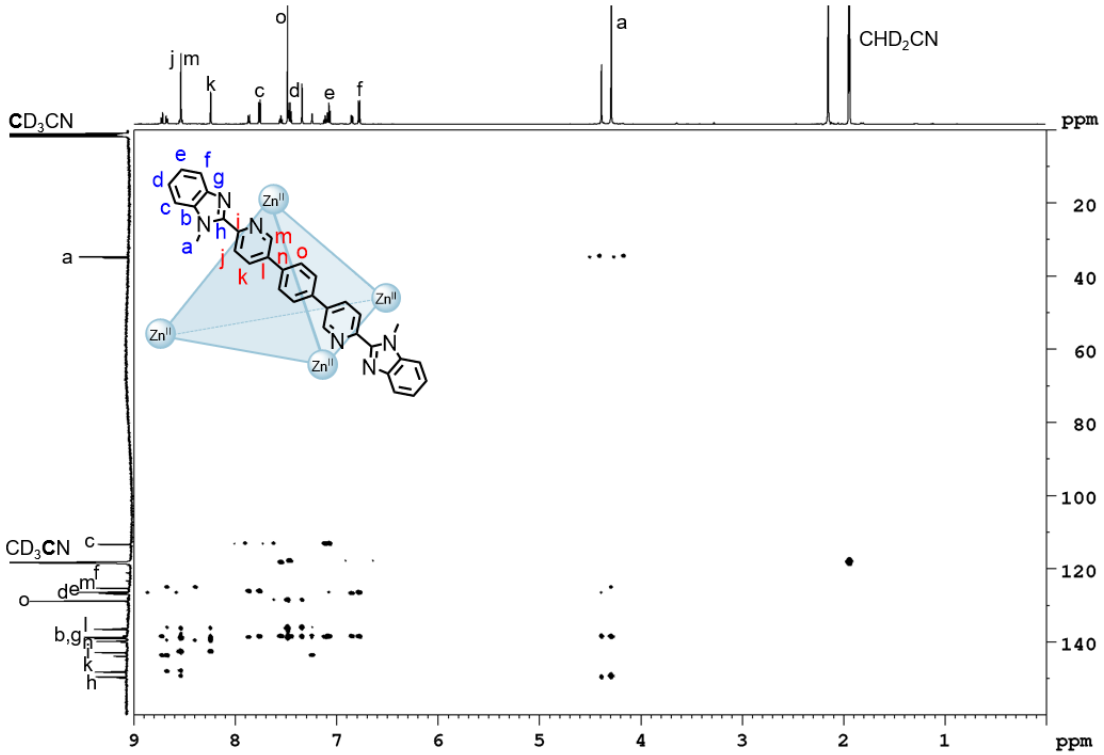

Figure S126. ^{1}H-^{13}C HMBC NMR spectrum (600 MHz/151 MHz, CD_3CN, 298 K) of cage **40a** and helicate **40b**. For clarity, only the signals for cage **40a** are labelled.

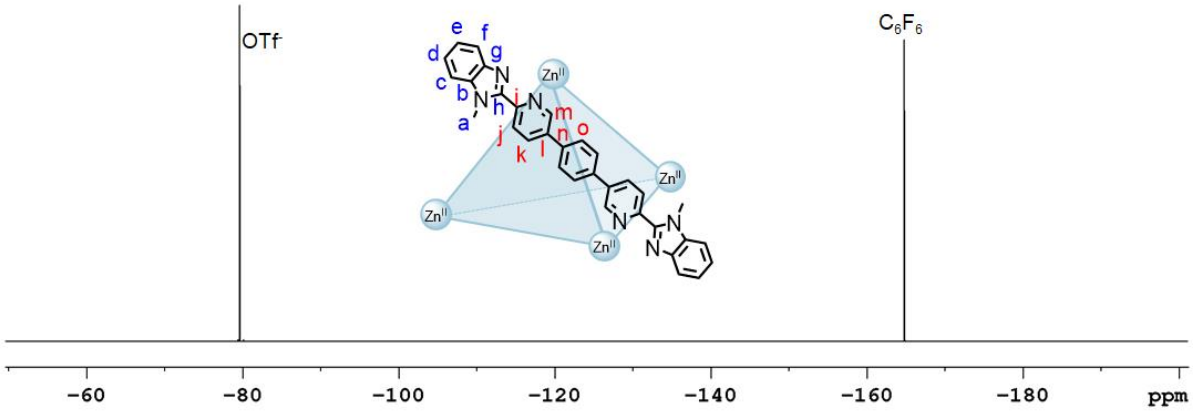

Figure S127. ^{19}F NMR spectrum (471 MHz, CD_3CN, 298 K, C_6F_6) of cage **40a** and helicate **40b**. For clarity, only cage **40a** is depicted.

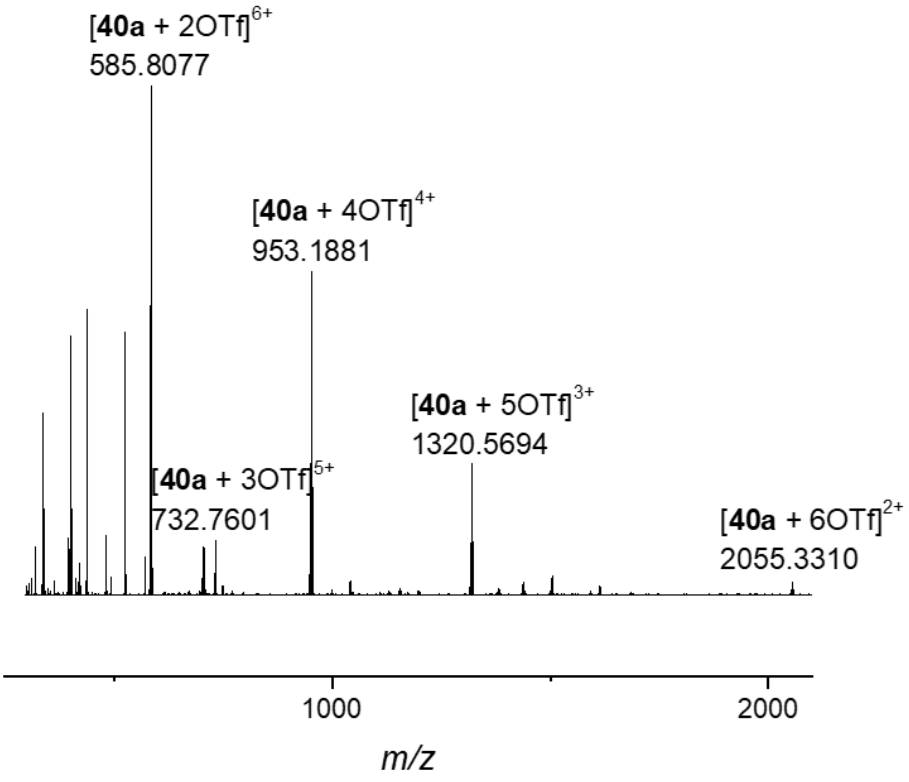

Figure S128. High resolution ESI mass spectrum of cage **40a** and helicate **40b**.

a)

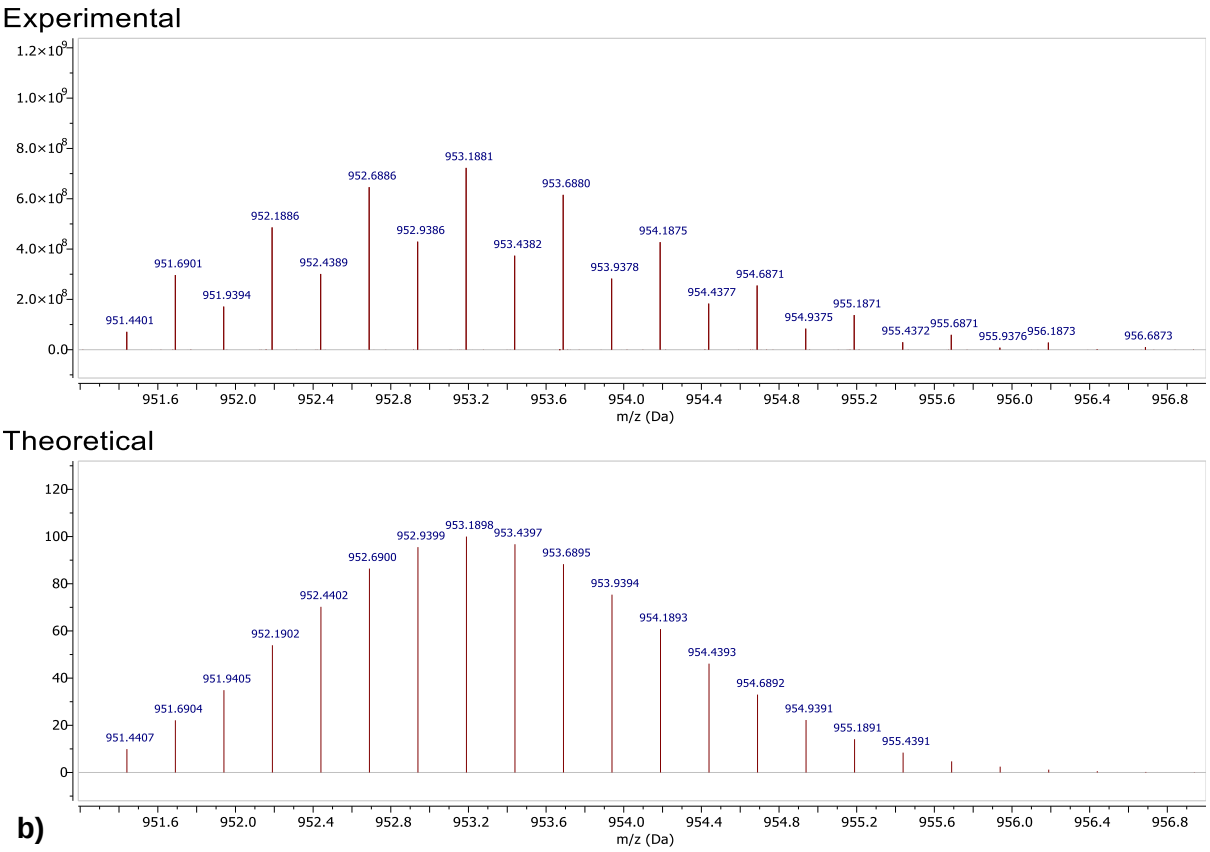

b)

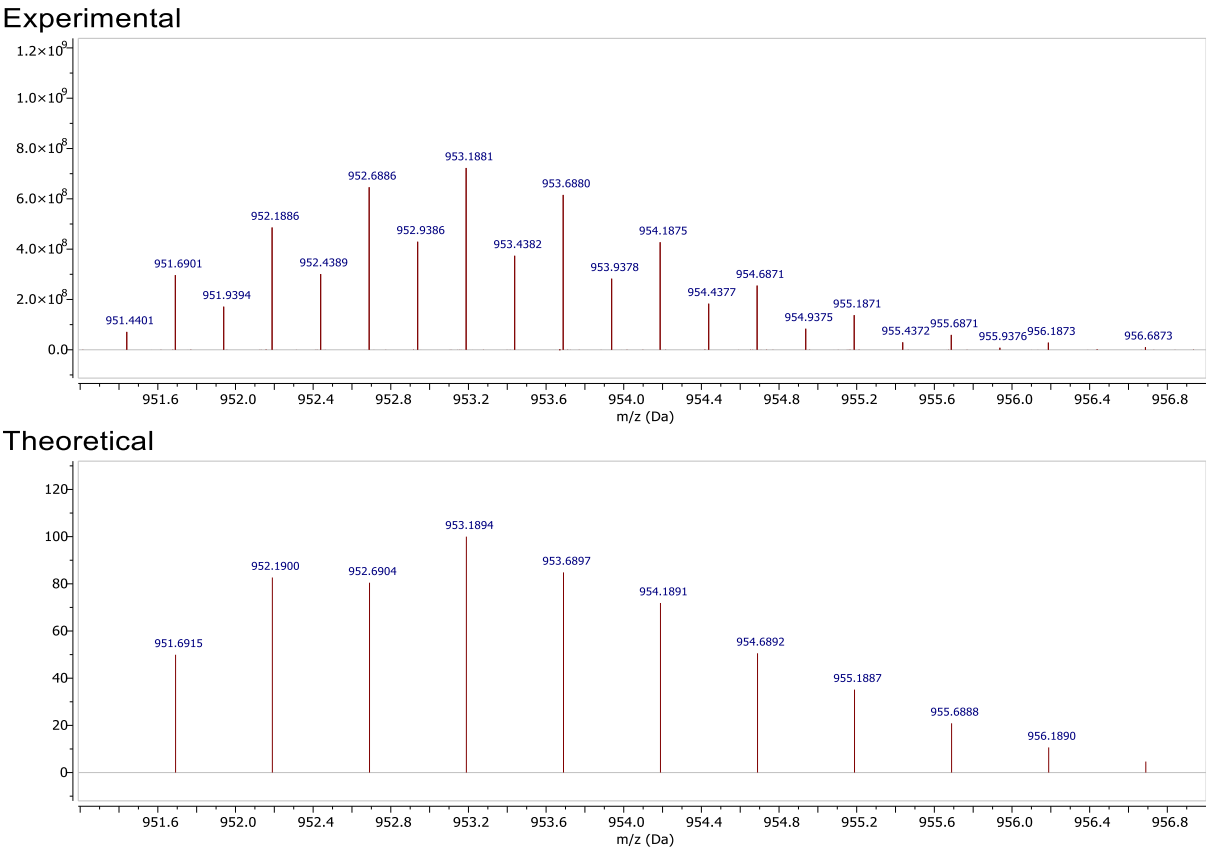

Figure S129. Isotopic patterns for a) cage **40a** and b) helicate **40b**: experimental (top) and theoretical (bottom).

3.8 Cage 41a and Helicate 41b

Zinc(II) triflate (2.06 mg, 5.67 µmol) and 1,4-di(6''-(1'-methyl-1*H*-benzo[*d*]imidazol-2'-yl)pyridin-3''-yl)-2,5-difluorobenzene (**32**) (4.36 mg, 8.25 µmol) were dissolved in CD_3CN (500 µL) and heated for 24 h at 50 °C to prepare cage **41a** and helicate **41b** *in situ*.

3.8.1 Cage **41a**

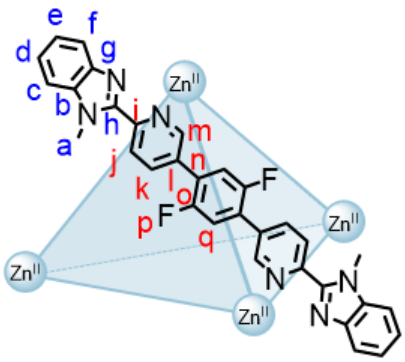

^{1}H NMR (600 MHz, CD_3CN, 298 K) δ (ppm): 8.48 (d, ^3J = 8.5 Hz, 12H, H_j), 8.38 (d, ^4J = 2.2 Hz, 12H, H_m), 8.33 (dd, ^3J = 8.5 Hz, ^4J = 2.2 Hz, 12H, H_k), 7.75 (dt, ^3J = 8.4 Hz, ^4J = 0.9 Hz, 12H, H_c), 7.46 (ddd, ^3J = 8.4 Hz, ^3J = 7.3 Hz, ^4J = 0.9 Hz, 12H, H_d), 7.32 (t, ^3J = 8.7 Hz, 12H, H_q), 7.09 (ddd, ^3J = 8.4 Hz, ^3J = 7.3 Hz, ^4J = 0.9 Hz, 12H, H_e), 6.80 (dt, ^3J = 8.4 Hz, ^4J = 0.9 Hz, 12H, H_f), 4.27 (s, 36H, H_a).

^{13}C NMR (151 MHz, CD_3CN, 298 K) δ (ppm): 157.5 ($C_{n/o}$), 155.9 ($C_{n/o}$), 150.1 (C_m), 149.4 (C_h), 143.3 (C_i), 141.6 (C_k), 138.7 (C_g), 138.6 (C_b), 133.9 (C_l), 126.9 (C_d), 126.5 (C_e), 125.3 (C_j), 118.2 (C_f), 113.4 (C_c), 34.5 (C_a).

^{19}F NMR (471 MHz, CD_3CN, 298 K, C_6F_6) δ (ppm): -79.7 (OTf^-), -122.9 (F_p).

HRMS (ESI): *m/z* = 2163.7752 [**41a** + 6OTf]$^{2+}$, 1392.5314 [**41a** + 5OTf]$^{3+}$, 1007.1598 [**41a** + 4OTf]$^{4+}$, 775.9372 [**41a** + 3OTf]$^{5+}$, 621.4557 [**41a** + 2OTf]$^{6+}$, 511.8260 [**41a** + OTf]$^{7+}$, 428.8537 [**41a**]$^{8+}$.

While the signals at *m/z* 511.8260 and 428.8537 are consistent with the 7+ and 8+ charges, respectively for the cage, the theoretical isotopic pattern do not match, possibly due to fragmentation in the gas phase or overlap with other signals.

3.8.2 Helicate **41b**

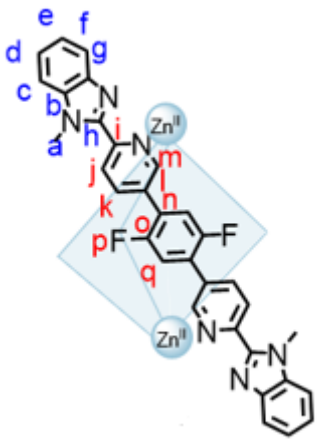

Due to the low quantity of helicate present, full characterisation of the helicate by NMR spectroscopy was not possible.

HRMS (ESI): *m/z* = 1007.1598 [**41b** + 2OTf]$^{2+}$, 621.4557 [**41b** + OTf]$^{3+}$, 428.8546 [**41b**]$^{4+}$.

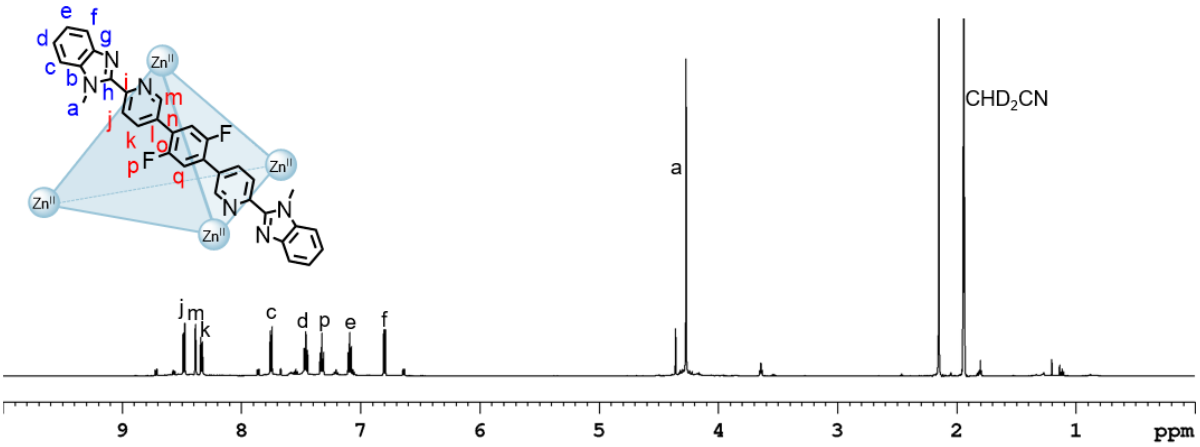

Figure S130. ^{1}H NMR spectrum (600 MHz, CD_3CN, 298 K) of cage **41a** and helicate **41b**. For clarity, only the signals for cage **41a** are labelled.

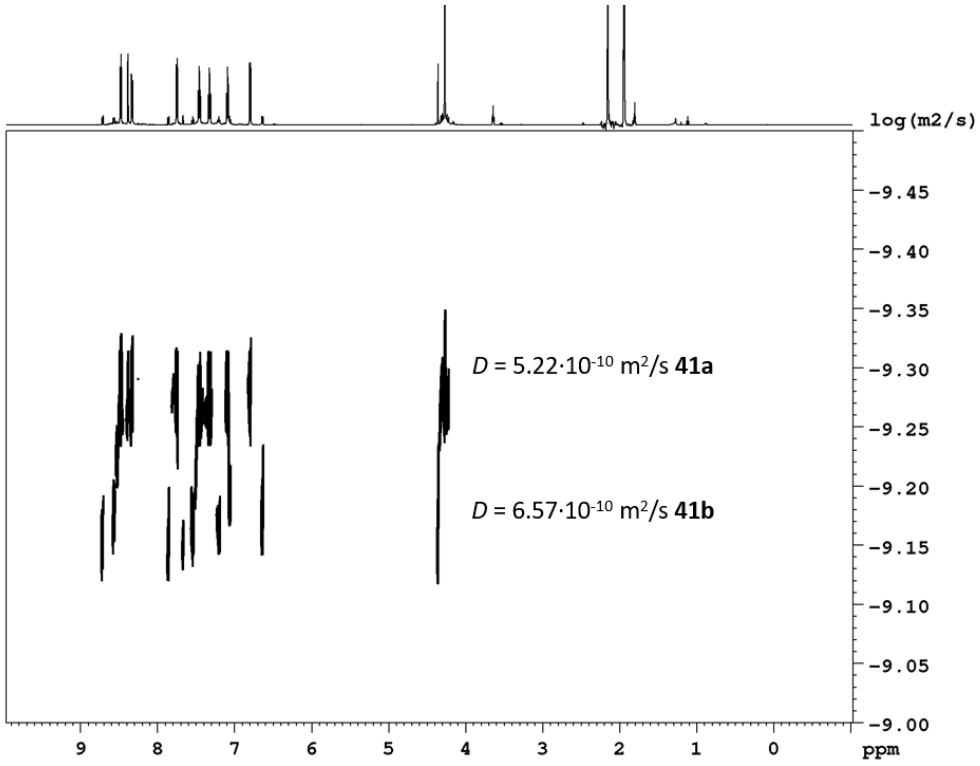

Figure S131. ^{1}H DOSY spectrum (600 MHz, CD_3CN, 298 K) of cage **41a** (D = 5.22·10^{-10} m^2/s) and helicate **41b** (D = 6.57·10^{-10} m^2/s).

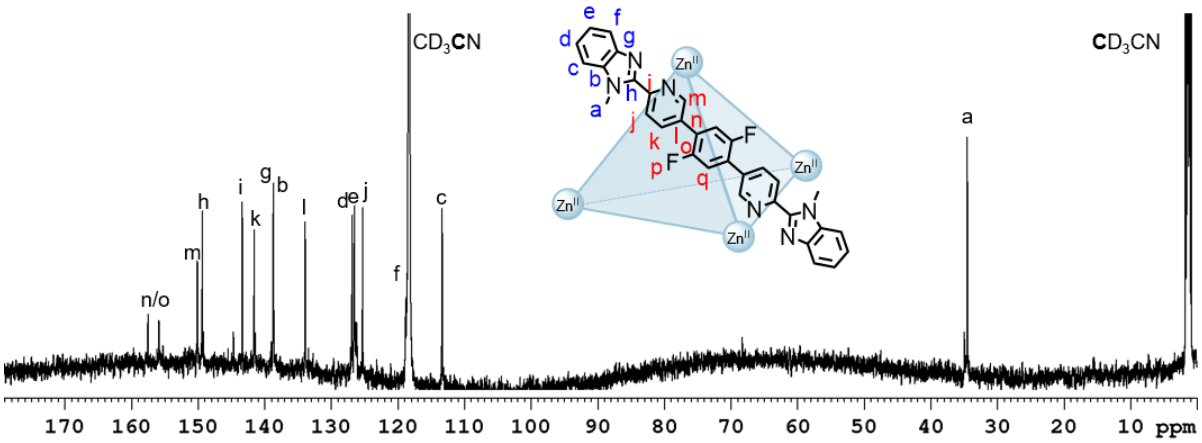

Figure S132. ^{13}C NMR spectrum (151 MHz, CD_3CN, 298 K) of cage **41a** and helicate **41b**. For clarity, only the signals for cage **41a** are labelled.

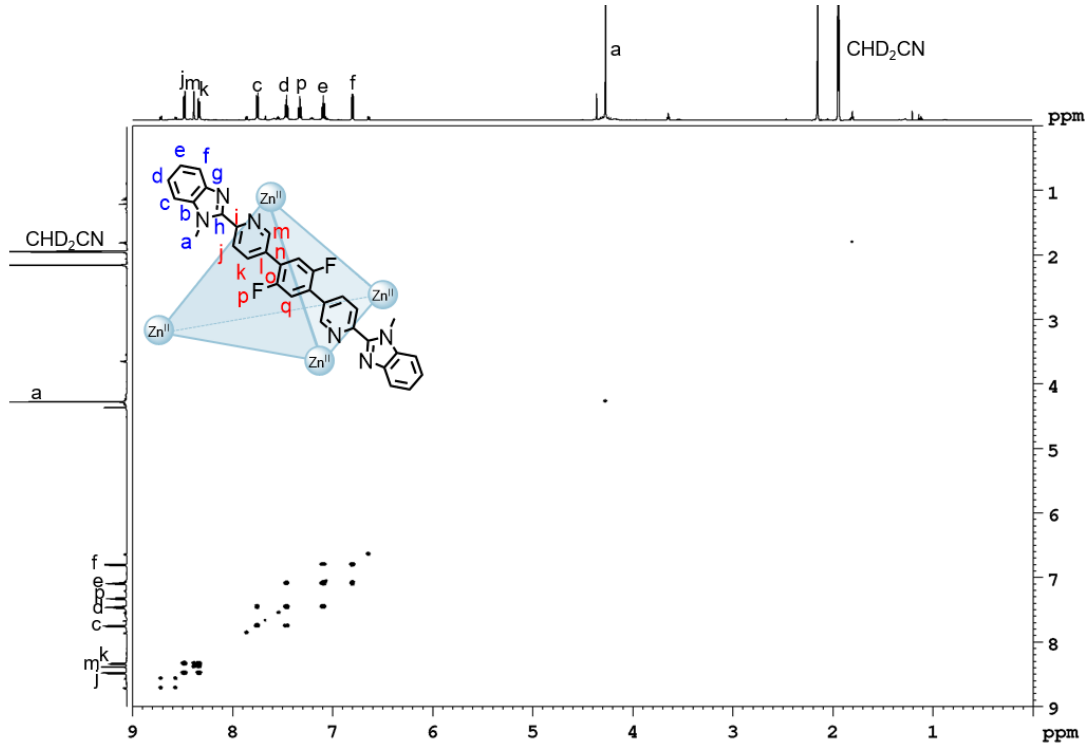

Figure S133. ^{1}H-^{1}H COSY NMR spectrum (600 MHz, CD_3CN, 298 K) of cage **41a** and helicate **41b**. For clarity, only the signals for cage **41a** are labelled.

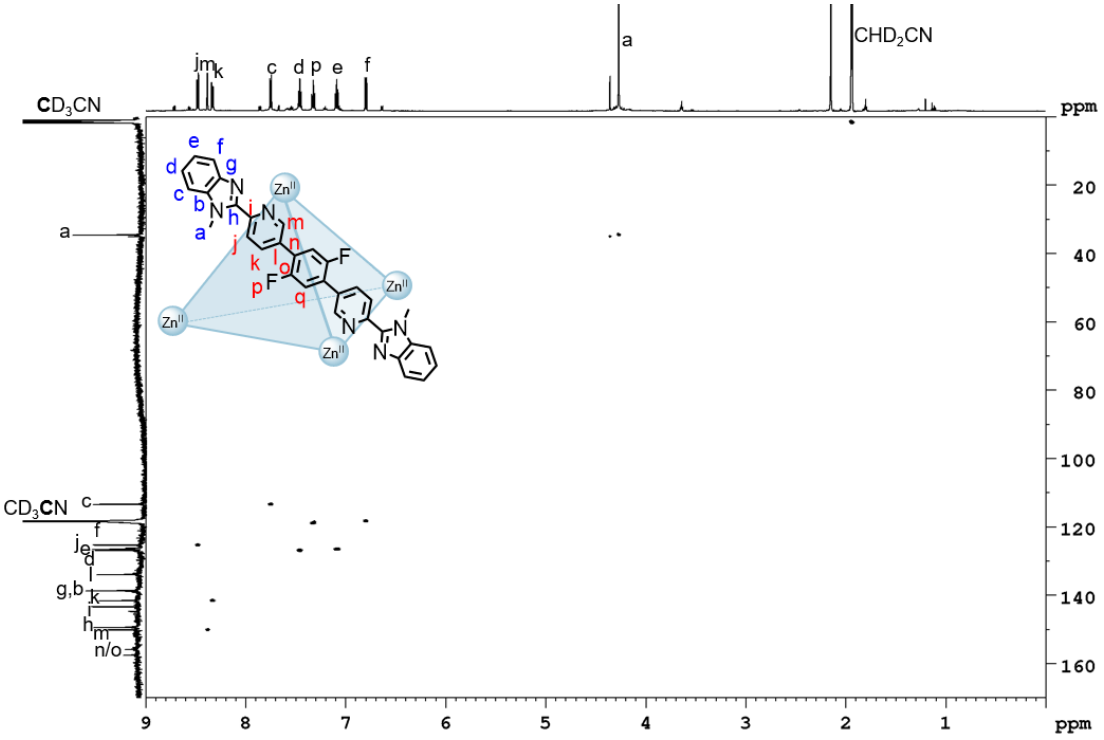

Figure S134. ^{1}H-^{13}C HSQC NMR spectrum (600 MHz/151 MHz, CD_3CN, 298 K) of cage **41a** and helicate **41b**. For clarity, only the signals for cage **41a** are labelled.

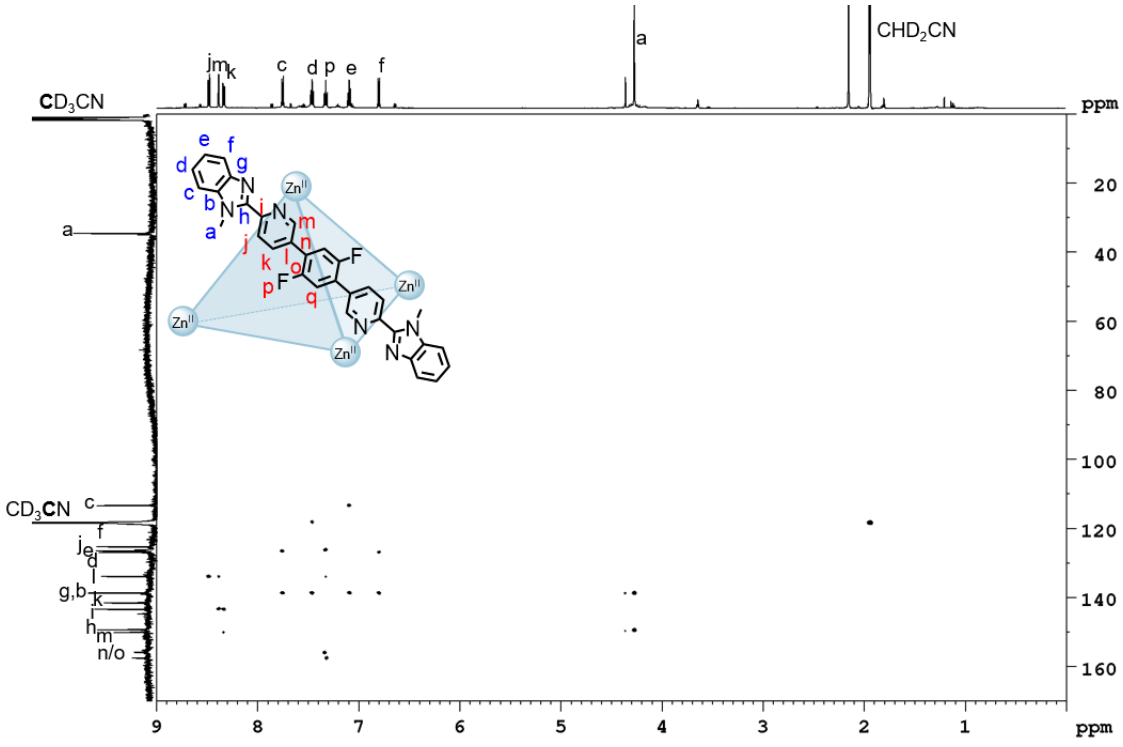

Figure S135. ^{1}H-^{13}C HMBC NMR spectrum (600 MHz/151 MHz, CD_3CN, 298 K) of cage **41a** and helicate **41b**. For clarity, only the signals for cage **41a** are labelled.

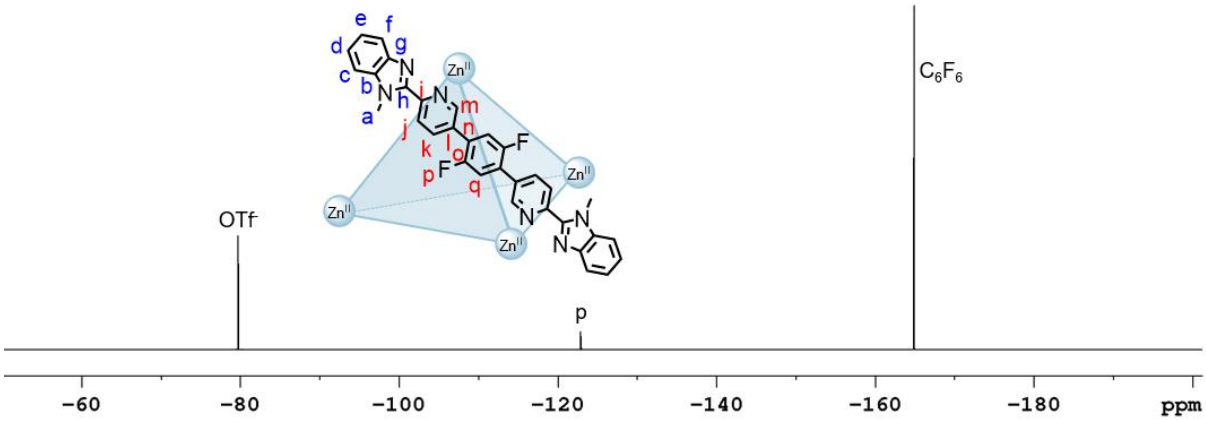

Figure S136. ^{19}F NMR spectrum (471 MHz, CD_3CN, 298 K, C_6F_6) of cage **41a** and helicate **41b**. For clarity, only cage **41a** is depicted.

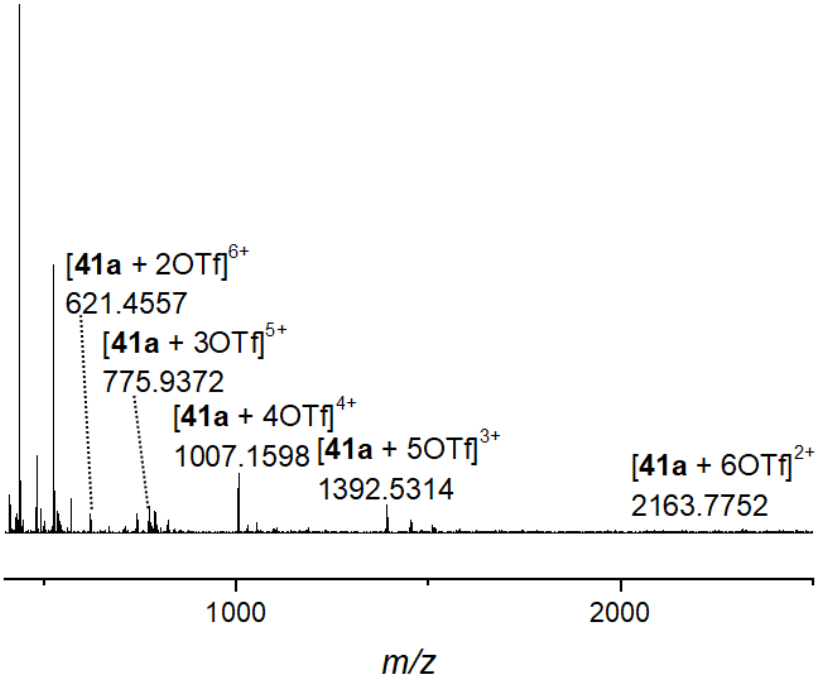

Figure S137. High resolution ESI mass spectrum of cage **41a** and helicate **41b**.

a)

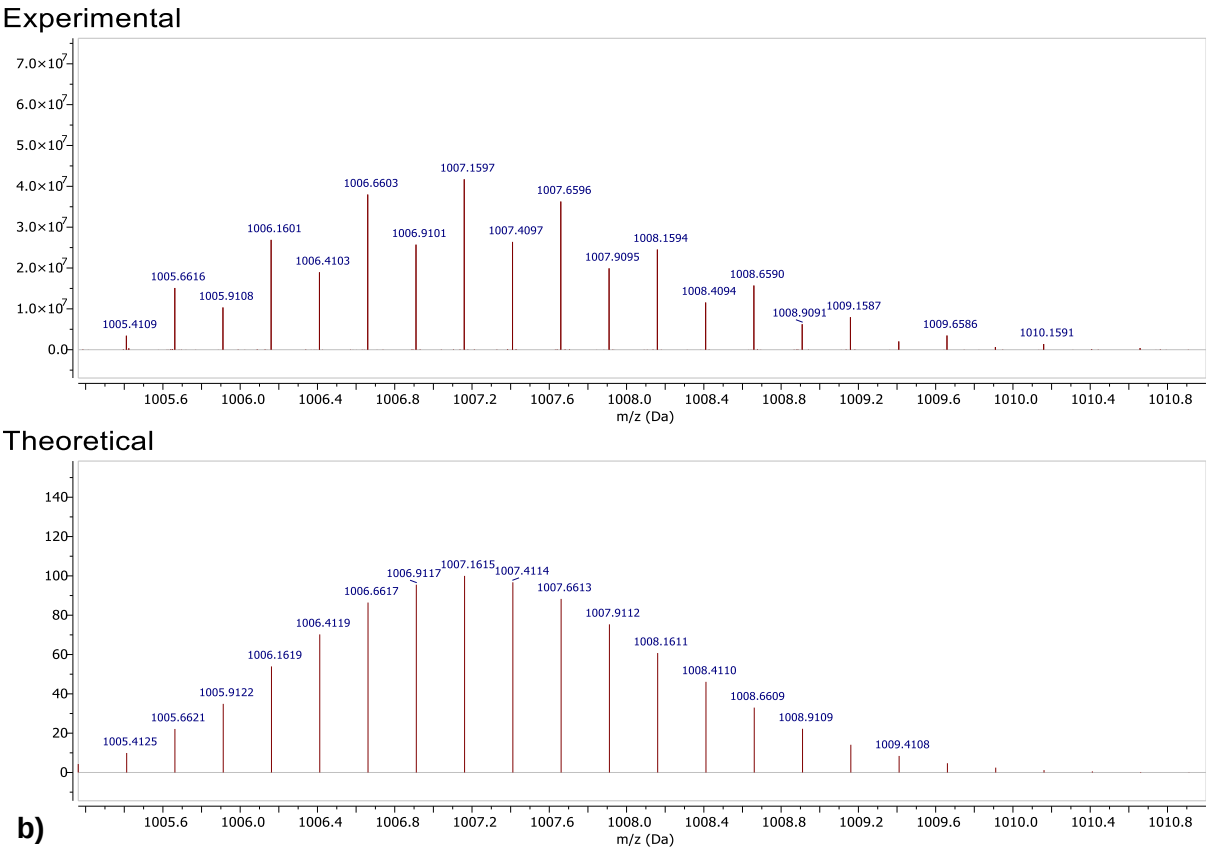

b)

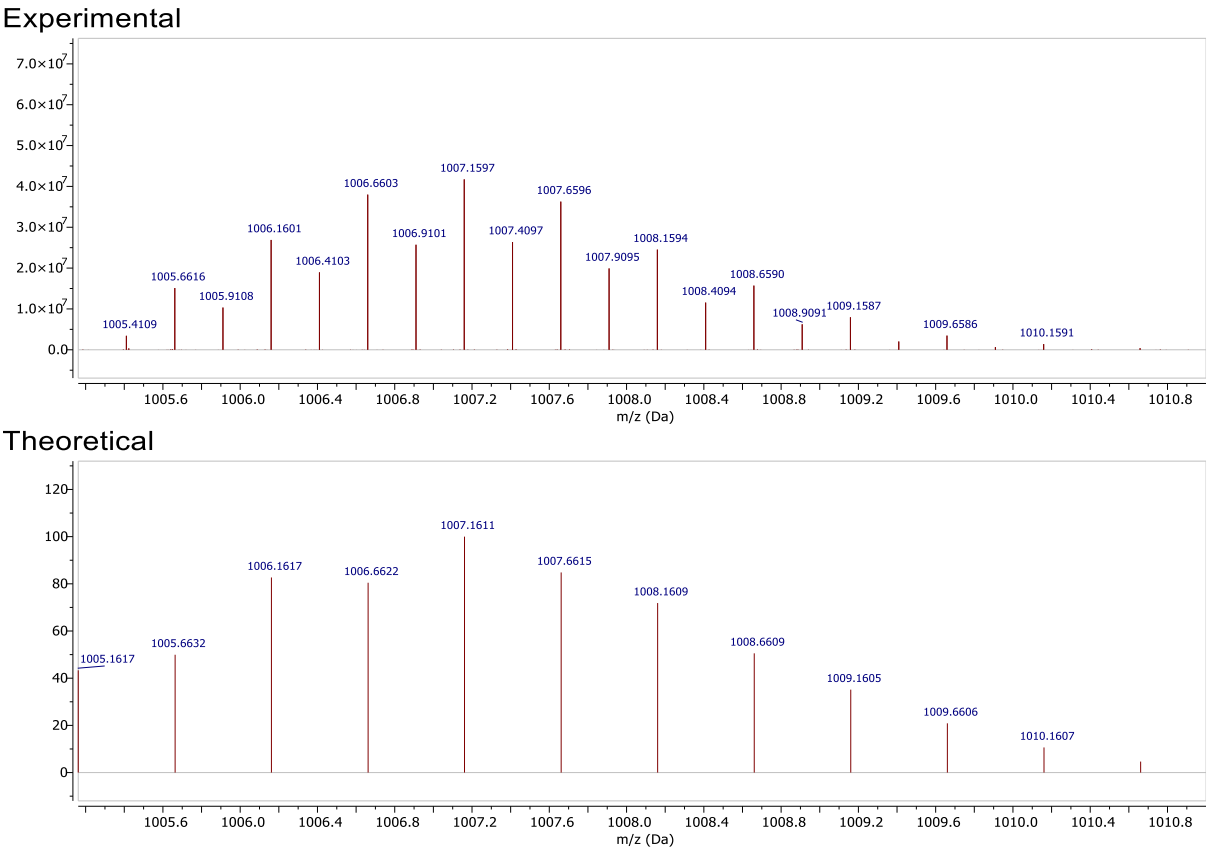

Figure S138. Isotopic patterns for a) cage **41a** and b) helicate **41b**: experimental (top) and theoretical (bottom).

3.9 Cage 42

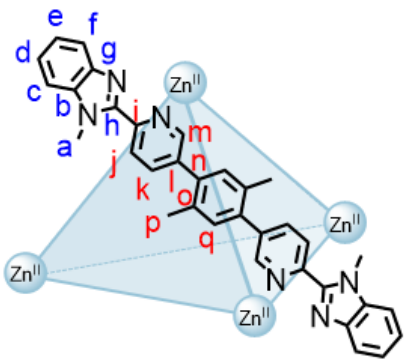

Zinc(II) triflate (2.00 mg, 5.50 µmol) and 1,4-di(6''-(1'-methyl-1*H*-benzo[*d*]imidazol-2'-yl)pyridin-3''-yl)-2,5-dimethylbenzene (**30**) (4.30 mg, 8.25 µmol) were dissolved in CD_3CN (500 µL) and heated for 24 h at 50 °C to prepare cage **42** *in situ*.

^{1}H NMR (500 MHz, CD_3CN, 298 K) δ (ppm): 8.40 (dd, ^3J = 8.4 Hz, ^5J = 0.7 Hz, 12H, H_j), 8.35 (dd, ^4J = 2.2 Hz, ^5J = 0.7 Hz, 12H, H_m), 8.11 (dd, ^3J = 8.4 Hz, ^4J = 2.2 Hz, 12H, H_k), 7.75 (dt, ^3J = 8.4 Hz, ^4J = 1.0 Hz, 12H, H_c), 7.45 (ddd, ^3J = 8.4 Hz, ^3J = 7.3 Hz, ^4J = 1.0 Hz, 12H, H_d), 7.06 (ddd, ^3J = 8.4 Hz, ^3J = 7.3 Hz, ^4J = 1.0 Hz, 12H, H_e), 7.06 (s, 12H, H_q), 6.63 (dt, ^3J = 8.4 Hz, ^4J = 1.0 Hz, 12H, H_f), 4.23 (s, 36H, H_a), 1.92 (s, 36H, H_p).

^{13}C NMR (125 MHz, CD_3CN, 298 K) δ (ppm): 149.8 (C_m), 149.5 (C_h), 142.7 (C_i), 142.5 (C_k), 140.8 (C_l), 138.7 (C_b), 138.6 (C_g), 137.0 (C_n), 134.4 (C_o), 133.4 (C_q), 126.7 (C_d), 126.5 (C_e), 125.2 (C_j), 118.1 (C_f), 113.3 (C_c), 34.6 (C_a), 20.0 (C_p).

^{19}F NMR (471 MHz, CD_3CN, 298 K, C_6F_6) δ (ppm): -79.6 (OTf^-).

HRMS (ESI): *m/z* = 2139.9267 [**42** + 6OTf]$^{2+}$, 1376.6328 [**42** + 5OTf]$^{3+}$, 995.2357 [**42** + 4OTf]$^{4+}$, 766.3980 [**42** + 3OTf]$^{5+}$, 613.5062 [**42** + 2OTf]$^{6+}$, 504.4410 [**42** + OTf]$^{7+}$, 422.8914 [**42**]$^{8+}$.

While the signals at *m/z* 504.4410 and 422.8914 are consistent with the 7+ and 8+ charges, respectively for the cage, the theoretical isotopic pattern do not match, possibly due to fragmentation in the gas phase or overlap with other signals.

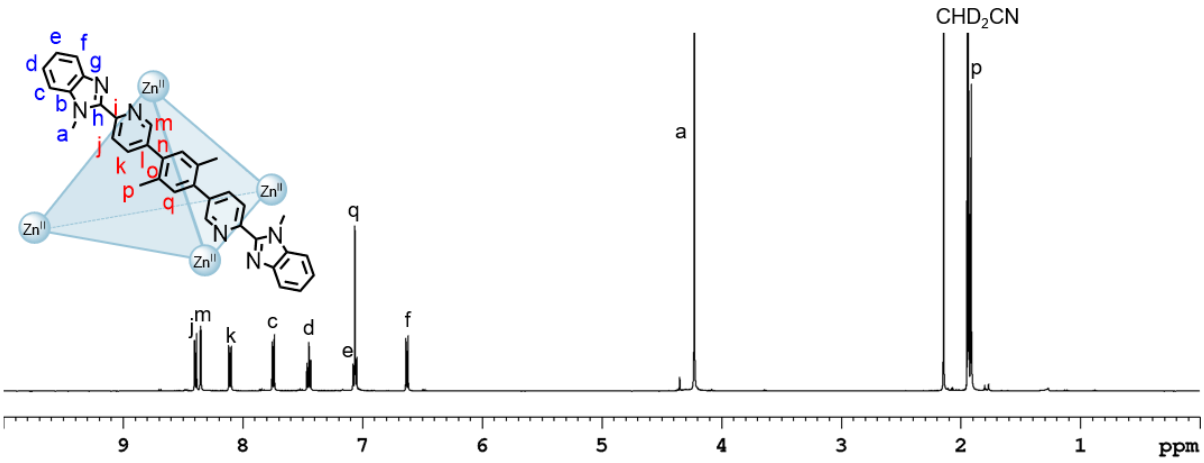

Figure S139. ^{1}H NMR spectrum (500 MHz, CD_3CN, 298 K) of cage **42**.

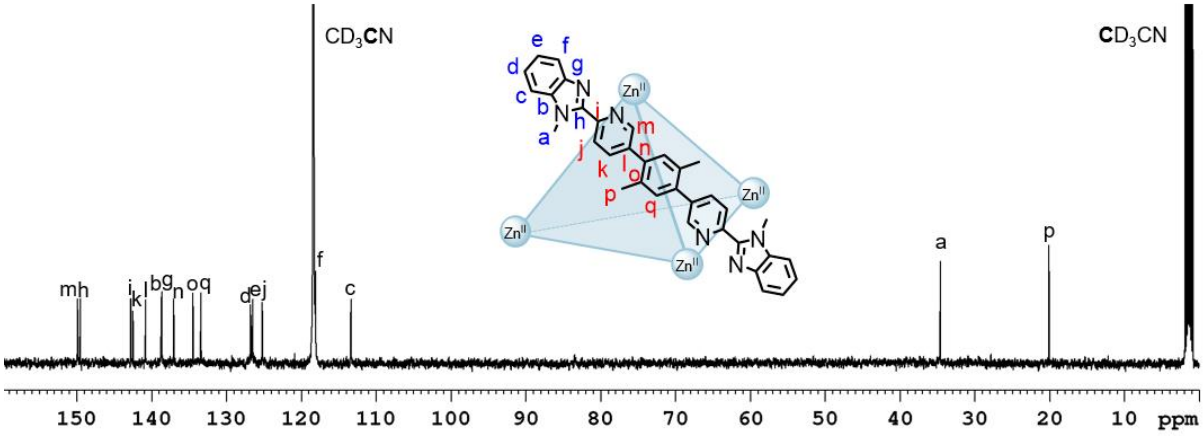

Figure S140. ^{13}C NMR spectrum (125 MHz, CD_3CN, 298 K) of cage **42**.

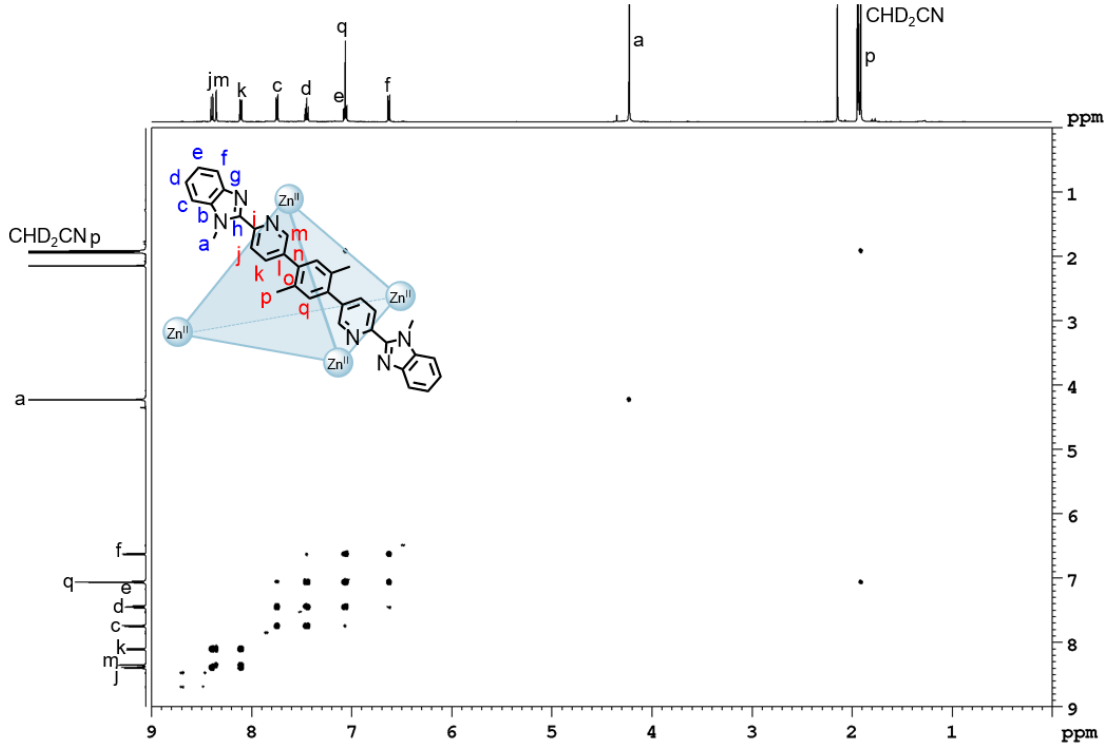

Figure S141. ^{1}H-^{1}H COSY NMR spectrum (500 MHz, CD_3CN, 298 K) of cage **42**.

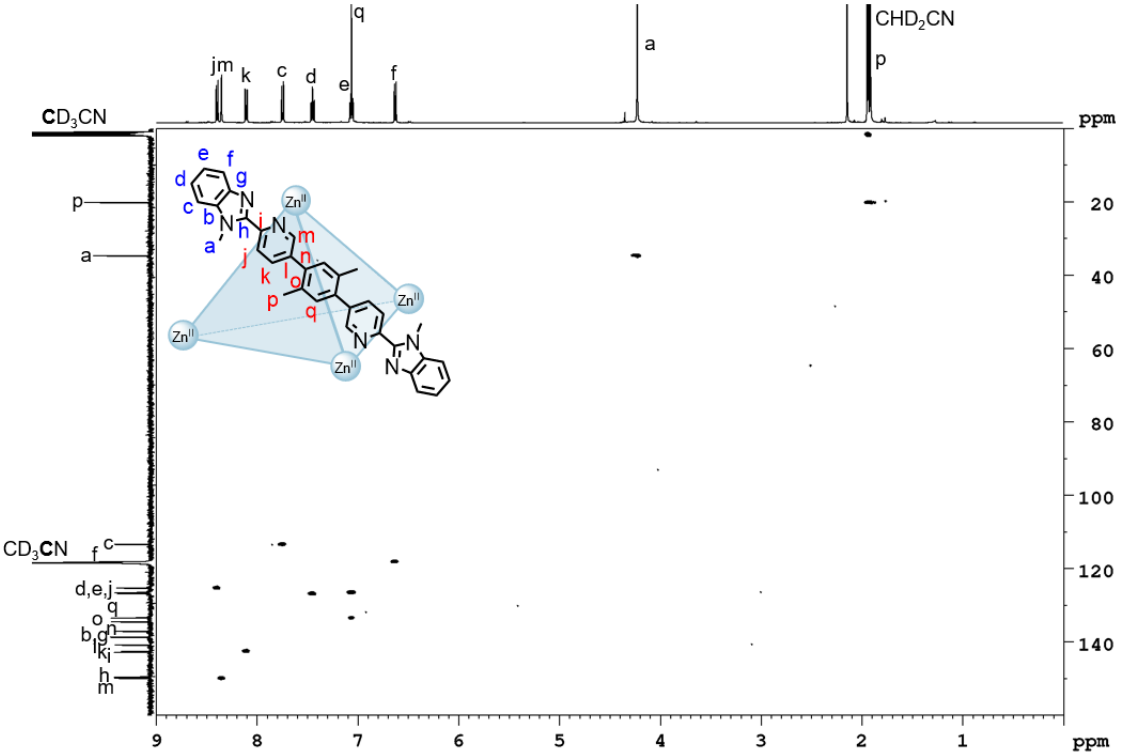

Figure S142. ^{1}H-^{13}C HSQC NMR spectrum (500 MHz/125 MHz, CD_3CN, 298 K) of cage **42**.

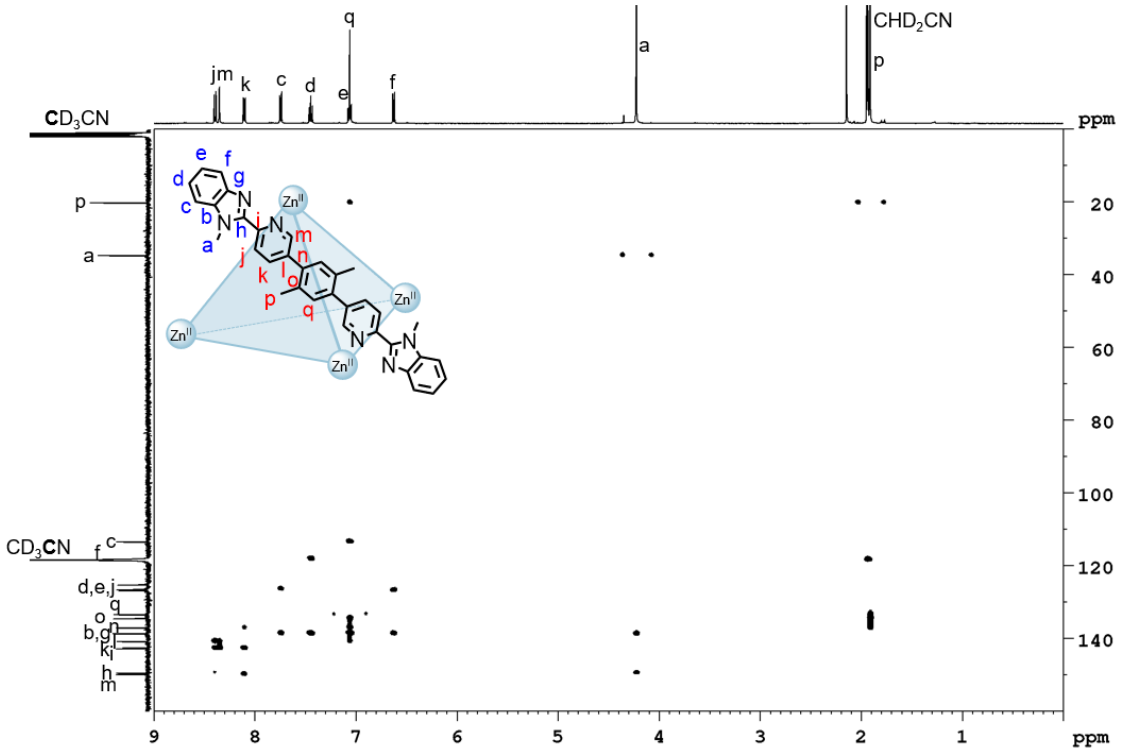

Figure S143. ^{1}H-^{13}C HMBC NMR spectrum (500 MHz/125 MHz, CD_3CN, 298 K) of cage **42**.

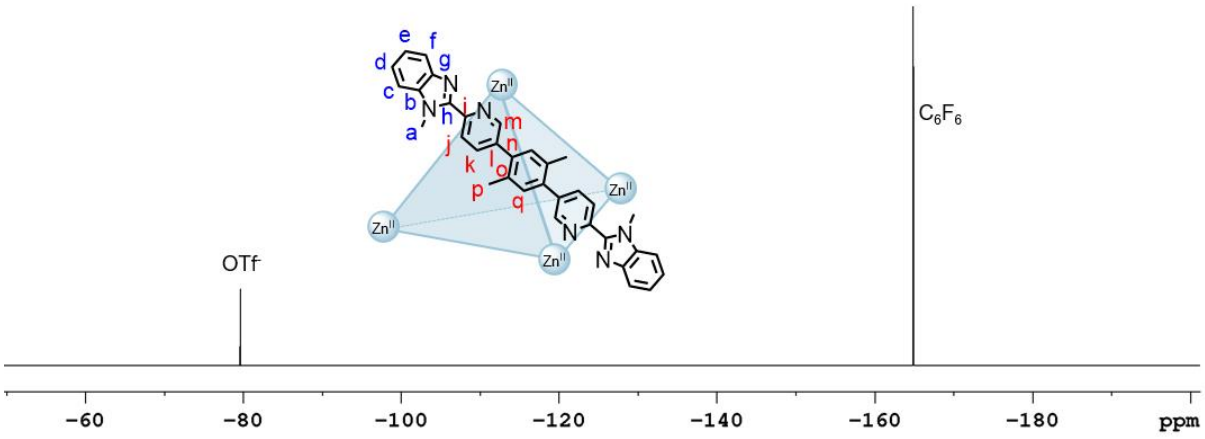

Figure S144. ^{19}F NMR spectrum (471 MHz, CD_3CN, 298 K, C_6F_6) of cage **42**.

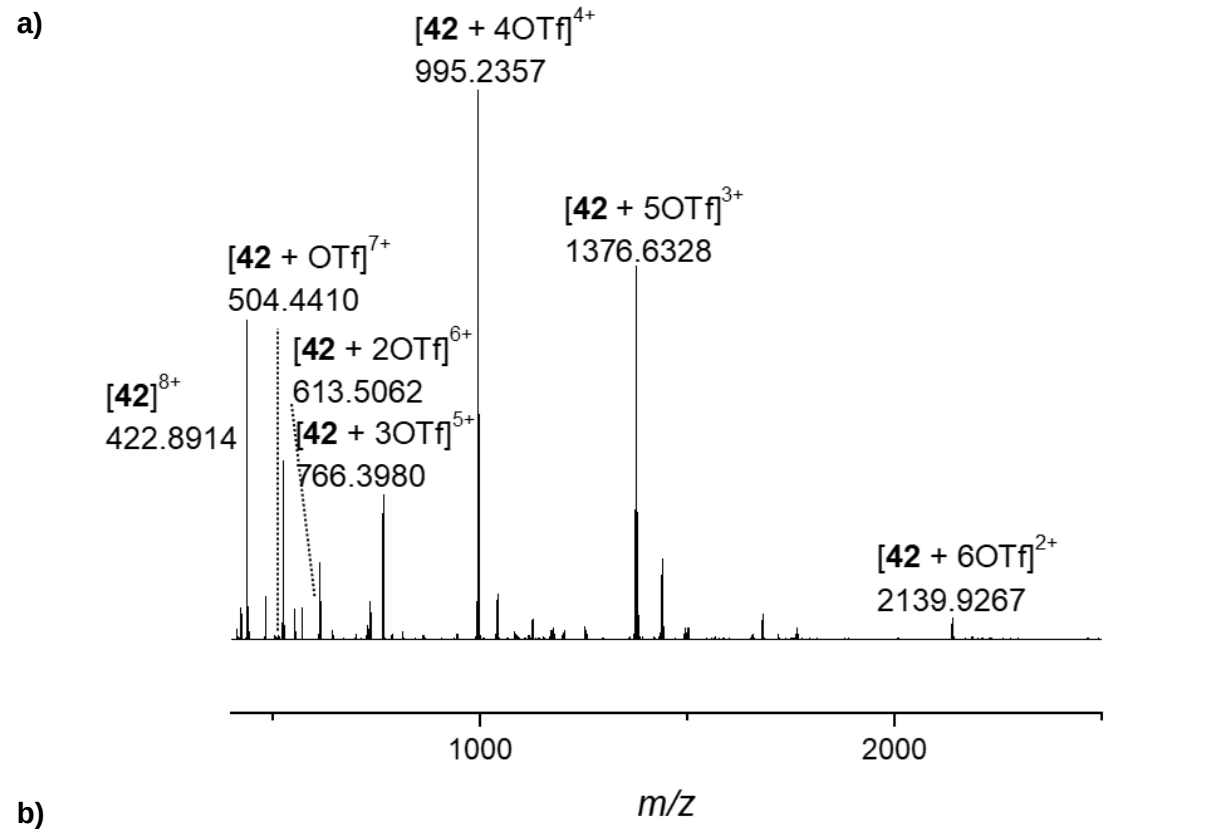

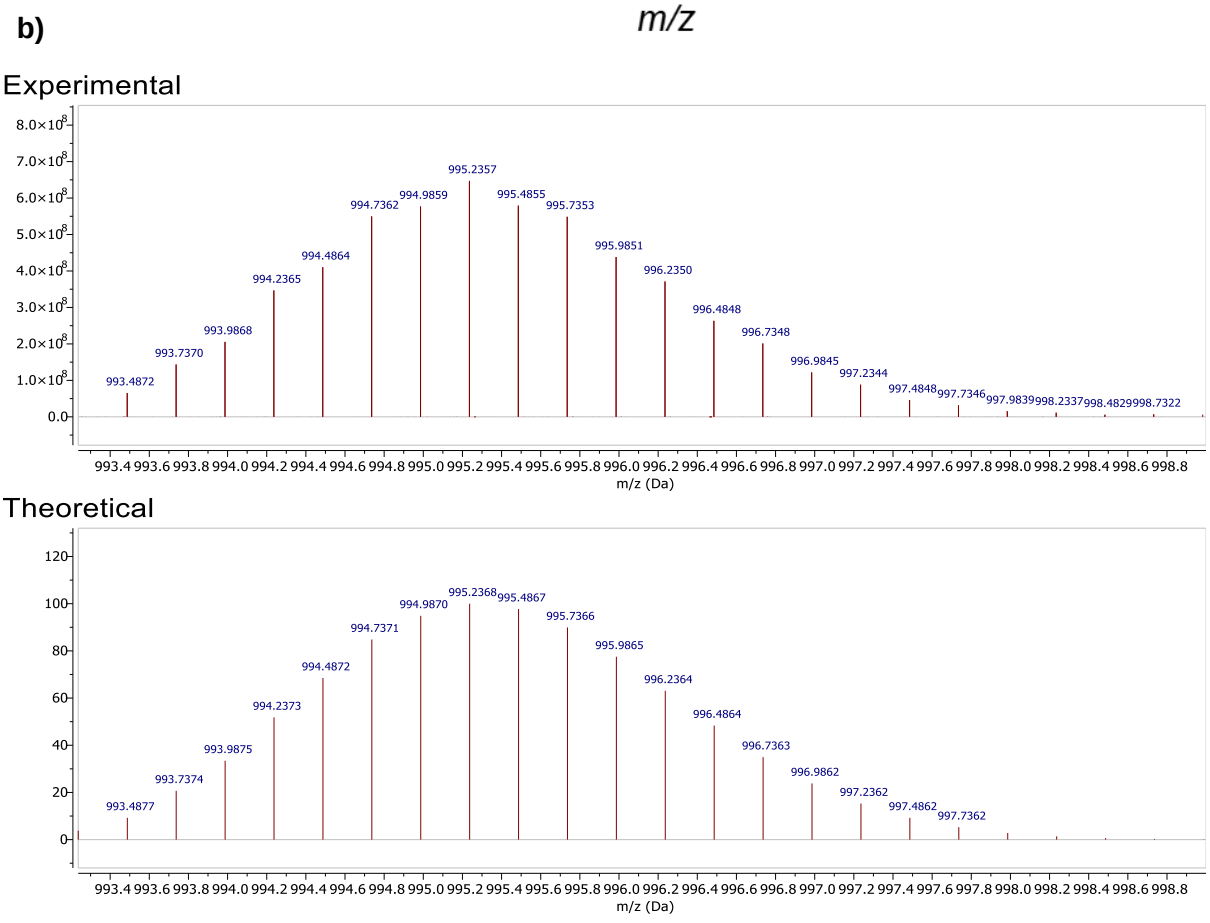

Figure S145. a) High resolution ESI mass spectrum of cage **42** and b) isotopic patterns of cage **42**: experimental (top) and theoretical (bottom).

3.10 Cage 43a and Helicate 43b

Zinc(II) triflate (1.99 mg, 5.47 µmol) and 1,2-di(4''-methyl-6''-(1'-methyl-1*H*-benzo[*d*]pyridine-2'-yl)pyridine-3''-yl)ethyne (**22**) (3.85 mg, 8.22 µmol) were dissolved in CD_3CN (500 µL) and heated for 74.5 h at 50 °C to prepare cage **43a** and helicate **43b** *in situ*.

3.10.1 Cage 43a

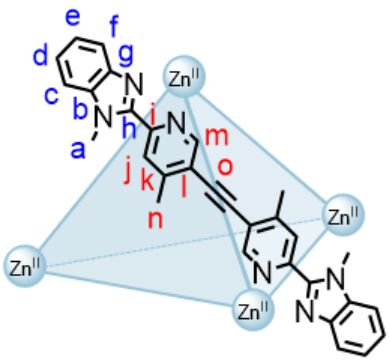

^{1}H NMR (500 MHz, CD_3CN, 298 K) δ (ppm): 8.18 (s, 12H, H_j), 7.97 (s, 12H, H_m), 7.77 (dt, ^3J = 8.6 Hz, ^4J = 0.9 Hz, 12H, H_c), 7.47 (ddd, ^3J = 8.6 Hz, ^3J = 7.3 Hz, ^4J = 0.9 Hz, 12H, H_d), 7.09 (ddd, ^3J = 8.4 Hz, ^3J = 7.3 Hz, ^4J = 0.9 Hz, 12H, H_e), 6.73 (dt, ^3J = 8.4 Hz, ^4J = 0.9 Hz, 12H, H_f), 4.25 (s, 36H, H_a), 2.48 (s, 36H, H_n).

^{13}C NMR (125 MHz, CD_3CN, 298 K) δ (ppm): 156.6 (C_k), 152.0 (C_m), 149.4 (C_h), 143.2 (C_i), 138.7 ($C_{b,g}$), 127.1 (C_d), 126.7 (C_e), 125.6 (C_j), 123.2 (C_l), 118.2 (C_f), 113.5 (C_c), 94.0 (C_o), 34.7 (C_a), 21.3 (C_n).

^{19}F NMR (471 MHz, CD_3CN, 298 K, C_6F_6) δ (ppm): -79.6 (OTf^-).

HRMS (ESI): *m/z* = 1983.3310 [**43a** + 6OTf]$^{2+}$, 1272.5697 [**43a** + 5OTf]$^{3+}$, 917.1887 [**43a** + 4OTf]$^{4+}$, 703.7607 [**43a** + 3OTf]$^{5+}$, 561.8079 [**43a** + 2OTf]$^{6+}$.

While the signal at *m/z* 561.8079 is consistent with the 6+ charge for the cage, the theoretical isotopic pattern does not match, possibly due to fragmentation in the gas phase or overlap with other signals.

3.10.2 Helicate 43b

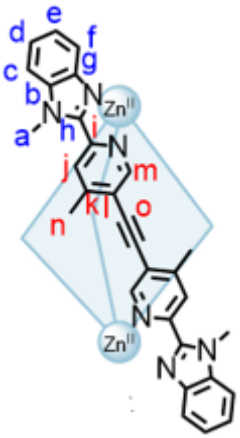

Due to the low quantity of helicate present and overlapping signals with cage **43a**, full characterisation of the helicate was not possible. Therefore, the NMR data below only includes proton and carbon atoms that could be assigned.

^{1}H NMR (500 MHz, CD_3CN, 298 K) δ (ppm): 8.41 (s, 6H, H_j), 7.82 (d, ^{3}J = 8.5 Hz, 6H, H_c), 7.52 (unres. ddd, 6H, H_d), 7.42 (s, 6H, H_m), 6.75 (unres. d, 6H, H_f), 4.31 (s, 18H, H_a), 2.65 (s, 18H, H_n).

^{13}C NMR (125 MHz, CD_3CN, 298 K) δ (ppm): 152.3 (C_m), 126.9 ($C_{j,d}$), 113.6 (C_c), 35.0 (C_a), 21.2 (C_n).

^{19}F NMR (471 MHz, CD_3CN, 298 K, C_6F_6) δ (ppm): -79.6 (OTf^-).

HRMS (ESI): *m/z* = 1982.3328 [**43b** + 3OTf]$^{+}$, 916.1884 [**43b** + 2OTf]$^{2+}$, 561.1414 [**43b** + OTf]$^{3+}$, 383.6179 [**43b**]$^{4+}$.

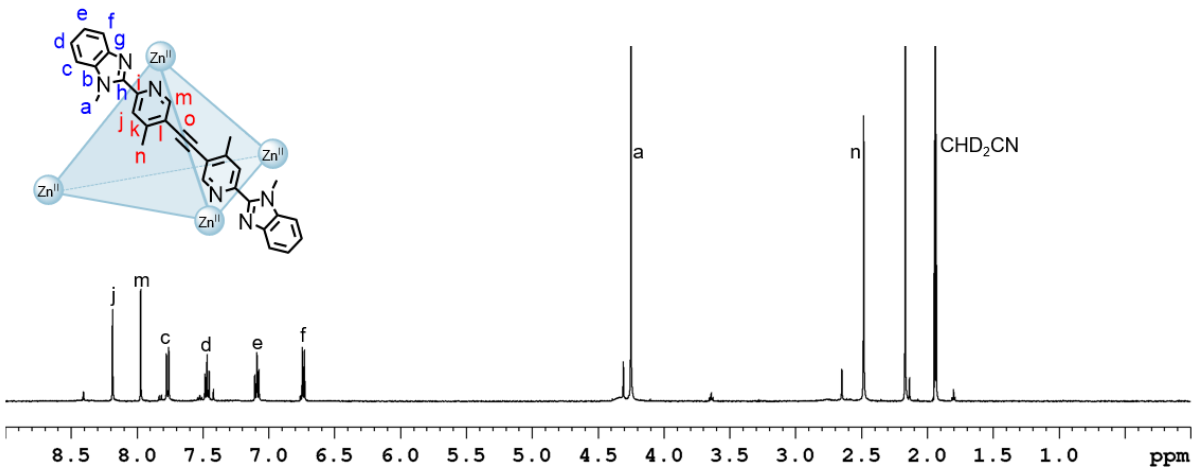

Figure S146. ^{1}H NMR spectrum (500 MHz, CD_3CN, 298 K) of cage **43a** and helicate **43b**. For clarity, only the signals for cage **43a** are labelled.

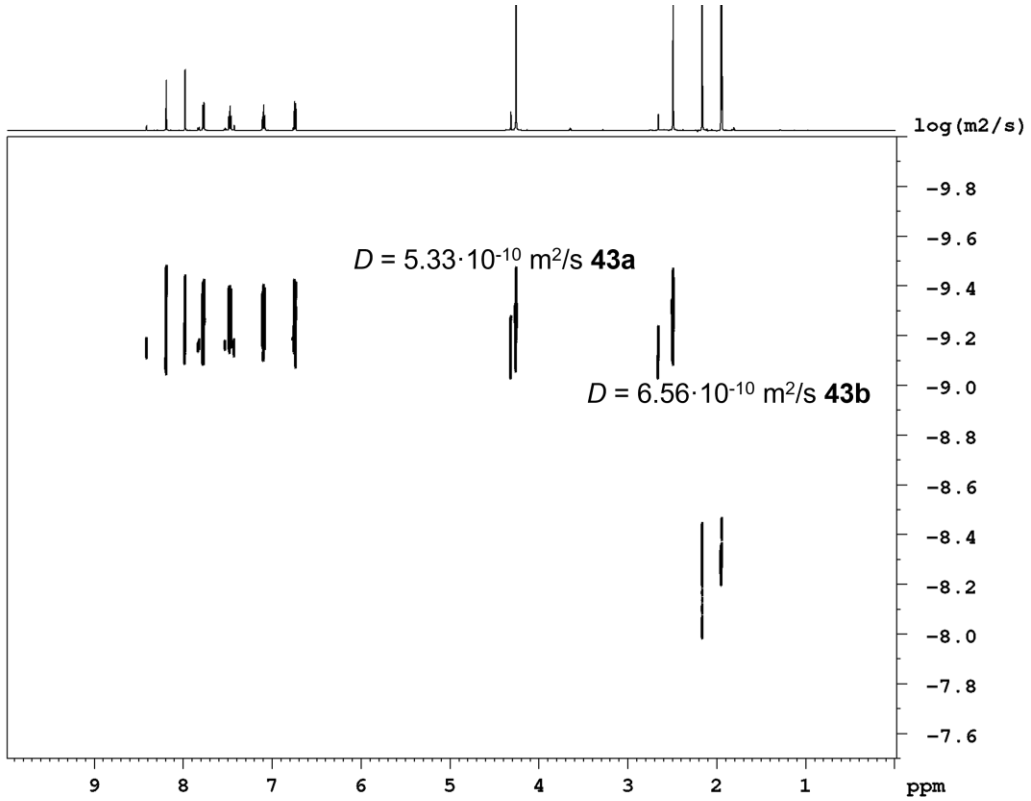

Figure S147. ^{1}H DOSY spectrum (600 MHz, CD_3CN, 298 K) of cage **43a** (D = 5.33·10^{-10} m^2/s) and helicate **43b** (D = 6.56·10^{-10} m^2/s).

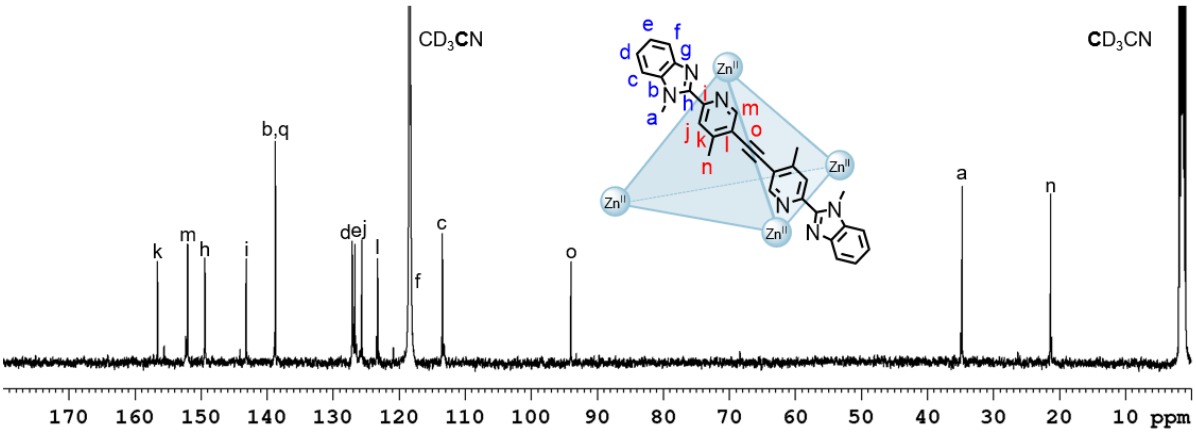

Figure S148. ^{13}C NMR spectrum (125 MHz, CD_3CN, 298 K) of cage **43a** and helicate **43b**. For clarity, only the signals for cage **43a** are labelled.

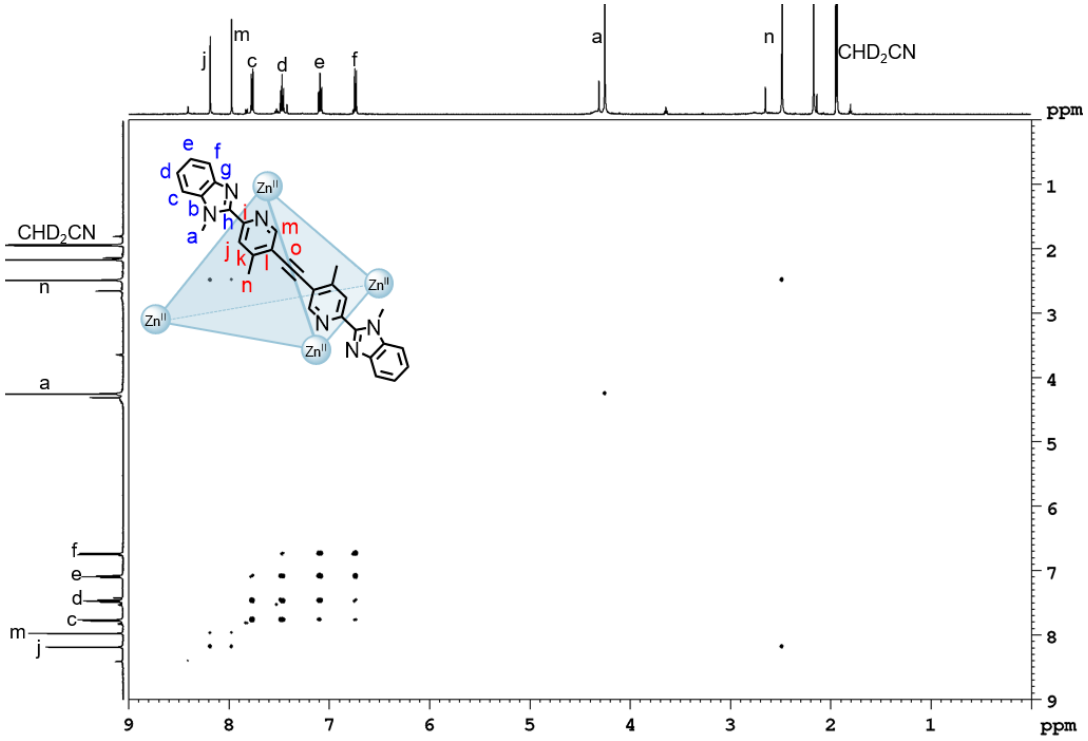

Figure S149. ^{1}H-^{1}H COSY NMR spectrum (500 MHz, CD_3CN, 298 K) of cage **43a** and helicate **43b**. For clarity, only the signals for cage **43a** are labelled.

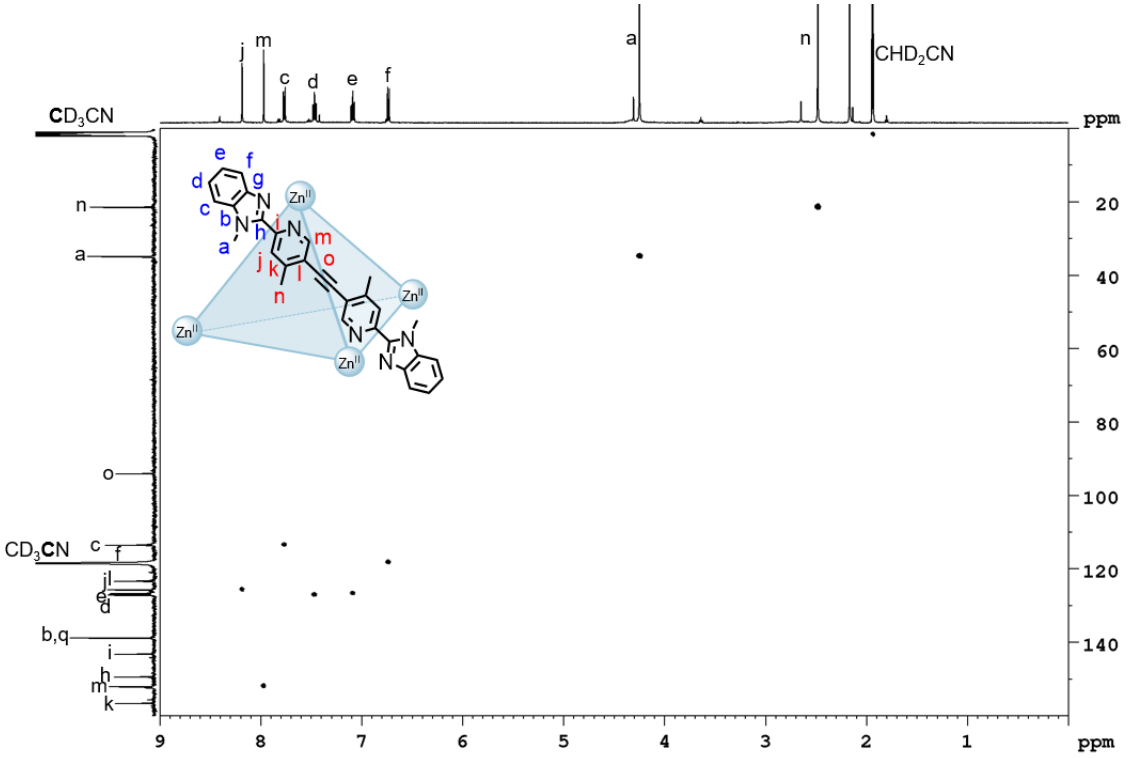

Figure S150. ^{1}H-^{13}C HSQC NMR spectrum (500 MHz/125 MHz, CD_3CN, 298 K) of cage **43a** and helicate **43b**. For clarity, only the signals for cage **43a** are labelled.

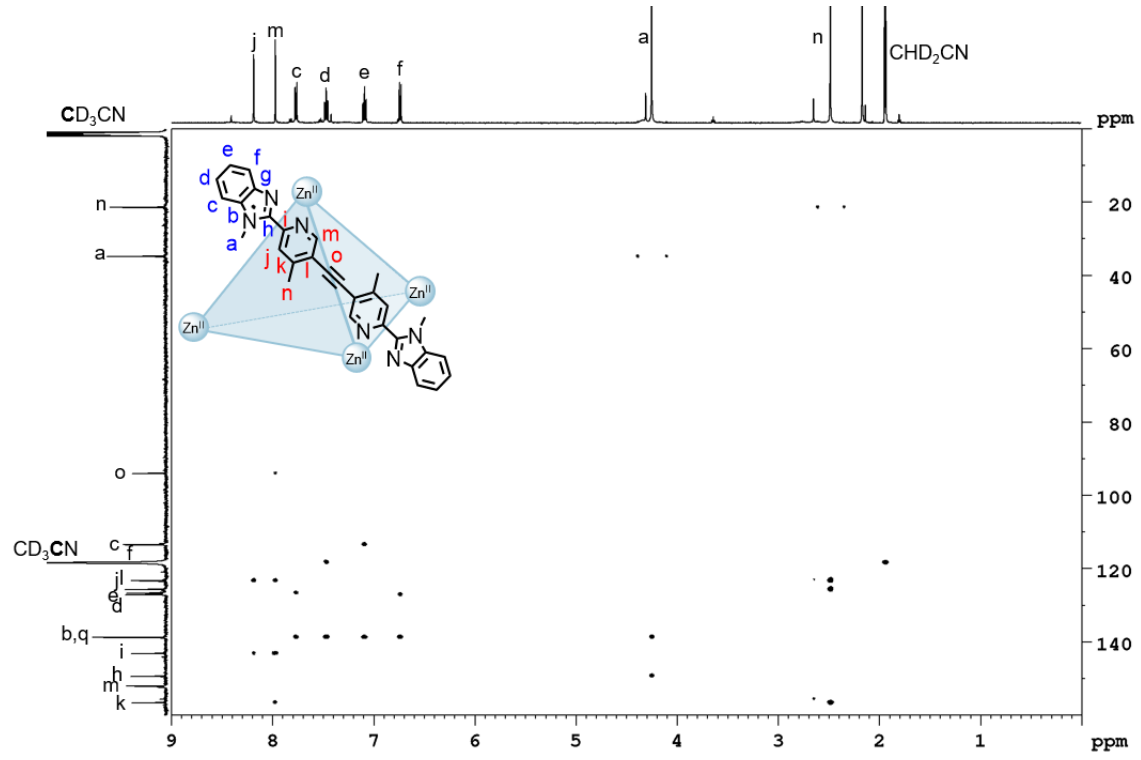

Figure S151. ^{1}H-^{13}C HMBC NMR spectrum (500 MHz/125 MHz, CD_3CN, 298 K) of cage **43a** and helicate **43b**. For clarity, only the signals for cage **43a** are labelled.

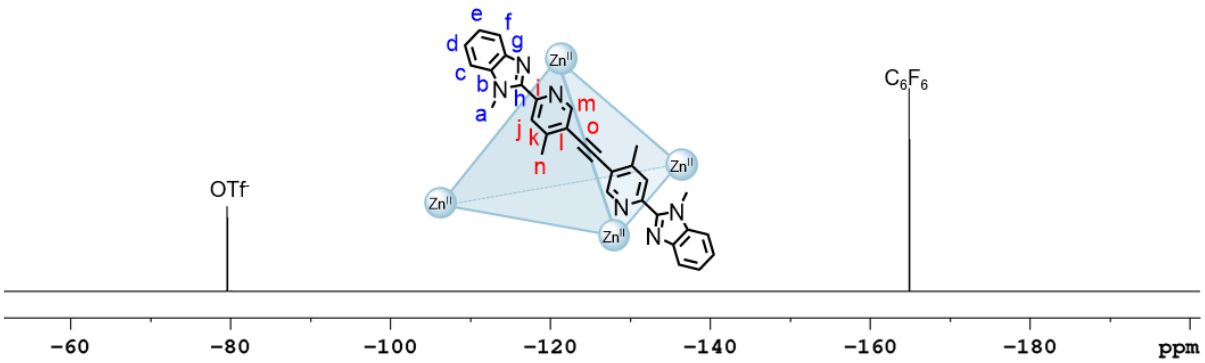

Figure S152. ^{19}F NMR spectrum (471 MHz, CD_3CN, 298 K, C_6F_6) of cage **43a** and helicate **43b**. For clarity, only cage **43a** is depicted.

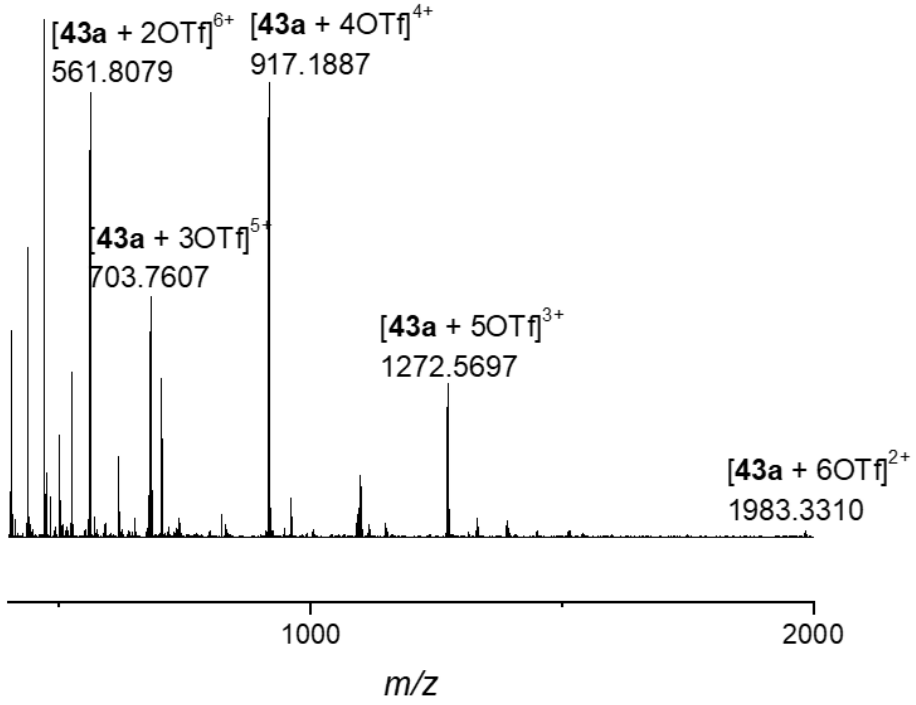

Figure S153. High resolution ESI mass spectrum of cage **43a** and helicate **43b**.

a)

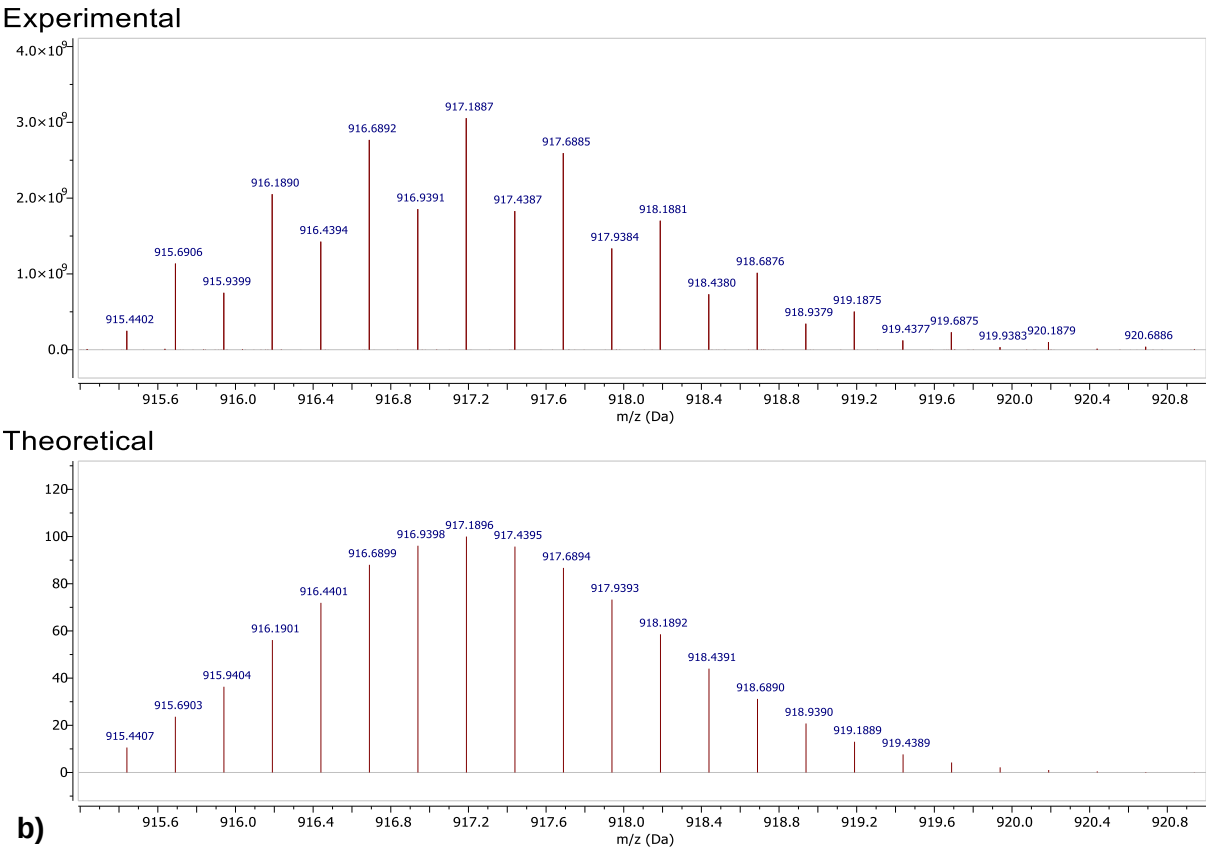

b)

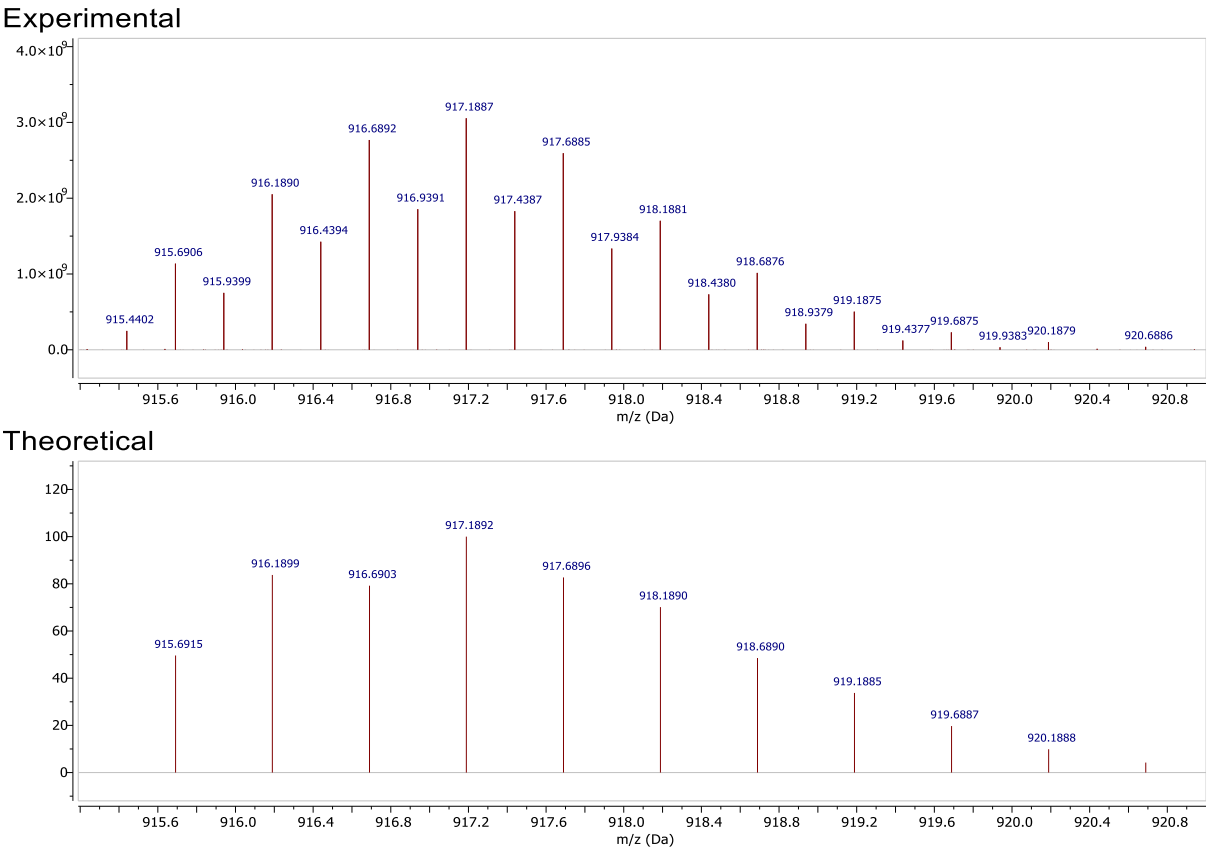

Figure S154. Isotopic patterns for a) cage **43a** and b) helicate **43b**: experimental (top) and theoretical (bottom).

3.11 Cage 44

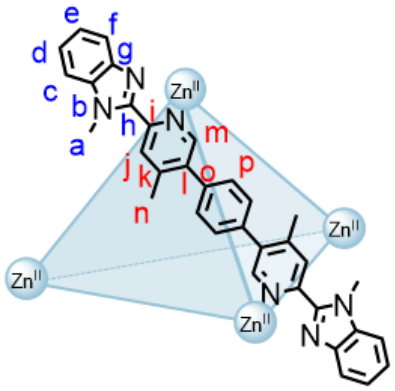

Zinc(II) triflate (2.00 mg, 5.50 µmol) and 1,4-bis(4''-methyl-6''-(1'-methyl-1*H*-benzo[*d*]imidazol-2'-yl)pyridin-3''-yl)benzene (**33**) (4.30 mg, 8.26 µmol) were dissolved in CD_3CN (500 µL) to prepare cage **44** *in situ*.

^{1}H NMR (500 MHz, CD_3CN, 298 K) δ (ppm): 8.46 (s, 12H, H_j), 7.83 (dt, ^3J = 8.5 Hz, ^4J = 0.9 Hz, 12H, H_c), 7.70 (s, 12H, H_m), 7.51 (ddd, ^3J = 8.5 Hz, ^3J = 7.3 Hz, ^4J = 0.9 Hz, 12H, H_d), 7.08 (s, 24H, H_p), 7.05 (ddd, ^3J = 8.3 Hz, ^3J = 7.3 Hz, ^4J = 0.9 Hz, 12H, H_e), 6.63 (dt, ^3J = 8.3 Hz, ^4J = 0.9 Hz, 12H, H_f), 4.36 (s, 36H, H_a), 2.63 (s, 36H, H_n).

^{13}C NMR (125 MHz, CD_3CN, 298 K) δ (ppm): 151.9 (C_m), 149.9 (C_h), 149.7 (C_i), 143.1 (C_k), 139.8 (C_l), 139.0 (C_b), 138.8 (C_g), 136.8 (C_n), 130.4 (C_o), 127.8 (C_q), 126.8 (C_d), 126.3 (C_e), 118.4 (C_j), 113.3 (C_f), 35.0 (C_c), 21.0 (C_a).

^{19}F NMR (471 MHz, CD_3CN, 298 K, C_6F_6) δ (ppm): -79.7 (OTf^-).

HRMS (ESI): *m/z* = 1375.9668 [**44** + 5OTf]$^{3+}$.

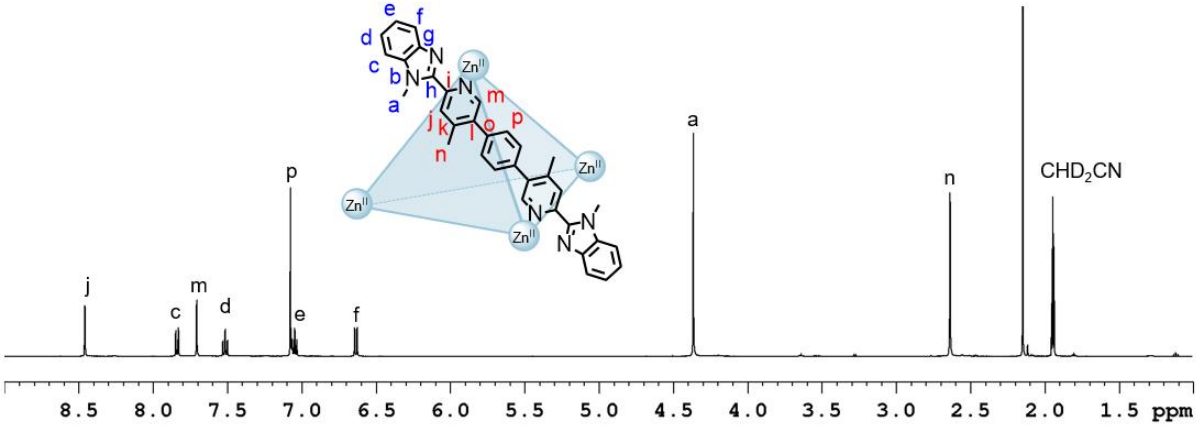

Figure S155. ^{1}H NMR spectrum (500 MHz, CD_3CN, 298 K) of cage **44**.

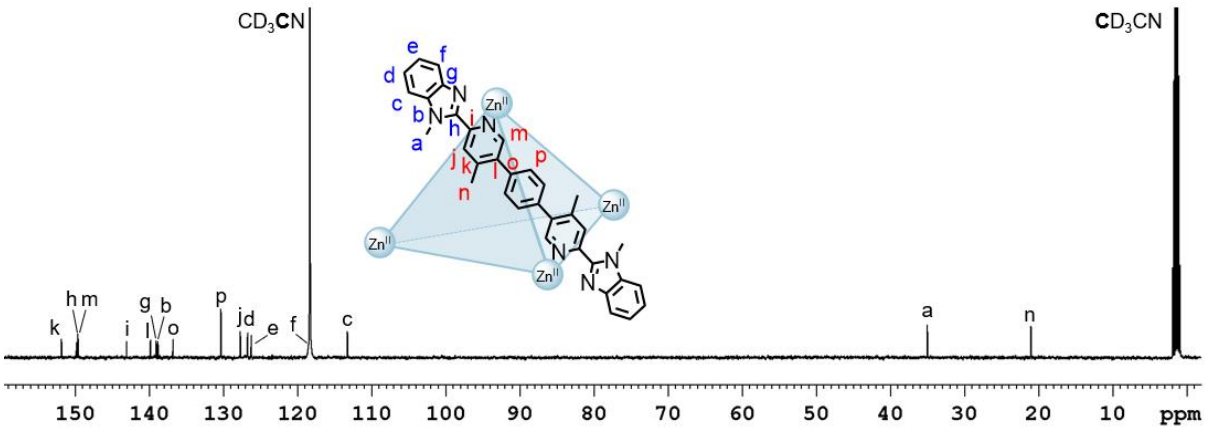

Figure S156. ^{13}C NMR spectrum (125 MHz, CD_3CN, 298 K) of cage **44**.

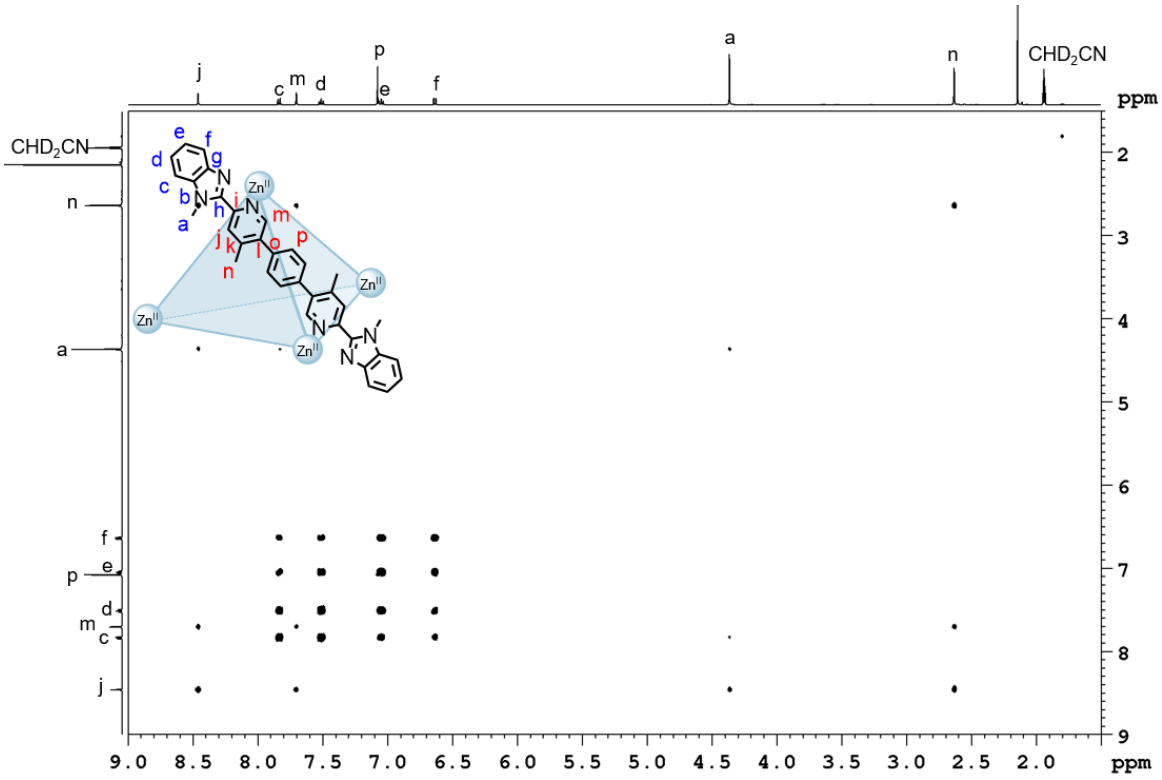

Figure S157. ^{1}H-^{1}H COSY NMR spectrum (500 MHz, CD_3CN, 298 K) of cage **44**.

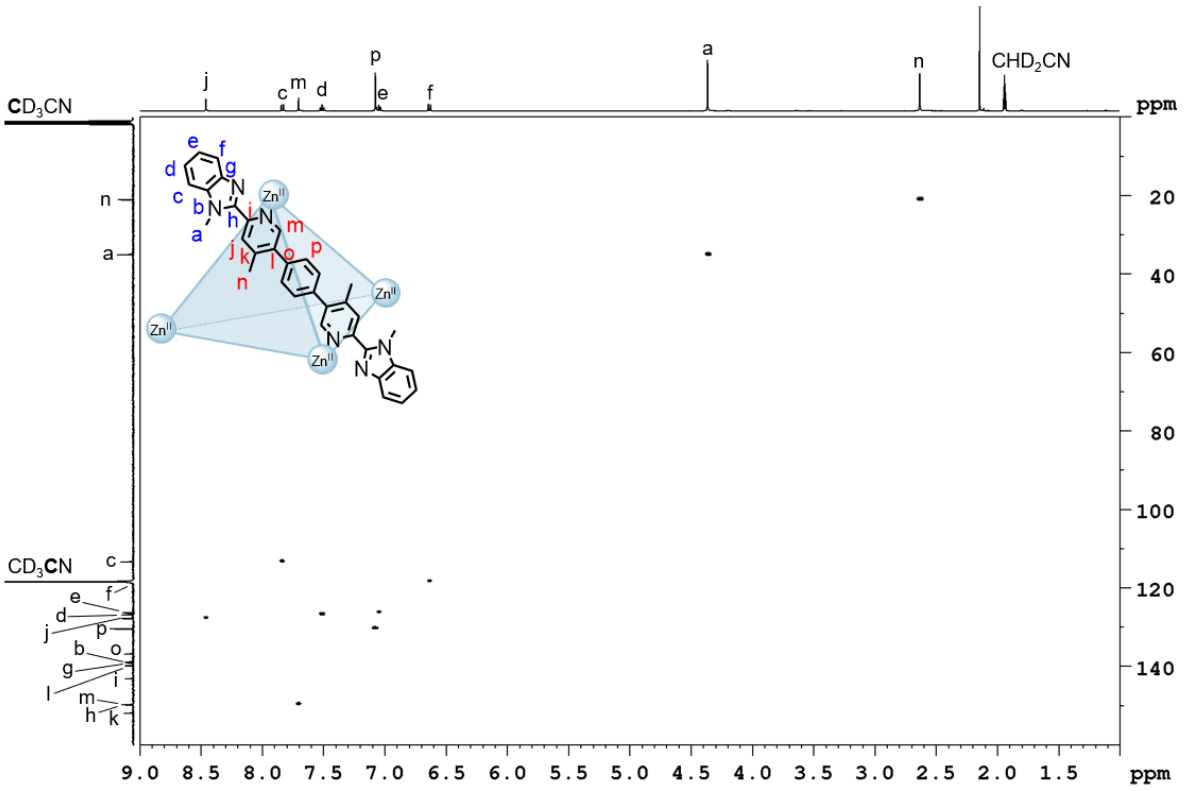

Figure S158. ^{1}H-^{13}C HSQC NMR spectrum (500 MHz/125 MHz, CD_3CN, 298 K) of cage **44**.

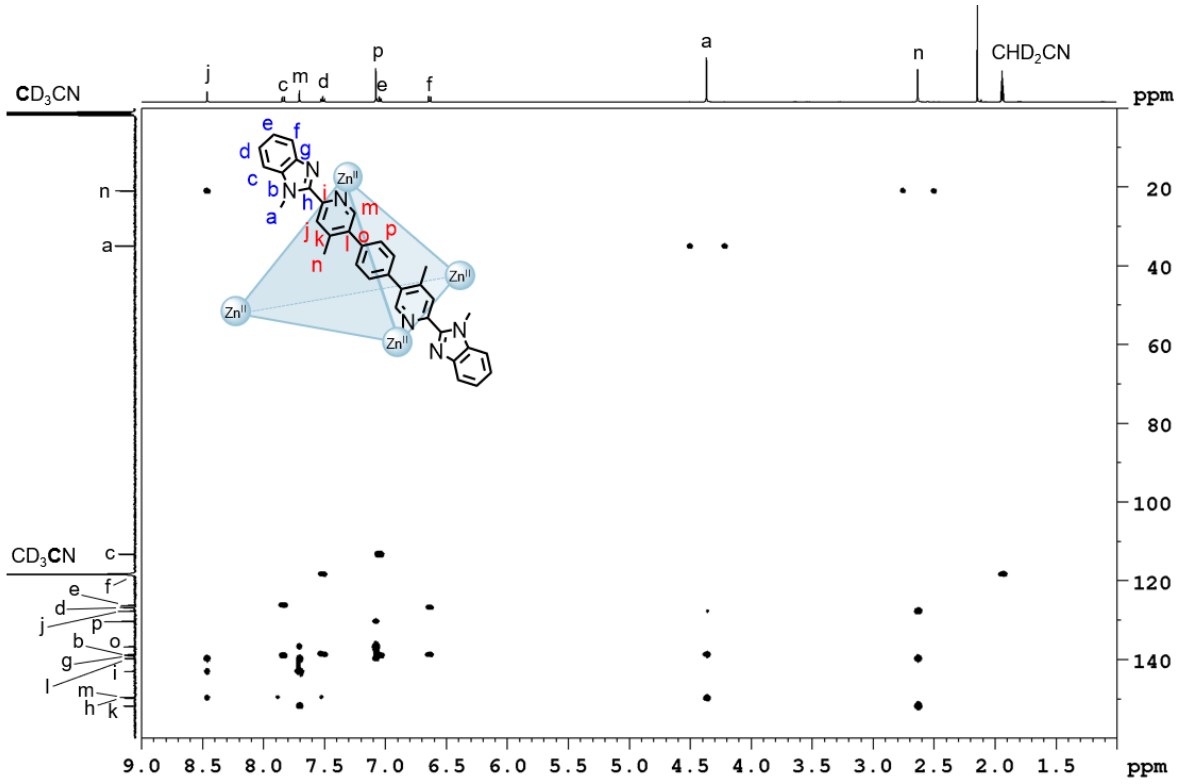

Figure S159. ^{1}H-^{13}C HMBC NMR spectrum (500 MHz/125 MHz, CD_3CN, 298 K) of cage **44**.

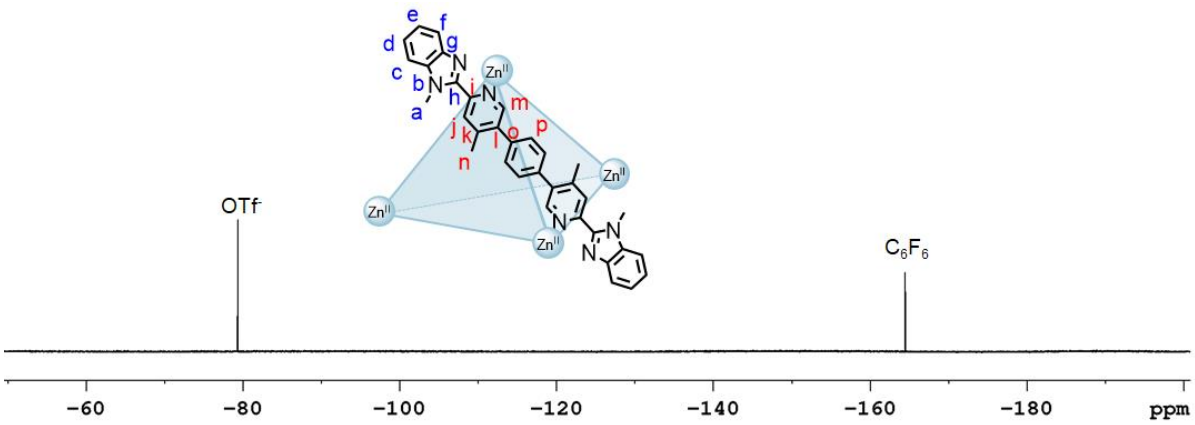

Figure S160. ^{19}F NMR spectrum (471 MHz, CD_3CN, 298 K, C_6F_6) of cage **44**.

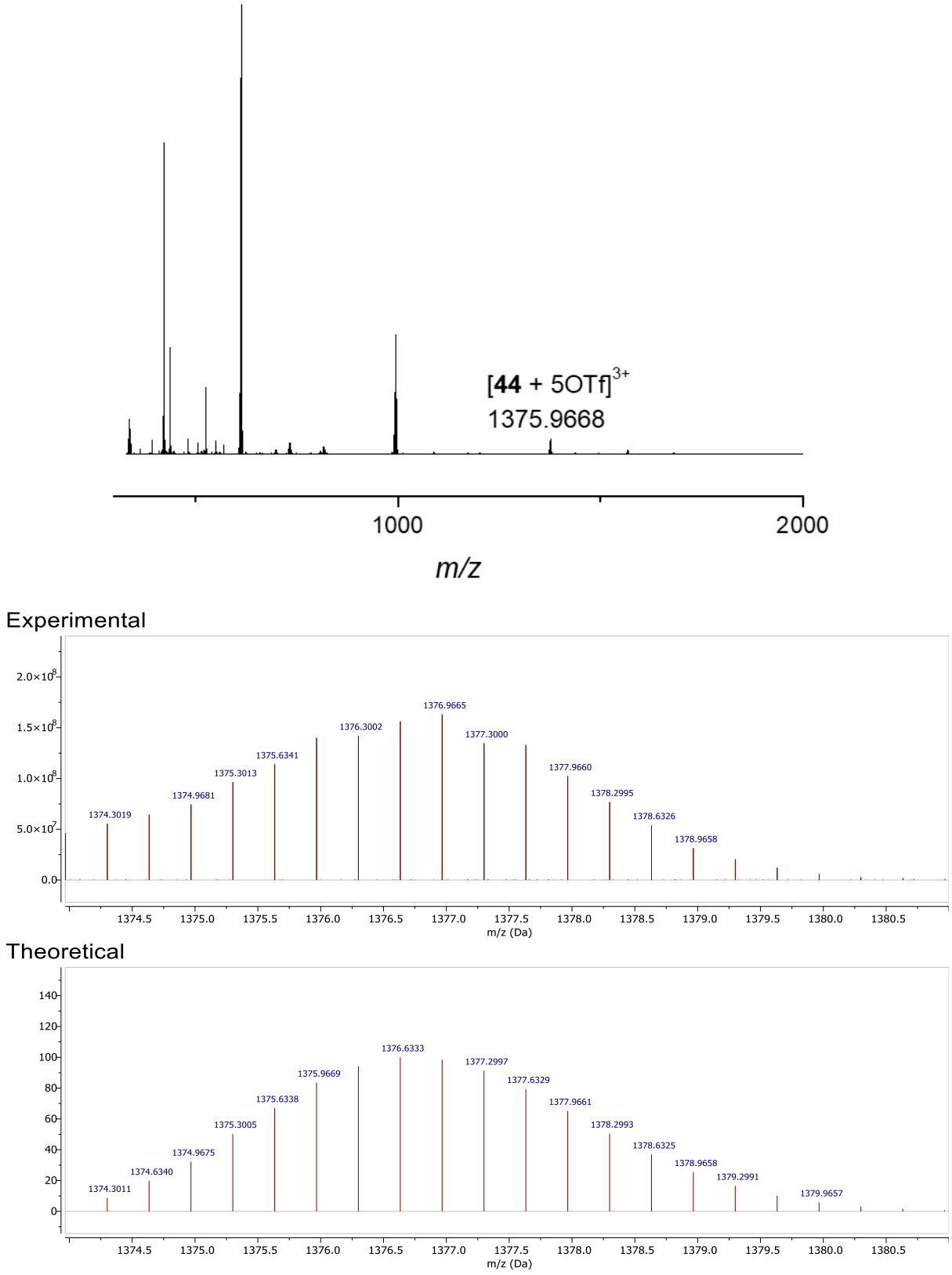

Figure S161. a) High resolution ESI mass spectrum of cage **44** and b) isotopic patterns of cage **44**: experimental (top) and theoretical (bottom).

4 Fe_4L_6 Metal-Organic Cages

Metal-organic cages based on Fe^{II} were self-assembled using six equivalents of the appropriate ligand and four equivalents of iron(II) triflate. The cages were prepared according to the procedures described in Sections 4.1-4.11. Characterisation using NMR spectroscopy and ESI-MS was consistent with the self-assembly of Fe_4L_6 cages. Elemental analysis of the cages was attempted in some cases, but the results were not satisfactory, most likely due to solvent that could not be removed by drying.

General procedure:

The ligands and $Fe(OTf)_2$ were dried *in vacuo* before weighing the appropriate amounts. Before transfer to the glovebox the ligand was stored at 110 °C for 1 h and $Fe(OTf)_2$ was stored under vacuum. The Fe^{II}-based cages were prepared using dried CD_3CN. Cage **2** was precipitated outside of the glovebox using diethyl ether, centrifuged and dried *in vacuo* before transfer back to the glovebox (For further details see Section 4.2).

4.1 Cage 1

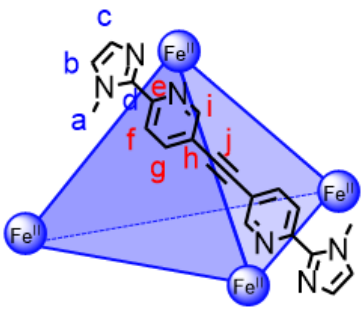

Iron(II) triflate (2.32 mg, 5.57 µmol) and 1,2-bis(6''-(1'-methyl-1*H*-imidazol-2'-yl)pyridin-3''-yl)ethyne (**14**) (2.85 mg, 8.37 µmol) were dissolved in dry CD_3CN (500 µL).

^{1}H NMR (600 MHz, CD_3CN, 298 K) δ (ppm): 8.22 (d, ^3J = 8.6 Hz, 12H, H_f), 8.00 (d, ^3J = 8.6 Hz, 12H, H_g), 7.75 (br, 12H, H_i), 7.43 (s, 12H, H_b), 6.33 (s, 12H, H_c), 4.22 (s, 36H, H_a).

^{13}C NMR (151 MHz, CD_3CN, 298 K) δ (ppm): 158.8 (C_i), 152.0 (C_h), 147.5 (C_e), 140.9 (C_g), 131.6 (C_c), 130.7 (C_b), 122.4 (C_f), 120.5 (C_d), 90.4 (C_j), 37.4 (C_a).

^{19}F NMR (471 MHz, CD_3CN, 298 K, C_6F_6) δ (ppm): -78.8 (OTf^-).

HRMS (ESI): *m/z* = 1003.7862 [**1** + 5OTf]$^{3+}$, 715.3524 [**1** + 4OTf]$^{4+}$.

While the signal at *m/z* 1003.7862 is consistent with the 3+ charge for the cage, the theoretical isotopic pattern does not match, possibly due to fragmentation in the gas phase or overlap with other signals.

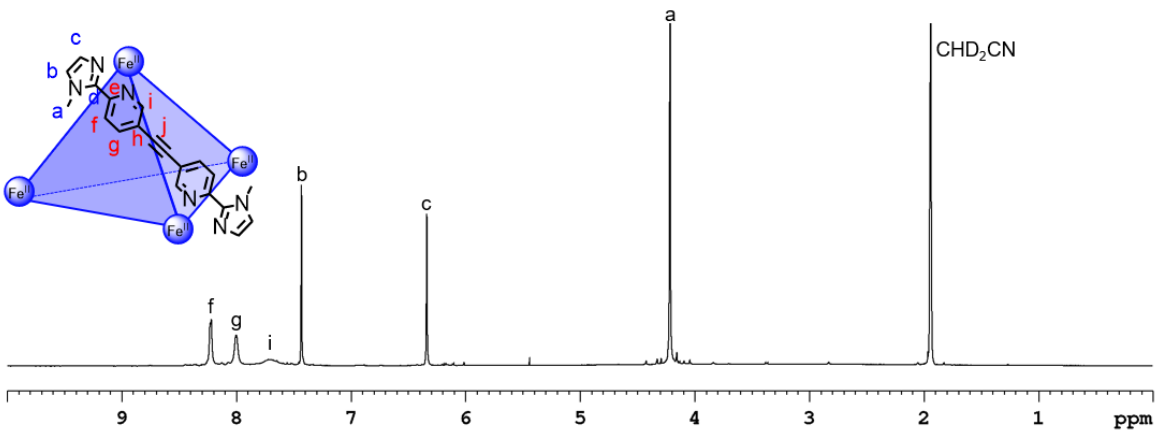

Figure S162. ^{1}H NMR spectrum (600 MHz, CD_3CN, 298 K) of cage **1**.

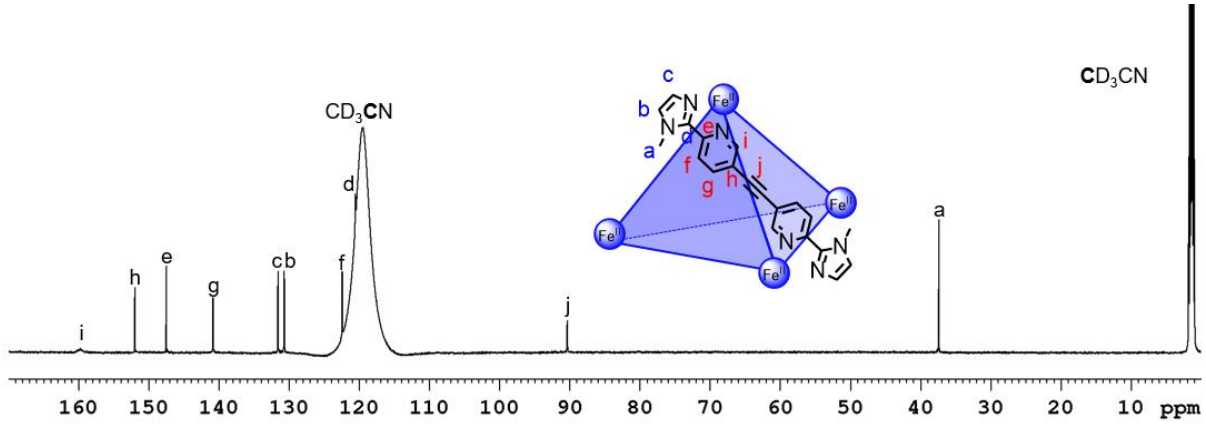

Figure S163. ^{13}C NMR spectrum (151 MHz, CD_3CN, 298 K) of cage **1**.

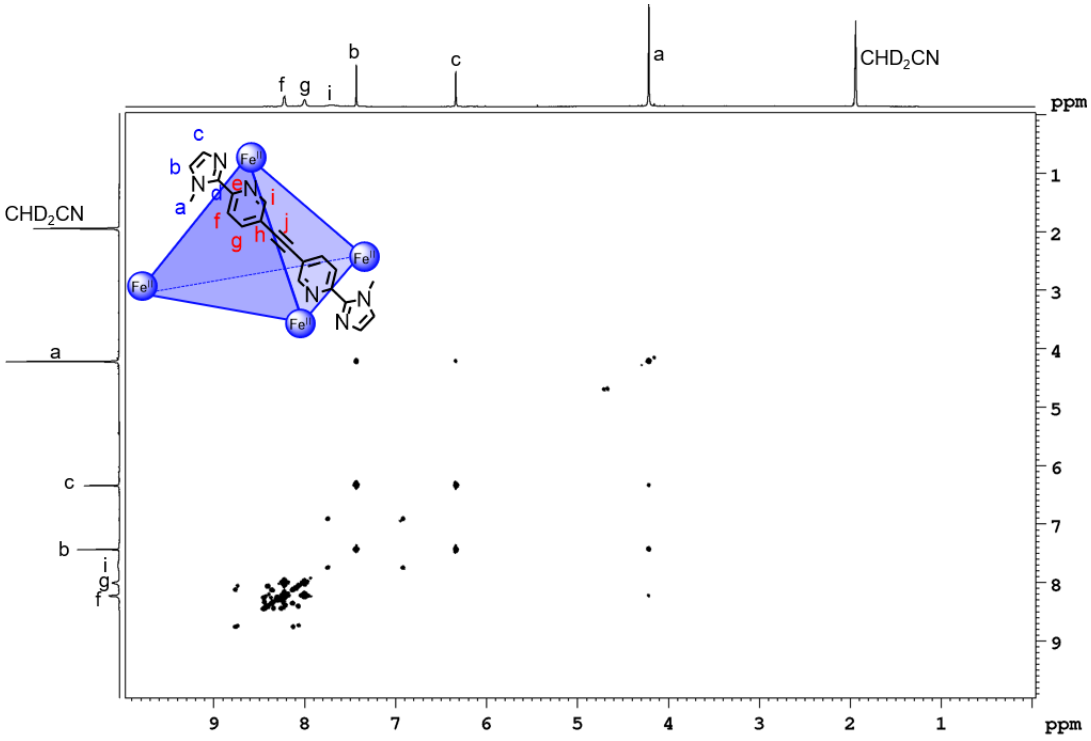

Figure S164. ^{1}H-^{1}H COSY NMR spectrum (600 MHz, CD_3CN, 298 K) of cage **1**.

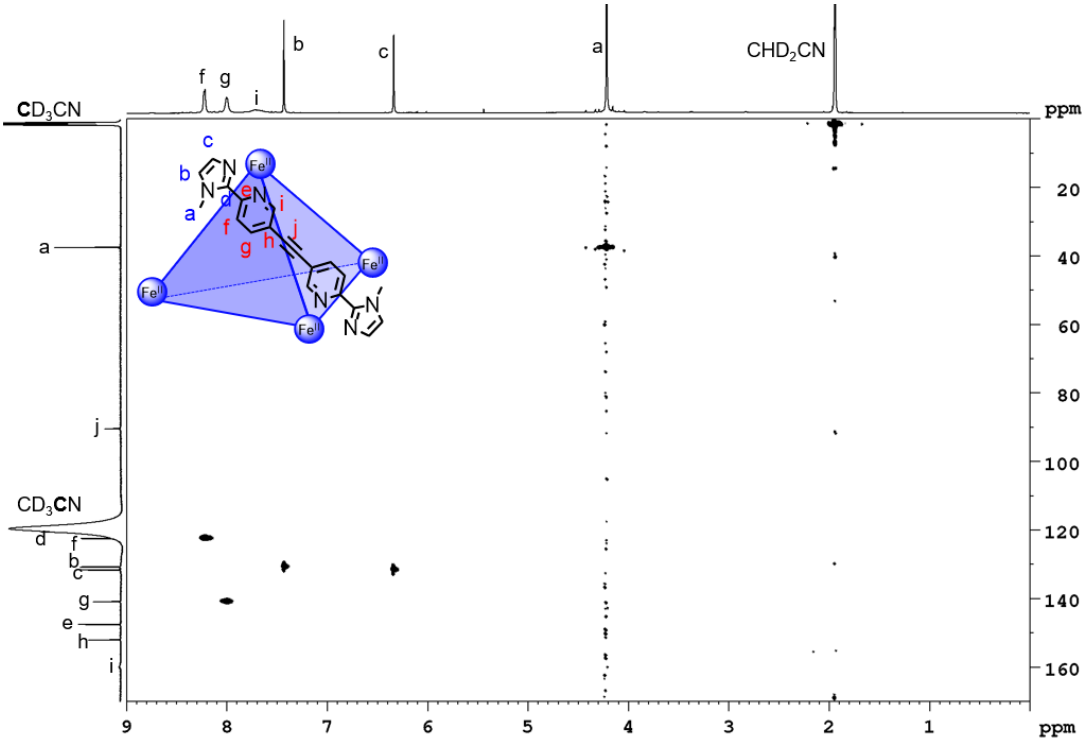

Figure S165. ^{1}H-^{13}C HSQC NMR spectrum (600 MHz/151 MHz, CD_3CN, 298 K) of cage **1**.

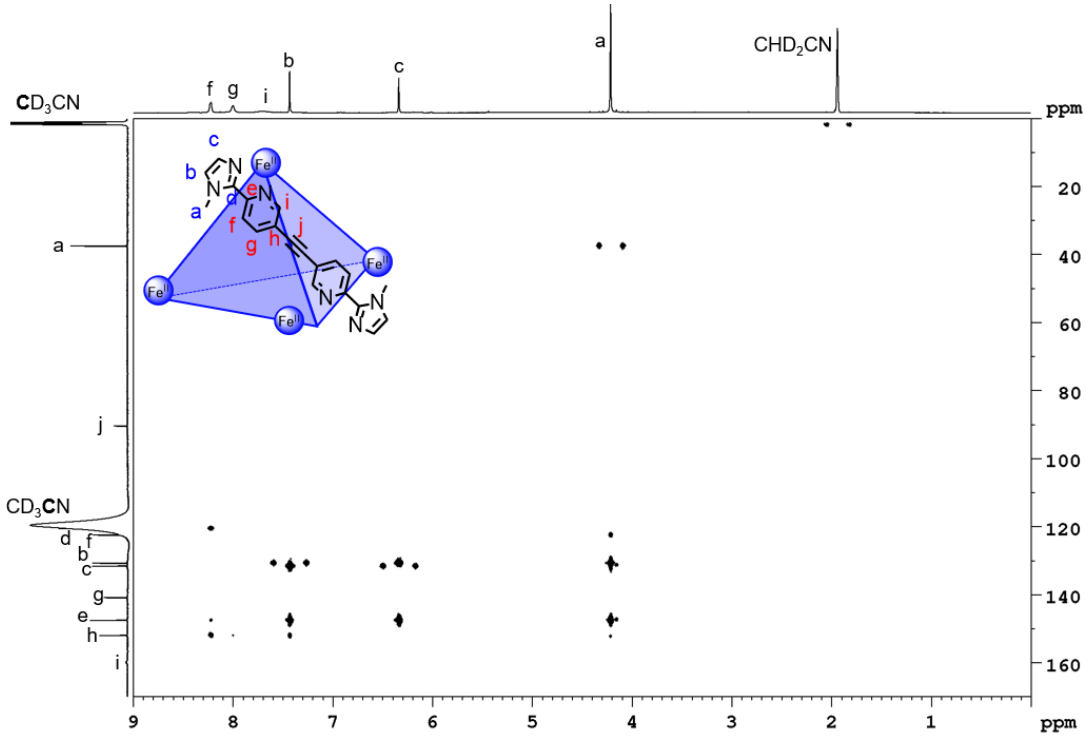

Figure S166. ^{1}H-^{13}C HMBC NMR spectrum (600 MHz/151 MHz, CD_3CN, 298 K) of cage **1**.

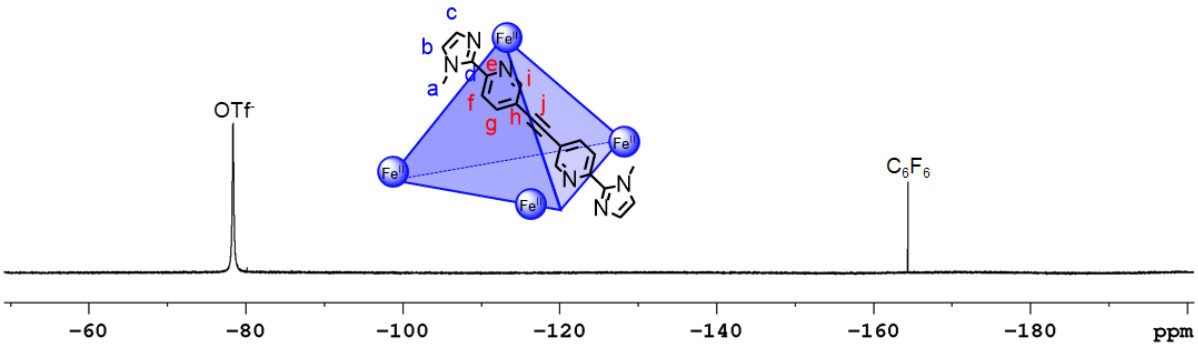

Figure S167. ^{19}F NMR spectrum (471 MHz, CD_3CN, 298 K) of cage **1**.

a)

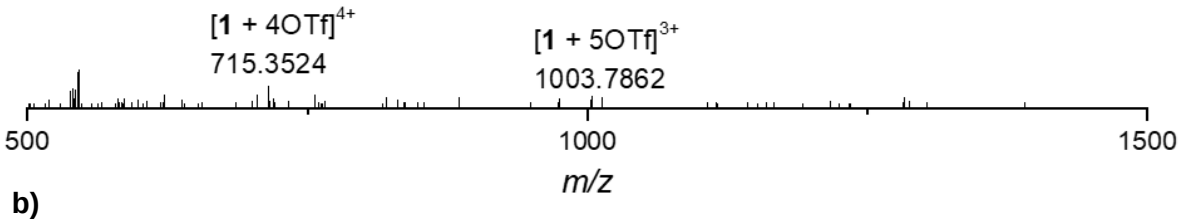

b)

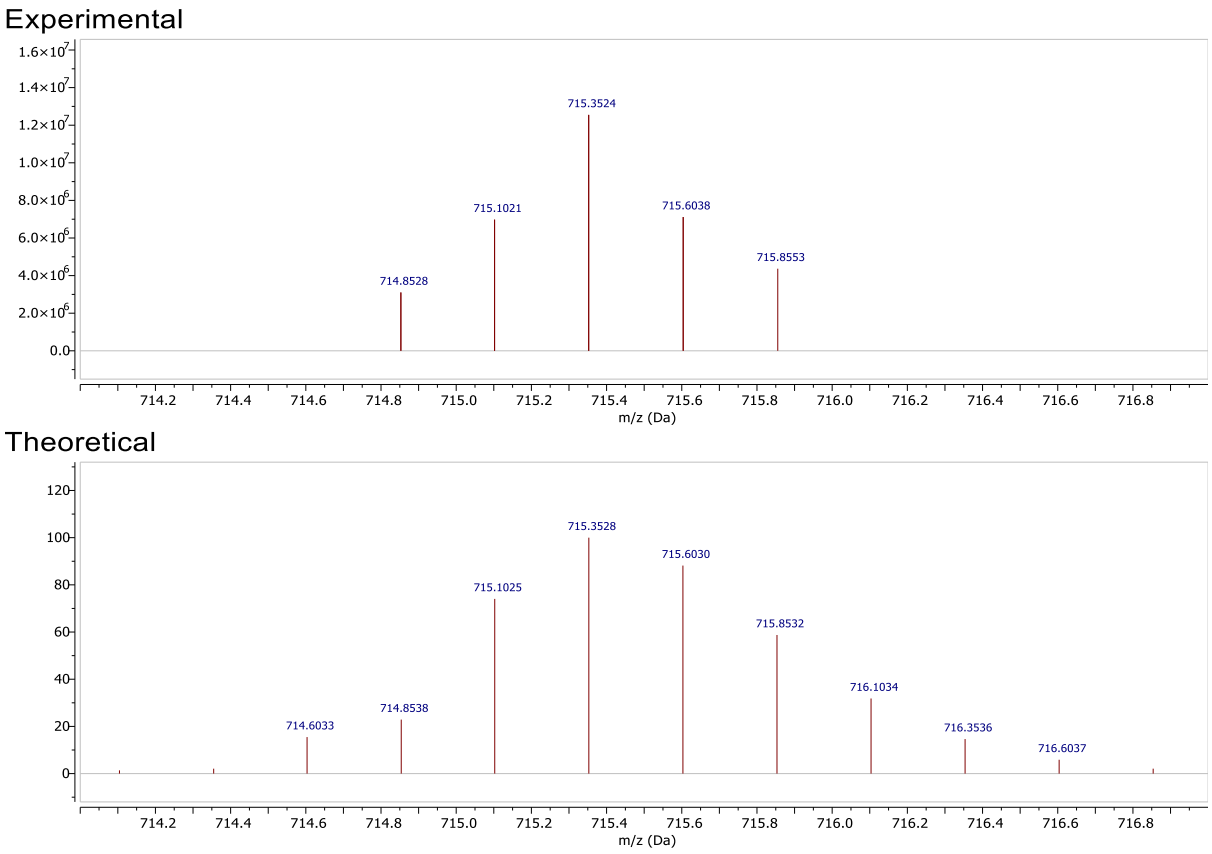

Figure S168. a) High resolution ESI mass spectrum of cage **1** and b) isotopic patterns of cage **1**: experimental (top) and theoretical (bottom).

4.2 Cage 2

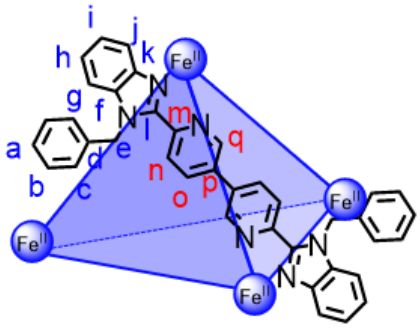

Iron(II) triflate (11.6 mg, 27.9 µmol) and 6',6''-di(1-benzyl-1*H*-benzo[*d*]imidazol-2-yl)-3',3''-bipyridine (**26**) (23.7 mg, 41.7 µmol) were dissolved in acetonitrile (3 mL) and the mixture was left to stand at room temperature for 3 h. The solution was poured into diethyl ether (10 mL), centrifuged, and the ether was decanted. Additional diethyl ether (10 mL) was added, and the suspension was centrifuged, decanted, and dried under vacuum (18.0 mg, 3.73 µmol, 53%).

^{1}H NMR (600 MHz, CD_3CN, 298 K) δ (ppm): 8.61 (d, ^{3}J = 8.4 Hz, 12H, H_n), 7.85 (d, ^{3}J = 7.9 Hz, 12H, H_g), 7.49 (t, ^{3}J = 7.9 Hz, 12H, H_h), 7.44 (dd, ^{3}J = 8.4 Hz, ^{4}J = 1.2 Hz, 12H, H_o), 7.29-7.25 (m, 24H, H_b), 7.24-7.20 (m, 36H, $H_{a,c}$), 7.18 (s, 12H, H_q), 7.09 (t, ^{3}J = 7.9 Hz, 12H, H_i), 6.76 (d, ^{2}J = 18.0 Hz, 12H, H_e), 6.13 (d, ^{3}J = 7.9 Hz, 12H, H_j), 6.07 (d, ^{2}J = 18.0 Hz, 12H, H_e).

^{13}C NMR (151 MHz, CD_3CN, 298 K) δ (ppm): 156.4 (C_q), 152.6 (C_l), 150.7 (C_m), 145.5 (C_k), 141.0 (C_f), 139.6 (C_o), 136.4 (C_p), 136.0 (C_d), 130.2 (C_b), 129.3 (C_a), 128.0 (C_h), 127.0 (C_c), 126.6 (C_i), 125.6 (C_n), 117.6 (C_j), 114.4 (C_g), 49.2 (C_e).

HRMS (ESI): *m/z* = 2264.4426 [**2** + 6OTf]$^{2+}$,1459.9767 [**2** + 5OTf]$^{3+}$, 1057.7428 [**2** + 4OTf]$^{4+}$.

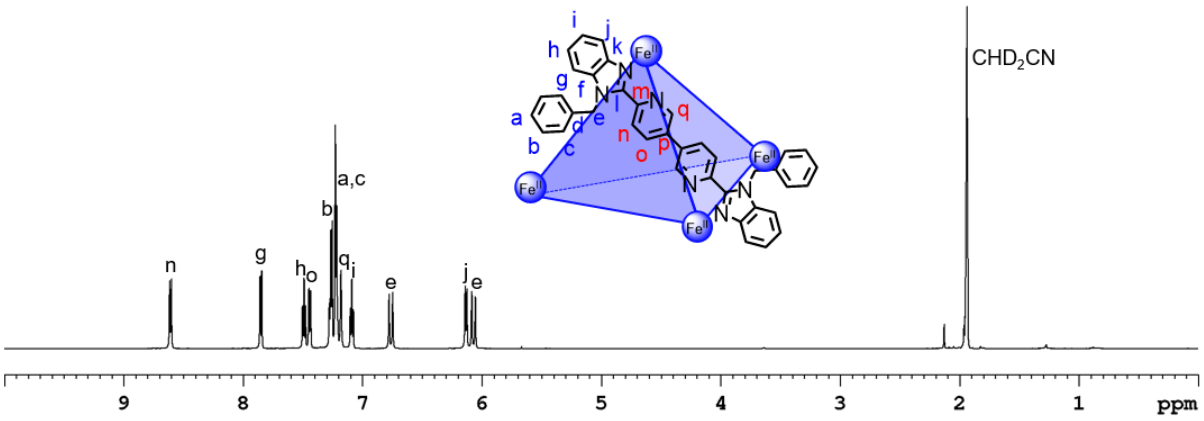

Figure S169. ^{1}H NMR spectrum (600 MHz, CD_3CN, 298 K) of cage **2**.

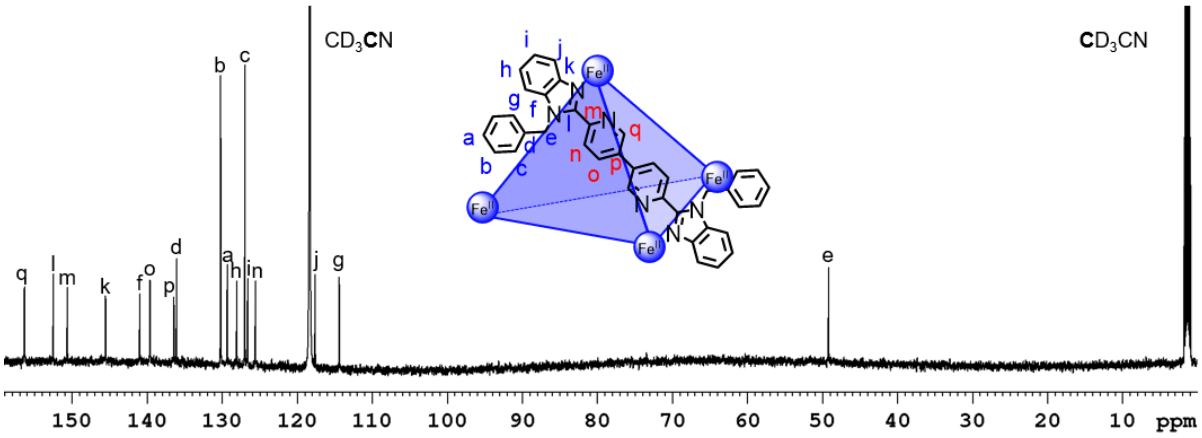

Figure S170. ^{13}C NMR spectrum (151 MHz, CD_3CN, 298 K) of cage **2**.

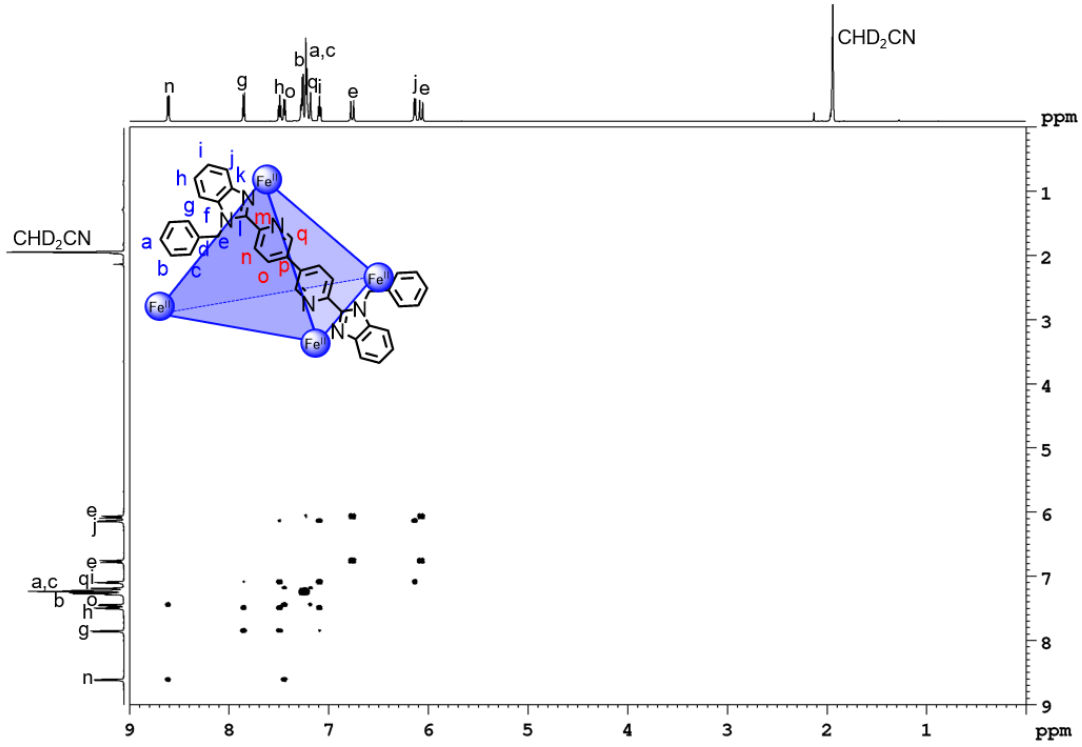

Figure S171. ^{1}H-^{1}H COSY NMR spectrum (600 MHz, CD_3CN, 298 K) of cage **2**.

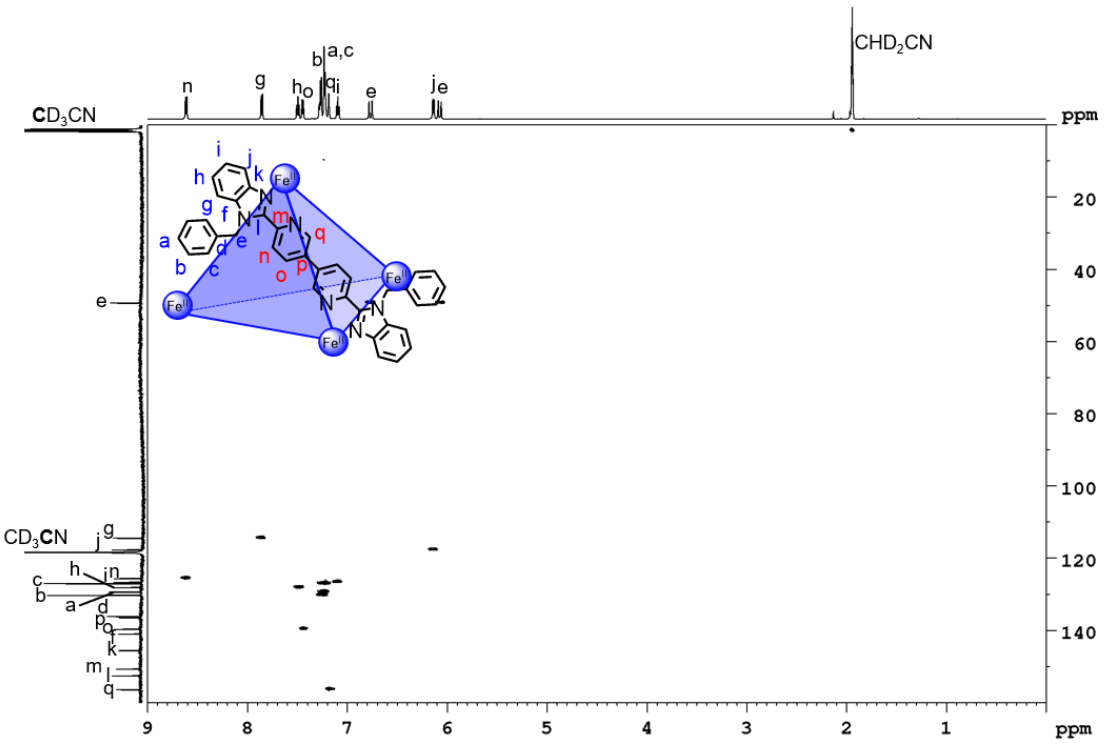

Figure S172. ^{1}H-^{13}C HSQC NMR spectrum (600 MHz/151 MHz, CD_3CN, 298 K) of cage **2**.

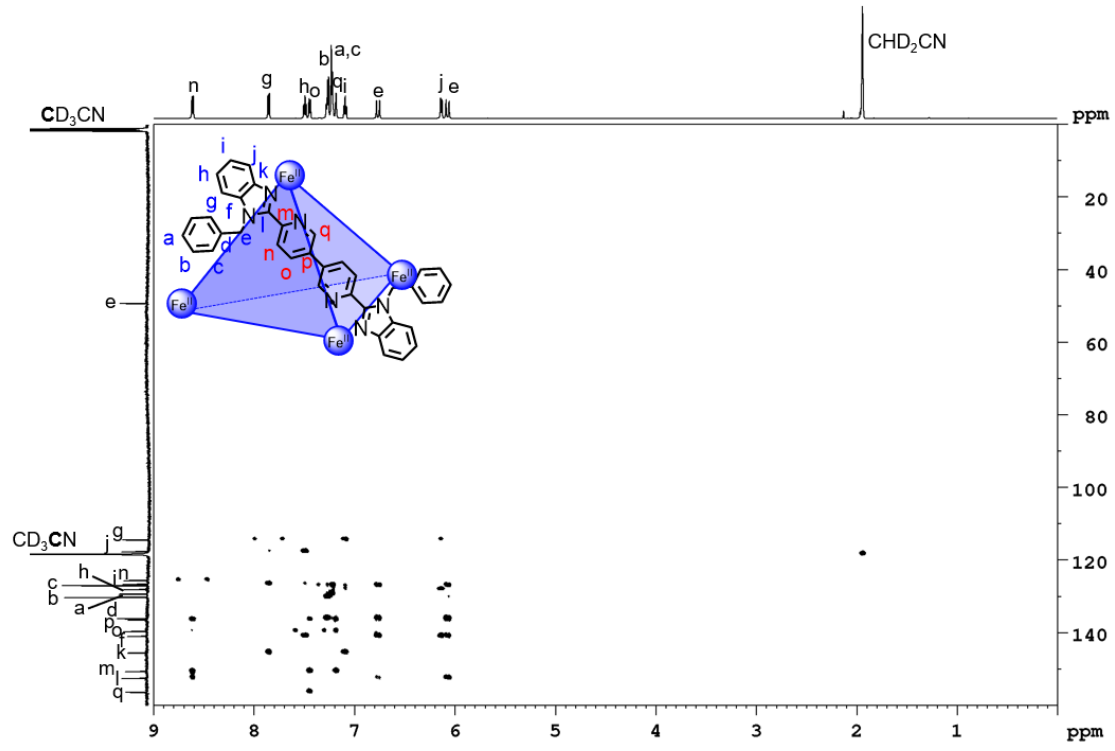

Figure S173. ^{1}H-^{13}C HMBC NMR spectrum (600 MHz/151 MHz, CD_3CN, 298 K) of cage **2**.

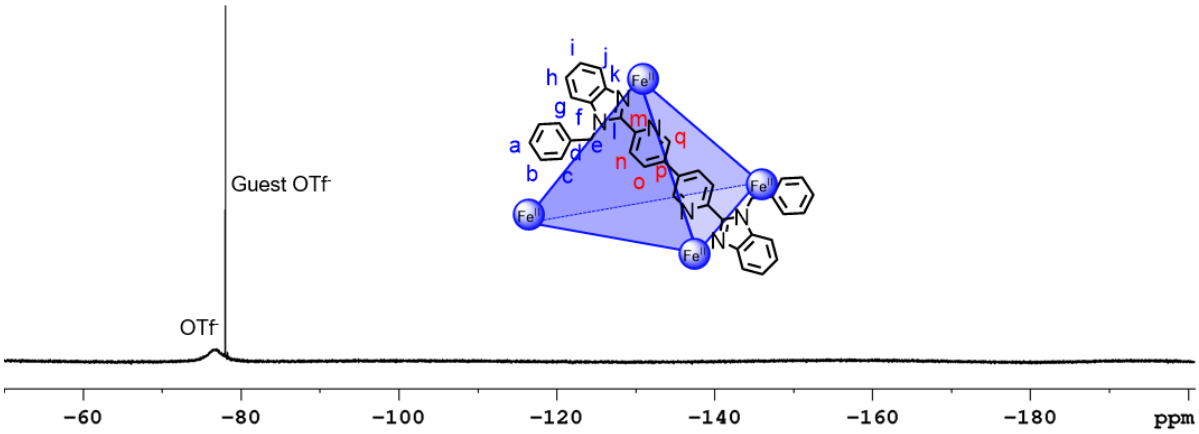

Figure S174. ^{19}F NMR spectrum (471 MHz, CD_3CN, 298 K) of cage **2**.

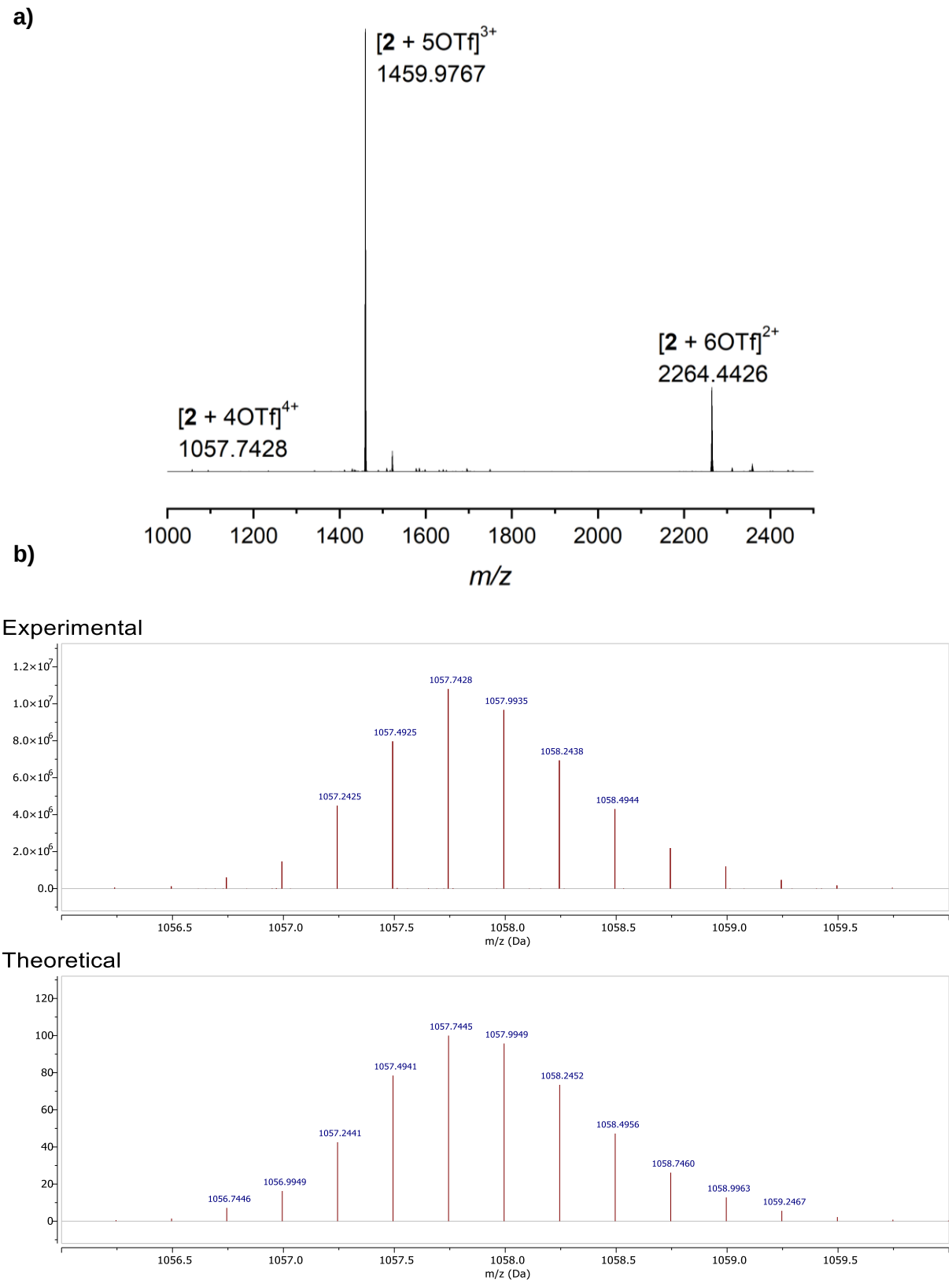

Figure S175. a) High resolution ESI mass spectrum of cage **2** and b) isotopic patterns of cage **2**: experimental (top) and theoretical (bottom).

4.3 Cage 3

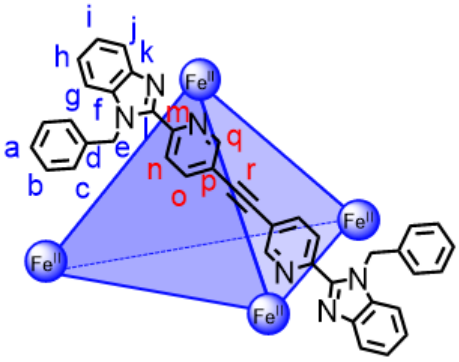

Iron(II) triflate (21.7 mg, 52.1 µmol) and 1,2-di(6''-(1'-benzyl-1*H*-benzo[*d*]imidazole-2'-yl)pyridin-3''-yl)ethyne (**19**) (46.2 mg, 78.0 µmol) were dissolved in acetonitrile (5 mL) and the mixture was left to stand at room temperature for 3 h. The solution was poured into diethyl ether (15 mL), centrifuged, and the ether was decanted. The precipitated cage was washed with additional diethyl ether (15 mL), centrifuged, decanted, and dried extensively under vacuum (49.4 mg, 8.21 µmol, 63%).

^{1}H NMR (600 MHz, CD_3CN, 298 K) δ (ppm): 10.03 (unres. d, 12H, H_n), 8.86 (br, 12H, H_q), 8.54 (d, ^{3}J = 8.1 Hz, 12H, H_g), 7.57 (d, ^{3}J = 8.3 Hz, 12H, H_o), 7.42 (t, ^{3}J = 8.1 Hz, 12H, H_h), 7.38 (t, ^{3}J = 7.4 Hz, 24H, H_b), 7.32 (d, ^{3}J = 7.4 Hz, 24H, H_c), 7.22 (t, ^{3}J = 7.4 Hz, 12H, H_a), 6.84 (t, ^{3}J = 6.6 Hz, 12H, H_i), 6.72 (d, ^{2}J = 17.9 Hz, 12H, H_e), 6.61 (d, ^{2}J = 17.9 Hz, 12H, H_e), 4.91 (unres. d, 12H, H_j).

^{13}C NMR (151 MHz, CD_3CN, 298 K) δ (ppm): 158.8 (C_k), 157.5 (C_q), 154.7 (C_f), 148.9 (C_m), 142.4 (C_o), 140.3 (C_p), 135.4 (C_d), 135.0 (C_l), 130.3 (C_n), 129.2 (C_b), 128.2 (C_a), 127.0 (C_h), 125.8 (C_c), 125.0 (C_i), 117.4 (C_j), 116.0 (C_g), 93.9 (C_r), 51.5 (C_e).

HRMS (ESI): *m/z* = 1508.3126 [**3** + 5OTf]$^{3+}$, 1093.9949 [**3** + 4OTf]$^{4+}$, 662.7292 [**3** + 3OTf]$^{5+}$, 527.4492 [**3** + 2OTf]$^{6+}$, 430.8211 [**3** + OTf]$^{7+}$.

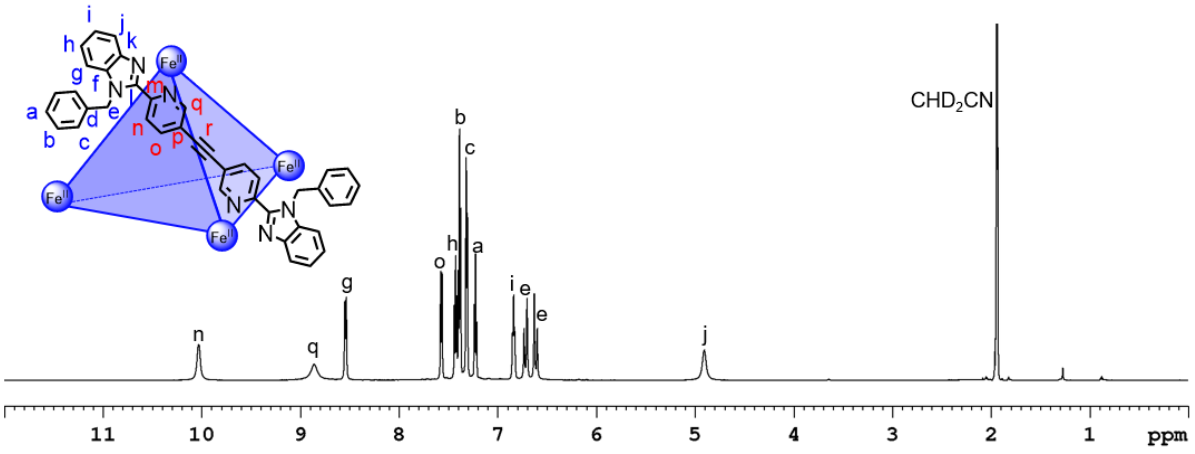

Figure S176. ^{1}H NMR spectrum (600 MHz, CD_3CN, 298 K) of cage **3**.

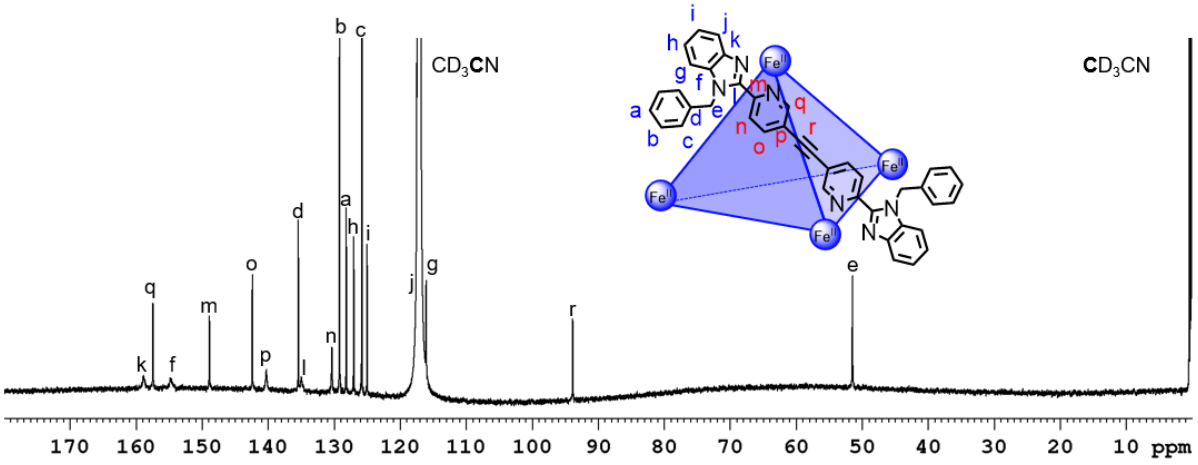

Figure S177. ^{13}C NMR spectrum (151 MHz, CD_3CN, 298 K) of cage **3**.

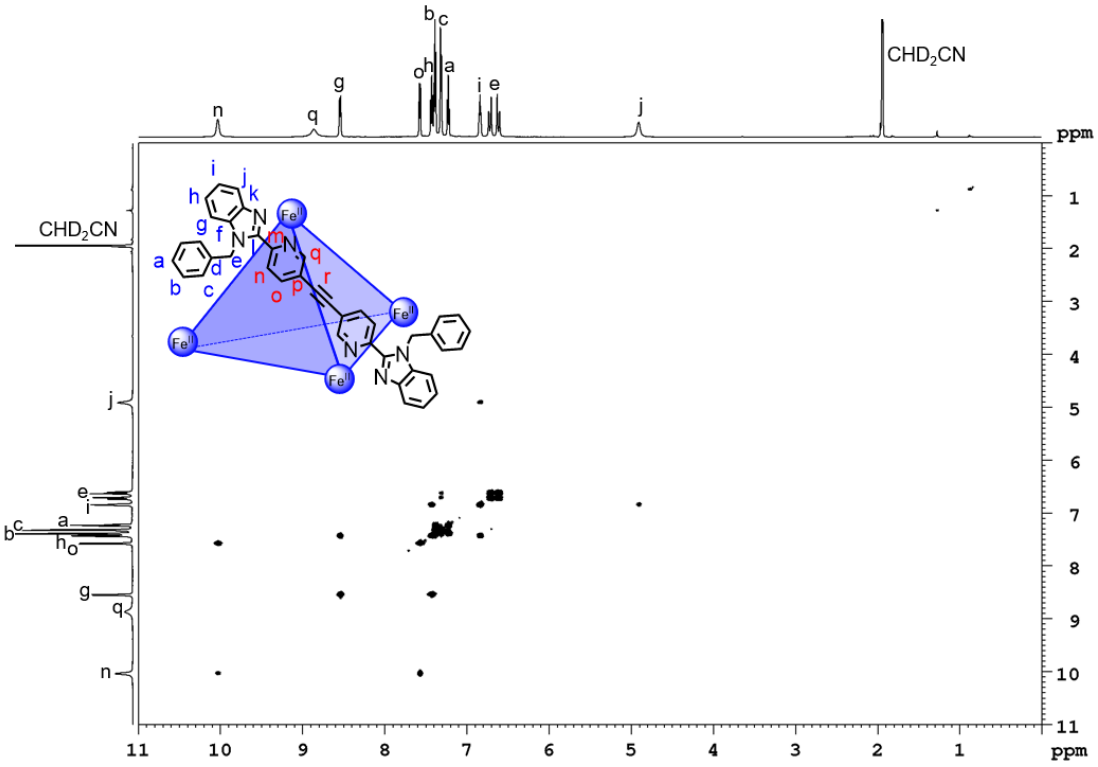

Figure S178. ^{1}H-^{1}H COSY NMR spectrum (600 MHz, CD_3CN, 298 K) of cage **3**.

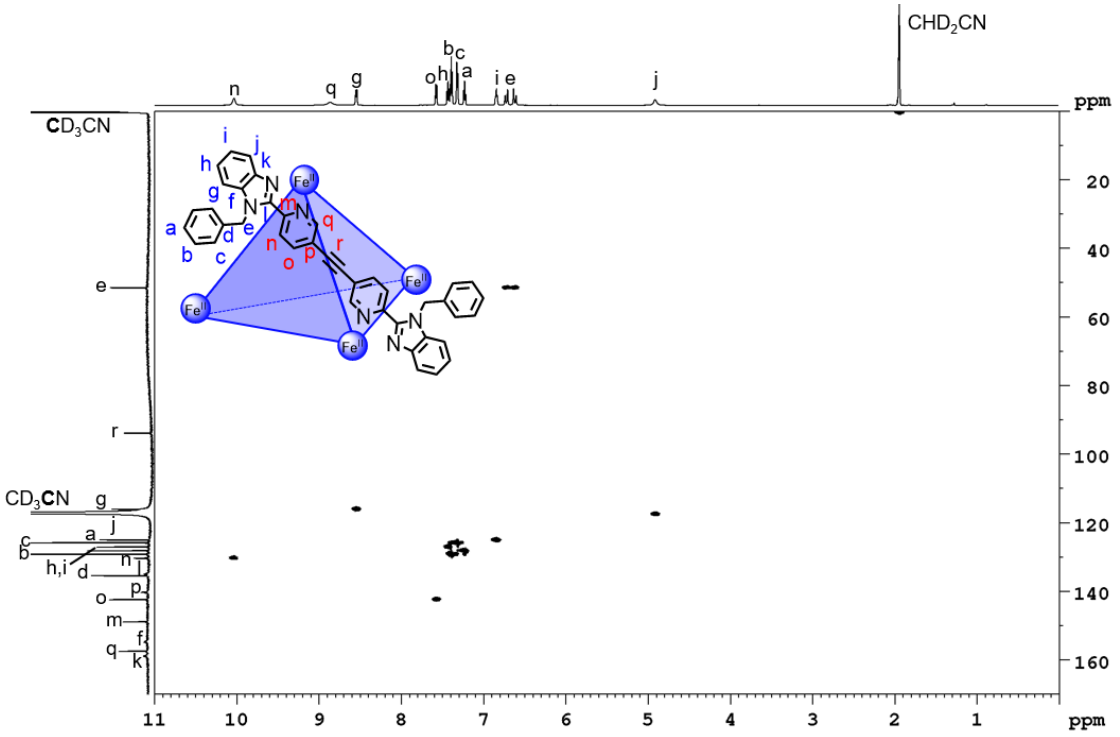

Figure S179. ^{1}H-^{13}C HSQC NMR spectrum (600 MHz/151 MHz, CD_3CN, 298 K) of cage **3**.

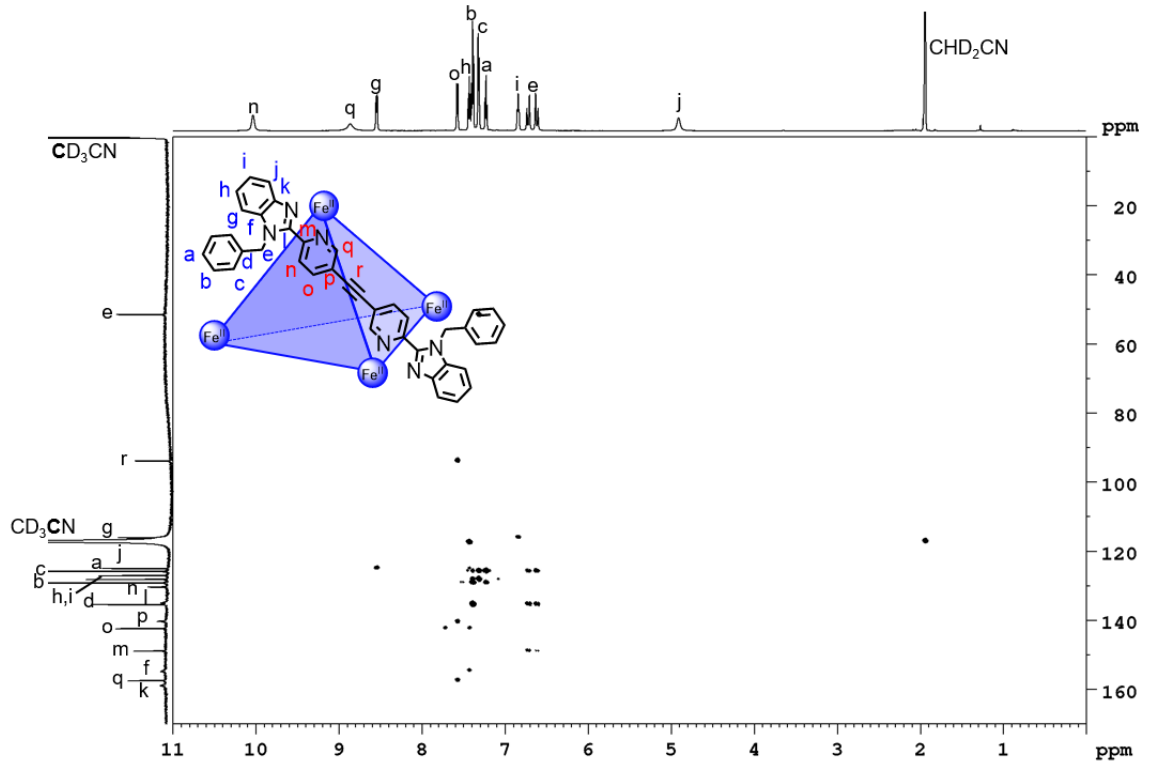

Figure S180. ^{1}H-^{13}C HMBC NMR spectrum (600 MHz/151 MHz, CD_3CN, 298 K) of cage **3**.

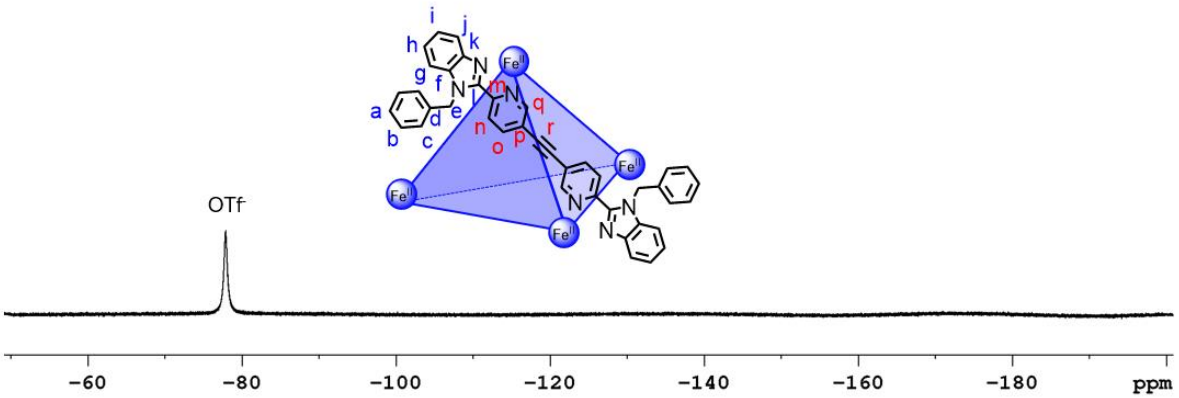

Figure S181. ^{19}F NMR spectrum (471 MHz, CD_3CN, 298 K) of cage **3**.

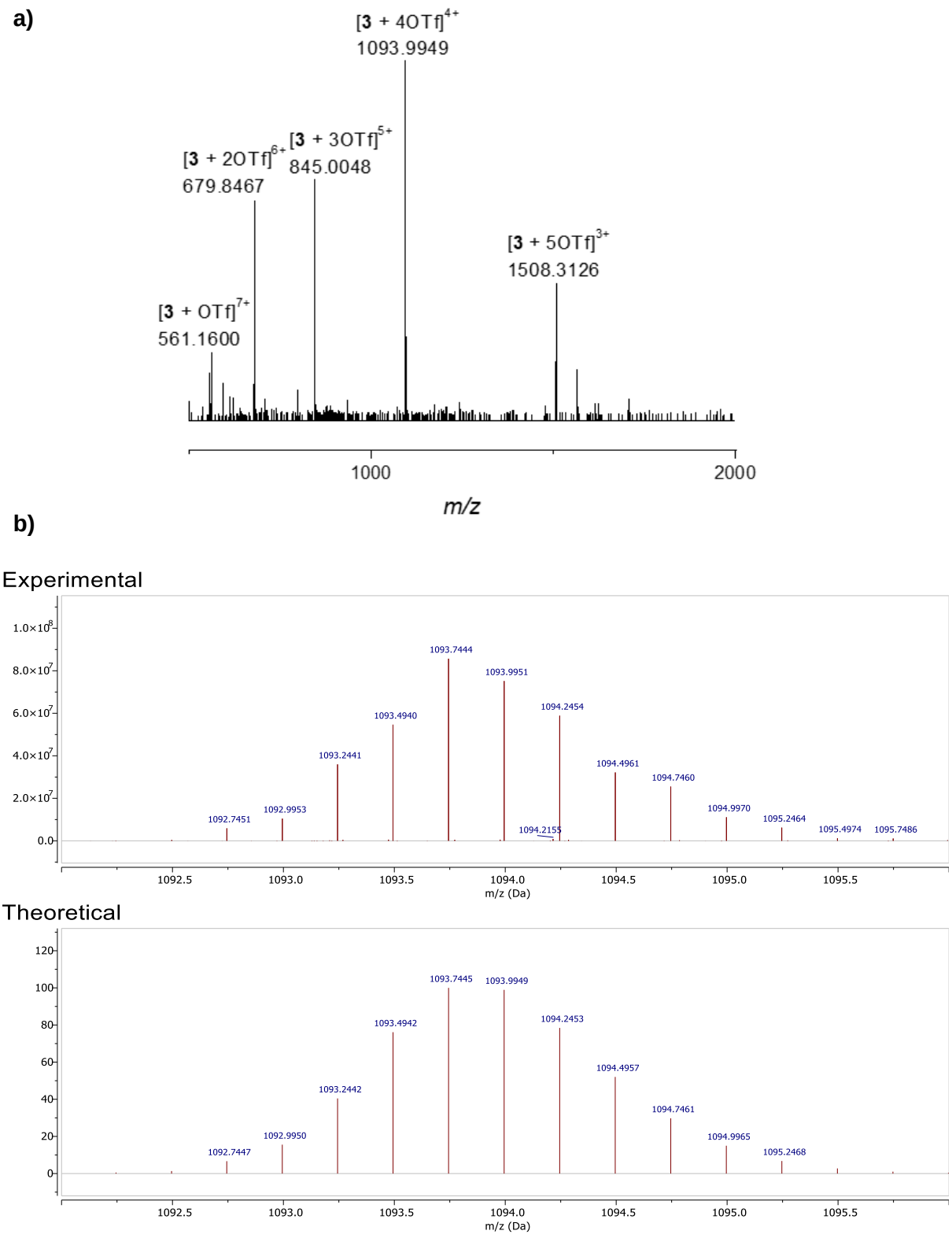

Figure S182. a) High resolution ESI mass spectrum of cage **3** and b) isotopic patterns of cage **3**: experimental (top) and theoretical (bottom).

4.4 Cage 4

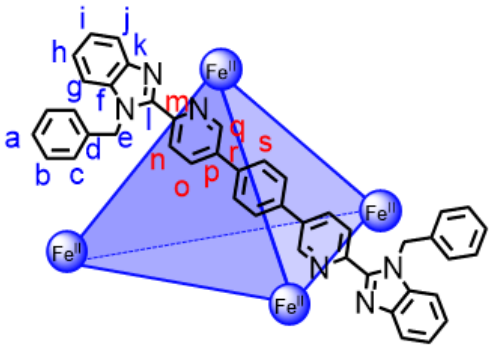

Iron(II) triflate (2.30 mg, 5.52 µmol) and 1,4-di(6''-(1'-benzyl-1*H*-benzo[*d*]imidazol-2'-yl)pyridin-3''-yl)benzene (**28**) (5.34 mg, 8.28 µmol) were dissolved in dry CD_3CN (500 µL).

^{1}H NMR (600 MHz, CD_3CN, 298 K) δ (ppm): 9.89 (s, 12H, H_n), 8.93 (br, 12H, H_q), 8.40 (d, ^3J = 8.3 Hz, 12H, H_g), 8.09 (d, ^3J = 8.1 Hz, 12H, H_o), 7.44 (unres. dt, 12H, H_h), 7.28 (d, ^3J = 7.3 Hz, 24H, H_c), 7.24 (t, ^3J = 7.3 Hz, 24H, H_b), 7.13 (t, ^3J = 7.3 Hz, 12H, H_a), 6.91 (t, ^3J = 7.3 Hz, 12H, H_i), 6.70 (s, 12H, H_s), 6.55 (d, ^2J = 18.0 Hz, 12H, H_e), 6.49 (d, ^2J = 18.0 Hz, 12H, H_e), 5.29 (s, 12H, H_j).

^{13}C NMR (151 MHz, CD_3CN, 298 K) δ (ppm): 157.1 (C_k), 153.9 (C_m), 152.8 (C_f), 150.3 (C_l), 147.1 (C_p), 143.1 (C_q), 138.5 (C_o), 137.2 (C_r), 136.6 (C_d), 130.7 (C_n), 130.5 (C_b), 129.3 (C_a), 128.2 (C_s), 127.9 (C_h), 127.0 (C_c), 126.2 (C_i), 118.5 (C_j), 116.5 (C_g), 52.2 (C_e).

HRMS (ESI): *m/z* = 2492.5379 [**4** + 6OTf]$^{2+}$, 1612.3752 [**4** + 5OTf]$^{3+}$, 1171.7921 [**4** + 4OTf]$^{4+}$, 907.6427 [**4** + 3OTf]$^{5+}$, 731.5433 [**4** + 2OTf]$^{6+}$, 605.7585 [**4** + OTf]$^{7+}$.

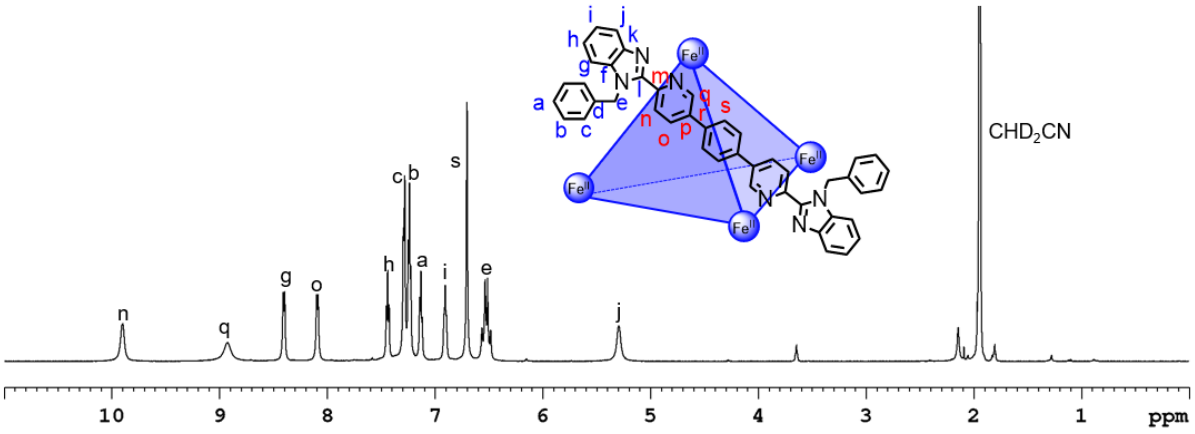

Figure S183. ^{1}H NMR spectrum (600 MHz, CD_3CN, 298 K) of cage **4**.

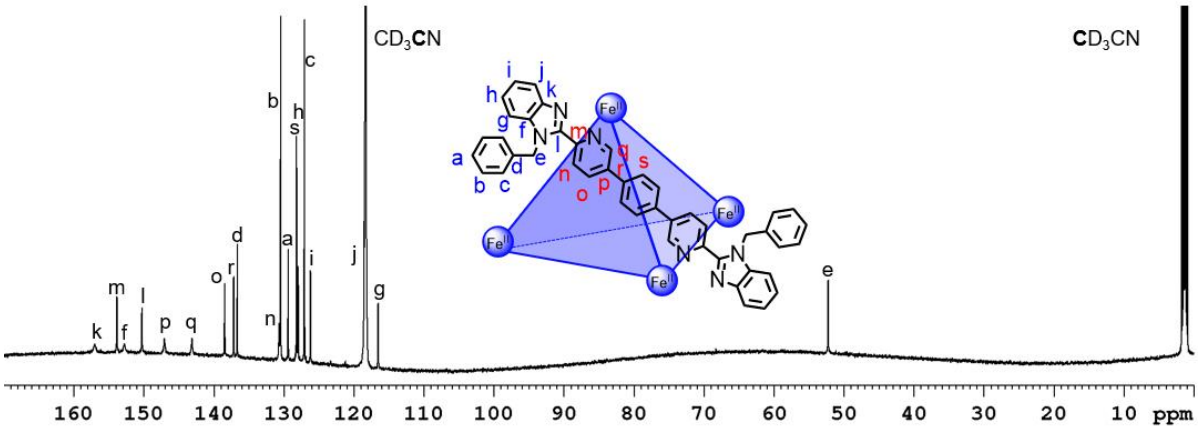

Figure S184. ^{13}C NMR spectrum (151 MHz, CD_3CN, 298 K) of cage **4**.

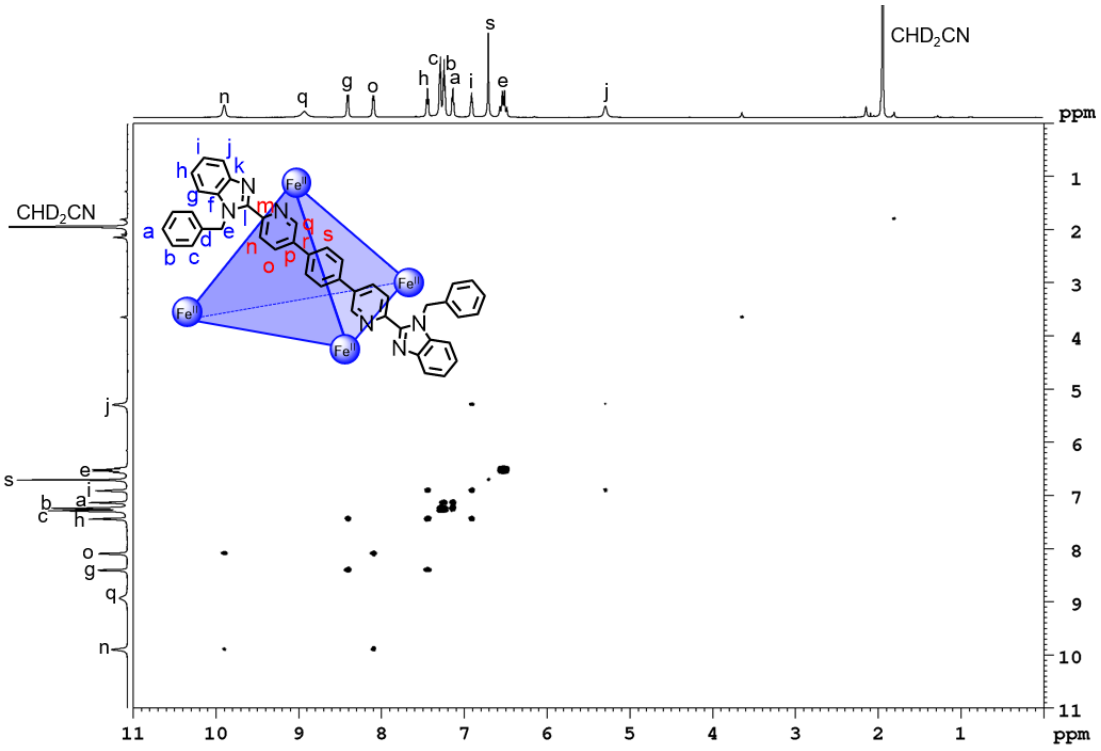

Figure S185. ^{1}H-^{1}H COSY NMR spectrum (600 MHz, CD_3CN, 298 K) of cage **4**.

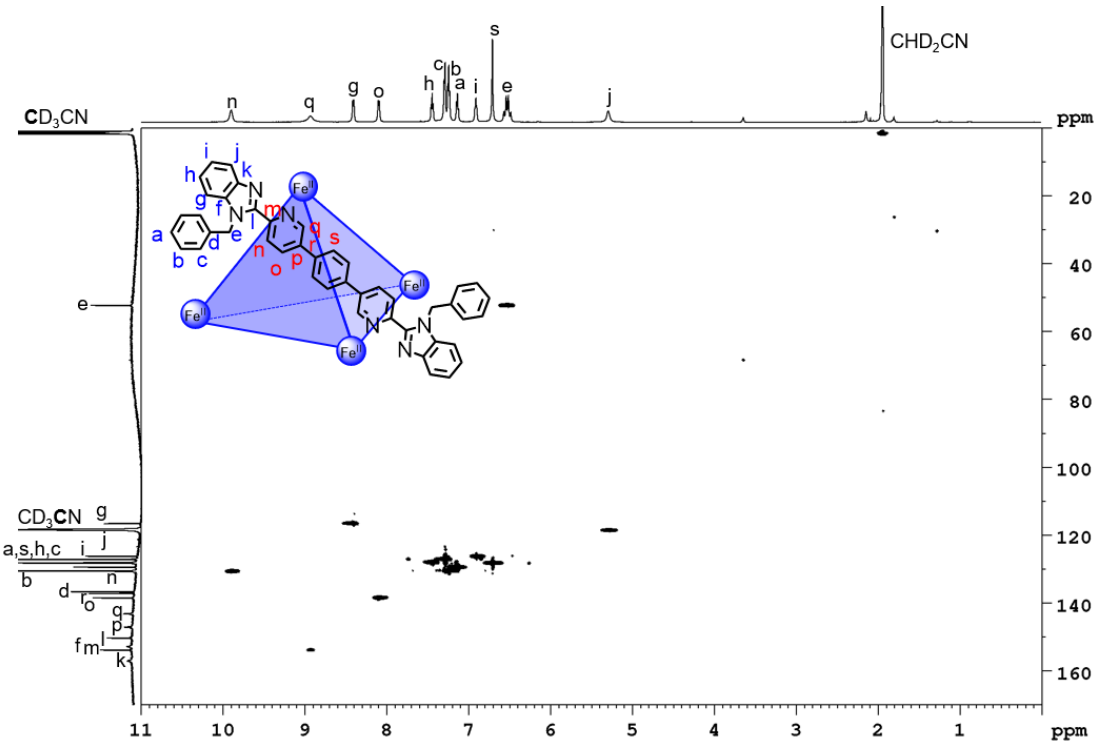

Figure S186. ^{1}H-^{13}C HSQC NMR spectrum (600 MHz/151 MHz, CD_3CN, 298 K) of cage **4**.

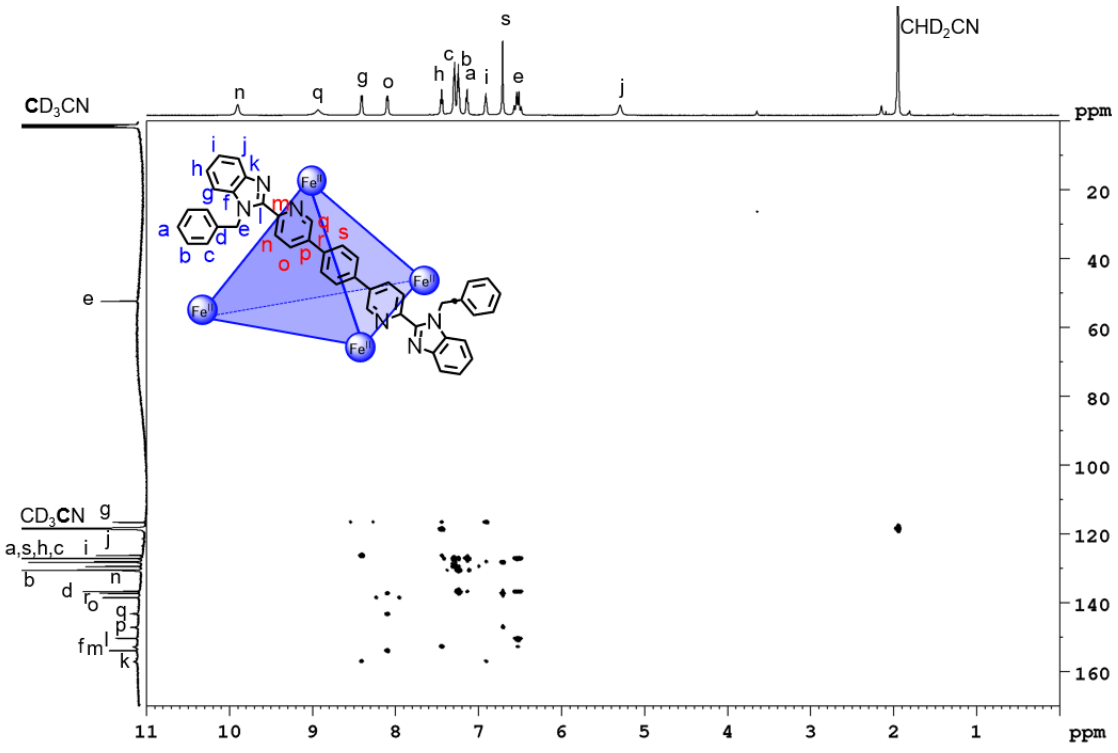

Figure S187. ^{1}H-^{13}C HMBC NMR spectrum (600 MHz/151 MHz, CD_3CN, 298 K) of cage **4**.

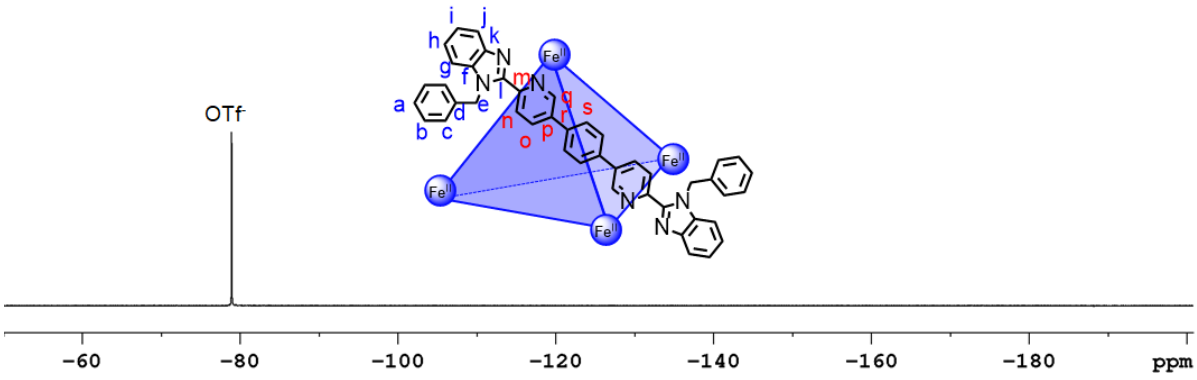

Figure S188. ^{19}F NMR spectrum (471 MHz, CD_3CN, 298 K) of cage **4**.

a)

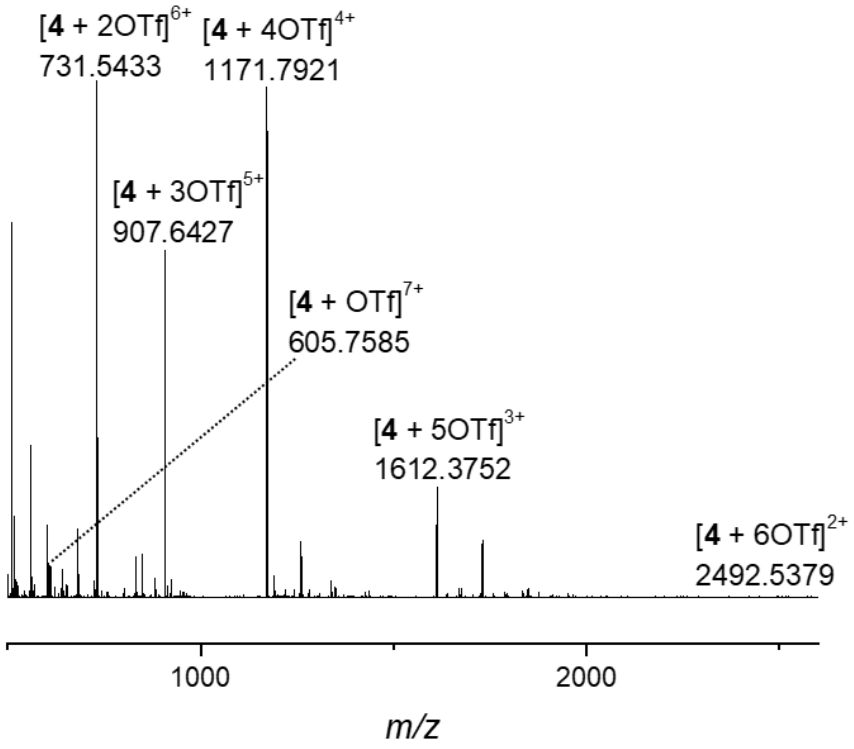

b)

Experimental

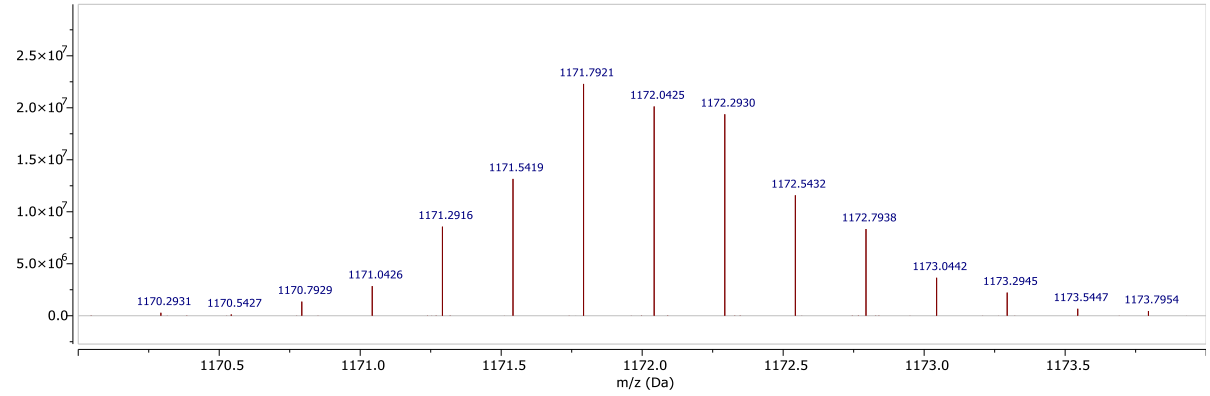

Theoretical

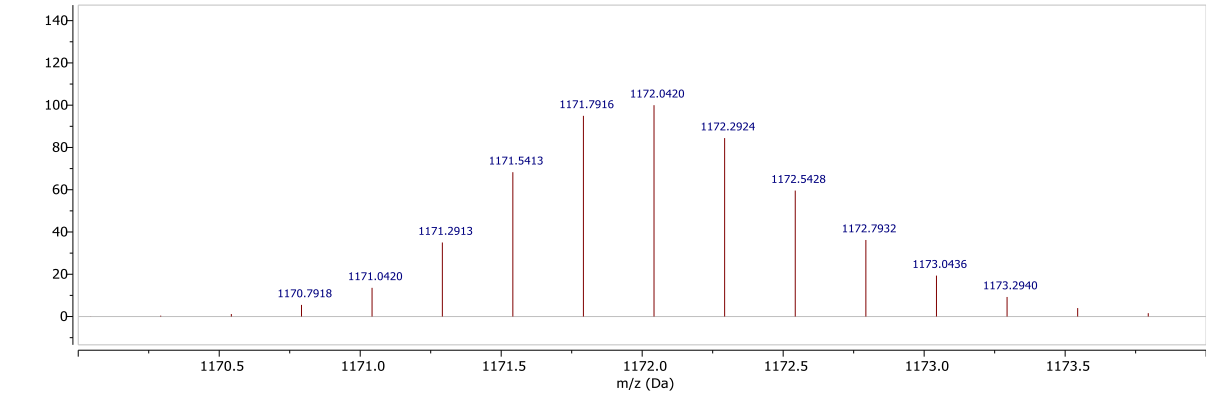

Figure S189. a) High resolution ESI mass spectrum of cage **4** and b) isotopic patterns of cage **4**: experimental (top) and theoretical (bottom).

4.5 Cage 5

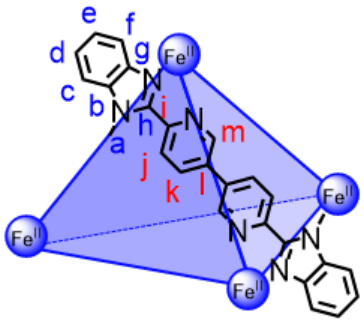

Iron(II) triflate (2.31 mg, 5.55 µmol) and 6',6''-di(1-methyl-1*H*-benzo[*d*]imidazol-2-yl)-3',3''-bipyridine (**24**) (3.46 mg, 8.31 µmol) were dissolved in dry CD_3CN (500 µL).

^{1}H NMR (600 MHz, CD_3CN, 298 K) δ (ppm): 11.41 (s, 12H, H_j), 9.72 (br, 12H, H_m), 8.87 (d, ^3J = 8.4 Hz, 12H, H_c), 7.41 (d, ^3J = 8.2 Hz, 12H, H_j), 7.30 (dd, ^3J = 8.4 Hz, ^3J = 7.4 Hz, 12H, H_d), 6.46 (unres. dd, 12H, H_e), 5.59 (s, 36H, H_a), 4.14 (br, 12H, H_f).

^{13}C NMR (151 MHz, CD_3CN, 298 K) δ (ppm): 163.6 (C_b), 156.5 (C_i), 151.4 (C_h), 141.0 (C_k), 137.5 (C_l), 134.3 (C_j), 127.0 (C_d), 124.9 (C_e), 119.1 (C_c), 118.6 (C_f), 38.3 (C_a).

HRMS (ESI): *m/z* = 1807.7483 [**5**+ 6OTf]$^{2+}$, 1155.8488 [**5** + 5OTf]$^{3+}$, 829.6484 [**5** + 4OTf]$^{4+}$, 633.7276 [**5** + 3OTf]$^{5+}$.

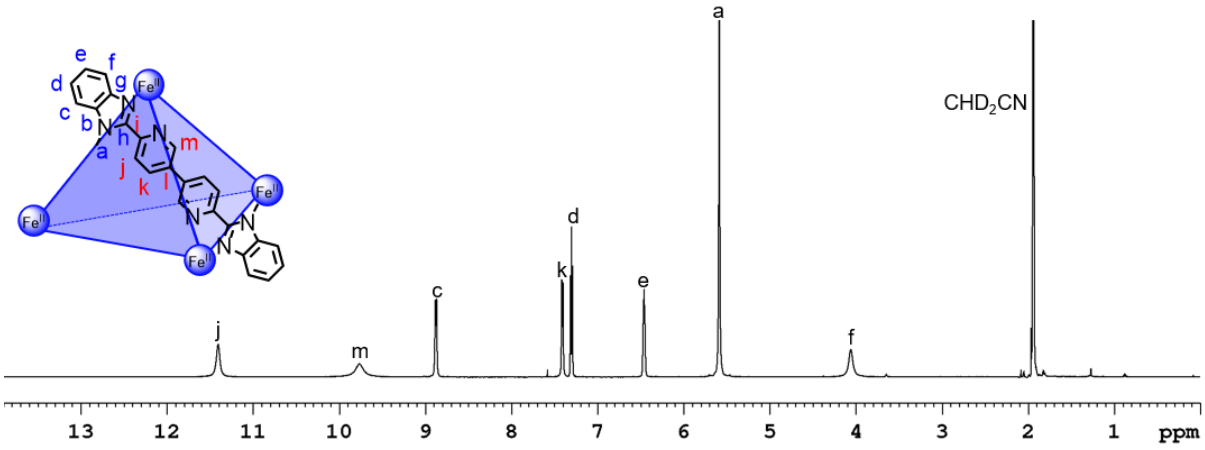

Figure S190. ^{1}H NMR spectrum (600 MHz, CD_3CN, 298 K) of cage **5**.

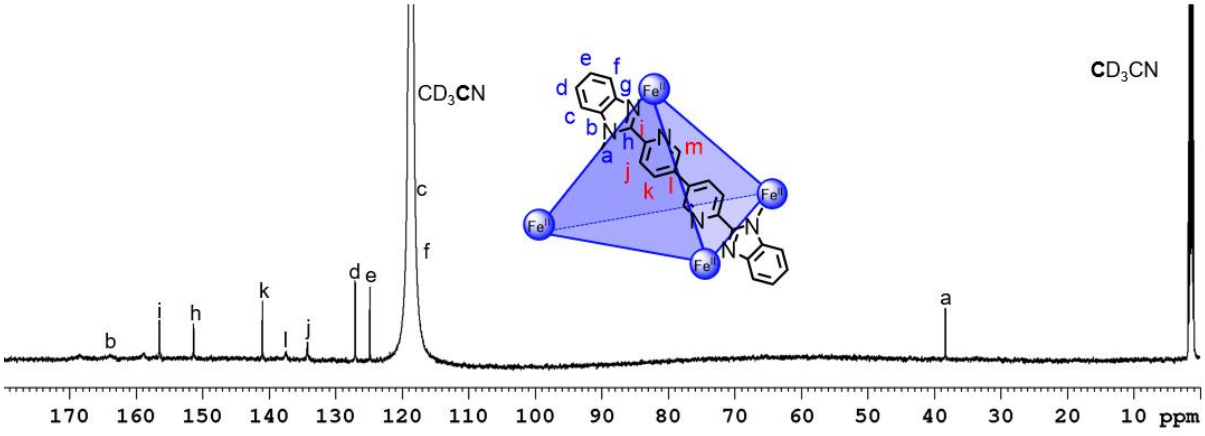

Figure S191. ^{13}C NMR spectrum (151 MHz, CD_3CN, 298 K) of cage **5**.

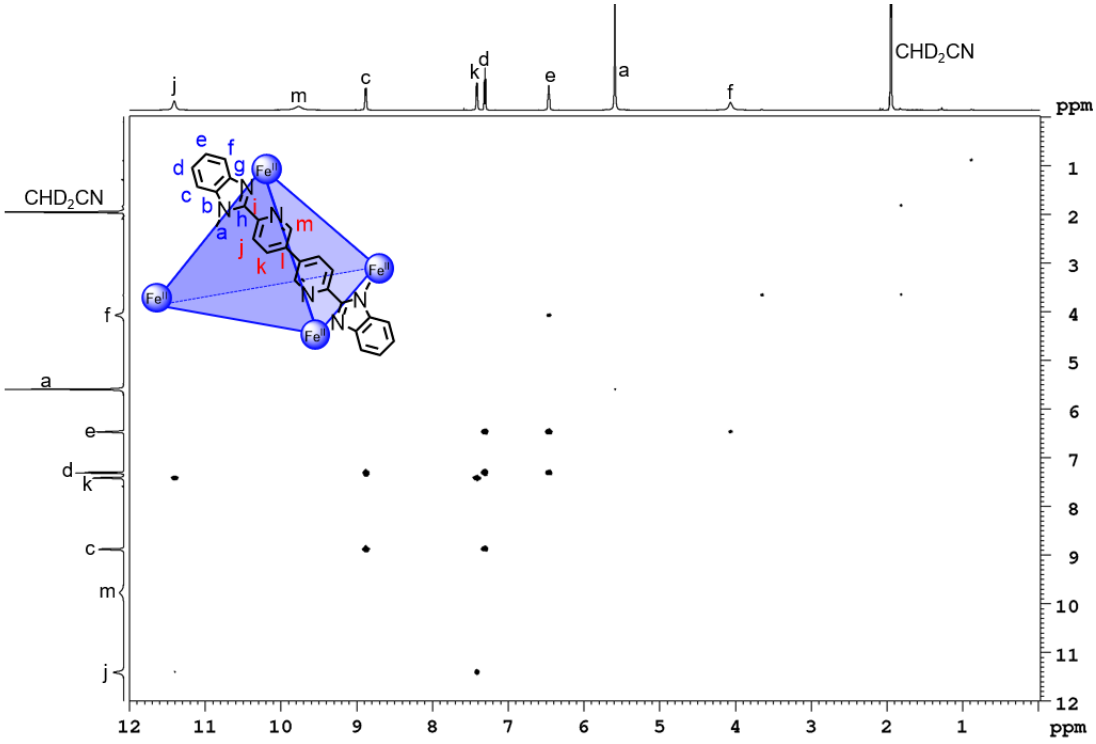

Figure S192. ^{1}H-^{1}H COSY NMR spectrum (600 MHz, CD_3CN, 298 K) of cage **5**.

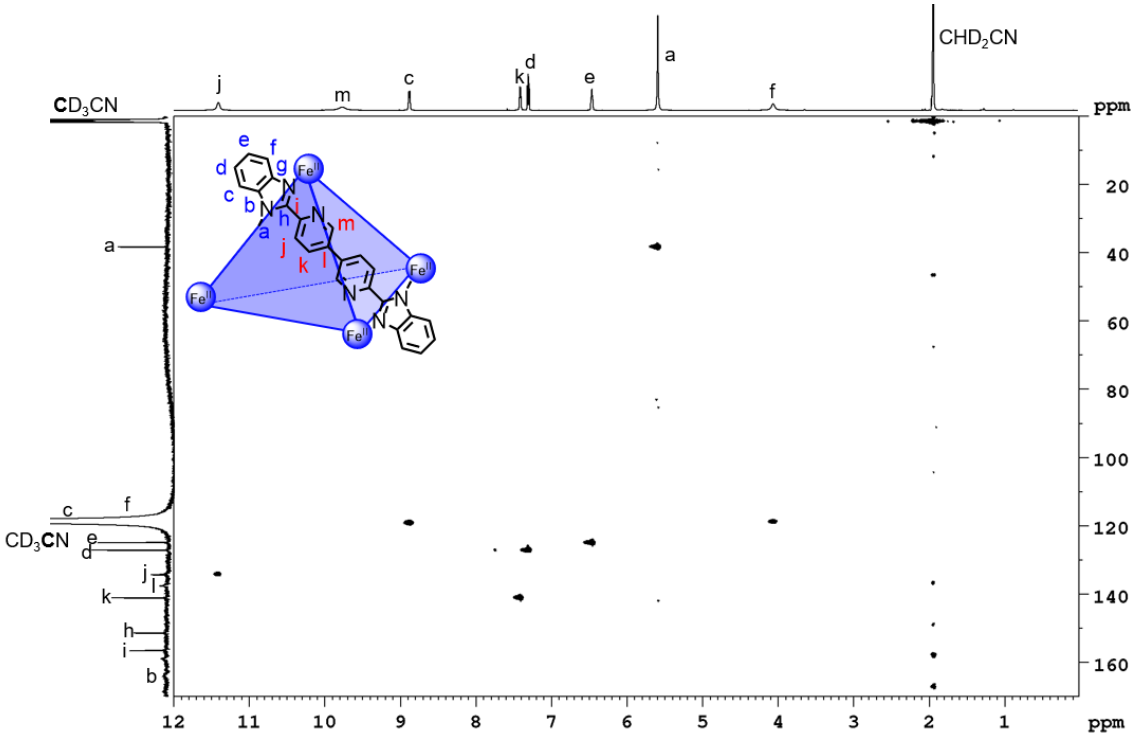

Figure S193. ^{1}H-^{13}C HSQC NMR spectrum (600 MHz/151 MHz, CD_3CN, 298 K) of cage **5**.

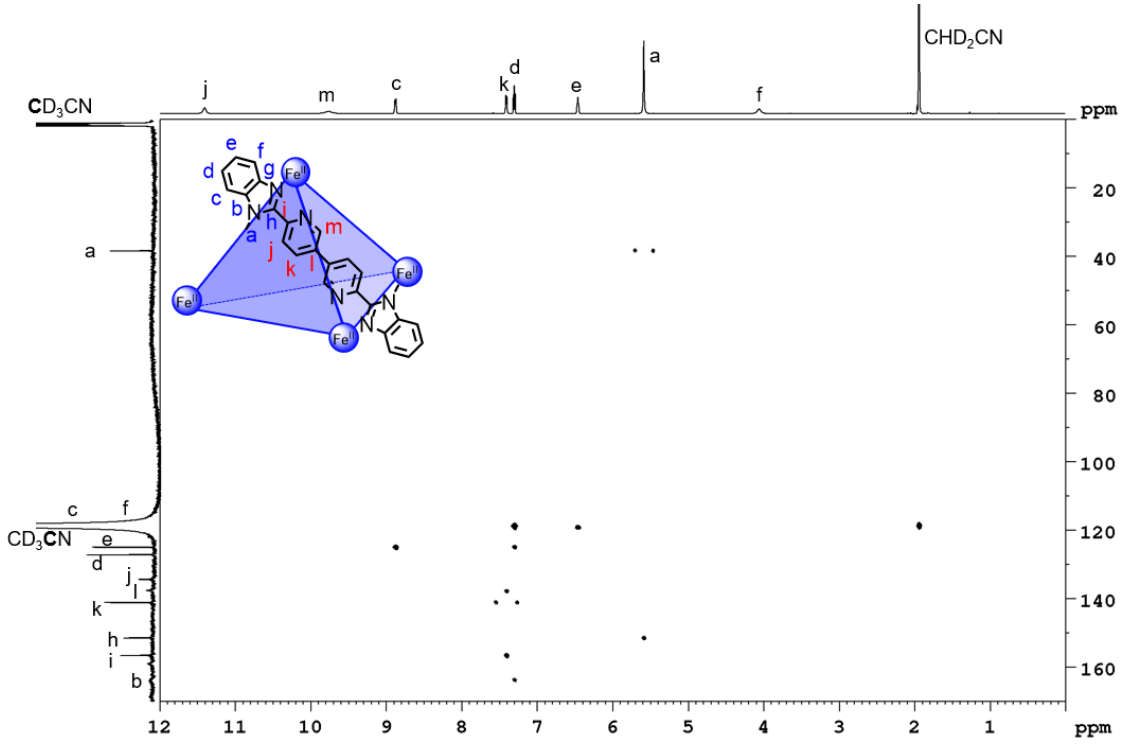

Figure S194. ^{1}H-^{13}C HMBC NMR spectrum (600 MHz/151 MHz, CD_3CN, 298 K) of cage **5**.

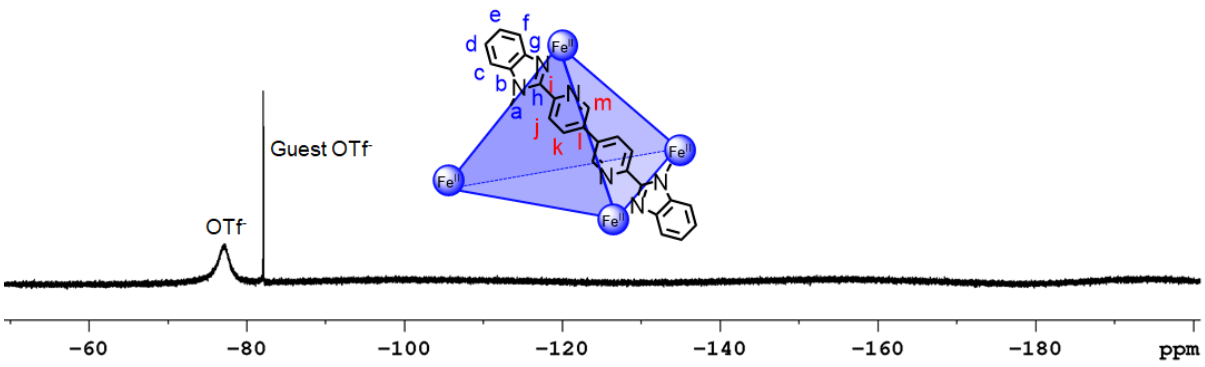

Figure S195. ^{19}F NMR spectrum (471 MHz, CD_3CN, 298 K) of cage **5**.

a)

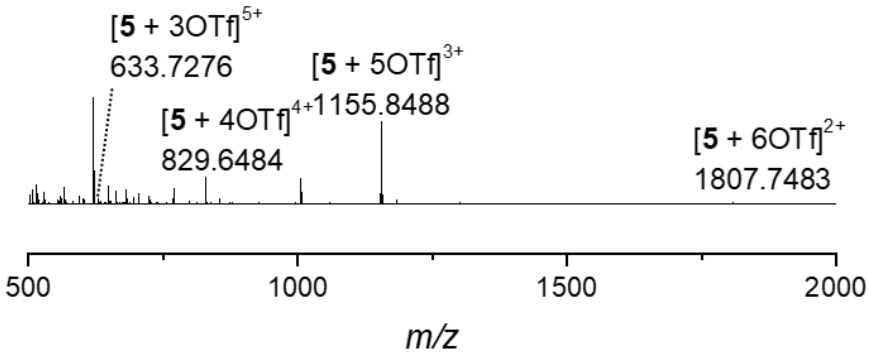

b)

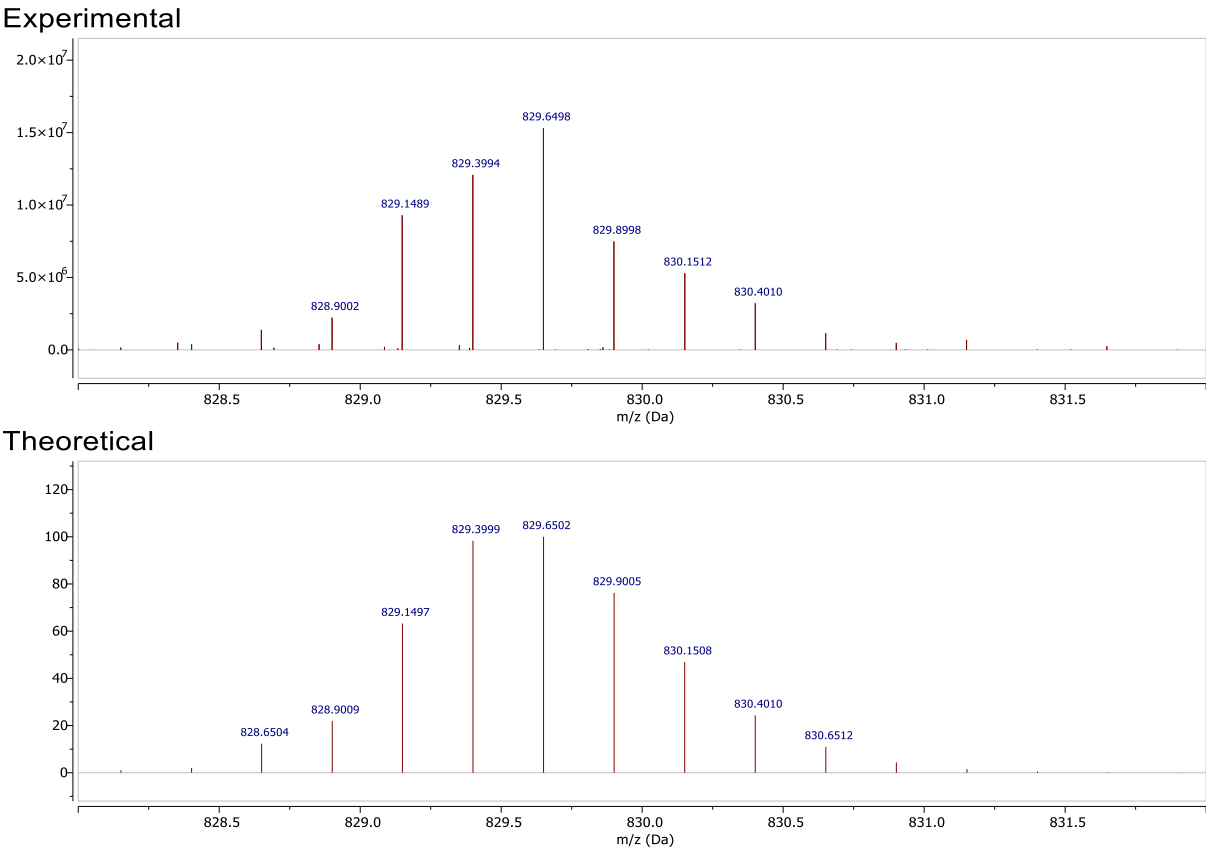

Figure S196. a) High resolution ESI mass spectrum of cage **5** and b) isotopic patterns of cage **5**: experimental (top) and theoretical (bottom).

4.6 Cage 6

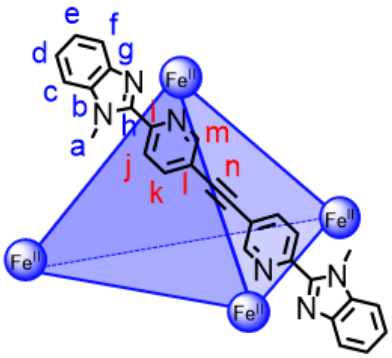

Iron(II) triflate (2.31 mg, 5.55 µmol) and 1,2-di(6''-(1'-methyl-1*H*-benzo[*d*]imidazole-2'-yl)pyridin-3''-yl)ethyne (**17**) (3.67 mg, 8.33 µmol) were dissolved in dry CD_3CN (500 µL) and heated for 143 h at 50 °C to prepare cage **6** *in situ*.

^{1}H NMR (600 MHz, CD_3CN, 298 K) δ (ppm): 16.3 (s, 12H, H_j), 15.1 (br, 12H, H_m), 10.8 (s, 12H, H_c), 7.19 (s, 48H, $H_{a,k}$), 6.97 (s, 12H, H_d), 5.75 (s, 12H, H_e), 1.05 (s, 12H, H_f).

^{13}C NMR (151 MHz, CD_3CN, 298 K) δ (ppm): 213.2 (s, C_{quart}), 209.8 (s, C_{quart}), 184.6 (s, C_{quart}), 157.2 (d, ^1J = 191 Hz, C_m), 152.1 (d, ^1J = 164 Hz, C_j), 148.1 (d, ^1J = 175 Hz, C_k), 140.3 (s, C_{quart}), 128.2 (d, ^1J = 167 Hz, C_c), 126.5 (d, ^1J = 165 Hz, C_d), 122.2 (d, ^1J = 162 Hz, C_e), 120.9 (d, ^1J = 165 Hz, C_f), 108.6 (s, C_{quart}), 105.8 (s, C_{quart}), 46.0 (d, ^1J = 143 Hz, C_a).

HRMS (ESI): *m/z* = 1880.2554 [**6** + 6OTf]$^{2+}$, 1203.8511 [**6** + 5OTf]$^{3+}$, 865.6493 [**6** + 4OTf]$^{4+}$, 662.7292 [**6** + 3OTf]$^{5+}$, 527.4492 [**6** + 2OTf]$^{6+}$, 430.8211 [**6** + OTf]$^{7+}$.

While the signal at *m/z* 430.8211 is consistent with the 7+ charge for the cage, the theoretical isotopic pattern does not match, possibly due to fragmentation in the gas phase or overlap with other signals.

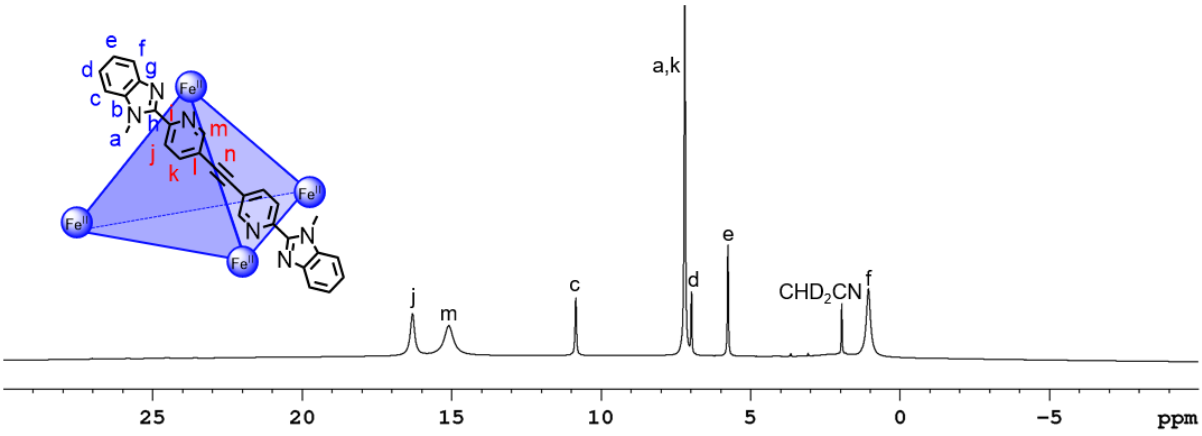

Figure S197. ^{1}H NMR spectrum (600 MHz, CD_3CN, 298 K) of cage **6**.

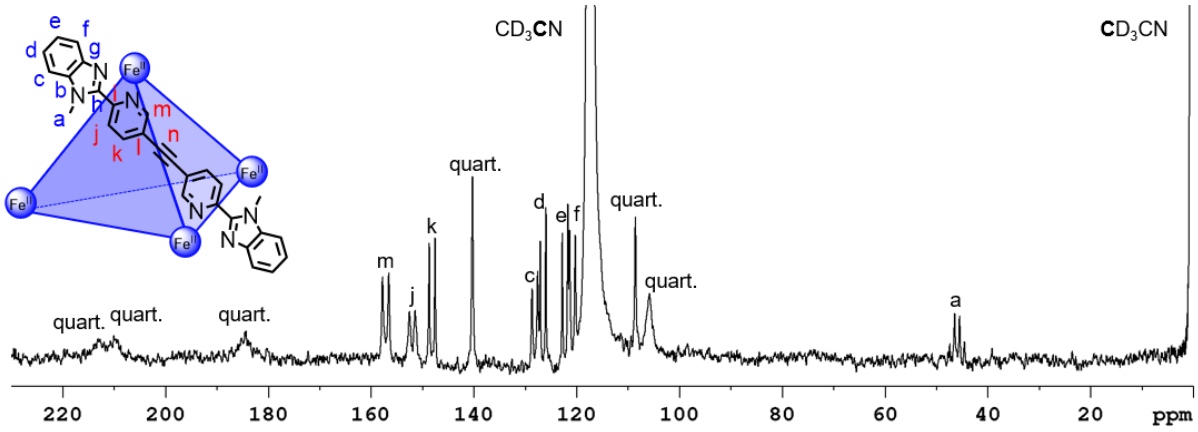

Figure S198. ^{13}C NMR spectrum (151 MHz, CD_3CN, 298 K) of cage **6**.

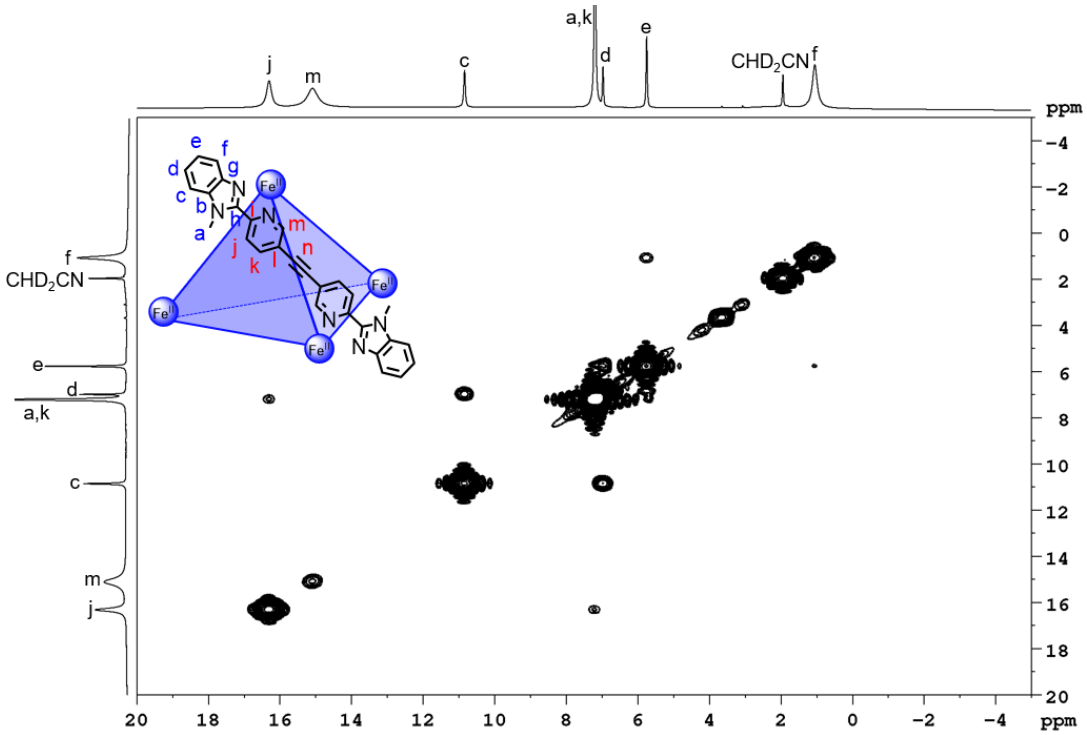

Figure S199. ^{1}H-^{1}H COSY NMR spectrum (600 MHz, CD_3CN, 298 K) of cage **6**.

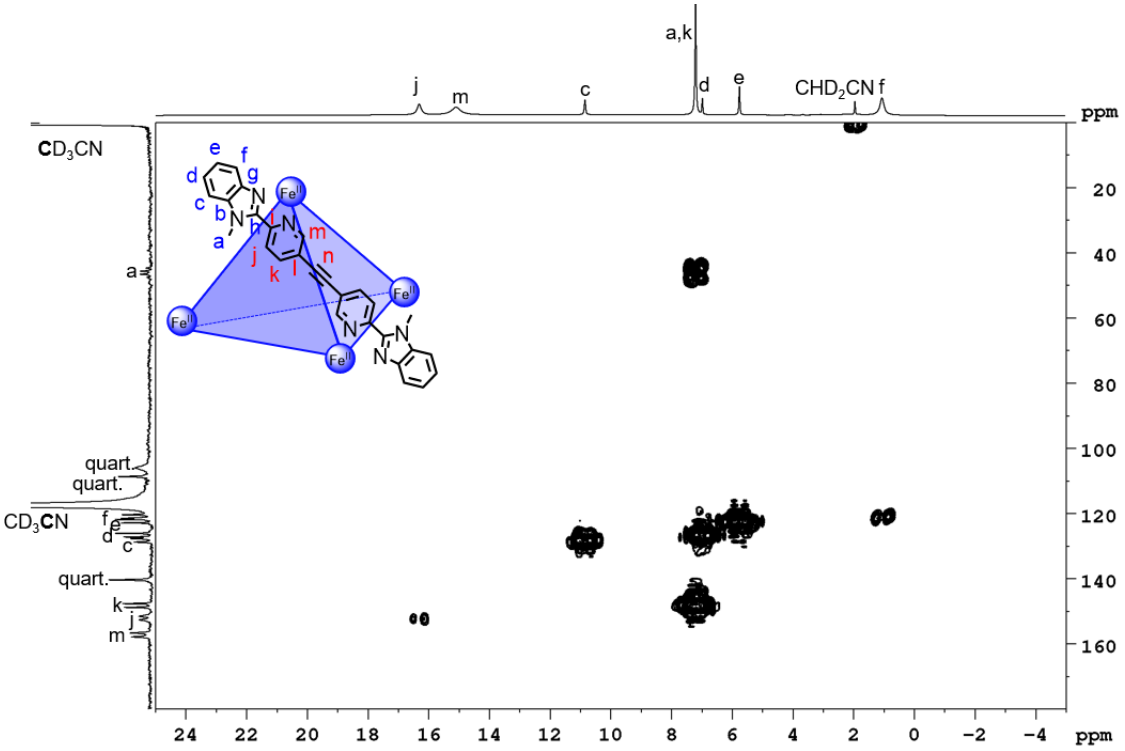

Figure S200. ^{1}H-^{13}C HMQC NMR spectrum (600 MHz/151 MHz, CD_3CN, 298 K) of cage **6**.

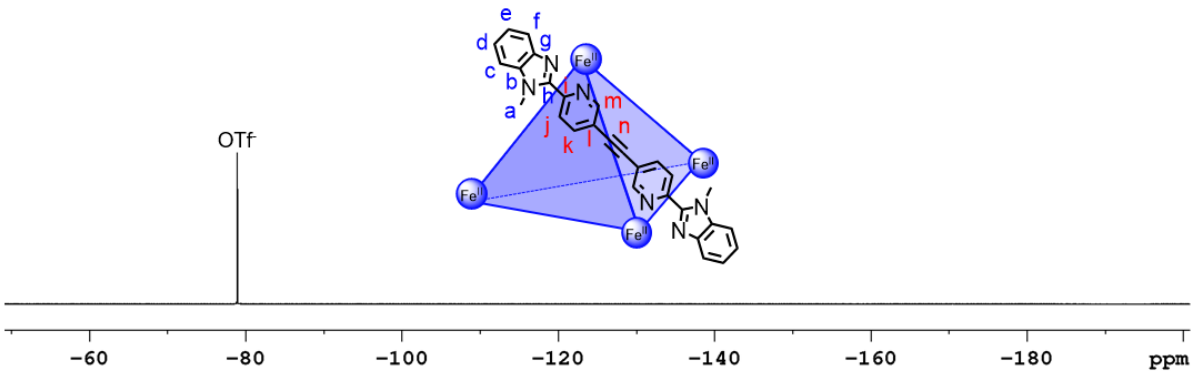

Figure S201. ^{19}F NMR spectrum (471 MHz, CD_3CN, 298 K) of cage **6**.

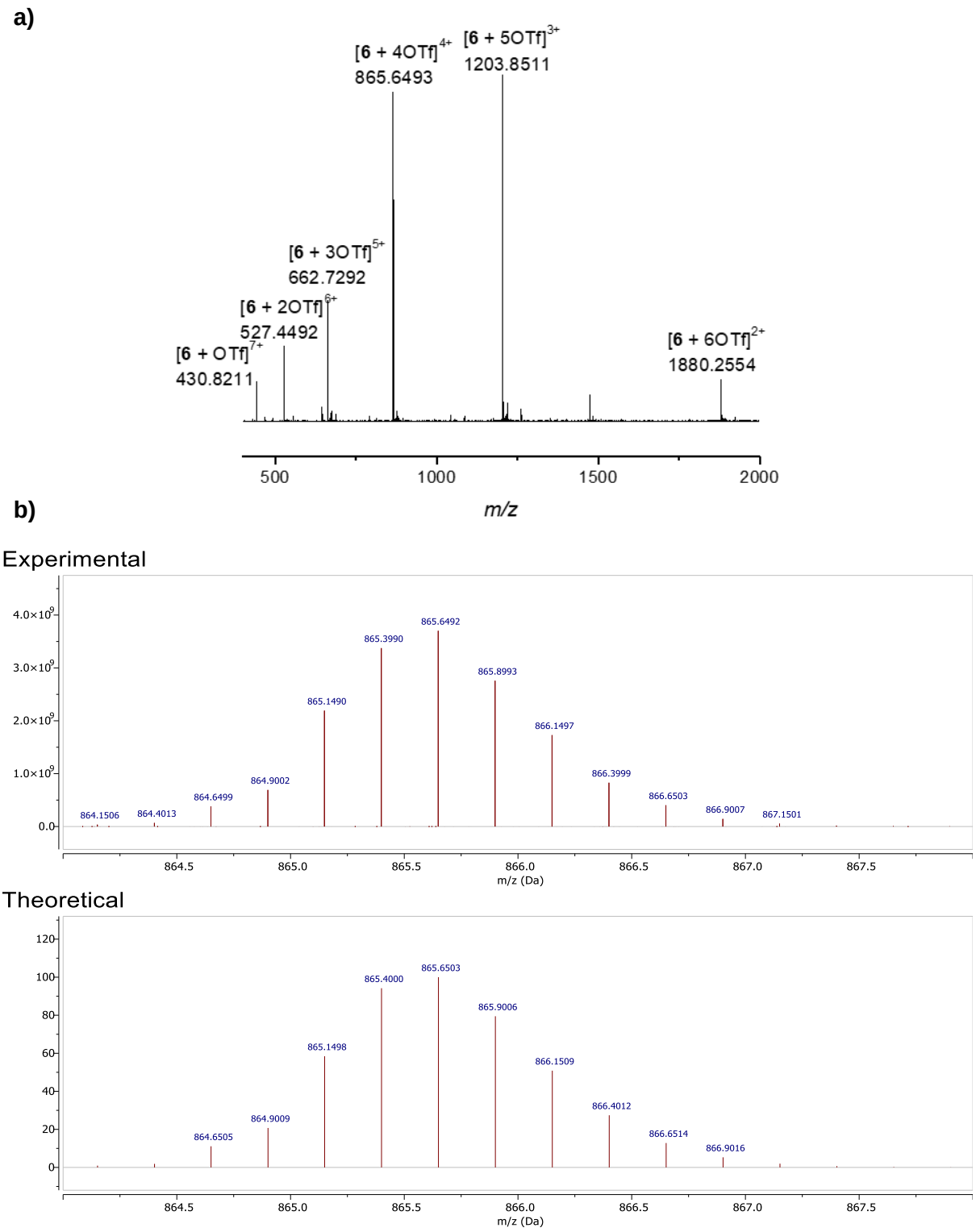

Figure S202. a) High resolution ESI mass spectrum of cage **6** and b) isotopic patterns of cage **6**: experimental (top) and theoretical (bottom).

4.7 Cage 7

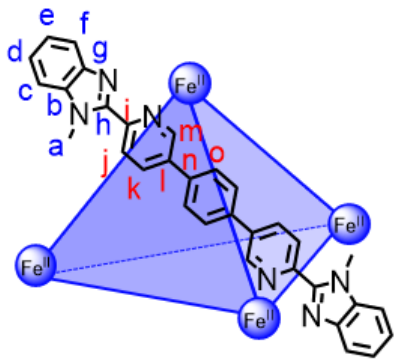

Iron(II) triflate (2.33 mg, 5.59 µmol) and 1,4-di(6''-(1'-methyl-1*H*-benzo[*d*]imidazol-2'-yl)pyridin-3''-yl)benzene (**27**) (4.14 mg, 8.40 µmol) were dissolved in dry CD_3CN (500 µL).

^{1}H NMR (500 MHz, CD_3CN, 298 K) δ (ppm): 13.10 (s, 12H, H_j), 12.2 (br, 12H, H_m), 9.44 (d, ^3J = 8.1 Hz, 12H, H_c), 7.86 (d, ^3J = 8.4 Hz, 12H, H_k), 7.14 (t, ^3J = 7.6 Hz, 12H, H_d), 6.75 (s, 24H, H_o), 6.26 (unres. dd, 12H, H_e), 5.86 (s, 36H, H_a), 3.22 (s, 12H, H_f).

^{13}C NMR (126 MHz, CD_3CN, 298 K) δ (ppm): 152.5 ($C_{quart.}$), 144.6 ($C_{quart.}$), 141.4 ($C_{quart.}$), 140.2 (C_o), 128.7 (C_s), 127.2 (C_d), 124.3 (C_e), 122.5 (C_c), 120.0 (C_f), 41.7 (C_a).

HRMS (ESI): *m/z* = 2036.3478 [**7** + 6OTf]$^{2+}$, 1307.9146 [**7** + 5OTf]$^{3+}$, 943.6976 [**7** + 4OTf]$^{4+}$, 724.9670 [**7** + 3OTf]$^{5+}$, 579.4813 [**7** + 2OTf]$^{6+}$.

While the signal at *m/z* 579.4813 is consistent with the 6+ charge for the cage, the theoretical isotopic pattern does not match, possibly due to fragmentation in the gas phase or overlap with other signals.

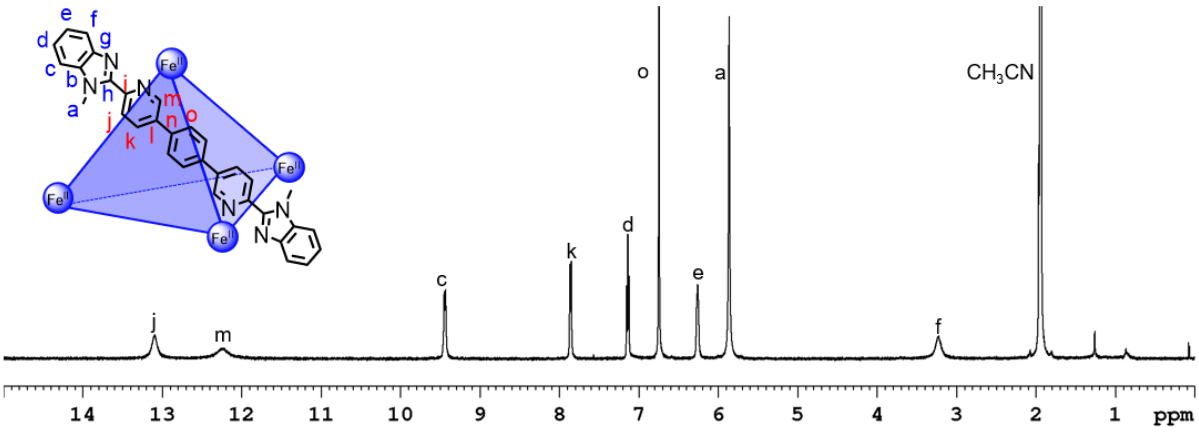

Figure S203. ^{1}H NMR spectrum (500 MHz, CD_3CN, 298 K) of cage **7**.

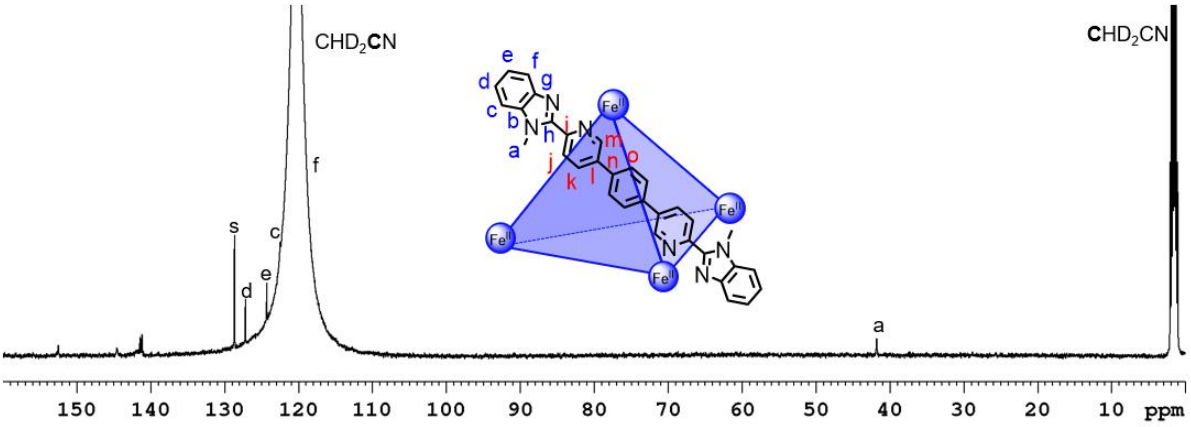

Figure S204. ^{13}C NMR spectrum (126 MHz, CD_3CN, 298 K) of cage **7**.

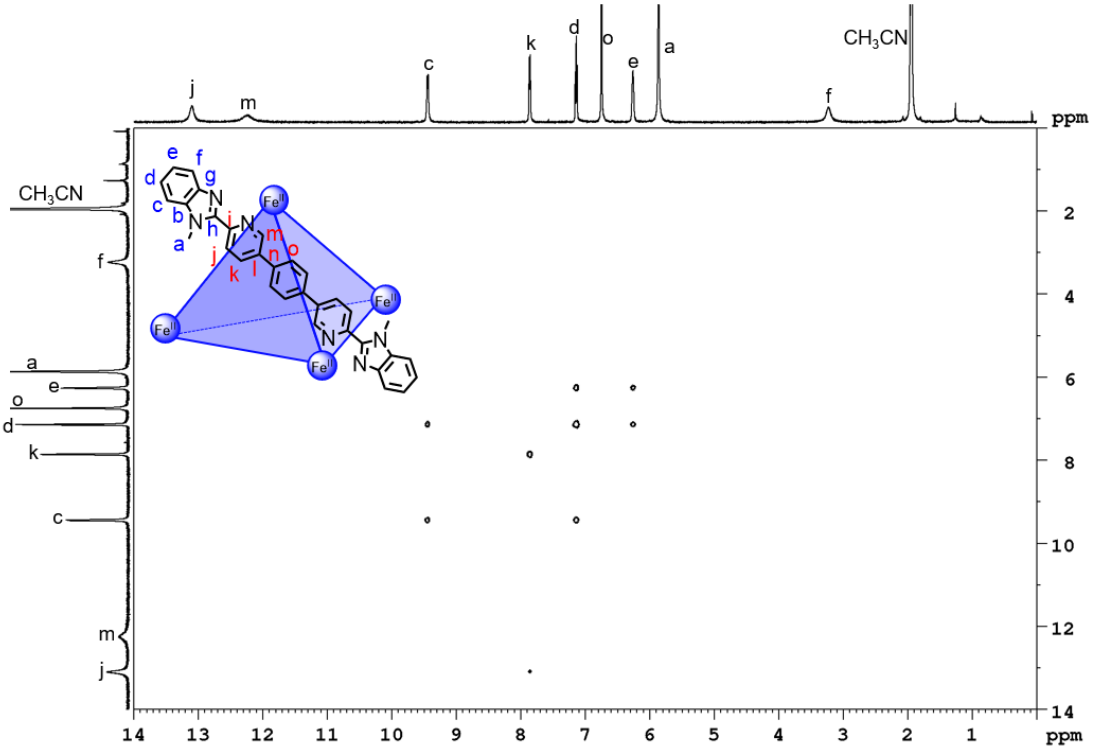

Figure S205. ^{1}H-^{1}H COSY NMR spectrum (500 MHz, CD_3CN, 298 K) of cage **7**.

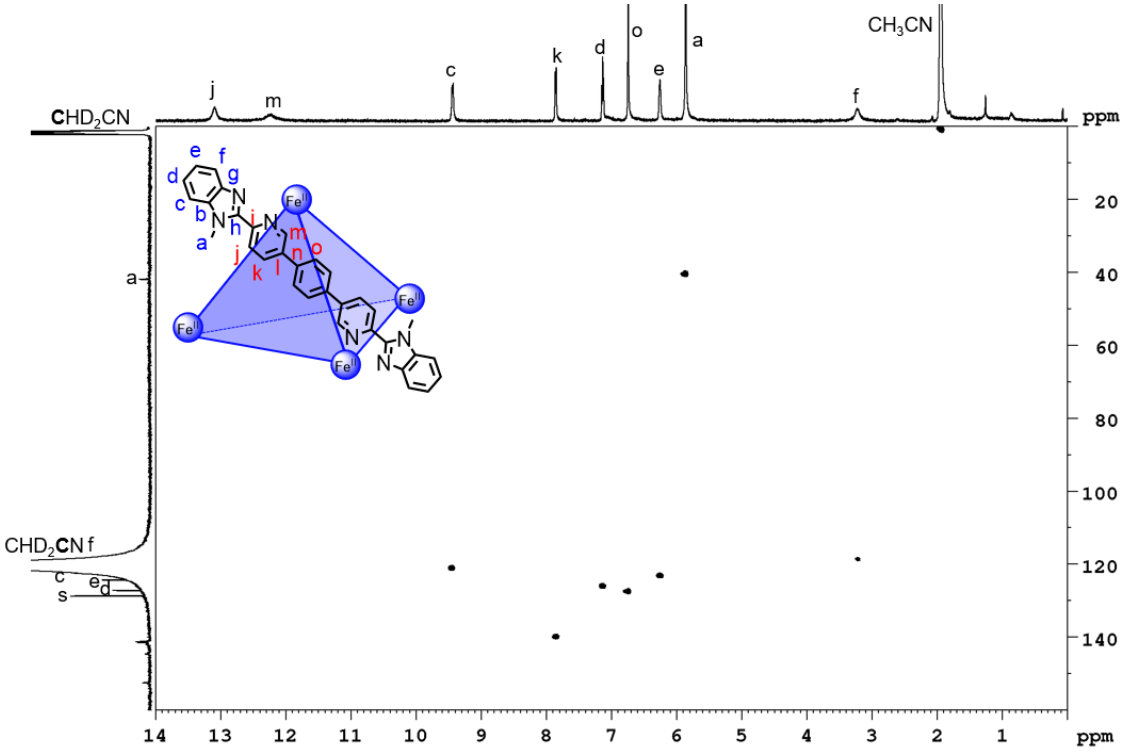

Figure S206. ^{1}H-^{13}C HSQC NMR spectrum (500 MHz/126 MHz, CD_3CN, 298 K) of cage **7**.

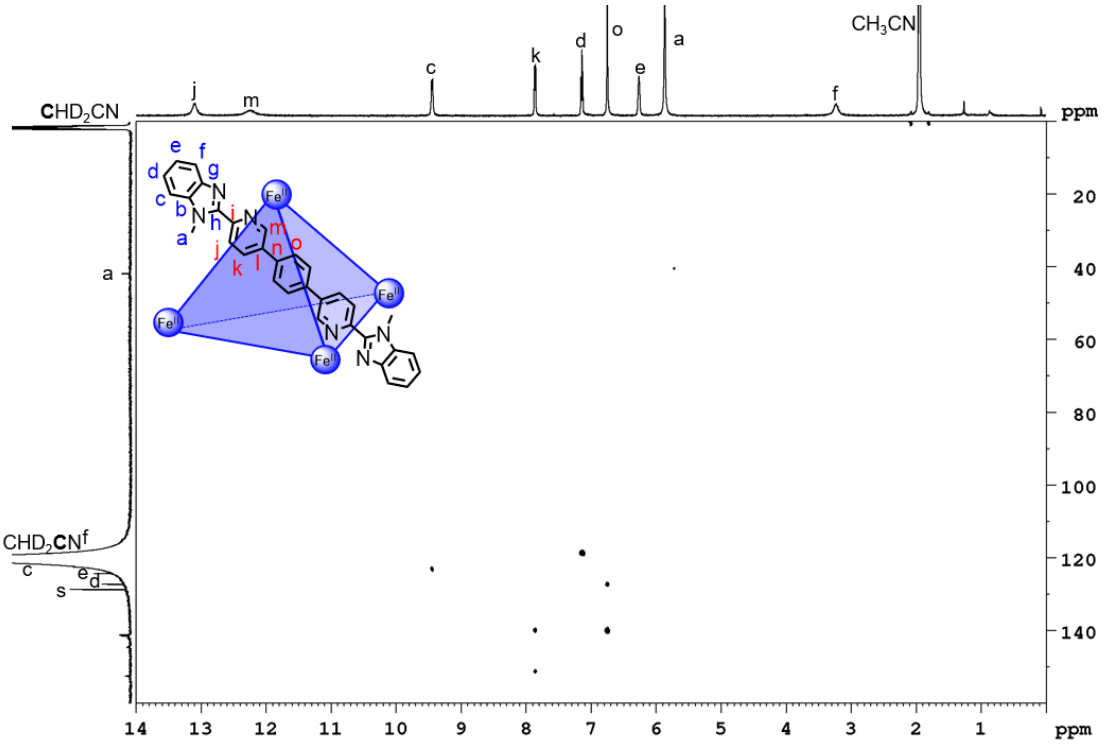

Figure S207. ^{1}H-^{13}C HMBC NMR spectrum (500 MHz/126 MHz, CD_3CN, 298 K) of cage **7**.

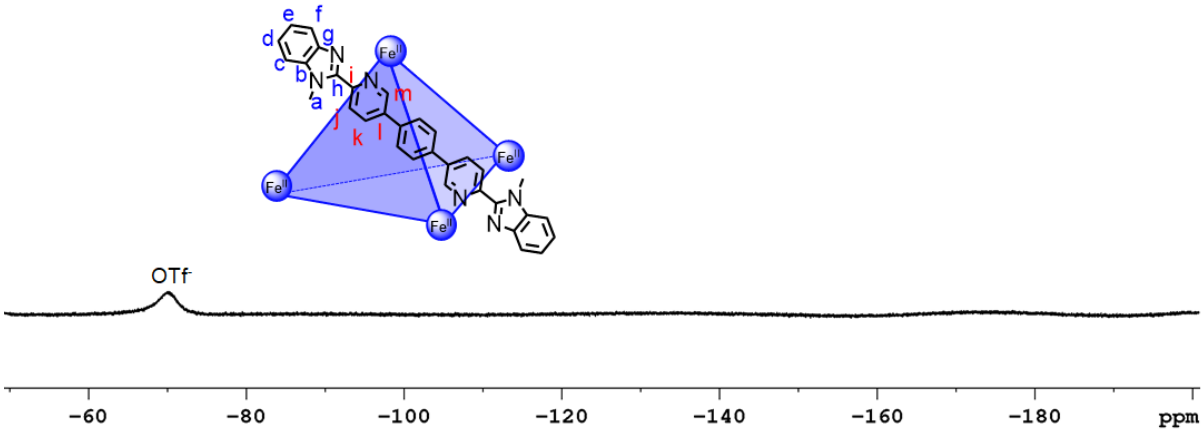

Figure S208. ^{19}F NMR spectrum (471 MHz, CD_3CN, 298 K) of cage **7**.

a)

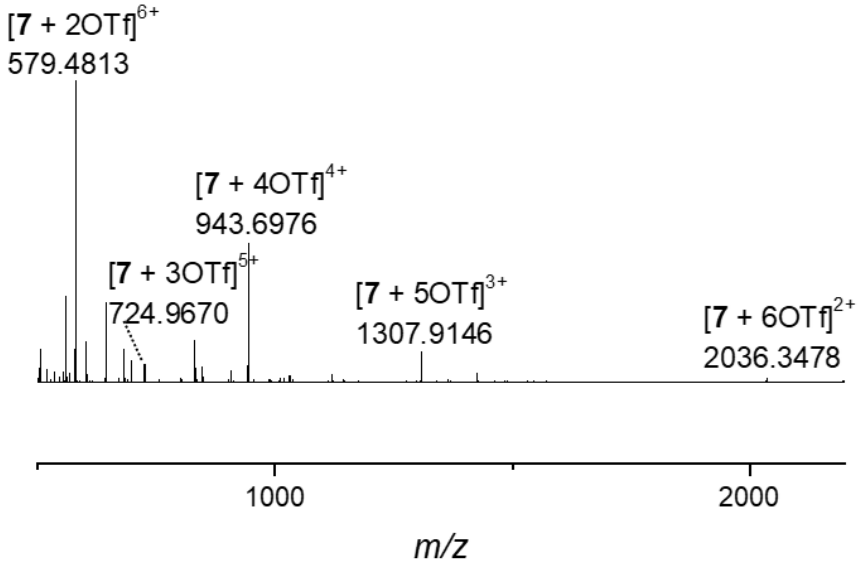

b)

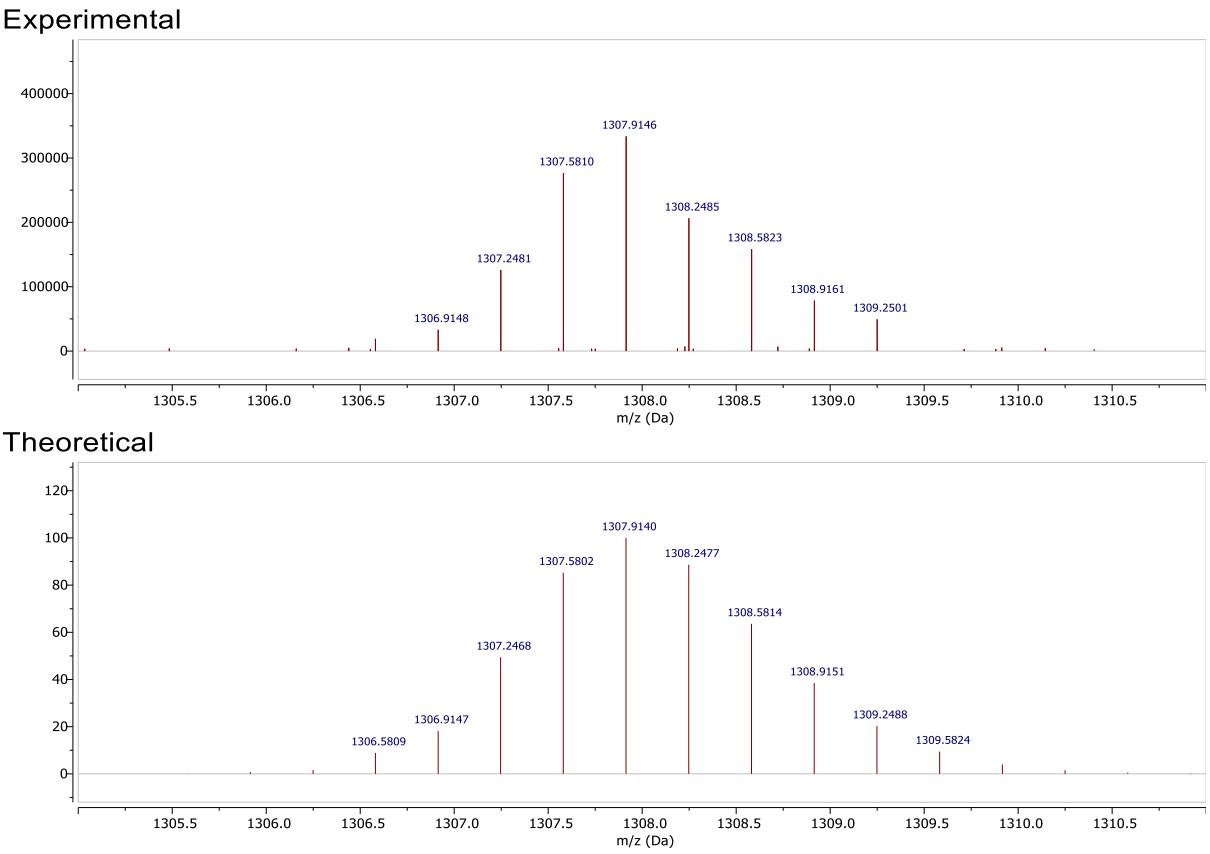

Figure S209. a) High resolution ESI mass spectrum of cage **7** and b) isotopic patterns of cage **7**: experimental (top) and theoretical (bottom).

4.8 Cage 8

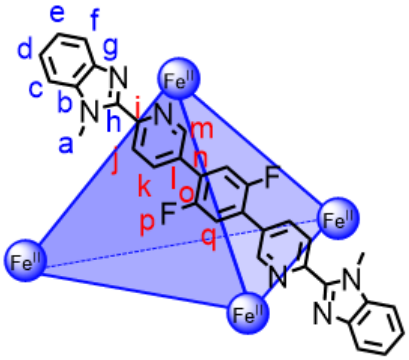

Iron(II) triflate (2.31 mg, 5.55 µmol) and 1,4-di(6''-(1'-methyl-1*H*-benzo[*d*]imidazol-2'-yl)pyridin-3''-yl)-2,5-difluorobenzene (**32**) (4.40 mg, 8.32 µmol) were dissolved in dry CD_3CN (500 µL).

^{1}H NMR (600 MHz, CD_3CN, 298 K) δ (ppm): 17.5 (br, 12H, H_m), 17.1 (s, 12H, H_j), 11.0 (s, 12H, H_c), 7.17 (d, ^3J = 6.5 Hz, 12H, H_k), 7.06 (s, 36H, H_a), 7.00 (t, ^3J = 7.5 Hz, 12H, H_d), 6.61 (unres. dt, 12H, H_q), 5.97 (unres. d, 12H, H_e), 2.28 (br, 12H, H_f).

^{13}C NMR (151 MHz, CD_3CN, 298 K) δ (ppm): 156.8 ($C_{quart.}$), 155.2 ($C_{quart.}$), 154.8 ($C_{quart.}$), 146.2 (C_k), 136.1 ($C_{quart.}$), 133.8 ($C_{quart.}$), 129.0 (C_c), 126.2 (C_d), 121.8 (C_e), 121.4 ($C_{quart.}$), 46.4 (C_a).

HRMS (ESI): *m/z* = 2144.2912 [**8** + 6OTf]$^{2+}$, 1379.8754 [**8** + 5OTf]$^{3+}$, 997.6674 [**8** + 4OTf]$^{4+}$, 768.3437 [**8** + 3OTf]$^{5+}$, 615.4611 [**8** + 2OTf]$^{6+}$, 506.1155 [**8** + OTf]$^{7+}$.

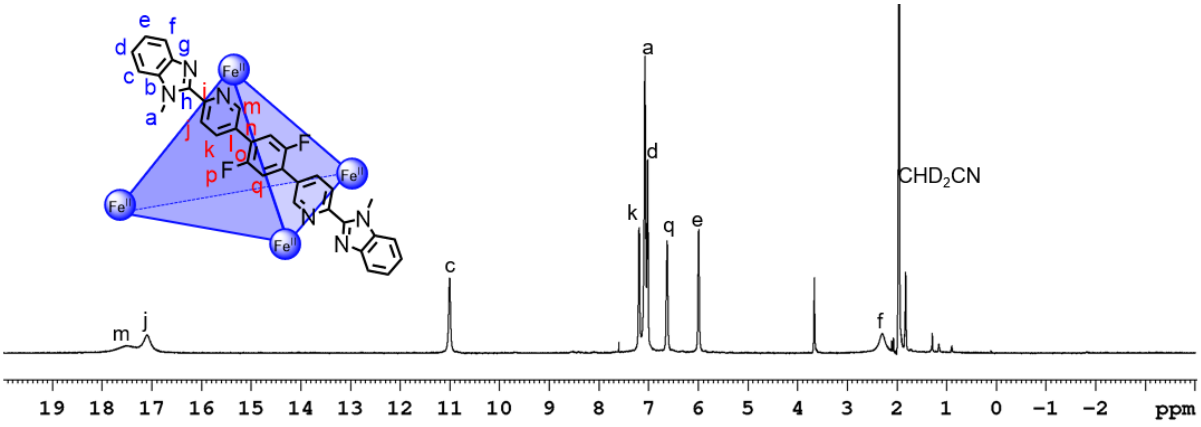

Figure S210. ^{1}H NMR spectrum (600 MHz, CD_3CN, 298 K) of cage **8**.

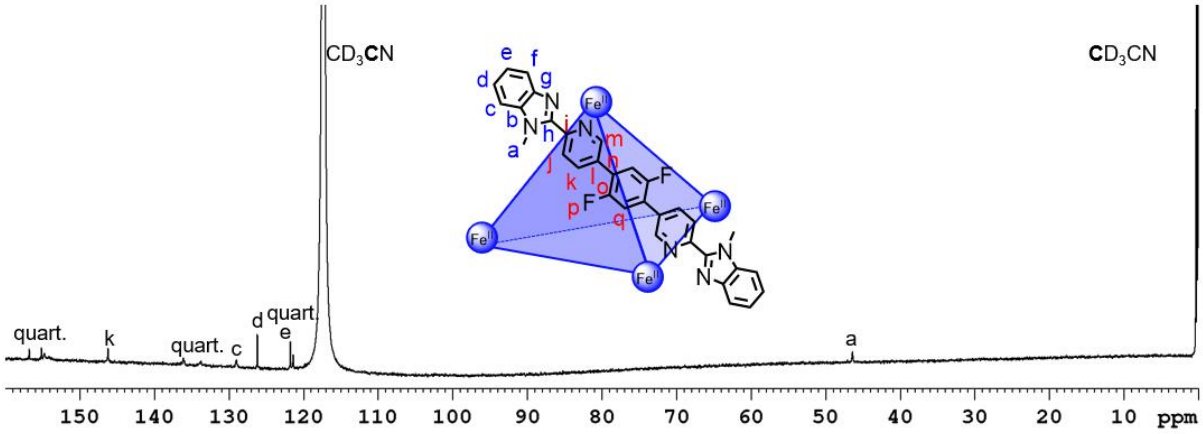

Figure S211. ^{13}C NMR spectrum (151 MHz, CD_3CN, 298 K) of cage **8**.

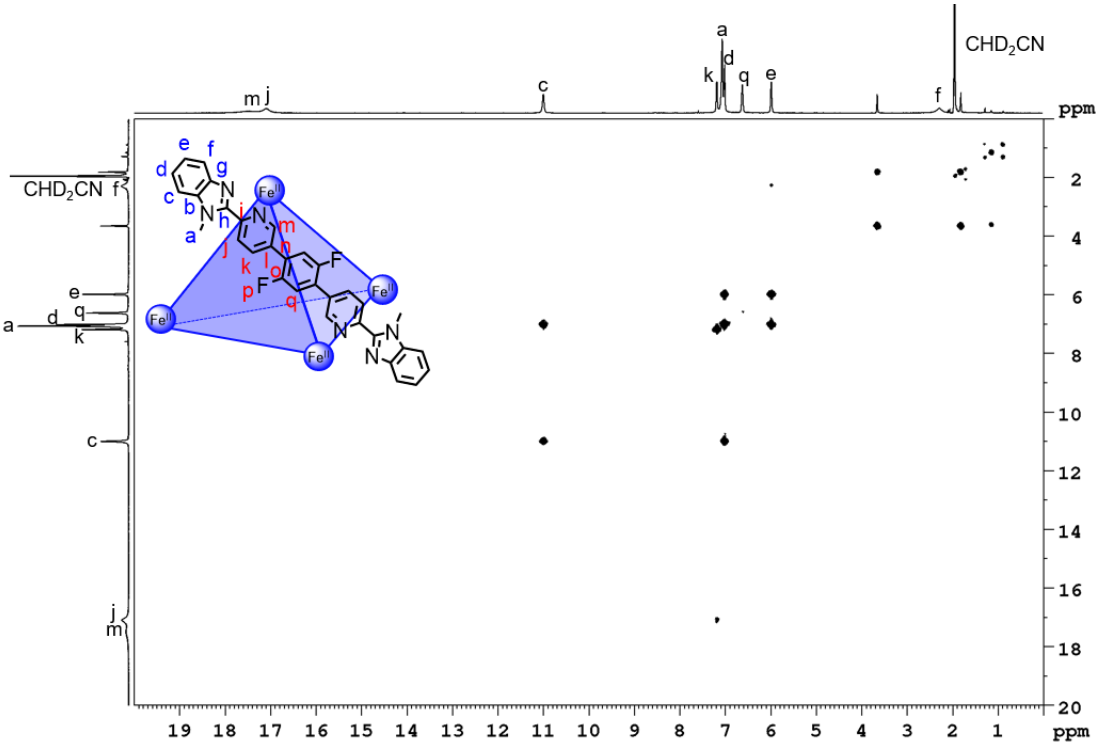

Figure S212. ^{1}H-^{1}H COSY NMR spectrum (600 MHz, CD_3CN, 298 K) of cage **8**.

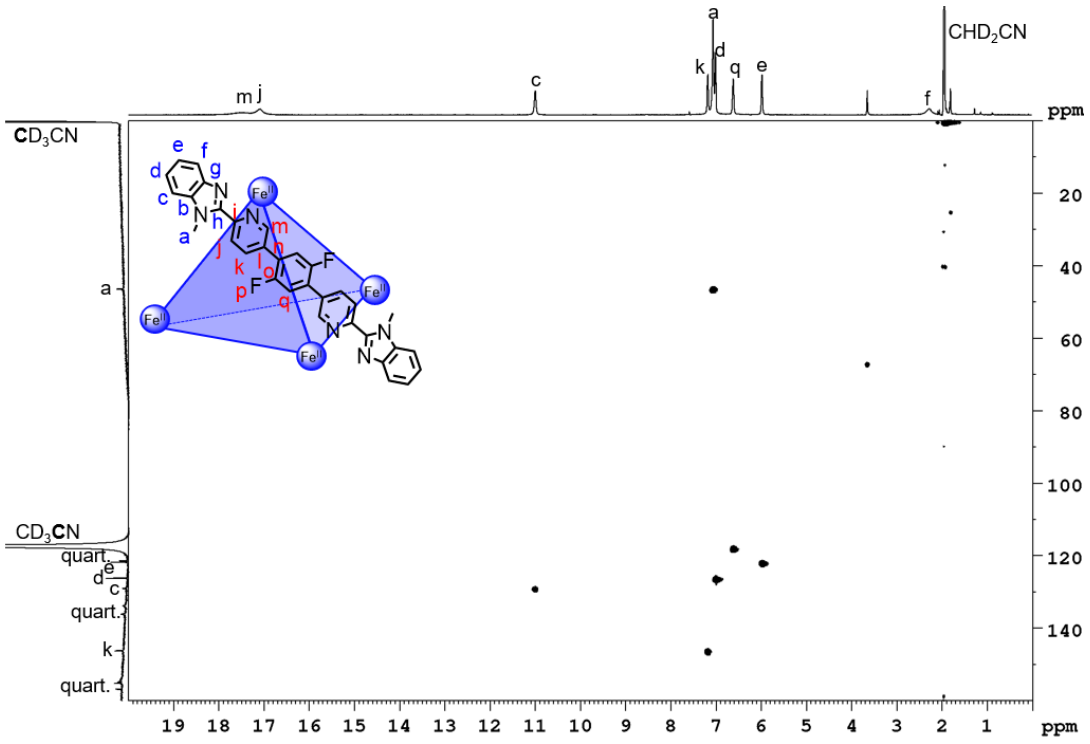

Figure S213. ^{1}H-^{13}C HSQC NMR spectrum (600 MHz/151 MHz, CD_3CN, 298 K) of cage **8**.

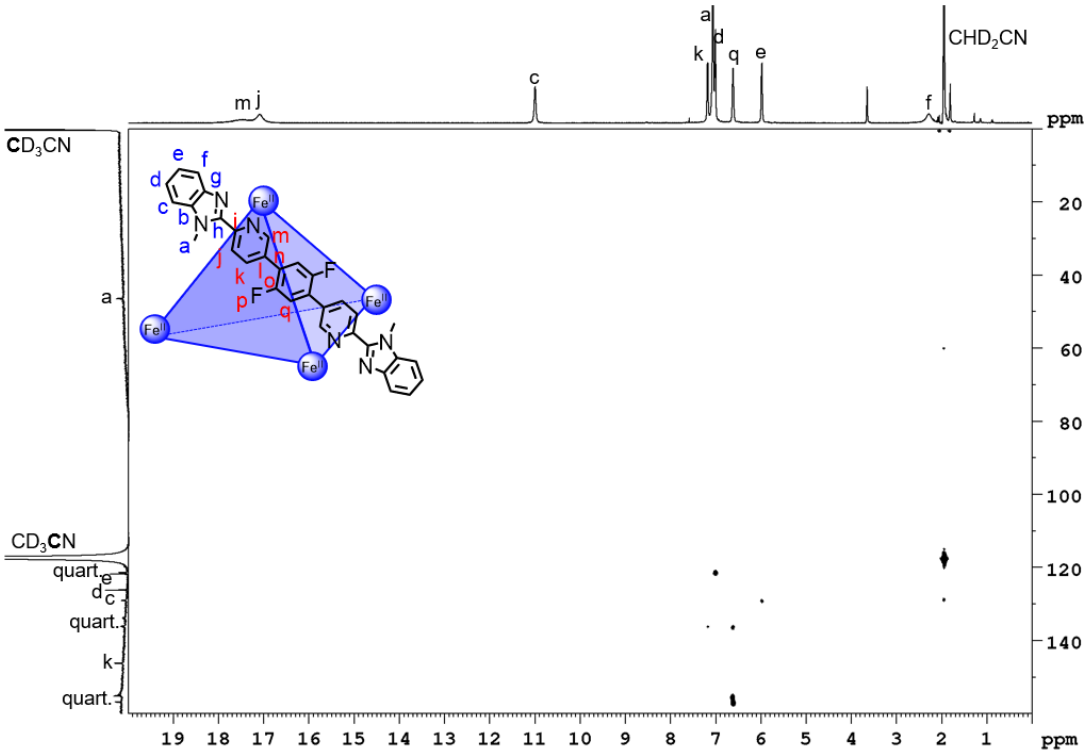

Figure S214. ^{1}H-^{13}C HMBC NMR spectrum (600 MHz/151 MHz, CD_3CN, 298 K) of cage **8**.

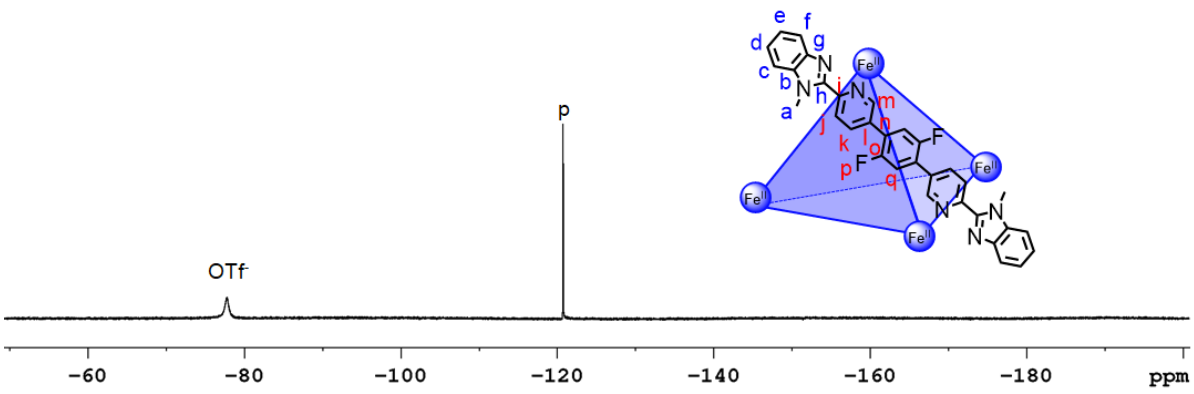

Figure S215. ^{19}F NMR spectrum (471 MHz, CD_3CN, 298 K) of cage **8**.

a)

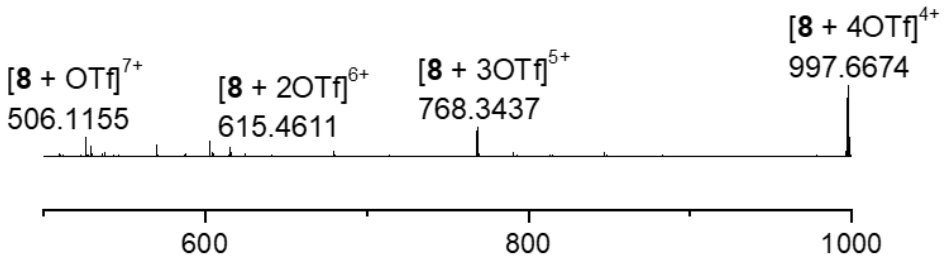

b)

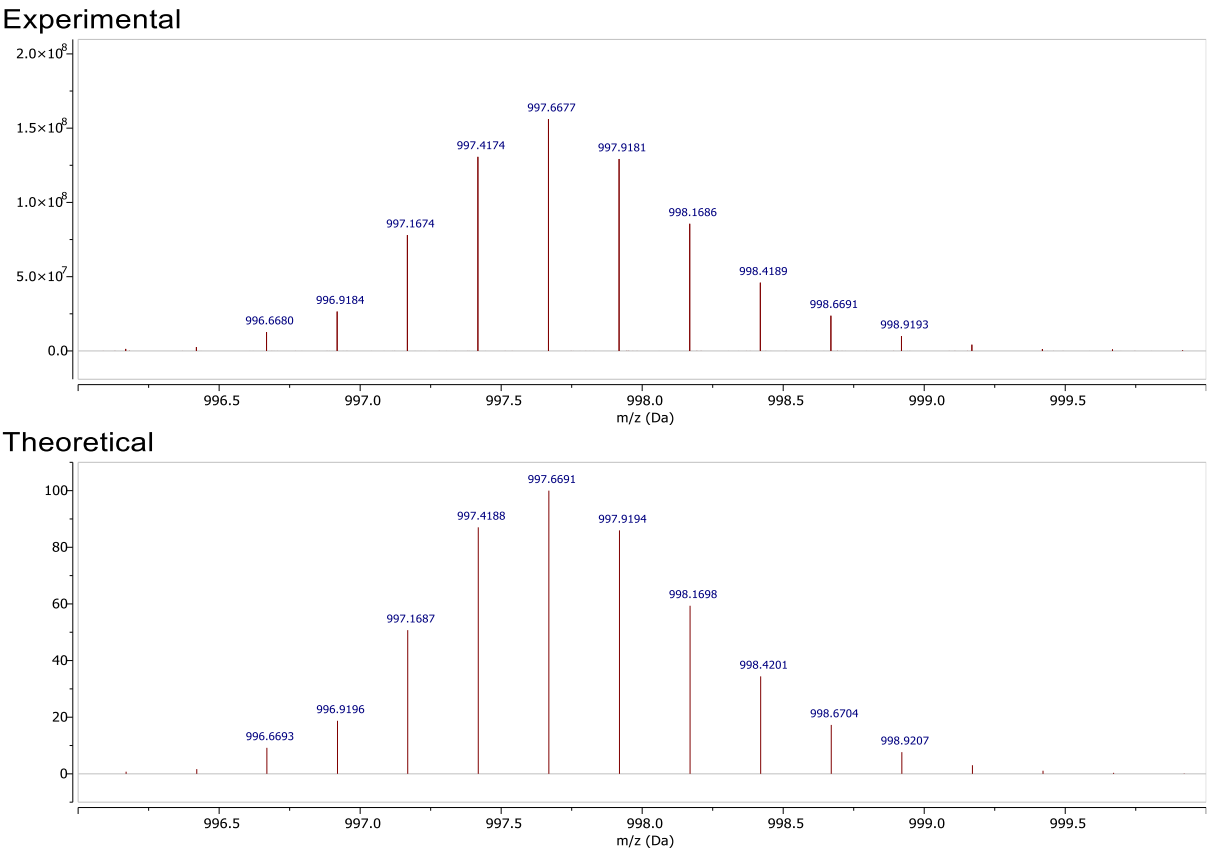

Figure S216. a) High resolution ESI mass spectrum of cage **8** (range *m/z* 500-1000) and b) isotopic patterns of cage **8**: experimental (top) and theoretical (bottom).

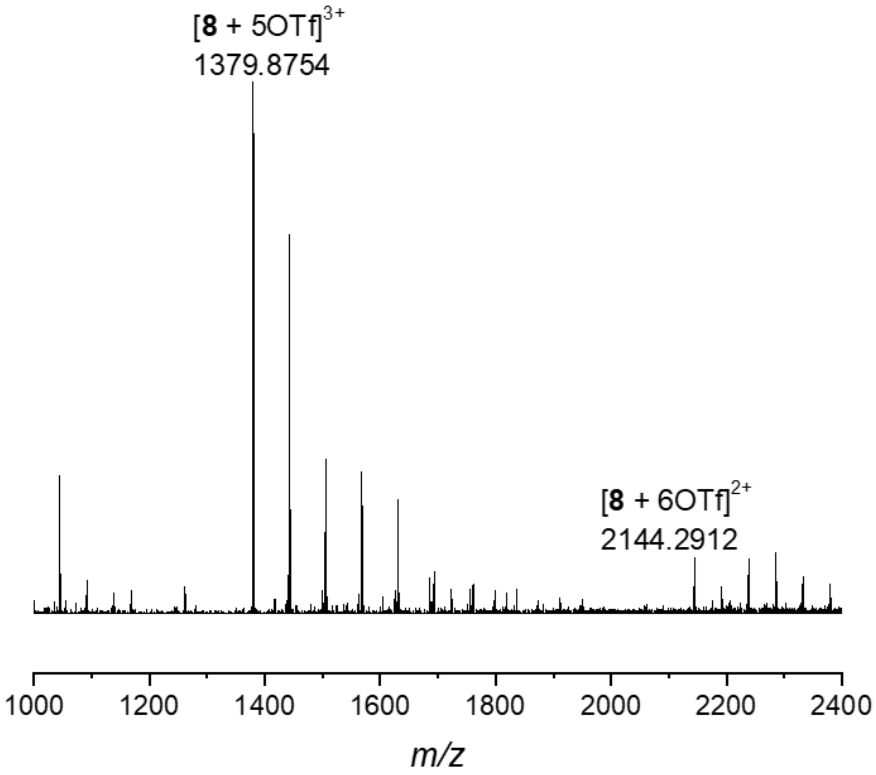

Figure S217. High resolution ESI mass spectrum (range *m/z* 1000-2400) of cage **8**.

4.9 Cage 9

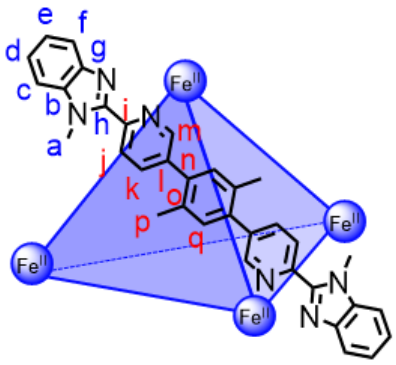

Iron(II) triflate (2.36 mg, 5.67 µmol) and 1,4-di(6''-(1'-methyl-1*H*-benzo[*d*]imidazol-2'-yl)pyridin-3''-yl)-2,5-dimethylbenzene (**30**) (4.43 mg, 8.51 µmol) were dissolved in dry CD_3CN (500 µL).

^{1}H NMR (600 MHz, CD_3CN, 298 K) δ (ppm): 28.5 (br, 12H, H_m), 25.9 (s, 12H, H_j), 14.6 (s, 12H, H_c), 9.52 (s, 36H, H_a), 6.51 (unres. dt, 12H, H_d), 5.61 (s, 12H, H_k), 5.27 (s, 12H, H_q), 5.23 (s, 12H, H_e), 0.21 (s, 36H, H_p), -0.06 (s, 12H, H_f).

^{13}C NMR (151 MHz, CD_3CN, 298 K) δ (ppm): 159.7 (C_k), 148.8 (C_c), 134.4 ($C_{quart.}$), 133.4 (C_q), 130.2 ($C_{quart.}$), 128.4 (C_d), 120.0 (C_e), 62.9 (C_a), 18.7 (C_p).

HRMS (ESI): *m/z* = 2121.4451 [**9** + 6OTf]$^{2+}$, 1363.9768 [**9** + 5OTf]$^{3+}$, 985.7433 [**9** + 4OTf]$^{4+}$, 758.8041 [**9** + 3OTf]$^{5+}$, 607.5114 [**9** + 2OTf]$^{6+}$, 499.4451 [**9** + OTf]$^{7+}$.

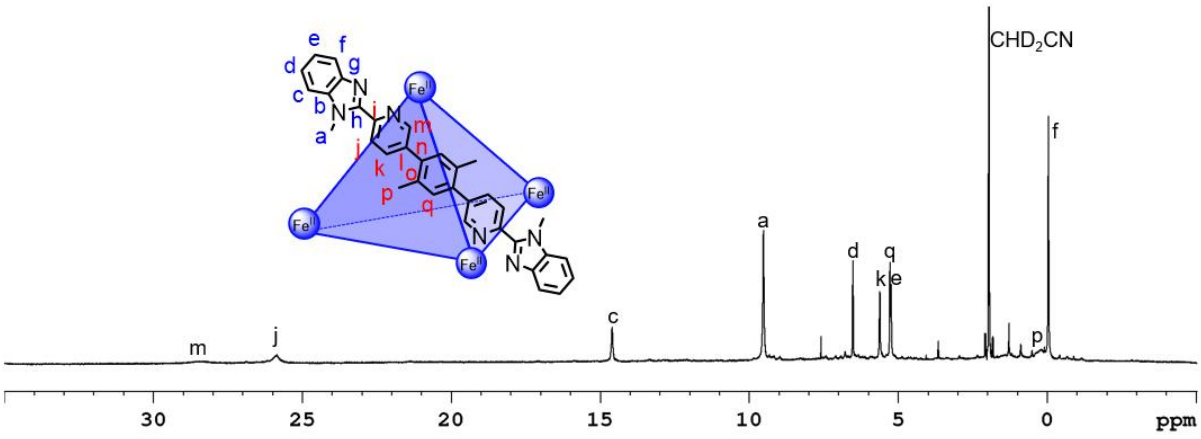

Figure S218. ^{1}H NMR spectrum (600 MHz, CD_3CN, 298 K) of cage **9**.

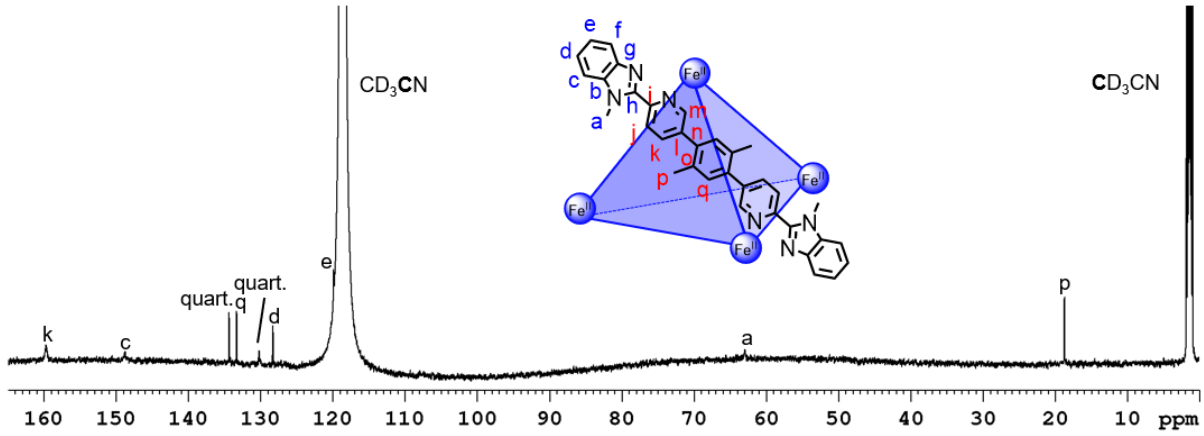

Figure S219. ^{13}C NMR spectrum (151 MHz, CD_3CN, 298 K) of cage **9**.

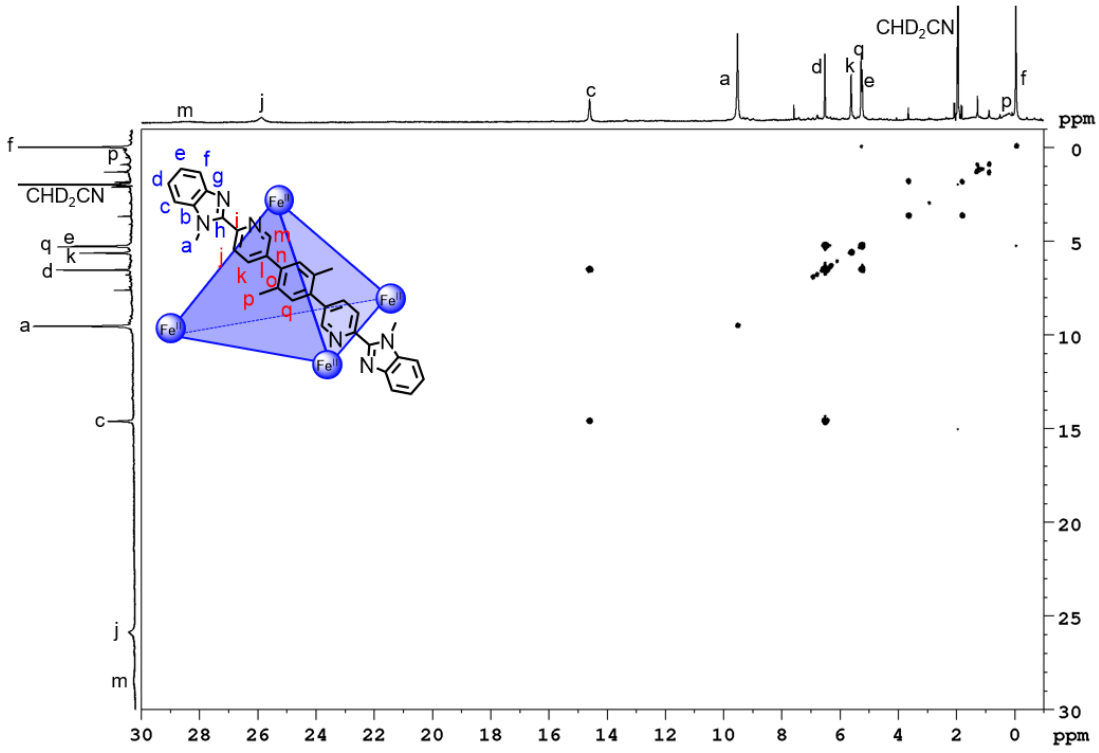

Figure S220. ^{1}H-^{1}H COSY NMR spectrum (600 MHz, CD_3CN, 298 K) of cage **9**.

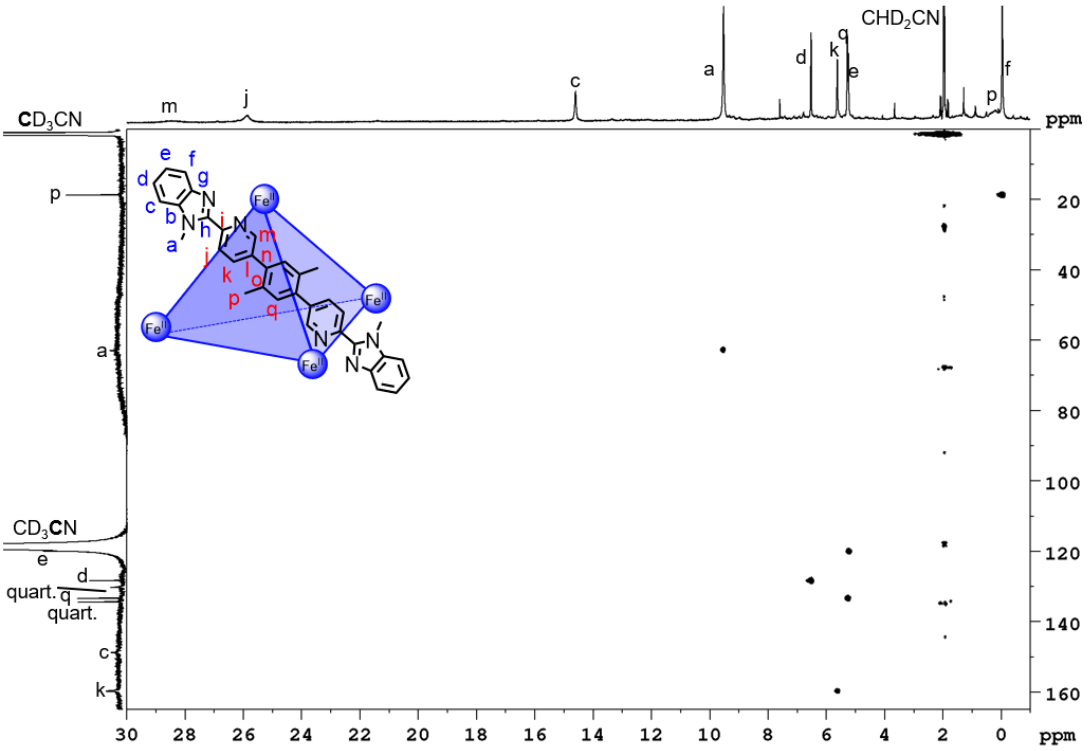

Figure S221. ^{1}H-^{13}C HSQC NMR spectrum (600 MHz/151 MHz, CD_3CN, 298 K) of cage **9**.

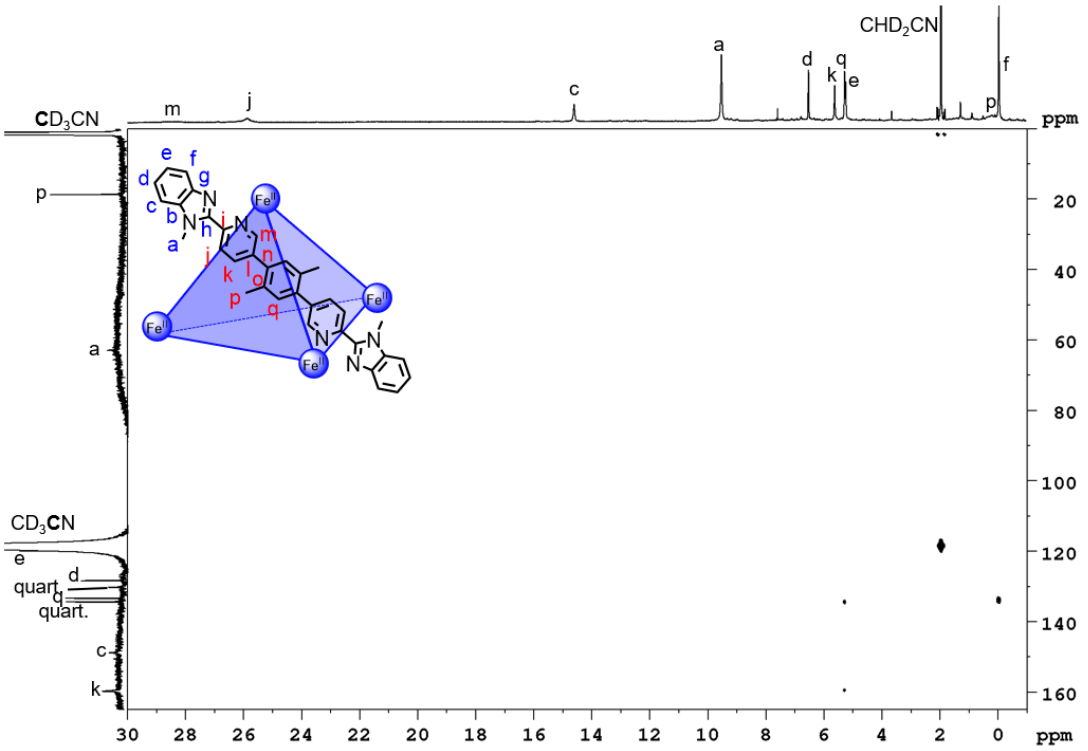

Figure S222. ^{1}H-^{13}C HMBC NMR spectrum (600 MHz/151 MHz, CD_3CN, 298 K) of cage **9**.

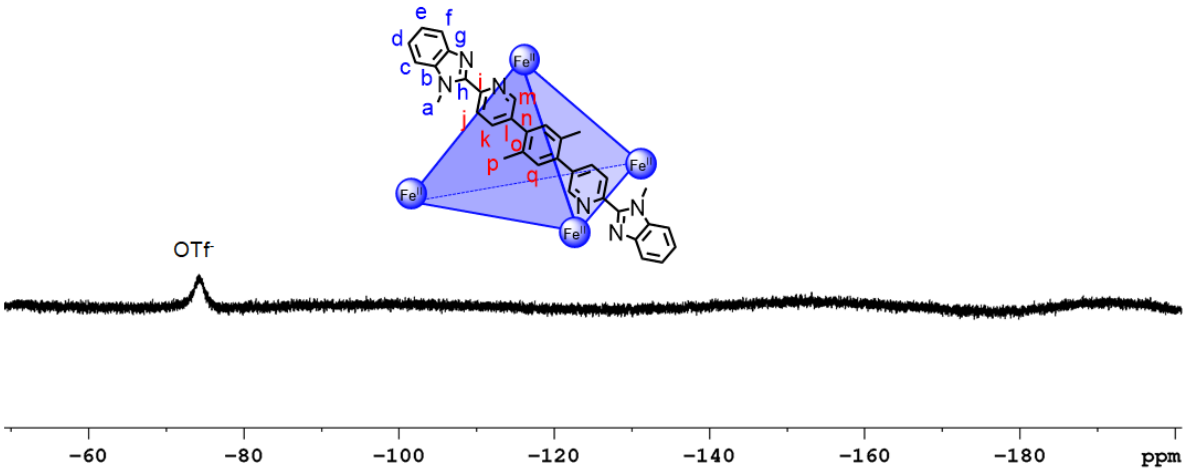

Figure S223. ^{19}F NMR spectrum (471 MHz, CD_3CN, 298 K) of cage **9**.

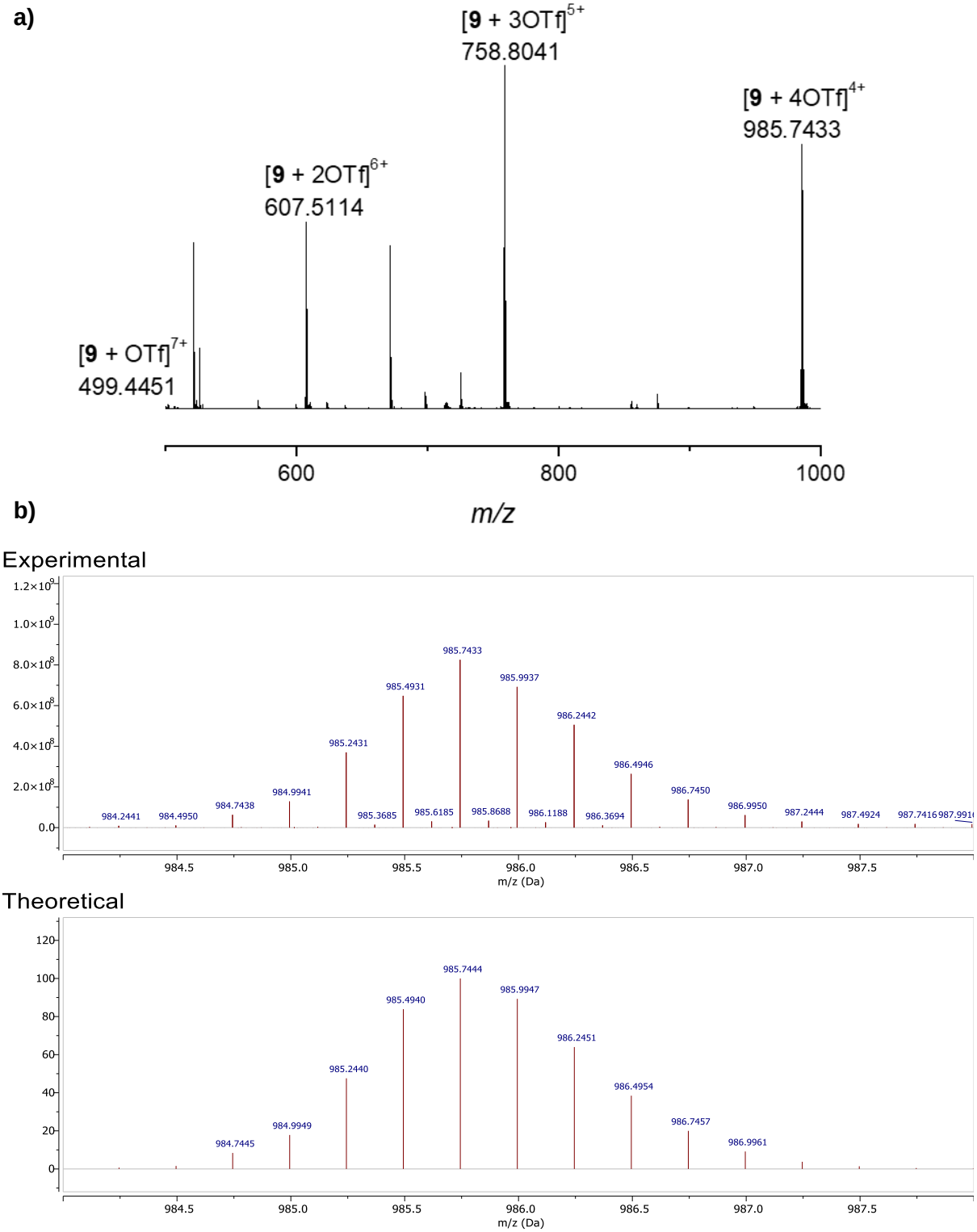

Figure S224. a) High resolution ESI mass spectrum of cage **9** (range *m/z* 500-1000) and b) isotopic patterns of cage **9**: experimental (top) and theoretical (bottom).

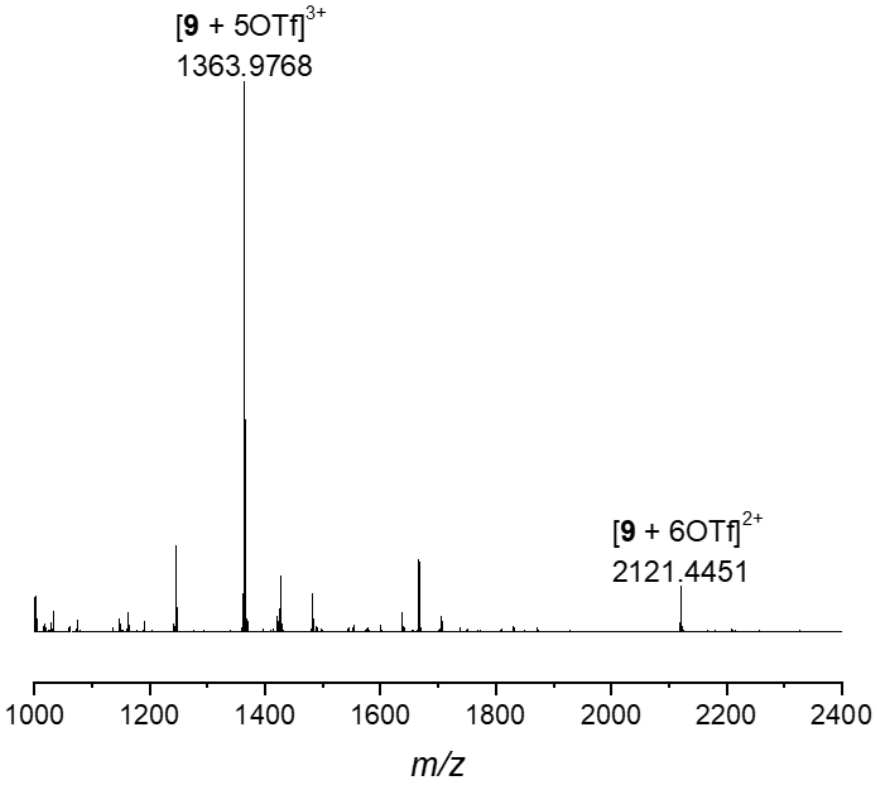

Figure S225. High resolution ESI mass spectrum (range *m/z* 1000-2400) of cage **9**.

4.10 Cage 10

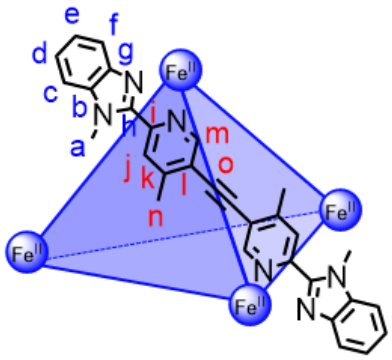

Iron(II) triflate (2.30 mg, 5.52 µmol) and 1,2-di(4''-methyl-6″-(1′-methyl-1*H*-benzo[*d*]imidazol-2′-yl)pyridin-3″-yl)ethyne (**22**) (3.88 mg, 8.28 µmol) were dissolved in dry CD_3CN (500 µL).

^{1}H NMR (600 MHz, CD_3CN, 298 K) δ (ppm): 19.4 (s, 12H, H_j), 19.1 (br, 12H, H_m), 12.2 (s, 12H, H_c), 8.25 (s, 36H, H_a), 6.84 (s, 12H, H_d), 5.46 (s, 12H, H_e), 2.93 (s, 36H, H_n), 0.18 (s, 12H, H_f).

^{13}C NMR (151 MHz, CD_3CN, 298 K) δ (ppm): 163.9 (s, $C_{quart.}$), 163.0 (s, $C_{quart.}$), 160.7 (d, ^1J = 182 Hz, $C_{j/m}$), 135.4 (d, ^1J = 166 Hz, C_c), 131.2 (s, $C_{quart.}$), 126.7 (d, ^1J = 160 Hz, C_d), 123.6 (s, $C_{quart.}$), 122.6 (s, $C_{quart.}$), 121.1 (d, ^1J = 161 Hz, C_e), 119.3 (unres. d, C_f), 85.0 (s, C_o), 52.0 (q, ^1J = 144 Hz, C_a), 18.5 (q, ^1J = 137 Hz, C_n).

HRMS (ESI): *m/z* = 1964.3488 [**10** + 6OTf]$^{2+}$, 1259.9138 [**10** + 5OTf]$^{3+}$, 907.6967 [**10** + 4OTf]$^{4+}$, 696.3669 [**10** + 3OTf]$^{5+}$, 555.4804 [**10** + 2OTf]$^{6+}$.

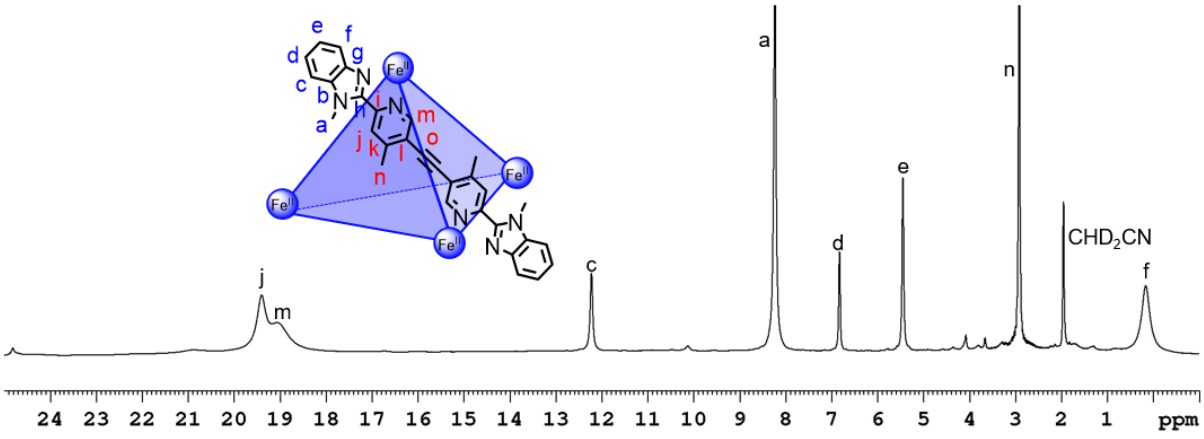

Figure S226. ^{1}H NMR spectrum (600 MHz, CD_3CN, 298 K) of cage **10**.

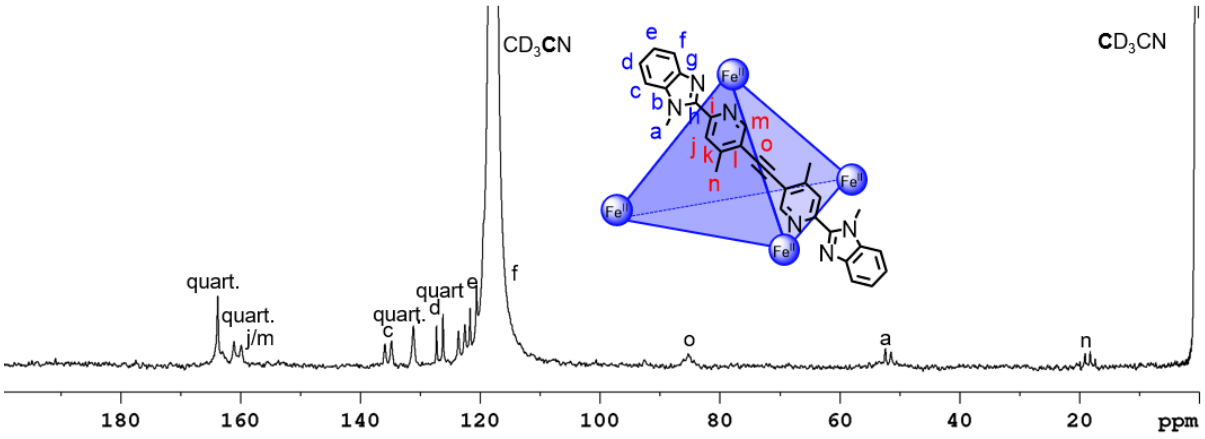

Figure S227. ^{13}C NMR spectrum (151 MHz, CD_3CN, 298 K) of cage **10**.

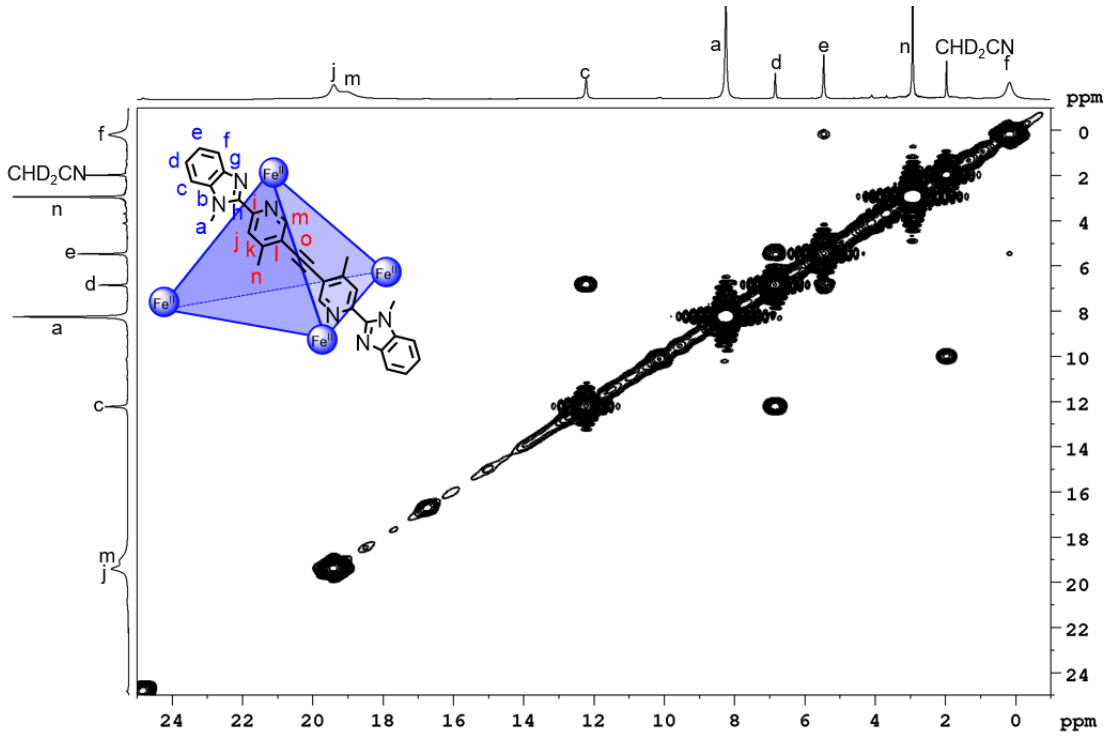

Figure S228. ^{1}H-^{1}H COSY NMR spectrum (600 MHz, CD_3CN, 298 K) of cage **10**.

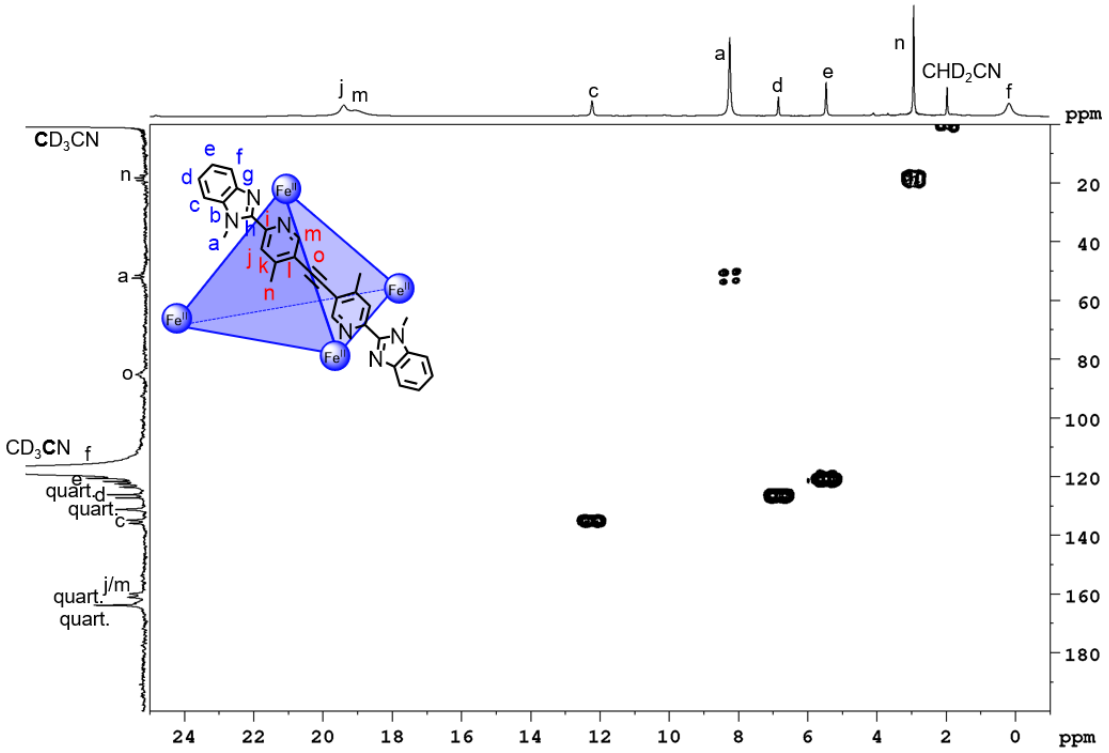

Figure S229. ^{1}H-^{13}C HMQC NMR spectrum (600 MHz/151 MHz, CD_3CN, 298 K) of cage **10**.

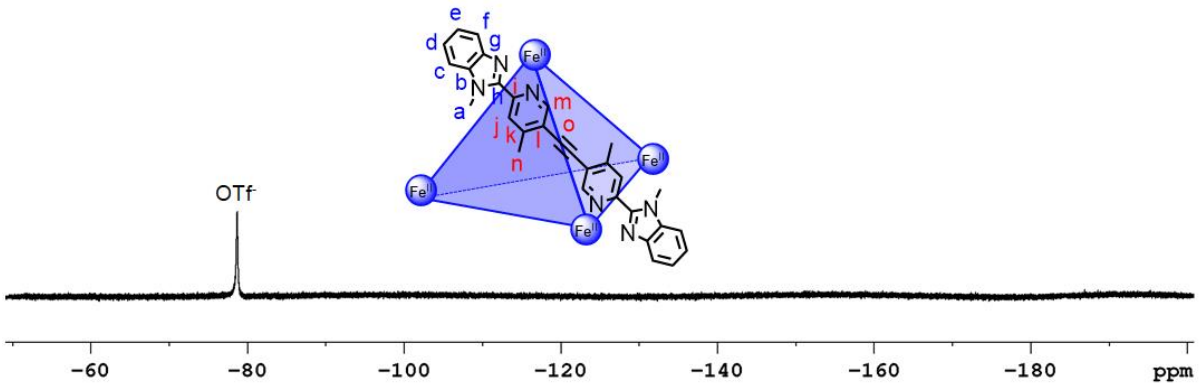

Figure S230. ^{19}F NMR spectrum (471 MHz, CD_3CN, 298 K) of cage **10**.

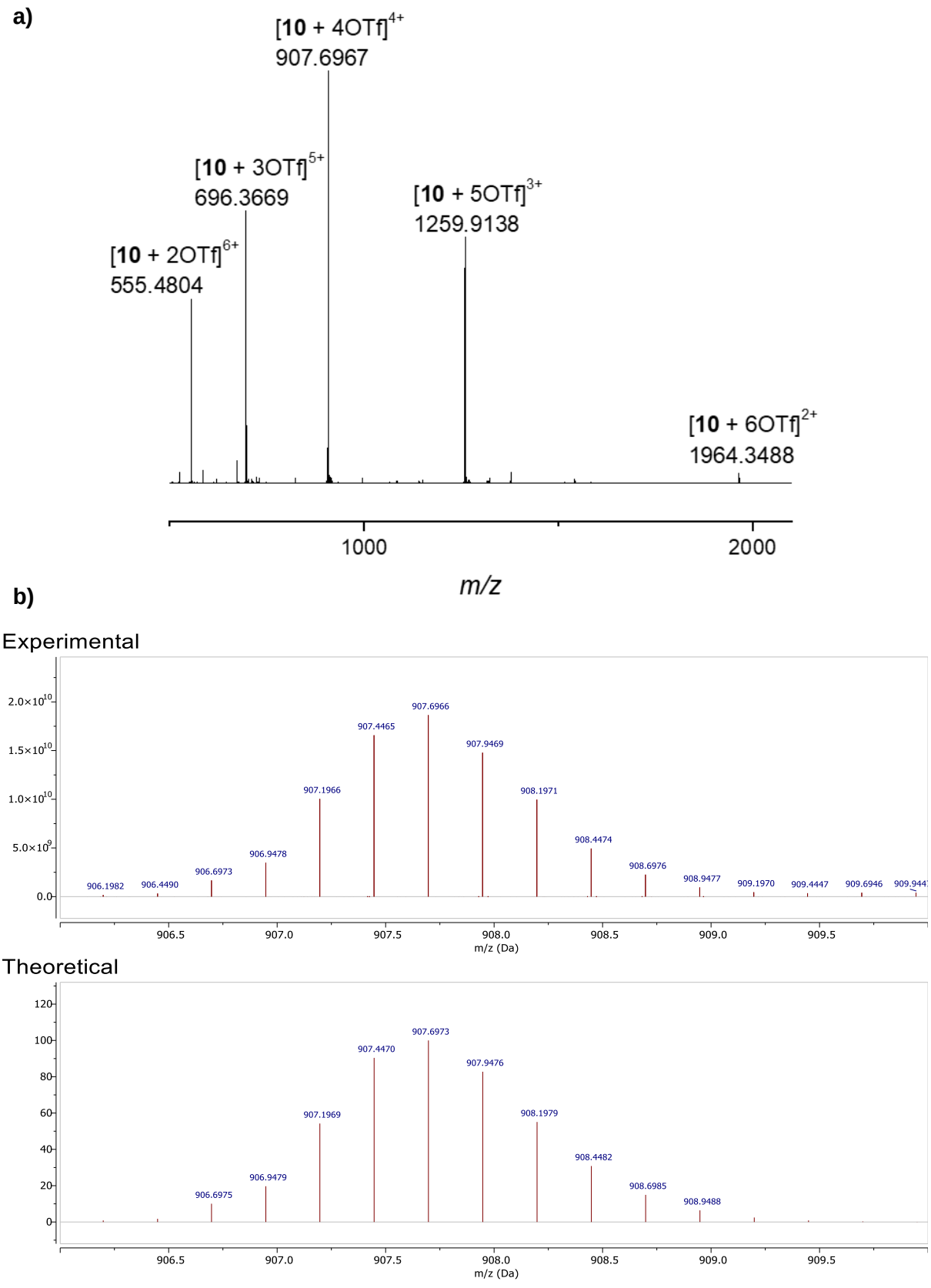

Figure S231. a) High resolution ESI mass spectrum of cage **10** and b) isotopic patterns of cage **10**: experimental (top) and theoretical (bottom).

4.11 Cage 11

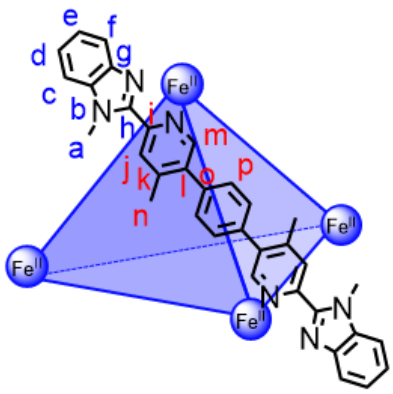

Iron(II) triflate (2.31 mg, 5.55 µmol) and 1,4-bis(4''-methyl-6''-(1'-methyl-1*H*-benzo[*d*]imidazol-2'-yl)pyridin-3''-yl)benzene (**33**) (4.34 mg, 8.34 µmol) were dissolved in dry CD_3CN (500 µL).

^{1}H NMR (600 MHz, CD_3CN, 298 K) δ (ppm): 58.3 (s, 12H, H_j), 32.8 (br, 12H, H_m), 24.9 (s, 12H, H_c), 22.1 (s, 36H, H_a), 4.81 (s, 36H, H_n), 2.80 (s, 12H, H_d), -3.32 (s, 12H, H_e), -6.19 (s, 24H, H_p), -29.3 (s, 12H, H_f).

^{13}C NMR (151 MHz, CD_3CN, 298 K) δ (ppm): 205.0 (C_c), 192.0 ($C_{quart.}$), 180.0 ($C_{quart.}$), 123.7 (C_p), 122.6 (C_d), 112.9 (C_a), 104.3 (C_e), 51.9 ($C_{quart.}$), 8.6 (C_n).

HRMS (ESI): *m/z* = 2120.4434 [**11** + 6OTf]$^{2+}$, 1363.9764 [**11** + 5OTf]$^{3+}$, 985.7422 [**11** + 4OTf]$^{4+}$, 607.5106 [**11** + 3OTf]$^{5+}$.

While the signals at *m/z* 985.7422 and 607.5106 are consistent with the 4+ and 5+ charges, respectively, for the cage, the theoretical isotopic pattern does not match, possibly due to fragmentation in the gas phase or overlap with other signals.

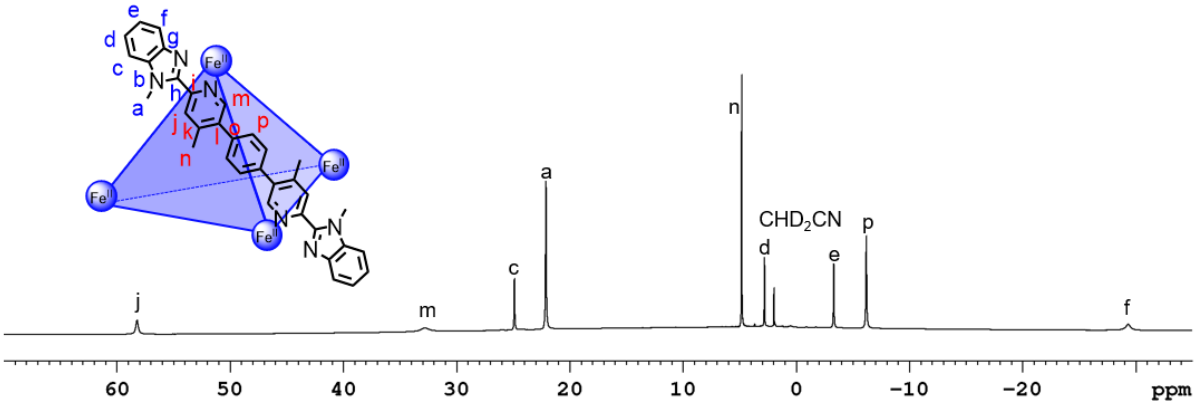

Figure S232. ^{1}H NMR spectrum (600 MHz, CD_3CN, 298 K) of cage **11**.

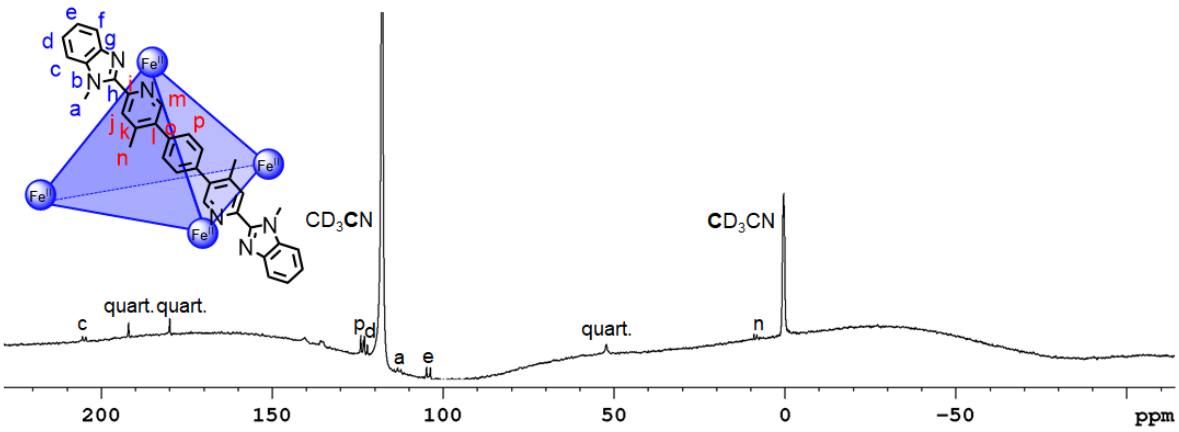

Figure S233. ^{13}C NMR spectrum (151 MHz, CD_3CN, 298 K) of cage **11**.

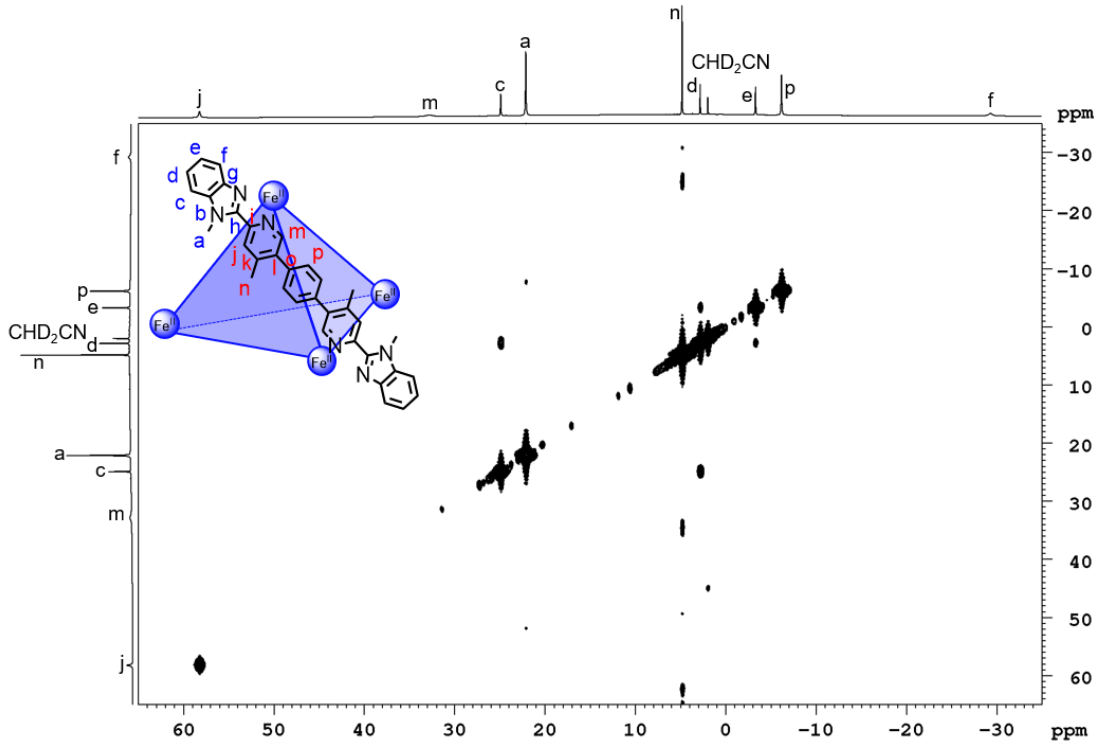

Figure S234. ^{1}H-^{1}H COSY NMR spectrum (600 MHz, CD_3CN, 298 K) of cage **11**.

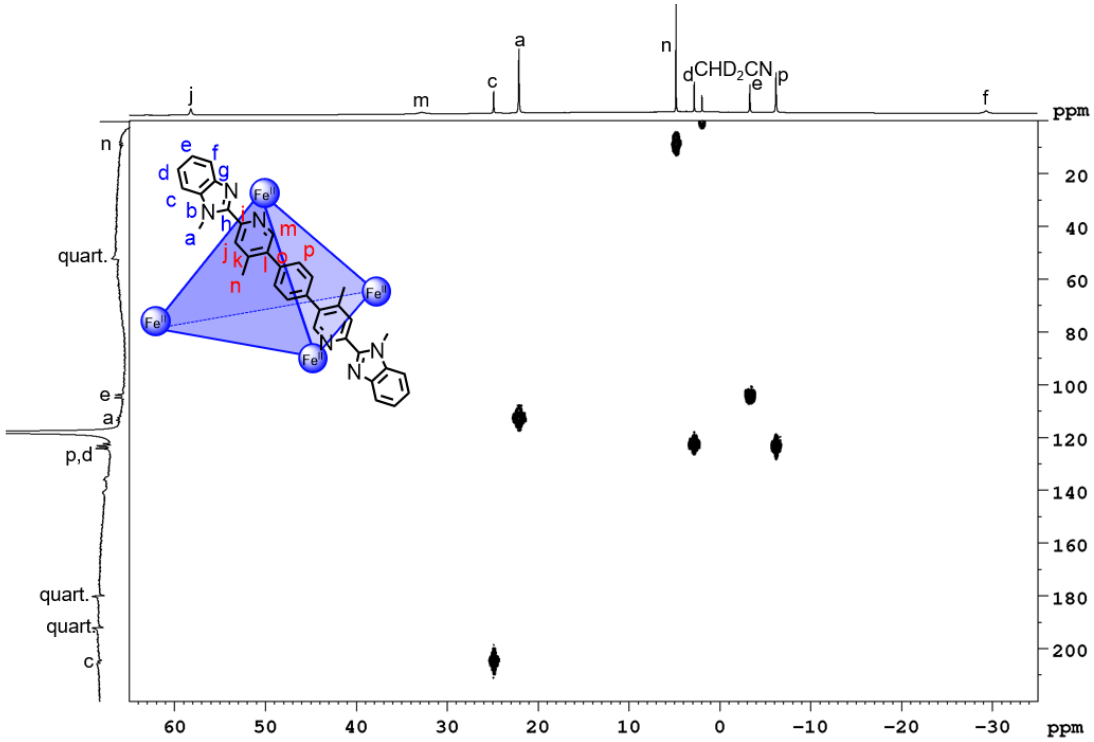

Figure S235. ^{1}H-^{13}C HMQC NMR spectrum (600 MHz/151 MHz, CD_3CN, 298 K) of cage **11**.

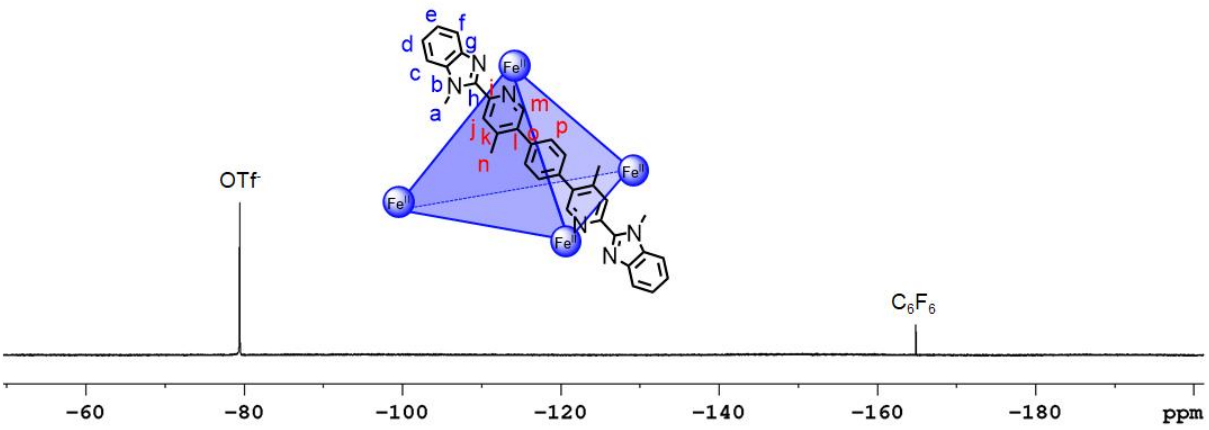

Figure S236. ^{19}F NMR spectrum (471 MHz, CD_3CN, 298 K) of cage **11**.

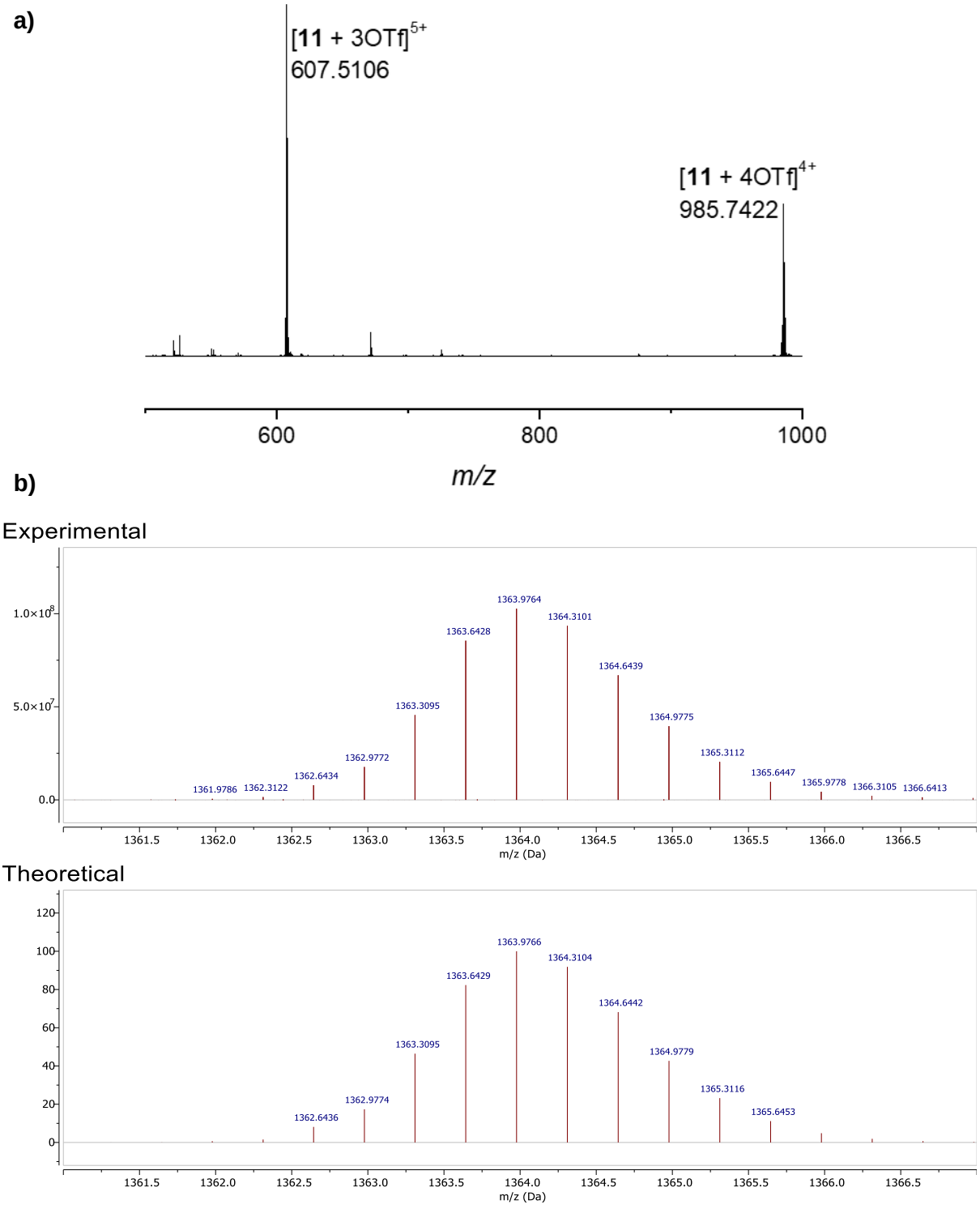

Figure S237. a) High resolution ESI mass spectrum (range *m/z* 500-1000) of cage **11** and b) isotopic patterns of cage **11**: experimental (top) and theoretical (bottom).

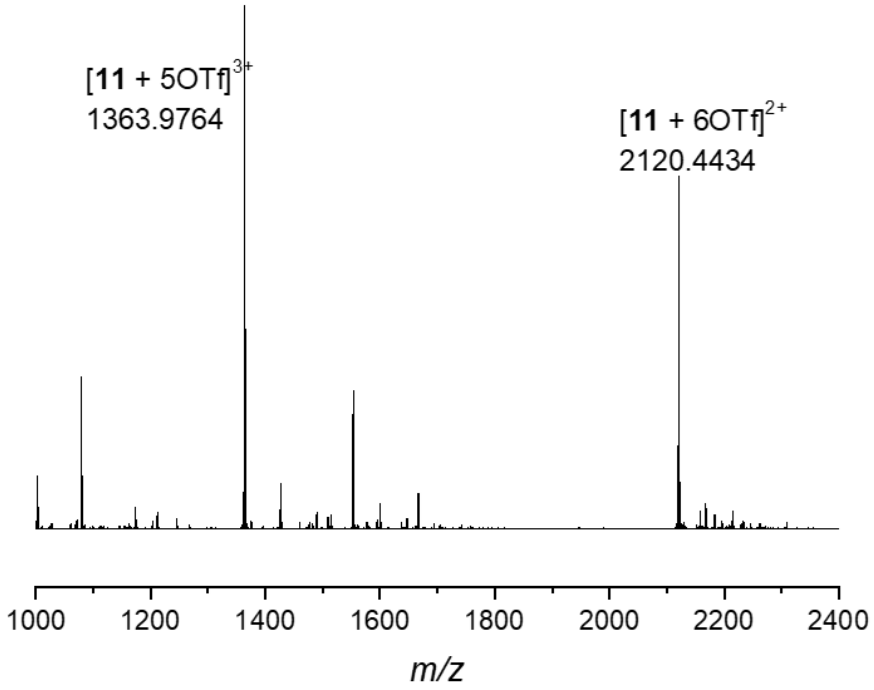

Figure S238. High resolution ESI mass spectrum (range *m/z* 1000-2400) of cage **11**.

5 Spin-Crossover Studies

5.1 Evans Method

For the determination of the magnetic susceptibility by the Evans method, a standard is required. Since the standard could potentially bind in the cavity of the cages, *p*-xylene was chosen[9] over other smaller commonly used standards *t*-BuOH and cyclohexane. However, preliminary studies with cage **6** suggested guest binding based on the chemical shift changes upon the addition of *p*-xylene, thus making it unsuitable as a standard (Figure S239). Since the ideal solution model does not require the use of a standard, the spin-crossover properties of the $Fe^{II}_4L_6$ cages were determined using this method.

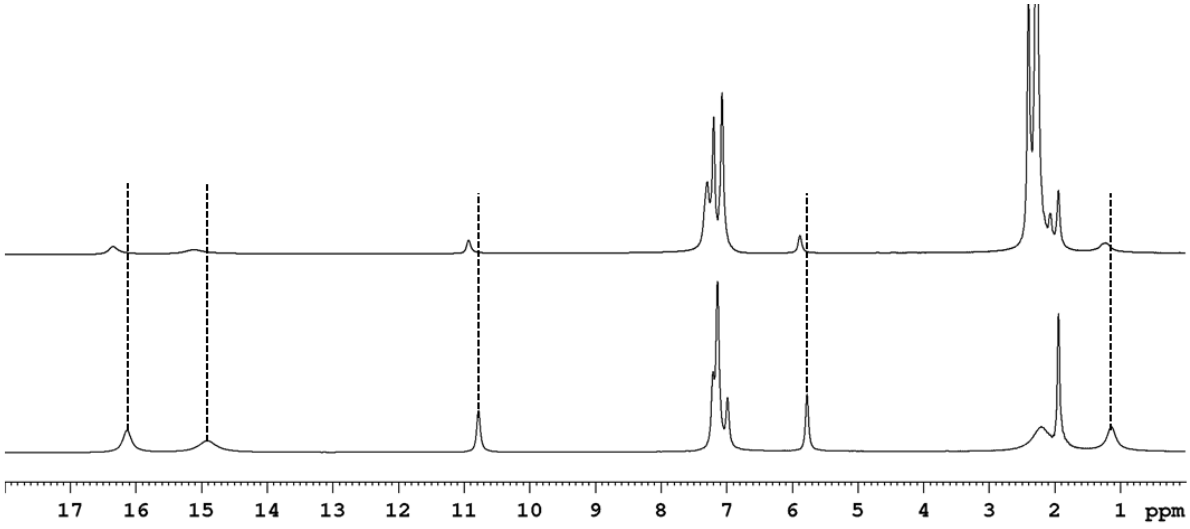

Figure S239. ^{1}H NMR spectra (500 MHz, CD_3CN, 298 K) of cage **6** with (top) and without (bottom) *p*-xylene.

5.2 Ideal Solution Model

The ideal solution model[10] can be used to determine the spin-crossover temperature $T_{1/2}$ by fitting δ (the chemical shift of the spin-crossover compound) as a function of temperature (T) to Eq. 1 using Origin (with R as 8.31446 J/mol·K) to calculate the values of C, ΔH, ΔS and δ_{LS} (the chemical shift of the low-spin state). In initial fits, δ_{LS} was not fixed and the fitting gave large errors or did not converge (Table S1, Sections 5.3-5.13). Therefore, δ_{LS} was fixed in subsequent fittings as the diamagnetic shift of the $Zn^{II}_4L_6$ analogue (Table S1) and a control VT experiment with cage **44** revealed the chemical shift of this proton (j) remained constant within the investigated temperature range (Figure S240).

$$\delta = \delta_{LS} + \frac{C}{T + T \cdot \exp\left(\frac{\Delta H - T\Delta S}{RT}\right)} \tag{1}$$

For the calculation of $T_{1/2}$ from the obtained ΔH and ΔS values, Eq. 2 describing K_{eq}, the equilibrium constant for the spin transition, is needed. By assuming that [HS] and [LS] (the high spin-state and low spin-state concentrations, respectively) are equal at $T_{1/2}$, Eq. 2 can be simplified to Eq. 3.

$$K_{eq} = \frac{[HS]}{[LS]} = exp\left(\frac{-\Delta G}{RT}\right) = 1 \tag{2}$$

$$1 = \exp\left(\frac{-\Delta G}{RT}\right) \equiv \Delta G = 0 \tag{3}$$

Insertion of Eq. 3 into Eq. 4 gives the spin-transition temperature $T_{1/2}$ as a function of ΔH and ΔS.

$$\Delta G = \Delta H - T\Delta S \tag{4}$$

$$T_{1/2} = \frac{\Delta H}{\Delta S} \tag{5}$$

Furthermore, the spin-state fractions γ_{LS} and γ_{HS} can be calculated for the high-spin and low-spin state, respectively, at any given temperature (Eq. 6).

$$\gamma_{LS} = \frac{[LS]}{[LS] + [HS]} \tag{6}$$

Reorganization of Eq. 2 as Eq. 7 and insertion into Eq. 6 gives Eq. 8. Following simplification, the spin-state fraction γ_{LS} can be calculated using the Gibbs energy (Eq. 9).

$$[HS] = K_{eq}\,[LS] \tag{7}$$

$$\gamma_{LS} = \frac{[LS]}{[LS] + [LS]K_{eq}} \equiv \frac{[LS]}{[LS]\left(1 + exp\left(\frac{-\Delta G}{RT}\right)\right)} \tag{8}$$

$$\gamma_{LS} = \frac{1}{1 + exp\left(\frac{-\Delta G}{RT}\right)} \tag{9}$$

Since the sum of the spin-state fractions equals 1 (Eq. 10), the spin-state fraction γ_{HS} can also be obtained (Eq. 11).

$$\gamma_{LS} + \gamma_{HS} = 1 \tag{10}$$

$$\gamma_{HS} = 1 - \frac{1}{1 + \exp\left(\frac{-\Delta G}{RT}\right)} \quad (11)$$

Table S1. Thermodynamic data from variable temperature NMR experiments (248-348 K)

Cage	Unfixed δ_{LS}			Fixed δ_{LS}		
	ΔH [kJ/mol][a]	ΔS [J/molK][a]	δ_{LS} [ppm][b]	ΔH [kJ/mol][a]	ΔS [J/molK][a]	$T_{1/2}$ [K]
1	[c]	[c]	-	[c]	[c]	[c]
2	[d]	[d]	7.78	[d]	[d]	[d]
3	[d]	[d]	8.02	[d]	[d]	[d]
4	[d]	[d]	8.18	[d]	[d]	[d]
5	[d]	[d]	8.34	[d]	[d]	[d]
6	22.88 ± 1.63	53.31 ± 8.07	8.43	24.46 ± 0.58	60.94 ± 3.00	401
7	28.46 ± 2.29	68.42 ± 11.0	8.70	27.71 ± 0.91	64.48 ± 5.78	430
8	29.98 ± 2.21	83.33 ± 7.85	8.48	27.22 ± 0.93	72.61 ± 4.00	375
9	19.55 ± 1.26	56.27 ± 4.69	8.40	21.79 ± 0.48	64.32 ± 2.00	339
10	31.14 ± 2.64	91.14 ± 8.97	8.18	27.44 ± 1.12	77.65 ± 4.40	353
11	[d]	[d]	8.46	20.78 ± 0.22	85.05 ± 0.93	244

[a] Determined from fitting the chemical shift change between 248 K and 348 K according to Eq. 1. [b] Chemical shift of the Zn(II) cage analogue. [c] Low spin cage. [d] Could not be determined since fitting did not converge.

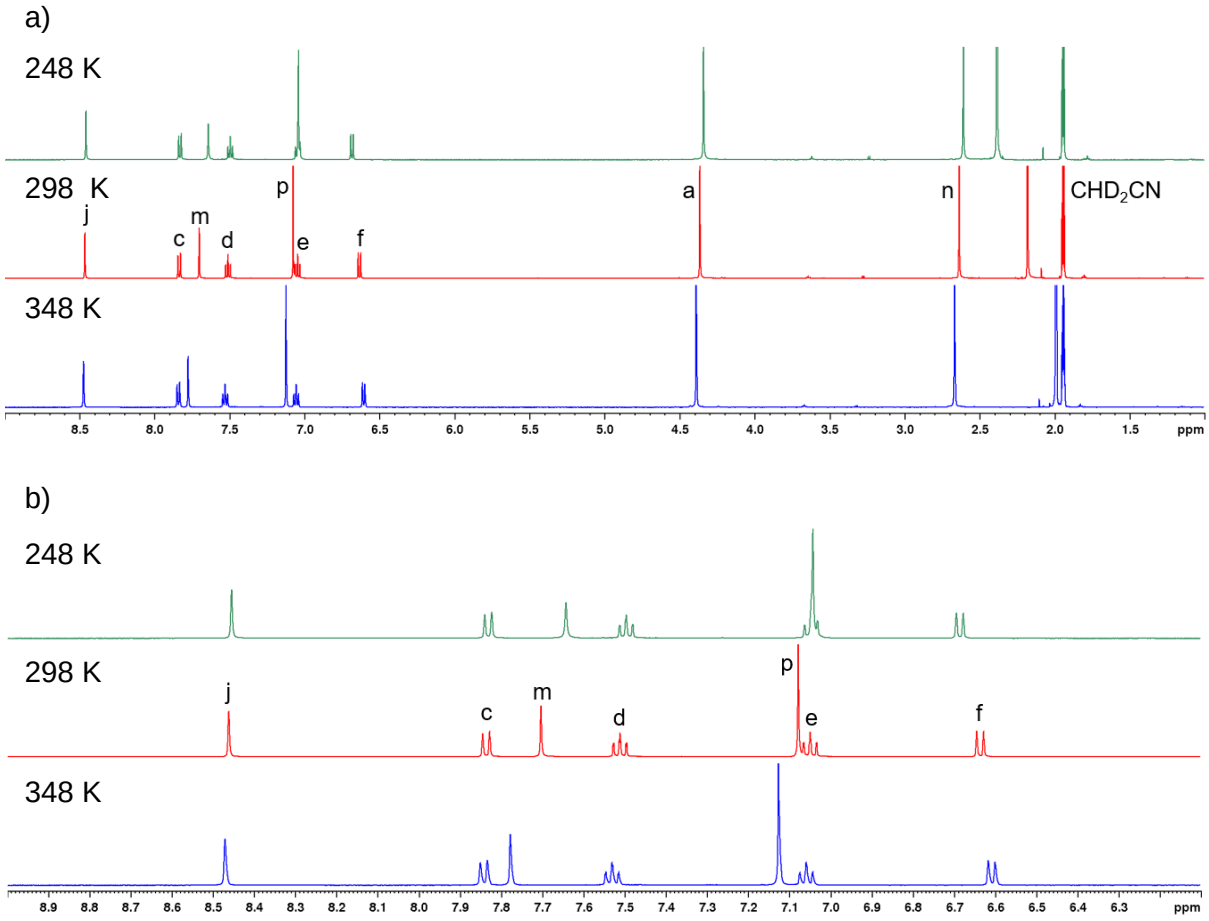

Figure S240. a) Chemical shift changes in the range of 248 K to 348 K for diamagnetic cage **44** with b) an expansion of the aromatic region.

5.3 Cage 1

Cage **1** was predominantly low spin between 248 K and 348 K.

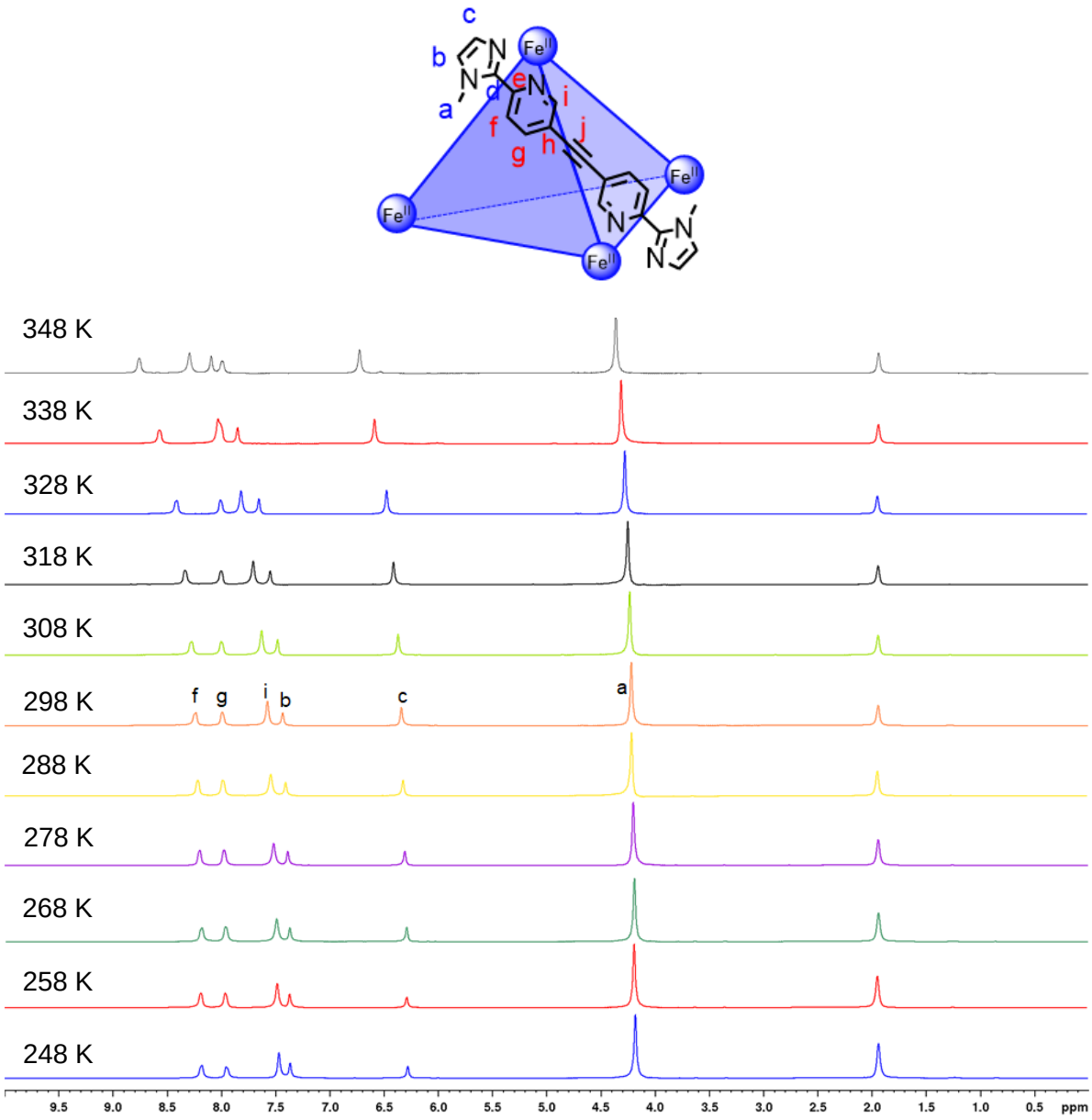

Figure S241. Chemical shift changes in the range of 248 K to 348 K for cage **1**.

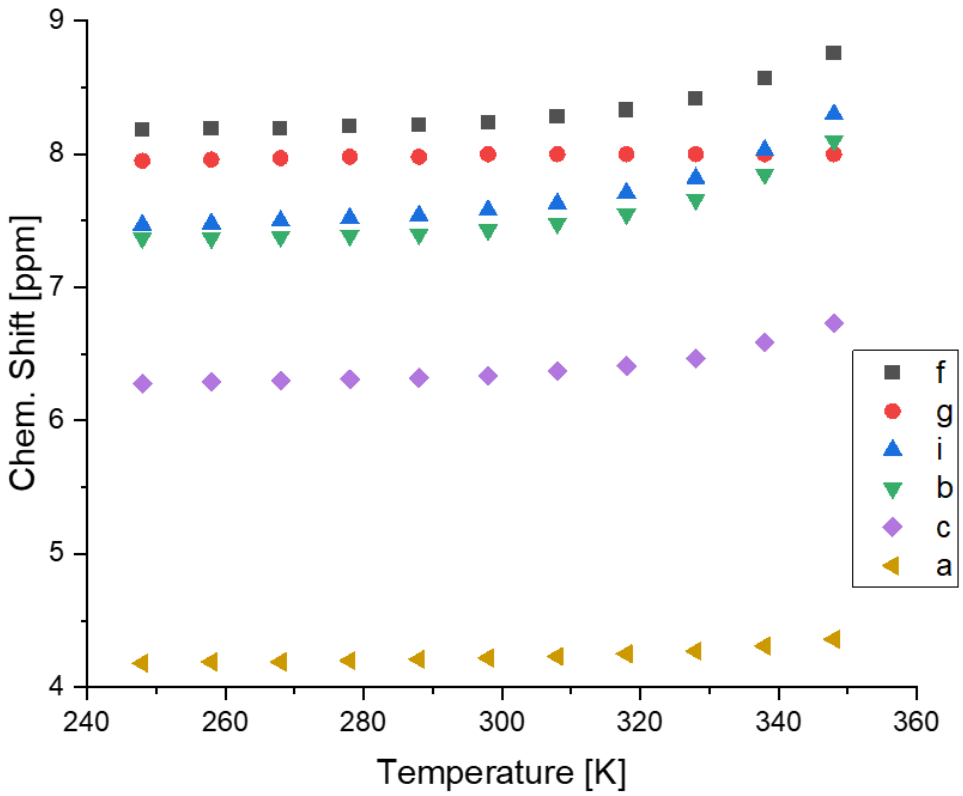

Figure S242. Chemical shift changes from 248 K to 348 K for cage **1**.

5.4 Cage 2

Cage **2** was predominantly low spin between 248 K and 348 K. Fitting did not converge with or without fixing δ_{LS}.

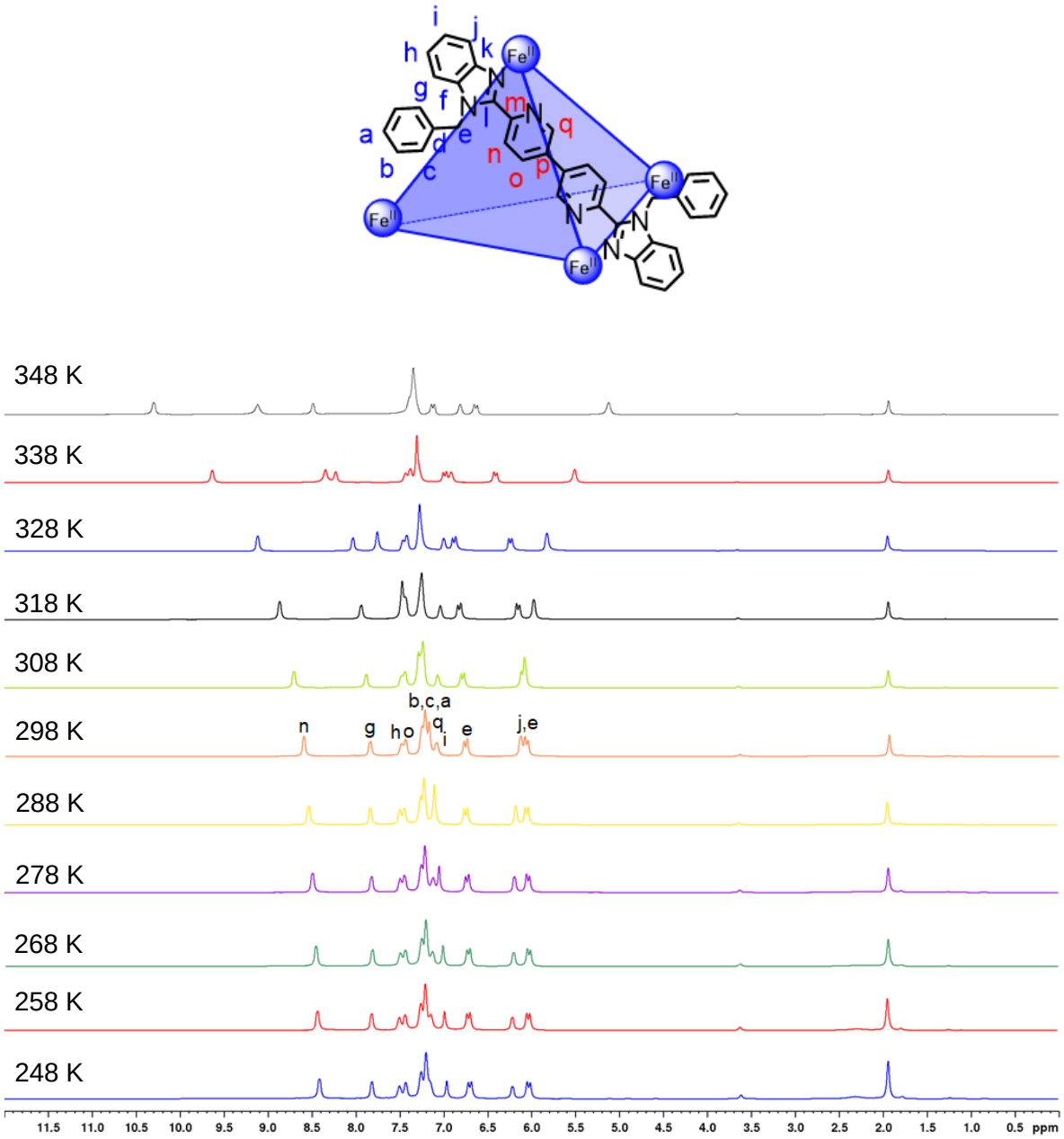

Figure S243. Chemical shift changes in the range of 248 K to 348 K for cage **2**.

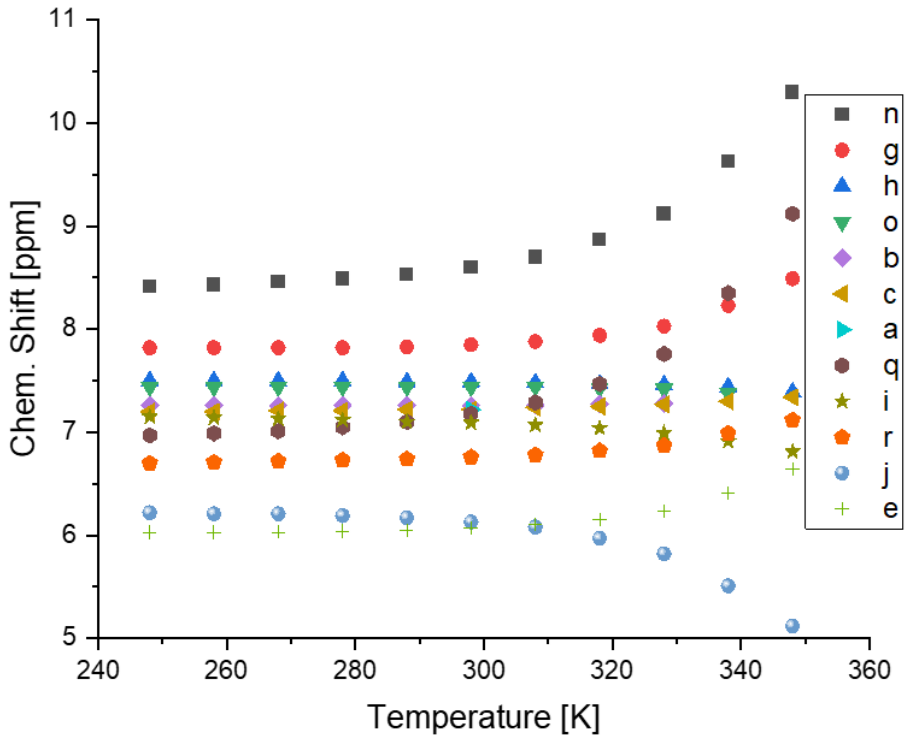

Figure S244. Chemical shift changes in the range of 248 K to 348 K for cage **2**.

5.5 Cage 3

Cage **3** was predominantly low spin between 248 K and 348 K. Fitting did not converge with or without fixing δ_{LS}.

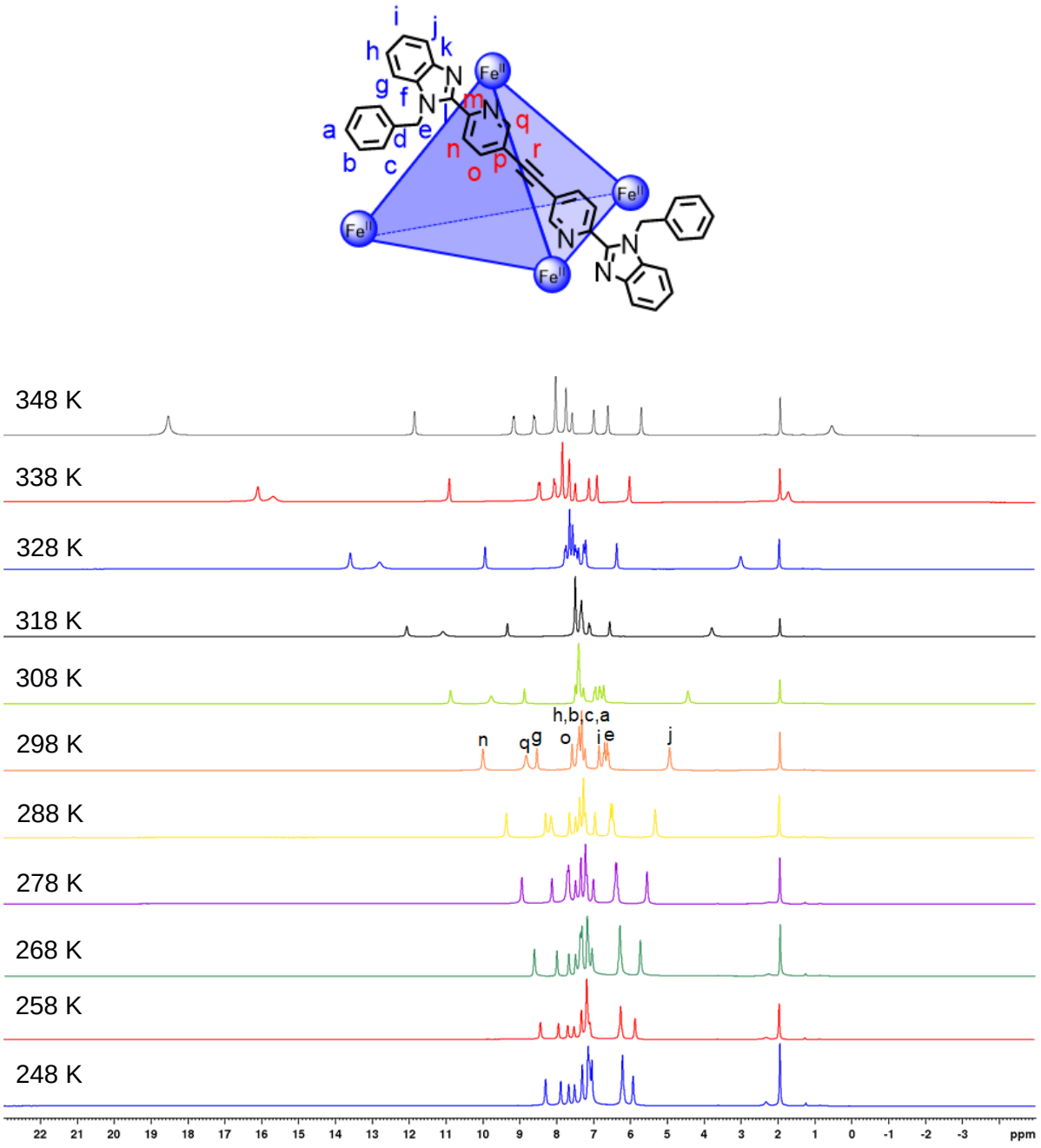

Figure S245. Chemical shift changes in the range of 248 K to 348 K for cage **3**.

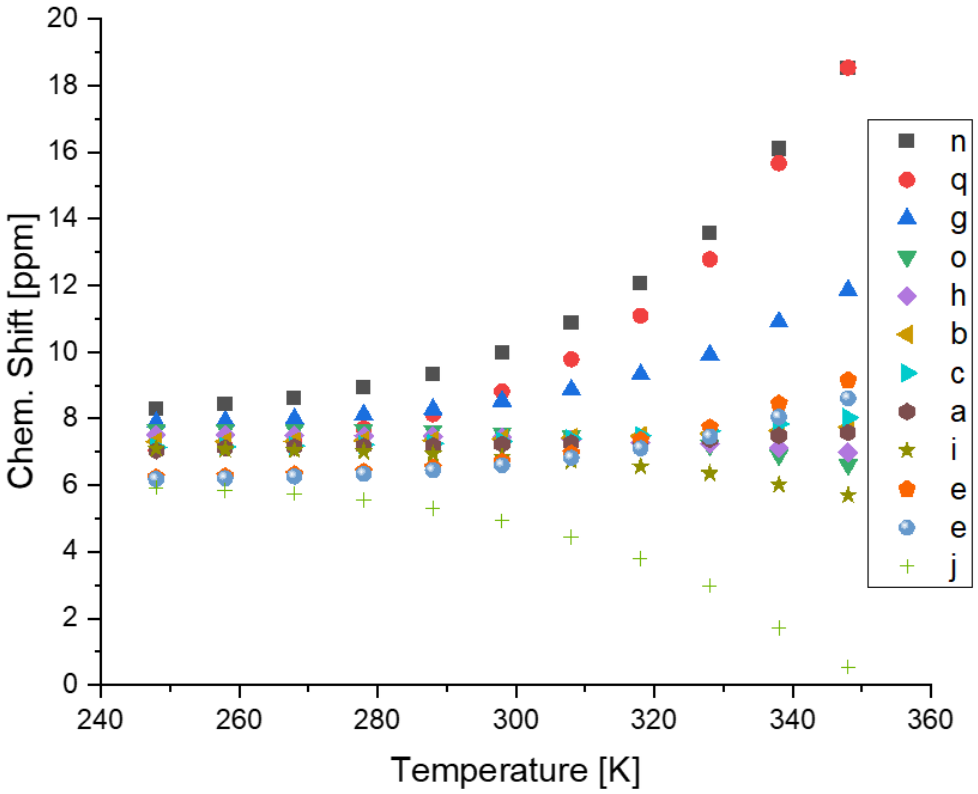

Figure S246. Chemical shift changes in the range of 248 K to 348 K for cage **3**.

5.6 Cage 4

Cage **4** was predominantly low spin between 248 K and 348 K. Fitting did not converge with or without fixing δ_{LS}.

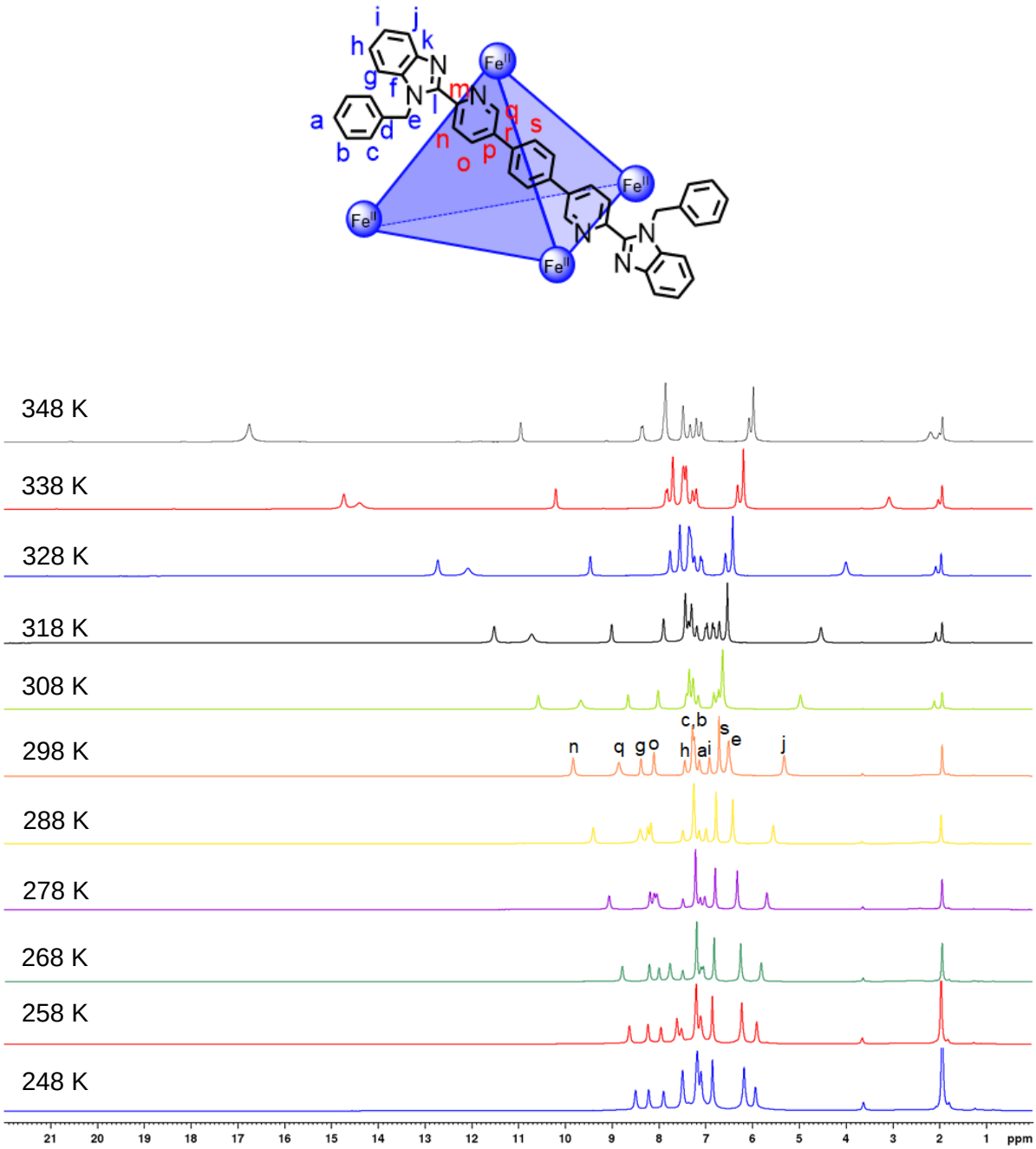

Figure S247. Chemical shift changes in the range of 248 K to 348 K for cage **4**.

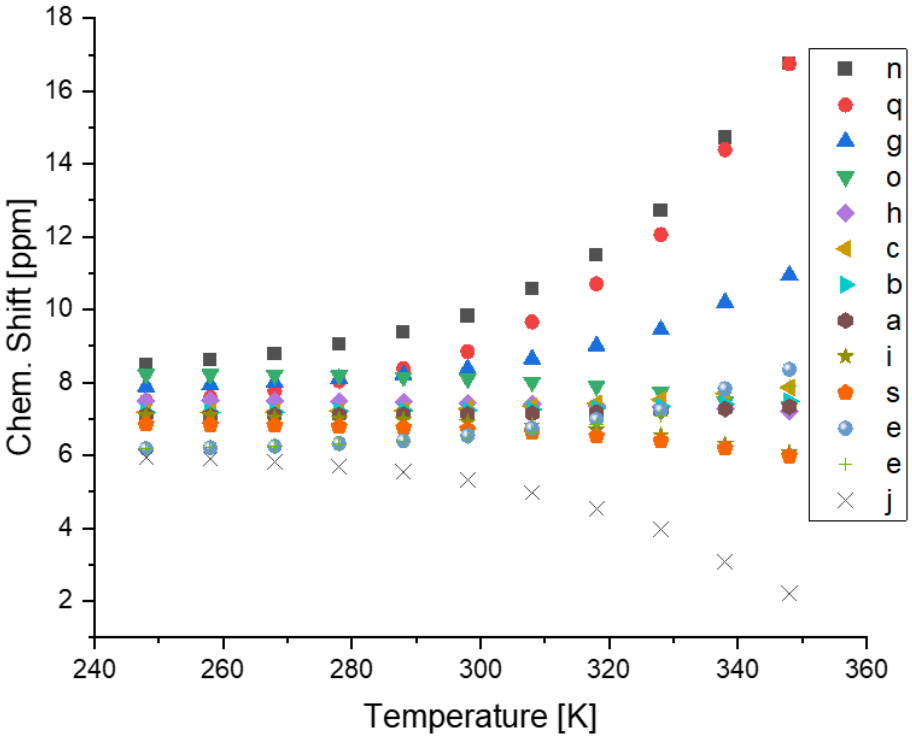

Figure S248. Chemical shift changes in the range of 248 K to 348 K for cage **4**.

5.7 Cage 5

Cage **5** was predominantly low spin between 248 K and 348 K. Fitting did not converge with or without fixing δ_{LS}.

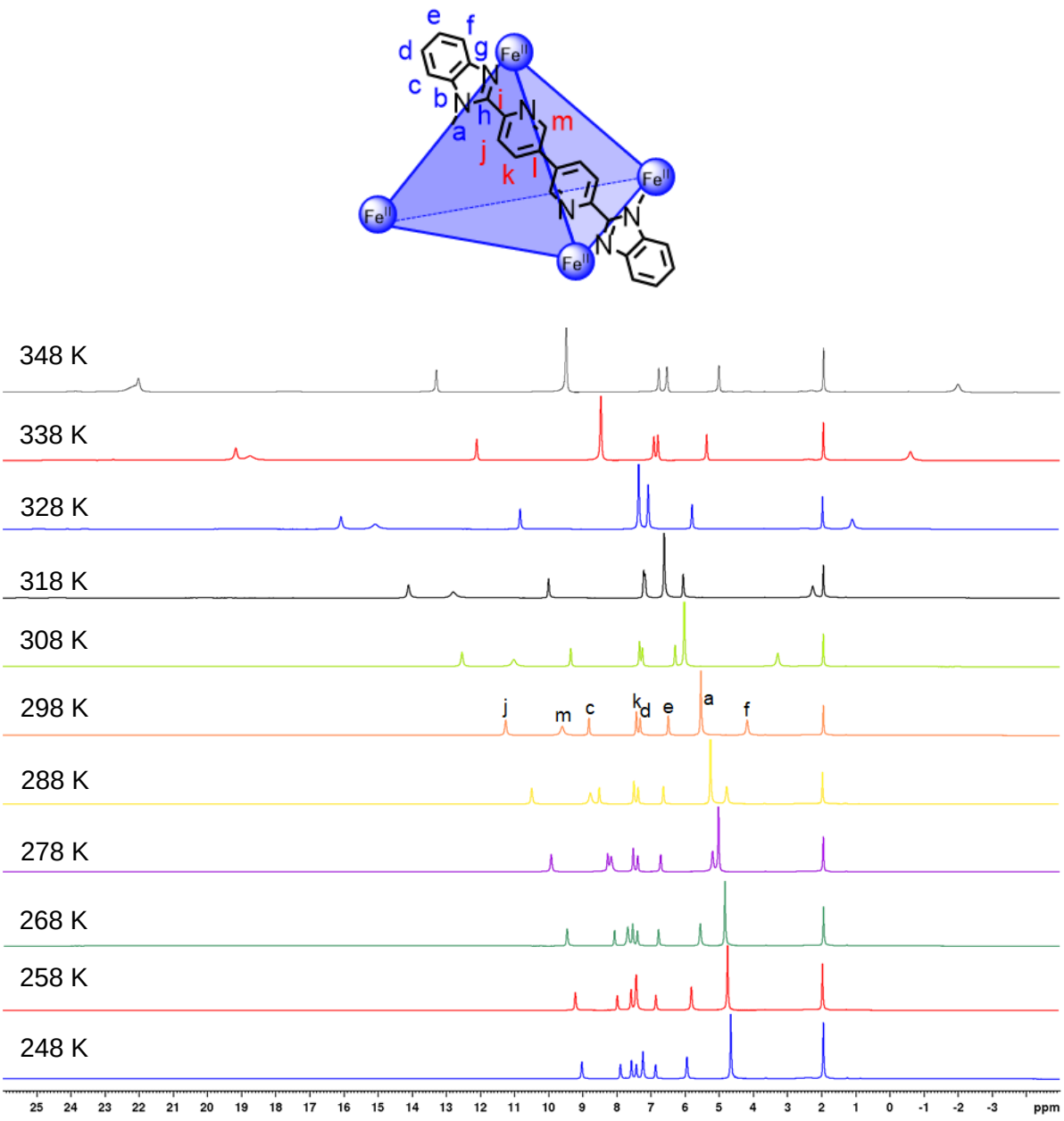

Figure S249. Chemical shift changes in the range of 248 K to 348 K for cage **5**.

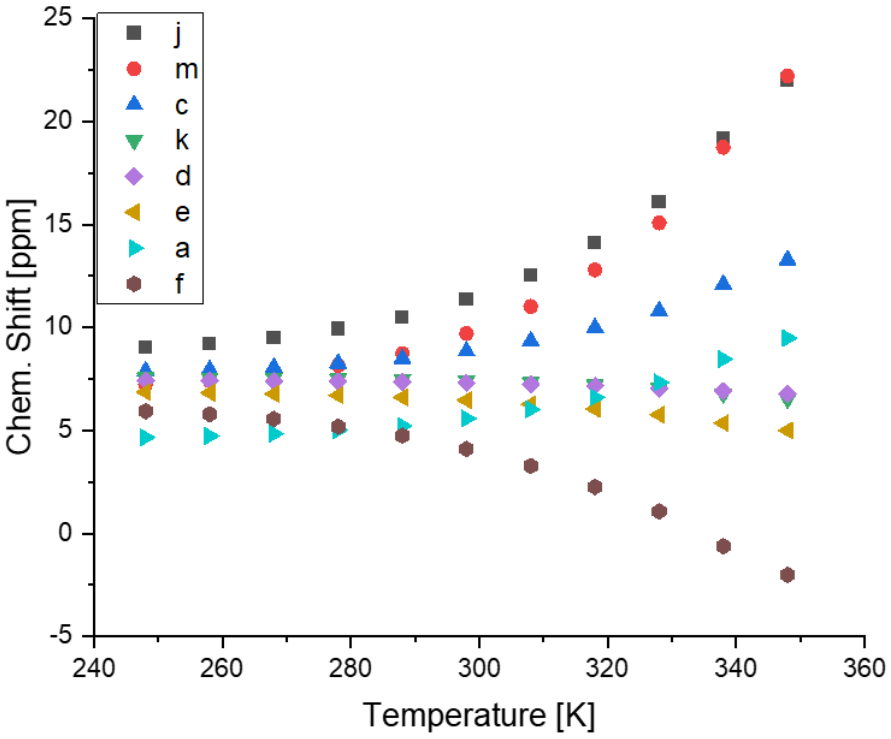

Figure S250. Chemical shift changes in the range of 248 K to 348 K for cage **5**.

5.8 Cage 6

While fitting converged with and without fixing δ_{LS}, large errors were obtained for the fit without a fixed δ_{LS}. A spin-crossover temperature of 401 K was obtained from the fitting with δ_{LS} fixed as 8.43 ppm.

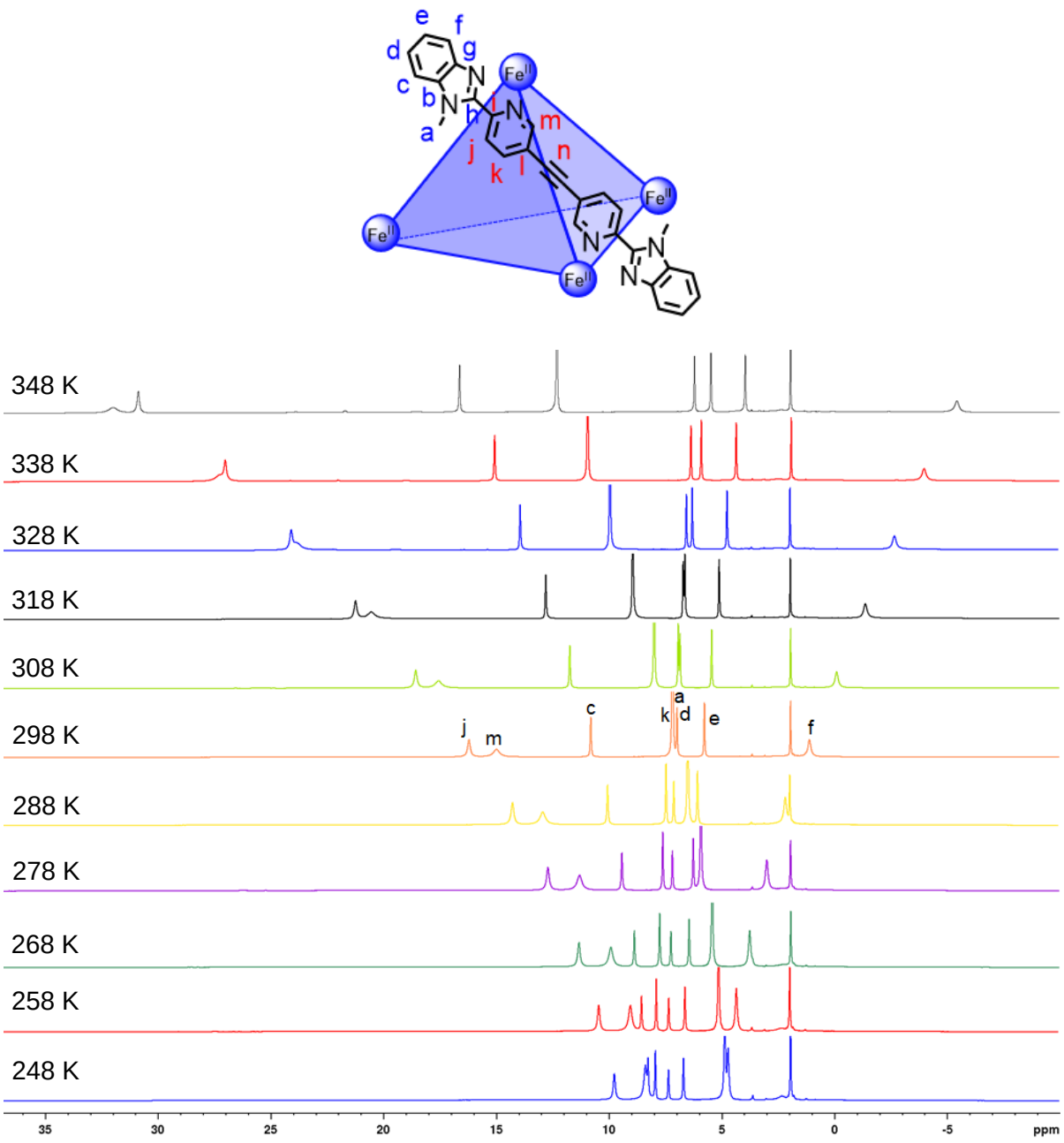

Figure S251. Chemical shift changes in the range of 248 K to 348 K for cage **6**.

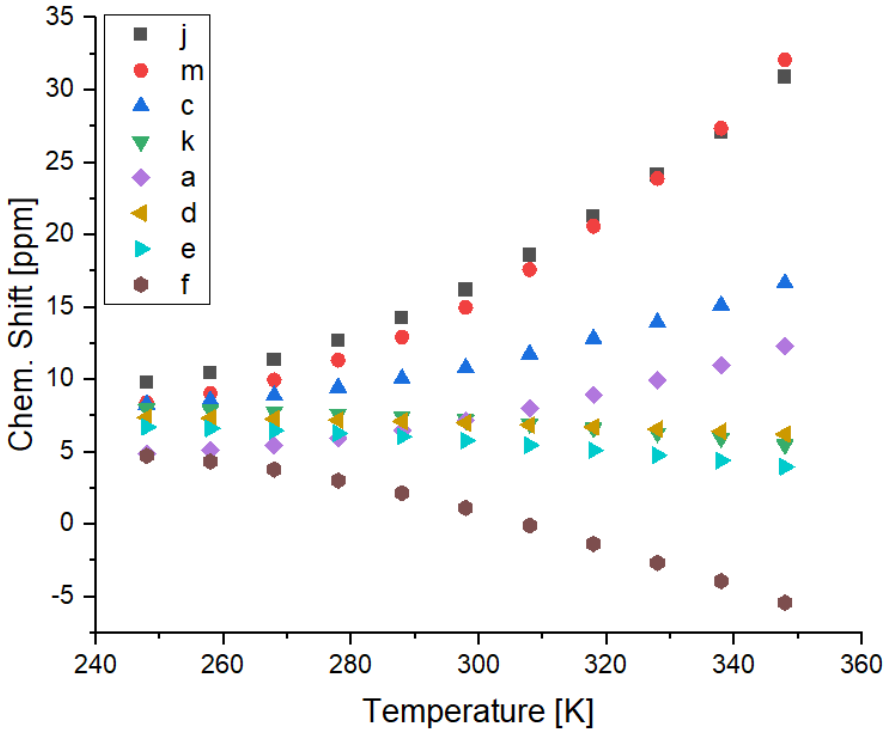

Figure S252. Chemical shift changes in the range of 248 K to 348 K for cage **6**.

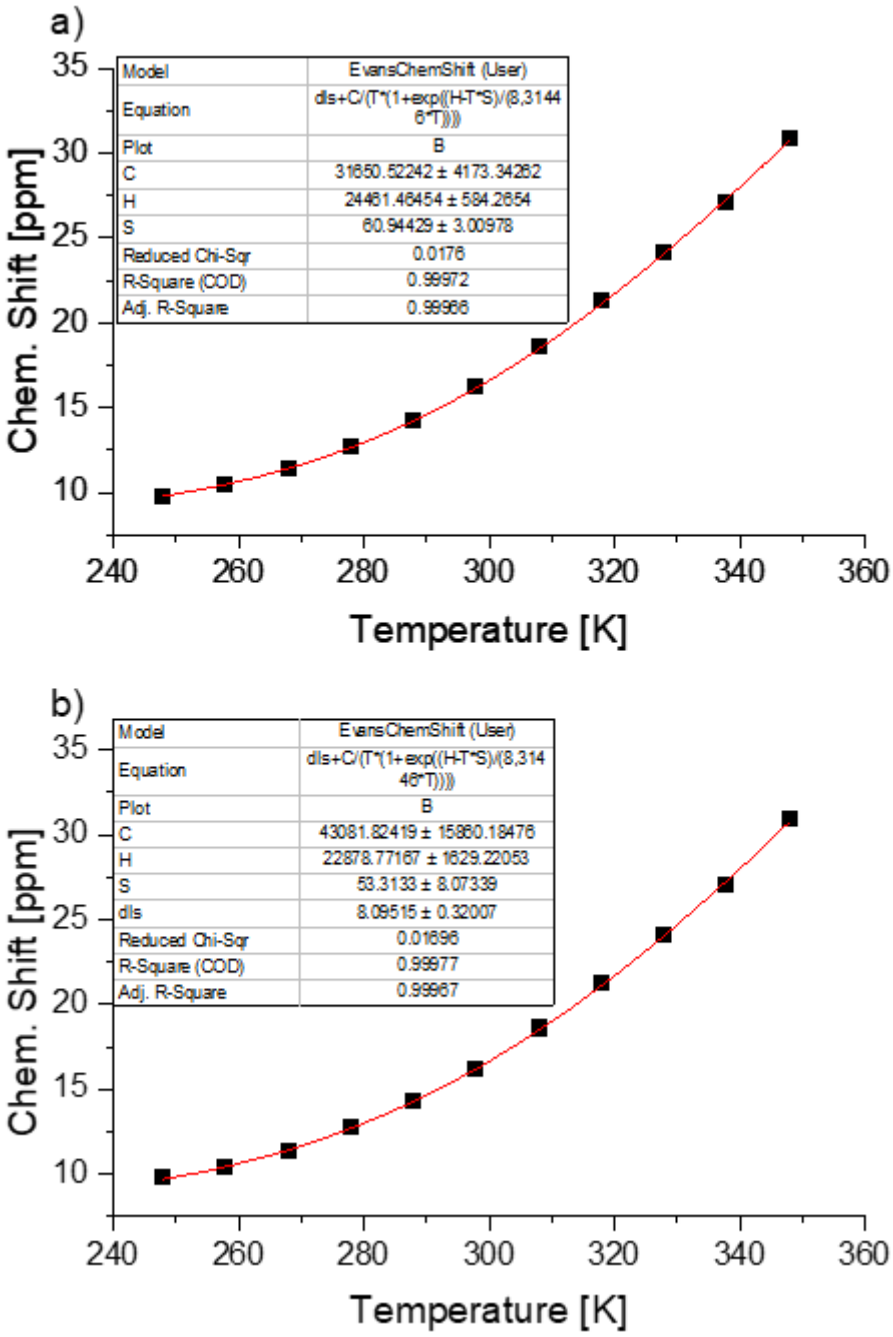

Figure S253. Fitting of the chemical shift versus temperature data for cage **6** where δ_{LS} was a) fixed as 8.43 ppm b) unfixed.

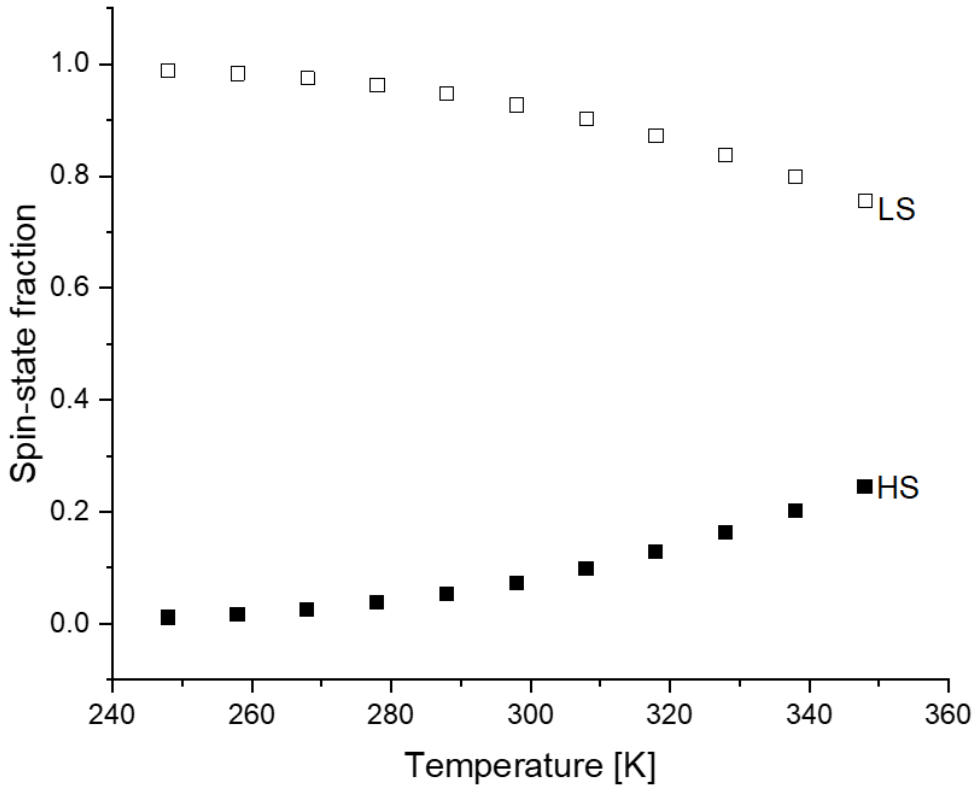

Figure S254. Spin-state population of cage **6**.

5.9 Cage 7

While fitting converged with and without fixing δ_{LS}, large errors were obtained for the fit without fixing δ_{LS}. A spin-crossover temperature of 430 K was obtained from the fitting with δ_{LS} fixed as 8.70 ppm.

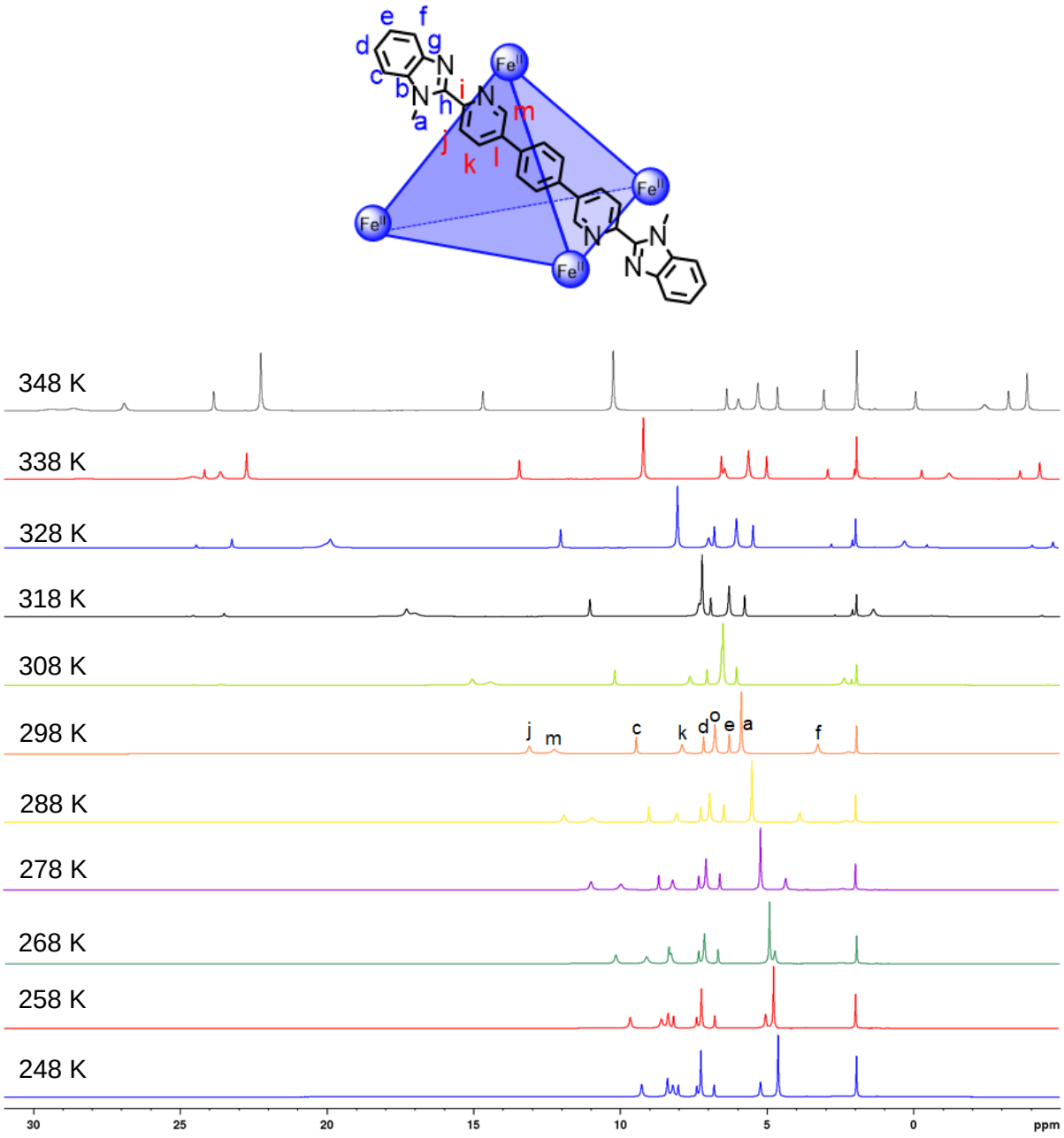

Figure S255. Chemical shift changes in the range of 248 K to 348 K for cage **7**. The appearance of additional signals above 318 K is attributed to the formation of other species, possibly due to the lability of the metal-ligand bonds at the elevated temperatures.

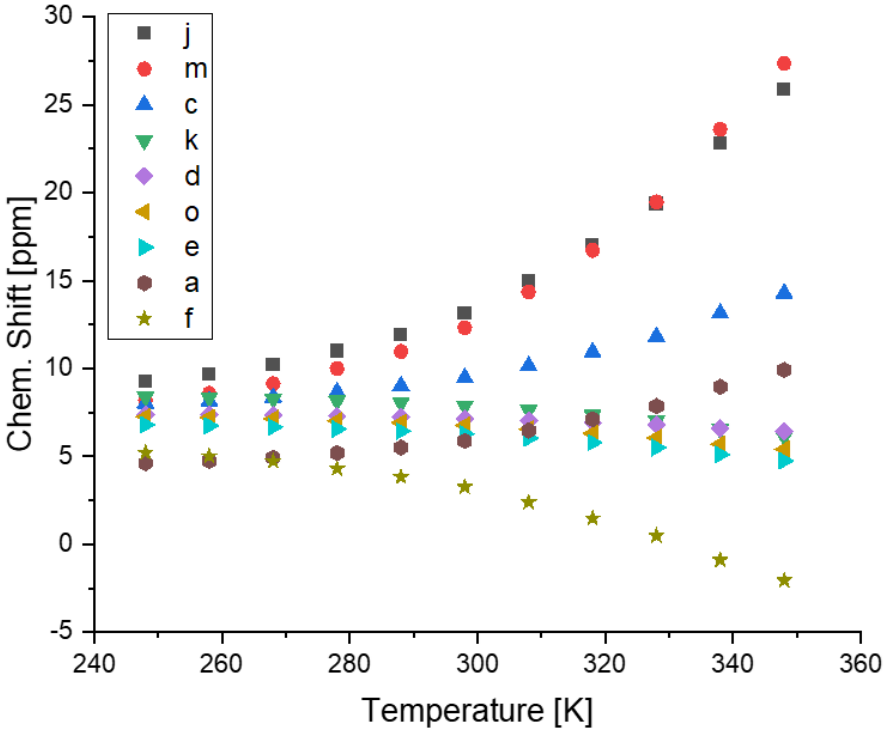

Figure S256. Chemical shift changes in the range of 248 K to 348 K for cage **7**.

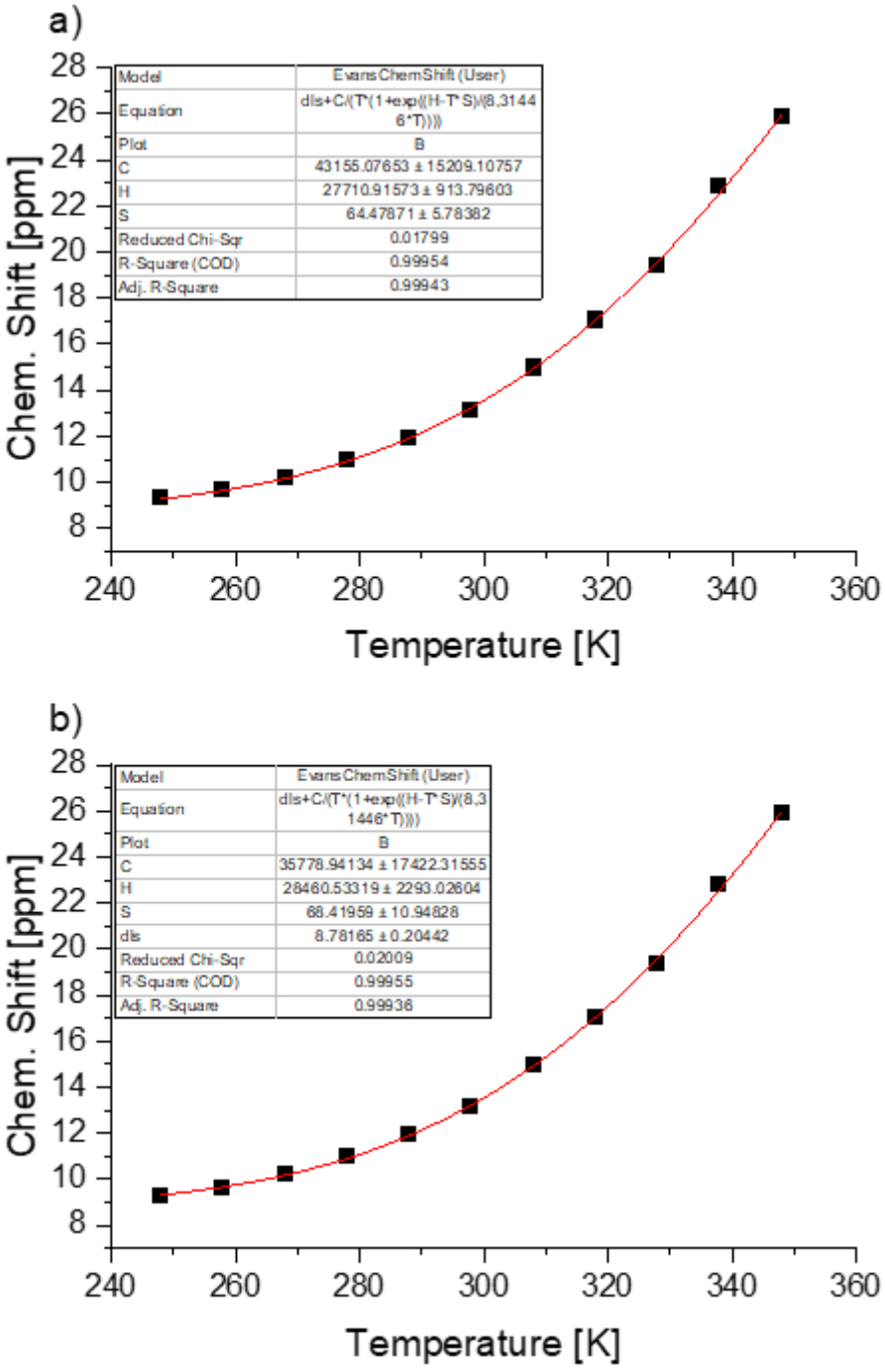

Figure S257. Fitting of the chemical shift versus temperature data for cage **7** where δ_{LS} was a) fixed as 8.70 ppm b) unfixed.

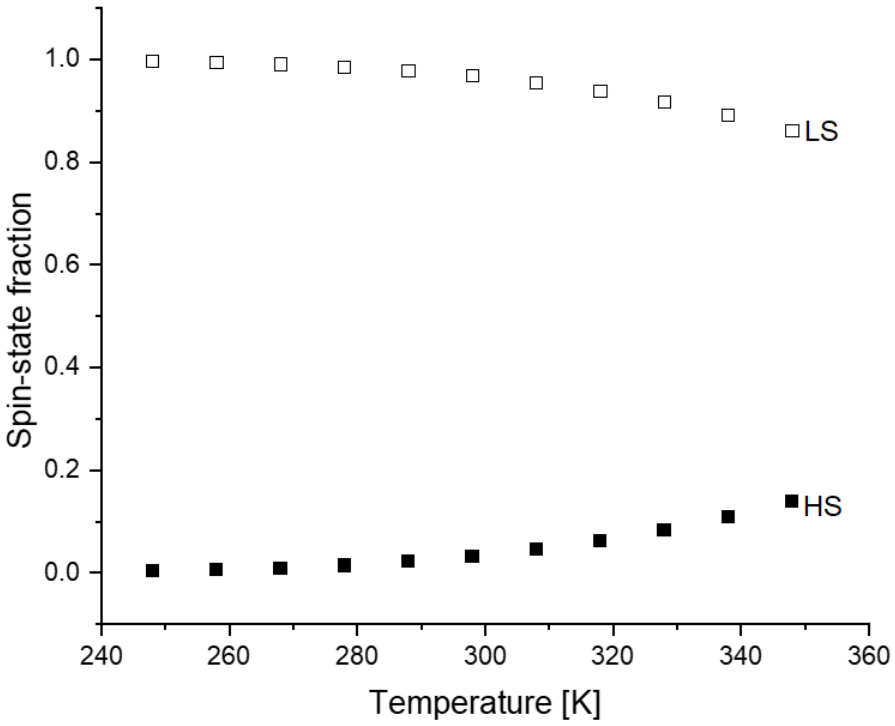

Figure S258. Spin-state population of cage **7**.

5.10 Cage 8

While fitting converged with and without fixing δ_{LS}, large errors were obtained for the fit without fixing δ_{LS}. A spin-crossover temperature of 375 K was obtained from the fitting with δ_{LS} fixed as 8.48 ppm.

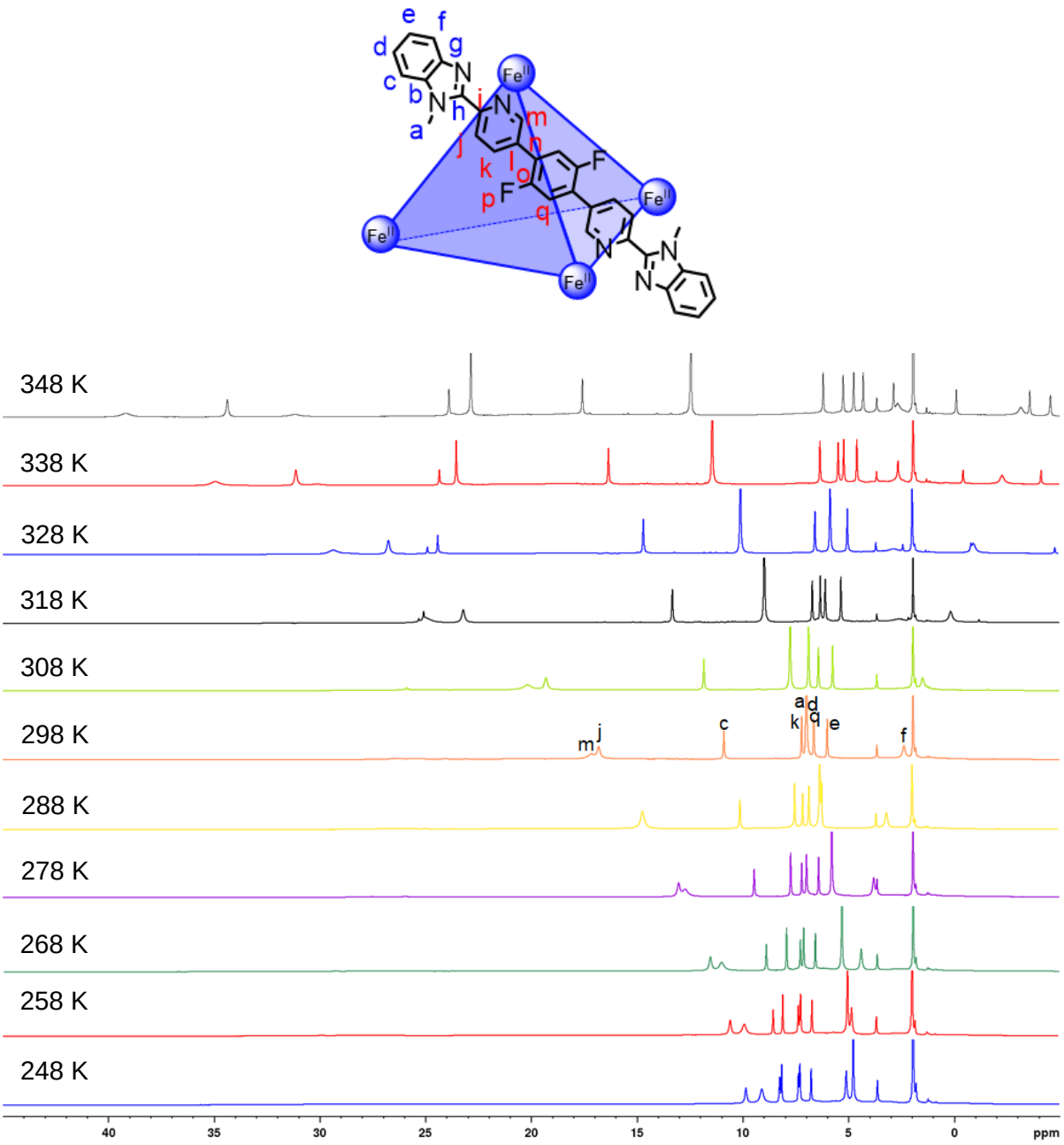

Figure S259. Chemical shift changes in the range of 248 K to 348 K for cage **8**. The appearance of additional signals above 308 K is attributed to the formation of other species, possibly due to the lability of the metal-ligand bonds at the elevated temperatures.

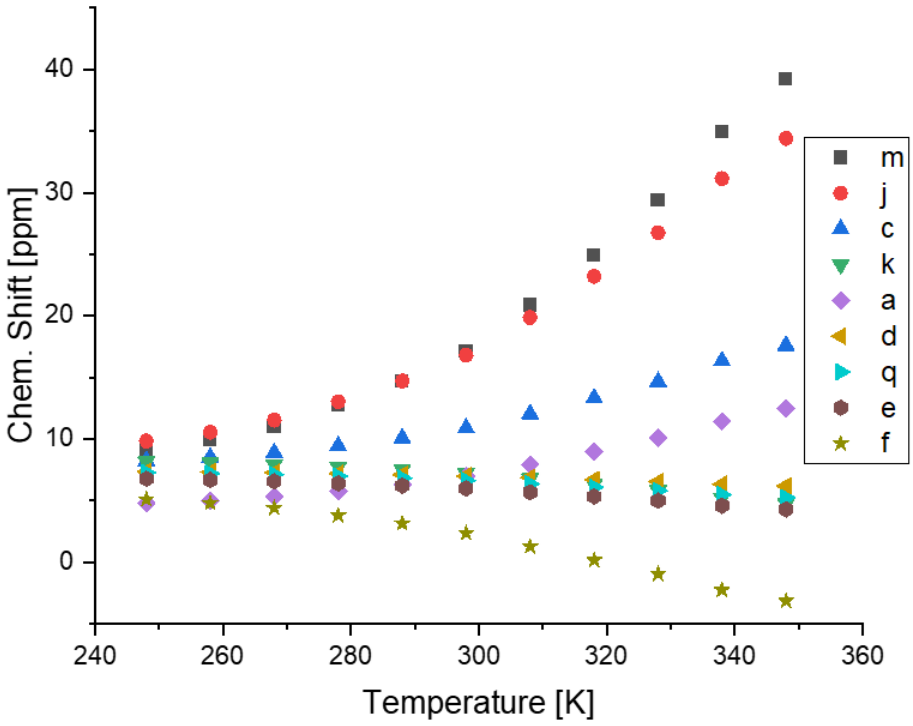

Figure S260. Chemical shift changes in the range of 248 K to 348 K for cage **8**.

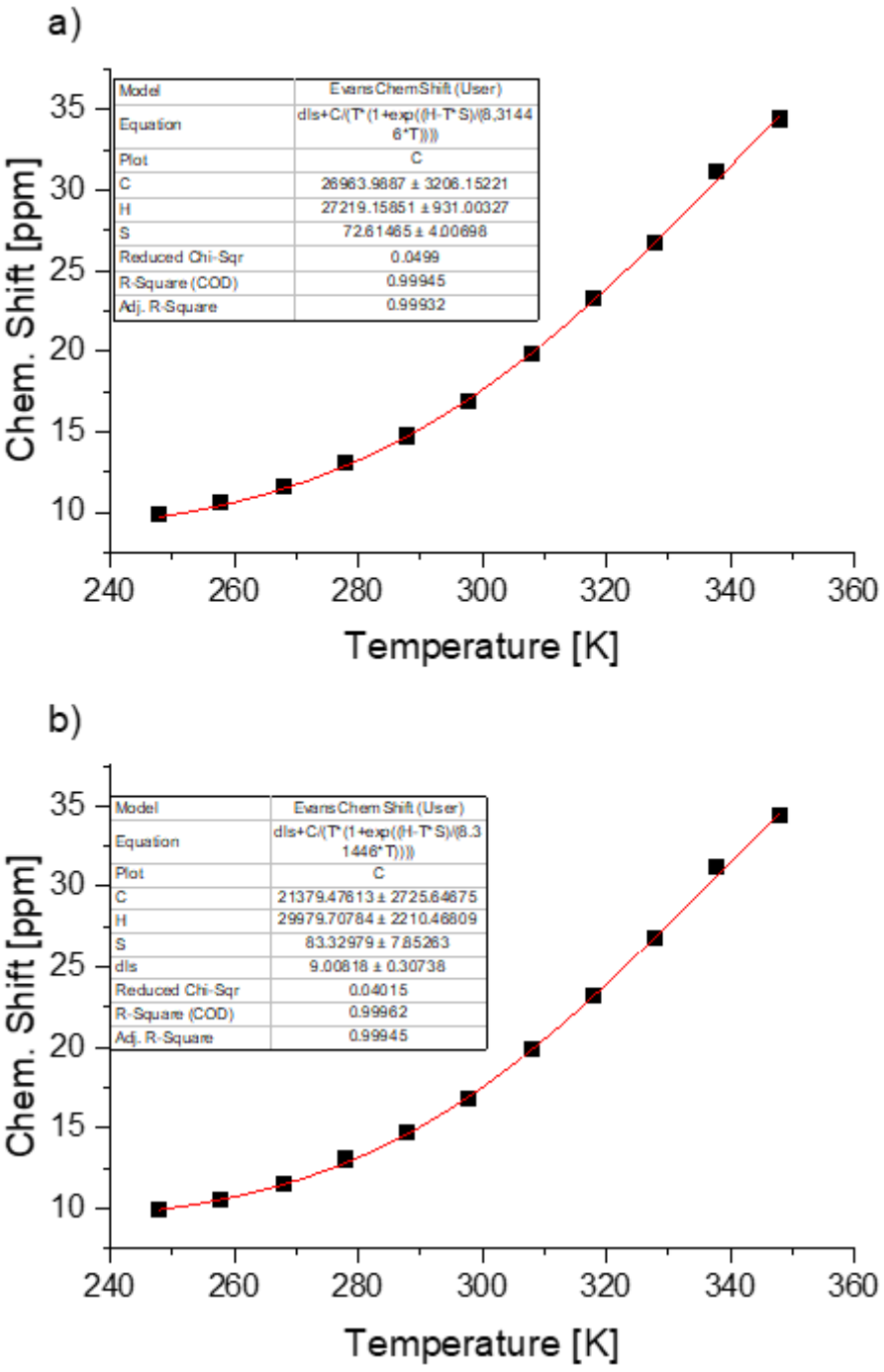

Figure S261. Fitting of the chemical shift versus temperature data for cage **8** where δ_{LS} was a) fixed as 8.48 ppm b) unfixed.

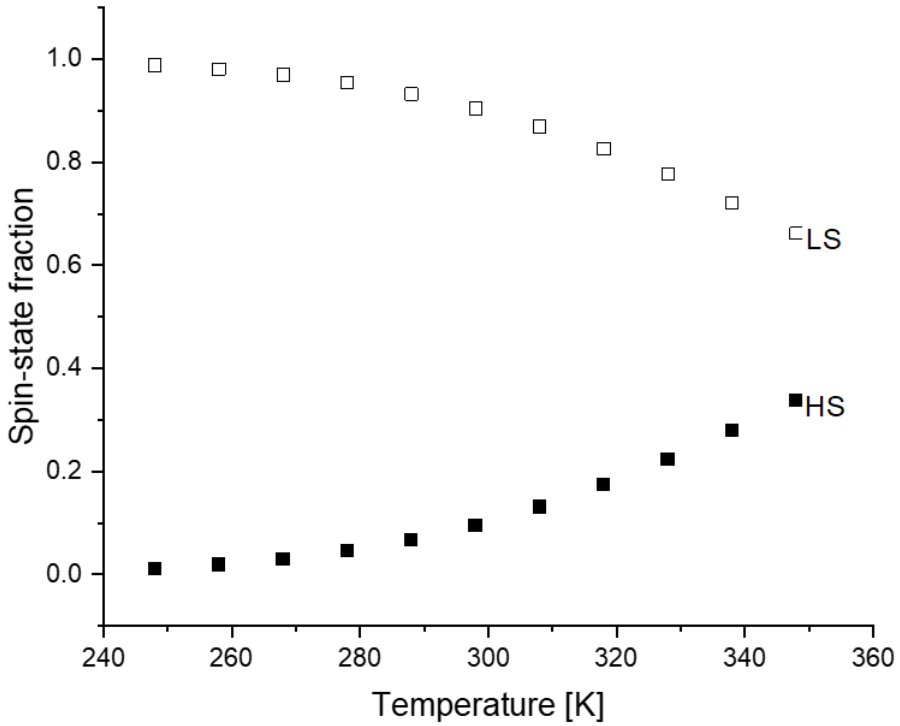

Figure S262. Spin-state population of cage **8**.

5.11 Cage 9

While fitting converged with and without fixing δ_{LS}, large errors were obtained for the fit without fixing δ_{LS}. A spin-crossover temperature of 339 K was obtained from fitting with δ_{LS} fixed as 8.40 ppm.

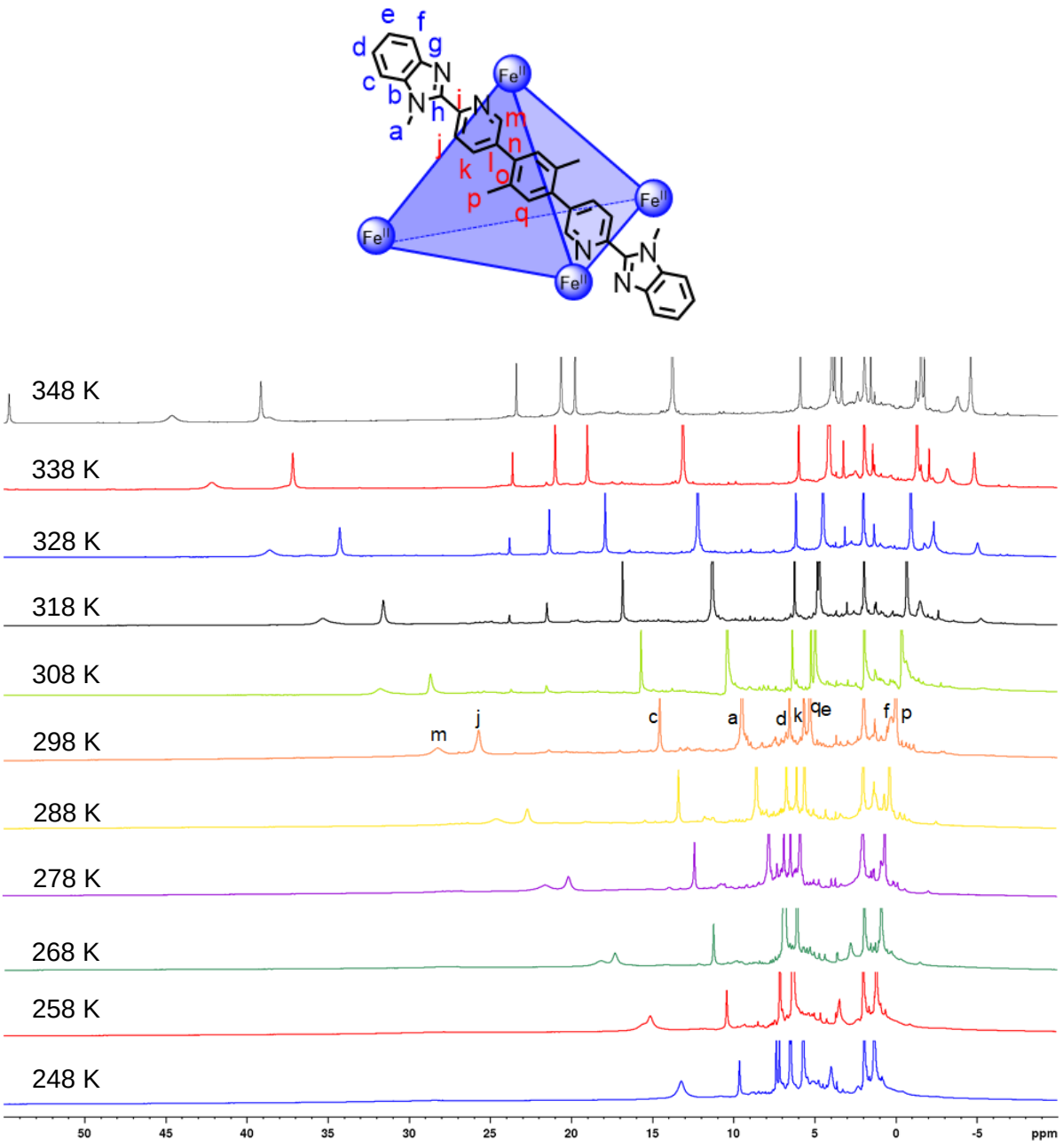

Figure S263. Chemical shift changes in the range of 248 K to 348 K for cage **9**. The appearance of additional signals above 308 K is attributed to the formation of other species, possibly due to the lability of the metal-ligand bonds at the elevated temperatures.

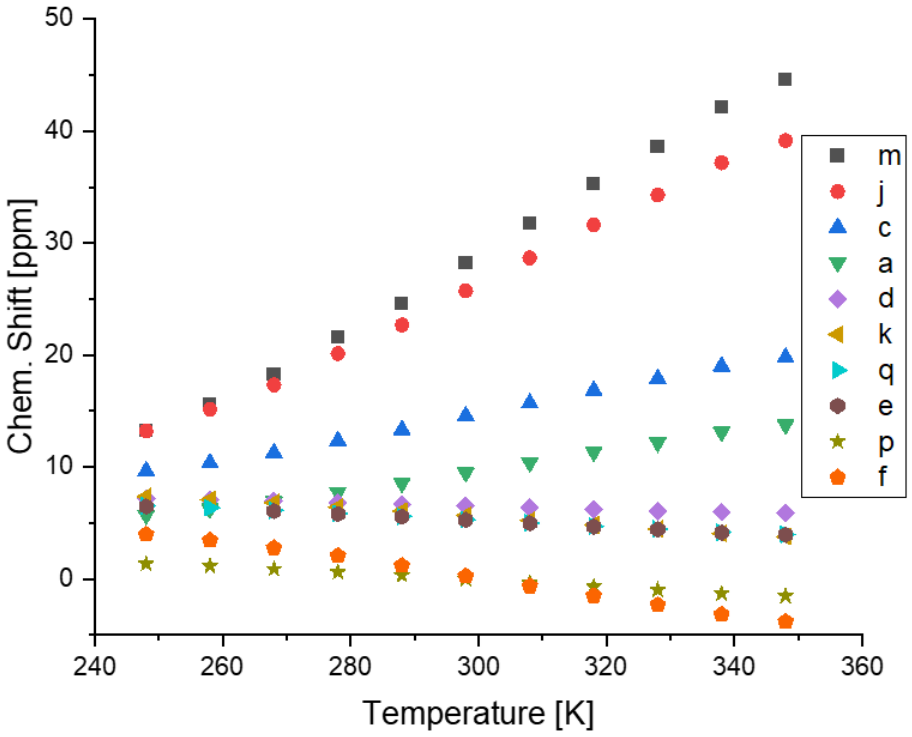

Figure S264. Chemical shift changes in the range of 248 K to 348 K for cage **9**.

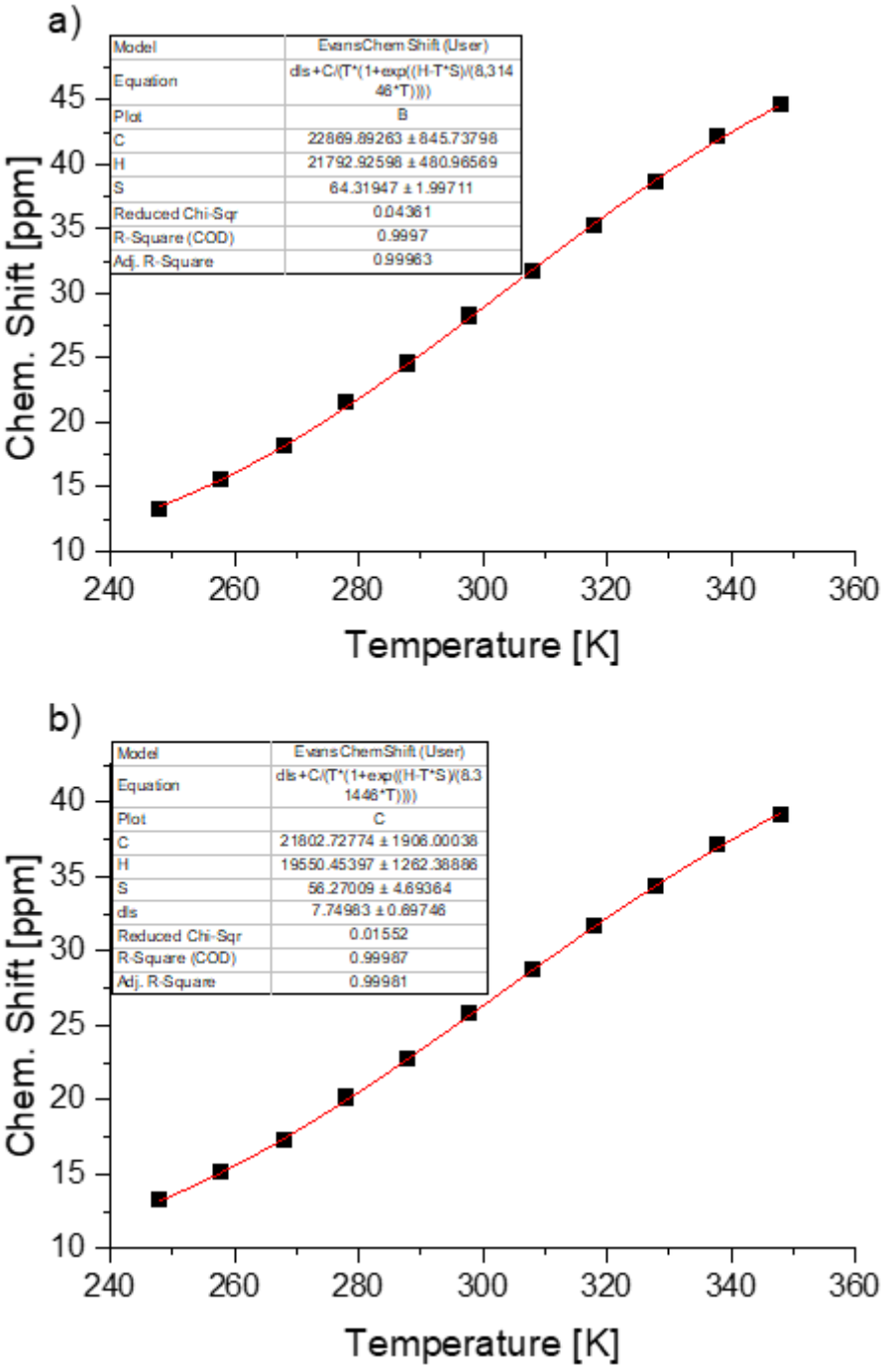

Figure S265. Fitting of the chemical shift versus temperature data for cage **9** (proton j) where δ_{LS} was a) fixed as 8.40 ppm b) unfixed.

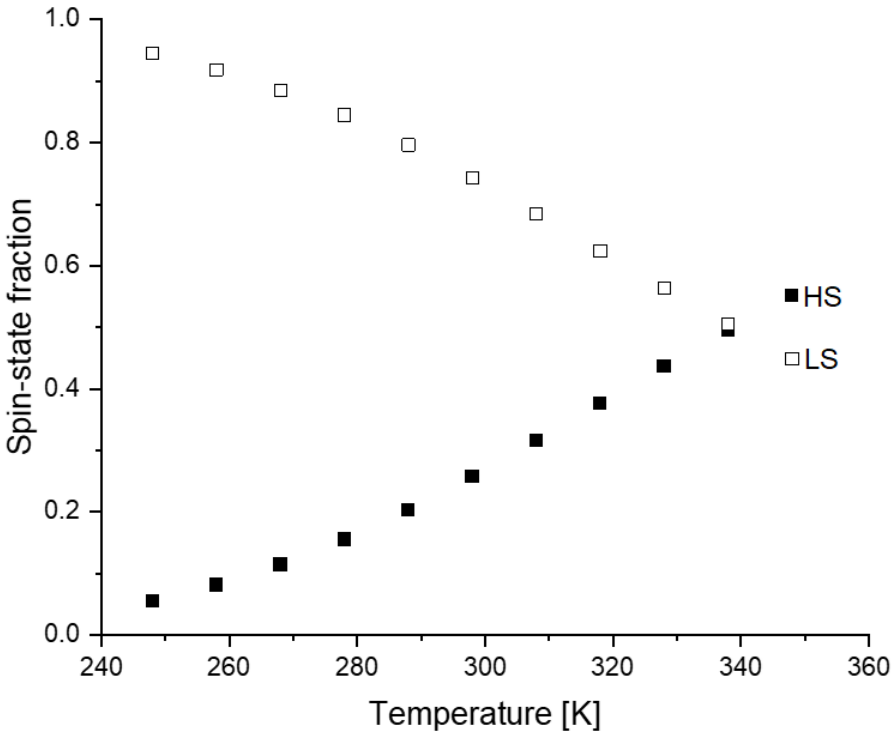

Figure S266. Spin-state population of cage **9**.

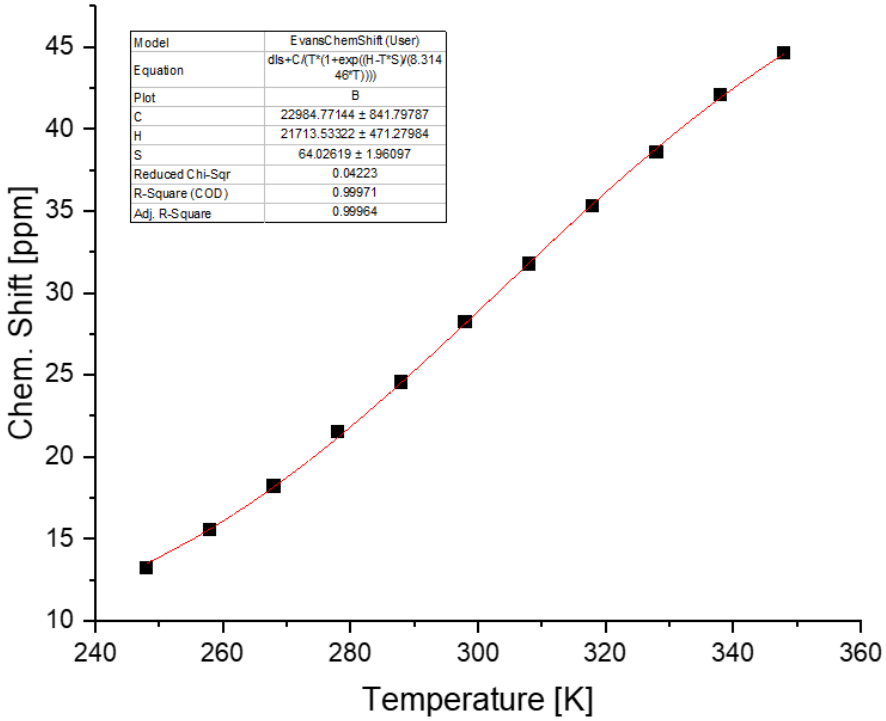

Figure S267. Fitting of the chemical shift versus temperature data for cage **9** (proton m) where δ_{LS} was fixed as 8.35 ppm.

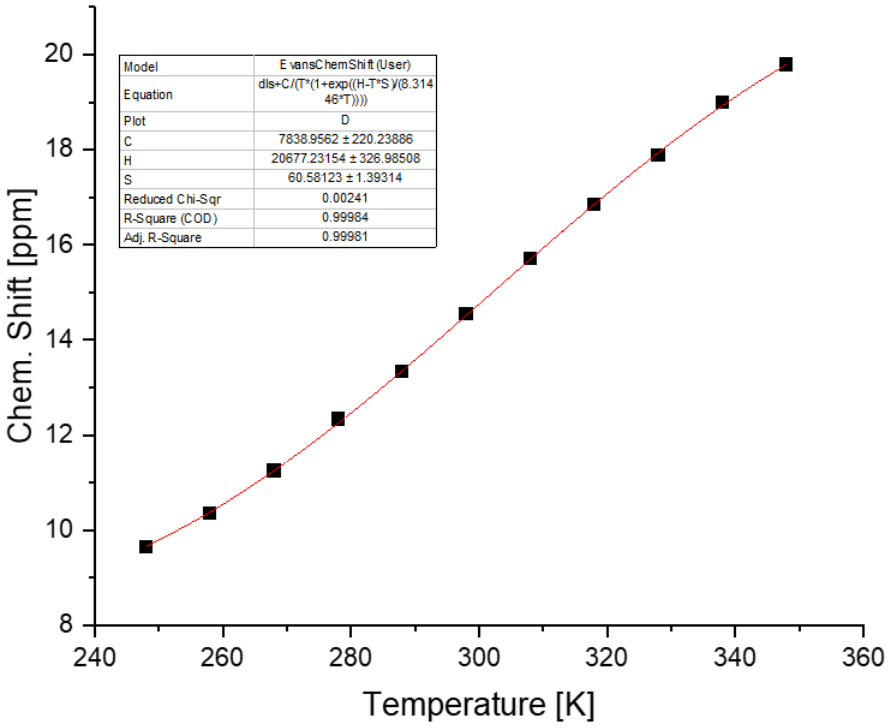

Figure S268. Fitting of the chemical shift versus temperature data for cage **9** (proton c) where δ_{LS} was fixed as 7.75 ppm.

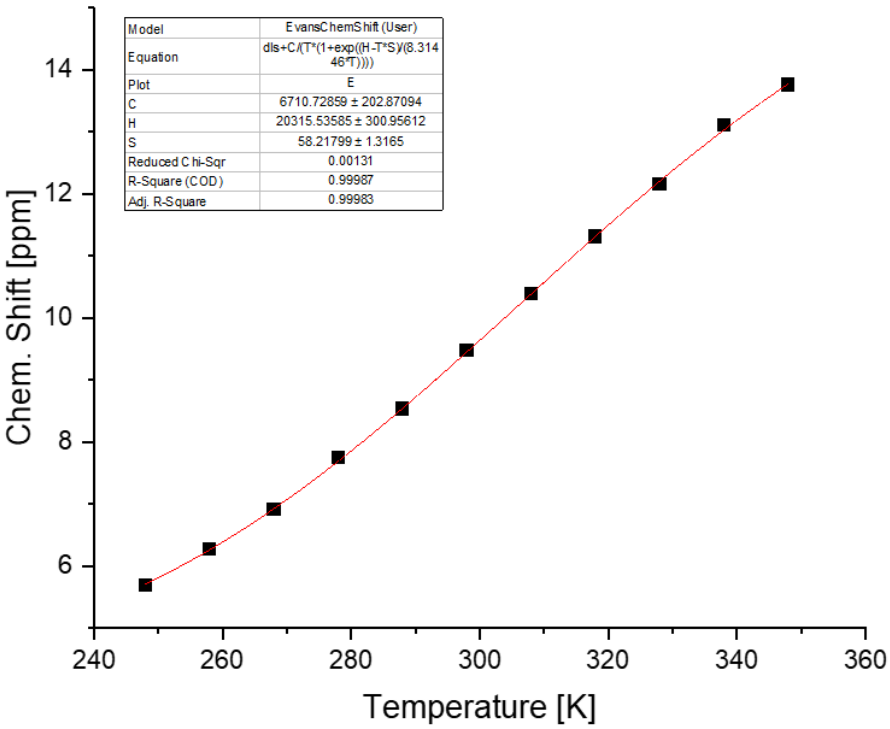

Figure S269. Fitting of the chemical shift versus temperature data for cage **9** (proton a) where δ_{LS} was fixed as 4.23 ppm.

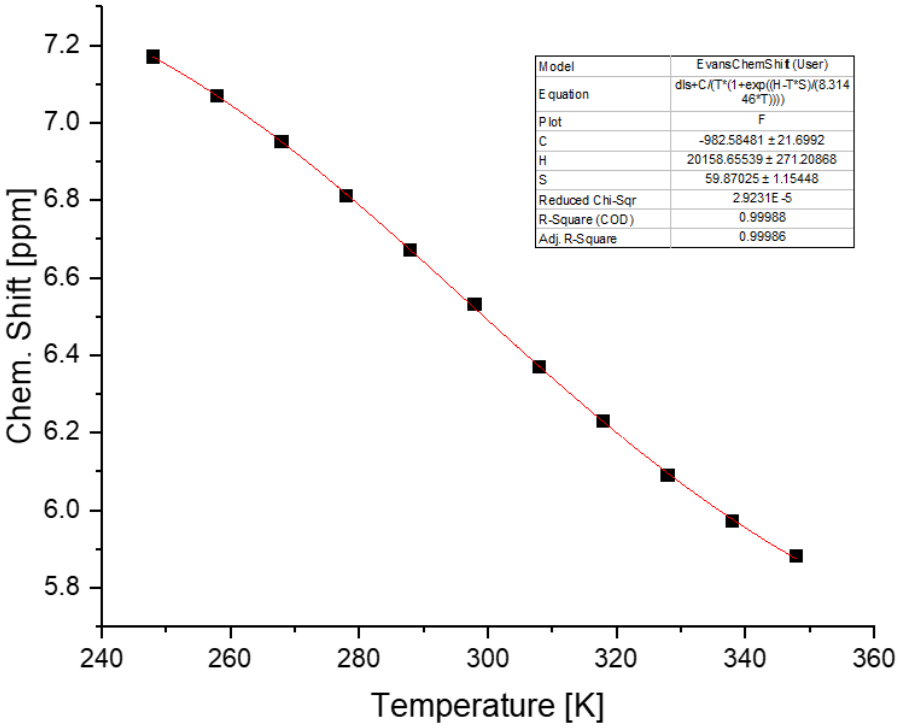

Figure S270. Fitting of the chemical shift versus temperature data for cage **9** (proton d) where δ_{LS} was fixed as 7.45 ppm.

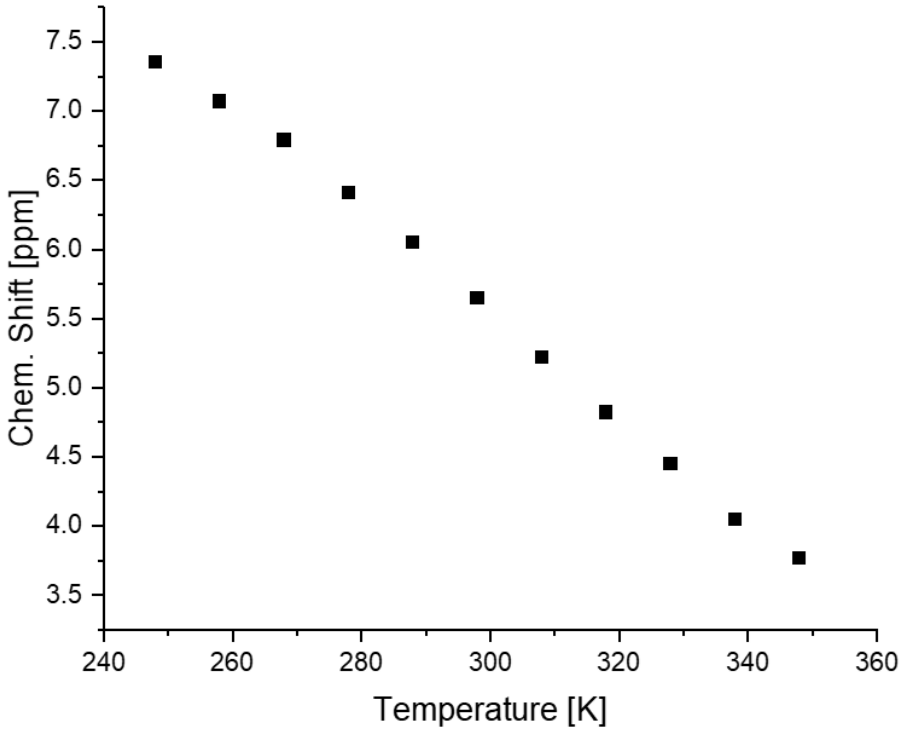

Figure S271. Fitting of the chemical shift versus temperature data for cage **9** (proton k) where δ_{LS} was fixed as 8.11 ppm. The fitting did not converge.

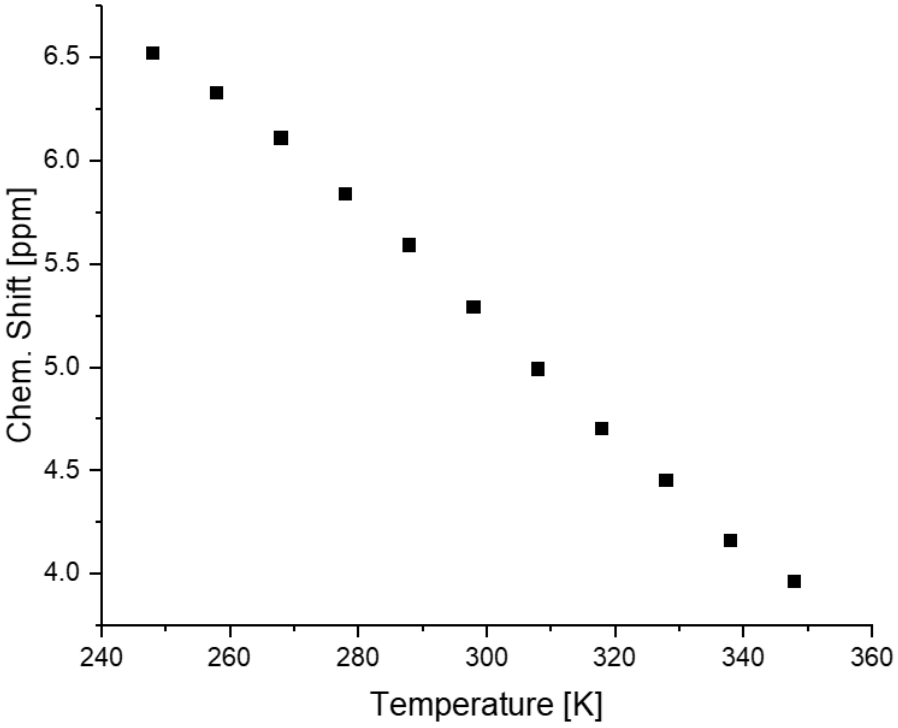

Figure S272. Fitting of the chemical shift versus temperature data for cage **9** (proton q) where δ_{LS} was fixed as 7.06 ppm. The fitting did not converge.

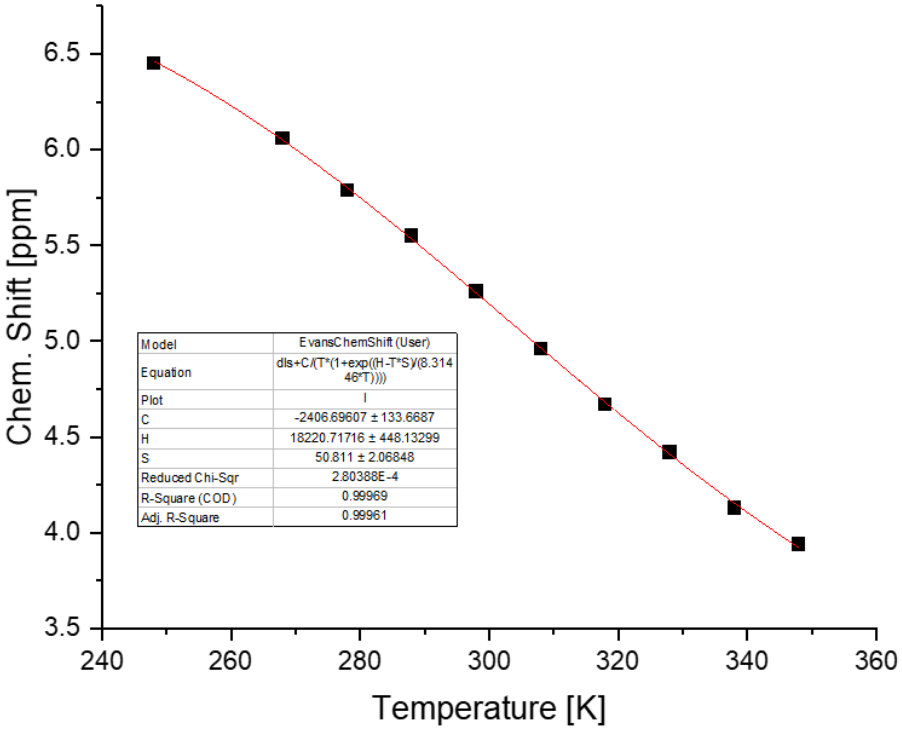

Figure S273. Fitting of the chemical shift versus temperature data for cage **9** (proton e) where δ_{LS} was fixed as 7.06 ppm.

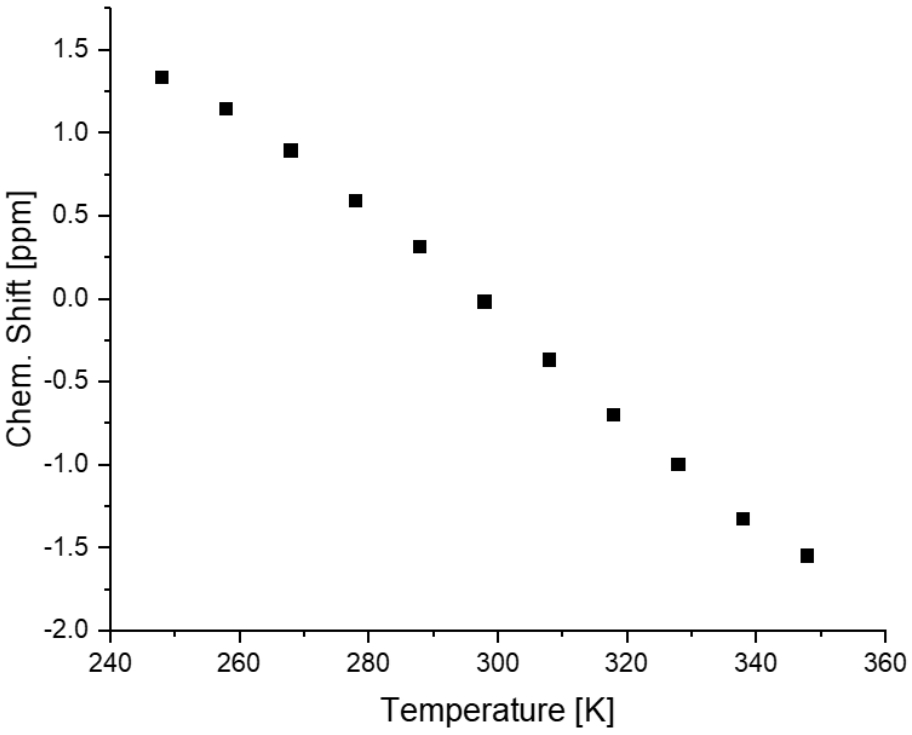

Figure S274. Fitting of the chemical shift versus temperature data for cage **9** (proton p) where δ_{LS} was fixed as 1.92 ppm. The fitting did not converge.

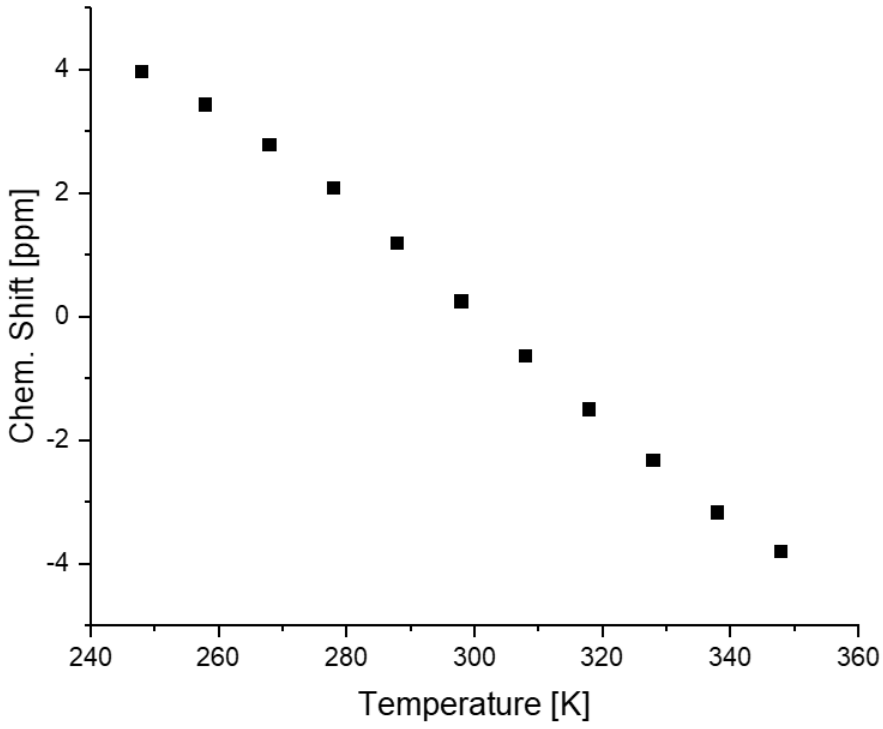

Figure S275. Fitting of the chemical shift versus temperature data for cage **9** (proton f) where δ_{LS} was fixed as 6.63 ppm. The fitting did not converge.

Table S2. Spin-crossover temperatures from variable temperature NMR experiments (248-348 K) for cage **9** fitting different protons.

Proton	Cage 9	
	$T_{1/2}$ [K]	δ_{LS} [ppm][a]
m	339	8.35
j	339	8.40
c	341	7.75
a	349	4.23
d	226	7.45
k	[b]	8.11
q	[b]	7.06
e	358	7.06
p	[b]	1.92
f	[b]	6.63

[a] Chemical shift of the Zn(II) cage analogue. [b] Could not be determined since fitting did not converge.

5.12 Cage 10

While fitting converged with and without fixing δ_{LS}, large errors were obtained for the fit without fixing δ_{LS}. A spin-crossover temperature of 353 K was obtained from the fitting with δ_{LS} fixed as 8.18 ppm.

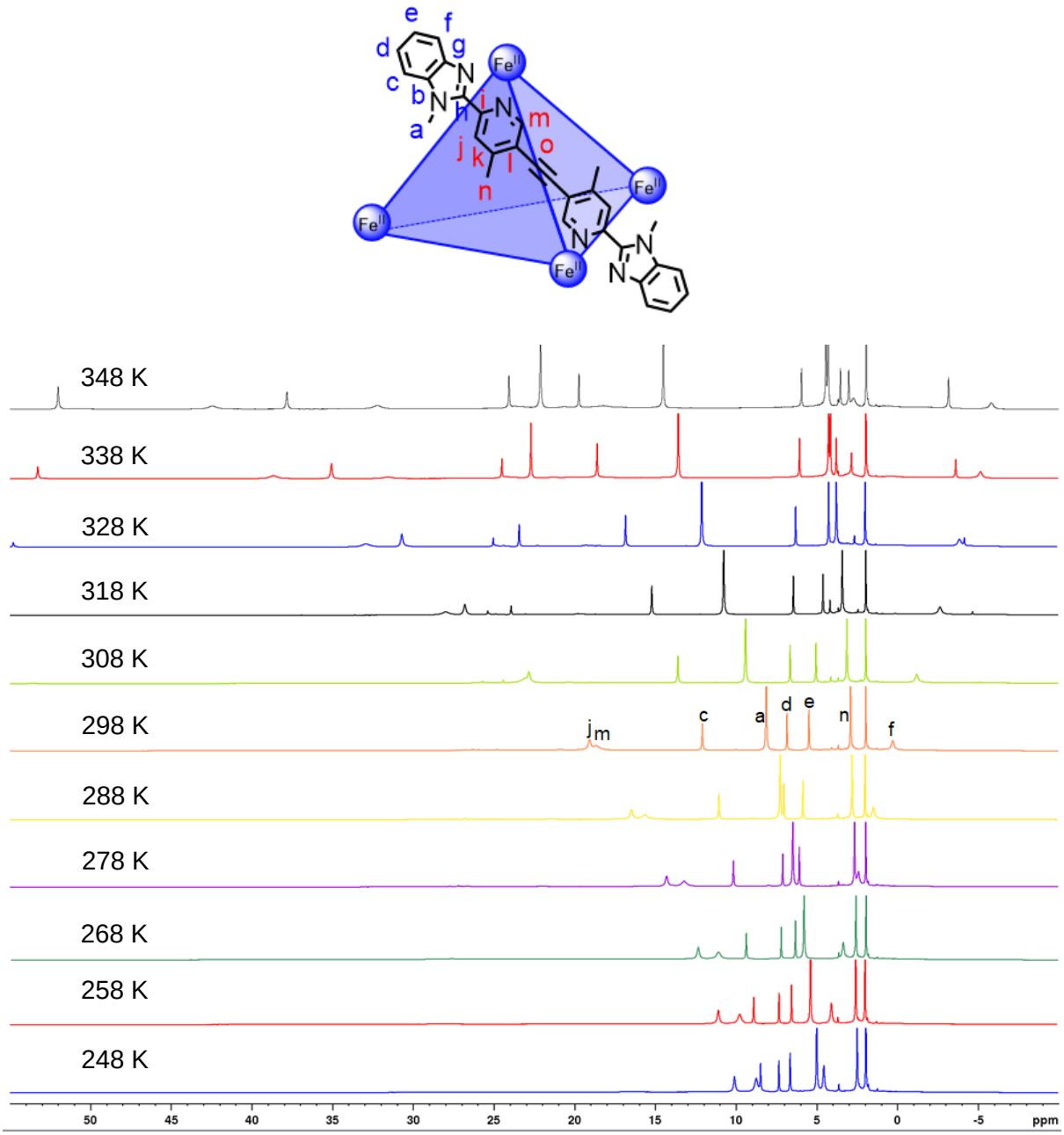

Figure S276. Chemical shift changes in the range of 248 K to 348 K for cage **10**. The appearance of additional signals above 318 K is attributed to the formation of other species, possibly due to the lability of the metal-ligand bonds at the elevated temperatures.

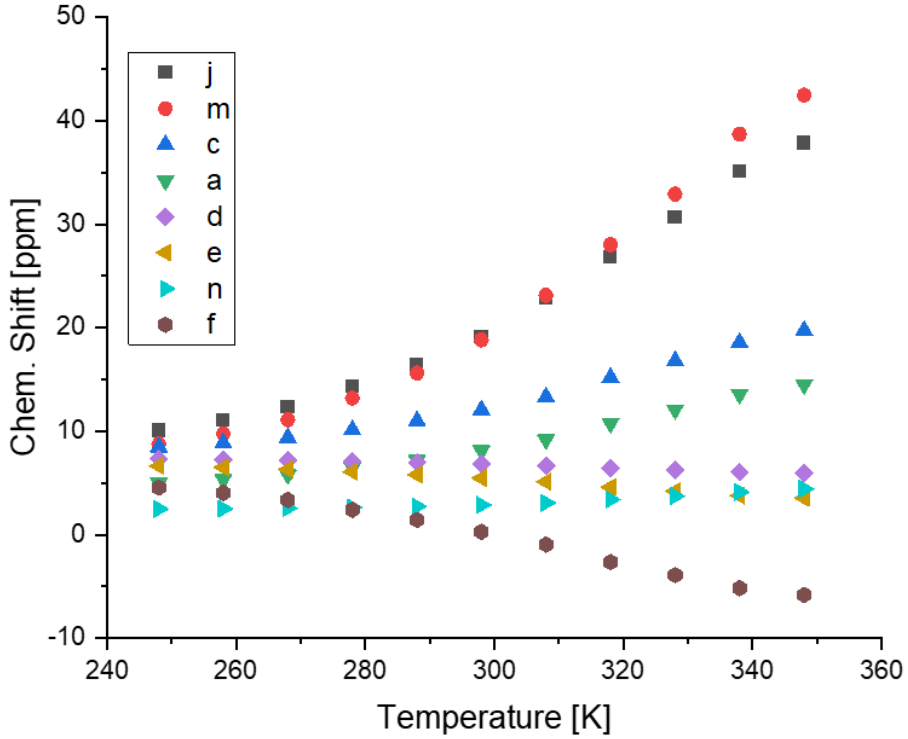

Figure S277. Chemical shift changes in the range of 248 K to 348 K for cage **10**.

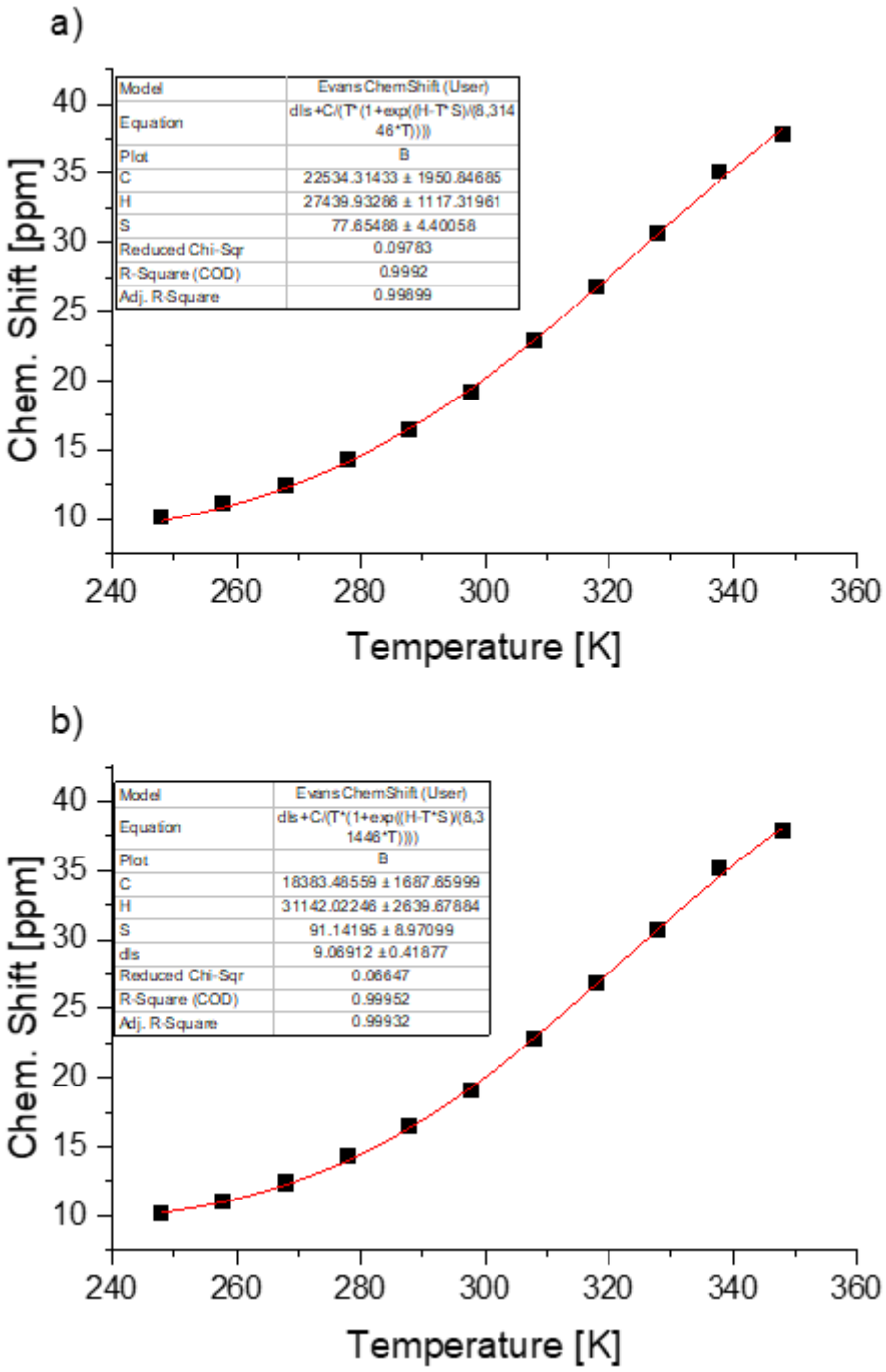

Figure S278. Fitting of the chemical shift versus temperature data for cage **10** where δ_{LS} was a) fixed as 8.18 ppm b) unfixed.

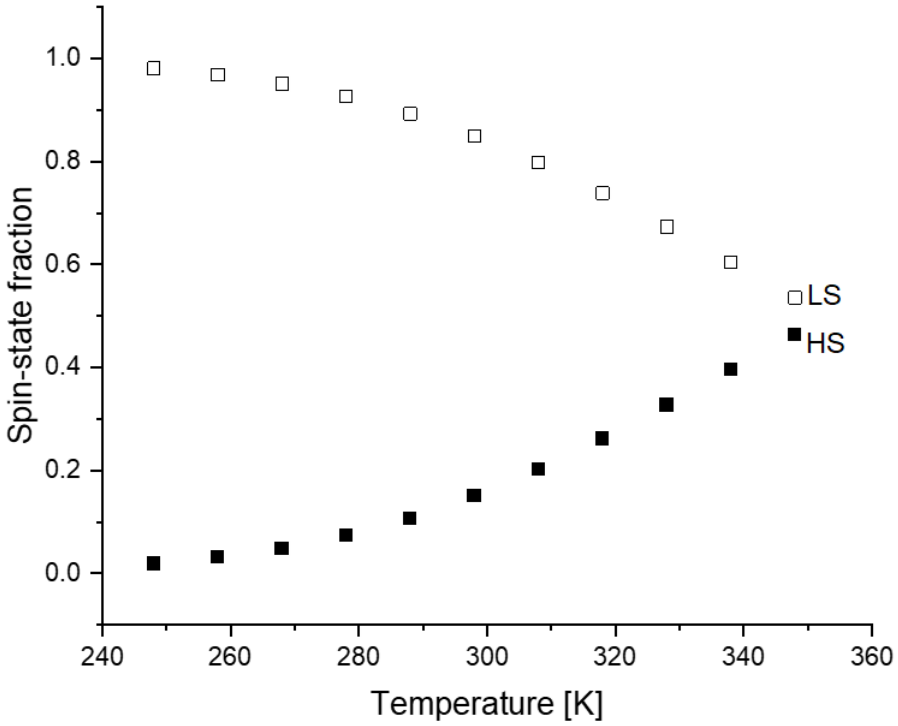

Figure S279. Spin-state population of cage **10**.

5.13 Cage 11

Cage **11** was predominantly high spin above 248 K and showed Curie-Weiss behavior above 310 K. Therefore, fitting was performed for data between 248 K and 308 K. While fitting converged with δ_{LS} fixed as 8.48 ppm giving a spin-crossover temperature of 244 K, the fitting did not converge when δ_{LS} was not fixed.

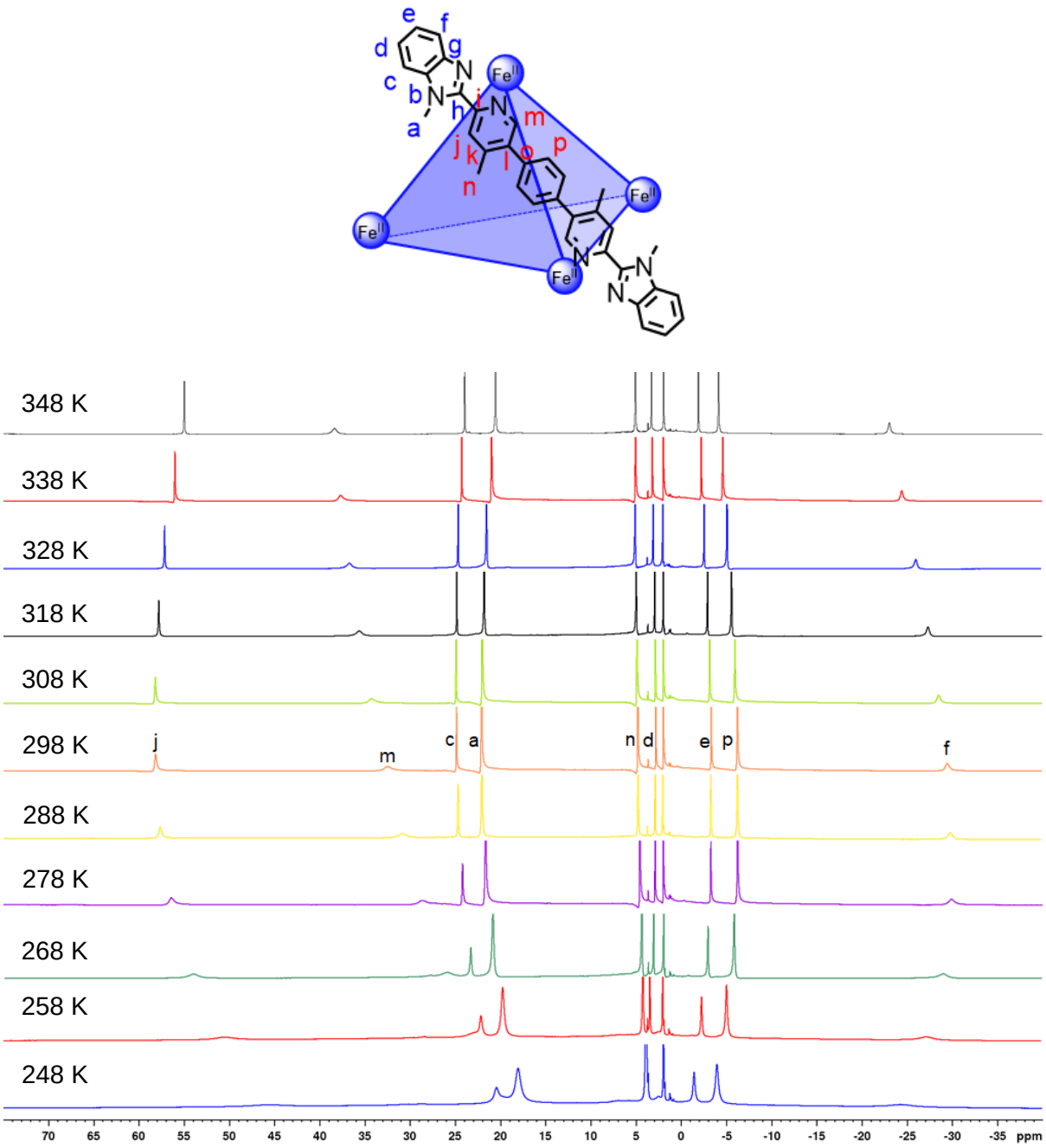

Figure S280. Chemical shift changes in the range of 248 K to 348 K for cage **11**.

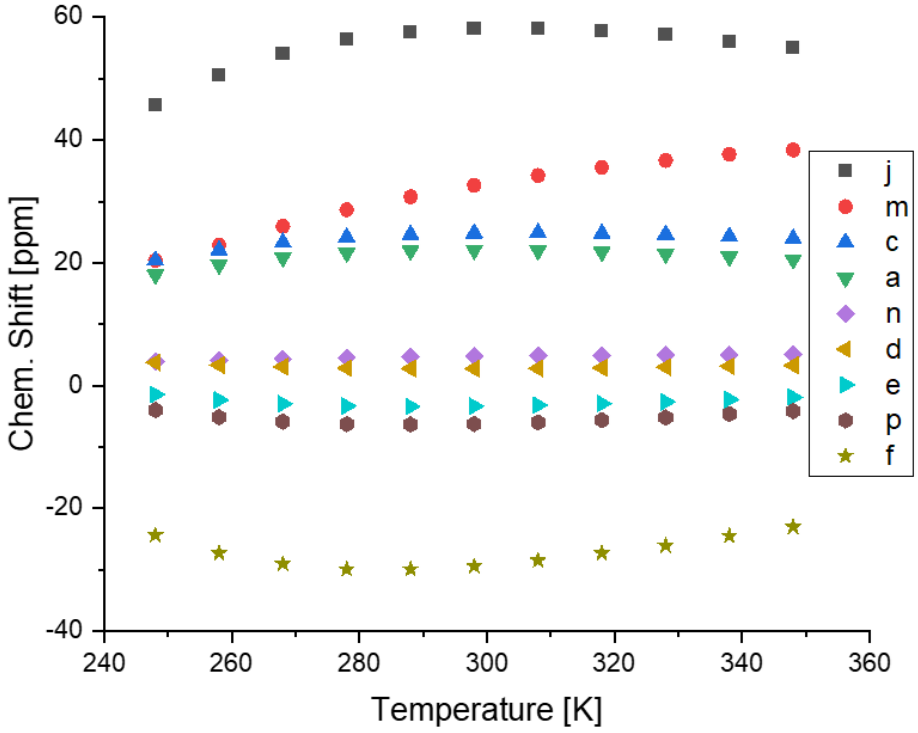

Figure S281. Chemical shift changes in the range of 248 K to 348 K for cage **11**.

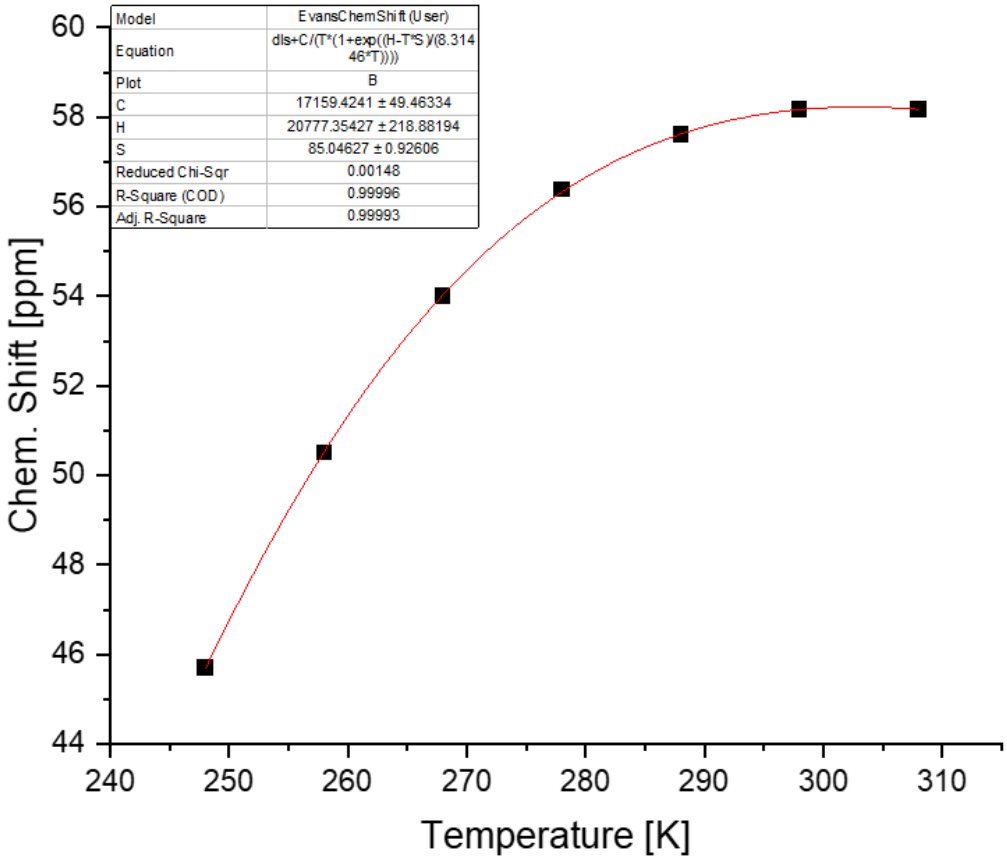

Figure S282. Fitting of the chemical shift versus temperature data for cage **11** (proton j) where δ_{LS} was fixed as 8.46 ppm. The fitting without fixing δ_{LS} did not converge.

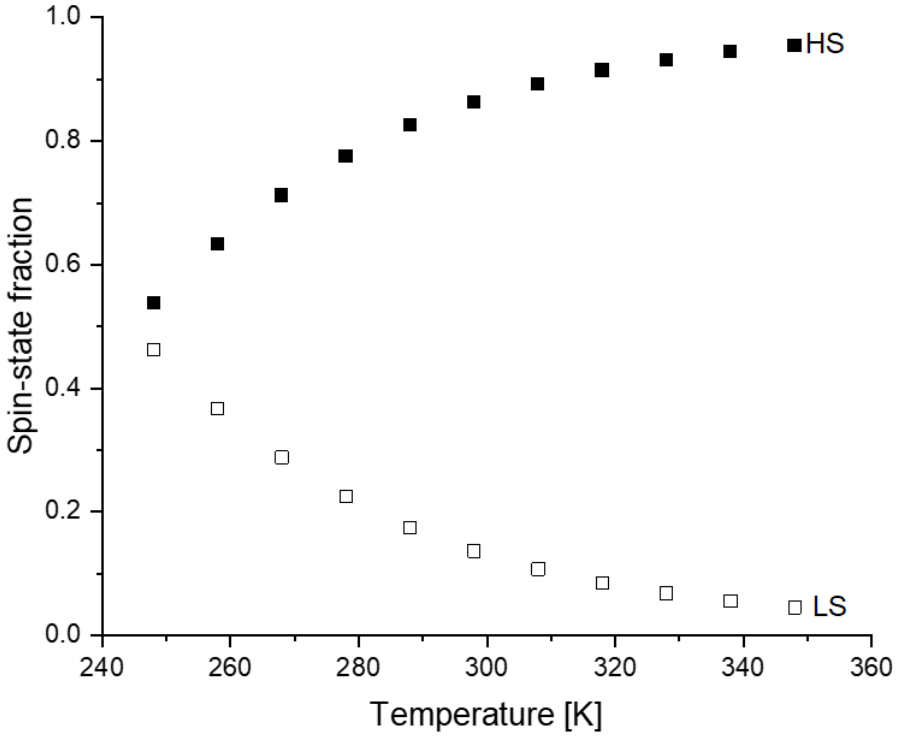

Figure S283. Spin-state population of cage **11**.

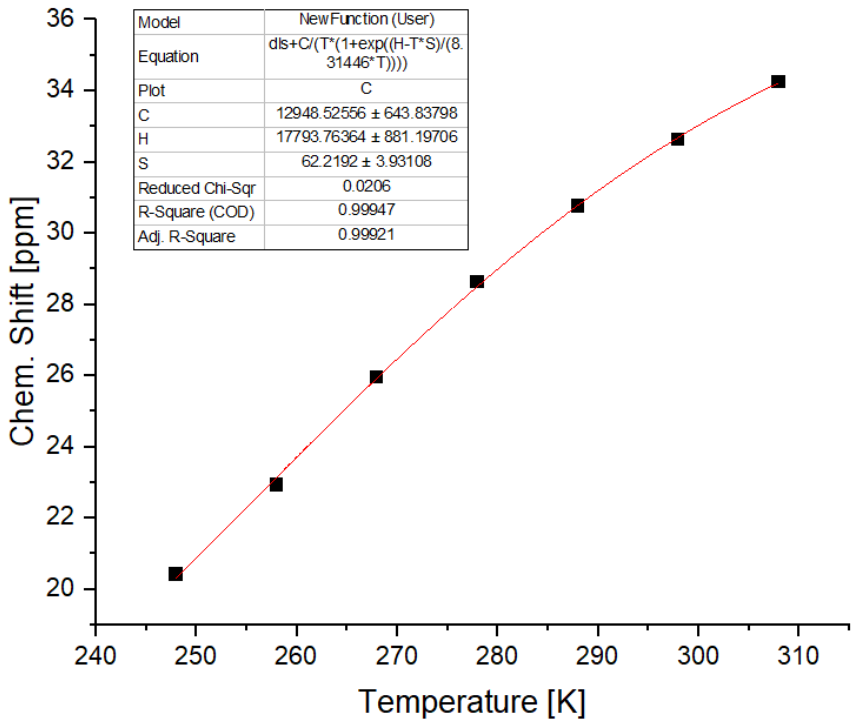

Figure S284. Fitting of the chemical shift versus temperature data for cage **11** (proton m) where δ_{LS} was fixed as 7.70 ppm.

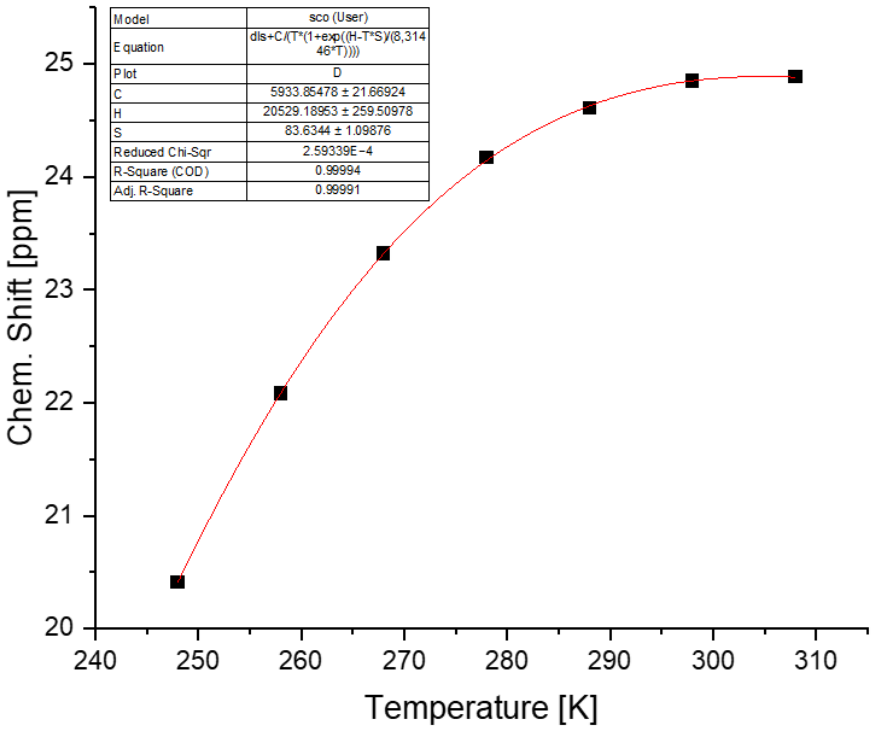

Figure S285. Fitting of the chemical shift versus temperature data for cage **11** (proton c) where δ_{LS} was fixed as 7.83 ppm.

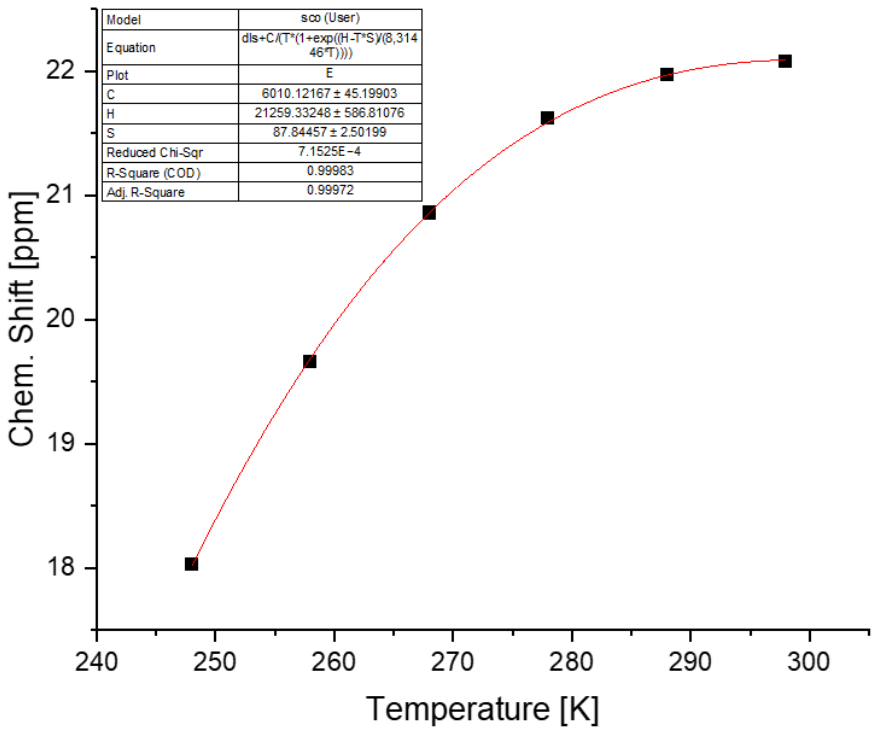

Figure S286. Fitting of the chemical shift versus temperature data for cage **11** (proton a) where δ_{LS} was fixed as 4.36 ppm.

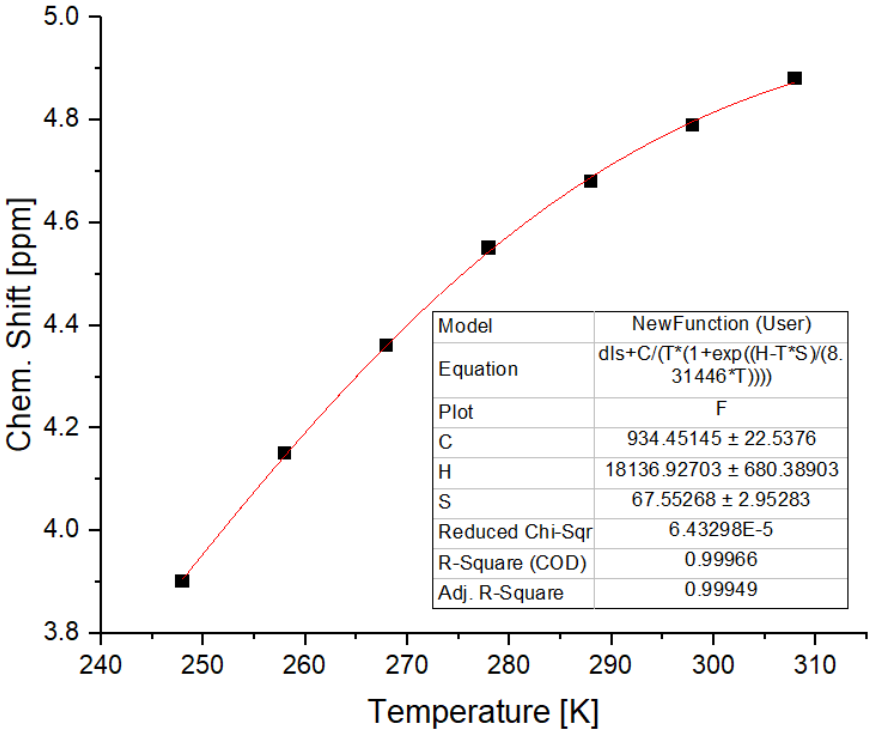

Figure S287. Fitting of the chemical shift versus temperature data for cage **11** (proton n) where δ_{LS} was fixed as 2.63 ppm.

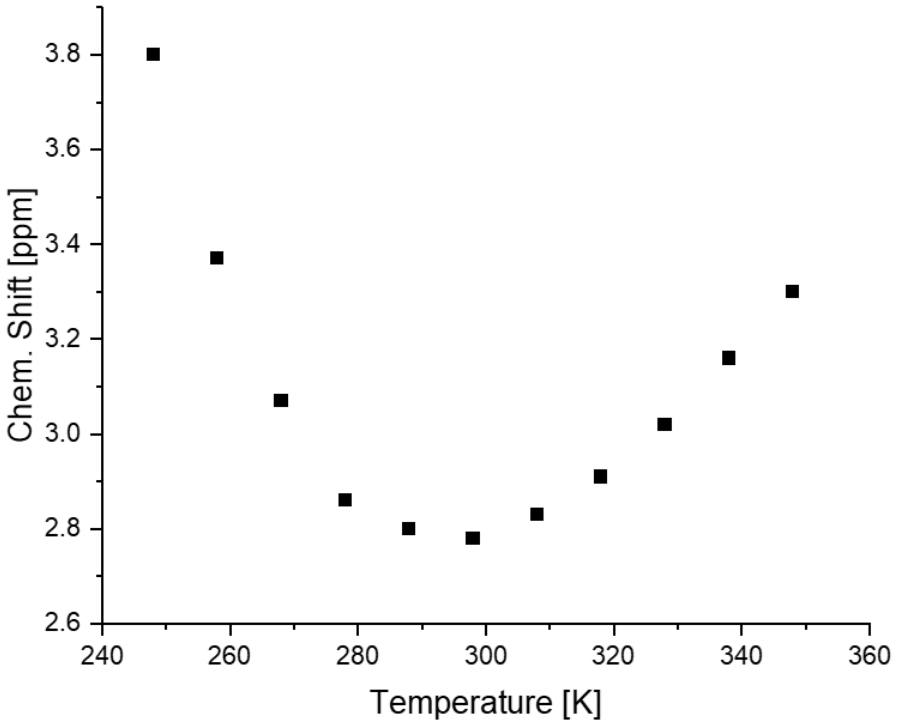

Figure S288. Fitting of the chemical shift versus temperature data for cage **11** (proton d) where δ_{LS} was fixed as 7.51 ppm. The fitting did not converge.

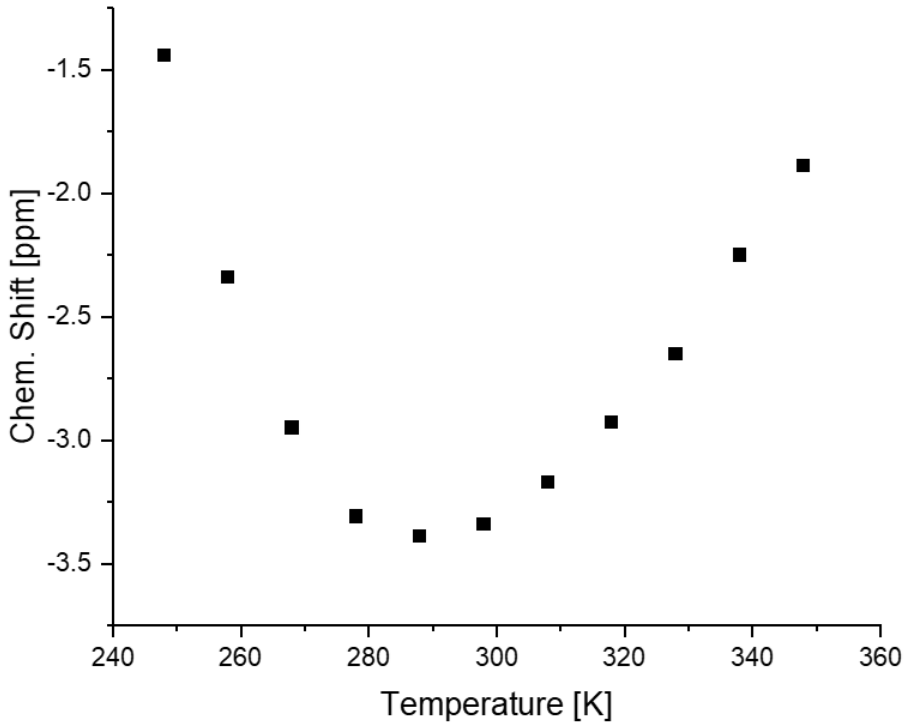

Figure S289. Fitting of the chemical shift versus temperature data for cage **11** (proton e) where δ_{LS} was fixed as 7.05 ppm. The fitting did not converge.

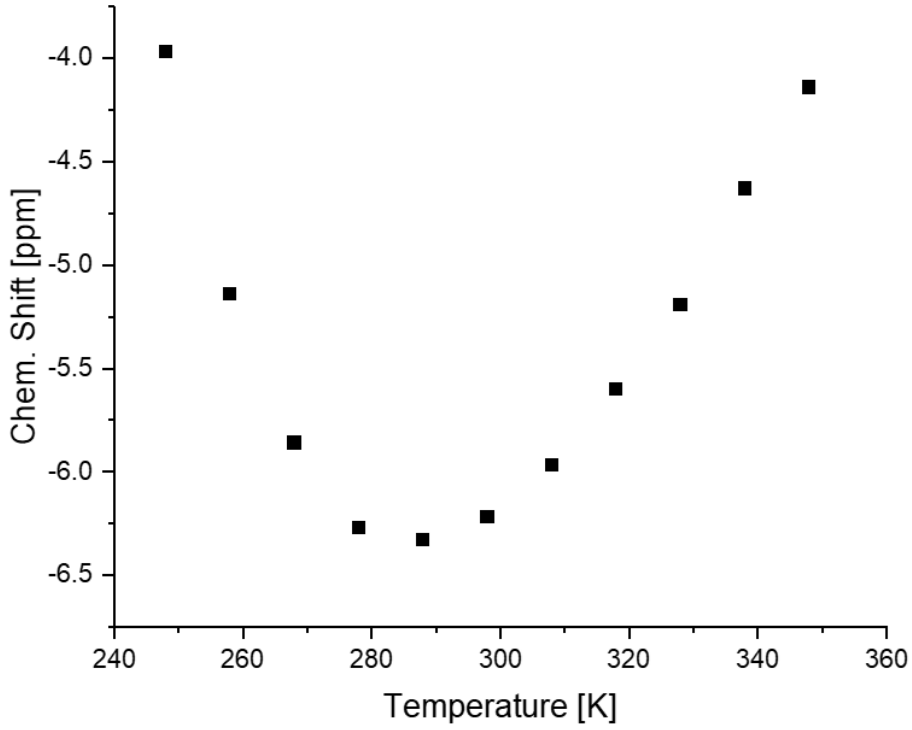

Figure S290. Fitting of the chemical shift versus temperature data for cage **11** (proton p) where δ_{LS} was fixed as 7.08 ppm. The fitting did not converge.

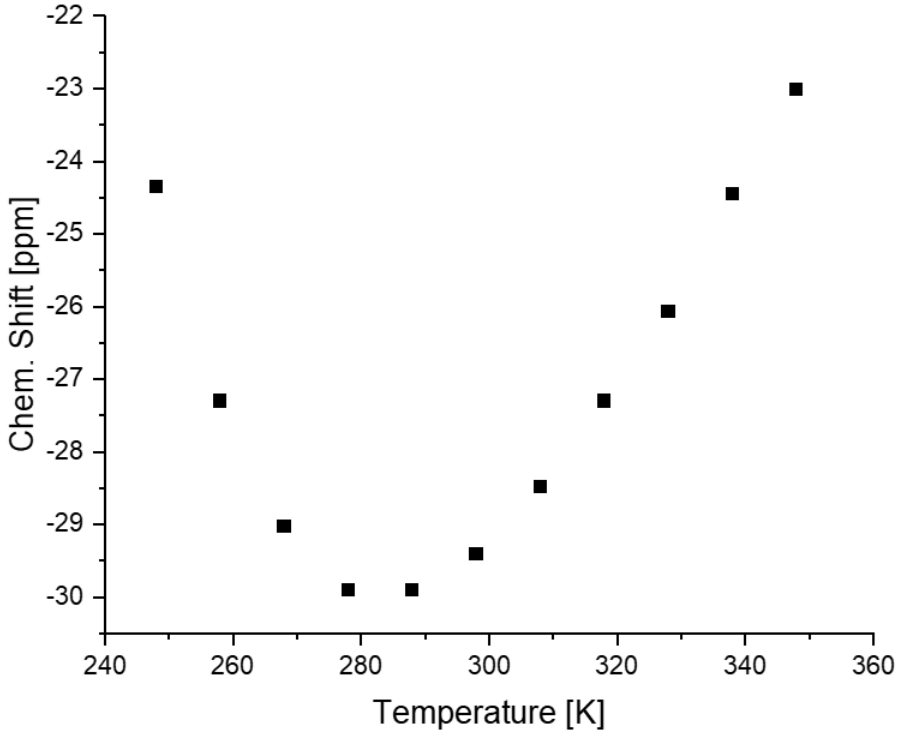

Figure S291. Fitting of the chemical shift versus temperature data for cage **11** (proton f) where δ_{LS} was fixed as 6.63 ppm. The fitting did not converge.

Table S3. Spin-crossover temperatures from variable temperature NMR experiments (248-308 K) for cage **11** for different protons.

Proton	Cage 11	
	$T_{1/2}$ [K]	δ_{LS} [ppm][a]
j	244	8.46
m	286	7.70
c	247	7.83
a	244	4.36
n	268	2.63
d	[b]	7.51
e	[b]	7.05
p	[b]	7.08
f	[b]	6.63

[a] Chemical shift of the Zn(II) cage analogue. [b] Could not be determined since fitting did not converge.

6 X-Ray Crystallography

Data collection for compound **18**, cages **5** and **7** was performed with a XtaLAB Synergy, Dualflex, HyPix diffractometer with CuKα radiation (λ = 1.54184). The structures were solved with SHELXT[11] and refined with SHELXL[12] using Least Squares minimisation. All non-hydrogen atoms were refined anisotropic. The C-H H atoms were positioned with idealized geometry and were refined isotropic with $U_{iso}(H) = 1.2\ U_{eq}(C)$. The crystal of cage **7** was racemically twinned and therefore, a twin refinement was performed leading to a BASF parameter of 0.455(8). In cage **5** six of the eight anions were located, whereas none of them can be located in cage **7**. Therefore, the contribution of the missing anions to the electron density map was removed but they were considered in the calculation of the molecular formula. The anions but also all other atoms have extremely high components of the anisotropic displacement parameters indicating for disorder. Several attempts were made to find a reasonable split model without any success but to reach convergence much of restraints must be used. All these problems can be traced back to the very poor crystal quality. Even on extremely long exposure times, especially cage **7** do not diffract below about 1.2 Å.

A table with selected crystal data and results for the structure refinement can be found in Tables S2 and S3.

CCDC-2207255 (compound **18**), CCDC-2207256 (cage **5**) and CCDC-2207257 (cage **7**) contain the supplementary crystallographic data for this paper. These data can be obtained free charge from the Cambridge Crystallographic Data Centre via http://www.ccdc.cam.ac.uk/data_request/cif.

Preparation of the single crystals

Crystals of compound **18** were obtained from slow evaporation of a solution in acetone. Crystals of cages **5** and **7** were obtained by vapour diffusion of diethyl ether into a CD_3CN solution of the cages.

Table S4. Selected crystal data and details of the structure refinements for compound **18**, cage **5** and cage **7**.

Compound	**Compound 18**	**Cage 5**	**Cage 7**
formula	$C_{19}H_{14}BrN_3$	$C_{162}H_{120}F_{24}Fe_4N_{36}O_{24}S_8$	$C_{200}H_{144}Fe_4N_{36}O_{24}F_{24}S_8$
MW / g mol^{-1}	364.24	3890.81	4371.38
crystal system	triclinic	orthorhombic	orthorhombic
space group	*P-1*	*Pccn*	*Pna*2$_1$
a / Å	10.6730(1)	67.4664(11)	38.3429(5)
b / Å	11.4988(2)	17.1648(4)	18.0379(4)
c / Å	12.9614(2)	32.7981(2)	37.1508(6)
α / °	73.861(1)	3290	90
β / °	85.843(1)	90	90
γ / °	87.851(1)	90	90
V / Å^3	1523.75(4)	37981.7(11)	25694.5(7)
T / K	100.00(1)	100.0(1)	100.0 (1)
Z	4	8	4
D_{calc} / g cm^{-3}	1.588	1.361	1.130
μ / mm^{-1}	3.685	4.041	3.040
Crystal size /mm^3	0.18×0.06×0.03	0.05×0.24×0.25	0.2×0.22×0.3
$2\theta_{max}$ / deg	159.914	159.708	133.198
measured refl.	20304	115736	88529
R_{int}	0.0169	0.0882	0.0596
unique refl.	6503	39182	36631
refl. $F_0>4\sigma(F_0)$	6385	29968	21859
parameter	416	2210	2091
R_1 [$F_0 > 4\sigma F_0$)]	0.0274	0.1603	0.1165
wR_2 [all data]	0.0764	0.4511	0.3504
GOF	1.098	1.807	1.185
$\Delta\rho_{max/min}$ / e Å^{-3}	0.58/-0.52	2.62/ −0.1.66	0.61/ −0.45

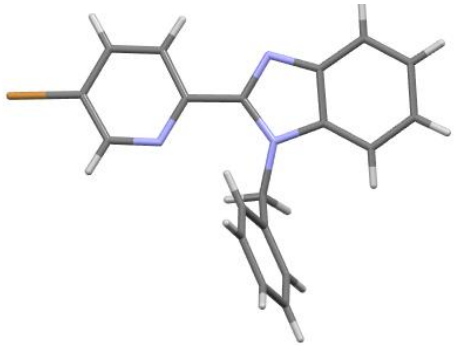

Figure S292. Crystal structure of compound **18**.

According to Shatruk and co-workers,[13] the N-N distance from an X-ray crystal structure of a

ligand can be used to predict the spin-state of the corresponding Fe^{II} homoleptic complex. Based on the N-N distance (2.81 Å) in compound **18**, Fe^{II} homoleptic complexes based on this coordination motif should show spin-crossover.

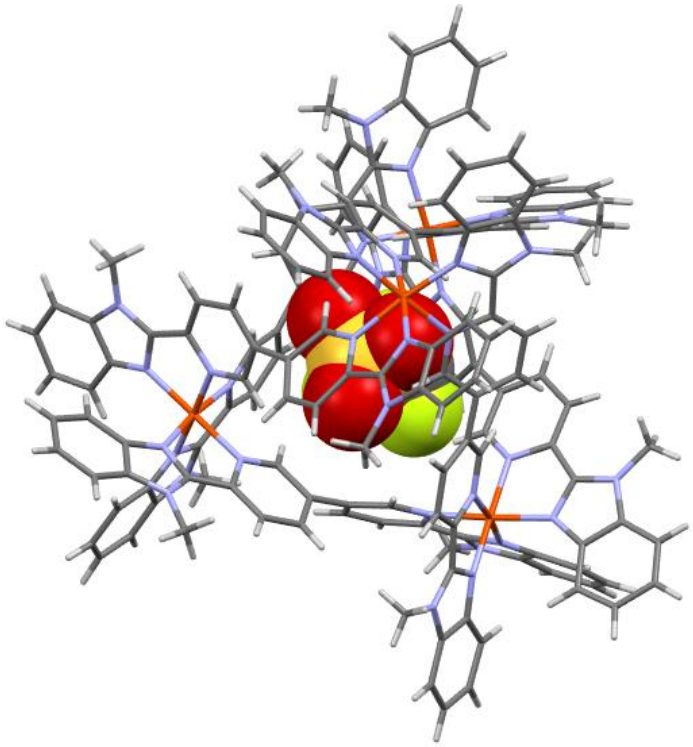

Figure S293. Crystal structure of cage **5**. Hydrogen atoms and non-encapsulated anions are omitted for clarity. The triflate anion was observed to bind in the cavity.

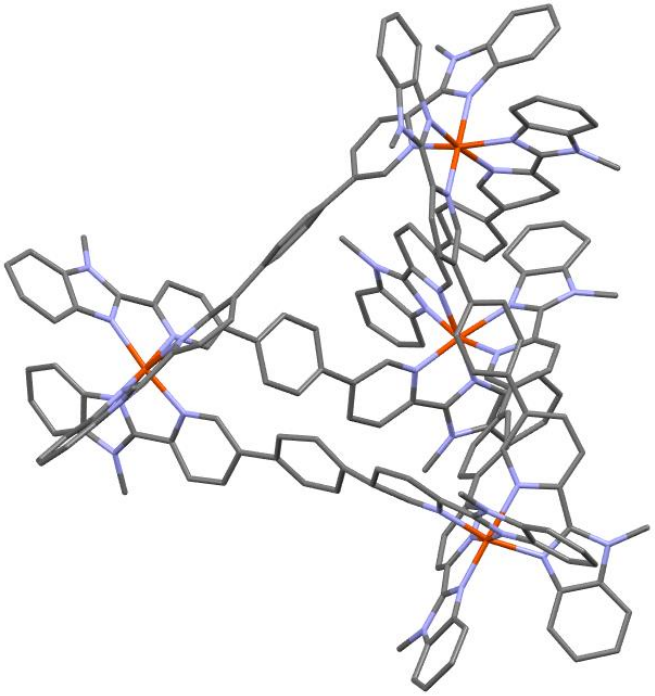

Figure S294. Crystal structure of cage **7**. Hydrogen atoms are omitted for clarity and the anions could not be located during refinement.

7 Anion Binding Studies

Cages **7** and **11** were prepared according to Section 4.7 and 4.11 and the ^{1}H and ^{19}F NMR spectra were measured at 298 K and 248 K. Afterwards, 8 equivalents (relative to the cage) of either $TBABF_4$ (3.65 mg, 11.1 µmol) or $TBANTf_2$ (5.80 mg, 11.1 µmol) were added and the solutions were directly analysed by NMR spectroscopy.

7.1 Cage 7 + BF_4^-

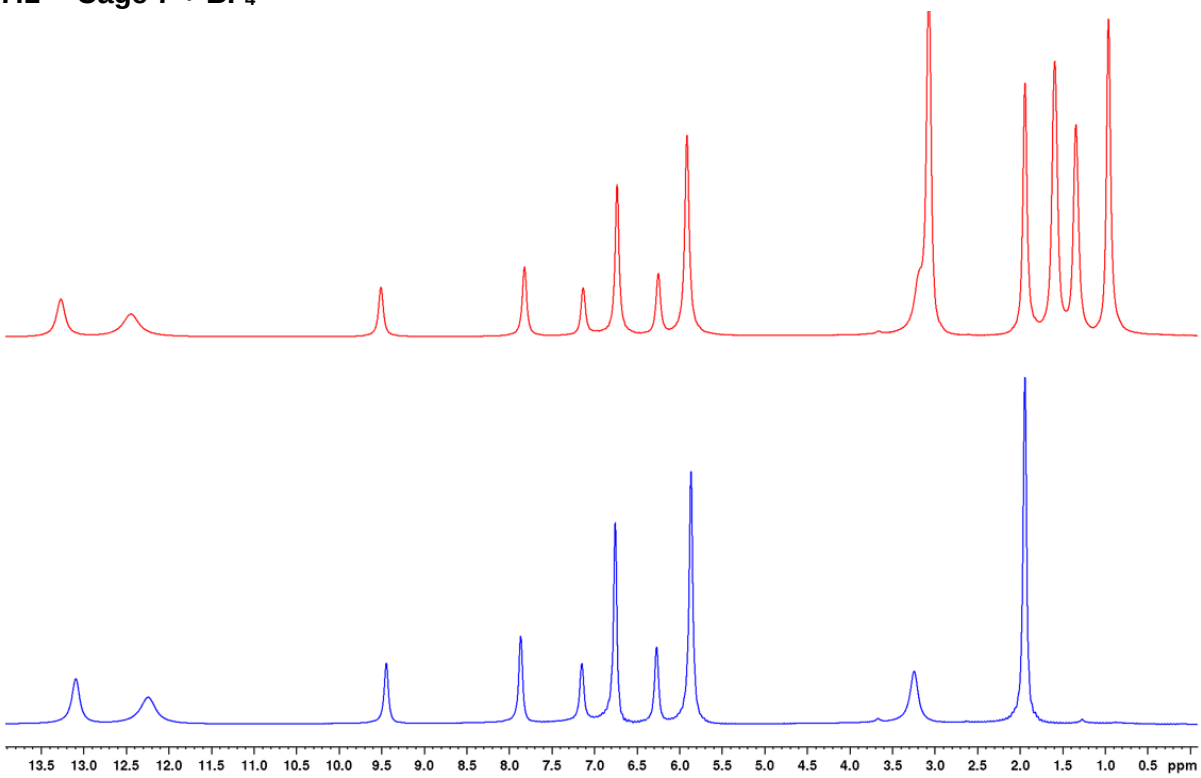

Figure S295. ^{1}H NMR spectra (500 MHz, CD_3CN, 298 K) of cage **7** before (bottom) and after addition of 8 equivalents $TBABF_4$ (top).

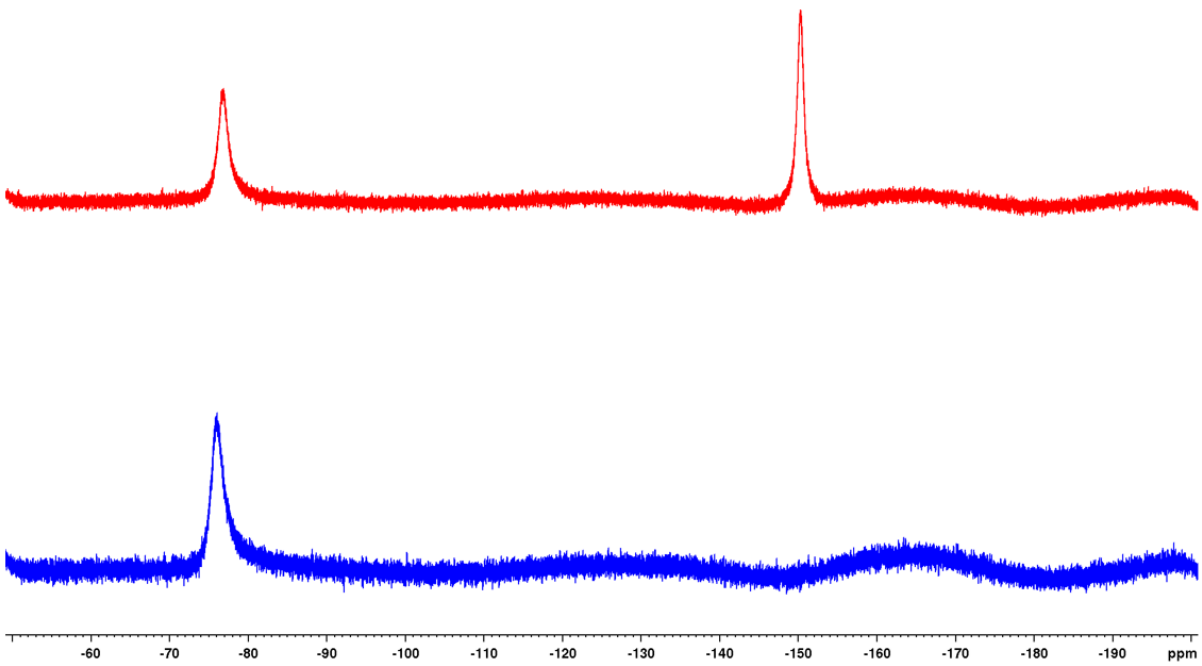

Figure S296. ^{19}F NMR spectra (471 MHz, CD_3CN, 298 K) of cage **7** before (bottom) and after addition of 8 equivalents $TBABF_4$ (top).

7.2 Cage 11 + BF_4^-

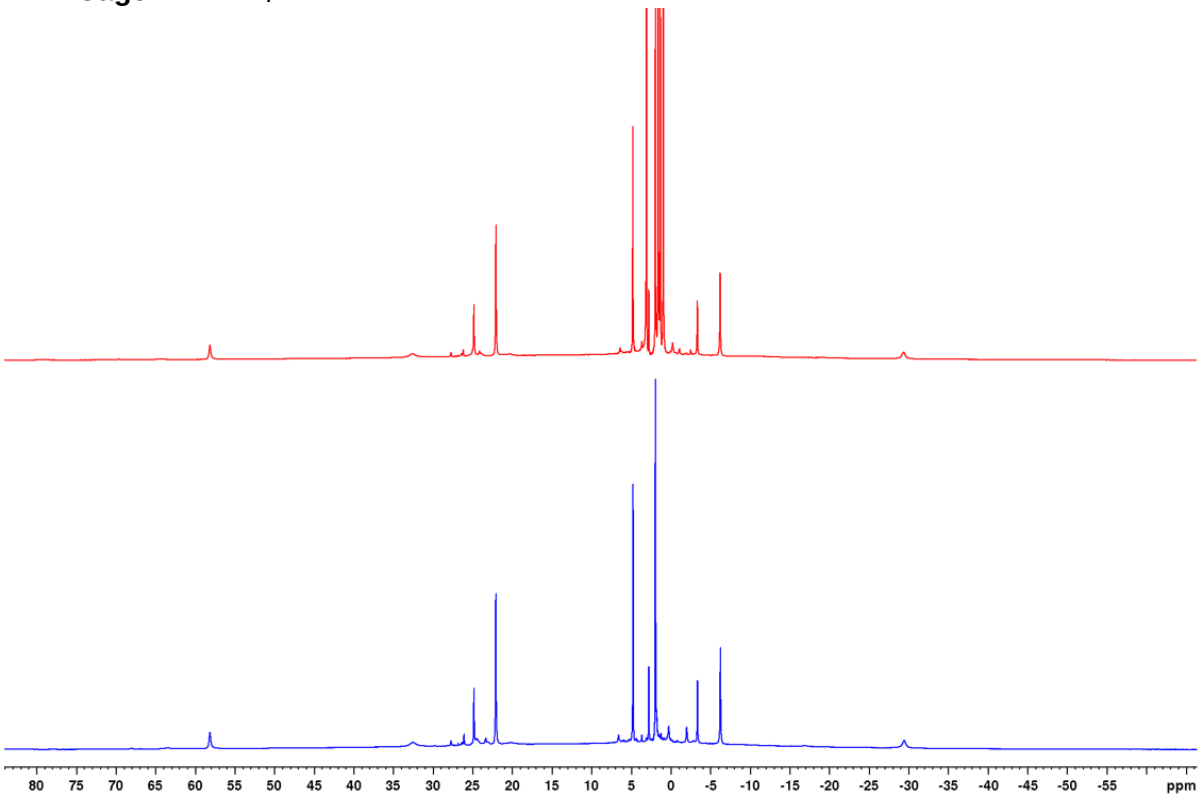

Figure S297. ^{1}H NMR spectra (500 MHz, CD_3CN, 298 K) of cage **11** before (bottom) and after addition of 8 equivalents $TBABF_4$ (top).

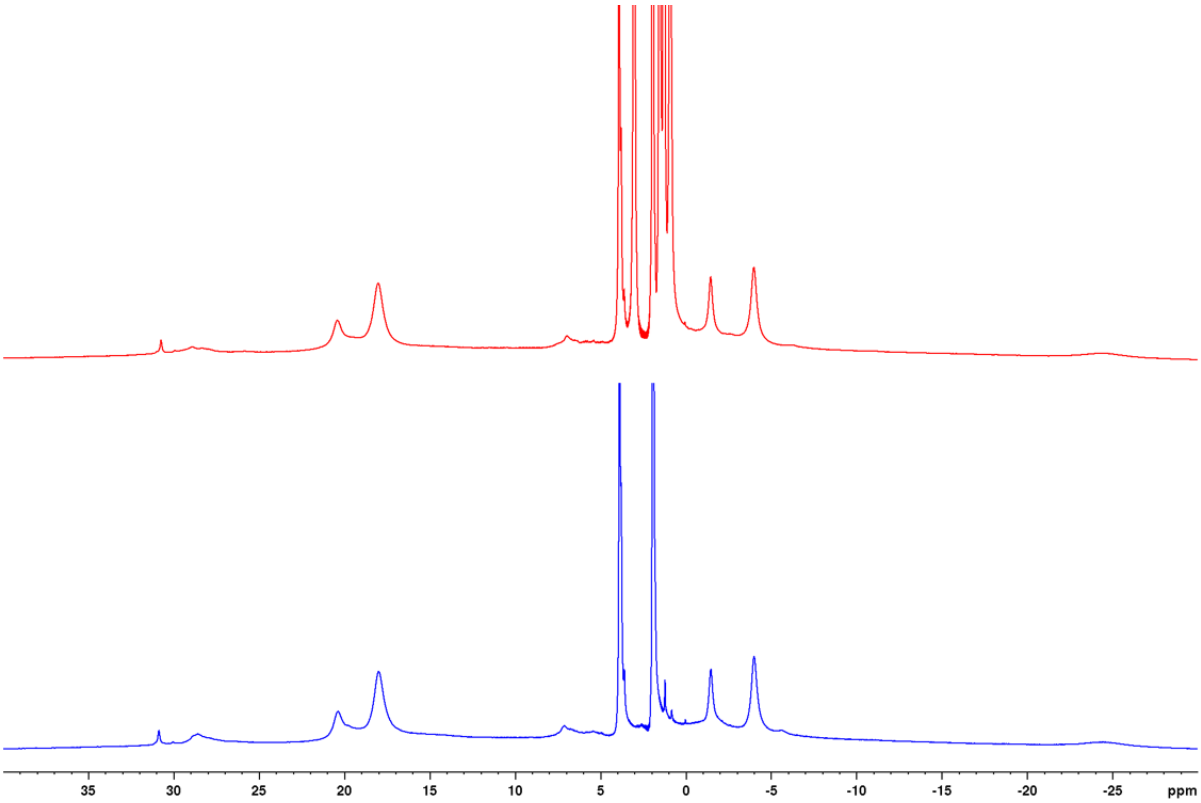

Figure S298. ^{1}H NMR spectra (500 MHz, CD_3CN, 248 K) of cage **11** before (bottom) and after addition of 8 equivalents $TBABF_4$ (top).

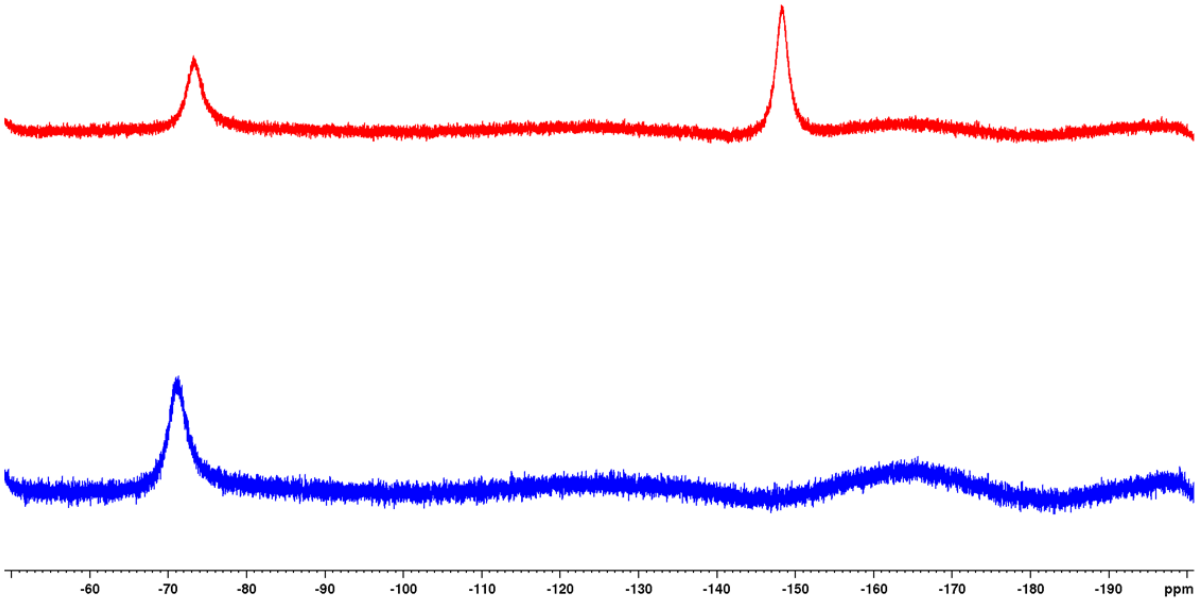

Figure S299. ^{19}F NMR spectra (471 MHz, CD_3CN, 298 K) of cage **11** before (bottom) and after addition of 8 equivalents $TBABF_4$ (top).

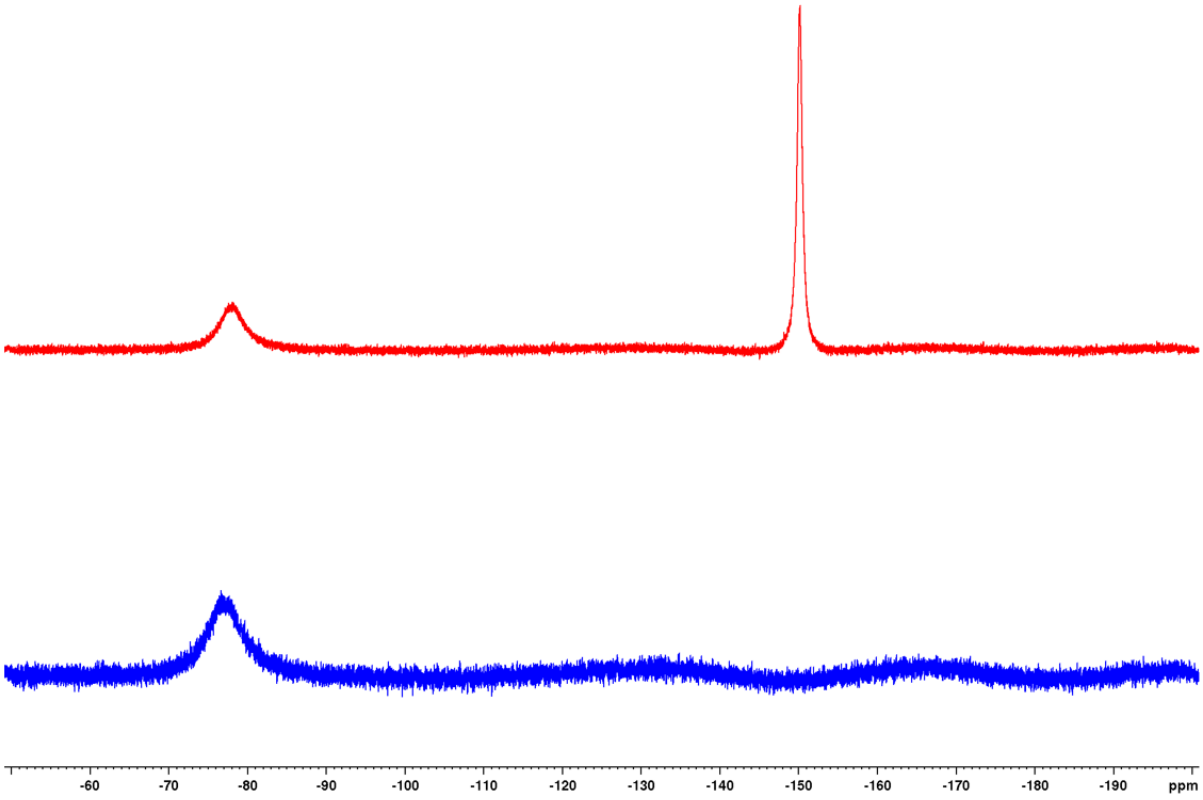

Figure S300. ^{19}F NMR spectra (471 MHz, CD_3CN, 248 K) of cage **11** before (bottom) and after addition of 8 equivalents $TBABF_4$ (top).

7.3 Cage 7 + NTf_2^-

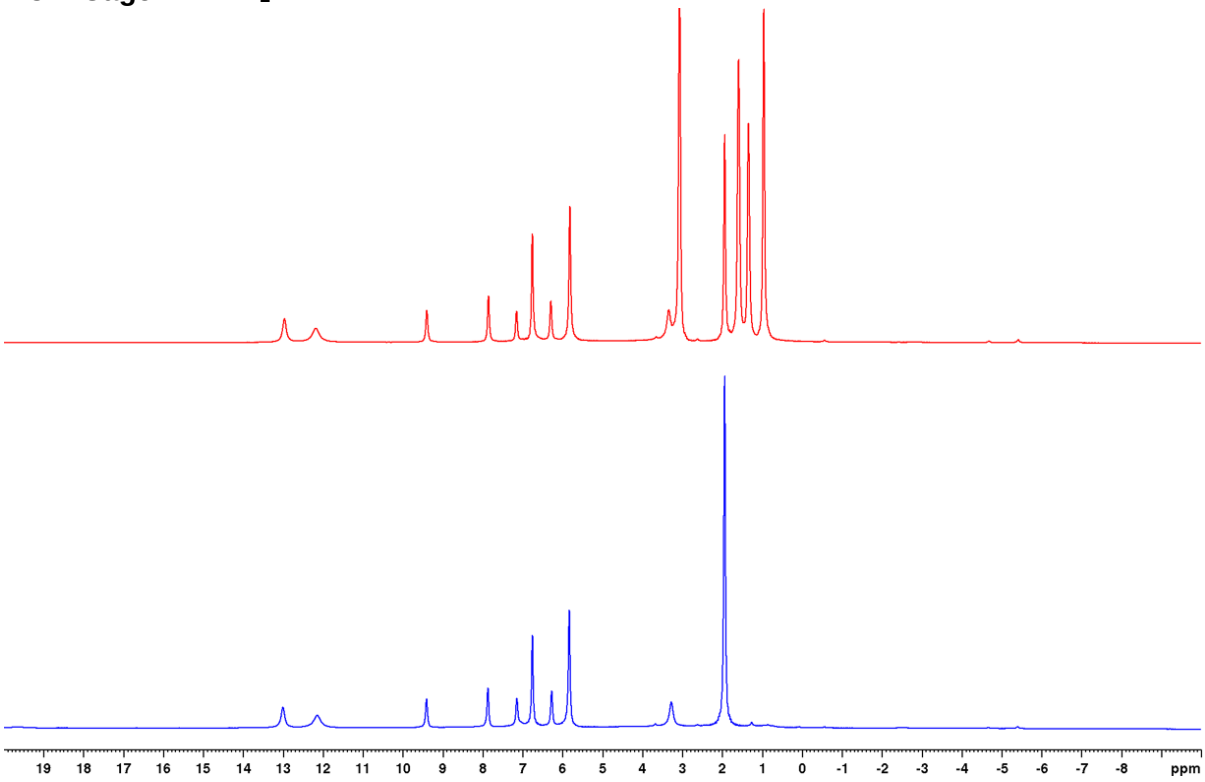

Figure S301. ^{1}H NMR spectra (500 MHz, CD_3CN, 298 K) of cage **7** before (bottom) and after addition of 8 equivalents $TBANTf_2$ (top).

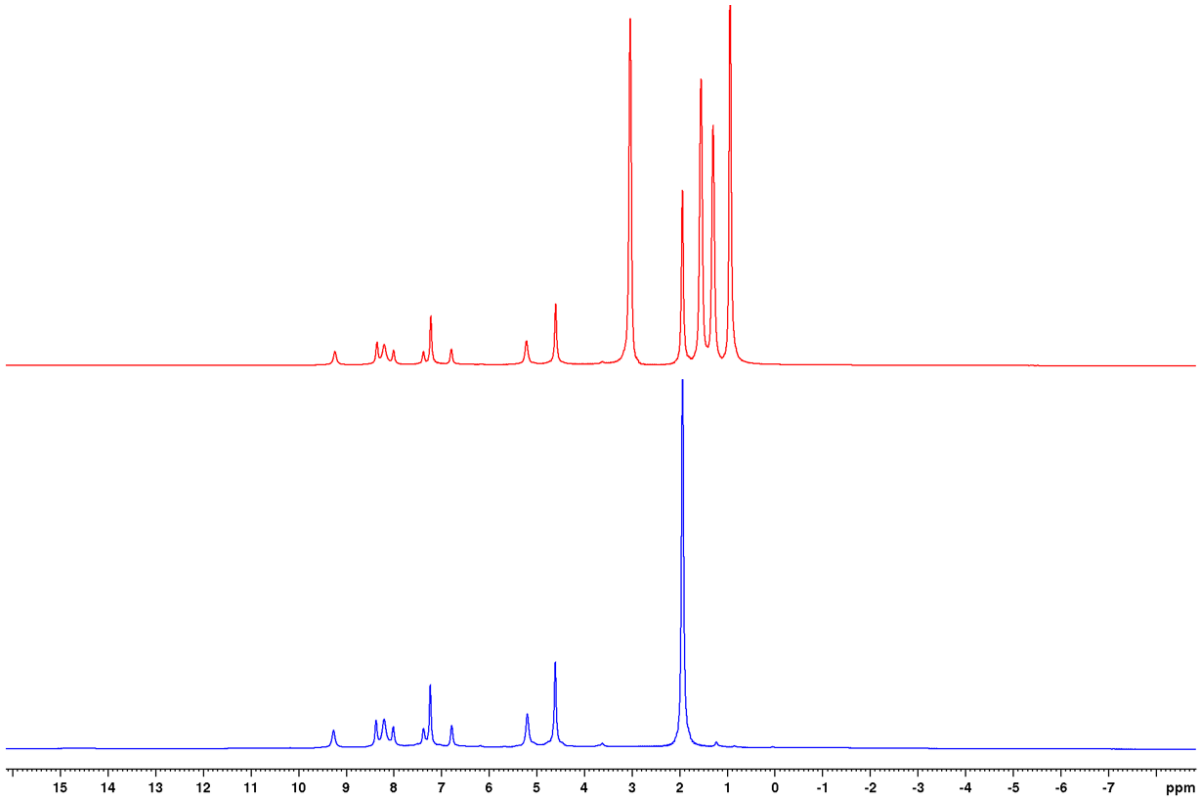

Figure S302. ^{1}H NMR spectra (500 MHz, CD_3CN, 248 K) of cage **7** before (bottom) and after addition of 8 equivalents $TBANTf_2$ (top).

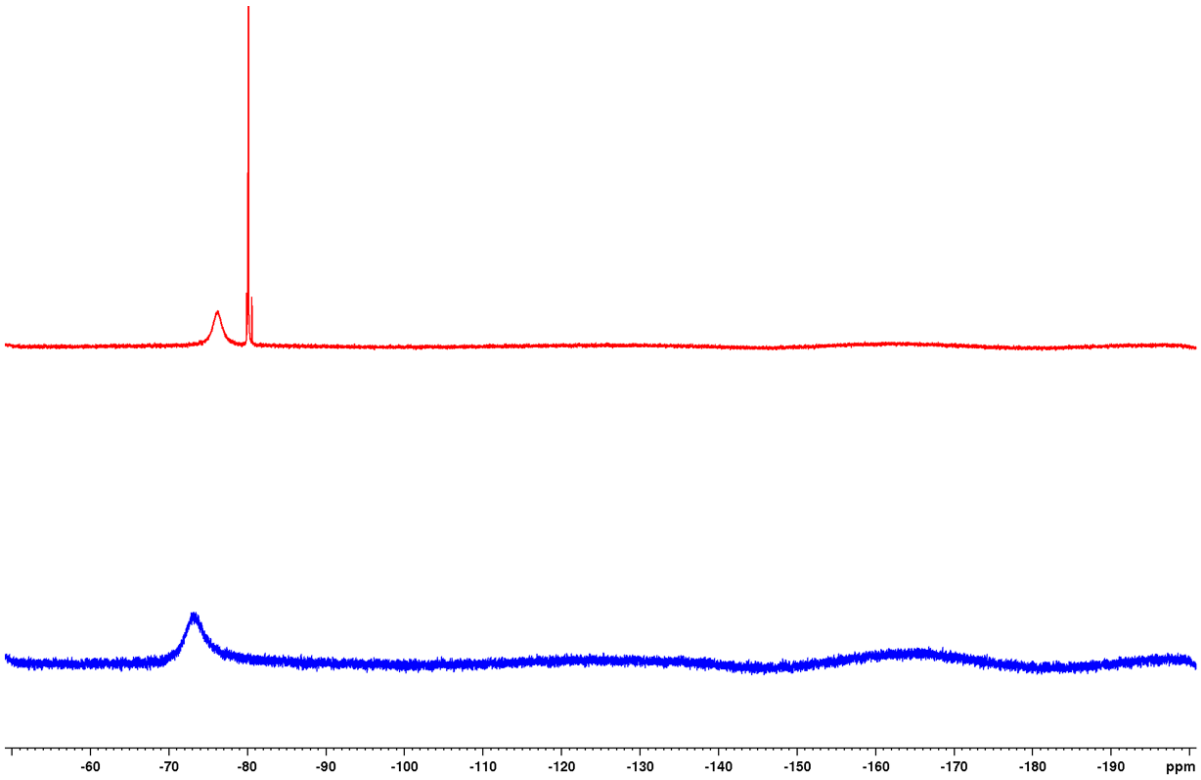

Figure S303. ^{19}F NMR spectra (471 MHz, CD_3CN, 298 K) of cage **7** before (bottom) and after addition of 8 equivalents $TBANTf_2$ (top).

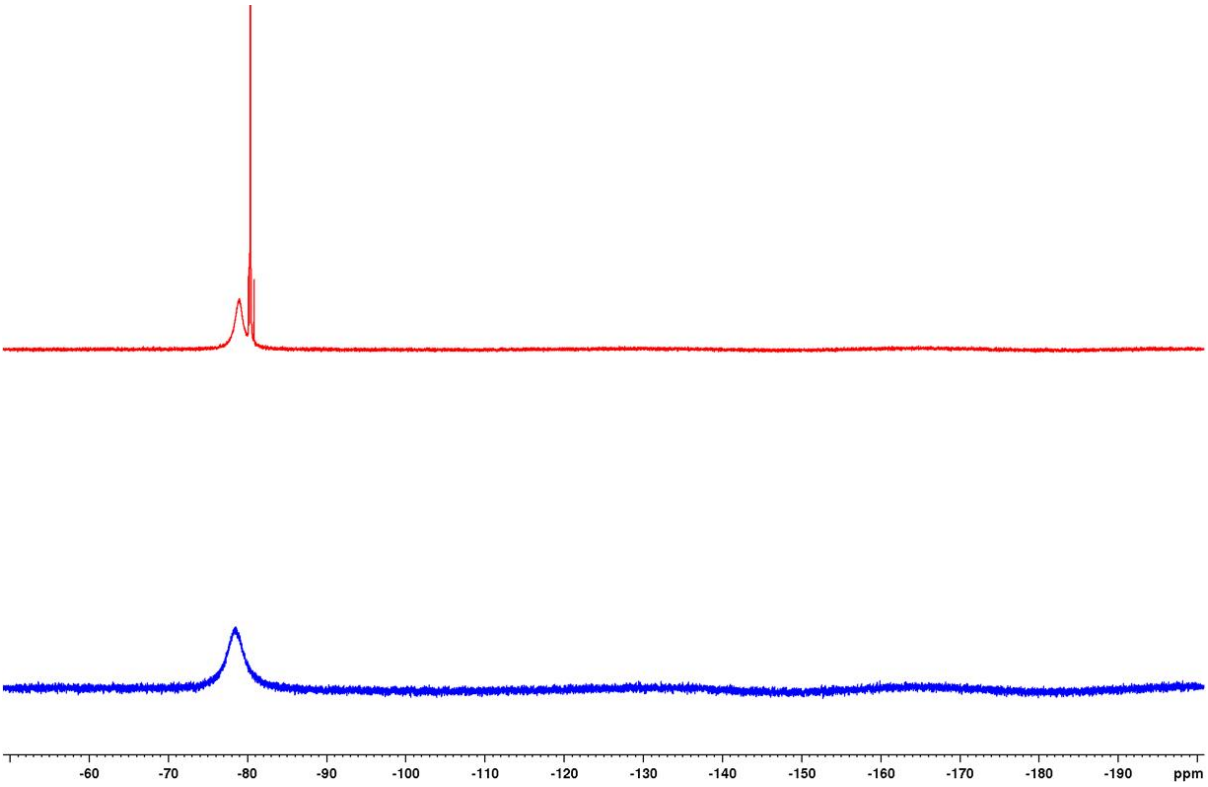

Figure S304. ^{19}F NMR spectra (471 MHz, CD_3CN, 248 K) of cage **7** before (bottom) and after addition of 8 equivalents $TBANTf_2$ (top).

8 References

[1] M. Lehr, T. Paschelke, E. Trumpf, A.-M. Vogt, C. Näther, F. D. Sönnichsen, A. J. McConnell, *Angew. Chem. Int. Ed.* **2020**, *59*, 19344-19351.

[2] M. Lehr, T. Paschelke, V. Bendt, A. Petersen, L. Pietsch, P. Harders, A. J. McConnell, *Eur. J. Org. Chem.* **2021**, 2728-2735.

[3] a) J. Jia, C. Jiang, X. Zhang, Y. Jiang, D. Ma, *Tetrahedron Lett.* **2011**, *52*, 5593-5595; b) M. E. Voss, C. M. Beer, S. A. Mitchell, P. A. Blomgren, P. E. Zhichkin, *Tetrahedron* **2008**, *64*, 645-651.

[4] M. Lin, Q. Tang, H. Zeng, G. Xing, Q. Ling, *Russ. J. Gen. Chem.* **2016**, *86*, 1747-1752.

[5] Q. Cao, D. S. Bailie, R. Fu, M. J. Muldoon, *Green Chem.* **2015**, *17*, 2750-2757.

[6] C.-C. Ko, W.-M. Kwok, V. W.-W. Yam, D. L. Phillips, *Chem. Eur. J.* **2006**, *12*, 5840-5848.

[7] E. Giraldi, A. B. Depallens, D. Ortiz, F. Fadaei-Tirani, R. Scopelliti, K. Severin, *Chem. Eur. J.* **2020**, *26*, 7578-7582.

[8] M. J. Burke, G. S. Nichol, P. J. Lusby, *J. Am. Chem. Soc.* **2016**, *138*, 9308-9315.

[9] A. J. McConnell, C. M. Aitchison, A. B. Grommet, J. R. Nitschke, *J. Am. Chem. Soc.* **2017**, *139*, 6294-6297.

[10] W. Kläui, W. Eberspach, P. Gütlich, *Inorg. Chem.* **1987**, *26*, 3977-3982.

[11] G. M. Sheldrick, *Acta Cryst., Sect. A: Found. Adv.* **2015**, *71*, 3-8.

[12] G. M. Sheldrick, *Acta Cryst., Sect. C: Struct. Chem.* **2015**, *71*, 3-8.

[13] H. Phan, J. J. Hrudka, D. Igimbayeva, L. M. L. Daku, M. Shatruk, *J. Am. Chem. Soc.* **2017**, *139*, 6437-6447.